Local Calibration of the MEPDG for Flexible Pavement Design

FINAL REPORT

Submitted to the North Carolina Department of Transportation
(Research Project No. HWY-2007-07)

Submitted by

Y. Richard Kim, Ph.D., P.E.
Campus Box 7908
Department of Civil, Construction, & Environmental Engineering
North Carolina State University
Raleigh, NC 27695-7908
Tel: 919-515-7758, Fax: 919-515-7908
E-mail: kim@ncsu.edu

Fadi M. Jadoun, Ph.D., P.E.
Campus Box 7908
Department of Civil, Construction, & Environmental Engineering
North Carolina State University
Raleigh, NC 27695-7908
Tel: 919-827-3877, Fax: 919-515-7908
E-mail: fmjadoun@ncsu.edu

Tian Hou
Former Graduate Research Assistant
Department of Civil, Construction, & Environmental Engineering
North Carolina State University

Naresh Muthadi
Civil Engineer
HNTB Corporation
2900 S Quincy Street, Suite 200
Arlington, VA, 22206

Department of Civil, Construction, & Environmental Engineering
North Carolina State University
Raleigh, NC

October 2011

Technical Report Documentation Page

1. Report No. FHWA\NC\2007-07	2. Government Accession No.	3. Recipient's Catalog No.
4. Title and Subtitle Local Calibration of the MEPDG for Flexible Pavement Design		5. Report Date October 2011 6. Performing Organization Code
7. Author(s) Y. Richard Kim, Fadi M. Jadoun, T. Hou, and N. Muthadi		8. Performing Organization Report No.
9. Performing Organization Name and Address Campus Box 7908, Dept. of Civil, Construction, & Environmental Engrg. NCSU, Raleigh, NC 27695-7908		10. Work Unit No. (TRAIS) 11. Contract or Grant No.
12. Sponsoring Agency Name and Address NC Department of Transportation Research and Analysis Group 1 South Wilmington Street Raleigh, NC 27601		13. Type of Report and Period Covered Final Report July 2006 – August 2009 14. Sponsoring Agency Code 2007-07
15. Supplementary Notes		

16. Abstract

In an effort to move toward pavement designs that employ mechanistic principles, the AASHTO Joint Task Force on Pavements initiated an effort in 1996 to develop an improved pavement design guide. The project called for the development of a design guide that employs existing state-of-the-practice mechanistic-based models and design procedures. The product of this initiative became available in 2004 in the form of software called the Mechanistic-Empirical Pavement Design Guide (MEPDG). The performance prediction models in the MEPDG were calibrated and validated using performance data measured from hundreds of pavement sections across the United States. However, these nationally calibrated performance models in the MEPDG do not necessarily reflect local materials, local construction practices, and local traffic characteristics. Therefore, in order to produce accurate pavement designs for the State of North Carolina, the MEPDG distress prediction models must be recalibrated using local materials, traffic, and environmental data. The North Carolina Department of Transportation (NCDOT) has decided to adopt the MEPDG for future pavement design work and has awarded a series of research projects to North Carolina State University. The primary objective of this study is to calibrate the MEPDG performance prediction models for local materials and conditions using the data and findings generated from this series of research projects.

The work presented in this report focuses on four major topics: (1) the development of a GIS-based methodology to enable the extraction of local subgrade soils data from a national soils database; (2) the rutting and fatigue cracking performance characterization of twelve asphalt mixtures commonly used in North Carolina; (3) the characterization of local North Carolina traffic; and (4) calibration of the flexible pavement distress prediction models in the MEPDG to reflect local materials and conditions.…

Continued next page.

17. Key Words MEPDG, Local Calibration, Flexible, Pavement Design	18. Distribution Statement		
19. Security Classif. (of this report) Unclassified	20. Security Classif. (of this page) Unclassified	21. No. of Pages 528	22. Price

Form DOT F 1700.7 (8-72) **Reproduction of completed page authorized**

Abstract (Continued)

The scope of this research is limited to rutting and fatigue cracking. The total number of sections available for this study is 46 sections: 22 long-term pavement performance (LTPP) sections (6 SPS and 16 GPS sites) and 24 non-LTPP sites. Because the LTPP sites have more complete distress and materials information available than the other sites, the research team used all the LTPP sites for calibration and used the 24 non-LTPP sites for validation. Some of the LTPP sections and many of the NCDOT sections were found to lack data, however, so MEPDG defaults and engineering judgment were used to populate the missing data.

For the subgrade soil characterization, a GIS-based methodology was developed so that NCDOT engineers can superimpose road sections of interest on the NCHRP 9-23A soil maps and find the corresponding alphanumeric soil unit code that is required to extract the related soil information. Material-specific hot mix asphalt (HMA) rutting and fatigue cracking model coefficients were developed for the twelve most commonly used HMA mixtures in North Carolina using data obtained from the triaxial repeated load permanent deformation (TRLPD) test and the direct tension cyclic test, respectively. These test data, in addition to the dynamic modulus data determined from the HWY-2003-09 project, *Typical Dynamic Moduli for North Carolina Asphalt Concrete Mixes*, have resulted in the North Carolina MEPDG materials database.

A North Carolina MEPDG traffic database has been established based on the research efforts from the HWY-2008-11 project, *Development of Traffic Data Input Resources for the Mechanistic Empirical Pavement Design Process*, and from this study. This database was developed based on a multi-dimensional clustering methodology and a pavement damage-based approach in order to characterize local traffic and to develop traffic catalogs for the traffic parameters required as inputs in the MEPDG.

The initial MEPDG verification runs reveal that, when the MEPDG national default calibration values are used, the rut depth and fatigue cracking predictions are significantly different from the measured values. Two approaches were used to calibrate the rutting and fatigue cracking models for local conditions and materials. The first approach uses the generalized reduced gradient (GRG) method, whereas the second approach uses the genetic algorithm (GA) optimization technique. The GA-based approach is found to result in statistically better total rut depth and alligator cracking predictions than the GRG method.

The local calibration of the MEPDG is found to reduce bias and standard error between the predicted and measured rut depth and fatigue cracking percentage values. However, the improvement is not enough to accept the null hypothesis that the measured values are equal to the predicted values at the 95% confidence interval. The calibration results demonstrate the importance of using material-specific performance test results, having detailed and reliable distress data, and taking permanent deformation measurements from individual layers through forensic investigation. This study results in a set of local calibration factors for the permanent deformation and fatigue cracking performance prediction models in the MEPDG for the State of North Carolina and the North Carolina MEPDG User Reference Guide, along with a list of future research recommendations.

DISCLAIMER

The contents of this report reflect the views of the authors and are not necessarily the views of North Carolina State University. The authors are responsible for the facts and the accuracy of the data presented herein. The contents do not necessarily reflect the official views or policies of the North Carolina Department of Transportation at the time of publication. This report does not constitute a standard, specification, or regulation.

ACKNOWLEDGEMENTS

This research was sponsored by the North Carolina Department of Transportation. The Steering and Implementation Committee was comprised of Clark Morrison, Ph.D., P.E. (Chair), Jack E. Cowsert, P.E., Michael J. Kneis, P.E., James (Jim) Phillips, P.E., Kent L. Taylor, P.E., Njoroge W. Wainaina, P.E., and Todd W. Whittington, P.E. Friends of the committee include Moy Biswas, Ph.D., P.E., Judith Corley-Lay, Ph.D., P.E., Robert S. Foyle, P.E., Cecil L. Jones, P.E., C. K. Su, Emily O. McGraw, P.E., Joseph (Max) Tate, P.E., and Mustan Kadibhai, P.E. These advisors have given invaluable direction and support to the research team throughout the project.

TABLE OF CONTENTS

LIST OF TABLES

LIST OF FIGURES

LIST OF ACRONYMS

Acronym	Meaning
AADTT	Annual Average Daily Truck Traffic
AASHTO	American Association of State Highway and Transportation Officials
ABC	Aggregate Base Course
AC	Asphalt Concrete
ALDF	Axle Load Distribution Factors
APT	Number of Axles per Truck
ATB	Asphalt Treated Base
AVC	Automatic Vehicle Classification
CTB	Cement Treated Base
DARWin-ME	Design, Analysis and Rehabilitation for Windows-Mechanistic Empirical
$\|E^*\|$	Dynamic modulus of asphalt concrete
EICM	Enhanced Integrated Climatic Model
FHWA	Federal Highway Administration
$\|G^*\|$	Dynamic shear modulus of asphalt binder
GIS	Geographic Information System
GUI	Graphical User Interface
HDF	Hourly Distribution Factors
HMA	Hot Mix Asphalt
IRI	International Roughness Index
LDF	Lane Distribution Factor
LOE	Line of Equality
M&T Unit	Materials and Tests Unit
MAF	Monthly Adjustment Factors
MEPDG	Mechanistic Empirical Pavement Design Guide
NMAS	Nominal Maximum Aggregate Size
NRCS	National Resources Conservation Service
PMS	Pavement Management Systems
PMU	Pavement Management Unit
SI	Serviceability Index
SWCC	Soil Water Characteristics Curve
TPB	Traffic Planning Branch
TSU	Traffic Survey Unit
USDA	United States Department of Agriculture
WIM	Weigh-in-Motion

CHAPTER 1 INTRODUCTION

1.1 Background

In 1958, the American Association of State Highway Officials (AASHO) sponsored the construction of a multi-million dollar project (the AASHO road test) in Ottawa, Illinois to study the performance of asphalt and Portland cement concrete pavements under different traffic loads and speeds. Although the main goal of the project was to quantify the amount of damage caused by trucks for tax purposes, the information gained from the project was crucial in advancing the knowledge of pavement structural design and performance, load equivalencies, climate effects, etc. However, the AASHO test road comprised limited layer material types, only a single type of subgrade material, a single climatic region, 1958 truck axle configurations and tire pressures, and more site-specific parameters that warrant a careful utilization of such information.

Based on the information obtained from the AASHO road test, the American Association of State Highway and Transportation Officials (AASHTO) was able to develop empirical structural design tools for designing flexible and rigid pavement structures. The most recent version of the AASHTO design guide was made available in 1993, and since that time, it has served as the most widely used design tool among state highway agencies in the United States to create the nation's highway network.

Due to the limitations of the aforementioned AASHO road test and its inherent empirical design procedures, the AASHTO Joint Task Force on Pavements (JTFP), which is responsible for the development and implementation of pavement design technologies, initiated an effort in 1996 to develop an improved AASHTO pavement design guide by the year 2002. As part of this effort, the JTFP sponsored a workshop in March 1996 in Irvine, California to develop a framework for improving the design guide. The participants were charged with identifying the means to develop an AASHTO mechanistic-empirical pavement design procedure by the 2002 deadline. Based on the conclusions of this meeting, NCHRP project 1-37A, *Development of the 2002 Guide for Design of New and Rehabilitated Pavement Structures: Phase II*, was awarded in 1998 to the ERES Consultants Division of Applied Research Associates, Inc. The project called for the development of a design guide that employs existing state-of-the-practice mechanistic-based models and design procedures (NCHRP, 2004a). The product of the NCHRP 1-37A project first became available in 2004 as the Mechanistic Empirical Pavement Design Guide (MEPDG). The mechanistic component of the MEPDG calculates pavement critical responses (i.e., stresses, strains, and deflections) based on layer material properties and climatic conditions. The empirical side of the design method bridges the gap between laboratory and field performance, which, in turn, reflects local construction practices and other field-related variables.

Recently, the MEPDG became an AASHTO official product. The software to convert the research product, MEPDG, into a production design tool was given the name DARWin-ME to differentiate it from the computer version of the AASHTO 1993 design guide called

DARWin (design, analysis, and rehabilitation for Windows). DARWin-ME will be available commercially early in 2011. (Note: the design guide is referred to as the MEPDG throughout this report, because the name change is not yet in effect.)

1.2 Research Needs and Significance

The performance models in the MEPDG were calibrated and validated using pavement performance data obtained mainly from the long-term pavement performance (LTPP) database (NCHRP, 2009). The LTPP program was established in 1987 by the Strategic Highway Research Program (SHRP) to study in-service pavements. More than 2,400 asphalt and Portland cement concrete pavement test sections across the United States and Canada have been monitored through this program.

The nationally calibrated performance models in the MEPDG do not necessarily reflect local conditions, however. Different highway agencies may have different policies regarding pavement preservation and maintenance techniques. They may also have different material types and specifications, various climatic regions, and different traffic stream characteristics. All these differences between local conditions and national averages, coupled with the recommendations of the NCHRP 1-40B project panel for local calibration, warrant the need for a state-level local calibration and validation guide. Distress prediction models must be calibrated properly prior to their adoption and use for design purposes. The accuracy of performance prediction models depends on an effective process of calibration and subsequent validation using independent data sets. This calibration/validation process is, in the end, critical for designers to be able to have confidence in the recommended design procedure (NCHRP, 2009).

The North Carolina Department of Transportation (NCDOT) decided to adopt the new MEPDG for future pavement design work. It then awarded a series of research projects to North Carolina State University (NCSU), including:

- HWY-2005-28 project *Implementation Plan for the New Mechanistic-Empirical Pavement Design Guide*
- HWY-2003-09 project *Typical Dynamic Moduli for North Carolina Asphalt Concrete Mixes*
- HWY-2008-11 project *Development of Traffic Data Input Resources for the Mechanistic Empirical Pavement Design Process*
- HWY-2007-07 project *Local Calibration of the MEPDG for Flexible Pavement Design*

Material databases were established from the HWY-2003-09 and HWY-2007-07 projects, whereas the HWY-2008-11 project characterized local traffic and prepared traffic catalogs for the traffic parameters required as inputs in the MEPDG. These local data were used in the HWY-2007-07 project to calibrate the MEPDG for local conditions. This report describes the research efforts made in the MEPDG local calibration using these data.

1.3 Research Objective

The primary objective of this research project is to calibrate the MEPDG for flexible pavements using typical local layer materials, typical pavement structures, and North Carolina climatic and traffic data. Within the scope of this objective, a materials database will be developed for the twelve most commonly used asphalt concrete mixtures in North Carolina. The local traffic data are assembled by the HWY-2008-11 project using the data collected from 46 weigh-in motion (WIM) stations across the state to develop data catalogs for the traffic parameters required as inputs to the MEPDG. These materials database and traffic catalogs will facilitate the design process by providing the designers with different sets of materials and traffic data that are required by the MEPDG for designing different types of pavement structures to be built in various locations across the state.

For calibrating the flexible pavement performance models, the scope of this research project is limited to alligator fatigue cracking (or so-called *bottom-up cracking*) and permanent deformation (or so-called *rutting*). Based on numerous test sections, the NCHRP 1-40B and NCHRP 9-30A project panels found that the MEPDG performance prediction model for longitudinal cracking (or so-called *top-down cracking*) has yet to be confirmed in order for it to actually predict surface-initiated load-related cracks. Therefore, longitudinal cracking is not addressed in this report.

1.4 Report Organization

This report consists of nine chapters and eight appendices. Chapter 1 presents background information regarding the new MEPDG as well as research needs and objectives. Chapter 2 focuses on material sources and acquisition. Chapter 3 addresses mixture verification procedures and target air voids development for fabricating performance specimens. Chapter 4 deals with unbound materials characterizations and the use of NCHRP 9-23A soils product. Chapter 5 presents in detail permanent deformation (rutting) characterization, and Chapter 6 presents fatigue cracking characterization. Chapter 7 presents a general overview and definitions of the traffic parameters that are required as inputs to the MEPDG. In addition, Chapter 7 summarizes the final local traffic input parameters as determined from the NCDOT HWY-2008-11 project. Chapter 8 discusses the calibration of the MEPDG performance models, and finally, Chapter 9 provides conclusions learned from this research in addition to future recommendations.

Appendix A includes a complete database of the structures, materials, location, and traffic information for all calibration and validation sections. Appendix B presents the dynamic modulus database for 18 of the most commonly used asphalt concrete mixtures in North Carolina. Appendix C presents the dynamic shear modulus database for three binder grades that are typically used in North Carolina. Appendix D summarizes the permanent deformation (rutting) database for the 12 most commonly used asphalt concrete mixtures in North Carolina as characterized using the triaxial repeated load permanent deformation (TRLPD) test method. Appendix E presents the bottom-up fatigue cracking (or so-called: alligator cracking) database for the twelve most commonly used asphalt concrete mixtures in North Carolina. Appendix F is a paper published in the Transportation Research Record

(TRR) that summarizes verification results and the results of the paper-based local calibration effort using level-3 materials data input. Appendix G is a complete subgrade soils database for the different soil profiles in North Carolina as determined by the NCHRP 9-23A project. Finally, Appendix H includes a *North Carolina MEPDG User Reference Guide* that assimilates the products of this research into a simplified user-friendly manual for use by NCDOT engineers to design asphalt concrete pavements.

CHAPTER 2 MATERIALS ACQUISITION

2.1 Identification of Twelve Most Commonly used Asphalt Mixtures in North Carolina

In the early stages of this research work, the NCDOT identified twelve of the most commonly used Superpave asphalt concrete mixtures that are typically produced and paved in North Carolina. Six of these mixes include reclaimed asphalt pavement (RAP). Job mix formula (JMF) and mix design (MD) sheets for these twelve mixtures have been acquired from the Materials and Tests (M&T) Unit at the NCDOT. The twelve mixtures were characterized in the lab, and the results were used to develop local calibration factors for the permanent deformation and alligator cracking performance prediction models currently embedded in the MEPDG. Significant effort was made in acquiring the aggregate materials and asphalt binders for these twelve mixtures from various quarries and asphalt production plants across North Carolina and South Carolina. Table 2.1 summarizes the selected twelve most commonly used mixtures along with their respective asphalt binder type, asphalt binder source, and aggregate source. Section 2.2 explains the mix type designation currently used by the NCDOT and shown in Table 2.1.

2.2 NCDOT Asphalt Mixture Designations

In 1998, the NCDOT implemented the Superpave (*Su*perior *per*forming asphalt *pave*ments) mix design method for the design of asphalt concrete mixtures. Superpave was developed through the Strategic Highway Research Program (SHRP), a five-year, applied research initiative that was authorized in 1987 by the United States Congress to evaluate techniques and technologies to combat the deteriorating conditions of the nation's highways. The NCDOT developed Superpave-based local specifications that include nomenclature to describe the various Superpave HMA mix types, such as those shown in Table 2.1. This naming convention is explained below.

Each Superpave mix name has a four-component structure. For example, the Superpave mix name RS9.5C has the following four components:

1) "R", when included, indicates the presence of RAP in the mixture.
2) "S", in this case, or "I" or "B" indicates the pavement structure layer for which the mix is designed; "S" stands for the *surface* layer, "I" stands for the *intermediate* (or binder) layer, and "B" stands for the *base* layer.
3) "9.5" is the nominal maximum aggregate size (NMAS) of the mixture. The NMAS is defined according to Superpave as one sieve size larger than the first sieve to retain more than 10 percent of the material. This research employs four NMAS mixtures: 9.5 mm, 12.5 mm, 19.0 mm, and 25 mm.
4) "C", in this case, or "A", "B", or "D", indicates the traffic level that this mixture was designed to handle. Table 2.2 shows the different Superpave mix types with their corresponding traffic level and binder grade that could be used. The scope of this research includes traffic levels "B" and "C", which are the most widely used levels in North Carolina.

Table 2.1. Summary of the Twelve Most Commonly Used HMA Mixes in North Carolina

Mix Type	PG Grade	Binder Source	Aggregate Source
S9.5B	PG64-22	Associated Asphalt/Inman - SC # 6	Vulcan - Morganton
S9.5C	PG70-22	Associated Asphalt - Greensboro	Vulcan / N. - Winston Salem
RS9.5C	PG70-22	Citgo - Wilmington # 31	Martin Marietta - Garner
			Rea Contractors - Garner
S12.5C	PG70-22	Citgo - Charlotte # 11	Vulcan - Rockingham
I19.0B	PG64-22	Associated Asphalt/Inman - SC # 6	Vulcan - Morganton
RI19.0B	PG64-22	Associated Asphalt/Inman - SC # 6	Martin Marietta - Pomona
			Martin Marietta - Central Rock
			G.S Materials - Emery
			Blythe Construction - Greensboro
B25.0B	PG64-22	Associated Asphalt - Salisbury # 12	Martin Marietta - Pomona
RB25.0B	PG64-22	Citgo - Wilmington # 31	Martin Marietta - Garner
			S.T. Wooten Corp. - Clayton
RS9.5B	PG64-22	Citgo - Wilmington # 31	Martin Marietta - Garner
			Rea Contractors -Garner
RS12.5C	PG70-22	Citgo - Wilmington # 31	Vulcan - Pineville
			Blythe Brothers - Charlotte
I19.0C	PG64-22	Citgo - Charlotte # 11	Vulcan - Rockingham
			Rea Contractors - Graham
RI19.0C	PG64-22	Citgo - Wilmington # 3	Vulcan - Pineville
			Blythe Construction - Pineville

Table 2.2. Recommended Superpave HMA Mix Types Based on Traffic Levels

Mix Type	Loading Range (80 KN) or 18 kip-(ESALs) during Pavement Design Life	Asphalt Binder Grade
Surface		
S9.5A	< 300,000	PG64-22
S9.5B	< 3 Million	PG64-22
S9.5C	3 to 10 Million	PG70-22
S12.5B	< 3 Million	PG64-22
S12.5C	3 to 30 Million	PG70-22
S12.5D	> 30 Million	PG76-22
Intermediate		
I19.0B	< 3 Million	PG64-22
I19.0C	3 to 30 Million	PG64-22
I19.0D	> 30 Million	PG70-22
Base		
B25.0B	< 3 Million	PG64-22
B25.0C	>= 3 Million	PG64-22
B37.5C	>= 3 Million	PG64-22

CHAPTER 3 MIXTURE VERIFICATION PROCEDURE AND TARGET AIR VOIDS DEVELOPMENT

3.1 Introduction

The overall goal of this part of the research is to build a future database that includes material properties and performance characteristics of the twelve most commonly used asphalt mixtures in North Carolina. When replicating the JMF using the recently acquired materials (hereafter referred to as *new* materials), the goal is to fabricate a mixture that is similar to the one that a contractor would produce using the same JMF and materials. Therefore, mixture verification criteria are needed to consider the field variables. This Chapter presents the steps necessary to develop these mixture verification criteria. Prior to fabricating the test specimens needed to characterize the twelve mixtures, verification must be undertaken to ensure that the current JMF will still produce mixtures that satisfy the developed criteria when used with the new materials.

3.2 Mixture Verification Procedure

For consistency, the following procedure has been developed to all twelve mixtures.

- If RAP is one of the stockpiles for a certain mixture, three representative RAP samples are burned to determine the percentage of asphalt cement that is RAP. The average value is then compared with the corresponding number in the JMF to determine the appropriate amount of additional binder necessary to achieve the optimal binder content.
- A wet sieve analysis is carried out for each stockpile, including RAP aggregates (after burning) for mixtures that include RAP.
- The aggregate bulk-specific gravities for each stockpile are measured.
- Using the optimal asphalt content and aggregate gradations presented in the JMF for each mixture, three mix design specimens (150 mm in diameter and 115 mm in height) are fabricated with target air voids of 4.0 percent.
- At least two maximum theoretical specific gravity (G_{mm}) replicates are prepared for each mixture, and average G_{mm} values are determined.
- Mixture bulk-specific gravities (G_{mb}) are then measured for all three replicates.
- Voids in mineral aggregate (VMA), voids filled with asphalt (VFA), and the percentage of air voids (V_a) are calculated and compared with Superpave design criteria.
- When all criteria are met, the fabrication of performance test specimens can begin.
- For mixtures that fail to meet the criteria, new mix designs are developed.

3.2.1 Development of a Mix Verification Acceptance Criteria

Because the properties of the component materials may be different from those used in developing the JMF, it is necessary to verify that hot mix asphalt (HMA) mixtures made from the new materials will satisfy the acceptance criteria. This verification process ensures that the mixtures used in this study represent the mixtures that have been and will be used in actual pavement construction.

In efforts to develop acceptance mix verification criteria, the 2008 version of the NCDOT Hot Mix Asphalt / Quality Management System (HMA/QMS) publication (NCDOT, 2008) has been consulted. This publication contains the control limits recommended by the NCDOT for plant mix production. Table 3.1 summarizes these control limits. Note that the moving average limit is not applicable to this study.

Table 3.1. NCDOT Control Limits for Mix Production

Mix Control Criteria	Target Source	Moving Average Limit	Individual Limit
No. 8 Sieve	JMF	± 4.0%	± 8.0%
No. 200 Sieve	JMF	± 1.5%	± 2.5%
% AC	JMF	± 0.3%	± 0.7%
% V_a @ N_{design}	JMF	± 1.0%	± 2.0%
VMA @ N_{design}	Min. Spec. Limit	- 0.50%	- 1.00%
$P_{0.075}/P_{be}$	1.0	± 0.4%	± 0.8%
% G_{mm} @ $N_{initial}$	Max. Spec. Limit	N/A	+ 2.0%
TSR	Min. Spec. Limit	N/A	- 15%

In addition to the information presented in Table 3.1, the NCDOT has its own HMA assessment program that was consulted to evaluate the work performed by quality control (QC) and quality assurance (QA) personnel. Table 3.2 summarizes the volumetric criteria that have been developed by the NCDOT for this program to achieve a good correlation between the values determined from the NCDOT M&T laboratory and the values obtained by the QC/QA personnel.

Table 3.2. NCDOT Assessment Program Criteria

Mix Control Criteria	Allowable Deviation
% AC	± 0.6%
G_{mm}	± 0.020
G_{mb}	± 0.030
G_{mb}-core	± 0.050

As part of the NCHRP 9-34 project, *Improved Conditioning and Testing Procedures for HMA Moisture Susceptibility*, Solaimanian et al. (2007) developed HMA mixture verification criteria. The first part of this research included mixture verification for all the mixes to ensure that they were all within the allowable deviation from the submitted mix designs. Table 3.3 summarizes these criteria. Note that data presented in Table 3.3 reflect the AASHTO Materials Reference Laboratory (AMRL) multi-laboratory precision statements. Although the allowable ranges shown in Table 3.3 correspond to 12.5 mm mixture sizes, other mixture sizes, including 9.5 mm and 19.0 mm, also were judged according to these criteria. In addition, Table 3.3 is applicable for mixtures fabricated with non-absorptive aggregates only. Furthermore, the mixture verification process, derived from the NCHRP 9-34 project, relates to the JMF numbers and not to the Superpave mix criteria.

Table 3.3. AASHTO Materials Reference Laboratory Multi-laboratory Precision Limits

Mix Control Criteria	Allowable Deviation
G_{mb} @ N_{design}	± 0.088
G_{mm}	± 0.021
% V_a @ N_{design}	± 3.5

Based on the information regarding mixture verification criteria, and taking into consideration the current criteria used by the NCDOT and the scope of the current research, the final mixture verification criteria to be used for this project have been assimilated and are summarized in Table 3.4.

Table 3.4. Mix Verification Criteria Developed for Local Calibration Project

Mix Control Criteria	Target Source	Allowable Deviation
G_{mm}	JMF	± 0.020
G_{mb} @ N_{design}	JMF	± 0.030
% V_a @ N_{design}	JMF	± 2.0
% VMA @ N_{design}	Min. Spec. Limit	- 1.0
% VFA @ N_{design}	Spec. Range	± 2.0
$P_{0.075}$ / P_{be}	1.0	± 0.8
% G_{mm} @ $N_{initial}$	Max. Spec. Limit	+ 2.0

For direct application of the developed criteria, Table 3.5 was constructed and customized for all twelve HMA mix types selected for this study.

Table 3.5. Mix Verification Criteria for the Twelve Most Commonly used Mix Types in NC

Mix Type	G_{mm}	G_{mb} @ $N_{design.}$	% V_a @ N_{design}	% VMA @ N_{design}	% VFA @ N_{design}	$P_{0.075}$ / P_{be}	% G_{mm} @ $N_{initial}$
S9.5B	2.527 - 2.567	2.415 - 2.475	2.0-6.0	≥ 14	63-80	0.2-1.8	≤ 92.5
S9.5C	2.583 - 2.623	2.469 - 2.529		≥ 14	71-78		≤ 91.0
RS9.5C	2.382 - 2.422	2.276 - 2.336		≥ 14	71-78		≤ 91.0
S12.5C	2.464 - 2.504	2.355 - 2.415	2.0-6.0	≥ 13	63-77	0.2-1.8	≤ 91.0
I19B[1]	2.588 - 2.628	2.474 - 2.534		≥ 12	63-80		≤ 92.5
RI19B	2.550 - 2.590	2.437 - 2.497		≥ 12	63-80		≤ 92.5
B25B	2.556 - 2.596	2.443 - 2.503		≥ 11	63-80		≤ 92.5
RB25B	2.450 - 2.490	2.341 - 2.401		≥ 11	63-80		≤ 92.5
RS9.5B[2]	2.413 - 2.453	2.306 - 2.366		≥ 14	63-80		≤ 92.5
RS12.5C	2.688 - 2.728	2.570 - 2.630		≥ 13	63-77		≤ 91.0
I19C	2.486 - 2.526	2.376 - 2.436		≥ 12	63-77		≤ 91.0
RI19C	2.688 - 2.728	2.570 - 2.630		≥ 12	63-77		≤ 91.0

[1]The mix design sheet for this mix shows a traffic level of "less than 0.3 million" ESALs. This number is a mistake that has been corrected to become "less than 3 million".

[2]This JMF replaces the one submitted to NCSU in an early stage of this research; the original JMF mix is no longer in production.

The volumetrics for each mixture were determined and compared with the corresponding criteria outlined in Table 3.5. Performance test specimens were fabricated for mixtures that satisfied the mixture verification criteria. A new mixture design was performed for mixtures that failed the mixture verification criteria shown in Table 3.5.

3.2.2 Wet Sieve Analysis

Aggregate stockpiles for all twelve mixes were analyzed for gradation following ASTM C136-06 test standards (ASTM, 2006). Table 3.6 compares the combined gradations determined from the wet sieve analysis (WSA) and the corresponding JMF numbers.

Table 3.6 Combined Aggregate Gradations Obtained from Wet Sieve Analysis vs. JMF

Sieve Size	S9.5B		RS9.5B		S9.5C		RS9.5C		S12.5C		RS12.5C	
	WSA	JMF	WSA	JMF	WSA	JMF	WSA	JMF	WSA	JMF	WSA	JMF
1"	100	100	100	100	100	100	100	100	100	100	100	100
3/4"	100	100	100	100	100	100	100	100	99	100	99	100
1/2"	100	100	100	100	100	100	100	100	99	100	99	100
3/8"	98	96	97	96	98	97	97	97	88	89	89	89
No.4	72	67	79	75	71	68	83	79	68	66	67	72
No.8	48	48	56	57	48	48	65	59	47	49	46	52
No.16	38	37	38	44	34	34	47	43	32	35	31	34
No.30	31	30	26	30	25	25	32	32	21	25	23	25
No.50	23	21	17	21	17	18	20	21	13	15	16	16
No.100	12	11	10	12	11	12	10	12	7	8	9	9
No.200	6	6	6	6	6	6	5	7	5	5	5	5
Sieve Size	I19B		RI19B		I19C		RI19C		B25B		RB25B	
	WSA	JMF	WSA	JMF	WSA	JMF	WSA	JMF	WSA	JMF	WSA	JMF
1"	100	100	100	100	100	100	100	100	100	99	99	98
3/4"	100	100	97	99	100	100	98	97	84	83	85	82
1/2"	100	100	80	84	100	100	87	85	68	69	72	71
3/8"	74	73	70	75	76	78	76	75	62	63	68	68
No.4	51	50	48	51	55	52	39	39	46	45	53	48
No.8	37	36	36	38	40	38	22	24	34	30	38	35
No.16	29	28	29	31	30	29	17	19	23	19	27	26
No.30	24	23	19	24	20	20	13	15	16	13	19	19
No.50	18	16	10	14	12	11	10	11	11	9	13	14
No.100	10	9	6	8	7	7	7	8	8	6	8	7
No.200	5	5	4	5	5	5	5	5	5	4	5	4

The data shown in Table 3.6 are a valuable part of the future material database, especially given that the twelve mixes had undergone different types of testing.

Table 3.7 summarizes the percentage of differences in combined stockpile gradations between the corresponding numbers in the JMF and those measured.

Table 3.7. Percentage Differences between JMF and Measured Combined Gradations

Sieve Size	Mixture ID					
	S9.5B	RS9.5B	S9.5C	RS9.5C	S12.5C	RS12.5C
1"	0	0	0	0	0	0
3/4"	0	0	0	0	-1	-1
1/2"	0	0	0	0	-1	-1
3/8"	2	1	1	0	-1	0
No.4	7	5	4	5	3	-7
No.8	0	-2	0	10	-4	-12
No.16	3	-14	0	9	-9	-9
No.30	3	-13	0	0	-16	-8
No.50	10	-19	-6	-5	-13	0
No.100	9	-17	-8	-17	-13	0
No.200	0	0	0	-29	0	0
Sieve Size	Mixture ID					
	I19B	RI19B	I19C	RI19C	B25B	RB25B
1"	0	0	0	0	1	1
3/4"	0	-2	0	1	1	4
1/2"	0	-5	0	2	-1	1
3/8"	1	-7	-3	1	-2	0
No.4	2	-6	6	0	2	10
No.8	3	-5	5	-8	13	9
No.16	4	-6	3	-11	21	4
No.30	4	-21	0	-13	23	0
No.50	13	-29	9	-9	22	-7
No.100	11	-25	0	-13	33	14
No.200	0	-20	0	0	25	25

Table 3.7 suggests that the percentage of differences between the JMF and measured values is smaller for coarse aggregates (retained on # 4 sieve) than for fine aggregates (passing # 4 sieve). The percentage of differences among coarse aggregates ranges between zero percent and 10 percent, whereas for fine aggregates, differences range between zero percent and 29 percent. These differences could be attributed to changes in the crushing and handling equipment at the different quarries. Soft aggregate might be crushed such that it exhibits different gradations even though the same equipment is used. Differences also could be caused by reaching a different layer in the aggregate stockpile or the changes in the aggregate quarry.

These differences in the gradations between the JMF and actual stockpiles make it difficult to obtain the same target gradation in the JMF. That is, if the stockpile percentages in the JMF were used with the materials obtained for this research, the gradation of the blended aggregate would be different from the blended gradation in the JMF. It is noted that the goal of this laboratory experimental program is to produce mixtures that are as similar as possible to those that contractors would produce in the field using the same materials and JMFs. In actual construction, contractors would apply the stockpile percentages in the JMF to the materials they acquire for the paving job. Therefore, the same approach, i.e., using the stockpile percentages in the JMF, was chosen for this study.

3.2.3 Measurement of Aggregate Dry Bulk-Specific Gravity (G_{sb})

With the scope of this research work in mind, the dry bulk-specific gravity (G_{sb}) values from the JMF were used in calculating the volumetrics of the mixtures. Again, the goal is to simulate the expected outcome in the field when a contractor takes a current JMF and uses it with the available materials. Therefore, to best characterize all twelve representative mixtures chosen for this project, the current JMF numbers were used with the currently available materials. As mentioned earlier, for mixtures that did not meet the criteria, a modification was made to the mixtures or a new mixture design was created prior to the fabrication of any performance specimens.

The measured G_{sb} values represent the correct bulk-specific gravity for the current materials. Correct G_{sb} values are vital for two reasons:

- First, they are used to populate the database with the appropriate specific gravities for completeness, soundness, and future use.
- Second, they are used to check the effects of the differences in G_{sb}, i.e., between the JMF numbers and the measured numbers, on the volumetrics of the mixtures.

Because of the imperative role that the bulk-specific gravity plays in mixture design and volumetrics, and because of the two reasons cited, the M&T Unit at the NCDOT was asked to measure the bulk-specific gravity of all the stockpiles for each of the twelve mixes. Aggregate stockpiles were sampled in the field following AASHTO T2 standards (AASHTO-a) to obtain enough materials for all characterization testing. Samples were then reduced in size for bulk-specific gravity testing.

Table 3.8 summarizes the bulk-specific gravity test results as measured by the NCDOT and compares these results to the values reported in the JMF.

Table 3.8. Change in Dry Bulk-Specific Gravity (G_{sb}) Over Time

Mix Type	JMF Effective Date	Materials Acquisition Date	JMF G_{sb}	NCDOT G_{sb}	Change in G_{sb}
S9.5B	1/11/2007	9/20/2007	2.781	2.824	0.043
S9.5C	4/4/2005	2/1/2008	2.828	2.793	-0.035
RS9.5C	3/31/2005	3/8/2007	2.606	2.625	0.019
S12.5C	9/20/2006	8/18/2008	2.680	2.687	0.007
I19B	1/11/2007	7/28/2008	2.796	2.844	0.048
RI19B	8/23/2006	9/25/2007	2.735	2.715	-0.020
B25B	10/25/2004	3/25/2008	2.769	2.773	0.004
RB25B	8/29/2003	2/27/2009	2.621	2.583	-0.038
RS9.5B	3/17/2008	2/27/2009	2.630	2.570	-0.060
RS12.5C	12/4/2003	2/9/2009	2.925	2.882	-0.043
I19C	10/31/2006	8/18/2008	2.664	2.674	0.010
RI19C	11/30/2006	2/9/2009	2.901	2.887	-0.014

Worth mentioning is that the M&T Unit measured only the bulk-specific gravity for the stockpiles; however, sieve analysis information, needed to calculate the combined aggregate specific gravities, was obtained at NCSU through a complete wet sieve analysis. In addition to bulk-specific gravity results, Table 3.8 also summarizes the JMF's effective dates and the date the new aggregate materials were acquired.

Table 3.9 summarizes the effects that changes in the bulk-specific gravity values have on mix volumetrics, i.e., the voids in mineral aggregates (*VMA*), voids filled with asphalt (*VFA*), and the dust proportion (DP), defined as the ratio of dust divided by effective binder content. The shaded fields in Table 3.9 correspond to volumetrics that did not satisfy the criteria presented in Table 3.5. Table 3.9 shows that out of the twelve mixtures, mixture I19B and mixture RS9.5B both failed the criteria. Therefore, these two mixtures need to be re-designed to meet the criteria in Table 3.5.

Table 3.9. Effect of the Change in Dry Bulk-Specific Gravity on HMA Mix Volumetrics

Mix Type	Volumetrics using JMF G_{sb}			Volumetrics using NCDOT G_{sb}		
	VMA	*VFA*	Dust/Binder	*VMA*	*VFA*	Dust/Binder
S9.5B	15.6	78.8	1.1	16.8	80.4	1
S9.5C	15.6	75.7	1.2	14.6	73.9	1.4
RS9.5C	16.5	77.6	1.3	17.1	78.4	1.2
S12.5C	16.2	73.2	0.9	16.4	73.6	0.9
I19B	13.6	81.9	1	15	83.6	0.9
RI19B	14.1	72.4	1.2	13.4	71	1.2
B25B	14.8	67.3	1	15	67.8	0.9
RB25B	13.7	67.9	1.1	12.4	64.6	1.2
RS9.5B	17.9	65.3	1.1	16	61.2	1.3
RS12.5C	15.8	69	1.1	14.6	66.3	1.2
I19C	14.1	69.1	1.2	14.4	69.8	1.2
RI19C	14.9	68.3	1.2	14.5	67.4	1.3

3.2.4 Reclaimed Asphalt Pavement (RAP) Materials

Six out of the twelve mixtures in this research have a RAP component. These mixtures are RS9.5B, RS9.5C, RS12.5C, RI19B, RI19C, and RB25B. To check the amount of asphalt that comes from these RAP materials, the ASTM D 6307-98 test method (ASTM, 1998) that utilizes a Troxler NTO asphalt burner was used to burn three representative samples from each RAP stockpile. Table 3.10 summarizes the results and compares them to the corresponding numbers reported in the JMF. Results suggest that very little difference exists between the RAP asphalt content measured in the lab and that reported in the JMF, with the exception of the RAP component of the RB25B mixture, which suggests a decrease in the amount of binder of about 1.2 percent.

Table 3.10. Summary of Asphalt Binder Content for HMA Mixes with RAP

Mix Type	% AC - Manual Weighing	% AC - Machine	% AC - Average	% AC Reported in JMF
RS9.5B	5.59	5.58	5.6	5.6
RS9.5C	5.28	5.22	5.3	5.2
RS12.5C	4.40	4.33	4.4	4.5
RI19B	4.45	4.80	4.6	4.6
RI19.0C	4.52	4.55	4.5	4.5
RB25.0B	4.34	4.31	4.3	5.5

3.2.5 Mixture Verification Results

One-point mixture verification tests were performed for each of the twelve mixtures prior to fabricating any performance test specimens. New materials were batched according to the JMF stockpile gradations and percentages in an attempt to simulate mixtures that would be produced in the field if similar JMF were used. Table 3.11 summarizes the one-point verification test results by showing all measured and calculated mixture volumetrics. The shaded fields in Table 3.11 correspond to the parameters that failed the criteria presented in Table 3.5.

Table 3.11 shows that three of the twelve mixtures failed the criteria for one component or another. The mixtures that failed are S9.5B, I19.0B, and RS9.5B. The I19.0B and RS9.5B mixtures have failed the criteria in Table 3.9. Using the same aggregate structures reported in the JMF, four-point mixture designs were carried out for these three mixtures, and new values for the total asphalt content were recommended. Table 3.12 presents the four-point mixture design results for the S9.5B, I19.0B, and RS9.5B mixtures. Table 3.12 shows the new recommended asphalt contents for these three mixtures.

Table 3.11. One-Point Mix Verification Test Results

Mix Type	G_{mm}	G_{mb} @ N_{design}	% V_a @ N_{design}	% VMA @ N_{design}	% VFA @ N_{design}	$P_{0.075}/P_{be}$	% G_{mm} @ $N_{initial}$
S9.5B	2.587	2.501	3.3	15.6	78.8	1.1	90.3
S9.5C	2.616	2.517	3.8	15.6	75.7	1.2	87.8
RS9.5C	2.414	2.324	3.7	16.5	77.6	1.3	89.6
S12.5C	2.495	2.376	4.3	16.2	73.2	0.9	89.3
I19B	2.633	2.544	2.5	13.6	81.9	1.0	91.2
RI19B	2.558	2.458	3.9	14.1	72.4	1.2	90.1
B25B	2.593	2.467	4.8	14.8	67.3	1.0	86.5
RB25.0B	2.472	2.361	4.4	13.7	67.9	1.1	88.7
RS9.5B	2.417	2.282	6.2	17.9	65.3	1.1	87.1
RS12.5C	2.712	2.575	4.9	15.8	69	1.1	88.1
I19C	2.519	2.397	4.3	14.1	69.1	1.2	89.5
RI19.0C	2.722	2.58	4.7	14.9	68.3	1.2	85.3

Table 3.12. Four-Point Mix Design Test Results and Recommended Asphalt Contents

Mix Type	New % AC	G_{mm}	G_{mb} @ N_{design}	% V_a @ N_{design}	% *VMA* @ N_{design}	% *VFA* @ N_{design}	$P_{0.075}/P_{be}$	% G_{mm} @ $N_{initial}$
S9.5B	5.9	2.574	2.501	4	15.4	74	1.1	90.3
I19B	4.8	2.641	2.534	4	13.7	71	1.1	89.9
RS9.5B	6	2.397	2.3	4	17.8	77	0.9	88.9

After the mixture design verification process was completed successfully for all twelve mixtures, a target air content was determined for the performance test specimens. Section 3.3 presents the process for determining this target air content.

3.3 Selection of a Target Air Void Percentage for Performance Test Specimens

The process of selecting the proper target air void percentage for performance specimens has two important dimensions. First, the effective calibration and validation of the distress prediction models employed by the MEPDG require the air void percentage at the time of construction (also referred to as *as-constructed* or *original* air voids). Second, the air voids to be used in the experimental program must be a representative value of the HMA layers in future construction, because the performance model coefficients to be determined from this study will form the basis for the Level 2 database for future use in the MEPDG.

In order to have a consistent target air content that can be used with all mixtures throughout this project, a literature review was carried out to search for national field mixture densification data that could help in identifying an air void level that is both representative of the initial stage after construction and that also promises successful specimen fabrication in the laboratory.

In the NCHRP 9-9 project, *Superpave Mix Design: Verifying Gyration Level in the N_{design} Table*, Prowell and Brown (2007) attempted to verify the N_{design} levels in the field. Samples were collected from 40 field projects at the time of construction. These field projects were located in 16 states and represent a wide range of traffic levels, asphalt binder grades, aggregate types, and gradations. The final report (NCHRP 573) contains a table that presents the changes in the percentage of the maximum specific gravity, G_{mm}, over time.

Table 3.13 summarizes the average changes in air void levels over two years using the data collected from all 16 states. Table 3.14 is a modification of the table documented in NCHRP 573 and presents the changes in air void levels over time instead of the changes in percentage of G_{mm}. The shaded fields in Table 3.14 correspond to data anomalies, which were ignored when calculating the averages reported in Table 3.13.

Table 3.13. Changes in Air Void Levels over Time – Results from 16 States

Time	Construction	3 months	6 months	1 year	2 years
% Air Voids	8.3	6.3	6.2	5.6	5.2

Taking into consideration the information presented in Table 3.14 and the in-laboratory verifications that were undertaken at NCSU, the decision was made to adopt a target air void level of 5.5% to be used for fabricating all the performance specimens for of all the mixtures throughout this project.

Table 3.14. Project NCHRP 9-9 Average In-Place Air Voids

Project ID	Roadway	Average Percentage of Air Voids				
		Construction	3 months	6 months	1 year	2 years
AL-1	Hwy 157	11.3	6.8	6.4	7.0	6.1
AL-2	Hwy 168	11.7	9.7	9.8	9.8	8.2
AL-3	Hwy 80	10.3	7.2	6.8	6.7	6.4
AL-4	Hwy 84	11.6	7.2	6.9	7.4	5.7
AL-5	Hwy 167	10.3	6.4	6.2	6.9	5.4
AL-6	Andrews Rd.	8.2	6.9	7.3	6.9	6.7
AR-1	I-40	8.0	6.9	6.5	5.9	5.8
AR-2	I-55	10.6	9.1	8.6	8.2	8.2
AR-3	I-40	8.5	5.4	5.2	5.2	5.3
AR-4	I-30	9.1	5.8	6.5	5.5	5.5
CO-1	Hwy 9	6.2	3.1	3.5	2.8	1.9
CO-2	Hwy 82	5.3	3.4	3.4	3.1	2.9
CO-3	I-70	6.5	5.4	4.0	4.4	4.3
CO-4	Hwy 13	6.3	6.7	7.2	5.8	5.8
CO-5	Hwy 82	8.4	6.4	6.3	5.8	6.2
FL-1	Davis Hwy	8.2	5.8	5.2	5.7	4.8
GA-1	Buford Hwy	5.0	4.3	4.2	4.0	3.5
IL-1	I-57	9.0	6.1	6.2	5.8	5.6
IL-2	I-64	8.2	5.8	5.9	5.6	4.8
IL-3	I-70	7.8	5.7	6.1	5.6	5.5
IN-1	US 136	8.7	9.7	9.7	37.7	6.5
IN-2	I-69	8.6	9.3	8.3	5.3	5.9
KS-1	I-70	10.1	8.8	7.9	6.4	6.4
KY-1	CR 1796	14.5	12.7	13.3	12.3	11.5
KY-2	I-64	7.8	6.8	6.7	6.1	5.9
KY-3	CR 1779	7.4	6.9	6.3	5.7	5.8
MI-1	I-75	8.7	7.9	7.2	6.6	5.2
MI-2	Hwy 50	6.9	4.8	3.9	3.2	3.2
MI-3	Hwy 52	7.0	6.3	5.5	N/A	3.5
MO-1	I-70	6.6	3.6	4.4	4.2	3.5
MO-2	Hwy 65	7.4	5.8	7.3	5.6	4.9
MO-3	I-44	6.5	5.6	5.7	4.7	4.4
NC-1	I-85	9.9	7.2	8.3	7.0	6.6
NE-1	Hwy 8	7.4	4.6	4.5	4.7	4.3
NE-2	Hwy 77	7.0	4.8	5.0	4.7	4.3
NE-3	Hyw 8	9.0	5.2	4.9	5.0	4.6
NE-4	I-80	7.8	5.1	4.8	3.3	2.8
TN-1	Hwy 171	8.9	6.9	6.9	5.9	5.7
UT-1	Hwy 150	8.1	6.5	6.8	N/A	6.3
WI-1	US 45	7.6	6.2	6.2	5.6	5.7

CHAPTER 4 UNBOUND MATERIALS CHARACTERIZATION

4.1 Introduction

The scope of this research work includes the characterization of asphalt concrete materials for rutting and fatigue distresses that occur in flexible pavements. Unbound base and subgrade layers have not been characterized as part of this research work. However, a GIS-based methodology has been developed to take advantage of the product of the NCHRP 9-23A project to determine subgrade soil properties for any location in North Carolina. Details regarding this methodology are presented in the following Section 4.2. For unbound base materials, the research team recommends that a separate project should be funded to characterize the most commonly used unbound base and sub-base materials in North Carolina. In the meantime, the research team recommends that the MEPDG default values should be used for unbound base and sub-base materials.

4.2 GIS-Based Implementation Methodology for the NCHRP 9-23A Recommended Soil Parameters for Use as Input to the MEPDG

4.2.1 Introduction

Compared to the empirically-based AASHTO design guide, the MEPDG adopts a mechanistic component into the design process in which pavement responses, i.e., stresses, strains, and deflections, are calculated. The response of unbound materials to a load is highly dependent on moisture content. Moisture has two distinct effects on unbound materials; first, it may alter the soil structure through the destruction of the cementation between the soil particles; and second, moisture can affect the stress state through suction or pore water pressure (ARA, 2004). In the MEPDG, the effect of moisture and temperature on the performance of different pavement layers is handled by the enhanced integrated climatic model (EICM). The EICM is a heat and moisture flow program that simulates changes in the characteristics of bound and unbound materials over the pavement design life (ARA, 2004). The EICM requires several input parameters that are classified under two main categories: climatic information and unbound material properties. Hourly climatic information, including air temperature, relative humidity, precipitation, wind speed and sunshine percentage, is already available from 851 weather stations (20 in North Carolina) and embedded into the MEPDG. Unbound material properties, on the other hand, are available for Level 3 input only, in which correlations are used to calculate the soil index properties and soil water characteristics curve (SWCC) parameters. These correlations are weak because they were derived based on a limited number of site correlation studies (Zapata, 2010).

In order to solve this problem, Dr. Claudia Zapata from Arizona State University (ASU) carried out the NCHRP 9-23A project (Zapata, 2010) with the objective of developing a national soils database that includes soil properties as required by the EICM in the MEPDG. Among the various required soil properties, the SWCC parameters are the focus of this project. The SWCC represents a measure of the water-holding capacity of a soil for different suction values. Soil suction and water content are important parameters that control many geotechnical properties of unsaturated soils, including permeability, volume change, deformability and shear strength (Barbour, 1998).

The product of the NCHRP 9-23A project comes in the form of a Microsoft Excel-based interface through which users can select a state and region of interest, after which a soils unit regional map is displayed showing color-coded soil polygons with unique alphanumeric labels. Users can then locate the road section of interest on the map to find the numeric code of the soil unit in which the road section is located. Each alphanumeric label is associated with a soils profile that might contain anywhere from one to ten soil horizons (layers). The soil properties associated with each soil profile are displayed in a table format that can be printed out.

In this research work, a GIS-based methodology has been developed for NCDOT engineers so that they may accurately superimpose road sections of interest on the NCHRP 9-23A soil maps and find the corresponding alphanumeric soil unit code required to extract related soil information. The proposed methodology uses ESRI's ArcGIS® 9.2 software (ESRI, 2010) and soil shape files downloaded from the website of the Natural Resources Conservation Service (NRCS) of the United States Department of Agriculture (USDA, 2010). Detailed procedures for this process are presented in subsequent sections.

4.2.2 Problem Statement

Currently, the main challenge in the implementation of the NCHRP 9-23A product is the absence of an easy and reliable method that can superimpose a road section on a soil map region and, consequently, allow the most accurate and appropriate soil unit code input to be selected. This challenge is especially evident with short road sections, such as the 500 ft sections in the LTPP program (FHWA, 2010). Short road sections require a high degree of accuracy to be superimposed correctly on a map. Moreover, the 9-23A product contains many GIS-based soil maps (shape files) that have been transformed into image files and stored as PDF documents. The fact that the actual shape files are unavailable makes it difficult to use georeferencing techniques to superimpose road sections on these maps.

4.2.3 Objective and Scope

The objective of this section is three-fold. The first part briefly introduces the hierarchical input levels available for unbound materials in the MEPDG and presents the soil parameters that are required by the EICM in order for it to predict the environmental factors. The importance of the SWCC parameters on pavement performance is also discussed. The second part introduces a detailed GIS-based methodology that can be followed by the NCDOT to superimpose road sections on the NCHRP 9-23A soil maps and, hence, select the most appropriate soils available for these sections. In addition, the development of a Microsoft Excel-based MEPDG soils data generator is introduced. The third part compares the AASHTO soils classification output of the NCHRP 9-23A database with that of the LTPP database and discusses any differences that may exist. It is vital to mention that the NCDOT has always conducted site-specific subgrade investigations, mainly for new location projects and for substantial widening projects. However, the NCDOT expects to benefit from the NCHRP 9-23A soils database in situations where detailed coring and test results are unavailable, such as for low volume roadways, relatively short bridge projects, and projects where widening is relatively narrow. The NCDOT also expects to use the NCHRP 9-23A data for preliminary designs.

4.2.4 MEPDG Unbound Materials Hierarchical Input Levels

The MEPDG offers a unique hierarchical input level approach that provides users with flexibility in selecting project design inputs based on the size, importance, and available resources for the particular project. This hierarchical approach is employed in the MEPDG in terms of traffic, materials, and environmental inputs (ARA, 2004). In this Section 4.2.4, only the available hierarchical levels for the environmental inputs and especially those required by the EICM are presented.

Three hierarchical levels of unbound material inputs are utilized by the EICM. Level 1 requires comprehensive lab and/or field testing to determine the index and volumetric properties of both saturated and unsaturated soils, mainly the SWCC parameters. Level 2 also requires the measurement of index and volumetric properties but uses correlations to determine the unsaturated soil properties. Level 3 is the least demanding level, requiring only index properties to be measured. In Level 3, saturated and unsaturated soil properties are determined through correlations. All correlations used in Levels 2 and 3 are embedded in the MEPDG and are employed automatically based on the input level and unbound material type selected by the user. Table 4.1 lists the input parameters required for each of the input levels.

Table 4.1. EICM Data Requirements for Unbound Materials Hierarchical Input Levels

<table>
<tr><th colspan="3">Input Level</th><th>Input Category</th><th>Input Parameters</th></tr>
<tr><td rowspan="8">Level 1</td><td rowspan="7">Level 2</td><td rowspan="3">Level 3</td><td>Soils Gradation</td><td>Index properties are calculated within the MEPDG</td></tr>
<tr><td rowspan="2">Atterberg Limits</td><td>Plasticity Index (PI)</td></tr>
<tr><td>Liquid Limit (LL)</td></tr>
<tr><td rowspan="4"></td><td rowspan="4">Compacted Soil Properties</td><td>Max. Dry Unit Weight (pcf)</td></tr>
<tr><td>Soils Specific Gravity, Gs</td></tr>
<tr><td>Saturated Hydraulic Conductivity (Permeability) (ft/hr)</td></tr>
<tr><td>Opt. Gravimetric Water Content (%)</td></tr>
<tr><td colspan="2"></td><td>SWCC Parameters</td><td>(a_f, b_f, c_f, and h_r)*</td></tr>
</table>

* Soil Water Characteristics Curve Parameters, see Equation (4.1) below.

Additional parameters required by the EICM are the depth of the water table and the project location, i.e., longitude and latitude, for each of the three input levels. With regard to data, the soils data obtained for the NCHRP 9-23A project are considered in the MEPDG to be Level 2 input data, because they do not necessarily represent actual field samples that have been tested in the lab. With regard to analysis, however, the NCHRP 9-23A soils data are considered Level 1 input data, because the index properties and SWCC parameters have been measured directly, or have been calculated, from measured soils data and not from weak correlations.

4.2.5 Soil Water Characteristics Curve (SWCC)

The SWCC, also called the soil water retention curve (SWRC), represents one of the most important relationships that affect moisture flow in partially saturated soils. The SWCC is the relationship between the amount of water in the soil and soil suction. In other words, the SWCC reflects the water-holding capacity of a soil for different suction values. Soil suction and water content are important parameters that control many geotechnical properties of unsaturated soils, including permeability, volume change, deformability and shear strength (Barbour, 1998). Because of the important role that the SWCC plays in overall pavement performance, it has been included as part of the EICM. Among the various models proposed to define the SWCC, the 1994 Fredlund and Xing model (Fredlund and Xing, 1994) is the one that has been selected for use in the MEPDG. Equation (4.1) shows the form of the model, and Figure 4.1 shows an example of a SWCC.

$$\theta_w = C(h) \times \left[\frac{\theta_s}{\left[\ln \left[\exp(1) + \left(\frac{h}{a_f} \right)^{b_f} \right] \right]^{c_f}} \right] \qquad (4.1)$$

where

$$C(h) = \left[1 - \frac{\ln\left(1 + \frac{h}{h_r}\right)}{\ln\left(1 + \frac{10^6}{h_r}\right)} \right]$$

θ_w = volumetric water content;

h= soil matric suction, kPa;

a_f =a soil parameter, function (air entry value, kPa);

b_f = a soil parameter, function (rate of water extraction from the soil);

c_f = a soil parameter, function (residual water content); and

h_r = a soil parameter, function (suction at which residual water content occurs, kPa).

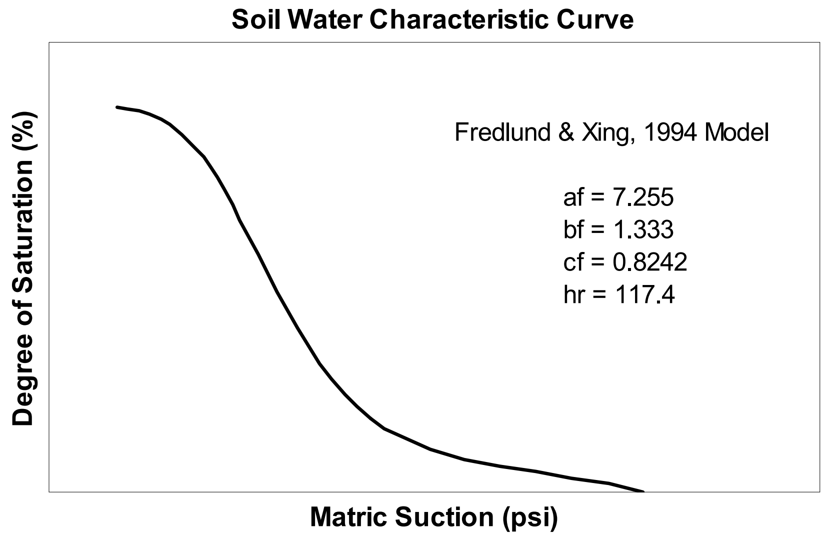

Figure 4.1. Example of a soil water characteristics curve.

4.2.6 Methodology to Superimpose Road Sections on NCHRP 9-23A Soil Maps

4.2.6.1 Background

Spatial and tabular soils data that are used in the NCHRP 9-23A project were obtained from the USDA's NRCS website. The downloaded information includes data for 1,227,117 soils throughout the United States and Puerto Rico (Zapata, 2010). Data from the NRCS are available at three levels of detail: first is the soil survey geographic (SSURGO) database, which has the most detailed soil information; second is the state soil geographic (STATSGO) database, which comes second in terms of soil information detail; and third is the national soil geographic (NATSGO) database, which has the least amount of detail and has been the choice of the NCHRP 9-23A research team for developing a national catalogue of soils data. The downloaded database includes spatial data in the form of shape files that contain spatial information required to locate geographic regions for different surveyed soil areas, and tabular data that include the various available soil properties within each of these geographic regions. Using the available shape files and tabular data, GIS-based soil maps for the entire United States and Puerto Rico have been created under the NCHRP 9-23A project.

4.2.6.2 Terminology used in the NCHRP 9-23A Project

Utilizing the shape files and their associated tabular data, geographic areas that have been identified as having soils that share the same or similar characteristics have been named *components* and are grouped together into *map units*. In the geographic sense, these so-called map units are soil polygons with identified boundaries. Each map unit might contain one or more soil components, which in turn might contain one or more soil *profiles*. Each soil profile contains soil *horizons* (layers) that range in number from 3 to 11 and range in thickness from several inches to 100 inches. Soils within the same soil profile might have a different AASHTO classification and different properties or might have a similar classification but different properties. In other words, two soils might be classified as A-4, but their resilient modulus values might be significantly different from each other. Furthermore, each *state map* is divided into a numbered grid that allows users to narrow the search to a smaller region within the particular state. The number of grids depends on the state's size and shape. For example, North Carolina is divided into 16 soil map regions. One of the major assumptions made during the NCHRP 9-23A project is that "the component with the largest percentage of coverage was representative of the entire map unit" (Zapata, 2010). This assumption was made in order to reduce the size of the database so that it was manageable. This assumption has shortcomings that are explained in subsequent sections.

4.2.6.3 Development of an EICM Soils Data Generator

To simplify the process of extracting soils data from the NCHRP 9-23A soils database and inputting them to the MEPDG, a simple user interface was developed in Microsoft Excel using visual basic for applications (VBA) programming language. This tool prepares files that contain soil properties required by the EICM in a format that can be imported directly from within the MEPDG. To use this tool effectively, all North Carolina soils data must first be extracted from the NCHRP 9-23A database, which was done by the research team as part of this research work. Once a soil alphanumeric unit code is entered into this tool, the tool extracts the desired soil properties that can then be exported to a file in the MEPDG format. Figure 4.2 is a screen capture of this interface where the soil unit code Z76 was selected. The following three-step procedure is required to use this simple Microsoft Excel tool to generate the required MEPDG input files:

1) Enter the alphanumeric soil unit code obtained through ArcMap® into the appropriate field. Upon entering the code and clicking *Enter*, the program will query the NCHRP 9-23A North Carolina soils database and extract data for up to nine different soil horizons. In the example shown in Figure 4.2, road sections within the soil unit code Z76 have three distinct horizons that are 5.1, 59.1, and 11.8 inches in thickness, respectively. Entering an alphanumeric soil unit code will return multiple Level 1 soil properties, such as Atterberg limits, index properties and properties of saturated and unsaturated soils, and other values that are required as inputs into the MEPDG, such as layer thickness, AASHTO classification, and the resilient modulus value or California bearing ratio (CBR).

2) Select whether or not the soils are compacted. For each of the horizons, Figure 4.2 shows that users have this choice. Figure 4.2 shows these fields in a light green color. As soon as users left-click their mouse in any of these fields, a drop-down menu appears. Users can then select *Yes* if the soil horizon is compacted or *No* if the soil horizon is uncompacted.

Enter Soil Unit Code from ArcMap =>>	Z76

Horizon 1 (Top)	Compacted ?	Horizon 2	Compacted ?	Horizon 3	Compacted ?
	Yes		No		No
AASHTO Classification	A-6		A-7-6		A-6
Thickness (in)	5.1		59.1		11.8
Resilient Modulus (psi)	10,969		7,096		10,353
CBR (%)	10		5		9

	Horizon 1		Horizon 2		Horizon 3
*Version Number	0.9	*Version Number	0.9	*Version Number	0.9
*Units	US	*Units	US	*Units	US
*Plasticity Index	11.5	*Plasticity Index	25.5	*Plasticity Index	17
*Liquid Limit	30	*Liquid Limit	45	*Liquid Limit	35.5
*Compacted Layer	1	*Compacted Layer	0	*Compacted Layer	0
*Unit Weight		*Unit Weight		*Unit Weight	
*Specific Gravity		*Specific Gravity		*Specific Gravity	
*Permeability	1.08E-01	*Permeability	1.08E-02	*Permeability	2.75E-02
*Optimum WC		*Optimum WC		*Optimum WC	
*af	5.9076	*af	12.8086	*af	0.6392
*bf	0.9922	*bf	1.1293	*bf	1.1482
*cf	0.6456	*cf	0.2516	*cf	0.3995
*hr	2999.6548	*hr	2999.9480	*hr	2995.9483
Grain Size Distribution		Grain Size Distribution		Grain Size Distribution	
0.001mm		0.001mm		0.001mm	
0.002mm	22.5	0.002mm	47.5	0.002mm	30.0
0.020mm		0.020mm		0.020mm	
#200	80.0	#200	76.5	#200	60.0
#100		#100		#100	
#80		#80		#80	
#60		#60		#60	
#50		#50		#50	
#40	95.0	#40	95.0	#40	95.0
#30		#30		#30	
#20		#20		#20	
#16		#16		#16	
#10	99.0	#10	99.0	#10	99.0
#8		#8		#8	
#4	100.0	#4	100.0	#4	100.0
3/8"		3/8"		3/8"	
1/2"		1/2"		1/2"	
3/4"		3/4"		3/4"	
1"		1"		1"	
1 1/2"		1 1/2"		1 1/2"	
2"		2"		2"	
2 1/2"		2 1/2"		2 1/2"	
3"		3"		3"	
3 1/2"		3 1/2"		3 1/2"	

Click to Export Horizon-1 Soil Data | Click to Export Horizon-2 Soil Data | Click to Export Horizon-3 Soil Data

Figure 4.2. A screen capture of the MEPDG EICM soils data generator.

3) Click the *Click to Export* button to generate a soils input file that can be imported through the MEPDG interface. Repeat this step for each of the soil horizons separately. Note that the MEPDG allows multiple subgrade layers to be entered. If

the alphanumeric soil unit code was available for a certain project location, Appendix G can be consulted to find the soil properties for that location. Appendix G is a comprehensive subgrade soils database for every soil unit code available in North Carolina.

4.2.6.4 Comparison between Soil Classifications from the NCHRP 9-23A Project and the LTPP Database

In order to validate the outputs of the NCHRP 9-23A database in terms of AASHTO soil classifications and compare the outputs to those obtained from the LTPP database, the proposed GIS-based methodology was used to superimpose 22 local LTPP sections on the NCHRP 9-23A soils maps to find the recommended soil profiles. The AASHTO soil classifications for these LTPP sites were extracted directly from the LTPP database. Table 4.2 summarizes the AASHTO soil classifications obtained from both sources along with the thicknesses of horizons for the NCHRP 9-23A soil profiles.

Before a comparison can be made, it is important to note that the NCHRP 9-23A database offers soil profiles that might contain more than one soil horizon. In fact, the average number of soil horizons within each soil profile typically ranges from three to five (Zapata, 2010). For each of these horizons, a thickness, when available in the original NRCS data, is given. On the other hand, the LTPP database contains only one AASHTO soil classification for each LTPP site. Soil horizons reported in the LTPP database generally are considered infinitely thick unless bedrock is present. Moreover, AASHTO soil classifications reported in the LTPP database are for representative soil types found at each LTPP site. When comparing the two databases, pavement designers should take a close look not only at the reported AASHTO classifications, but also at the thickness of each soil horizon. In some cases, the soil profiles recommended by the NCHRP 9-23A database might show multiple layers that share the same AASHTO classification. These layers, however, may have differences in their soil index properties, SWCC parameters, and other characteristics.

Looking only at AASHTO soil classifications, soil properties excluded, Table 4.2 shows that AASHTO soil classifications obtained using the NCHRP 9-23A database generally are in agreement with those extracted from the LTPP database. However, data for Sections 371030 and 371028 do not match well. A possible reason for this mismatch is that the NCHRP 9-23A database developers assumed that “the component with the largest percentage of coverage was representative of the entire map unit” (Zapata, 2010). The two sites mentioned above, 371030 and 371028, might be located in components that are not large; hence, the soil classification was mismatched. To avoid this possible issue, the research team recommends that borehole soil samples are obtained from the field and tested in the laboratory for more reliable and accurate results.

Table 4.2 also shows that the NCHRP 9-23A database does not include soils data for Section 371028, which belongs to the soil unit with the alphanumeric code Z81. Note that Z81 is a soil unit zone that could occur in any location in and outside of North Carolina. Furthermore, the NCHRP 9-23A database does not have soil information for four (Caswell, Cherokee, Iredell and Swain) of the 100 North Carolina counties.

Table 4.2. Comparison between Soil Classifications from the NCHRP 9-23A Project and the LTPP Database

Section ID	371006		371024		371030		371040	
9-23A Soil Unit Code	AA2		AB4		Z76		AB4	
Horizon #	AASHTO Classification and Layer Thickness (in.) as Determined from 9-23A							
1	A-4	7.1	A-4	7.1	A-6	5.1	A-4	7.1
2	A-4	3.9	A-4	18.1	A-7-6	59.1	A-4	18.1
3	A-7-6	39.0	A-4	4.7	A-6	11.8	A-4	4.7
Total Thickness (in.)	------	50.0	------	29.9	------	76.0	------	29.9
LTPP Classification	A-7-5	------	A-5	------	A-3	------	A-4	------

Section ID	371352		371645		371801		371802	
9-23A Soil Unit Code	Z97		Z93		Z69		AA6	
1	A-4	9.1	A-4	5.1	A-4	9.1	A-4	7.9
2	A-7-6	39.0	A-6	17.7	A-7-6	39	A-6	3.1
3	A-7-6	20.1	A-6	42.1	A-6	37	A-7-6	22
Total Thickness (in.)	------	68.2	------	64.9	------	85.1	------	33.0
LTPP Classification	A-4	------	A-4	------	A-4	------	A-2-6	------

Section ID	371803		371814		371817		371992	
9-23A Soil Unit Code	AC2		Z69		AA2		Z97	
1	A-5	11.0	A-4	9.1	A-4	7.1	A-4	9.1
2	A-6	9.8	A-7-6	39	A-4	3.9	A-7-6	39
3	A-4	5.1	A-6	37	A-7-6	39	A-7-6	20.1
Total Thickness (in.)	------	25.9	------	85.1	------	50.0	------	68.2
LTPP Classification	A-4	------	A-3	------	A-7-5	------	A-7-5	------

Section ID	372819		372824		372825		370801	
9-23A Soil Unit Code	AA5		AA0		AA7		Z78	
1	A-2-4	9.1	A-4	9.8	A-4	7.1	A-3	35.8
2	A-7-6	26.0	A-4	4.3	A-7-6	16.9	A-4	13
3	A-6	11.0	A-7-6	17.7	A-7-6	3.1	A-2	29.1
	------	------	A-6	28.0	------	------	------	------
Total Thickness (in.)	------	46.1	------	59.8	------	27.1	------	77.9
LTPP Classification	A-6	------	A-7-5	------	A-6	------	A-3	------

Section ID	370802		370859		37901		37902	
9-23A Soil Unit Code	Z78		Z78		Z95		Z95	
1	A-3	35.8	A-3	35.8	A-4	11.8	A-4	11.8
2	A-4	13.0	A-4	13	A-6	6.3	A-6	6.3
3	A-2	29.1	A-2	29.1	A-7-6	28.7	A-7-6	28.7
Total Thickness (in.)	------	77.9	------	77.9	------	46.8	------	46.8
LTPP Classification	A-3	------	A-3	------	A-4	------	A-6	------

Section ID	37903		371028		------		------	
9-23A Soil Unit Code	Z95		Z81		------		------	
1	A-4	11.8	------	------	------	------	------	------
2	A-6	6.3	------	------	------	------	------	------
3	A-7-6	28.7	------	------	------	------	------	------
Total Thickness (in.)	------	46.8	------	------	------	------	------	------
LTPP Classification	A-6	------	A-7-5	------	------	------	------	------

4.2.6.5 Recommendations for the Use of the NCHRP 9-23A Database

The following recommendations are made from this study:

- Whenever possible, it is highly recommended that soil samples from field boreholes should be acquired and tested in the laboratory to obtain soil index properties and SWCC parameters required by the EICM for Level 1 input and analysis.

- A GIS-based approach, similar the one proposed in this chapter, is recommended to superimpose road sections accurately on NCHRP 9-23A soil maps. This approach is critical for MEPDG local calibration where LTPP sections that are only 500 ft long are likely to be used.

- It is recommended that soils data extracted from the NCHRP 9-23A database should be evaluated against recent or historical soils data that were tested at or near a location of interest in order to ensure that these data are not out of range before using such data directly in the MEPDG.

- Realizing that the MEPDG allows for a maximum of ten layers to be input by users, including the asphalt, base, and subgrade layers, and because the NCHRP 9-23A soil profiles can have up to ten subgrade layers, NCDOT pavement designers must decide which subgrade layers to include or exclude in order to stay within the maximum allowable number of layers. If the number of layers becomes problematic, it is recommended that designers investigate neighboring soil profiles to gain information as to the soil type that is representative of the area. In addition, designers should consider the thickness of the layers when deciding which layers to keep and which ones to exclude. Thin layers with unique and localized soil properties should be excluded, whereas thick and dominant soil layers should be kept.

CHAPTER 5 PERMANENT DEFORMATION CHARACTERIZATION

5.1 Introduction

Permanent deformation (or so-called rutting) is a load-associated distress that occurs in flexible pavements. Rutting normally occurs under the wheel path and is considered a major factor that negatively affects rideability. Ruts filled with a substantial amount of water can cause vehicles to hydroplane, a situation where tires become separated from the pavement surface by a layer of water, thus causing the vehicle to slide. Figure 5.1 clearly shows an extreme case of permanent deformation of a flexible pavement.

Rutting is a manifestation of two mechanisms: densification and shear flow. Densification is associated with mixture volume changes and usually occurs early in the pavement life. Shear flow, on the other hand, is a type of plastic flow with no volume change. Shear flow starts when the aggregate structure of the mixture cannot withstand traffic loads, especially under high temperatures at which the stiffness of asphalt concrete mixtures drop. It is mainly because of shear flow that a pavement develops large rut depths that lead to the eventual failure of the pavement.

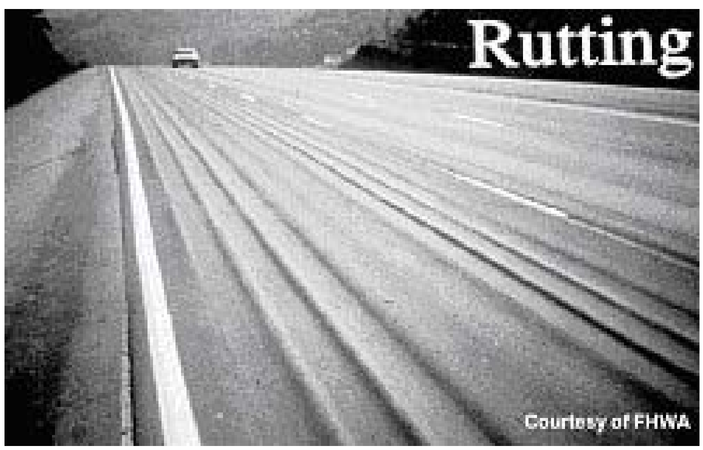

Figure 5.1. Example of a severe permanent deformation case in flexible pavement.

5.2 Rutting in the MEPDG

The MEPDG utilizes the incremental damage concept in predicting the total rut depth in a pavement structure. Total rut depth is calculated as the summation of rut depths accumulated in all unbound and bound layers. Equation (5.1) is used within the MEPDG to calculate the total rut depth.

$$RD = \sum_{i=1}^{n} \varepsilon_{p,i} h_i \qquad (5.1)$$

where

RD	=	total rut depth,
i	=	sublayer number,
n	=	total number of sublayers,
ε_{pi}	=	plastic strain in sublayer i, and
h_i	=	thickness of sublayer i.

Rutting is predicted at the mid-depth of each sublayer of the pavement system. Equation (5.2) and Equation (5.3) show the permanent deformation models currently embedded in the MEPDG for asphalt concrete layers and for unbound base and subgrade layers, respectively. The MEPDG permanent deformation prediction models assume that no rutting occurs in stabilized base and sub-base layers, e.g., cement- and lime-stabilized layers.

$$\frac{\varepsilon_p}{\varepsilon_r} = K_z * \beta_{r1} * 10^{kr1} T^{\beta_{r2} * k_{r2}} N^{\beta_{r3} * k_{r3}} \quad (5.2)$$

where

ε_p	=	Plastic strain (in./in.),
ε_r	=	Resilient strain (in./in.),
T	=	Temperature of layer at mid-depth ($°F$),
N	=	Number of load repetitions,
$\beta_{r1}, \beta_{r2}, \beta_{r3}$	=	Local calibration coefficients,
k_1, k_2, k_3	=	National coefficients, $k_1 = -3.35412, k_2 = 1.5606, k_3 = 0.4791$,
K_Z	=	Depth function = $(C_1 + C_2 \times D)(0.328196)^D$,
C_1	=	$-0.1039 \times h_{ac}{}^2 + 2.4868 \times h_{ac} - 17.342$,
C_2	=	$0.0172 \times h_{ac}{}^2 - 1.7331 \times h_{ac} + 27.428$, and
h_{ac}	=	Total thickness of asphalt layer(s).

$$\delta_a(N) = \beta_{gb}\, k_1\, \varepsilon_v h \left(\frac{\varepsilon_o}{\varepsilon_r}\right)\left(e^{-\left(\frac{\rho}{N}\right)^{\beta}}\right) \quad (5.3)$$

where

δ_a	=	Permanent deformation for the layer/sublayer (in.),
N	=	Number of traffic repetitions,
β_{s_1}	=	Local/state calibration factor,
k_1	=	National calibration factor for unbound materials,
	=	2.03 for granular materials and 1.67 for subgrade materials,
ε_v	=	Vertical strain (in./in.),
h	=	Thickness of the layer (in.),
$\varepsilon_o, \rho, \beta$	=	Material properties, and
ε_r	=	Resilient strain obtained from laboratory testing (in./in.).

During a TRLPD test, a specified number of repeated load cycles are applied on a cylindrical asphalt concrete specimen, and the cumulative permanent deformation as a function of the number of load cycles is recorded automatically for each load cycle. A load cycle consisting of a 0.1-second haversine pulse load and a 0.9-second dwell (i.e., rest) time is applied for the test duration, typically about three hours or 10,000 load cycles. Results usually are presented in terms of the cumulative permanent strain (ε_p) versus the number of loading cycles (N). In this study, the test duration was extended to 12,000 cycles or 50,000 microstrains, whichever occurred first, as an attempt to define the secondary region more accurately and to capture the tertiary flow, defined in the following paragraphs.

A typical TRLPD permanent strain versus number of cycles relationship is shown in Figure 5.2 and Figure 5.3 in arithmetic and log-log scales, respectively. Worth mentioning is that the model presented in Equation (5.2) is valid for the secondary region, which appears as a straight line in the log-log scale, as shown in Figure 5.3.

Figure 5.2 shows that the cumulative permanent strain curve is divided into the following three stages:

- Primary stage. A good representation of material densification is evident at this stage, and hence, this stage typically is associated with volumetric change. This stage is also responsible for the high initial level of rutting that typically is measured in the field within the first year or two of in-service pavement life.

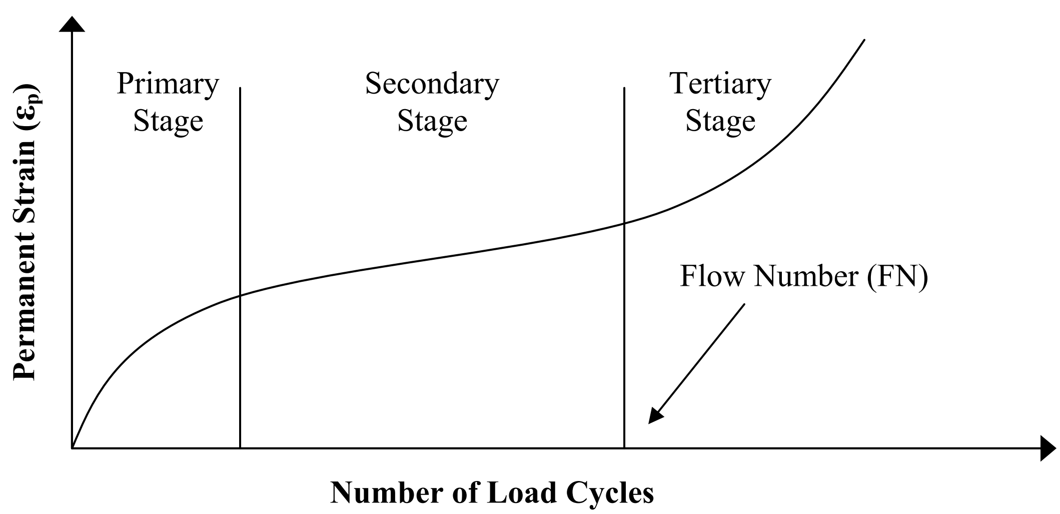

Figure 5.2. Typical TRLPD permanent strain vs. number of cycles graph in arithmetic scale.

- Secondary stage. Rutting during this stage typically is less than is observed in the primary stage, but it is still associated with small changes in volume. In addition, rutting during this stage typically accumulates at a constant rate. Good performing pavements are expected to stay within this stage most of their service life.

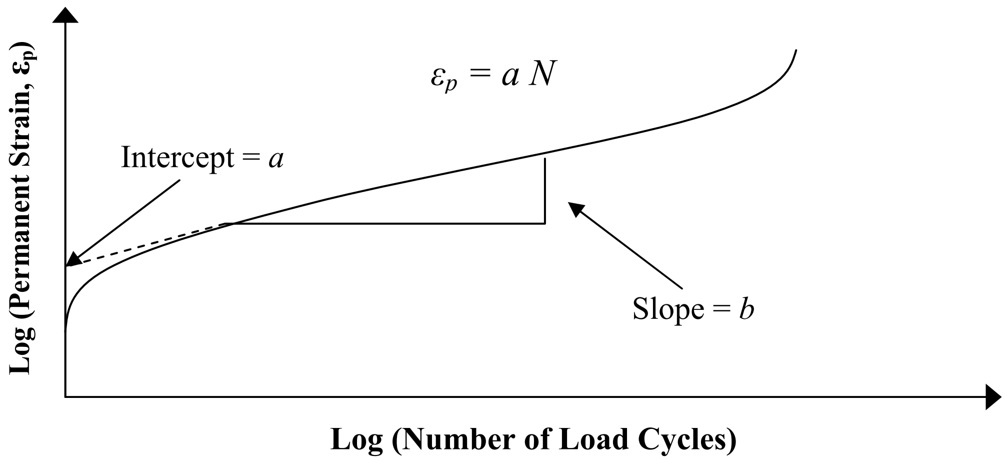

Figure 5.3. Typical TRLPD permanent strain vs. number of cycles graph in log-log scale.

- Tertiary stage. Rutting during this stage is caused mainly by shear deformation. The high level of rutting that accumulates during this stage typically is not associated with volumetric changes. The number of cycles that corresponds to the beginning of this stage is referred to as the *flow number* (FN). Asphalt concrete pavements that experience tertiary flow are undesirable, as the process of rutting occurs rapidly during this stage.

It is vital to mention that in addition to the permanent strain (ε_p), two other mixture parameters have been found to affect rutting behavior (NCHRP, 2002): the resilient modulus (M_R) and the permanent-to-resilient strain ratio ($\varepsilon_p/\varepsilon_r$). The resilient modulus is the ratio of the applied compressive stress to the resilient vertical strain (ε_r), which is the recoverable strain during the rest period between loading cycles. Figure 5.4 shows a strain response curve obtained from an actual lab test. Figure 5.4 also illustrates the permanent strain (ε_p) and resilient strain (ε_r) for one of the loading cycles

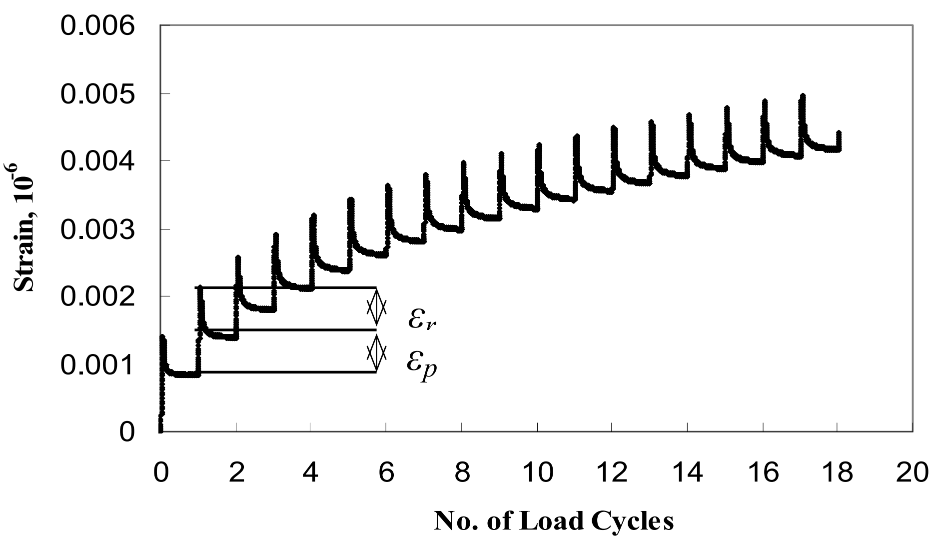

Figure 5.4. Typical TRLPD recorded strain vs. number of cycles during the primary stage.

5.3 Test Equipment

A servo-hydraulic universal testing machine, UTM-25, was used for all the TRLPD tests. UTM-25 is equipped with a 25 kN (5620 lbf) load cell and is capable of applying loads over a wide range of frequencies ranging from 0.01 Hz to 25 Hz. This machine is computer-controlled. All test data were acquired via customized Labview software that was developed at NCSU.

Four on-specimen linear variable differential transformers (LVDTs) were used to measure the vertical deformation of the specimen under cyclic loading. This method generally is preferred over using actuator LVDTs to measure vertical deformation. For accurate temperature measurements, two dummy specimens with temperature sensors centrally embedded in them were used. The first dummy specimen used is the same size as the tested specimens and is located inside the testing chamber but outside the triaxial cell, whereas the second dummy specimen is smaller and sits inside the triaxial cell.

5.4 Triaxial Stress State

Throughout this research, the emphasis has been on characterizing the layer materials in the laboratory using a similar stress state to that observed in real pavements under actual truck loading and environmental changes. Two main research efforts were consulted to help determine the triaxial stress state that best simulates the field conditions to use for all the TRLPD tests. These two studies are discussed below.

5.4.1.1 Effort by Von Quintus et al. under NCHRP 9-30A (2007)

Von Quintus et al. (NCHRP, 2007b) studied the effects of stress state and temperature on TRLPD test results as part of the NCHRP 9-30A project. They designed a testing matrix that incorporates partial factorial variations of temperature, confining pressure, and deviatoric stress. Table 5.1 shows the different test combinations used.

Table 5.1. NCHRP 9-30A Proposed Test Matrix for Repeated Load Testing Program

Deviatoric Stress, psi	Confining Pressure, psi								
	Unconfined			10 psi			20 psi		
	Test Temperature, °F								
	100	120	140	100	120	140	100	120	140
30					X				
50		X		X	X	X		X	
70					X				

The deviatoric stress was found to affect the slope and the value of the permanent strain relationship, especially at a high number of cycles (>1000) and for deviatoric stress values of 50 psi or more. At a low deviatoric stress of 30 psi, the maximum permanent strain values were found to be low, and the average slopes continued to decrease with increasing load cycles. At 50 psi deviatoric stress, no significant differences in the slopes were found compared to the 30 psi deviatoric stress. When 70 psi deviatoric stress was applied, a clear increase in permanent strain values was observed. Therefore, the NCHRP 9-30A team recommended the use of 70 psi deviatoric stress. Another finding of Von Quintus et al. is that a confining pressure of 10 psi reduced the permanent strain substantially throughout the test, whereas increasing the pressure to 20 psi slightly increased the permanent strain. Therefore, the Von Quintus et al. recommended the use of 10 psi for the confining pressure.

5.4.2 Effort by Gibson et al. (2009)

Gibson et al. (2009) simulated a three-layer flexible pavement structure under 18 different stress state combinations using KENLAYER multilayer linear elastic theory. The multiaxial stress measurements were taken at a series of points in a grid pattern distributed at varying depths and lateral positions under a dual tire configuration. To reduce the three-dimensional stress to two parameters, Gibson et al. (2009) used the first stress invariant, I_1, as a representation of normal (bulk) stress, and the second deviator stress invariant, $(J_{2D})^{0.5}$, as a representation of the shear conditions. To calculate the viscoplastic strains resulting from each stress state, Gibson et al. fed each three-dimensional principal stress condition into the three-dimensional viscoplastic model developed by Gibson and Schwartz (2006). Using the first and second stress invariants, Gibson et al. (2009) were able to determine a range of critical stress that the pavement would most likely encounter under wheel loads, as shown in Figure 5.5. Gibson et al. also showed the stress invariants that they calculated from stress values reported by Witczak et al., Monismith and Tayebali, Coree and Hislop, and Mallick et al., as seen in Figure 5.5. Based on their simulation analyses of real world conditions, Gibson et al. (2009) finally recommended a stress state of 10 psi (69 kPa) for confining pressure and 75 psi (523 kPa) for deviatoric stress. To accelerate lab testing, they recommended a stress state of 10 psi (69 kPa) for confining pressure and 120 psi (827 kPa) for deviatoric stress.

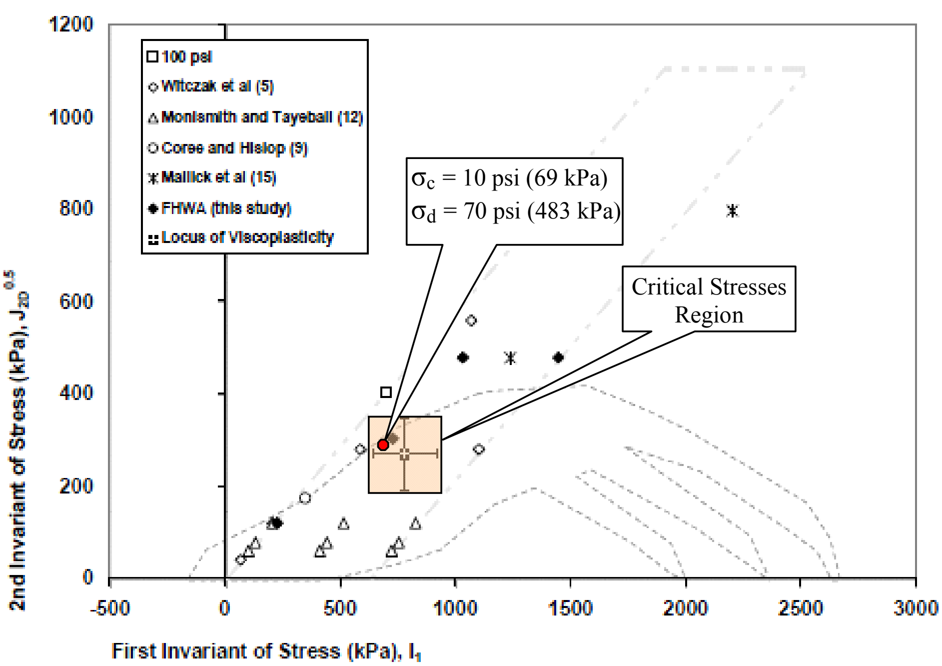

Figure 5.5. Critical stress region, as identified from the 3D viscoplastic model analysis of KENLAYER. (Figure from Gibson et al. 2009).

Based on the recommendations of the NCHRP 9-30A panel and the work by Gibson et al. (2009), the research team selected a stress state of 10 psi (69 kPa) confining pressure and 70 psi (483 kPa) deviatoric stress. This selected stress state was used for all confined cyclic tests throughout this project. For perspective, the location of the first and second invariants, I_1 = 100 psi (690 kPa) and $(J_{2D})^{0.5}$ = 40 psi (278 kPa), which correspond to the selected stress states, is superimposed on Figure 5.5.

5.5 TRLPD Test Temperatures

Based on the recommendations of the NCHRP 9-30A team, TRLPD testing is performed at three temperatures: a low temperature of 20°C (68°F); an intermediate temperature of 40°C (104°F), and a high LTPP-bind temperature, which is 54°C (130°F) for North Carolina.

5.6 TRLPD Test Results

TRLPD tests were conducted for all 12 mixtures included in this research work. Two test specimens with an air void percentage of 5.5 ± 0.5 were tested at each test temperature. However, in cases where variability among test results was high, a third specimen was tested, and the average of the three results was considered. In general, it was observed that the larger the aggregate size, the more the variability between different replicates. Similarly, mixtures with RAP tended to show variable test results because RAP contains random aggregate sizes, as it is typically scooped when batching; i.e., RAP typically is not sieved.

Figure 5.6 shows the relationship between permanent strain (ε_p) and the number of load cycles (N) for all 12 mixtures at 20°, 40°, and 54°C. Figure 5.7 shows the relationship between the permanent-to-resilient strain ratio and the number of load cycles (N). The relationships presented in Figure 5.6 and Figure 5.7 are shown in arithmetic and log-log scales. None of the mixes went into the tertiary stage during the tests and therefore the FN values are greater than 12,000 cycles, which is the number of loading cycles used in the TRLPD test. This observation indicates that these mixes are acceptable in terms of rutting performance.

To simplify the interpretation of Figure 5.6 and Figure 5.7, Table 5.2 and Table 5.3 summarize the rankings of the different mixtures with respect to permanent strain and permanent-to-resilient strain ratio, respectively. Note that Table 5.2 and Table 5.3 are based on the average measured values of the last 1,000 test cycles. This decision was made to overcome test noise, especially at low test temperatures. Detailed TRLPD test results for all 12 mixtures at 20°, 40°, and 54°C are reported in Appendix D of this report.

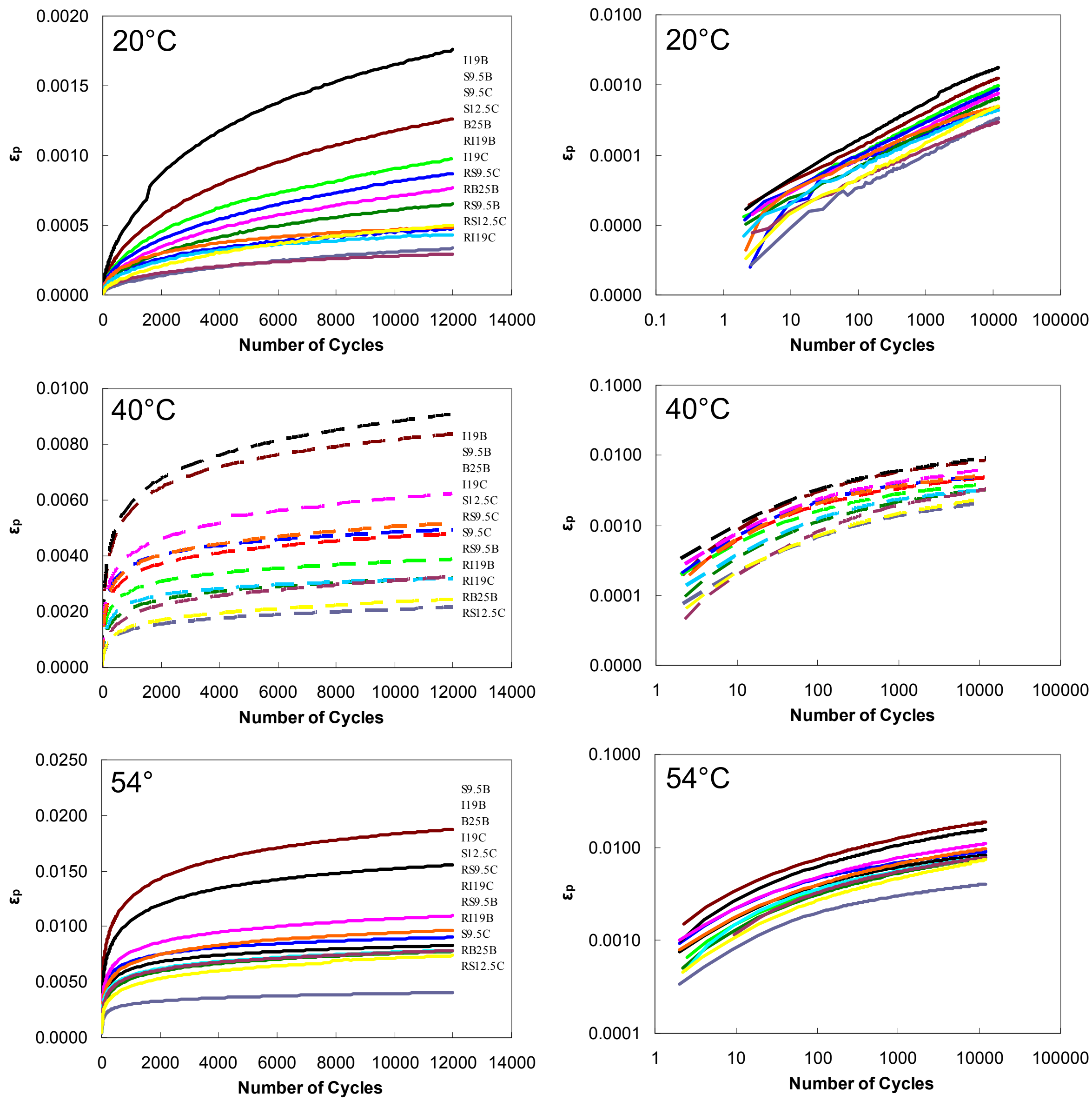

Figure 5.6. Average permanent strain vs. number of cycles at 20°, 40°, and 54°C.

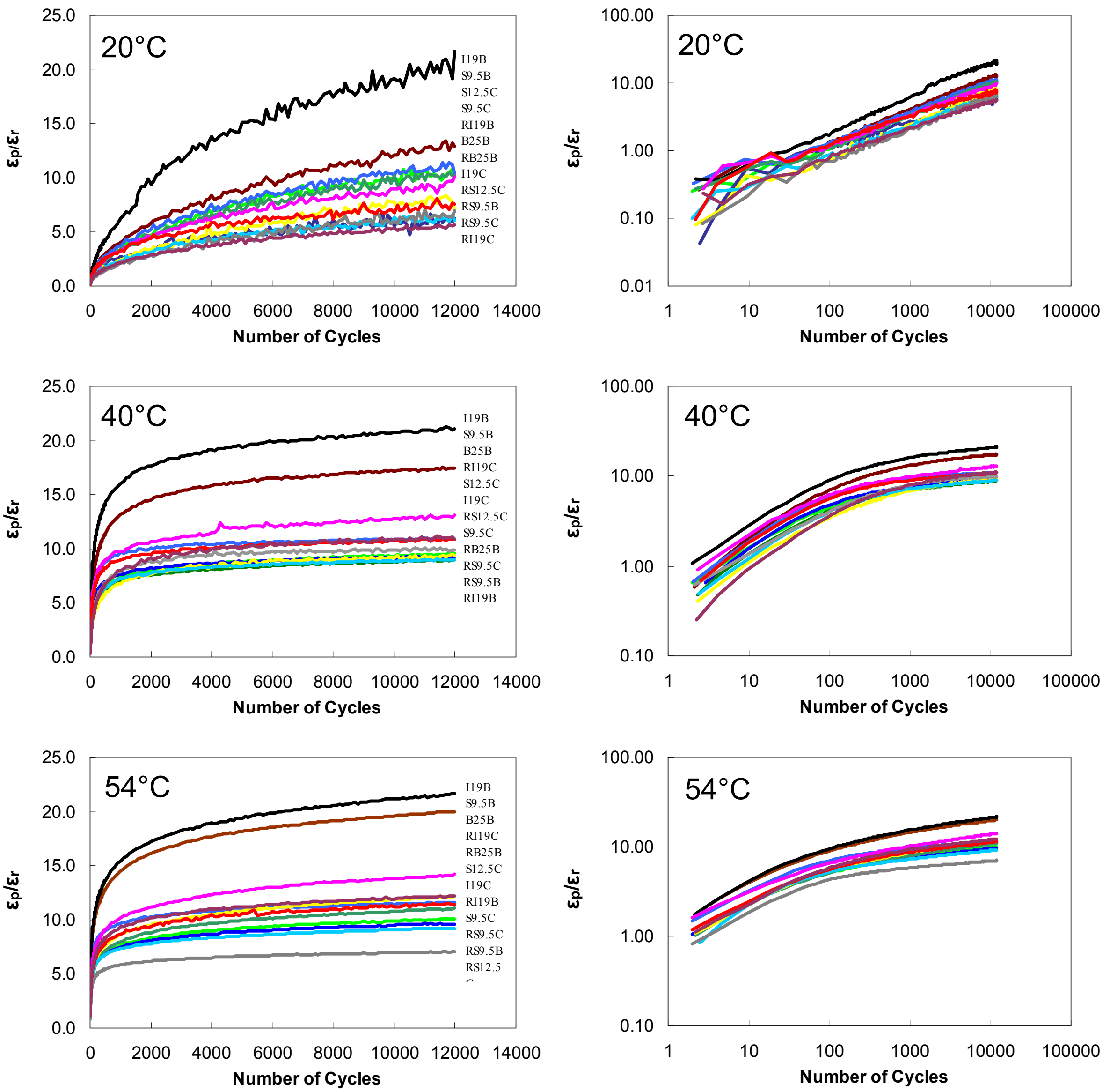

Figure 5.7. Average permanent-to-resilient strain ratio vs. number of cycles at 20°, 40°, and 54°C.

The TRLPD test results shown in Figure 5.6, Figure 5.7, Table 5.2, and Table 5.3 all suggest that the I19.0B and S9.5B mixtures perform the worst in resisting permanent deformation at all three test temperatures. On the other hand, the RS12.5C and RI19.0C mixtures both seem to show the best resistance to rutting, especially at higher temperatures. The rankings shown in Table 5.2 generally are good representations of the field rankings for the mixes tested, because all mixture types were tested in the lab under similar stress states, loads, and test temperatures as those experienced in the field.

Table 5.2. Mixture Ranking Based on Permanent Strain (Worst to Best)

Ranking, Worst to Best, Per Temperature		
20°C	40°C	54°C
I19.0B	I19.0B	S9.5B
S9.5B	S9.5B	I19.0B
S9.5C	B25.0B	B25.0B
S12.5C	I19.0C	I19.0C
B25.0B	S12.5C	S12.5C
RI19.0B	RS9.5C	RS9.5C
RB25.0B	S9.5C	RS9.5B
I19.0C	RI19.0C	RI19.0C
RS9.5C	RI19.0B	S9.5C
RS9.5B	RS9.5B	RI19.0B
RS12.5C	RB25.0B	RB25.0B
RI19.0C	RS12.5C	RS12.5C

Table 5.3. Mixture Ranking Based on Permanent-to-Resilient Strain Ratio (Worst to Best)

Ranking, Worst to Best, Per Temperature		
20°C	40°C	54°C
I19.0B	I19.0B	I19.0B
S9.5B	S9.5B	S9.5B
S12.5C	B25.0B	B25.0B
S9.5C	RI19.0C	RI19.0C
RI19.0B	S12.5C	RB25.0B
B25.0B	I19.0C	S12.5C
RB25.0B	RS12.5C	I19.0C
I19.0C	S9.5C	RI19.0B
RS12.5C	RB25.0B	S9.5C
RS9.5B	RS9.5C	RS9.5C
RS9.5C	RS9.5B	RS9.5B
RI19.0C	RI19.0B	RS12.5C

Figure 5.8 is a bar chart showing the average measured permanent strain values and permanent-to-resilient strain ratios for all the mixtures at the end of 12,000 test cycles. Figure 5.8 provides a succinct summary of each mixture's rutting performance.

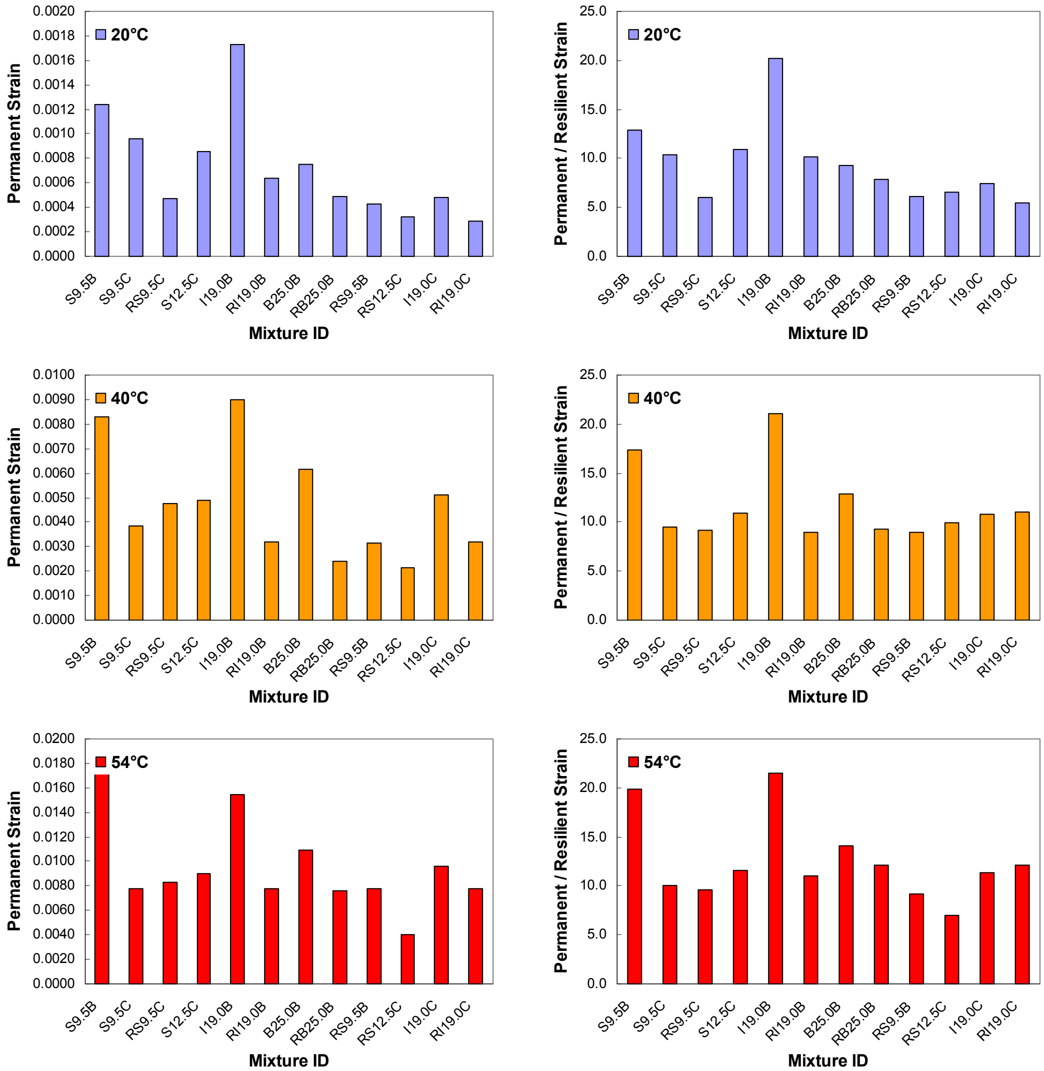

Figure 5.8. Final permanent strain values and permanent-to-resilient strain ratios at 20°, 40°, and 54°C.

Equation (5.2), presented in Section 5.2 suggests that the permanent-to-resilient strain ratio criterion should be used to model asphalt concrete, as this is the form of the model. However, Table 5.2 and Table 5.3 suggest that mixture rankings change depending on whether permanent strain is considered as the criterion versus the permanent-to-resilient strain ratio. For example, Table 5.3 suggests that at 54°C, when mixtures are ranked based on the permanent-to-resilient strain ratio, the I19.0B mixture performs slightly worse than the S9.5B mixture, whereas Table 5.2 suggests the opposite. It is vital to know that the proper ranking for field representation is the one that is based on permanent strain. The rationale behind the selection of this ranking criterion is that the ratio does not clearly explain whether the material experiences a large permanent strain or a small resilient strain, and vice versa. In other words, two mixtures could have similar permanent-to-resilient strain ratios, but one may have a large permanent strain and a small resilient strain compared to the other that may have a small permanent strain and very small resilient strain. The resilient strain parameter shown in Equation (5.2) is introduced primarily to tie the structural design to the mix design. Below is a list of a few observations that can be drawn from Table 5.2:

- For the most part, rutting performance is similar at 40°C and 54°C but different at 20°C.
- Mixtures with RAP clearly perform better in resisting permanent deformation than mixtures without RAP at all three test temperatures.
- For mixtures without RAP, “C” mixtures in general show better resistance to permanent deformation than “B” mixtures.
- The two mixtures that perform the worst at all temperatures, i.e., I19.0B and S9.5B, happen to share the same binder source (Associated Asphalt in Inman, SC), and the same aggregate quarry (Vulcan in Morganton, NC). However, there are not enough experimental data to prove that the source of these materials is the reason for this poor rutting performance.
- The three mixes that perform the best (RS12.5C, RI19.0C, and RB25.0B) happen to share the same binder source (Citgo in Wilmington, NC). The RI19C and RS12.5C mixtures also share the same aggregate quarry (Vulcan in Pineville, NC).

Figure 5.9 (a) and Figure 5.9 (b) show the numerical differences and percent differences respectively in permanent strain versus mix type and corresponding binder grade. Figure 5.9 is plotted to assess the sensitivity of different mixture types to temperature and to show the extent that the effect of this sensitivity has on measured permanent strain. Figure 5.9 (b) suggests that binder grade and/or stiffness have no clear effect on the measured permanent strain, which is evident when comparing, for example, the percentage of change in permanent deformation of the RS9.5C mixture that uses PG 70-22 binder and the I19.0B mixture that uses PG 64-22 binder. Figure 5.9 (b) suggests that when the test temperature changes from 20° to 40°C, the percentage of change in permanent strain for the RS9.5C mixture is almost double that of the I19.0B mixture, even though the RS9.5C mixture uses a stiffer binder than the I19.0B mixture uses. Note that the trend in percent change does not always agree with the numerical differences. To avoid any misleading conclusions, it is recommended to consider the information in Figure 5.9 (a) and (b) at the same time.

The random change in percentage of permanent strain could be attributed to the aggregate structure of the different mixtures. The binder effect might still be present, but it may be smeared with other factors. On the other hand, Figure 5.9 (b) suggests that when the test temperature changes from 40° to 54°C, the effect of binder stiffness and/or mixture type on the percentage of change in permanent strain becomes less noticeable.

The results shown in Figure 5.9 present a dilemma, however; that is, a given mix can be rated according to its rut resistance with respect to the other mixtures without considering that the same mixture type could behave differently if the sources of the mixture materials are different. For example, a B25.0B mixture that uses materials from source A might show excellent rut resistance compared to another B25.0B mixture that uses materials from source B. One preliminary idea to address this dilemma leans towards using predictive relationships in populating the behavior of different source mixtures in resisting permanent deformation.

A few steps in this direction were taken in an attempt to correlate the measured permanent strain values to the number of compaction gyrations recorded at the time of compaction and then correlate them to the measured air voids and aggregate properties.

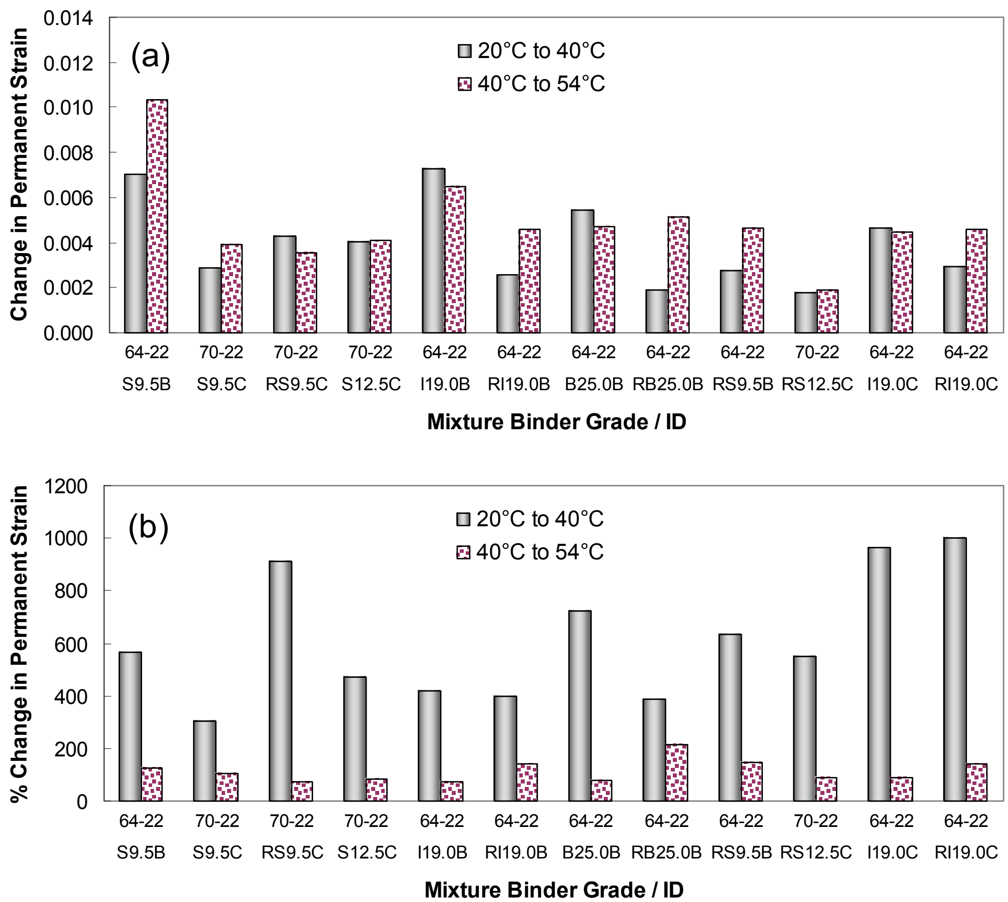

Figure 5.9. Effect of temperature and binder grade on permanent strain: (a) numerical difference; and (b) percent difference.

Figure 5.10 shows the permanent strains measured in the TRLPD tests at the end of 12,000 loading cycles versus the number of compaction gyrations and versus measured air voids. Different functions were plotted to obtain the best fit curves for the available data. The best function to fit the permanent strain versus number of gyrations relationship was found to be a logarithmic function in the semi-log scale, whereas the best function to fit the permanent strain versus percentage of air voids relationship was found to be a quadratic function in the arithmetic scale. The functions were fitted based on a limited number of data points obtained from the 12 mixtures that were tested in addition to other data that were available from other projects.

Figure 5.10 suggests that the measured permanent strain values after 12,000 loading cycles decrease as the number of gyrations required to compact the mixtures to a specific height increases. This observation is logical because a large number of gyrations indicates mixtures that are difficult to compact; hence, such mixtures are resistant to permanent deformation under repetitive loading. In addition, Figure 5.10 suggests that specimens with high air voids in general exhibit high permanent strain values. This observation is also logical and could be attributed to the densification effect under repetitive loading cycles. As mentioned earlier in this document, the acceptable range of air voids for each test specimen is between 5.0% and 6.0%, which is a 0.5% tolerance from the target air void of 5.5 percent.

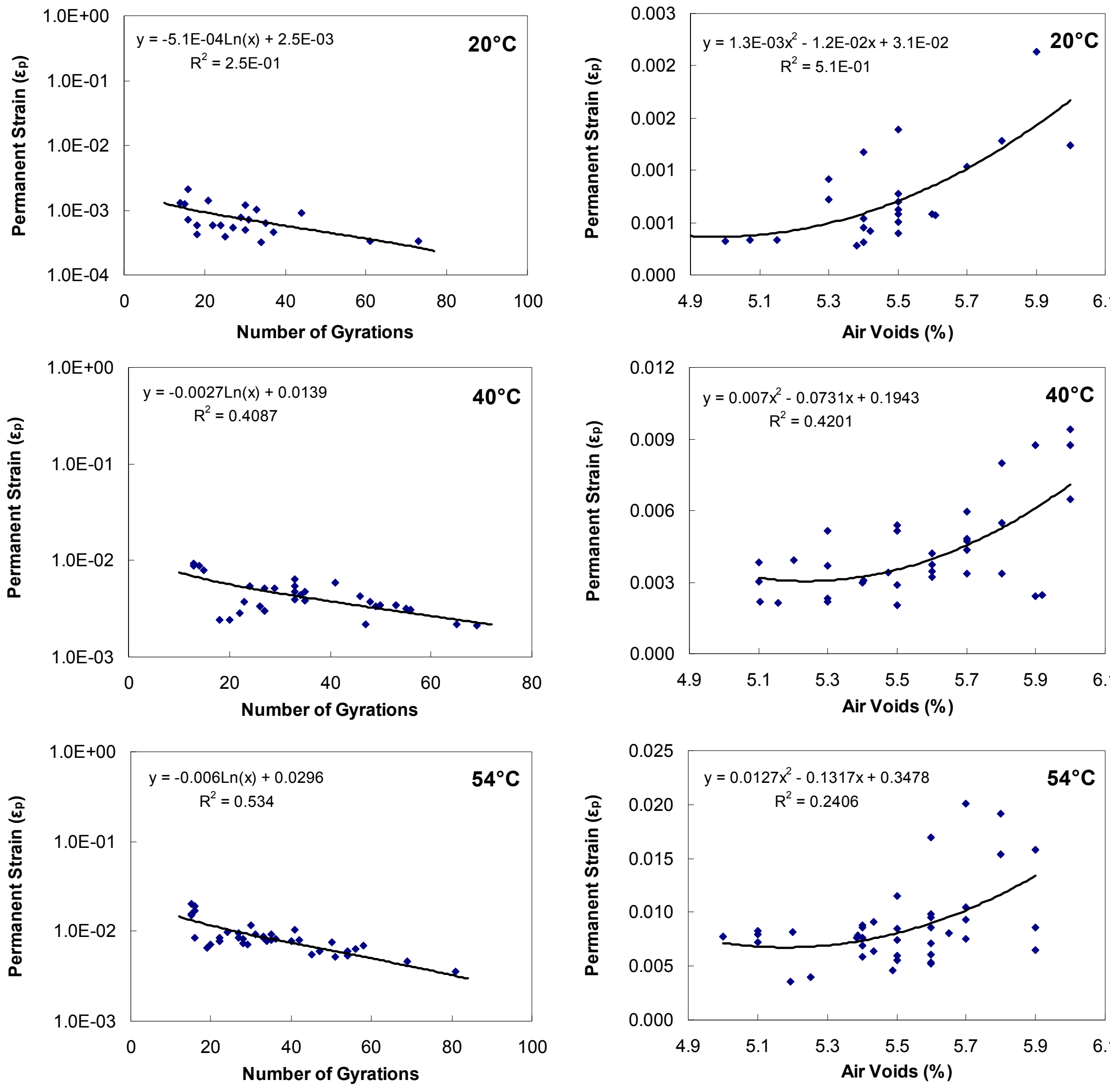

Figure 5.10. Effect of number of gyrations and specimen air void content on permanent strain.

Figure 5.10 also suggests a relatively strong relationship between permanent strain and number of gyrations and also between permanent strain and percentage of air voids at 40° and 54°C. However, these relationships are not as strong at 20°C, probably due to the nature of the TRLPD testing when the stiffness of the asphalt concrete at low temperatures is relatively high.

An AIMS (Aggregate Image Measurement System) machine became available to the research team through an inter-laboratory study that was organized by Pine Instruments, developers of this machine. This machine is capable of providing objective measurements of aggregate shape and texture properties. Samples from all aggregate stockpiles included in this project were tested using the AIMS machine. Various aggregate properties were measured, including aggregate surface texture, the percentage of flat and elongated aggregates, aggregate angularity, and sphericity.

Figure 5.11 shows the effects of texture and percentage of flat and elongated particles on the permanent strains measured after 12,000 loading cycles.

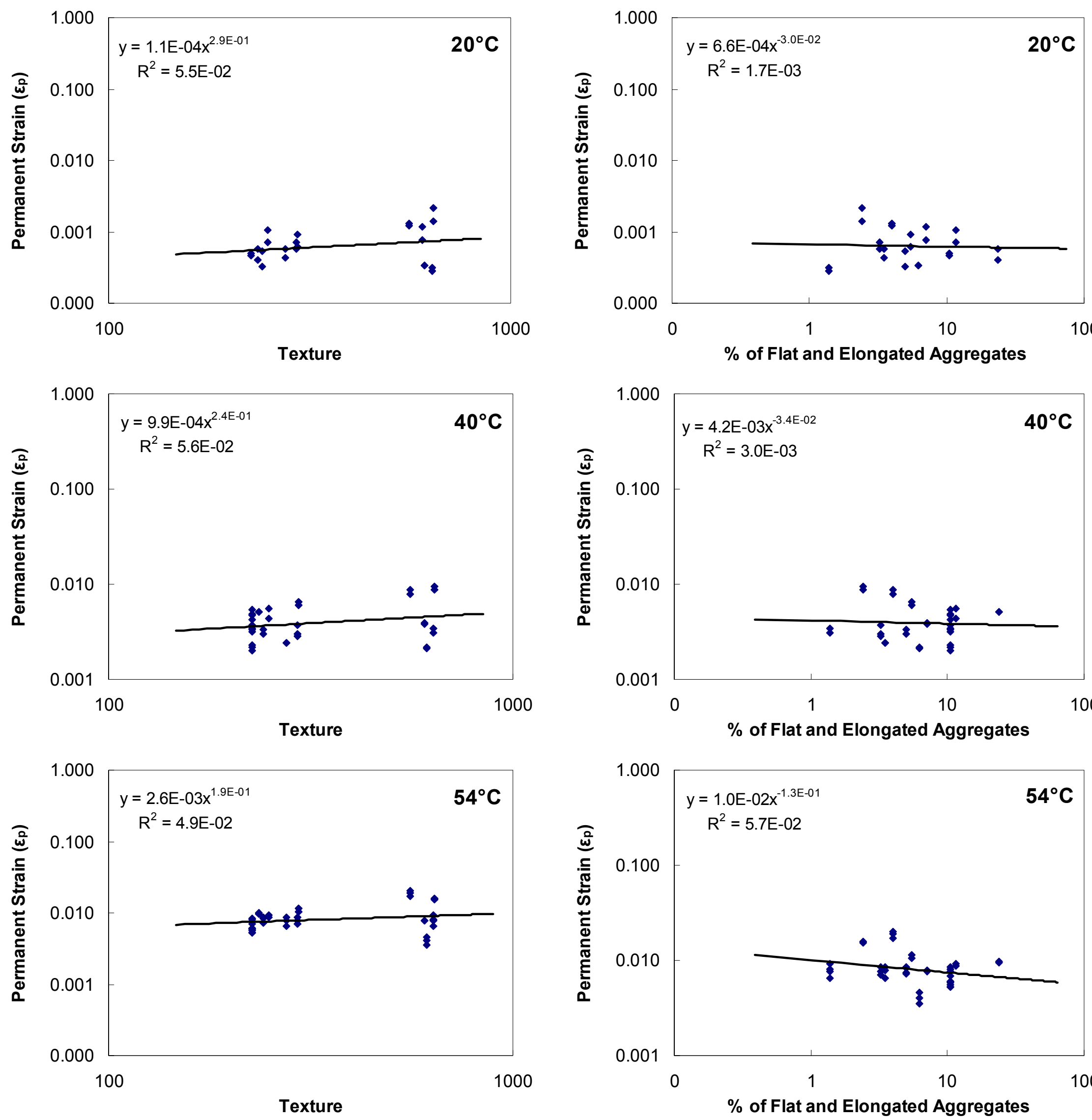

Figure 5.11. Effect of aggregate surface texture and percentage of flat and elongated aggregate on permanent strain.

With the limited amount of data used in this study, Figure 5.11 suggests that the differences in texture for the different aggregates used in the different mixes do not have a large effect on permanent strain at all three test temperatures. A similar observation can be made with regard to the effect of the percentage of flat and elongated particles on rutting performance. The results, at least in terms of texture, do not quite agree with the conclusion drawn by Sousa et al. (1991) that rough aggregates increase rutting resistance. This discrepancy could possibly be attributed to the fact that the surface textures measured for the different aggregates used in this study are not so different, and hence, the effect is not evident. In addition, only a limited number of aggregate stockpiles were tested because this testing was not a major part of the research plan.

The correlations presented in Figure 5.11 are not strong enough to warrant the development of a correlation between the source of the material and the rutting performance of the mixtures. Further experimental work is required in which similar mixtures with different aggregate and binder sources are tested. Such a significant effort is beyond the scope of this research work.

5.7 Rutting Characterization for the Twelve Most Commonly used Asphalt Mixtures in North Carolina

5.7.1 First Approach

The MEPDG uses the model shown in Equation (5.4) to evaluate the permanent deformation of asphalt concrete layers. Equation (5.4) has been presented earlier in this chapter as Equation (5.2). The same equation is reintroduced in this section with a slight modification to aid in understanding the steps used in finding the coefficients and exponents of the permanent deformation model. β_{r1}, β_{r2}, and β_{r3} in Equation (5.4) are called the *local calibration factors*, and their primary role is to adjust the predictions from the model to account for the differences between predicted permanent strain in the lab versus that measured in the field. k'_{r1}, k'_{r2}, and k'_{r3}, on the other hand, are material-specific coefficients that are determined from the TRLPD test results. The rearrangement steps shown below for Equation (5.4) summarizes the initial steps followed under this task to determine k'_{r1}, k'_{r2}, and k'_{r3}.

$$\frac{\varepsilon_p}{\varepsilon_r} = K_z * \beta_{r1} * 10^{k'_{r1}} T^{\beta_{r2} * k'_{r2}} N^{\beta_{r3} * k'_{r3}} \quad \text{.......}(5.4)$$

Let

$$\begin{aligned} K_1 &= K_z * \beta_{r1} * 10^{k'_{r1}} \\ K_2 &= k'_{r2}\, \beta_2 \qquad \text{.......}(5.5) \\ K_3 &= k'_{r3}\, \beta_3 \end{aligned}$$

Equation (5.4) becomes

$$\frac{\varepsilon_p}{\varepsilon_r} = K_1 T^{K_2} N^{K_3} \quad (5.6)$$

Let $K_1 T^{K_2} = A$ and take the log of both sides in Equation (5.6) to obtain

$$Log\left(\frac{\varepsilon_p}{\varepsilon_r}\right) = Log(A) + K_3 Log(N) \quad (5.7)$$

Also,

$$Log(A) = Log(K_1) + K_2 Log(T) \quad (5.8)$$

Note that Equation (5.7) and Equation (5.8) both have the form of a linear function. Hence, the values of K_1, K_2, and K_3 can all be obtained by plotting their linear functions, as shown in Figure 5.12. In this so-called *First Approach*, the three *Log*(*A*) values (the intersects) obtained from the $Log(\varepsilon_p/\varepsilon_r)$ versus *Log* (*N*) relationship at the three test temperatures are used to plot the relationship between *Log*(*A*) and *Log*(*T*). To differentiate between the K_3 values obtained from TRLPD tests performed at different temperatures, the following indicators were used: $K_{3\text{-}20}$ was used to denote the K_3 value obtained from tests performed at 20°C, whereas $K_{3\text{-}40}$, and $K_{3\text{-}54}$ indicate the K_3 values obtained from tests performed at 40°C and 54°C, respectively. Average K_3 values obtained at all temperatures are denoted simply as K_3.

Once the K_1, K_2, and K_3 values were determined, as shown in Figure 5.12, and assuming that all local calibration factors (β_{r1}, β_{r2}, and β_{r3}) are equal to one, the material-specific *k* values (k'_{r1}, k'_{r2}, and k'_{r3}) can all be determined.

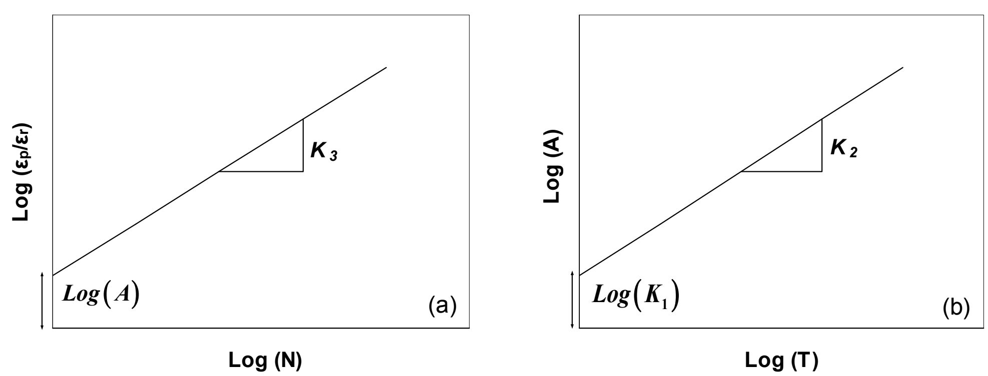

Figure 5.12. Approach followed for finding the rutting model coefficients: (a) $Log(\varepsilon_p/\varepsilon_r)$ vs. *Log* (*N*) relationship; and (b) *Log*(*A*) *vs.* *Log*(*T*) relationship.

5.7.2 Second Approach (Selected)

This *Second Approach* is similar to the first approach with one major difference. In this approach, the *Log* (*A*) values that were used to plot the relationship between *Log*(*A*) and *Log*(*T*) were not obtained from the $Log(\varepsilon_p/\varepsilon_r)$ versus *Log*(*N*) relationship, as was the case in the first approach; rather, these values were obtained using Microsoft Excel Solver numerical optimization routine. The optimization was undertaken to minimize the sum of squared errors (SSE) between both sides of Equation (5.7) by changing *Log*(*A*)*,* which is the objective function. The K_3 value that was used in Equation (5.7) is actually the average K_3 value obtained from tests performed at three temperatures; i.e., K_3 is the average of $K_{3\text{-}20}$, $K_{3\text{-}40}$, and $K_{3\text{-}54}$. These values were obtained from the $Log(\varepsilon_p/\varepsilon_r)$ versus *Log* (*N*) relationship, shown in Figure 5.12, at 20°C, 40°C, and 54°C, respectively.

In the second approach, the assumption is that the slope of the $Log(\varepsilon_p/\varepsilon_r)$ versus *Log*(*N*) relationship, i.e., the K_3 value, is constant at the three test temperatures. However, TRLPD test data from tests performed on local mixtures have shown, in general, that this assumption holds true at 40°C and 54°C, but not at 20°C. It was observed that the K_3 values are higher at 20°C than at 40°C and 54°C. Initially, this observation did not seem rational because K_3 represents the effect of loading cycles on the permanent-to-resilient strain ratio, as shown in Figure 5.12. The effects at low temperatures generally are expected to be smaller than at high temperatures. One possible reason for this observation is that the duration of the test (12,000 cycles) was not long enough to transfer the material from the initial stage to the secondary stage, which led to very stiff mixtures at 20°C. This observation may be because during the secondary stage, the material stabilized, and the effect of loading cycles on permanent deformation lessened.

Finally, the decision was made under this task to select the *Second Approach* to obtain material-specific *k* values because smaller differences were calculated between the permanent-to-resilient strain ratios measured from lab tests and those predicted using the rutting model shown in Equation (5.4). That is, the *Log*(*A*) values obtained through optimization provide a better prediction than those obtained from the linear relationship between $Log(\varepsilon_p/\varepsilon_r)$ and *Log*(*N*). In addition, it was decided, as will be discussed under Section 5.7.4, to include the 20°C data in the optimization work to determine the K_1, K_2, and K_3 values, and hence, to determine the material-specific *k* values.

Figure 5.13 shows a comparison between predicted and lab-measured permanent strains for the S9.5B mixture as an example. The predicted permanent strain curve shown in Figure 5.13 was obtained by following the *Second Approach* and by selecting one of four available optimization methods that could be used to fine-tune the results from the *Second Approach*, as will be discussed in Section 5.7.3.

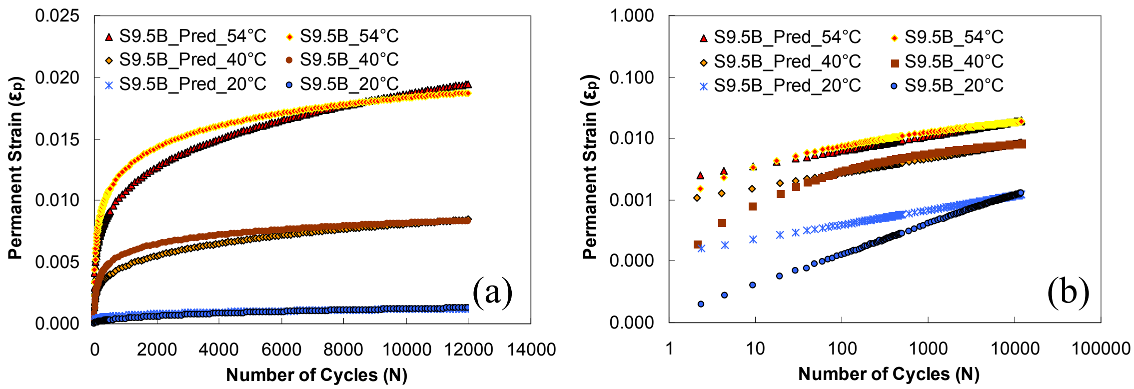

Figure 5.13. Comparison between predicted and lab-measured permanent strain values for the S9.5B mixture: (a) arithmetic scale; and (b) logarithmic scale.

Figure 5.14 is a comprehensive flow chart showing the procedure followed in each of the two approaches, i.e., the *First Approach* and *Second Approach*, to determine the K_1, K_2, and K_3 values. As explained earlier, Figure 5.14 shows that the only difference between the two approaches is the way the *Log*(A) parameter is determined. In the *First Approach*, the *Log*(A) parameter is determined as the intersect in the linear relationship between *Log*($\varepsilon_p/\varepsilon_r$) and *Log*($N$), whereas in the *Second Approach*, Microsoft Excel Solver numerical optimization routine was used to find a constant *Log*(A) that is closest to the lab-measured *Log*(A) at each of the three test temperatures. Section 5.7.2.1 presents the detailed procedure followed under the *Second Approach*.

5.7.2.1 Detailed Procedure of the Second Approach

This detailed procedure uses the S9.5B mixture as an example. A similar procedure was followed to determine material-specific k values for all the other mixtures involved in this study. The procedure is illustrated as part of Figure 5.14 and is explained in detail in the following steps:

1) TRLPD tests were carried out on the S9.5B mixture at three temperatures: 20°C, 40°C, and 54°C. A minimum of two specimens was tested at each temperature, and the average of the results was taken. For accurate temperature measurements, two dummy specimens were used (as explained under Section 5.3). TRLPD test data, including stress and strain values, were captured using LabView software with a customized acquisition program developed at NCSU.
2) MATLAB® software was then used with another customized program to analyze the acquired data in order to obtain permanent and resilient strain values at each loading cycle (N). A cycle is comprised of 0.9 second of loading time followed by a 0.1-second rest time. Figure 5.4 illustrates the definition of permanent strain (ε_p) and resilient strain (ε_r). Permanent-to-resilient strain ratios ($\varepsilon_p/\varepsilon_r$) were then calculated. Each test was allowed to run for 12,000 cycles or 50,000 micro strains, whichever occurred first.

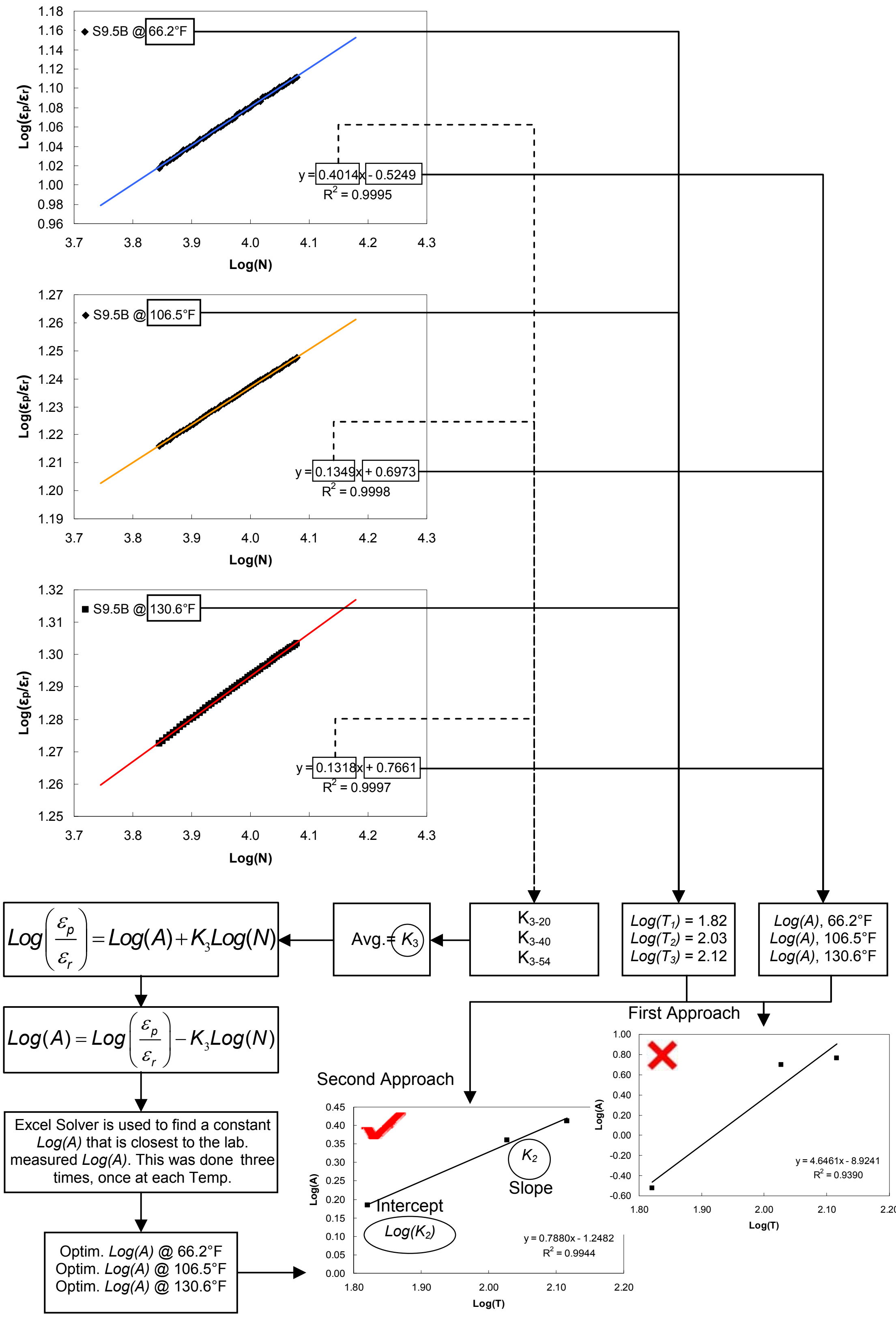

Figure 5.14. Schematic diagram showing the two approaches for finding rutting k values.

3) Because Equation (5.4) applies only to the secondary region of the TRLPD test curve, as explained in Section 5.2, it was necessary to determine this region before considering data for further optimization work. Initially, the task of defining the secondary stage was challenging because of the unclear and undefined transition between the initial stage and the secondary stage and between the secondary stage and the tertiary stage, as shown in Figure 5.3. The difficulty stems from the fact that finding the secondary stage depends on the log-log chart, which means that any error in the number of cycles could be magnified due to the log scale effect. However, because none of the 12 mixtures reached tertiary flow, as defined in Section 5.2, the latter transition was a moot issue; i.e., a transition from the secondary to tertiary region did not even occur. To ensure that the selected data were from the secondary region, only the last 5,000 cycles of each test were considered. Worth mentioning is that the primary region in most of the tested mixtures ended at about 1,000 to 2,000 cycles after starting the test; therefore, considering data within the last 5,000 cycles of the testing was a conservative assumption.
4) At each test temperature, the $Log\ (\varepsilon_p/\varepsilon_r)$ versus $Log(N)$ graph was plotted, as illustrated in Figure 5.14. In the log scale, the curve is a linear representation of the secondary stage. Again, the data plotted were those captured only within the last 5,000 cycles of each test.
5) The slope of the $Log\ (\varepsilon_p/\varepsilon_r)$ versus $Log(N)$ relationship is denoted as K_3 (see Equation (5.5)). Three K_3 values are defined in this context, as shown in Figure 5.14, one at each temperature. The K_3 values obtained at 20°C are denoted as $K_{3\text{-}20}$, and those obtained at 40°C and 54°C are denoted as $K_{3\text{-}40}$ and $K_{3\text{-}54}$, respectively. The average slope is denoted as K_3.
6) The K_3 value determined from Step 5 was substituted in Equation (5.7), and then Microsoft Excel Solver numerical optimization routine was used to find a constant $Log(A)$ value that was closest to the $Log(A)$ value calculated from the TRLPD test data measured in the lab. Solver optimization was repeated three times, once for each test temperature.
7) Knowing the three measured test temperatures and the optimized $Log(A)$ values at each of these temperatures, a figure similar to Figure 5.12 (b) was constructed, as shown in Figure 5.14. A form similar to that shown in Figure 5.12 (b) was used to obtain the K_1 and K_2 values, with $Log(K_1)$ being the intersect, and K_2 being the slope of the $Log(A)$ versus $Log(T)$ relationship.

Using the K_1 and K_2 values determined from Step 7 and the K_3 value from Step 5, the material-specific *k* values were determined as per their definitions in Equation (5.5).

As was discussed first in Section 5.7.2, the work undertaken in the *Second Approach* used the TRLPD test results at all three test temperatures, i.e., 20°C, 40°C, and 54°C. Section 5.7.4 discusses in detail the reasons that 20°C data are included. The next Section 5.7.3 discusses the different methods that were tried in an effort to fine-tune the material-specific *k* values determined from Step 7 above.

5.7.3 Methods Attempted to Fine-Tune the Material-Specific *k* Values

Four optimization methods were tested in an attempt to fine-tune the k'_{r1}, k'_{r2}, and k'_{r3} values obtained from the *Second Approach*. Two of the four methods use the Microsoft Excel Solver numerical optimization routine, and the other two methods use Evolver Genetic Algorithm (GA) numerical optimization routine. The goal is to find the best *beta* values that minimize the SSE between the measured permanent strain and the permanent strain predicted using the MEPDG rutting model, shown in Equation (5.4). The four optimization methods that were tested are:

1) Solver with SSE as the objective function,
2) Solver with log (SSE) as the objective function,
3) GA (Evolver) with SSE as the objective function, and
4) GA (Evolver) with log (SSE) as the objective function

where

$$SSE = \left(\varepsilon_{p-measured} - \varepsilon_{p-predicted}\right)^2 \quad (5.9)$$

$$Log(SSE) = \left(log(\varepsilon_{p-measured}) - log(\varepsilon_{p-predicted})\right)^2 \quad (5.10)$$

In all four methods, the β_{r1}, β_{r2}, and β_{r3} values in Equation (5.4) are constantly optimized until the search for an absolute minimum SSE or Log (SSE), as defined in Equations (5.9) and (5.10), has ended.

In some cases, *beta* values, and hence, material-specific *k* values, obtained using the four aforementioned optimization methods, were found to be close to each other and close to the material-specific *k* values obtained using the *Second Approach* before any fine-tuning was undertaken. In some other cases, however, the differences were found to be large. Considering all 12 mixtures tested under this task together, the most stable optimization method that was found to give consistent results among all the mixtures is the second method, which uses Microsoft Excel Solver numerical optimization routine to minimize the Log(SSE). The other methods performed well for some mixtures but not for others. The values of β_{r1}, β_{r2}, and β_{r3} that were obtained from an intermediate step during the application of the *Second Approach* were used as seeds for the four optimization methods mentioned above. This step was necessary, because in many cases the final optimization results were found to be dependent to a certain degree on the initial seed values.

Table 5.4 shows the effects of the four optimization methods on S9.5B material-specific *k* values. The shaded row in Table 5.4 corresponds to the values that were selected for the S9.5B mixture. As mentioned earlier, a similar approach was followed for the other 11 mixtures tested under this task.

Table 5.4. Effects of Different Optimization Methods on Rutting *k* Values for the S9.5B Mixture

Method	β_{r1}	β_{r2}	β_{r3}	Minimum *SSE*	Minimum *Log(SSE)*	k'_{r1}	k'_{r2}	k'_{r3}
Second Approach	127.613	0.505	0.465	0.000659	0.46498	-1.4595	0.9201	0.2227
Solver on SSE	127.745	0.515	0.441	0.000006	0.03227	-1.2478	0.8036	0.2112
Solver on log(SSE)	127.745	0.484	0.496	0.000008	0.01470	-1.2478	0.7555	0.2375
Evolver on SSE	462.182	0.430	0.293	0.000000	0.04161	-0.6893	0.6715	0.1406
Evolver on log(SSE)	147.711	0.483	0.465	0.000007	0.01453	-1.1847	0.7533	0.2227

As previously mentioned, the goal of this study is to find the best material-specific *k* values, i.e., k'_{r1}, k'_{r2}, and k'_{r3}, which will minimize the differences between predicted permanent strain and lab-measured permanent strain. The intent is that these *k* values will replace the national default *k* values, k_{r1} = -3.34412, k_{r2} = 1.5606, and k_{r3} = 0.4791, for calibration work and for implementation work as well.

Depending on the mixture type to be used in the design, different *k* values will be required for different mixtures. For pavement structures with more than a single asphalt layer, *k* values that correspond to different mixtures should be entered separately in the MEPDG. Worth mentioning is that Version 1.1 of the MEPDG, in its current form, does not allow users to enter different *k* values for different layers; however, the research team was able to obtain a different version of the MEPDG that allows this procedure to be possible. At the time of this analysis, the commercial version of the MEPDG (called DARWin-ME) that would be available in 2011 was expected to have the option of entering material-specific *k* values for each asphalt layer independently. However, it was found at the end of this project that DARWin-ME does not have an ability to input different rutting coefficients for different layers. There is no time to address this conflicting issue in this project, and it needs to be addressed through an additional study. The next Section 5.7.4 explains the rationale behind including 20°C data in the process of finding the best material-specific *k* values.

5.7.4 Effects of Including 20°C TRLPD Test Results on Material-Specific *k* Values

5.7.4.1 Background and Presentation of Similar Work Undertaken by Arizona State University (ASU)

As mentioned earlier, the slope of the *Log* ($\varepsilon_p/\varepsilon_r$) versus *Log*(*N*) curve at 20°C is steeper than that at 40°C and 54°C for all 12 mixtures tested under this task. This observation was not expected, but it may be related to the fact that at 20°C, none of the mixtures reached the secondary stage, even after 12,000 loading cycles. During the initial stage of loading, the slope typically is much steeper due to the rapid densification of the material under cyclic loading compared to the secondary stage during which the mixture is more stable. Initially, this observation suggested excluding the 20°C data from the work required to determine the material-specific *k* values. However, this section discusses in detail the reasons that the 20°C data are included and the benefits of doing so.

In order to determine the effects of including 20°C data on the calculated material-specific *k* values, the analysis was conducted twice, once with 20°C data and another without 20°C data. In addition, in order to judge whether the calculated *k* values in each case were reasonable, results from similar work performed by Kaloush at ASU (Kaloush, 2001) were examined for comparison. Further, the calculated *k* values were compared to the national default values, as explained later in this section.

Among the different parameters shown in Figure 5.12, Kaloush reported two parameters: the intercept (*Log*(*A*)) and the slope (K_3). In addition, Kaloush reported the resilient strain (ε_r) and the measured air content for each tested specimen. Table 5.5 summarizes a small portion of Kakoush's results and some back-calculated material-specific *k* values that the research team obtained using the *Second Approach* presented in Section 5.7.2.1.

Table 5.5. Back-Calculated Rutting Material-Specific *k* Values for Some MnRoad Mixtures

Experiment	Section	Meas. Va,%	Temp °F	Intercept	Slope	Resilient Strain	Back-Calculated Material-Specific *k* Values		
							k'_{r1}	k'_{r2}	k'_{r3}
MnRoad	16	7.5	100	0.1832	0.1560	0.0224	-0.592	0.387	0.224
		7.4	130	0.2273	0.2920	0.0352			
	17	7.3	100	0.0586	0.1845	0.0150	-0.643	0.351	0.203
		7.3	130	0.0986	0.2210	0.0262			
	18	5.0	100	0.0911	0.2220	0.0245	-0.159	0.125	0.295
		5.1	130	0.1054	0.3670	0.0431			
	20	6.2	100	0.0755	0.4095	0.0362	-0.161	0.118	0.455
		6.1	130	0.0889	0.5000	0.0501			
	22	5.6	100	0.0296	0.1655	0.0097	-0.350	0.190	0.194
		5.6	130	0.0512	0.2215	0.0230			

Table 5.5 includes the results of ten tests that Kaloush performed on some MnRoad mixtures. Only ten mixtures are included in this comparison because these mixtures are the only mixtures tested under conditions close to the conditions used at NCSU. Two differences between the test conditions used in Kaloush's work and those implemented under this task are: 1) the MnRoad mixtures tested by Kaloush and shown in Table 5.5 were tested at 120 psi deviatoric stress and 20 psi confining pressure compared to 70 psi deviatoric stress and 10 psi confining pressure for tests performed at NCSU; and 2) as Table 5.5 shows, six out of the ten specimens that Kaloush tested had higher air contents than the maximum limit allowed for tests performed at NCSU, i.e., 5.5 ± 0.5 percent. Note that because Kaloush did not perform any of the tests at 20°C, all the back-calculated *k* values reported in Table 5.5 were analyzed with this information in mind.

Again, the reason for comparing the data to the work performed at ASU and also to the MEPDG national default values is to evaluate the effects of including the 20°C TRLPD test data on the calculated rutting model *k* values and to determine if the obtained *k* values are reasonable.

Table 5.6 presents a summary of the rutting model *k* values obtained from four sources: 1) MEPDG national default values, 2) ASU results from ten tests on MnRoad mixtures, where no tests were performed at 20°C, 3) NCSU test results for 12 local mixtures with 20°C data included, and 4) NCSU test results for12 local mixtures with 20°C data excluded.

Table 5.6. Comparison of Rutting Model Coefficients among MEPDG, ASU, and NCSU Results

Organization	k_{r1}	k_{r2}	k_{r3}
MEPDG national default *k* values	-3.35412	1.5606	0.4791
ASU average *k* values from Table 5.5, without 20°C	-0.38100	0.2340	0.2740
NCSU average *k* values with 20°C	-1.00000	0.5780	0.2150
NCSU average *k* values without 20°C	-0.12900	0.2890	0.1470

An initial inspection of Table 5.6 reveals that the average ASU and NCSU *k* values are much different from the MEPDG national default values, but they are not as different when compared to each other. To better understand the information presented in Table 5.6, it is necessary to know that the k_{r2} exponent represents the effect of temperature on rutting, whereas the exponent k_{r3} represents the effect of number of loading cycles on rutting. From Table 5.6, it can be seen that the MEPDG national default *k* values overestimate the effects of temperature and number of loading cycles on rutting compared to the NCSU and ASU *k* values. This difference could be attributed in part to the fact that the MEPDG national default values have a field calibration factor built into them, which is obviously not the case with the data presented for ASU and NCSU that are dependent mainly on laboratory material testing without any correction factors or transfer functions.

When the ASU data are compared to the NCSU data, 20°C data excluded, Table 5.6 suggests that the average k_{r2} exponent obtained from the NCSU tests is relatively close to that from ASU, indicating that both sources give a roughly similar weight to the effect of temperature on mixture rutting performance. However, when the k_{r3} values are compared, Table 5.6 suggests that the rutting performance of the NCSU mixtures is less dependent on the number of loading cycles than that of the ten MnRoad mixtures tested at ASU. Furthermore, Table 5.6 suggests that when the 20°C TRLPD test data were included in the NCSU work, the k_{r2} exponent value went up compared to that reported for ASU and NCSU when 20°C data were excluded. This finding is expected because, again, k_{r2} represents the effect of temperature on the mixture rutting performance, so including the 20°C data made the temperature effect appear more pronounced.

From the information presented in the previous paragraphs, the research team decided that the 20°C TRLPD test data should be included in characterizing the rutting model *k* values. This decision was based on two factors: 1) the *k* values obtained when the 20°C data are included are actually closer to the MEPDG national default values that acknowledge field-to-lab differences, and 2) the *k* values obtained for the different mixtures appear to be more stable when 20°C data are included. In contrast, *k* values obtained when 20°C data are excluded vary significantly among the different mixtures, which did not appear to be rational, based on the experience of the research team. However, before the final decision was made to include the 20°C TRLPD test data in characterizing the rutting model coefficients, i.e., the *k* values, two more studies were carried out. These studies are presented and discussed in the next two subsections, 5.7.4.2 and 5.7.4.3.

5.7.4.2 Study 1: MEPDG Simulations to Evaluate the Effects of 20°C TRLPD Test Data

In this study, the MEPDG was utilized to evaluate the effect of the two *k* value sets, as reported in Table 5.7 for the S9.5B mixture, on rutting predictions for two different pavement structures, full depth (thick) and conventional aggregate base (thin), in three different climates (Cleveland, Ohio; Raleigh, North Carolina; and Houston, Texas). In addition, the MEPDG was executed to evaluate the effect of using the MEPDG national default *k* values (shown in Table 5.6) for the same pavement structures and environments. The latter evaluation was carried out to assess the differences in predicted rut depth when using lab-generated *k* values, i.e., the NCSU *k* values, versus national default *k* values that include a lab-to-field conversion factor. The total number of MEPDG runs was 18, i.e., 2 pavement structures x 3 locations x 3 sets of *k* values.

Table 5.7. Effect of Including 20°C TRLPD Test Data on S9.5B Rutting Model Coefficients

20°C TRLPD Test Data Included?	S9.5B Mix *k* Values		
	k'_{r1}	k'_{r2}	k'_{r3}
Yes	-1.248	0.756	0.238
No	-0.876	0.691	0.178

Figure 5.15 is a schematic of a cross-section of the two pavement structures that were used in these simulations.

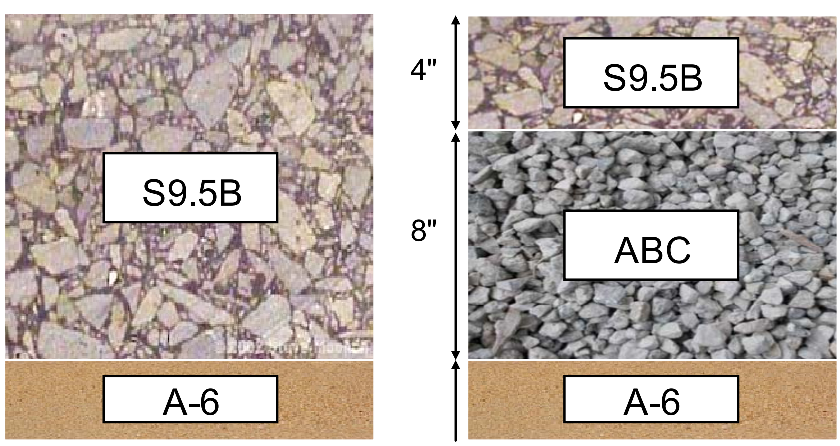

Figure 5.15. Pavement sections used in MEPDG simulation runs to check the effect of including 20°C TRLPD test data on pavement rutting.

The thick full-depth pavement is 12 inches of S9.5B mixture on top of A-6 subgrade, and the thin pavement structure is 4 inches of S9.5B mixture on top of 8 inches of aggregate base course (ABC) on top of A-6 subgrade. The thick full-depth pavement structure with 12 inches of the surface course was not realistic, but the research team did not have a means of entering different rutting model coefficients for different layers at the time of this evaluation. Because this study focuses on the effect of including 20°C TRLPD data, the reasonableness of the study pavement structure was not deemed to be critical.

Note that the full-depth structure might not be realistic in the sense that a single surface mixture (S9.5B) was used for the whole depth; however, this design was selected so that only one set of *k* factors was needed as input to the MEPDG. As mentioned earlier, if different asphalt concrete layers are used in a design, then separate sets of *k* values that correspond to the different asphalt layer types must be entered, which is beyond the scope of this exercise. The goal of this exercise is to gain insight into the effect of changing the rutting model coefficients on pavement predicted rut depth in different temperature zones rather than evaluating a realistic pavement design.

Table 5.8, Table 5.9, Figure 5.16 and Figure 5.17 summarize the results of the 18 MEPDG simulation runs based on the information given under *Study 1*. Table 5.8 summarizes two types of rutting predictions: the total rutting that accumulates on the pavement surface and rutting in the asphalt layer. It is realized that the rutting model *k* values obviously are associated with the rutting predicted in the asphalt layer only; however, the total rut depth is also reported in Table 5.8 to reflect the contribution of the asphalt layer rutting to the total rutting.

Table 5.8 and Figure 5.17 both show that the effect of including the 20°C TRLPD test data in developing the S9.5B rutting model *k* values is slightly more significant for thick pavements than thin pavements. Table 5.8 suggests an average percentage of difference in the predicted total rut depth of 1.4 % for thick pavements compared to 1.0% in thin pavements. Furthermore, Table 5.8 and Figure 5.17 both suggest that the effect of including 20°C TRLPD test data is much higher when the predicted rutting found only in the asphalt layers is considered. Table 5.8 suggests an average difference of 15.5% in thick pavements versus 12.3% in thin pavement. It is interesting to see that the variations in rutting predictions due to changes in the environment, i.e., project location, are slightly higher when the 20°C data are included. This finding is especially noticeable for asphalt layer rut predications where the maximum percentage of difference in predicted asphalt rutting is about 55% versus 52.9% for thick pavements, and 55.6% versus 50.0% for thin pavements, when including or excluding 20°C data, respectively. Furthermore, Table 5.8 suggests that the warmer the project location climate, the greater the effect of including 20°C data on predicted rut depth.

Table 5.8. Effect of Including 20°C TRLPD Test Data on Predicted Rut Depth for Different Pavement Sections with the S9.5B Mixture in Different Environments

City	Total Rut Depth in Thick Pavement (inch)			
	With 20°C	Without 20°C	% Difference	Absolute Difference
Cleveland	0.292	0.289	1.0	0.003
Raleigh	0.312	0.307	1.6	0.005
Houston	0.316	0.311	1.6	0.005
Max % Diff.	8.2	7.6	----------	----------
Average	----------	----------	1.4	0.004
City	Total Rut Depth in Thin Pavement (inch)			
	With 20°C	Without 20°C	% Difference	Absolute Difference
Cleveland	0.506	0.502	0.8	0.004
Raleigh	0.504	0.500	0.8	0.004
Houston	0.509	0.502	1.4	0.007
Max % Diff.	0.6	0.0	----------	----------
Average	----------	----------	1.0	0.005
City	AC Rut Depth in Thick Pavement (inch)			
	With 20°C	Without 20°C	% Difference	Absolute Difference
Cleveland	0.02	0.017	15.0	0.003
Raleigh	0.026	0.022	15.4	0.004
Houston	0.031	0.026	16.1	0.005
Max % Diff.	55.0	52.9	----------	----------
Average	----------	----------	15.5	0.004
City	AC Rut Depth in Thin Pavement (inch)			
	With 20°C	Without 20°C	% Difference	Absolute Difference
Cleveland	0.027	0.024	11.1	0.003
Raleigh	0.035	0.031	11.4	0.004
Houston	0.042	0.036	14.3	0.006
Max % Diff.	55.6	50.0	----------	----------
Average	----------	----------	12.3	0.004

Table 5.9. Effect of Using MEPDG Default Rutting *k* Values on Predicted Rut Depth for Different Pavement Sections with the S9.5B Mixture in Different Environments

City	Total Rut Depth (inch)		AC Rut Depth (inch)	
	Thick	Thin	Thick	Thin
Cleveland	0.501	0.751	0.228	0.273
Raleigh	0.619	0.849	0.333	0.38
Houston	0.708	0.947	0.422	0.481

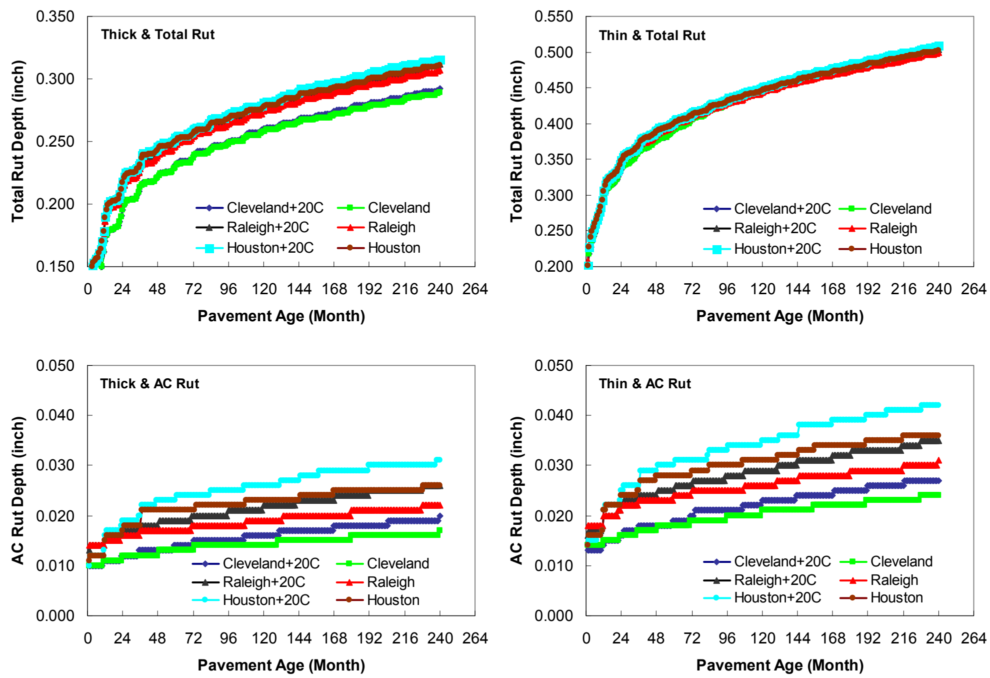

Figure 5.16. Effect of including 20°C data on predicted rut depth in thin and thick pavements in three temperature zones.

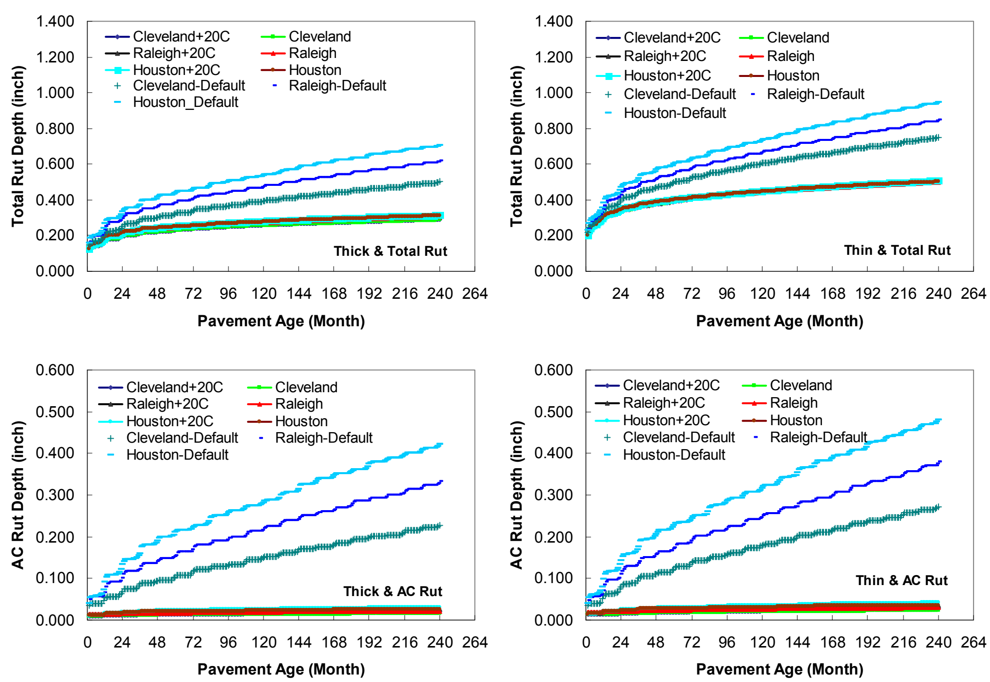

Figure 5.17. Effect of using the national default rutting *k* values compared to NCSU lab-generated *k* values on rutting predicted by the MEPDG.

Table 5.8 and Figure 5.17 both suggest that for any pavement type/location combination, the contribution of the asphalt layer to the total rut depth is small. This observation is not the case when the MEPDG default *k* values are used. Table 5.9 suggests that the average contribution of asphalt layer rutting to total rutting is about 50 percent. In other words, when the default *k* values are used, almost half of the total predicted rut depth comes from the asphalt layer. This observation is rational because of the field-to-lab conversion factor that is included in the national default *k* values, as mentioned earlier. This observation emphasizes the importance of the local calibration process in bridging the gap between lab predictions and field measurements. It is vital to remember that all the material-specific rutting *k* values presented so far are lab-based and do not include any calibration factors.

When looking at the differences in predicted rut depths that occur as a result of including or excluding the 20°C TRLPD test data, close attention should be given to the absolute differences in predicted rut depth as well as the percentages of difference. In this example, the absolute differences, as suggested by Table 5.8, are small (the maximum difference is 0.007 inch), indicating a difference that can be ignored. However, the percentages of difference might indicate the expected differences in rut depths if large rut depths are predicted for different structures and environments.

Based on the presented results of *Study 1*, the research team determined that it is acceptable to include the 20°C data in developing the rutting model material-specific *k* values for local mixtures. However, before the decision was finalized, the research team decided to conduct a final study to compare the effect of including 20°C data on the ranking of the local mixtures based on predicted permanent strain and lab-measured permanent strain.

5.7.4.3 Study 2: Evaluation of the Effects of including 20°C Data on Mixture Rankings

The goal of *Study 2* is to help the research team decide whether the 20°C TRLPD test data should or should not be included in characterizing the rutting model *k* values for each of the 12 most commonly used asphalt concrete mixtures in North Carolina. This study uses the ranking of each of these mixtures, which is based on the permanent strain (ε_p) and permanent-to-resilient strain ratio ($\varepsilon_p/\varepsilon_r$) at the end of 12,000 cycles, in addition to the actual measured strains, as the basis of comparison. Two sets of rutting model *k* values for each of 12 mixtures were determined. The first set was determined through considering only 40°C and 54°C TRLPD test data, whereas the second set of *k* values was determined considering 20°C, 40°C, and 54°C data.

For each of the 12 mixtures, there is a single lab-measured permanent strain and permanent-to-resilient strain ratio at the end of 12,000 cycles, and 2 predicted permanent strains and permanent-to-resilient strain ratios, one for each set of *k* values, also at the end of the 12,000 cycles. To decide whether to include or exclude the 20°C data in characterizing the rutting *k* values for each of the mixtures, the research team developed two criteria. The first criterion concerns the selection of the *k* value set that results in a ranking that is closest to that observed based for the measured data. The second criterion considers the actual predicted permanent strain values and permanent-to-resilient strain ratios and selects the *k* value set associated with the smaller percentages of difference between the predicted and measured permanent strain values and permanent-to-resilient strain ratios.

Table 5.10 shows the rankings of the 12 mixtures based on the three methods of calculating the permanent strain at each test temperature, 20°C, 40°C, and 54°C. The three methods are: (1) measured, (2) predicted, excluding the 20°C data, and (3) predicted, including 20°C data.

Table 5.10. Effect of 20°C TRLPD Test Data on Mixture Ranking Based on Predicted Permanent Strain (ε_p)

(ε_p) Values Measured at 20°C							
Measured		Predicted w/o 20°C		Ranking agree w/ measured?	Predicted w/ 20°C		Ranking agree w/ measured?
RI19.0C	0.00030	RB25.0B	0.0004	No	RI19.0C	0.0003	Yes
RS12.5C	0.00034	RI19.0B	0.0004	No	RS12.5C	0.0003	Yes
RS9.5B	0.00043	RI19.0C	0.0004	No	RS9.5B	0.0004	Yes
RS9.5C	0.00048	RS9.5B	0.0006	No	RS9.5C	0.0005	Yes
I19.0C	0.00049	RS9.5C	0.0006	No	RB25.0B	0.0005	No
RB25.0B	0.00050	I19.0C	0.0006	No	I19.0C	0.0005	No
RI19.0B	0.00065	S9.5C	0.0007	No	RI19.0B	0.0006	Yes
B25.0B	0.00077	S12.5C	0.0008	No	B25.0B	0.0007	Yes
S12.5C	0.00087	B25.0B	0.0009	No	S9.5C	0.0008	No
S9.5C	0.00097	RS12.5C	0.0011	No	S12.5C	0.0008	No
S9.5B	0.00126	S9.5B	0.0012	Yes	S9.5B	0.0012	Yes
I19.0B	0.00176	I19.0B	0.0018	Yes	I19.0B	0.0017	Yes
(ε_p) Values Measured at 40°C							
RS12.5C	0.00215	RS12.5C	0.0021	Yes	RS12.5C	0.0017	Yes
RB25.0B	0.00243	RB25.0B	0.0024	Yes	RB25.0B	0.0026	Yes
RI19.0C	0.00305	RI19.0C	0.0030	Yes	RI19.0C	0.0028	Yes
RS9.5B	0.00317	RS9.5B	0.0032	Yes	RS9.5B	0.0030	Yes
RI19.0B	0.00320	RI19.0B	0.0032	Yes	RI19.0B	0.0036	Yes
S9.5C	0.00387	S9.5C	0.0039	Yes	S9.5C	0.0039	Yes
RS9.5C	0.00478	RS9.5C	0.0048	Yes	RS9.5C	0.0046	Yes
S12.5C	0.00493	S12.5C	0.0049	Yes	I19.0C	0.0049	No
I19.0C	0.00515	I19.0C	0.0051	Yes	S12.5C	0.0051	No
B25.0B	0.00621	B25.0B	0.0062	Yes	B25.0B	0.0061	Yes
S9.5B	0.00835	S9.5B	0.0084	Yes	S9.5B	0.0084	Yes
I19.0B	0.00906	I19.0B	0.0090	Yes	I19.0B	0.0091	Yes
(ε_p) Values Measured at 54°C							
RS12.5C	0.00406	RS12.5C	0.0041	Yes	RS12.5C	0.0050	Yes
RB25.0B	0.00761	RB25.0B	0.0077	Yes	RI19.0B	0.0074	No
RI19.0B	0.00778	RI19.0B	0.0078	Yes	RB25.0B	0.0075	No
S9.5C	0.00782	RS9.5B	0.0078	No	S9.5C	0.0080	Yes
RI19.0C	0.00782	S9.5C	0.0079	No	RS9.5B	0.0084	No
RS9.5B	0.00785	RI19.0C	0.0079	No	RI19.0C	0.0085	No
RS9.5C	0.00830	RS9.5C	0.0083	Yes	RS9.5C	0.0088	Yes
S12.5C	0.00904	S12.5C	0.0091	Yes	S12.5C	0.0093	Yes
I19.0C	0.00966	I19.0C	0.0097	Yes	I19.0C	0.0101	Yes
B25.0B	0.01097	B25.0B	0.0110	Yes	B25.0B	0.0116	Yes
I19.0B	0.01555	I19.0B	0.0156	Yes	I19.0B	0.0160	Yes
S9.5B	0.01875	S9.5B	0.0191	Yes	S9.5B	0.0195	Yes

Table 5.11 shows the rankings based on permanent-to-resilient strain ratios at 20°C, 40°C, and 54°C following the same aforementioned three methods.

Table 5.11. Effect of 20°C TRLPD Test Data on Mixture Ranking Based on Predicted Permanent-to-Resilient Strain Ratios ($\varepsilon_p/\varepsilon_r$)

Measured		Predicted w/o 20°C		Ranking agree w/ measured?	Predicted w/ 20°C		Ranking agree w/ measured?
($\varepsilon_p/\varepsilon_r$) Values Measured at 20°C							
RI19.0C	5.50884	RI19.0B	5.6204	No	RI19.0C	5.5465	Yes
RS9.5B	6.24566	RB25.0B	5.7292	No	RS9.5C	6.1093	No
RS9.5C	6.25838	RI19.0C	8.1273	No	RS9.5B	6.3256	No
RS12.5C	6.62287	S9.5C	8.2651	No	RS12.5C	6.8522	Yes
I19.0C	7.38361	RS9.5C	8.3307	No	I19.0C	7.3975	Yes
RB25.0B	8.13010	RS9.5B	8.7702	No	RB25.0B	7.6879	Yes
B25.0B	9.76319	I19.0C	9.8146	No	S9.5C	8.3743	No
RI19.0B	10.28791	S12.5C	10.0086	No	B25.0B	9.3458	No
S9.5C	10.85754	B25.0B	10.9323	No	RI19.0B	9.6325	No
S12.5C	11.29710	S9.5B	12.7982	No	S12.5C	10.7441	Yes
S9.5B	12.93160	I19.0B	20.6323	No	S9.5B	12.4888	Yes
I19.0B	20.42983	RS12.5C	21.1060	No	I19.0B	19.8161	Yes
($\varepsilon_p/\varepsilon_r$) Values Measured at 40°C							
RS9.5B	9.07481	RI19.0B	9.0845	No	RS12.5C	8.0732	No
RI19.0B	9.10331	RS9.5B	9.0942	No	RS9.5B	8.4601	No
RS9.5C	9.38163	RS9.5C	9.3346	Yes	RS9.5C	8.9894	Yes
RB25.0B	9.60498	RB25.0B	9.5104	Yes	S9.5C	9.7530	No
S9.5C	9.60678	S9.5C	9.6239	Yes	RI19.0C	9.9411	No
RS12.5C	10.34256	RS12.5C	10.2043	Yes	RI19.0B	10.2553	No
RI19.0C	10.90906	RI19.0C	10.7959	Yes	RB25.0B	10.3262	No
I19.0C	11.02857	I19.0C	11.0185	Yes	I19.0C	10.4982	Yes
S12.5C	11.16347	S12.5C	11.1432	Yes	S12.5C	11.5562	Yes
B25.0B	13.11848	B25.0B	13.0866	Yes	B25.0B	12.8876	Yes
S9.5B	17.68184	S9.5B	17.7746	Yes	S9.5B	17.8892	Yes
I19.0B	21.44764	I19.0B	21.3563	Yes	I19.0B	21.4616	Yes
($\varepsilon_p/\varepsilon_r$) Values Measured at 54°C							
RS12.5C	7.10886	RS12.5C	7.1877	Yes	RS12.5C	8.7374	Yes
RS9.5B	9.29147	RS9.5B	9.2805	Yes	RS9.5B	9.9533	Yes
RS9.5C	9.64921	RS9.5C	9.7070	Yes	RS9.5C	10.2662	Yes
S9.5C	10.13396	S9.5C	10.2546	Yes	S9.5C	10.3922	Yes
RI19.0B	11.05930	RI19.0B	11.0744	Yes	RI19.0B	10.5237	Yes
I19.0C	11.51091	I19.0C	11.5434	Yes	S12.5C	11.9455	No
S12.5C	11.66838	S12.5C	11.7011	Yes	RB25.0B	11.9991	No
RB25.0B	12.17426	RB25.0B	12.3084	Yes	I19.0C	12.0854	No
RI19.0C	12.23793	RI19.0C	12.4391	Yes	RI19.0C	13.3010	Yes
B25.0B	14.16586	B25.0B	14.2168	Yes	B25.0B	14.9433	Yes
S9.5B	20.10812	S9.5B	20.4650	Yes	S9.5B	20.8719	Yes
I19.0B	21.56727	I19.0B	21.6753	Yes	I19.0B	22.2103	Yes

Table 5.10 and Table 5.11 show that at 20°C the rankings obtained by using the *k* value set that considers the 20°C data are in agreement with the rankings of the measured data at 20°C. This finding is true for both permanent strain and the permanent-to-resilient strain ratio.

Table 5.10 suggests that at 40°C both *k* value sets lead to rankings that are in agreement with the measured values, with the exception of two mixtures (S12.5C and I19C) that were switched in their rankings when the *k* value set that considers 20°C data was used. Looking at the predicted strain values for these two mixtures, however, it can be noticed that both mixtures end up with permanent strain values that are very close to each other: 0.0049 versus 0.0051 for the S12.5C and I19C mixtures, respectively. As for the permanent-to-resilient strain ratio, Table 5.11 suggests that both predicted measurements show some ranking disagreement when compared with the measured rankings; however, there are six mixtures whose predictions were based on the inclusion of the 20°C data that did not agree in ranking with the measured data compared to only two mixtures from the group that excluded the 20°C data.

Table 5.10 shows that at 54°C both *k* value sets result in some disagreement with the rankings that are based on the measured permanent strain. Again, looking more closely at the actual strain values, the ranking disagreement can be ignored. As for the permanent-to-resilient strain ratio, Table 5.11 suggests that including the 20°C data actually has caused three of the mixtures to disagree with the rankings of the measured data. However, the differences in predicted permanent-to-resilient strain values at the end of the 12,000 cycles are small, and the disagreement once again can be ignored.

Figure 5.18 was constructed to observe any trend changes between the measured and predicted permanent strains as well as between the measured and predicted permanent-to-resilient strain ratios. Figure 5.18 shows that, in general, predictions obtained using *k* values that include the 20°C data in their development are close to trends of the measured data mainly at 20°C. The arrows in Figure 5.18 indicate mixtures that are observed to deviate from the trend of the measured data. In general, Figure 5.18 suggests that including 20°C data produces more uniform and stable trends across the range of all three test temperatures, as compared to excluding the 20°C data that leads to unstable trends, especially at 20°C.

As mentioned earlier, the second criterion considers the actual predicted strain values and selects the *k* value set associated with the smaller percentage of difference between the predicted and measured permanent strain and permanent-to-resilient strain ratios. For each of the mixtures, Table 5.12 summarizes the percentages of difference between the measured strains and strains predicted using the two different sets of *k* values, the one that includes the 20°C data and the one that excludes them.

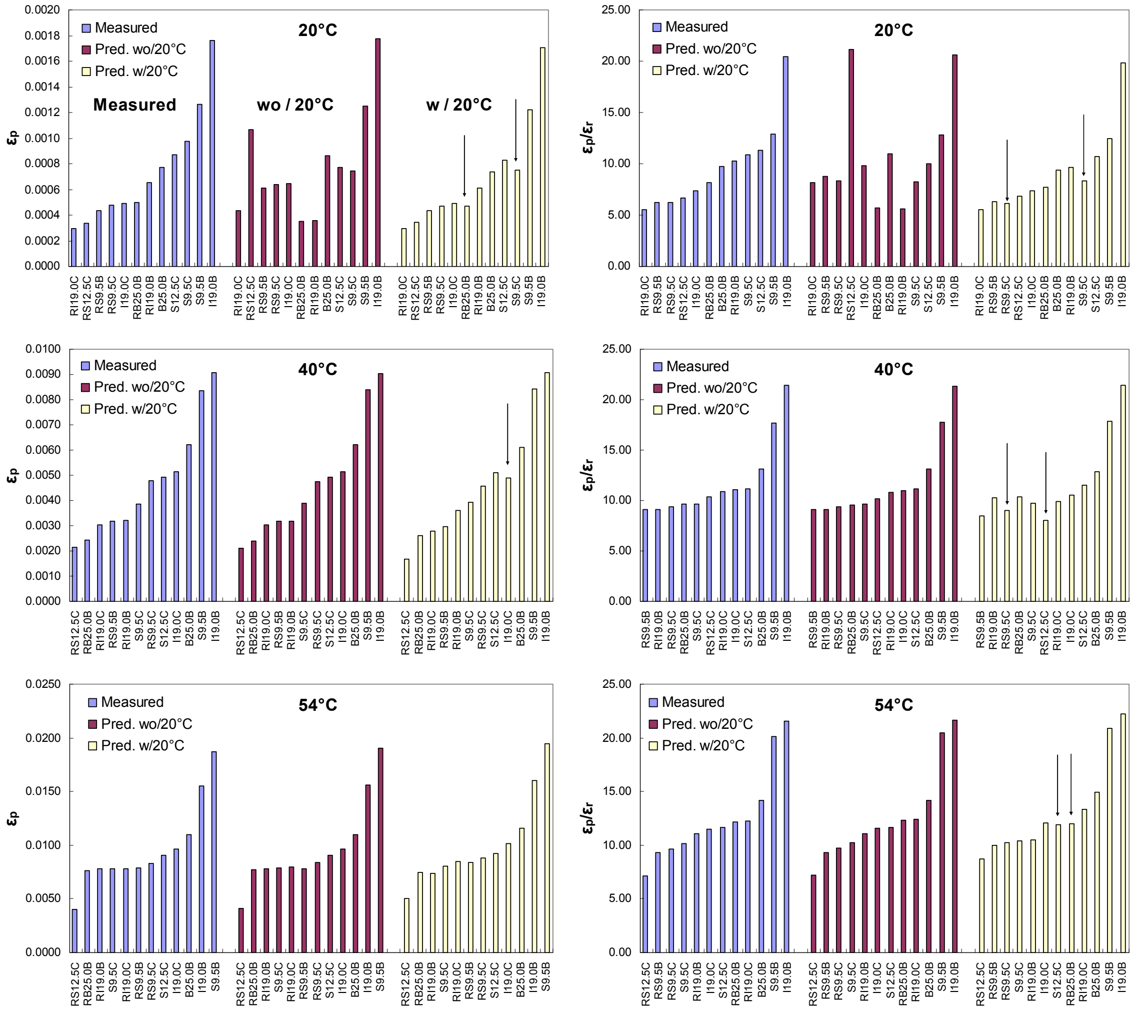

Figure 5.18. Effect of 20°C TRLPD test data on predicted permanent strain values (ε_p) and permanent-to-resilient strain ratios ($\varepsilon_p/\varepsilon_r$) compared to the measured values.

Table 5.12 shows that at 20°C, strain predictions that consider the 20°C TRLPD test data are much closer to the measured strain values with an average percentage of difference of 4.9% versus an average percentage of difference of 41.4% for predictions that do not consider the 20°C data. This result is expected because the consideration of a wide temperature range improves the predictions at a wide temperature range.

Table 5.12 shows that at 40°C and 54°C the percentages of difference between the measured and predicted strains, when 20°C TRLPD test data are not considered, are slightly smaller than those between the measured and predicted strains when 20°C TRLPD test data are considered: 0.5% and 0.8% (excluding 20°C data) versus 6.2% and 6.1% (including 20°C data) at 40°C and 54°C, respectively. However, the maximum difference of 6.2% between the predicted and lab-measured strains is considered by the research team to be acceptable.

Table 5.12. Effect of 20°C TRLPD Test Data on Percent Difference Between Measured and Predicted Permanent Strain (ε_p) and Permanent-to-Resilient Strain Ratios ($\varepsilon_p/\varepsilon_r$)

ε_p and $\varepsilon_p/\varepsilon_r$ % Difference (Meas.- Pred.)						
Mix Type	20°C		40°C		54°C	
	w/o 20°C	w/ 20°C	w/o 20°C	w/ 20°C	w/o 20°C	w/ 20°C
S9.5B	1.0	3.4	0.5	1.2	1.8	3.8
S9.5C	23.9	22.9	0.2	1.5	1.2	2.5
RS9.5C	33.1	2.4	0.5	4.2	0.6	6.4
S12.5C	11.4	4.9	0.2	3.5	0.3	2.4
I19.0B	1.0	3.0	0.4	0.1	0.5	3.0
RI19.0B	45.4	6.4	0.2	12.7	0.1	4.8
B25.0B	12.0	4.3	0.2	1.8	0.4	5.5
RB25.0B	29.5	5.4	1.0	7.5	1.1	1.4
RS9.5B	40.4	1.3	0.2	6.8	0.1	7.1
RS12.5C	218.7	3.5	1.3	21.9	1.1	22.9
I19.0C	32.9	0.2	0.1	4.8	0.3	5.0
RI19.0C	47.5	0.7	1.0	8.9	1.6	8.7
Average	41.4	4.9	0.5	6.2	0.8	6.1
Std. Dev.	58.1	6.0	0.4	6.2	0.6	5.7

At this point, it is clear that including the 20°C TRLPD test data for characterizing the rutting model coefficients for different mixtures leads to slightly better predictions at 40°C and 54°C. At 20°C, however, including the 20°C TRLPD test data improves the predictions considerably. So, based on the recommendation of the NCHRP 9-30A research team to consider the 20°C data, and based on the results of the work that was performed at ASU and presented in Section 5.7.4.1 and the two studies reported in Sections 5.7.4.2 and 5.7.4.3, the research team decided to include the 20°C TRLPD test data in developing the coefficients of the rutting model currently embedded in the MEPDG for each of the 12 most commonly used asphalt mixtures in North Carolina. The next Subsection 5.7.5 summarizes the coefficients that have been developed and that are recommended by the research team for each of the 12 mixtures.

5.7.5 Rutting Model Coefficients for Each of the 12 Most Commonly Used Mixtures in North Carolina

Table 5.13 summarizes the final rutting model coefficients for each of the 12 most commonly used mixtures in North Carolina.

The coefficients in Table 5.13 replace the national default *k* values currently embedded in MEPDG Version 1.1. To recapitulate, the coefficients in Table 5.13 were determined by considering the TRLPD test data at all three temperatures, i.e. 20°C, 40°C, and 54°C and by using Microsoft Excel Solver optimization routine to minimize the Log (SSE), as discussed in Section 5.7.3.

Table 5.13. Summary of the Rutting Model Material-Specific *k* Values for the MEPDG

Mix ID	k'_{r1}	k'_{r2}	k'_{r3}
S9.5B	-1.2478	0.7555	0.2375
RS9.5B	-1.1407	0.6839	0.1698
S9.5C	-0.5822	0.3304	0.2208
RS9.5C	-1.4252	0.7972	0.1849
S12.5C	-0.1356	0.1610	0.2138
RS12.5C	-0.8830	0.3910	0.2447
I19B	0.1150	0.1787	0.2093
RI19B	-0.1676	0.1336	0.2225
I19C	-1.1219	0.7279	0.1626
RI19C	-2.5412	1.3269	0.2104
B25B	-1.3474	0.7350	0.2378
RB25B	-1.5201	0.7123	0.2678

Since none of the “D” mixes were characterized in this research, the research team recommends that “D” mixes should be treated as “C” mixes in pavement design. For example, S9.5D mix can use the same material-specific *k* values that are recommended for S9.5C mix. This recommendation is based on the fact that “D” mixes were treated as “C” mixes in all the calibration work presented in. In other words, the differences between the performance of “D” and “C” mixes are smeared in the calibration factors. Similarly, some of the “C” mixes that were not characterized in this research, e.g., B25.0C mix, can use the specific *k* values of the B25.0B mix for the same aforementioned reason. For mixtures that are not included among the 12 most commonly used mixtures characterized in this research work, readers can refer to Table 8.3.

CHAPTER 6 FATIGUE CRACKING CHARACTERIZATION

6.1 Introduction

Fatigue cracking is a form of distress that can take either a pattern that resembles alligator skin covering part or most of the roadway, or a pattern that resembles longitudinal cracks in the traffic direction, mostly in the wheel path. Two types of fatigue cracking generally are recognized: bottom-up cracking (or so-called alligator cracking) and top-down cracking (or so-called longitudinal cracking).

Alligator cracks are caused mainly by tensile strains induced by truck wheel loads at the bottom of the asphalt bound layers. Alligator cracks initiate at the bottom of the asphalt layer and propagate their way up to the pavement surface to appear as multiple, short, longitudinal or transverse cracks in the wheel path. However, with continued truck traffic loadings, these cracks become interconnected, thus forming an alligator pattern. In the MEPDG, the amount of alligator cracking is calculated as a percentage of the total lane area (NCHRP 2009).

Longitudinal cracks, on the other hand, initiate at the surface of the pavement and propagate downward. Longitudinal cracks have three primary causes. The first cause is truck wheel loads with high tire pressure, which creates tension, torsion, and shear stresses at the surface of the pavement. The second cause is related to thermal loading. Daily and seasonal temperature variations, which tend to be extreme at the surface, cause tensile stress at the surface that can trigger the initiation of longitudinal cracks. The third cause of longitudinal cracks is aging. Over time, the asphalt binder component of the HMA ages, causing the asphalt mixture to lose its elasticity and become stiff. Stiff mixtures are prone to cracking. When they first appear, longitudinal cracks might look similar to alligator cracks, and it is difficult to distinguish between the two types of cracking. Longitudinal cracks, however, develop and become connected longitudinally with increased truck traffic loading. In the MEPDG, longitudinal cracks are calculated in terms of feet per mile. Figure 6.1 shows images of both types of cracks.

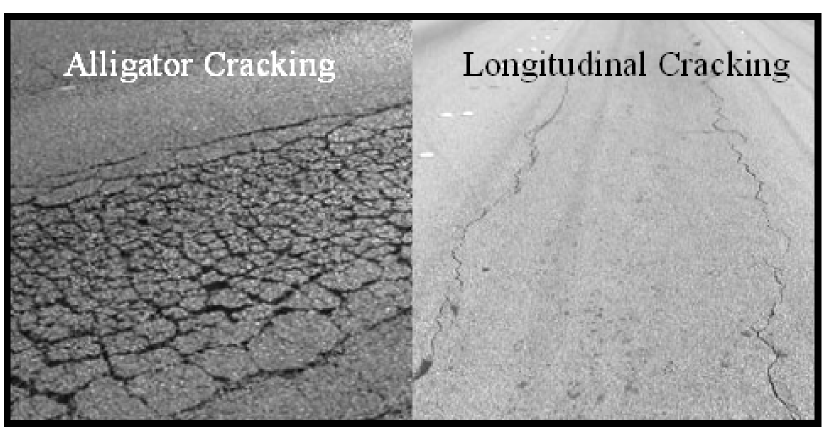

Figure 6.1. Real images of alligator cracking and longitudinal cracking.

The propagation of fatigue cracks throughout the asphalt layer eventually allows water to enter the unbound layer and causes deterioration of the pavement structure and its serviceability. Thus, an accurate description and prediction of fatigue resistance for HMA is extremely important to flexible pavement design and preservation.

Fatigue performance modeling is one the major topics in asphalt concrete modeling work. Currently, the only standard fatigue test available for asphalt concrete mixtures is the flexural bending fatigue test, AASHTO T-321. Several problems are associated with flexural fatigue testing, the most important of which is that the stress state is not uniform but varies over the depth of the specimen. In addition, equipment for fabricating beam specimens is not widely available. Viscoelastic continuum damage (VECD) fatigue testing is a promising alternative to flexural fatigue testing. Several researchers have successfully applied the VECD model to asphalt concrete mixtures using the constant crosshead rate direct tension test. However, due to the load level limitations of the new AMPT equipment, an immediate need has arisen to develop a model that can characterize fatigue performance quickly using cyclic test data. In this study, a simplified VECD (S-VECD) model developed at NCSU is applied to the 12 most commonly used asphalt concrete mixtures in North Carolina. It is shown that the simplified VECD model can predict fatigue tests accurately under various temperature conditions and strain levels. It is also shown that the model can be utilized to simulate both the strain-controlled direct tension fatigue test and the traditional beam fatigue test. In this report, simulation results are presented. Conclusions regarding the applicability of the new model are advanced as well as suggestions for further work. The subsequent sections discuss in detail available simulation fatigue test methods in addition to the available fatigue cracking performance prediction models.

6.2 Fatigue Tests and Fatigue Models for Asphalt Concrete

In order to simulate the fatigue performance of asphalt concrete in the field, several scientists and researchers have developed various laboratory fatigue tests and models. In this Section 6.2, two major fatigue test methods are discussed: the flexural bending test and the direct tension test.

6.2.1 Flexural Bending Test

The most commonly used flexural bending test is the standard beam fatigue test that measures the fatigue life of a compacted asphalt beam subjected to repeated flexural bending. The standard procedure for the beam fatigue test is described in the AASHTO T-321 standard and was adopted by researchers at the University of California Berkeley under the SHRP project (SHRP, 1994; Tayebali et al., 1995). The standard rectangular beam size used for the fatigue test is 380 mm long by 63 mm wide by 50 mm thick. The specimen dimensions and test configurations are illustrated in Figure 6.2.

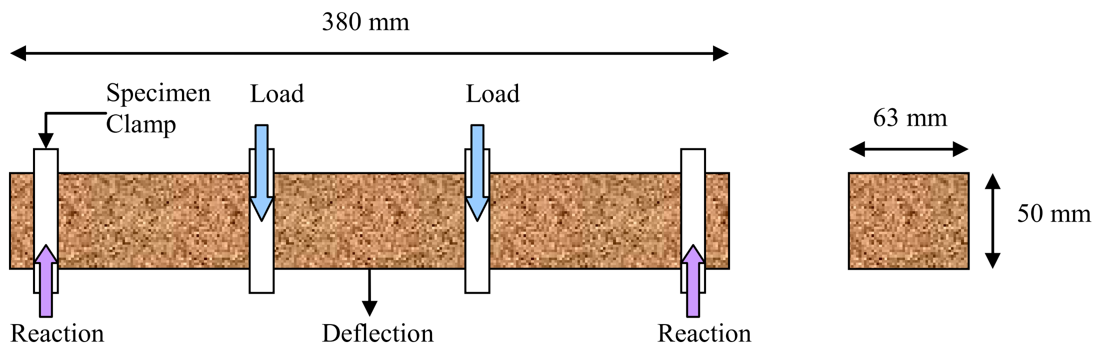

Figure 6.2. Beam fatigue test configuration and specimen dimensions.

To produce a uniformly distributed bending moment throughout the mid-span of the beam, loads are applied at two third points. During the test, the mid-span deflection, strain, and load are recorded at each cycle. A control and data acquisition system is used to adjust the load and to ensure that the test specimen undergoes a constant level of strain for each load cycle. The specimen stiffness at the 50th load cycle is used as an estimate of the initial stiffness, and the failure point is defined as the load cycle at which the specimen exhibits a 50% reduction in stiffness relative to the initial stiffness.

It has been accepted for many years that the fatigue performance of asphalt concrete mixtures can be characterized using either a strain-based method (Equation (6.1)) or stress-based method (Equation (6.2)).

$$N_f = k_1 \left(\frac{1}{\varepsilon_0} \right)^{k_2} \quad (6.1)$$

$$N_f = k_1 \left(\frac{1}{\sigma_0} \right)^{k_2} \quad (6.2)$$

where

N_f	=	number of cycles to failure;
ε_o, σ_o	=	initial strain and stress amplitudes, respectively; and
k_1, k_2	=	material constants.

Later, it was suggested by Monismith et al. (1985) to include the mixture stiffness term ($|E^*|$) in the equations so that the temperature effect can be taken into consideration, as shown in Equation (6.3). The k_1, k_2, and k_3 coefficients shown in Equation (6.3) are material constants. $|E^*|$ in Equation (6.3) should be measured at the temperature where the fatigue analysis is performed.

$$N_f = k_1 \left(\frac{1}{\varepsilon_0} \right)^{k_2} \left(|E^*| \right)^{k_3} \quad (6.3)$$

In the recently developed MEPDG, the mathematical model shown in Equation (6.3) was selected as an input to predict the fatigue performance of HMA, except that a laboratory-to-field adjustment factor was added in the MEPDG.

6.2.2 Simplified Fatigue Test Using the Viscoelastic Continuum Damage (VECD) Model

All the traditional fatigue tests, such as the beam fatigue test, are empirical in nature, which could introduce substantial errors when used in material performance prediction. Researchers and the asphalt industry are now moving toward mechanistic approaches that include rigorous theoretical considerations. The VECD model is a technique that makes use of materials' fundamental properties and helps develop a simplified laboratory test program.

The history of the VECD model begins with Kim and Little (1990), who first successfully applied Schapery's (1981) nonlinear viscoelastic constitutive theory for materials with distributed damage to sand asphalt under cyclic loading. Later, Lee and Kim (1998) developed the VECD model and proved that it can be applied to asphalt concrete under both controlled stress and controlled strain cyclic loading. The work of Daniel and Kim (2002) shows that damage in asphalt concrete is a material property and can be determined using a simplified procedure, such as the constant crosshead rate monotonic direct tension test. Later, Chehab et al. (2002, 2003) showed that the time-temperature superposition (t-TS) principle could be extended from a material's linear viscoelastic range to high damage levels, which helps reduce the required testing time significantly. The most recent work has been performed by Underwood (2006), who applied these principles to mixtures tested at the Federal Highway Administration Accelerated Load Facility (FHWA ALF) in McLean, VA. Underwood demonstrated the applicability of the modeling principles to both modified and unmodified asphalt concrete mixtures, and successfully predicted ALF mixture fatigue resistance rankings using the S-VECD model. The theoretical background for these test methods and models is discussed in detail in subsequent sections.

Despite the fact that the VECD model is much simpler than the traditional beam fatigue test for fatigue performance characterization, several shortcomings remain. One is that the characterization process requires constant rate tests, which are theoretically appropriate for the work potential theory formulation, but encompass certain practical constraints with regard to the load capacity requirements of the testing machine. This issue is particularly important because the capacity of the AMPT is nearly equal to the threshold value needed for constant rate testing. Thus, an immediate need has emerged to develop a model that not only is applicable to cyclic fatigue test data, but also allows quick and easy characterization using such tests.

Several researchers have worked to develop a simplified mechanistic model. Christensen and Bonaquist (2005) developed such a model based on the approach suggested by Kim et al. (2002) in which simplifications are made in the calculation of the pseudo strain and in the idealization of the input conditions. Kutay and Associates (2008) applied a form of the VECD model and showed that two different test protocols, controlled stress and controlled crosshead push-pull tests, yield the same damage characteristic relationship. Although these research efforts have shown positive results, they have certain faults that limit their applications. Underwood (2009) proposed a more rigorously accurate simplified model, which was able to correct the deficiencies in the other models. This model was developed to characterize asphalt concrete mixtures using cyclic fatigue testing.

The main advantages of using the S-VECD protocol for fatigue cracking evaluation are:

- The fatigue performance at different temperatures and different strain amplitudes can be determined from only a few cyclic tests;
- The test protocol can be performed in the AMPT; and
- The test specimens can be fabricated using the Superpave gyratory compactor.

The objective of this part of the research is to verify the S-VECD model by applying it to various types of asphalt concrete mixtures under various conditions and determine their model coefficients. In the latter part of this chapter, different applications of the simplified fatigue model are discussed and results of fatigue performance simulations are presented.

Figure 6.3 is a flow chart of the simplified fatigue test program with the help of the VECD model. The major advantages of this test program include: (1) a much shorter testing time than has been possible heretofore; (2) its ability to take into account numerous different conditions due to its theoretically-based nature; and (3) its ability to separate material properties from structural pavement response models, such as layered elastic analysis.

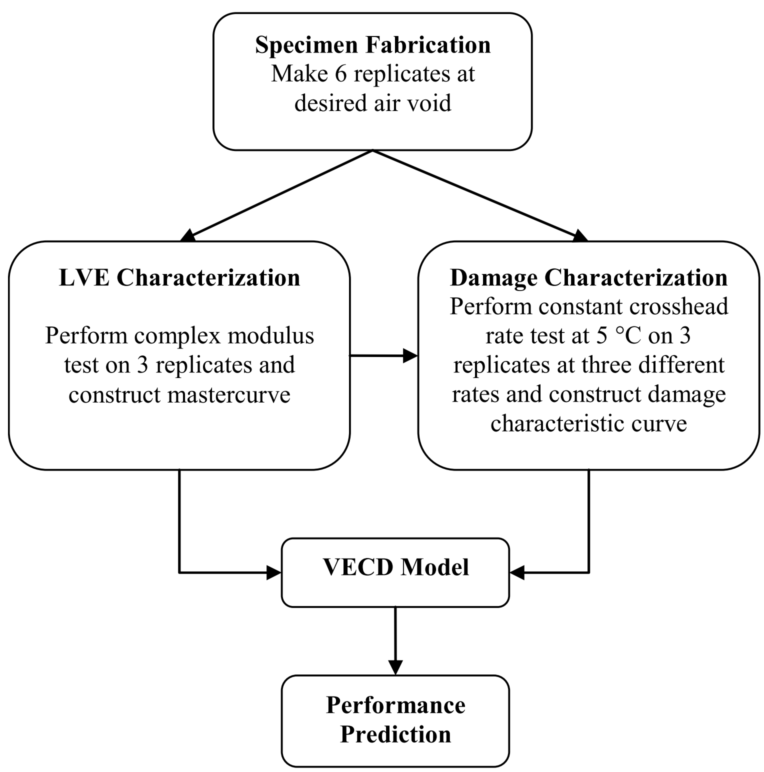

Figure 6.3. Flow chart of the simplified fatigue test program.

6.3 Theoretical Background

6.3.1 Linear Viscoelastic Theory

For linear elastic materials, the stress-strain relationship can be described simply using Hooke's Law; i.e., the stress and strain are linearly proportional to each other, and the materials' response is affected only by the current input. For viscoelastic materials, which exhibit time-dependent behavior, the response is affected not only by the current input, but also by the input history. For non-aging linear viscoelastic material, the stress-strain relationship can be expressed by the following two convolution integrals.

$$\sigma = \int_0^t E(t-\tau)\frac{d\varepsilon}{d\tau}d\tau \qquad (6.4)$$

$$\varepsilon = \int_0^t D(t-\tau)\frac{d\sigma}{d\tau}d\tau \qquad (6.5)$$

where

$E(t)$	=	relaxation modulus;
$D(t)$	=	creep compliance; and
t	=	integration variable.

6.3.2 Complex Modulus (E^*)

Besides the relaxation modulus ($E(t)$) and creep compliance ($D(t)$), the complex modulus (E^*) is another important parameter that can capture the linear viscoelastic behavior of asphalt concrete. The complex modulus is composed of two parts: the storage modulus (E') that represents the elastic portion, and the loss modulus (E'') that represents the viscous portion. In complex number notation, the complex modulus can be written in the form of Equation (6.6), and in the complex plane, it can be represented graphically as shown in Figure 6.4.

$$E^* = E' + iE'' \qquad (6.6)$$

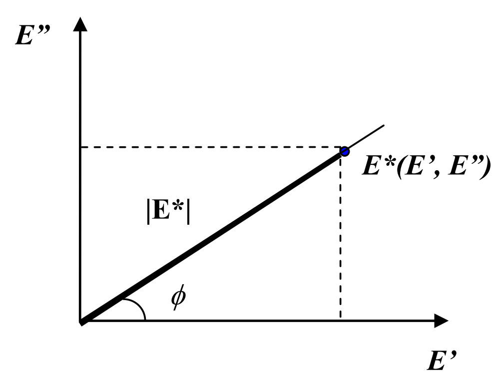

Figure 6.4. Graphical representation of the complex modulus in the complex plane.

6.3.3 Time-Temperature Superposition (t-TS) Principle

For viscoelastic material, such as asphalt concrete, stiffness is dependent on time (or rate of loading) and temperature. To capture the full range, stiffness tests need to be performed at multiple loading frequencies and temperatures. However, due to the limitations of machine capacity and testing time, such a task is difficult to accomplish. Applying the t-TS principle can help reduce the required testing time significantly.

According to the t-TS principle, the same stiffness value can be obtained either at low test temperatures and long loading times or at high test temperatures but short loading times. In other words, the time and temperature effects can be combined into a single parameter. This process can be undertaken by horizontally shifting the modulus values at different temperatures to a certain reference temperature, as shown in Figure 6.5. The shifted frequency is called *reduced frequency*, f_R, which can be obtained by multiplying the original frequency by a shift factor, as shown in Equation (6.7) and Equation (6.8). A single mastercurve can then be obtained, and it can be represented by a sigmoidal function, as shown in Equation (6.9). A typical dynamic modulus mastercurve and shift factor function curve are presented in Figure 6.6 and Figure 6.7, respectively. Any material for which a single mastercurve can be formed by such a shifting method is called *thermorheologically simple* (TRS) material.

$$f_R = f \times a_T \tag{6.7}$$

where

f = frequency in Hz; and
a_t = shift factor.

$$\log a_T = \alpha_1 T^2 + \alpha_2 T + \alpha_3 \tag{6.8}$$

where

a_1, a_2, a_3 = coefficients; and
T = temperature.

$$\log |E^*| = a + \frac{b}{1 + \dfrac{1}{e^{c+d*\log f_R}}} \tag{6.9}$$

where

$a, b, c,$ and d = coefficients; and
f_R = reduced frequency.

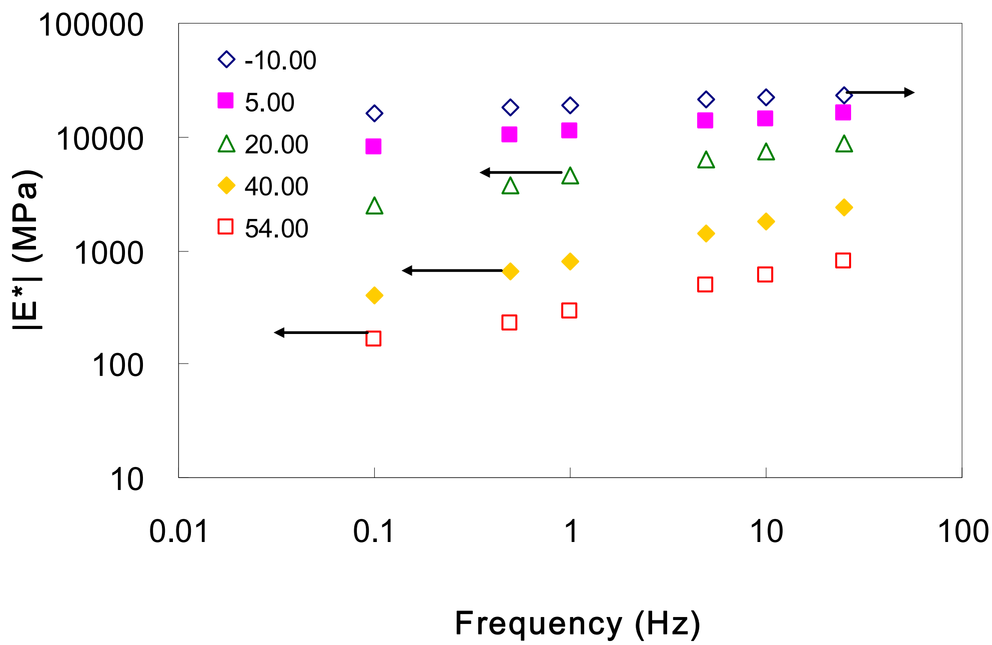

Figure 6.5. Horizontal shifting of the dynamic modulus (|E*|) value from different temperatures to the reference temperature (5°C).

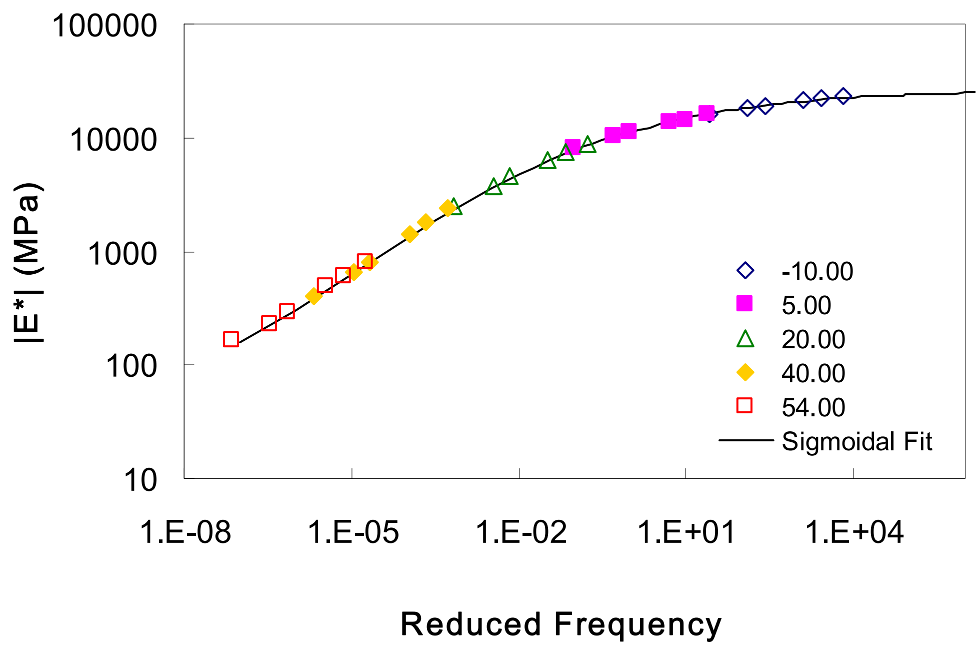

Figure 6.6. Typical example of a shifted dynamic modulus (|E*|) mastercurve.

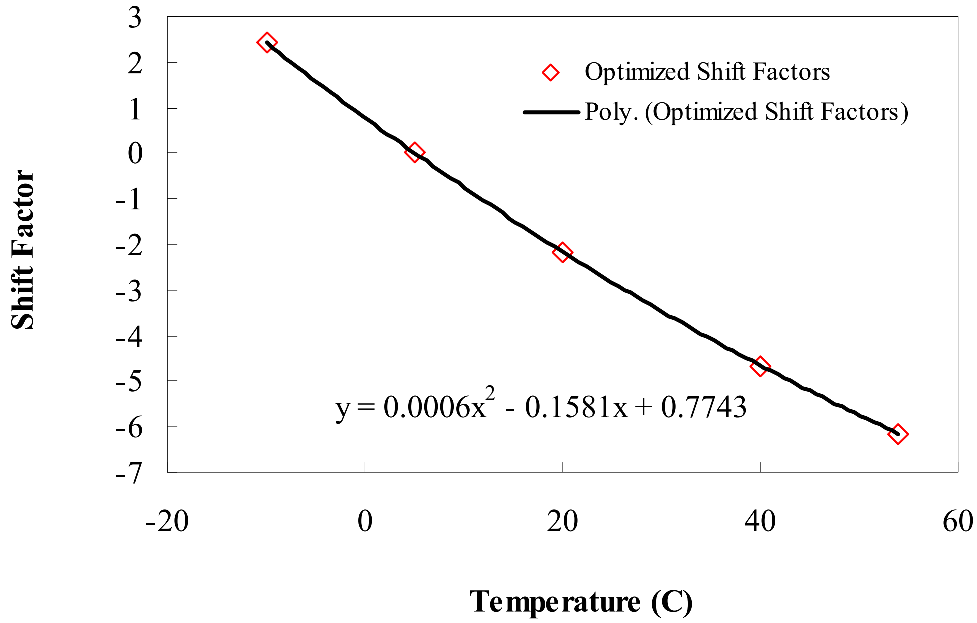

Figure 6.7. Example of time-temperature shift factor function.

6.3.4 Interconversion among Unit Response Functions

The relaxation modulus ($E(t)$), creep compliance ($D(t)$), and complex modulus (E^*) are all called *unit response functions*, as they are equivalent to the output due to a certain type of unit input. For example, the relaxation modulus is equivalent to the stress response due to a unit step strain input, and the creep compliance is equivalent to the strain response due to a unit step stress input. These two unit response functions are not easy to obtain experimentally in the time domain; however, they can be converted from the complex modulus in the frequency domain via linear viscoelastic theory. In this conversion process, the storage modulus (E') is first determined by Equation (6.10) and then expressed using Prony series representation in the angular frequency domain, as shown in Equation (6.11).

$$E' = |E^*| \cos\phi \qquad (6.10)$$

$$E'(\omega) = E_\infty + \sum_{i=1}^{m} \frac{\omega^2 \rho_i^2 E_i}{\omega^2 \rho_i^2 + 1} \qquad (6.11)$$

where

E = elastic modulus;
ω = angular frequency;
E_i = Prony coefficients; and
ρ_i = relaxation time.

Using experimentally obtained storage modulus values and the collocation method, the Prony coefficients (*Ei's*) can be determined. These coefficients are then used in Equation (6.12) to find the relaxation modulus.

$$E(t) = E_\infty + \sum_{i=1}^{m} E_i e^{-\frac{t}{\rho_i}} \qquad (6.12)$$

According to the theory of viscoelasticity, the exact relationship between the relaxation modulus and creep compliance is given in Equation (6.13).

$$\int_0^t E(t-\tau)\frac{dD(t)}{d\tau}d\tau = 1 \qquad (6.13)$$

Similar to the relaxation modulus, the creep compliance can also be written in Prony series form, as given in Equation (6.14).

$$D(t) = D_0 + \sum_{j=1}^{n} D_j\left(1 - e^{-\frac{t}{\tau_j}}\right) \qquad (6.14)$$

Substituting Equation (6.12) and Equation (6.14) into Equation (6.13), after simplification and rearrangement a linear algebraic term can be obtained, as shown in Equation (6.15).

$$[A]\{D\} = [B] \qquad (6.15)$$

where

$$[A] = \sum_{j=1}^{M}\left[\sum_{m=1}^{N}\frac{\rho_m E_m}{\rho_m - \tau_j}\left(e^{-\frac{t}{\rho_m}} - e^{-\frac{t}{\tau_j}}\right) + E_\infty\left(1 - e^{-\frac{t}{\tau_j}}\right)\right]$$

$\{D\} = D_j$; and

$$[B] = 1 - \frac{1}{E_\infty + \sum_{m=1}^{N} E_m}\left(E_\infty + \sum_{m=1}^{N} E_m e^{-\frac{t}{\rho_m}}\right)$$

This equation can then be solved, and the Prony coefficients can be determined to find the creep compliance.

6.3.5 Elastic-Viscoelastic Correspondence Principle

Schapery (1984) suggested that the constitutive equations for elastic media and viscoelastic media have identical forms, except that, for viscoelastic media, the stress and strain terms do not necessarily have any physical meaning. Instead, they are defined as pseudo variables in the form of convolution integrals. According to this correspondence principle, viscoelastic problems can be solved using elastic solutions when physical stress (or strain) is replaced by pseudo stress (strain). The formulation of pseudo strain is shown in Equation (6.16).

$$\varepsilon^R = \frac{1}{E_R}\int_0^t E(t-\tau)\frac{d\varepsilon}{d\tau}d\tau \quad (6.16)$$

where

ε^R	=	pseudo strain;
ε	=	actual strain;
E_R	=	reference modulus which is an arbitrary constant; and
$E(t)$	=	relaxation modulus.

Substitute Equation (6.16) into Equation (6.4) to obtain Equation (6.17).

$$\sigma = E_R\varepsilon^R \quad (6.17)$$

It is obvious that Equation (6.17) has a similar form as Hooke's Law for elastic media, and a correspondence can be found between the elastic and viscoelastic stress-strain constitutive relationships.

Moreover, a critical implication of pseudo strain is that it is equal to the corresponding stress when $E_R = 1$. In other words, the value of pseudo strain equals the stress response of linear viscoelastic material due to a certain strain input. This important property can be visualized clearly in the stress-pseudo strain plot for a monotonic tension test, as shown in Figure 6.8.

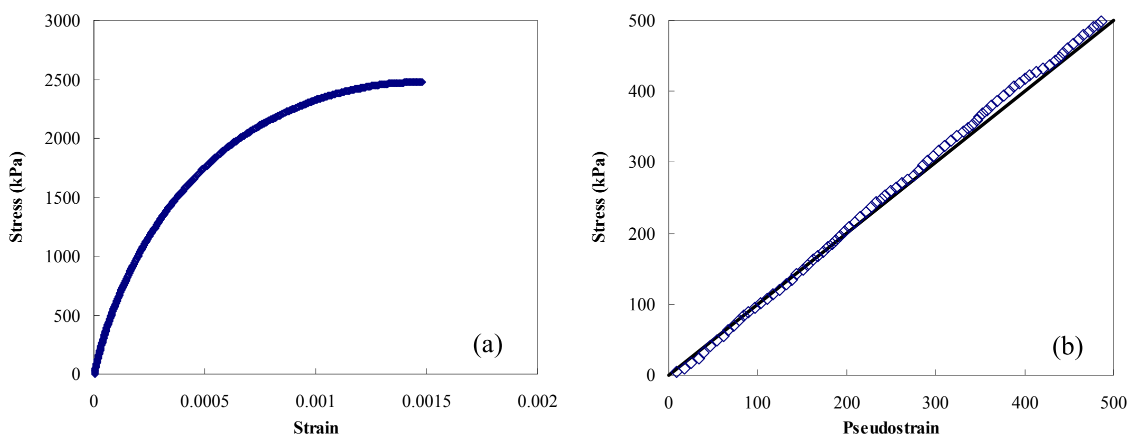

Figure 6.8. Typical test results from a constant crosshead rate tension test: (a) stress-strain plot; and (b) stress-pseudo strain plot.

6.3.6 Viscoelastic Continuum Damage Theory

Continuum damage theory ignores microscale behavior and characterizes materials using macroscale observations. The two essential parameters that continuum damage theory tries to quantify are effective stiffness and damage. The effective stiffness, which represents the material's structural integrity, can easily be assessed in the form of the instantaneous secant modulus; damage, on the other hand, is difficult to quantify and generally relies on rigorous theories. One of the theories is the work potential theory developed by Schapery (1990) for elastic materials with growing damage based on the thermodynamics of irreversible process. In Schapery's theory, damage is quantified by an internal state variable (ISV) that accounts for microstructural changes in the material. By using the correspondence principle described in Section 6.3.5, the work potential theory can then be extended to viscoelastic media. In summary, the VECD theory is composed of the following three basic equations.

1. Pseudo strain energy density function:

$$W^R = f(\varepsilon^R, S) \qquad (6.18)$$

2. Stress-pseudo strain relationship:

$$\sigma = \frac{\partial W^R}{\partial \varepsilon^R} \qquad (6.19)$$

3. Damage evolution law:

$$\frac{\partial S}{\partial t} = \left(-\frac{\partial W^R}{\partial S} \right)^{\alpha} \qquad (6.20)$$

where

W^R = pseudo strain energy density;
ε^R = pseudo strain;
S = damage parameter (internal state variable); and
a = damage evolution rate.

6.4 Experimental Program for Fatigue Characterization

6.4.1 Material

Detailed information regarding the aggregates and asphalt binders that were used in this study for fatigue specimen fabrication, in addition to mix verification results, can be found in Chapter 2 and Chapter 3 of this report.

6.4.2 Specimen Fabrication

All test specimens were compacted by a Superpave gyratory compactor (SGC) to a diameter of 150 mm and a height of 178 mm. To obtain homogeneous specimens and at the same time fulfill the representative volume element (RVE) requirement, all test samples were cored and cut to a diameter of 75 mm and a height of 150 mm for testing. Prior to testing, the air void ratio was determined for each specimen using the CoreLok method. As mentioned earlier, all test specimens used in this study have an air void content within the range of 5.5 ± 0.5%. To minimize the aging effect, specimens were sealed in plastic bags and stored carefully if they were not tested immediately after fabrication. No specimens were accepted for testing more than two weeks after they were cored and cut to avoid possible aging effects.

6.4.3 Test Set-Up

All test specimens were glued to metal plates at both ends using epoxy before they were set in the machine for testing. Four loose-core LVDTs were mounted around the specimen at intervals of 90 degrees, as shown in Figure 6.9. The gauge length is 100 mm. A MTS-810 closed-loop servo-hydraulic machine was used for all the tests. For complex modulus testing, a 2-kip load cell was used, and for controlled crosshead (CX) cyclic testing, a 5-kip load cell was used. The test temperature was maintained in an environmental chamber, together with liquid nitrogen and a feedback system. During the tests, the axial load, machine crosshead movement, and LVDT movement were recorded using a customized program with LabView software.

Figure 6.9. Test specimen inside the MTS-810 environmental chamber.

6.4.4 Test Methods

Two major types of tests were performed in this study: the complex modulus test and the CX cyclic test. Laboratory experiments were conducted according to the test protocols described in the coming section.

6.4.4.1 Complex Modulus Test

The tension-compression complex modulus tests were performed at five temperatures (-10°, 5°, 20°, 40°, and 54°C) and six frequencies (25, 10, 5, 1, 0.5, and 0.1 Hz). The testing order was from low to high temperatures and from high to low frequencies to minimize damage to the specimens. A five-minute rest period was allowed between every two adjacent frequencies, and at least two and half hours were allowed after the testing temperature was changed to achieve thermal equilibrium. The target strain level was within 50 to 70 microstrains. All tests were performed in stress-controlled mode according to AASHTO TP62-03. The complex modulus values were obtained from the final six cycles of each loading series, i.e., when the material reached a steady state. Figure 6.10 shows the stress and strain history plots in a typical complex modulus test.

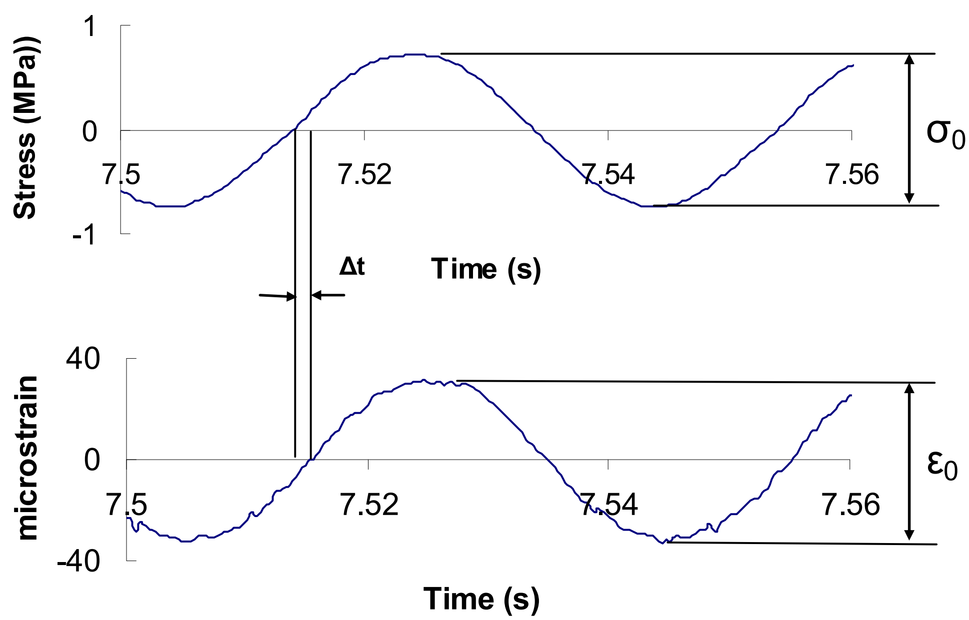

Figure 6.10. Stress and strain history plots in a typical tension-compression complex modulus test.

The dynamic modulus and phase angle were calculated using Equation (6.21) and Equation (6.22), respectively.

$$|E^*| = \frac{\sigma_0}{\varepsilon_0} \quad \text{......} \quad (6.21)$$

where

σ_o = steady state stress amplitude; and
ε_o = steady state strain amplitude.

$$\phi = \Delta t \cdot 2\pi f \quad (6.22)$$

where

f = testing frequency.

6.4.4.2 Controlled Crosshead (CX) Cyclic Test

Because a true controlled strain test using cylindrical specimens is difficult to run and can damage equipment if improperly performed, the CX cyclic test was used for fatigue performance characterization whereby the machine actuator's displacement was programmed to reach a constant peak level at each loading cycle. All the CX tests in this study were conducted at a constant frequency of 10 Hz. Due to machine compliance issues, the actual on-specimen strain was significantly less than the programmed level, as shown in Figure 6.11 (a). Even though the on-specimen strains remain tensile, both tensile and compressive stresses were applied on the specimen, with a decreasing mean stress, as shown in Figure 6.11 (b).

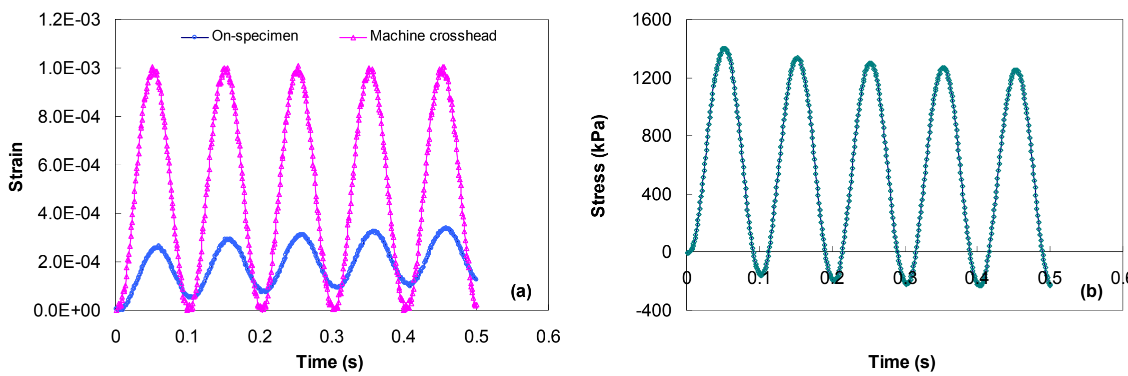

Figure 6.11. Strain and stress histories for first five cycles of a typical CX test.

This kind of test results in a mixed mode of loading that is neither controlled stress nor controlled strain. Christensen and Bonaquist (2005) proposed systems that allow users to perform true controlled strain testing of cylindrical specimens. However, these systems often do not allow the test to run to complete failure. In this study, the CX cyclic tests were performed to complete failure. The failure criterion is discussed in Section 6.4.5.

6.4.5 Failure Definition for Cyclic Testing

In CX cyclic testing, the dynamic modulus and phase angle are tracked throughout the entire fatigue life. The traditional fatigue analysis method defines *failure* as the point where the material's modulus drops to 50% of its initial value. However, this method is purely empirical, and a new approach suggested by Reese (1997) was used in this study whereby the cycle at which the phase angle shows a sharp decrease is defined as the number of cycles at failure (N_f). Figure 6.12 shows this failure definition from a typical CX cyclic test. This approach is strongly theoretically based, because it is believed that the drop in the phase angle is caused by macrocrack localization, which is normally caused by the coalescence of microcracks under repeated cycles of loading. When macrocracks develop, all the work input is concentrated at the crack tip, the remaining body relaxes, and therefore the time dependence of the global stress-strain behavior decreases. This reduction in time dependence causes the decrease in the phase angle.

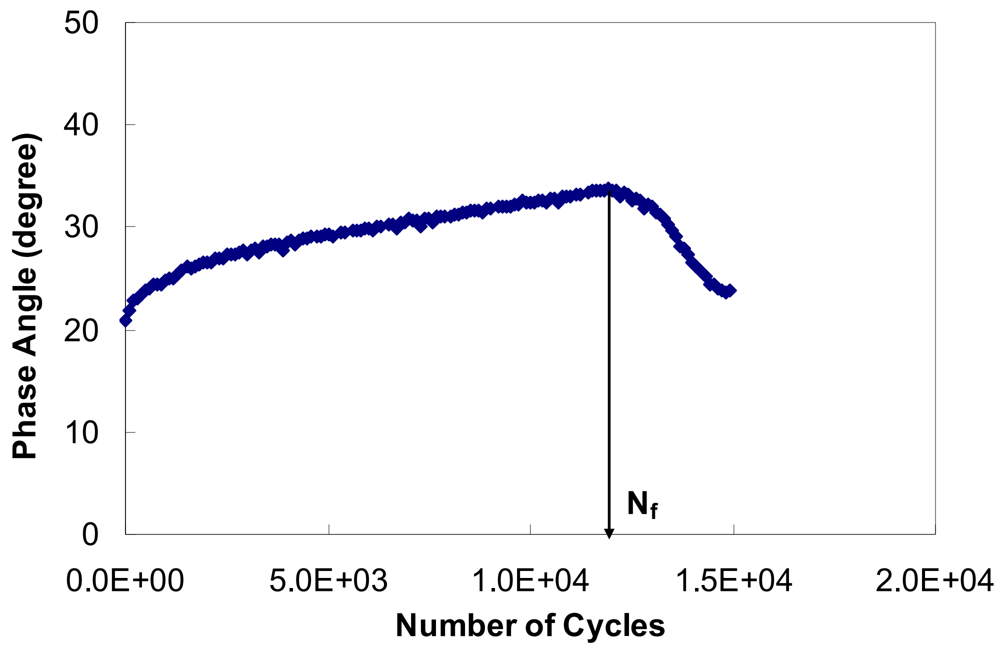

Figure 6.12. Fatigue life definition of a typical CX cyclic test indicating number of cycles to failure (N_f).

6.5 Simplified VECD Model

6.5.1 Rigorous Modeling Approach

In the rigorous VECD modeling approach, a material's effective stiffness is expressed as the secant modulus in the stress-pseudo strain plot, as shown in Equation (6.23).

$$C = \frac{\sigma}{\varepsilon^R} \qquad (6.23)$$

C is the pseudo stiffness, which is a function of damage (S). For the uniaxial mode of loading, the pseudo strain energy density function is given by Equation (6.24).

$$W^R = \frac{1}{2}(\varepsilon^R)^2 C \quad (6.24)$$

Because only C is a function of S in Equation (6.24), when it is substituted into Equation (6.20) the damage evolution law takes the form shown in Equation (6.25).

$$\frac{\partial S}{\partial t} = \left(-\frac{1}{2}(\varepsilon^R)^2 \frac{\partial C}{\partial S} \right)^{\alpha} \quad (6.25)$$

Several different methods have been used by researchers to solve the above damage evolution law. The chain rule method proposed by Lee and Kim (1998) is used throughout the work presented in this chapter. This method utilizes the chain rule shown in Equation (6.26) by substituting it into Equation (6.25).

$$\frac{dC}{dS} = \frac{dC}{dt}\frac{dt}{dS} \quad (6.26)$$

After simplification, the damage calculation from this rigorous modeling approach is given in Equation (6.27). Note that the time step term, Δt, is replaced by the reduced time interval, $\Delta\xi$, due to the verification of the t-TS principle with growing damage.

$$dS_i = \left(-\frac{1}{2}(\varepsilon^R)_i^2 \Delta C_i \right)^{\frac{\alpha}{1+\alpha}} \cdot (\Delta\xi)_i^{\frac{1}{1+\alpha}} \quad (6.27)$$

This model was applied successfully to constant crosshead rate monotonic test data. However, if this rigorous approach is applied to cyclic data, then it requires the pseudo strain, pseudo stiffness, and damage to be calculated and tracked for the entire loading history. An average test with 30,000 cycles to failure and 100 data points per cycle (to gain good cycle pulse definition and avoid computational irregularities) would then require the analysis of 3,000,000 data points. Although this task is possible using modern computers, it is cumbersome even when using advanced computational schemes. Further, experimental difficulties, such as data storage and electrical interference (noise and phase distortion), can lead to significant errors. One of the advantages of the simplified VECD model used in this work is that it alleviates these shortcomings.

6.5.2 Simplified Modeling Approach

The S-VECD model used in this research was developed by Underwood (2009). Before introducing this simplified modeling approach, a set of variables must be defined based on the schematic view of CX cyclic testing to distinguish those variables from those used in monotonic testing and the rigorous approach. These variables are summarized in Figure 6.13.

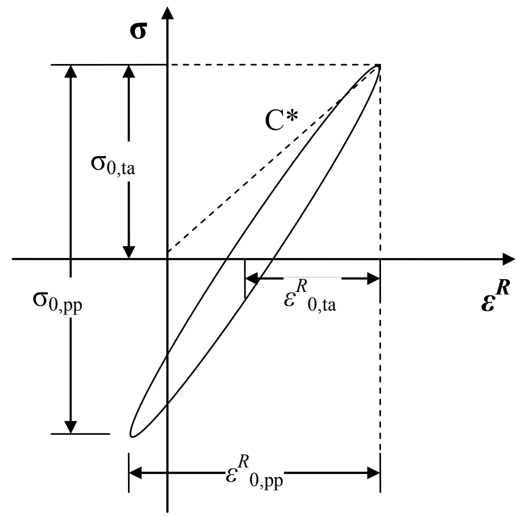

Figure 6.13. Schematic view of variables defined in the simplified VECD modeling approach for controlled crosshead cyclic testing.

Different from its role in the rigorous model, the pseudo stiffness term, C^*, as used in cyclic testing is a cyclic magnitude-based value that is equal to the ratio between tensile stress amplitude, $\sigma_{0,ta}$, and pseudo strain tension amplitude, $\varepsilon^{R}_{0,ta}$, for a given cycle, *i*. $\sigma_{0,pp}$ and $\varepsilon_{0,pp}$ stand for peak-to-peak stress and strain amplitude. These definitions will also affect the damage calculation, which is introduced later in this chapter.

6.5.2.1 Defining Alpha (α)

Based on theoretical arguments that employ the macrocracking phenomenon, the power, α, in the damage evolution law was found by Schapery (1990) to relate to linear viscoelastic time dependence. Motivated by earlier work on this subject (Lee and Kim, 1998a and b; Daniel and Kim, 2002; Chehab et al., 2003; and Underwood et al., 2006), in this study the maximum absolute value of the log-log slope of the relaxation modulus, m, is taken to represent the linear viscoelastic response. According to Schapery's theory, if the material's fracture energy and failure stress are constant, then $\alpha = 1 + 1/m$, but if the fracture process zone size and fracture energy are constant, then $\alpha = 1/m$. Although different researchers have used differing α values, the general suggestion of Lee and Kim (1998a and b), which is that it is most appropriate to use $\alpha = 1 + 1/m$ for the CX tests, was adopted in this research. This approach is supported by the work of Daniel and Kim (2002) that uses the constant failure stress and energy criteria for the CX tests.

6.5.2.2 Identification of Tensile Loading Time

Because crack growth is related strongly to tensile stress rather than compressive stress, it is critical to identify the actual time at which tensile loading starts and ends for a given cycle, as shown in Figure 6.14.

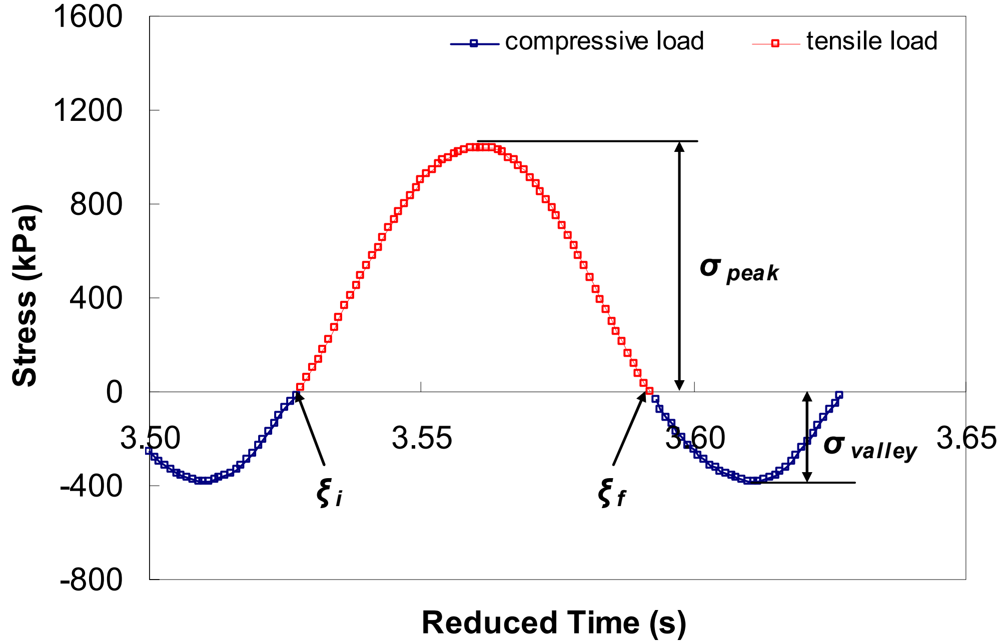

Figure 6.14. Loading history for a typical cycle during controlled crosshead (CX) cyclic testing.

In this research, the analytical function shown in Equation (6.28) is used to describe the stress history for any given cycle.

$$\frac{\sigma(t)}{\sigma_{0,ta}} = (\beta - \cos(\omega t))\frac{1}{\beta + 1} \qquad (6.28)$$

where

ω = angular frequency; and

$\beta_i = \dfrac{(\sigma_{peak})_i + (\sigma_{valley})_i}{|\sigma_{peak}|_i + |\sigma_{valley}|_i}$ for a given cycle *i*.

When $\beta = 1$, the entire stress history for that given cycle is tensile; when $\beta = 0$, half of the stress history is under tensile loading; and when $\beta = -1$, the entire stress history is compressive. As described earlier, in a general CX cyclic test, the β value starts from 1, then decreases and remains around 0 as the number of loading cycles increases.

From Equation (6.28), the starting time of tensile load, ξi, and the end time, ξf, can be found for any given cycle using Equation (6.29) and Equation (6.30).

$$\xi_i = \frac{\pi}{\omega} - \frac{\pi - \cos^{-1}(\beta)}{\omega} \qquad (6.29)$$

$$\xi_f = \frac{\pi}{\omega} + \frac{\pi - \cos^{-1}(\beta)}{\omega} \qquad (6.30)$$

6.5.2.3 Simplification and Adjustment Factor

The simplification process starts with the pseudo strain calculation. The rigorous approach solves the convolution integral, i.e., Equation (6.16), which provides an accurate calculation of the pseudo strain magnitude and tracks any permanent pseudo strain during the test. However, this is not a practical way to perform cyclic testing, which can easily have over 10 million data points. A simplified calculation method is given by Equation (6.31), which helps save a significant amount of computational time without introducing significant errors.

$$(\varepsilon_{0,ta}^R)_i = \frac{1}{E_R} \cdot \frac{\beta + 1}{2}((\varepsilon_{0,pp})_i \cdot |E^*|_{LVE}) \qquad (6.31)$$

The simplified approach used in this research assumes that Equation (6.32) can be used to simplify the more rigorous Equation (6.27) for damage calculation.

$$dS_i = \left(-\frac{1}{2}(\varepsilon_{0,ta}^R)_i^2 \Delta C_i^*\right)^{\frac{\alpha}{1+\alpha}} \cdot (\Delta\xi)_i^{\frac{1}{1+\alpha}} \cdot (K_1)^{\frac{1}{1+\alpha}} \qquad (6.32)$$

As compared with Equation (6.27), Equation (6.32) replaces pseudo strain, ε^R, with pseudo strain tension amplitude, $\varepsilon^R_{0,ta}$, replaces pseudo stiffness, C, with the cyclic-based value, C*, and replaces time step, $\Delta\xi$, with tensile loading time interval, ξi -ξf. This simplified model implicitly assumes that pseudo strain is some constant value within a cycle. This flaw was corrected by adding an adjustment factor, K_1, which is a rigorously defined parameter dependent on the time history of loading, $f(\xi)$, only. For the assumption that damage growth within an individual cycle is small, the factor, K_1, is given by Equation (6.33).

$$K_1 = \frac{1}{\xi_f - \xi_i} \int_{\xi_i}^{\xi_f} (f(\xi))^{2\alpha} d\xi \qquad (6.33)$$

where $f(\xi)$ is the loading history function, which has the same formulation as Equation (6.28).

6.5.2.4 Specimen-to-Specimen Variability

In all the previous VECD model characterization processes, the pseudo stiffness term is normalized for specimen-to-specimen variability by a factor, *I*, which is defined typically as the slope of the stress-pseudo strain curve for a stress level up to 500 kPa. In this study, the dynamic modulus ratio (DMR) is used for all the normalization processes instead of *I*.

It is found that the damage curves collapse better when using the DMR rather than *I* for all the mixtures included in this study; the graphical comparisons can be found in Appendix E.

To define the DMR, first the fingerprint test dynamic modulus value is computed using the final six cycles of the test, and is denoted as $|E^*|_{test}$. Then, the linear viscoelastic modulus for the particular temperature and frequency of that given fingerprint test is computed using the Prony coefficient function for the storage and loss moduli, as shown in Equation (6.34).

$$|E^*|_{LVE} = \sqrt{(E^{'})^2 + (E^{''})^2} \quad (6.34)$$

where

$$E' = E_\infty + \sum_{i=1}^{N} \frac{E_i \rho_i^2 (2\pi f)^2}{\rho_i^2 (2\pi f)^2 + 1} \text{; and}$$

$$E'' = \sum_{i=1}^{N} \frac{E_i \rho_i (2\pi f)}{\rho_i^2 (2\pi f)^2 + 1}$$

After $|E^*|_{test}$ and $|E^*|_{LVE}$ are obtained, the DMR is computed as the ratio of these two numbers, as shown in Equation (6.35).

$$DMR = \frac{|E^*|_{test}}{|E^*|_{LVE}} \quad (6.35)$$

6.5.2.5 Model Formulation

The S-VECD model used in this study uses a combined approach to take advantage of both the rigorous approach and the simplified approach. It is suggested that within the model the pseudo strain should be calculated piecewise, but the rigorous calculation was used for the first loading path. This portion of the loading history is important because damage growth in this first loading path can be substantial. But for all the other cycles, the simplified calculation was used, i.e., Equation (6.36). As a result of the piecewise definition of pseudo strain, the pseudo stiffness is also piecewise, as defined in Equation (6.37).

$$\varepsilon^R = \begin{cases} \varepsilon^R = \dfrac{1}{E_R} \displaystyle\int_0^\xi E(\xi - \tau) \frac{d\varepsilon}{d\tau} d\tau & \xi \le \xi_p \\ (\varepsilon_{0,ta}^R)_{cycle\ i} = \dfrac{1}{E_R} \cdot \dfrac{\beta + 1}{2} ((\varepsilon_{0,pp})_i \cdot |E^*|_{LVE}) & \xi > \xi_p \end{cases} \quad (6.36)$$

$$C = \begin{cases} C = \dfrac{\sigma}{\varepsilon^R \cdot DMR} & \xi \le \xi_p \\ C^* = \dfrac{\sigma_{0,ta}}{\varepsilon_{0,ta}^R \cdot DMR} & \xi > \xi_p \end{cases} \quad (6.37)$$

For a similar reason and because significant damage can occur along the first loading path, the rigorous calculation shown in Equation (6.27) was used. After this time, however, the simplified calculation method was used. For lack of a clearer term, this portion of the damage calculation is referred to as the *transient* calculation and the remaining calculations as the *cyclic* calculations, as shown in Equation (6.38).

$$dS = \begin{cases} (dS_{Transient})_{timestep\ j} = \left(-\frac{1}{2}(\varepsilon^R)_j^2 \frac{\partial C}{\partial S}\right)^{\alpha} \cdot (d\xi)_j & \xi \le \xi_p \\ (dS_{Cyclic})_{cycle\ i} = \left(-\frac{1}{2}(\varepsilon^R_{0,ta})_i^2 \frac{\partial C^*}{\partial S}\right)^{\alpha} \cdot (d\xi_p) \cdot (K_1) & \xi > \xi_p \end{cases} \qquad (6.38)$$

6.6 Test Results and Model Verification

6.6.1 Linear Viscoelastic Characterization

Three complex modulus tests were performed for each mixture to obtain the linear viscoelastic properties. The results were then averaged to obtain a representative mastercurve for each mixture. Figure 6.15 and Figure 6.16 show the average dynamic modulus mastercurves for all 12 mixes plotted in semi-log and log-log scale, respectively. Figure 6.15 and Figure 6.16 suggest that, in general, surface mixtures have low stiffness values, whereas intermediate mixtures and base mixtures show relatively high stiffness values. It can also be seen that the dynamic modulus values of the RAP mixes are higher than those of the non-RAP mixes, except for the RB25.0B mixture. Figure 6.17 and Figure 6.18 show the phase angle and shift factor test results, respectively, for all 12 mixtures.

The relaxation modulus and creep compliance values were calculated from the complex modulus using linear viscoelastic theory. The slope of the dynamic modulus mastercurve in log-log space, m, is another important property that relates directly to the damage evolution rate, α, in the continuum damage model. These properties are used for further modeling work presented in Section 6.6.2.

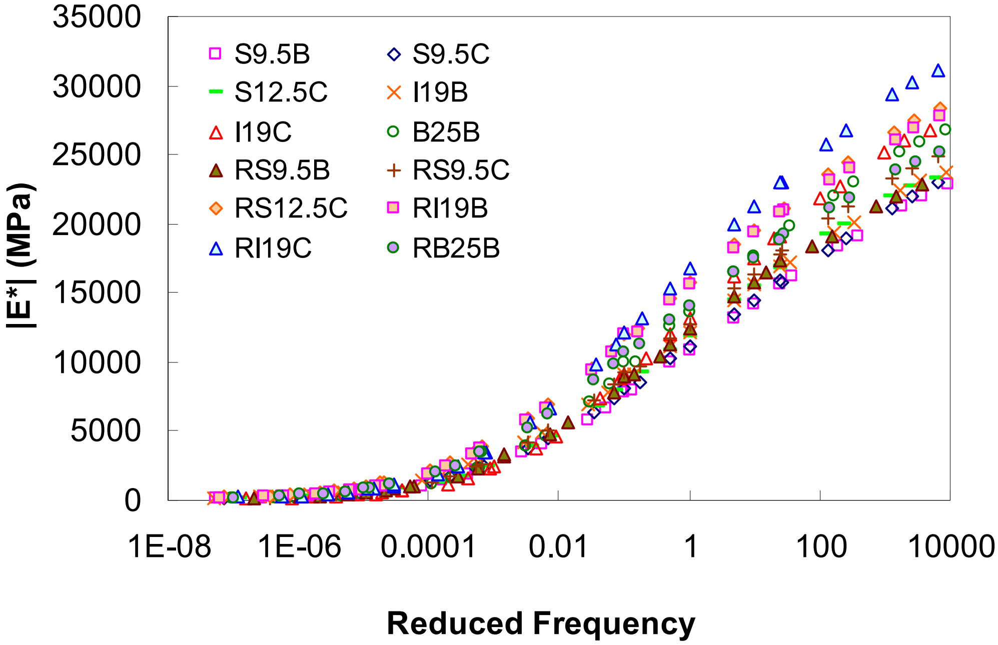

Figure 6.15. Average dynamic modulus mastercurves for all mixtures (semi-log).

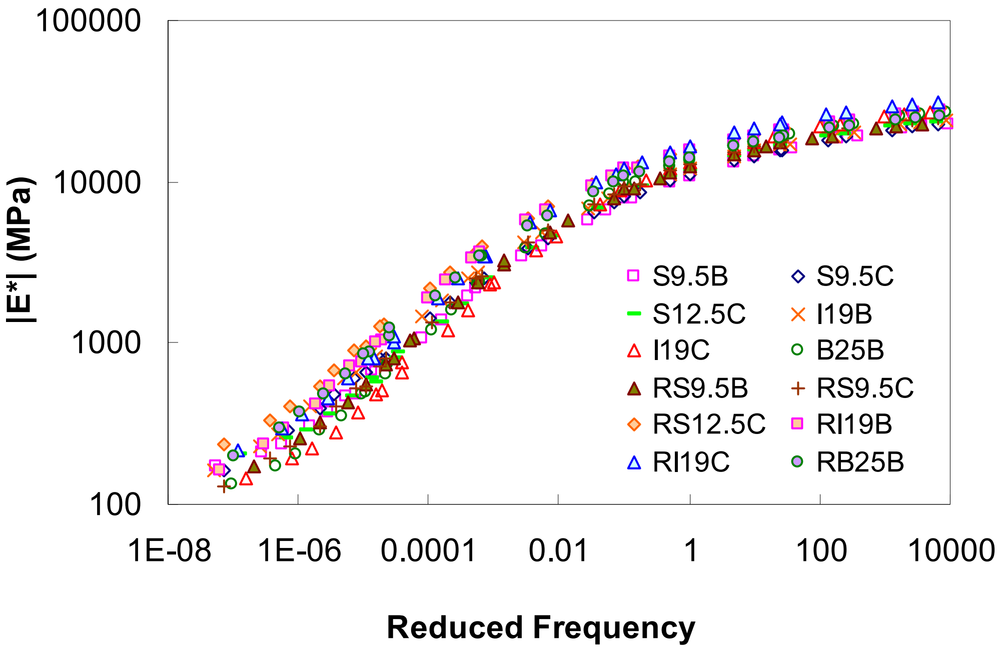

Figure 6.16. Average dynamic modulus mastercurves for all mixtures (log-log).

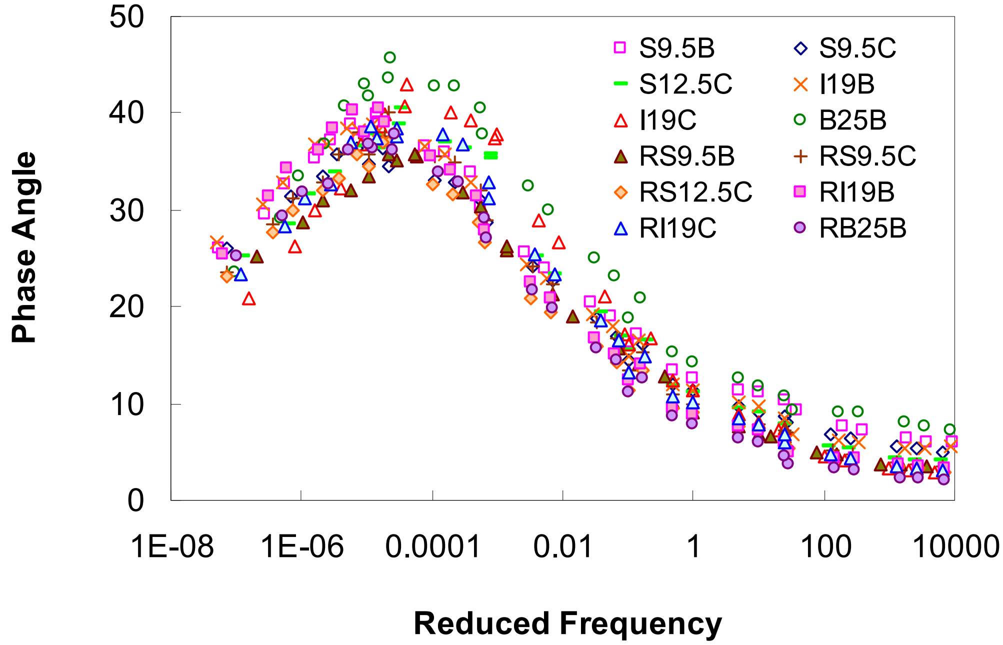

Figure 6.17. Average phase angle mastercurves for all mixtures (semi-log).

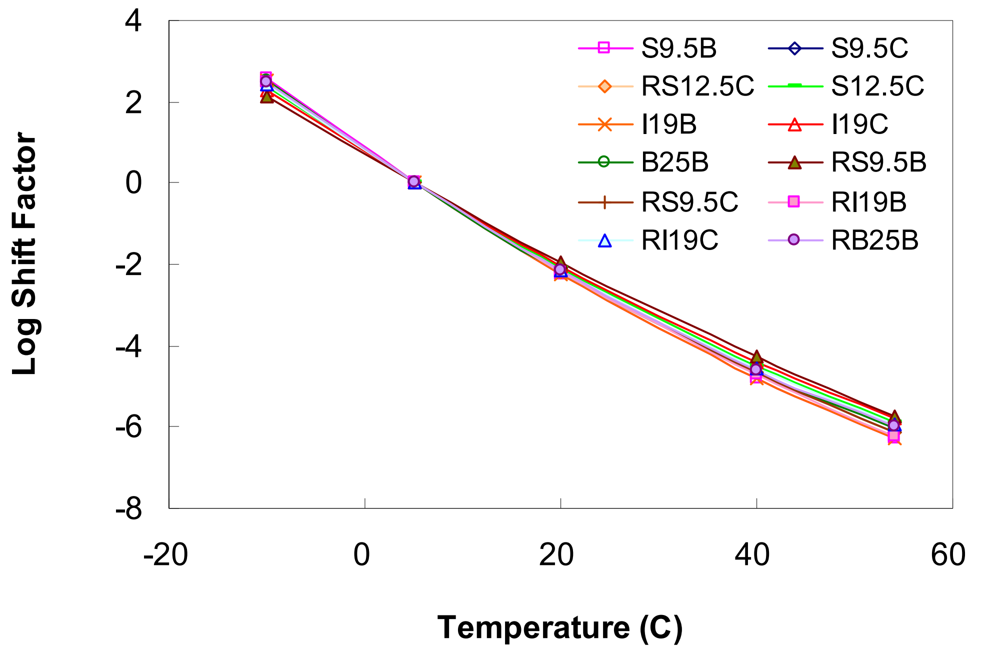

Figure 6.18. Shift factor functions for all mixtures.

6.6.2 Viscoelastic Damage Characterization

The viscoelastic damage was characterized by performing CX cyclic tests at different strain levels and under different temperature conditions. The choice of crosshead strain magnitude was based on experimental experience, because the relationship between machine crosshead strain and actual on-specimen strain can vary depending on mixture type and temperature. A proper determination of crosshead strain is important, because it directly affects the on-specimen strain level and, thus, the fatigue life of the specimen.

Of the 12 mixtures included in this study, the S9.5C mixture was chosen for the development of the simplified VECD model because of its fine-graded nature and, thus, low testing variability. For this particular purpose, 16 tests were performed on this mixture. After the model was developed, it was verified using four additional mixtures that cover a wide range of mixture types. The four verification mixtures used in this study are S9.5B, I19.0C, B25.0B and RS9.5C. For each of these four mixtures, six cyclic tests were performed at two different strain levels and three different temperatures. Once the model was verified, it was no longer necessary to perform fatigue tests for the remaining mixes under as many different conditions as for the first five mixtures. Instead, only two strain-level fatigue tests (one at a high strain level and the other at a low level) were performed at a single temperature (19°C), and the fatigue behavior from the other temperatures and strain levels was predicted using the simplified VECD model. Table 6.1 summarizes the cyclic test results for all 12 mixtures tested in this study. All tests were performed at a constant frequency of 10 Hz, and failure was defined as the point at which the phase angle starts to drop.

Table 6.1. Summary of Controlled Crosshead (CX) Cyclic Test Results

Material	Specimen Name	Crosshead Strain ($\mu\varepsilon$)	Test Designation	Initial Strain[a] ($\mu\varepsilon$)	Freq. (Hz)	Temperature (°C)	N_f
S9.5C	S9.5C-28	1500	27-CX-VH	668	10	26.80	1600
	S9.5C-29	1500	27-CX-VH (2)	638	10	26.80	420
	S9.5C-30	1000	27-CX-H	437	10	26.80	17500
	S9.5C-31	750	27-CX-L	303	10	26.60	86100
	S9.5C-37	1200	27-CX-H2	520	10	26.95	780
	S9.5C-38	600	27-CX-VL2	247	10	26.80	165000
	S9.5C-43	550	27-CX-VL	225	10	27.40	190000
	S9.5C-13	1000	19-CX-H	240	10	19.05	45000
	S9.5C-14	750	19-CX-VL	190	10	19.00	311000
	S9.5C-22	1600	19-CX-VH	402	10	18.50	2280
	S9.5C-39	1500	19-CX-H3	425	10	18.70	3780
	S9.5C-40	1200	19-CX-H2	332	10	18.80	12100
	S9.5C-26	1100	5-CX-H	150	10	5.00	70000
	S9.5C-27	1000	5-CX-L	126	10	4.90	140000
	S9.5C-41	1400	5-CX-VH	213	10	4.60	1430
	S9.5C-42	1200	5-CX-H2	189	10	5.30	1100

Table 6.1 (Continued)

S9.5B	S9.5B-4	950	27-CX-H	500	10	27.40	12100
	S9.5B-5	1200	19-CX-H	363	10	19.20	4570
	S9.5B-6	850	19-CX-L	266	10	19.30	47000
	S9.5B-7	750	27-CX-L	353	10	27.30	87900
	S9.5B-8	1150	5-CX-H	200	10	5.50	4600
	S9.5B-9	950	5-CX-L	166	10	5.50	198000
I19C	I19C-4	1000	19-CX-H	252	10	19.15	6500
	I19C-6	700	27-CX-H	264	10	27.40	19900
	I19C-7	550	27-CX-L	236	10	27.40	217000
	I19C-8	800	5-CX-VL-not fail	106	10	5.40	>277200[b]
	I19C-9	700	19-CX-L	232	10	19.50	27000
	I19C-10	950	5-CX-H	133	10	5.15	16600
B25B	B25B-5	1000	19-CX-H	240	10	19.10	4780
	B25B-11	730	19-CX-L	186	10	19.10	7160
	B25B-14	1000	5-CX-H	122	10	5.40	11000
	B25B-18	725	5-CX-L	112	10	5.15	73800
	B25B-20	400	27-CX-L	162	10	27.50	75000
	B25B-22	500	27-CX-H	256	10	27.40	11000
RS9.5C	RS9.5C-5	1100	19-CX-H	287	10	19.40	44000
	RS9.5C-6	950	19-CX-L	232	10	19.60	148000
	RS9.5C-7	900	27-CX-H	355	10	27.30	27500
	RS9.5C-8	1100	5-CX-VL-not fail	155	10	5.15	>168000[b]
	RS9.5C-9	800	27-CX-L	318	10	27.35	79000
	RS9.5C-10	1200	5-CX-H	174	10	5.35	41000
S12.5C	S12.5C-4	1150	19-CX-H	312	10	19.20	1250
	S12.5C-5	750	19-CX-L	192	10	19.20	74100
I19B	I19B-5	1000	19-CX-H	306	10	19.00	800
	I19B-6	650	19-CX-L	181	10	19.20	19000
RS12.5C	RS12.5C-4	900	19-CX-H	186	10	19.10	9330
	RS12.5C-5	750	19-CX-L	156	10	19.00	220000
RI19B	RI19B-4	900	19-CX-H	187	10	19.45	6000
	RI19B-5	650	19-CX-L	141	10	19.50	23700
RI19C	RI19C-4	900	19-CX-H	180	10	19.35	3450
	RI19C-6	700	19-CX-L	122	10	19.20	68900
RB25B	RB25B-4	700	19-CX-H	175	10	19.20	950
	RB25B-7	600	19-CX-L	133	10	19.20	7550
RS9.5B	RS9.5B-4	N/A	19-CX-H	276	10	19.4	13000
	RS9.5B-5	N/A	19-CX-L	254	10	19.2	52800

[a] On-specimen strain at the 50th loading cycle.
[b] Test was stopped at that number of loading cycle, and specimen did not fail.

After each fatigue test, the pseudo stiffness (*C**) and damage (*S*) were computed. Figure 6.19 shows the damage curves (*C** versus *S*) for the S9.5C, S9.5B, I19C, B25B, and RS9.5C mixtures. As mentioned earlier, these five mixtures were used for model development and verification, which require numerous tests under various test conditions.

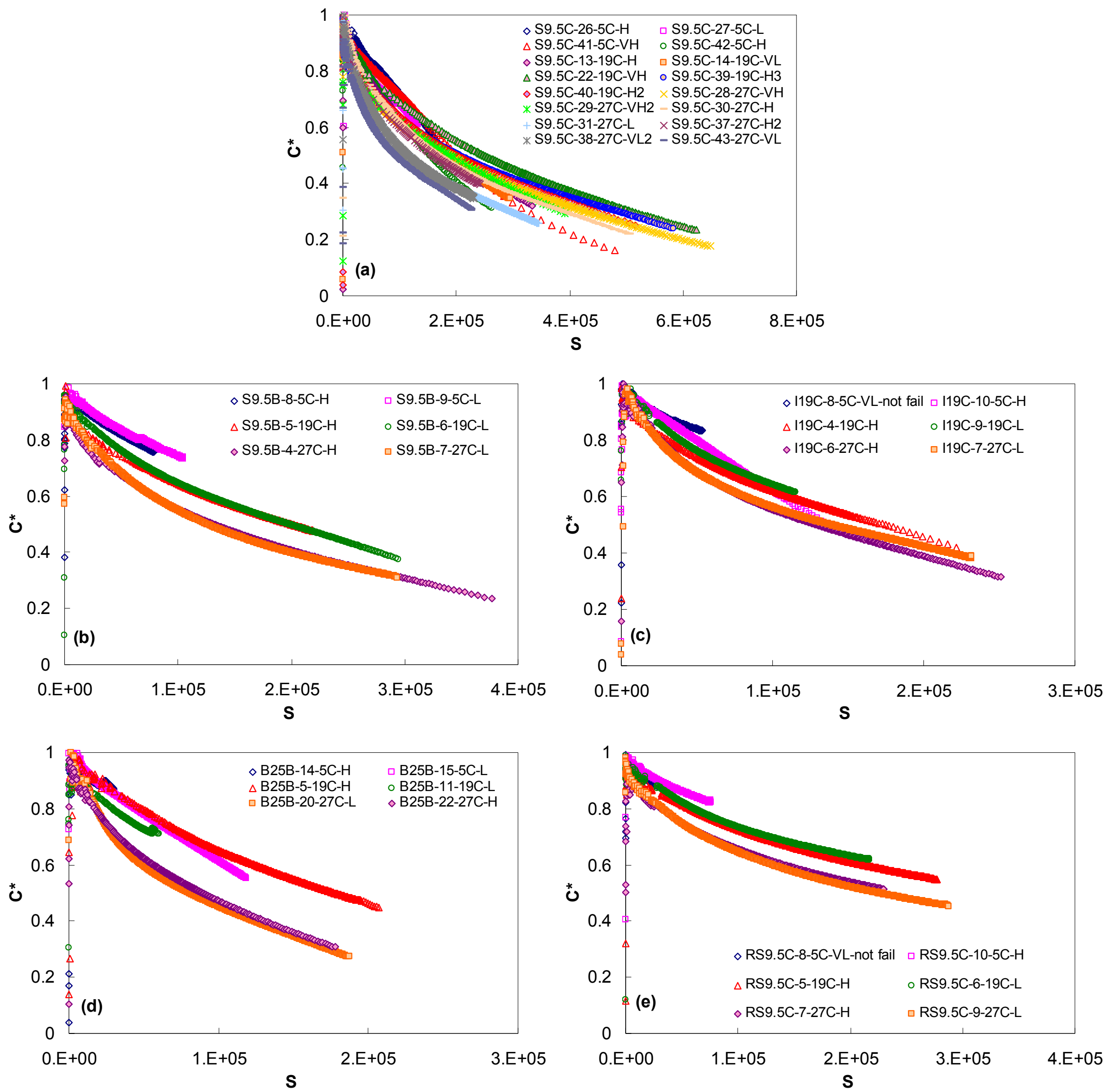

Figure 6.19. Damage curves for: (a) S9.5C; (b) S9.5B; (c) I19C; (d) B25B; and (e) RS9.5C mixtures.

The results in Figure 6.19 show that most of the 5°C and 19°C curves collapse well within each mixture, except S9.5B, for which the 5°C curves stay above the 19°C curves. In general, the 5°C curves are relatively short, indicating brittle behavior of the material at low temperatures. Another observation from Figure 6.19 is that all the 27°C curves stay near the bottom of the graph. This phenomenon is consistent with that observed by other researchers for low strain rate or high temperature monotonic tests, which can be explained by viscoplasticity.

Due to these reasons, the intermediate temperature, 19°C, was chosen as the testing temperature for the remaining mixtures after the model had been verified. It is believed that 19°C is a suitable temperature for the characterization of a material’s viscoelastic damage because the material is not as brittle as at low temperatures and the effect of viscoplasticity is negligible. Figure 6.20 shows the damage curves for the other seven mixtures, i.e., S12.5C, I19.0B, RS9.5B, RS12.5C, RI19.0B, RI19.0C, and RB25.0B.

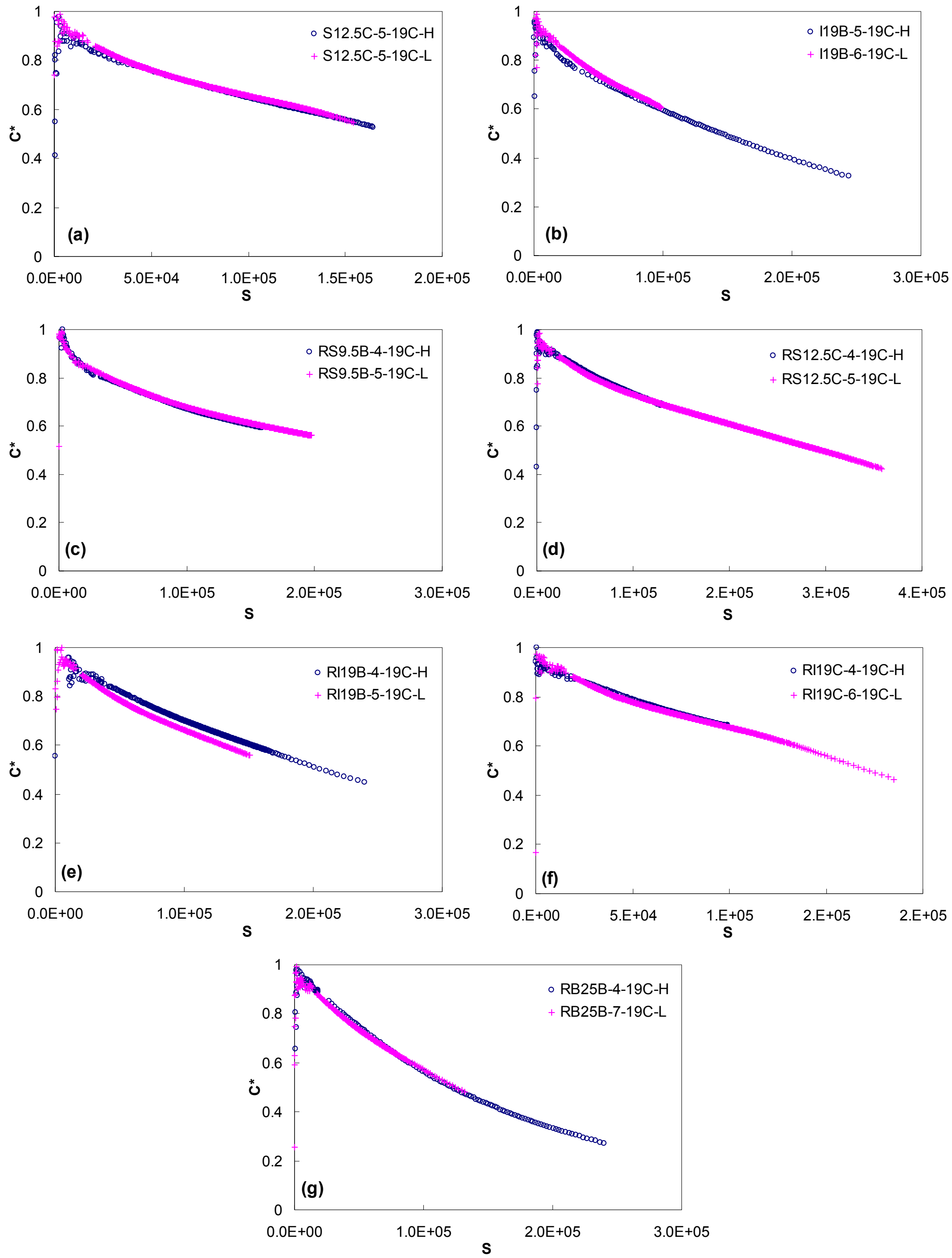

Figure 6.20. Damage curves for: (a) S12.5C; (b) I19.0B; (c) RS9.5B; (d) RS12.5C; (e) RI19.0B; (f) RI19.0C; and (g) RB25.0B.

Figure 6.20 shows that for all the mixtures, the two curves obtained from two distinct cyclic tests (one at a low strain level and the other at a high strain level) collapse very well. Of all the CX tests performed in this study, two failure patterns were observed, mid-failure and end-failure. Figure 6.21 illustrates the two failure patterns.

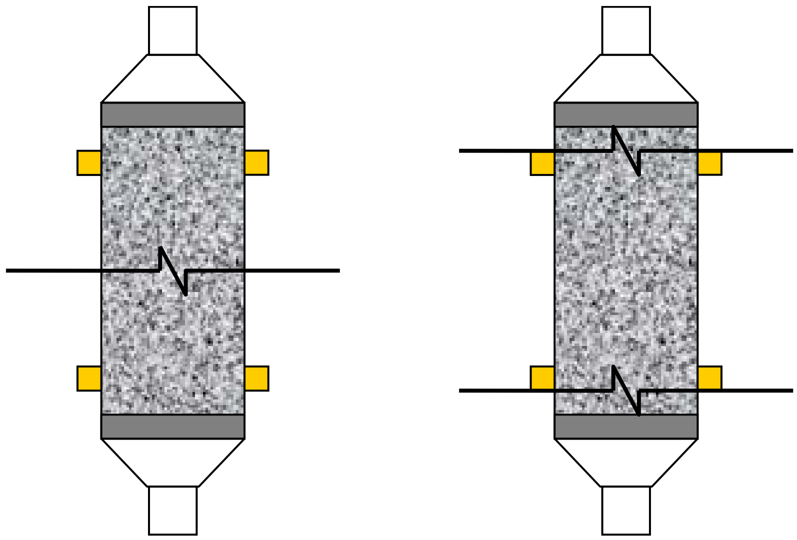

(a) **(b)**

Figure 6.21. Failure locations of CX cyclic tests: (a) mid-failure, and (b) end-failure.

Mid-failure tests are considered to be *good* tests, because the LVDTs are able to capture the major damage throughout the entire test. End-failure tests are not as successful as mid-failure tests because the macrocrack localizes beyond the experimental measurement range. For this reason, the material’s stiffness cannot be calculated accurately, at least not in late stages of the test. The failure locations of all the CX cyclic tests are summarized in Table 6.2.

For damage characterization purposes, end-failure test results can still be considered as valid, and this conclusion is substantiated by Figure 6.22 that shows 19°C damage curves generated from both mid-failure and end-failure tests for several mixtures. It can be observed from Figure 6.22 that end-failure tests result in shorter damage curves than the mid-failure tests; in other words, the end-failure tests result in a high measured pseudo stiffness value at failure. This result can be explained by the macrocrack localization phenomenon, as explained earlier in this section. Again, this result does not affect damage characterization, as the end-failure (short) curves follow the trend of the mid-failure (long) curves. Thus, it is proved that the material’s damage curve can be characterized by uniaxial CX cyclic tests, regardless of their failure locations.

Table 6.2. Summary of Failure Locations for CX Cyclic Tests

Specimen Name	Failure Location	Specimen Name	Failure Location	Specimen Name	Failure Location
S9.5C-13	middle	S9.5B-4	middle	RI19C-4	end
S9.5C-14	middle	S9.5B-5	end	RI19C-6	middle
S9.5C-22	middle	S9.5B-6	middle	B25B-5	end
S9.5C-26	middle	S9.5B-7	middle	B25B-11	end
S9.5C-27	middle	S9.5B-8	end	B25B-14	end
S9.5C-28	middle	S9.5B-9	end	B25B-18	middle
S9.5C-29	middle	RS9.5B-4	end	B25B-20	middle
S9.5C-30	middle	RS9.5B-5	end	B25B-22	middle
S9.5C-31	middle	S12.5C-4	end	RB25B-4	middle
S9.5C-37	middle	S12.5C-5	end	RB25B-7	middle
S9.5C-38	end	RS12.5C-4	end		
S9.5C-39	middle	RS12.5C-5	middle		
S9.5C-40	middle	I19B-5	middle		
S9.5C-41	middle	I19B-6	end		
S9.5C-42	middle	RI19B-4	Middle		
S9.5C-43	middle	RI19B-5	middle		
RS9.5C-5	end	I19C-4	middle		
RS9.5C-6	end	I19C-6	middle		
RS9.5C-7	end	I19C-7	end		
RS9.5C-9	end	I19C-9	end		
RS9.5C-10	end	I19C-10	middle		

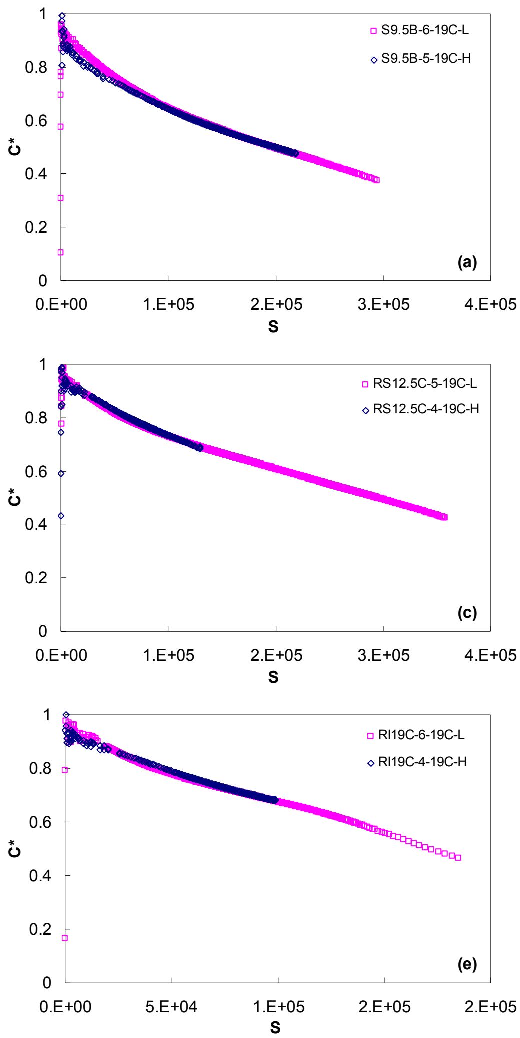

Figure 6.22. Damage curves for CX cyclic tests with different failure locations: (a) S9.5B; (b) I19.0C; (c) RS12.5C; (d) I19.B; and (e) RI19.C mixtures.

All the 19°C test curves were fitted to analytical forms to obtain the damage characteristic curves for each mixture, which were then used for predicting fatigue performance. The power law function suggested by Lee and Kim (1998), shown as Equation (6.39), was found to fit the experimental results better than the exponential function (Equation (6.40)) used by Underwood (2005).

$$C^* = 1 - C_{11} S^{C_{12}} \quad (6.39)$$

$$C^* = e^{aS^b} \quad (6.40)$$

The damage characteristic curves for all 12 mixtures are plotted together in Figure 6.23. Damage characteristic curves depict the mixture's resistance to damage. However, it is impossible to compare mixtures' fatigue performances simply by looking at the damage characteristic curves. A better comparison can be achieved by fatigue test simulations, which is discussed later in subsequent sections of this chapter.

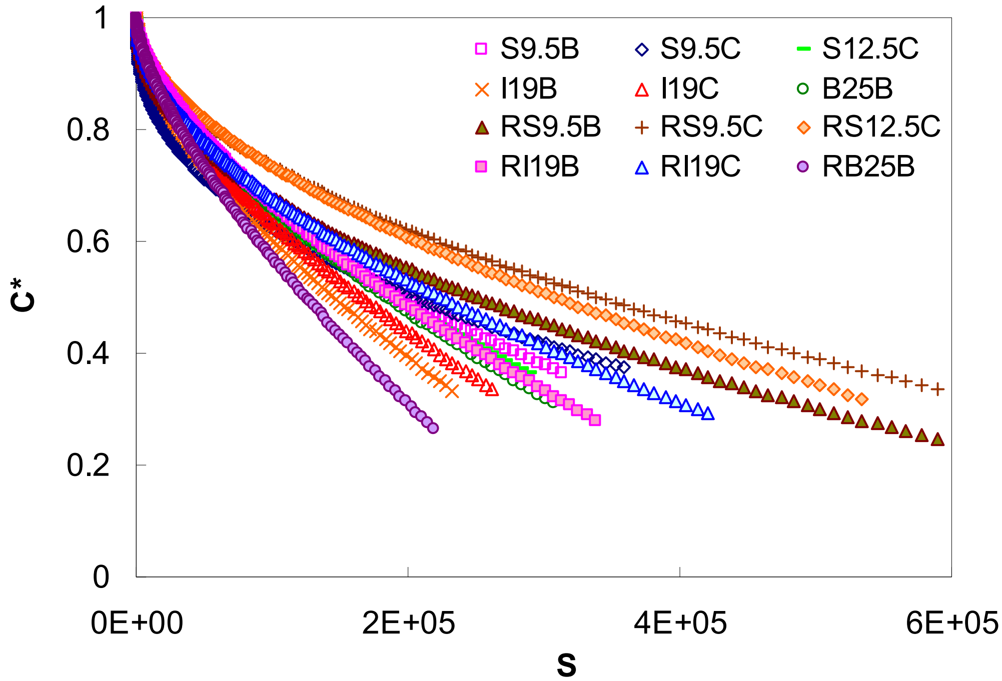

Figure 6.23. Damage characteristic curves for all mixtures.

6.7 Model Application

6.7.1 Simulation Failure Envelope

The simplified fatigue model does not account for changing time dependency, and therefore, it is not possible to observe a sudden decrease of the phase angle in simulations, which is used to define failure in the measured tests. For this reason, empirical observations of all the tested mixtures were used to determine the failure criterion. These observations are shown in Figure 6.24 where the pseudo stiffness at failure is plotted against the reduced frequency for multiple mixtures. Note that only mid-failure test results are used here, because the measured stiffness values are not reliable for end-failure tests, as explained earlier.

Figure 6.24 suggests that the pseudo stiffness at failure increases with reduced frequency. For non-RAP mixtures, when the reduced frequency is below 0.01 Hz, which corresponds to approximately 27°C at 10 Hz, failure for the cyclic tests occurs at a pseudo stiffness of approximately 0.28, a value similar to that observed by Daniel and Kim (2002) for their tests, which were performed at 25°C. As the reduced frequency increases, failure tends to occur at a higher level of pseudo stiffness. It is also observed that the rate of this increment is aggregate size-dependent; that is, as the NMAS increases, the rate of change in the pseudo stiffness at failure as a function of reduced frequency increases.

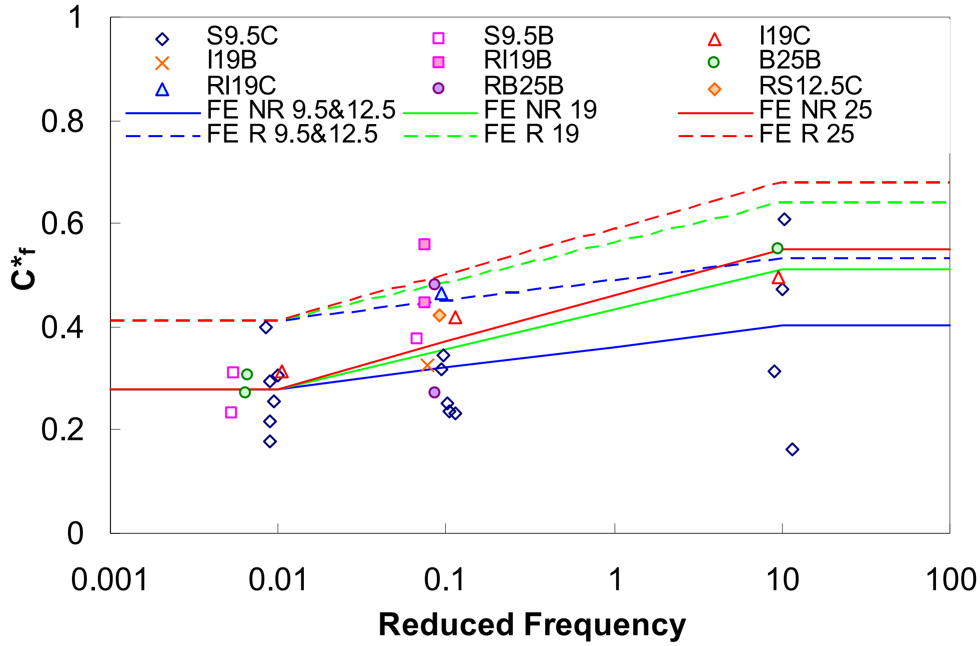

Figure 6.24. Failure envelope for fatigue test simulation.

Further, from the data around a reduced frequency of 0.1 Hz, it was found that RAP mixtures have a higher failure pseudo stiffness value than non-RAP mixtures. So in summary, the piecewise fitting function given in Equation (6.41) was applied for failure criterion development. Note that because calibration data are not available when the reduced frequency is greater than 10 Hz or less than 0.01 Hz, it is assumed that the failure pseudo stiffness neither increases nor decreases beyond this range. The failure envelope within this range is a linear function in semi-log space, whereas the slope is a function of NMAS, and the intercept is affected by the inclusion of RAP in the mixture. The coefficients of the fitting function are listed in Table 6.3.

$$C_f^* = \begin{cases} a \cdot \log(0.01) + b & f_R \leq 0.01 \\ a \cdot \log(f_R) + b & 0.01 < f_R < 10 \\ a \cdot \log(10) + b & f_R \geq 10 \end{cases} \qquad (6.41)$$

where

f_r = reduced frequency; and

a and b = coefficients.

Table 6.3. Coefficients for Failure Envelope

	NMAS	a	b
Non-RAP	9.5&12.5	0.040538	0.361945
	19	0.076546	0.433962
	25	0.090027	0.460924
RAP	9.5&12.5	0.040538	0.490049
	19	0.076546	0.562066
	25	0.090027	0.589027

6.7.2 Fatigue Test Prediction

Once the simplified VECD model was calibrated, i.e., the C_{11} and C_{12} coefficients in Equation (6.39) were found for each mixture, the analytical function of the damage characteristic curve could be substituted into Equation (6.38) for simulation purposes. So, the amount of damage can be calculated for a known pseudo strain history by assuming an initial damage value, e.g., 0.1. The predicted damage for a prescribed pseudo strain history becomes the form shown in Equation (6.42).

$$S_{i+1} = S_i + \left(\frac{1}{2} (\varepsilon_{0,ta}^R)^2 C_{11} C_{12} S^{C_{12}-1} \right)^{\alpha} K_1 (d\xi) \quad \text{(6.42)}$$

The corresponding pseudo stiffness history can then be predicted if the damage history is determined according to Equation (6.39). The predicted and measured pseudo stiffness values for a typical good prediction are shown in Figure 6.25, and results from a typical bad prediction are shown in Figure 6.26.

Finally, by applying the failure criterion developed in the previous Section 6.7.1, the fatigue life can be predicted for that particular cyclic test with a known pseudo strain history. By comparing the measured and predicted fatigue test results in strain versus fatigue life plots (Figure 6.27 and Figure 6.28), it can be seen that the model does a reasonable job of predicting failure at all temperatures.

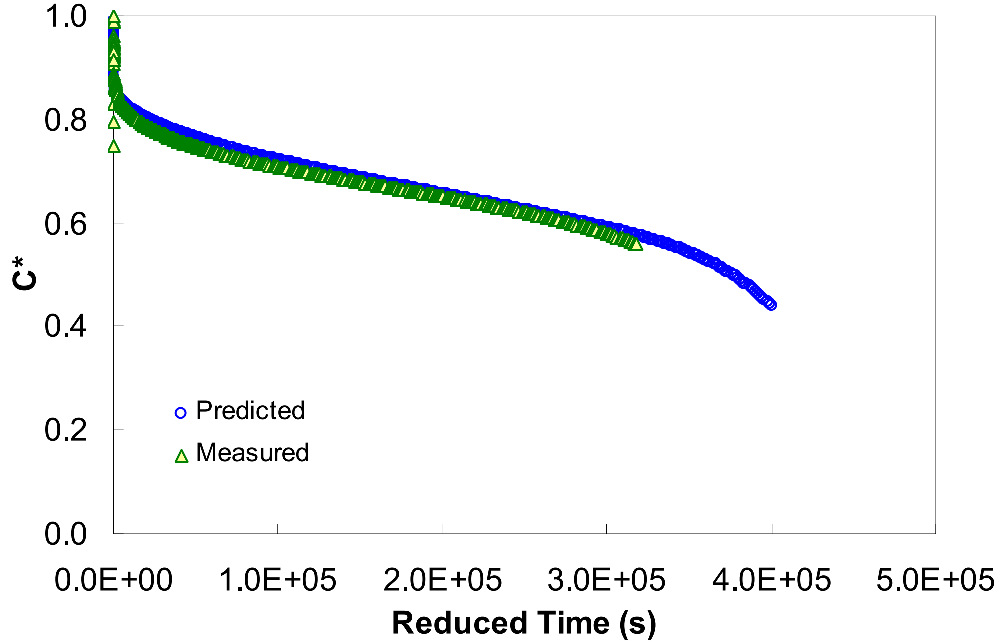

Figure 6.25. Typical good pseudo stiffness prediction (RI19B-5).

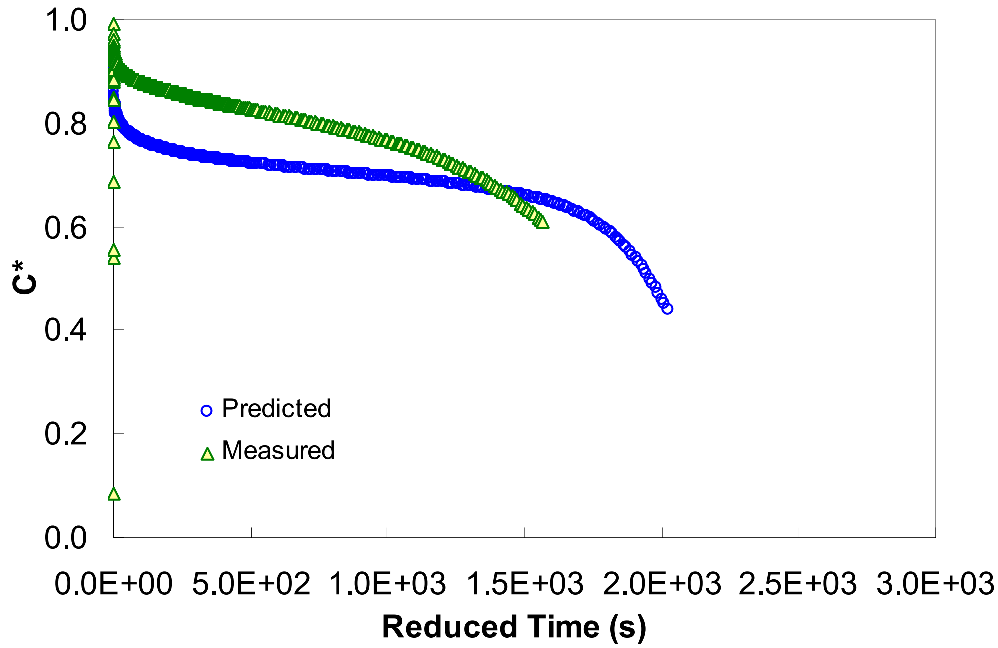

Figure 6.26. Typical bad pseudo stiffness prediction (I19C-10).

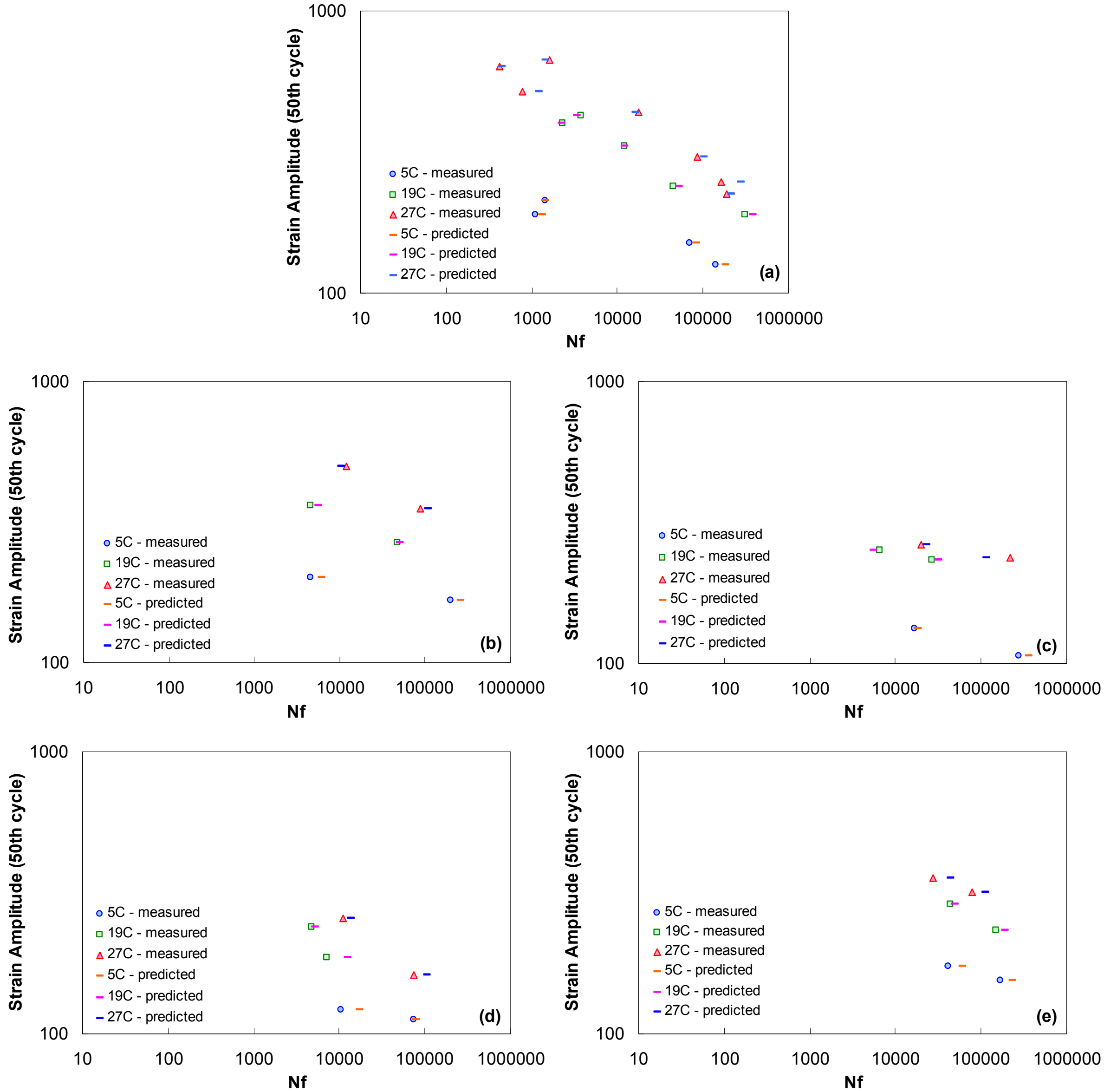

Figure 6.27. Controlled crosshead (CX) cyclic test simulation results for: (a) S9.5C; (b) S9.5B; (c) I19.0C; (d) B25.0B; and (e) RS9.5C mixtures.

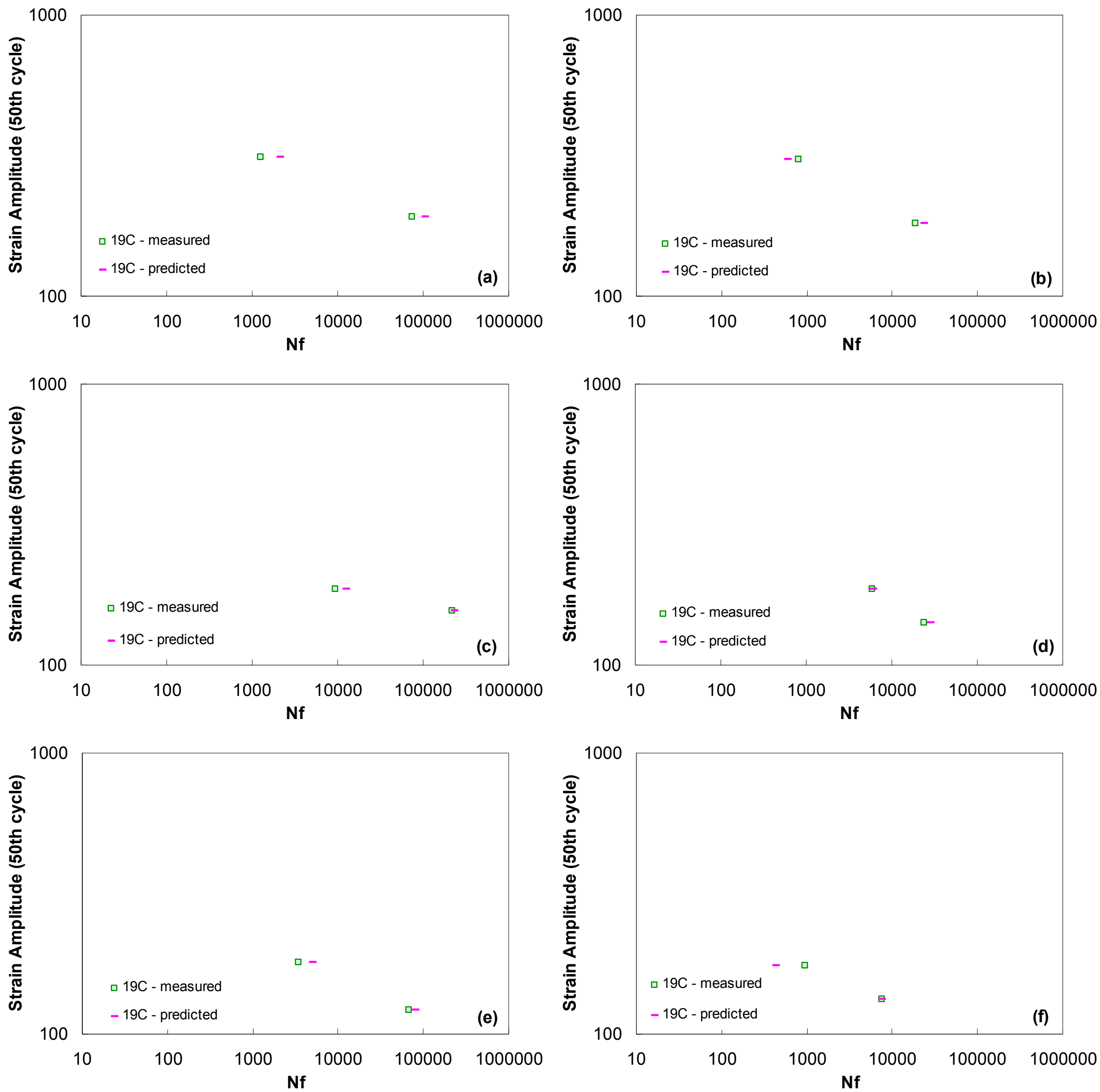

Figure 6.28. Controlled crosshead (CX) cyclic test simulation results for: (a) S12.5C; (b) I19.0B; (c) RS12.5C; (d) RI19.0B; (e) RI19.0C; and (f) RB25B mixtures.

By looking at the comparison of the measured and predicted fatigue lives shown in Figure 6.29, it was found that there is a slight tendency to overestimate the fatigue life. This overestimation can be attributed to the following reasons:

1. The power law function does not fit well with experimental damage curves. Some mixtures, such as RS12.5C and RI19.0C, have a rapid decrease in pseudo stiffness when the specimen is close to failure.
2. End-failure specimens, e.g., all the tests of the RS9.5C and S12.5C mixes, fail at a high pseudo stiffness value, whereas the simulation failure envelope is calibrated using mid-failure test results only.

3. Most of the 27°C test curves stay below the calibrated damage characteristic curve due to viscoplasticity. When using the damage characteristic curve to predict 27°C tests, it overpredicts the pseudo stiffness, and eventually overpredicts the fatigue life.

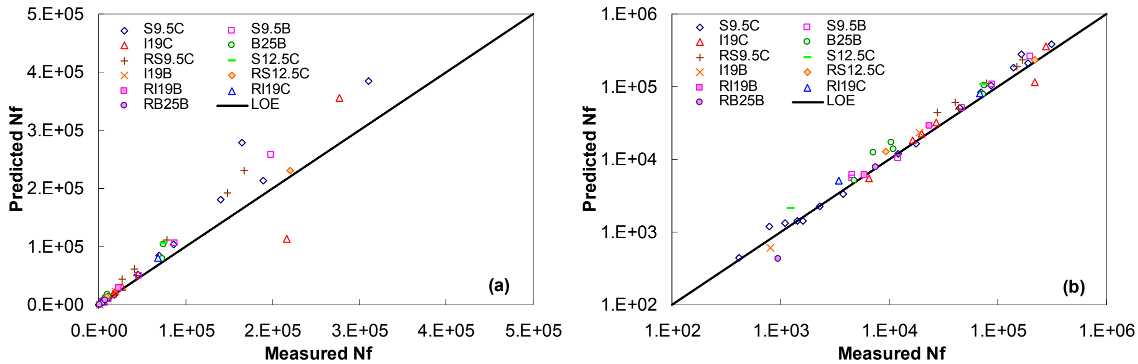

Figure 6.29. Comparison of measured and predicted fatigue lives in: (a) arithmetic scale, and (b) log scale.

6.7.3 Further Development of Failure Envelope Using an Optimization Technique

One approach to improve fatigue test prediction results is to develop a new failure envelope that can reduce the differences between the measured and predicted fatigue lives. For this reason, a general study on failure envelope development was made based on mid-failure cyclic test data using an optimization technique.

Based on observations, the desired shape of the failure envelope is similar to that developed in Section 6.7.1, and the equation is shown as follows:

$$C_f^* = \begin{cases} b & f_R < 0.01 \\ a \cdot (\log(f_R) - \log(0.01)) + b & 0.01 \le f_R < 10 \end{cases} \qquad (6.43)$$

where a is a function of NMAS, and b is a function of RAP mixture versus non-RAP mixture.

The shape of the failure envelope is unknown when the reduced frequency is greater than 10 Hz, due to the availability of data points. The optimization process was performed using Evolver Genetic Algorithm (GA) optimization routine. Two different objective functions were used: the total prediction error in arithmetic scale and in log scale. By changing the values of the coefficients in Equation (6.43), the SSEs are minimized, and the prediction results after optimization are shown in Figure 6.30 and Figure 6.31.

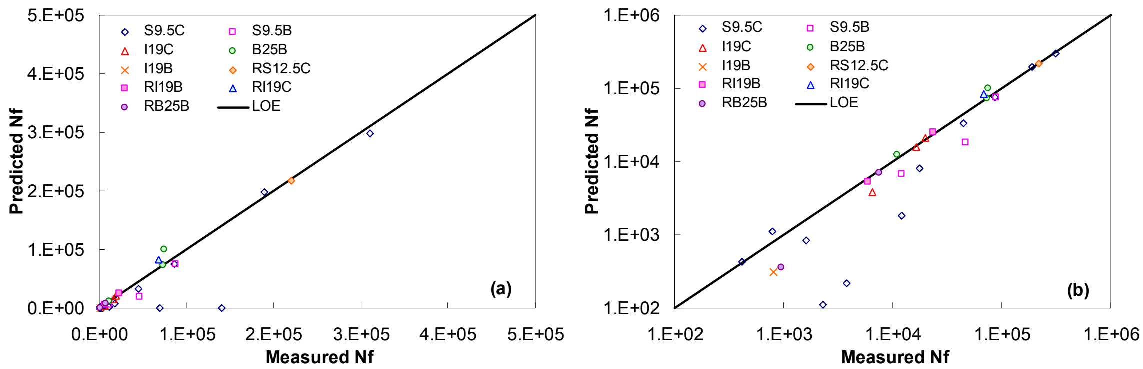

Figure 6.30. Fatigue life prediction results in: (a) arithmetic; and (b) log scales after minimizing the total prediction error in arithmetic scale.

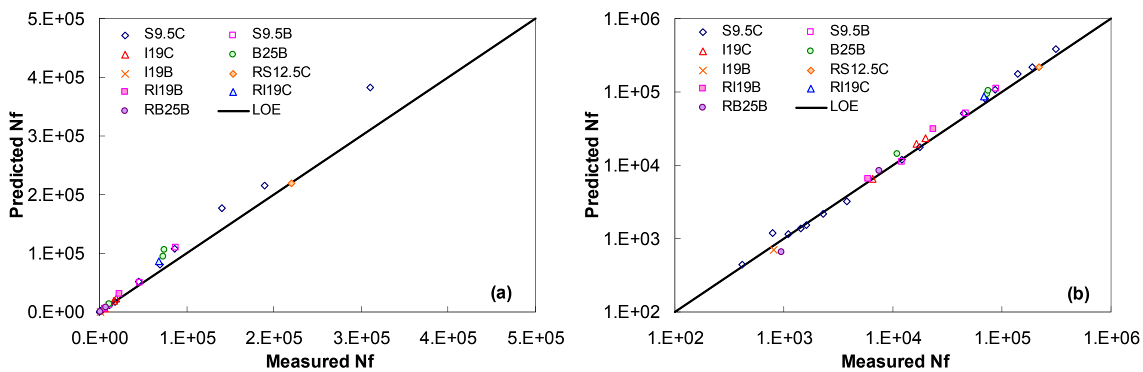

Figure 6.31. Fatigue life prediction results in: (a) arithmetic; and (b) log scales after minimizing the total prediction error in log scale.

By comparing the results after optimization using the two different objective functions, it is found that minimizing the total prediction error in log scale gives better overall prediction results than in arithmetic scale, so all further findings are based on this objective function. The optimization yields a group of coefficients, which are listed in Table 6.4, and the resulting failure envelope is presented in Figure 6.32.

Table 6.4. Optimized Failure Envelope Coefficients

Coefficient	NMAS/ RAP	Value
a	NMAS 9.5	0.073018
	NMAS 12.5	0.185247
	NMAS 19	0.033746
	NMAS 25	0.002675
b	Non-RAP	0.258598
	RAP	0.301445

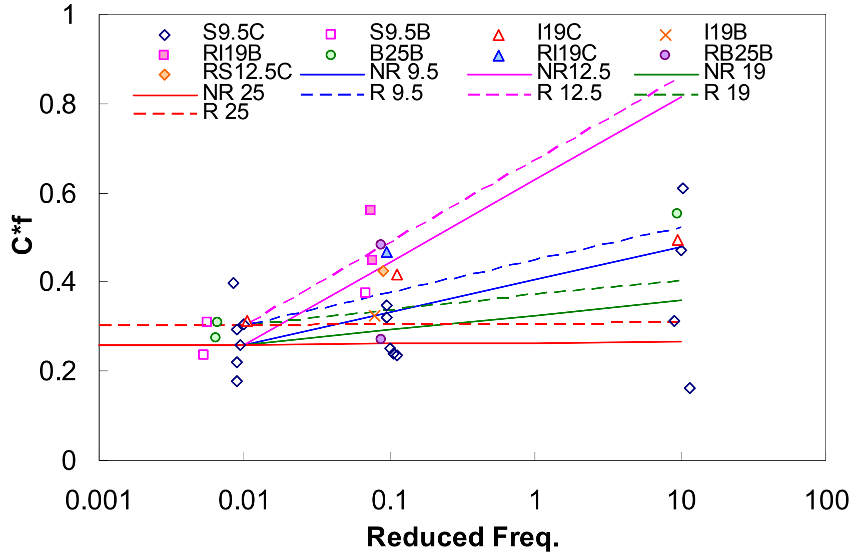

Figure 6.32. Optimized failure envelope.

Figure 6.32 shows that the optimized failure envelope matches with the experimental data points. The value of intercept coefficient, *b*, for RAP mixtures is greater than that for non-RAP mixtures. The value of slope coefficient, *a*, decreases with an increase in NMAS, except for the 12.5 mm mixture, which has a much greater value than all the other aggregate sizes. This phenomenon can be explained by the lack of sufficient experimental data points for the 12.5 mm mixtures, as only one RS12.5C data point is used in the optimization process.

A closer look at the relationship between slope coefficient and NMAS is presented in Figure 6.33, and a linear regression line is generated in the same graph.

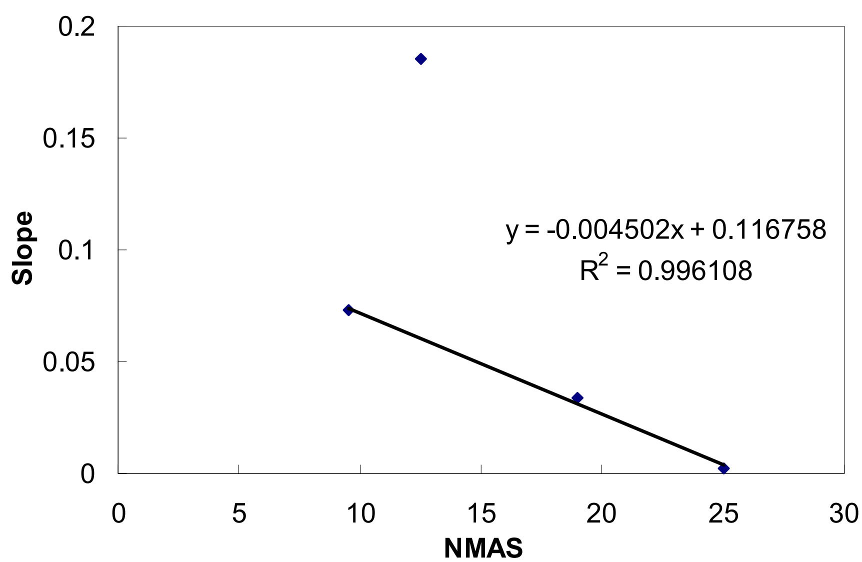

Figure 6.33. Optimized slope coefficients versus NMAS.

Note that due to the availability of experimental data, the results for the 12.5 mm mixture were not considered as reliable, and therefore, that mixture was not included in the regression analysis.

A final version of the failure envelope is proposed in Equation (6.44), and its graphical representation is illustrated in Figure 6.34. As a conclusion, this failure envelope covers a range of cyclic tests whose reduced frequencies are less than 10 Hz. It uses the pseudo stiffness value as the criterion to define failure. This value is assumed constant when the reduced frequency is less than 0.01 Hz, although it starts to increase as the reduced frequency goes beyond 0.01 Hz. In addition, the increasing rate is dependent on the mixture's NMAS. For mixtures with the same NMAS tested at a certain reduced frequency, the value of pseudo stiffness at failure for the RAP mixture is greater than for the non-RAP mixture. This final failure envelope is then applied to predict the fatigue life for the mid-failure cyclic tests, and the results are presented in Figure 6.35.

$$C_f^* = \begin{cases} b & f_R < 0.01 \\ a \cdot (\log(f_R) - \log(0.01)) + b & 0.01 \le f_R < 10 \end{cases} \quad (6.44)$$

where

$$a = -0.004502 NMAS + 0.116758; \text{ and}$$

$$b = \begin{cases} 0.258598 & RAP \\ 0.301445 & non-RAP \end{cases}$$

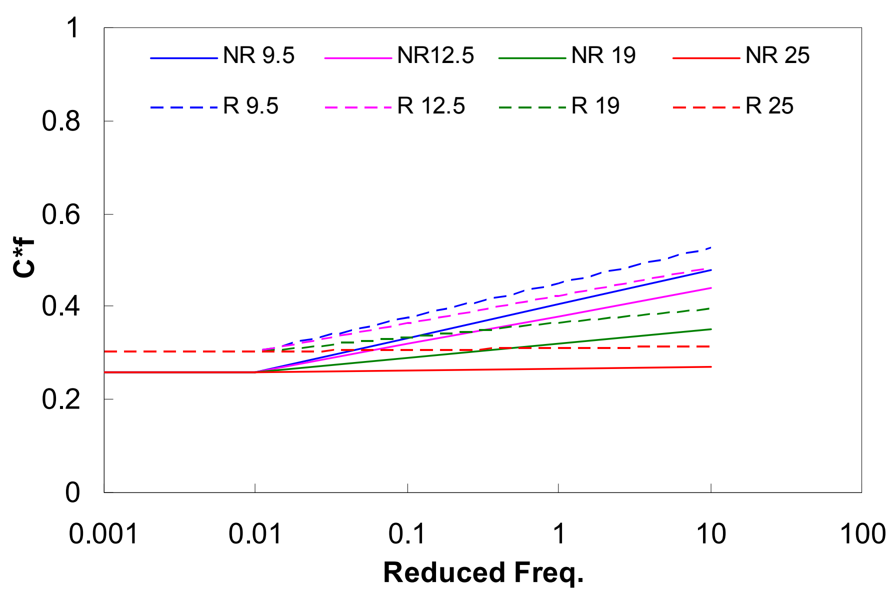

Figure 6.34. Fatigue failure envelope.

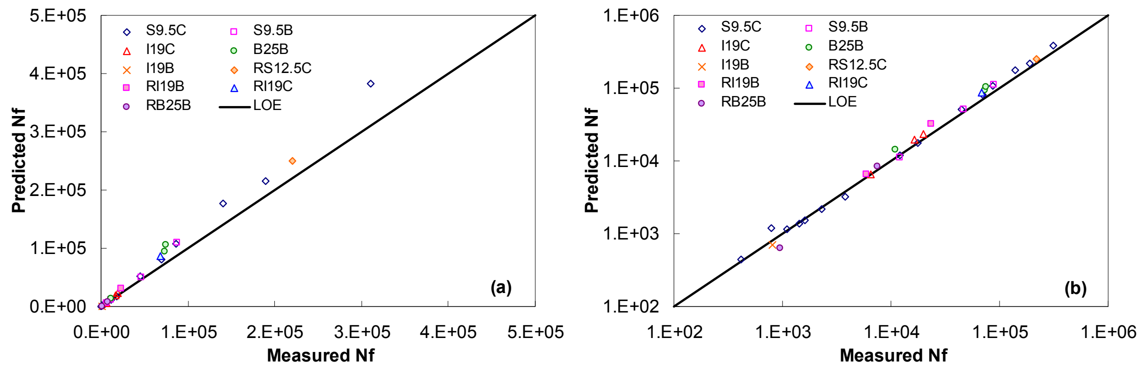

Figure 6.35. Fatigue life prediction results using failure envelope.

It is seen from Figure 6.35 that the prediction error can be reduced further by applying the new failure envelope, as compared to Figure 6.29, and the overprediction problem is alleviated by ignoring the end-failure tests. It should be noted that this failure envelope has not been validated yet due to the insufficiency of experimental data. Validation and improvement of the current failure envelope is part of recommended future research.

6.7.4 Direct Tension Fatigue Simulation

One application of the simplified VECD model is to simulate purely strain-controlled direct tension cyclic testing. The theoretical background is described by the following equation derivations. First, the damage calculation equation (Equation (6.38)) can be rewritten with respect to loading cycle, N, as shown in Equation (6.45).

$$dS = \left(-\frac{1}{2} (\varepsilon_{0,ta}^{R})^2 \frac{\partial C^*}{\partial S} \right)^{\alpha} K_1 \left(\frac{dN}{f_{red}} \right) \quad (6.45)$$

where f_{red} is the reduced frequency of loading in Hz. The relationship between pseudo stiffness and damage is known as the power law function in Equation (6.39), and the derivative of pseudo stiffness with respect to damage is

$$\frac{\partial C^*}{\partial S} = -C_{11} C_{12} S^{C_{12}-1} \quad (6.46)$$

Substituting Equation (6.46) into Equation (6.45) and isolating the terms relating to damage, Equation (6.47) can be obtained as

$$dS = \left(\frac{1}{2} (\varepsilon_{0,ta}^{R})^2 C_{11} C_{12} \right)^{\alpha} K_1 \left(\frac{dN}{f_{red}} \right) (S^{(C_{12}-1)})^{\alpha} \quad (6.47)$$

Thus,

$$(S^{(C_{12}-1)})^{-\alpha}\, dS = \left(\frac{1}{2}(\varepsilon_{0,ta}^{R})^2 C_{11}C_{12}\right)^{\alpha} K_1 \left(\frac{1}{f_{red}}\right) dN \quad (6.48)$$

Integrating Equation (6.48) on both sides gives

$$\int_{S_{ini}}^{S_f} (S^{(C_{12}-1)})^{-\alpha}\, dS = \int_{1}^{N_f} \left(\frac{1}{2}(\varepsilon_{0,ta}^{R})^2 C_{11}C_{12}\right)^{\alpha} K_1 \left(\frac{1}{f_{red}}\right) dN \quad (6.49)$$

$$\left.\frac{S^{\alpha-\alpha C_{12}+1}}{\alpha-\alpha C_{12}+1}\right|_{S_{ini}}^{S_f} = \left(\frac{1}{2}(\varepsilon_{0,ta}^{R})^2 C_{11}C_{12}\right)^{\alpha} K_1 \left(\frac{1}{f_{red}}\right)(N_f-1) \quad (6.50)$$

$$\frac{S_f^{\alpha-\alpha C_{12}+1}}{\alpha-\alpha C_{12}+1} - \frac{S_{ini}^{\alpha-\alpha C_{12}+1}}{\alpha-\alpha C_{12}+1} = \left(\frac{1}{2}(\varepsilon_{0,ta}^{R})^2 C_{11}C_{12}\right)^{\alpha} K_1 \left(\frac{1}{f_{red}}\right)(N_f-1) \quad (6.51)$$

Assuming that $S_{ini} << S_f$ and $N_f >> 1$, Equation (6.51) can be simplified as

$$\frac{S_f^{\alpha-\alpha C_{12}+1}}{\alpha-\alpha C_{12}+1} = \left(\frac{1}{2}(\varepsilon_{0,ta}^{R})^2 C_{11}C_{12}\right)^{\alpha} K_1 \left(\frac{1}{f_{red}}\right)(N_f) \quad (6.52)$$

Rearranging Equation (6.52), the fatigue life, N_f, becomes

$$N_f = \frac{(f_{red})(2^{\alpha})S_f^{\alpha-\alpha C_{12}+1}}{(\alpha-\alpha C_{12}+1)(C_{11}C_{12})^{\alpha}(\varepsilon_{0,ta}^{R})^{2\alpha} K_1} \quad (6.53)$$

Substituting the cyclic portion of the pseudo strain in Equation (6.36) into Equation (6.53) and recognizing that $E_R = 1$ yields

$$N_f = \frac{(f_{red})(2^{\alpha})S_f^{\alpha-\alpha C_{12}+1}}{(\alpha-\alpha C_{12}+1)(C_{11}C_{12})^{\alpha}\left[(\beta+1)(\varepsilon_{0,pp})(|E^*|_{LVE})\right]^{2\alpha} K_1} \quad (6.54)$$

For different strain amplitude, loading frequency and temperature, a different fatigue life can be obtained using the above Equation (6.54). The simulation results can then be fitted by the empirical model (Equation (6.3)). Figure 6.36 and Figure 6.37 show the simulation results of strain-controlled direct tension cyclic tests for all 12 mixtures at 5°C, 19°C and 27°C. Note that all the simulated tests are in a zero mean strain condition, i.e., $\beta=0$, and the loading frequency is 10 Hz. The failure criterion used in the simulations is the same as the one developed in Section 6.7.3, i.e., S_f is calculated from C^*_f through the power law function. Table 6.5 and Table 6.6 summarize the regression coefficients of the empirical model for all the mixtures as obtained from direct tension fatigue test simulations in KPa and psi-based units respectively.

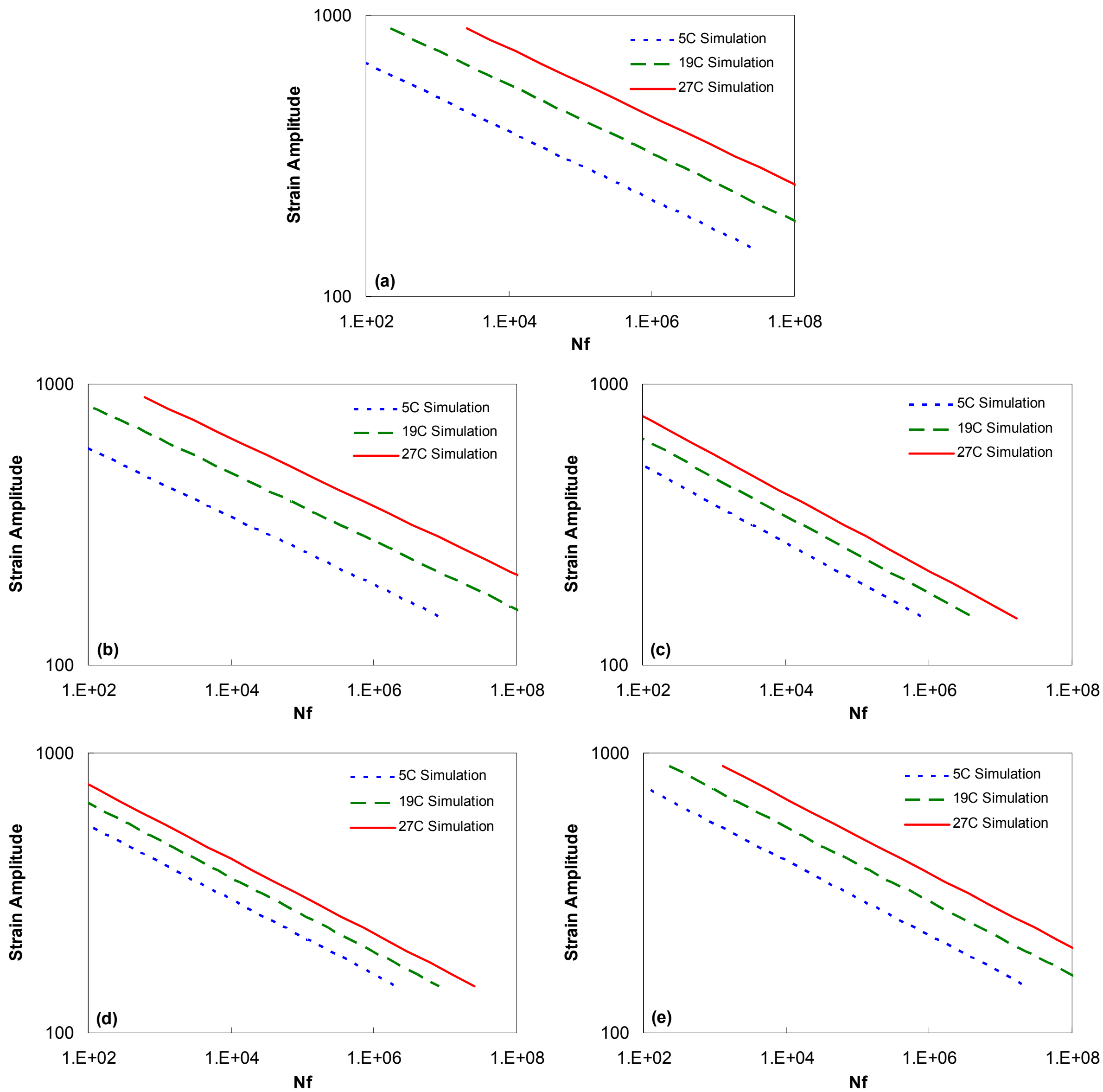

Figure 6.36. Strain-controlled direct tension fatigue test simulation results for: (a) S9.5C; (b) S9.5B; (c) I19.0C; (d) B25.0B; and (e) RS9.5C mixtures.

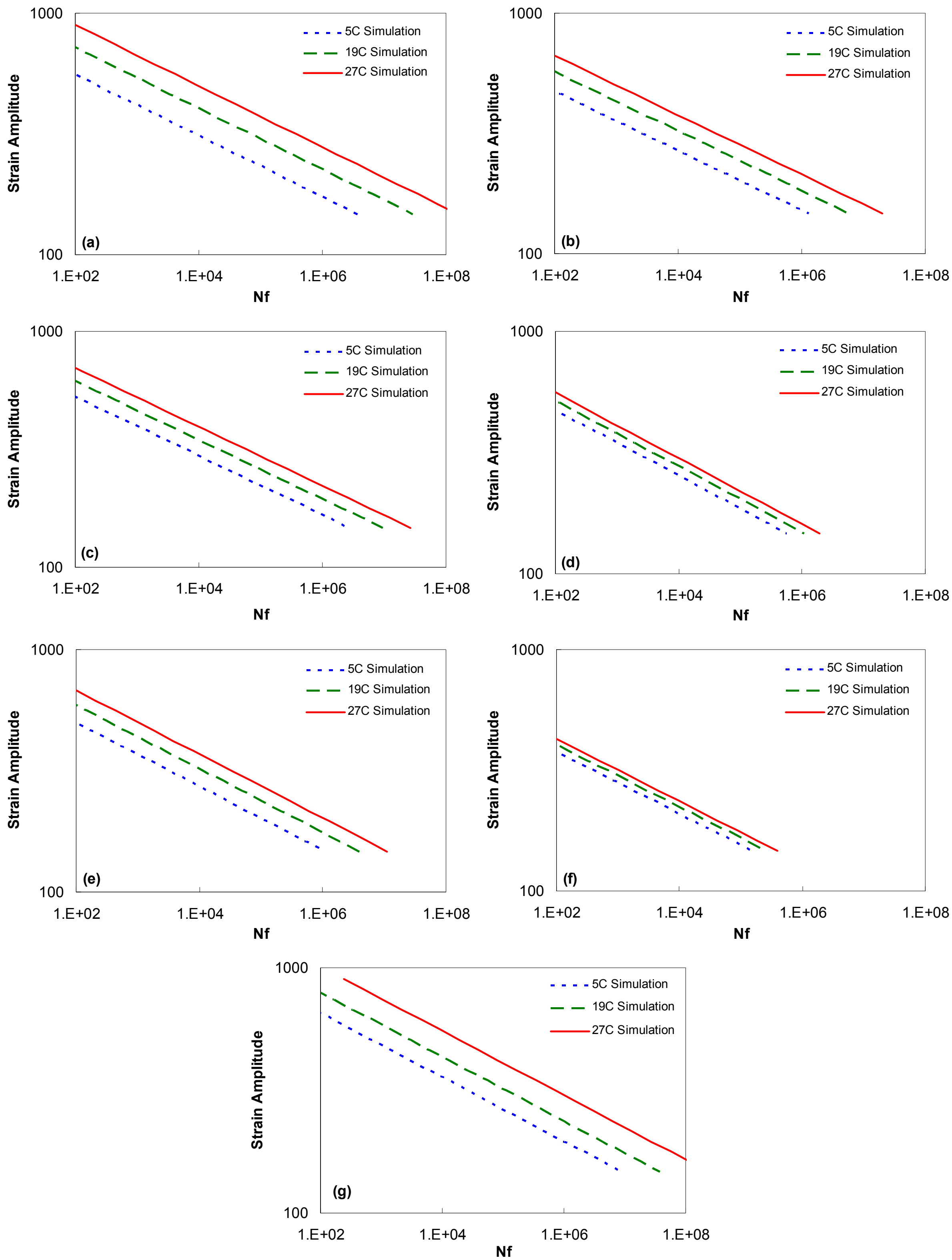

Figure 6.37. Strain-controlled direct tension fatigue test simulation results for: (a) S12.5C; (b) I19.0B; (c) RS12.5C; (d) RI19.0B; (e) RI19.0C; (f) RB25.0B; and (g) RS9.5B mixtures.

Table 6.5. Summary of Regression Coefficients for Empirical Model from Direct Tension Fatigue Simulation (KPa-based)

mixture	K_{f1}	K_{f2}	kf_3
S9.5B	1.895E+05	8.253	4.189
RS9.5B	1.682E+02	7.622	3.403
S9.5C	2.424E+11	8.253	4.972
RS9.5C	4.296E+02	7.547	3.354
S12.5C	5.021E-01	7.902	3.258
RS12.5C	1.128E-05	8.000	2.616
I19B	1.691E-08	8.090	2.385
RI19B	1.225E-14	7.392	1.191
I19C	1.815E-05	7.275	2.374
RI19C	2.813E-08	7.609	2.126
B25B	4.782E-09	7.507	1.951
RB25B	2.323E-18	7.762	0.958

Table 6.6. Summary of Regression Coefficients for Empirical Model from Direct Tension Fatigue Simulation (psi-based)

mixture	K_{f1}	K_{f2}	kf_3
S9.5B	5.82E+01	8.253	4.189
RS9.5B	2.36E-01	7.622	3.403
S9.5C	1.64E+07	8.253	4.972
RS9.5C	6.61E-01	7.547	3.354
S12.5C	9.31E-04	7.902	3.258
RS12.5C	7.22E-08	8.000	2.616
I19B	1.69E-10	8.090	2.385
RI19B	1.23E-15	7.392	1.191
I19C	1.85E-07	7.275	2.374
RI19C	4.64E-10	7.609	2.126
B25B	1.11E-10	7.507	1.951
RB25B	3.65E-19	7.762	0.958

Comparisons of simulation results at different temperatures (5°C, 19°C and 27°C) are presented in Figure 6.38, Figure 6.39, and Figure 6.40, respectively It is seen that at all three temperatures, a mixture's fatigue performance drops as its NMAS increases; i.e., the 9.5 mm mixtures exhibit the most fatigue resistance, whereas the 25 mm mixtures are the most prone to fatigue damage. It is observed also that, in general, non-RAP mixtures are more fatigue resistant than RAP mixtures at all temperatures, except that at 5°C the RS9.5C mixture exhibits better performance than the S9.5C mixture. In addition, the difference in fatigue performance among the mixtures increases with the test temperature. In other words, at a high temperature such as 27°C, an asphalt mixture's fatigue performance is more mixture type-dependent than at a low temperature.

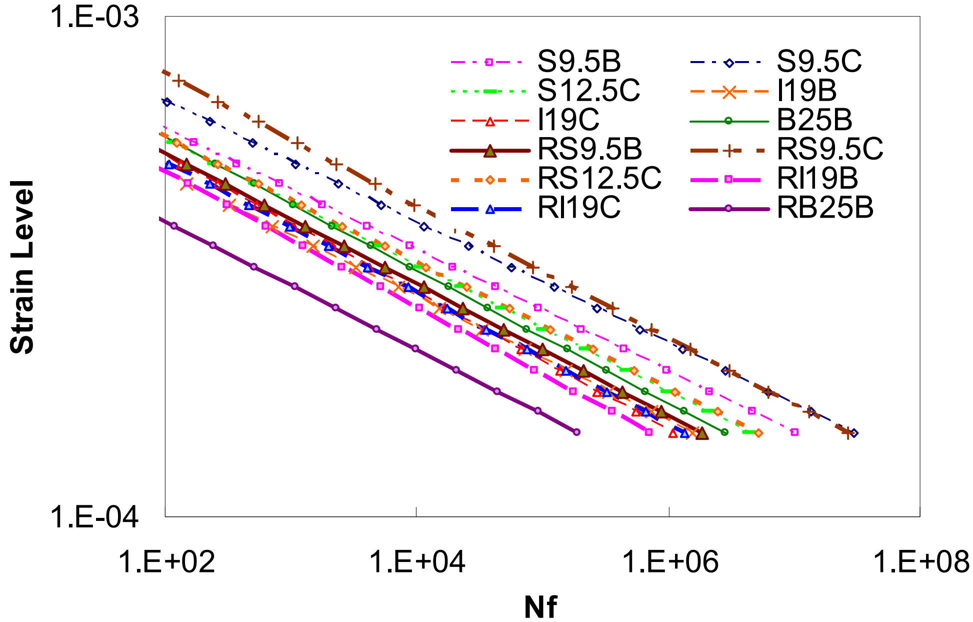

Figure 6.38. 5°C strain-controlled direct tension fatigue test simulations for all mixtures.

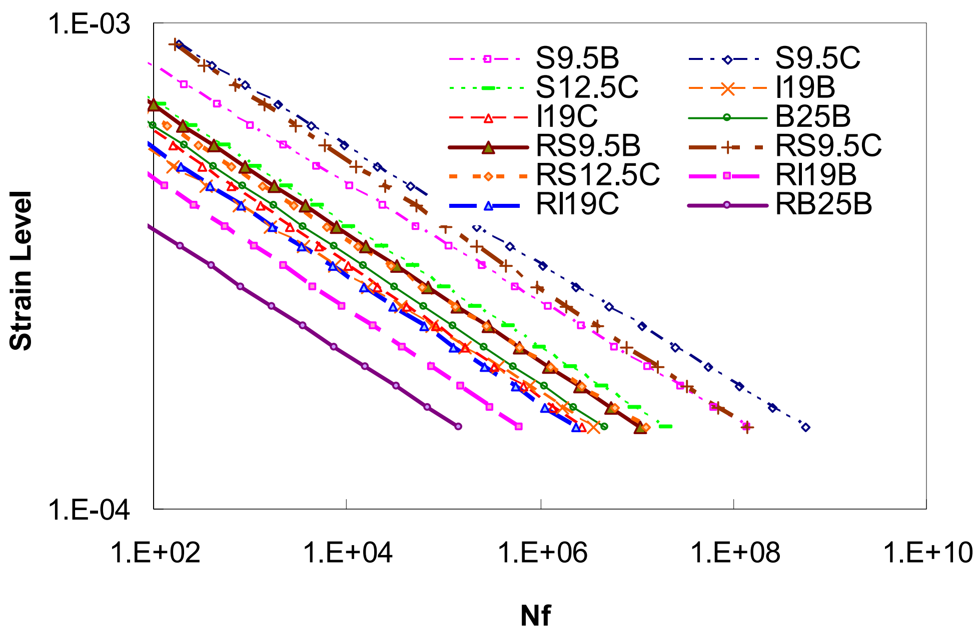

Figure 6.39. 19°C strain-controlled direct tension fatigue test simulations for all mixtures.

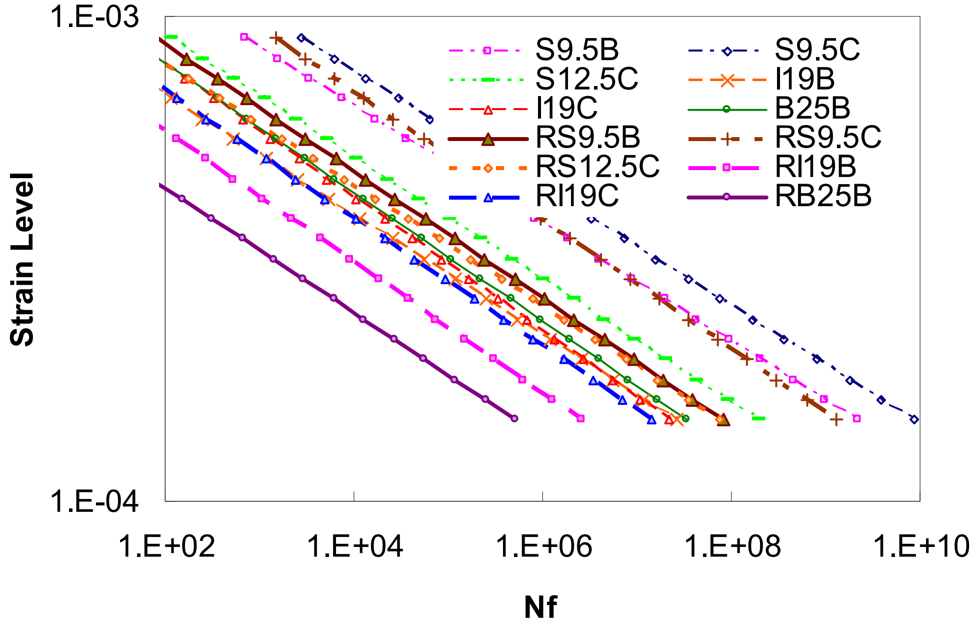

Figure 6.40. 27°C strain-controlled direct tension fatigue test simulations for all mixtures.

6.7.5 Beam Fatigue Simulation

Another important application of the simplified VECD model is to simulate the traditional beam fatigue test. In this study, the method proposed by Christensen and Bonaquist (2005) is used. During the analysis, a standard beam was divided into ten equal layers from top to bottom, each with a thickness of 5 mm. The test was simulated in strain-controlled mode; i.e., the tensile strain amplitude at the bottom of the beam reaches a constant peak value during each cycle and returns to zero at the end of each cycle. The entire loading history was divided into logarithmically spaced intervals, and the accumulated damage during each interval was calculated using Equation (6.47) for each layer. The cyclic portion of the pseudo strain calculation in Equation (6.36) was used. Note that β is equal to 1 in this case. The resulting pseudo stiffness can then be calculated at the end of each loading interval. The modulus of each layer was assumed not to change during the test; however, the effective width of each layer was adjusted proportionally to the pseudo stiffness due to the damaged caused in the previous interval; see Equation (6.55).

$$(w_{eff})_i = (w_{ini})_i \cdot C_i^* \quad (6.55)$$

where

W_{eff} = effective width;
W_{ini} = initial width; and
i = layer index.

A new moment of inertia and neutral axis were then calculated based on the new beam dimensions. Note that damage occurs only below the neutral axis; for the layers above the neutral axis, their effective widths remain constant, as they are subjected to compressive stress only. The simulation process is illustrated graphically in Figure 6.41.

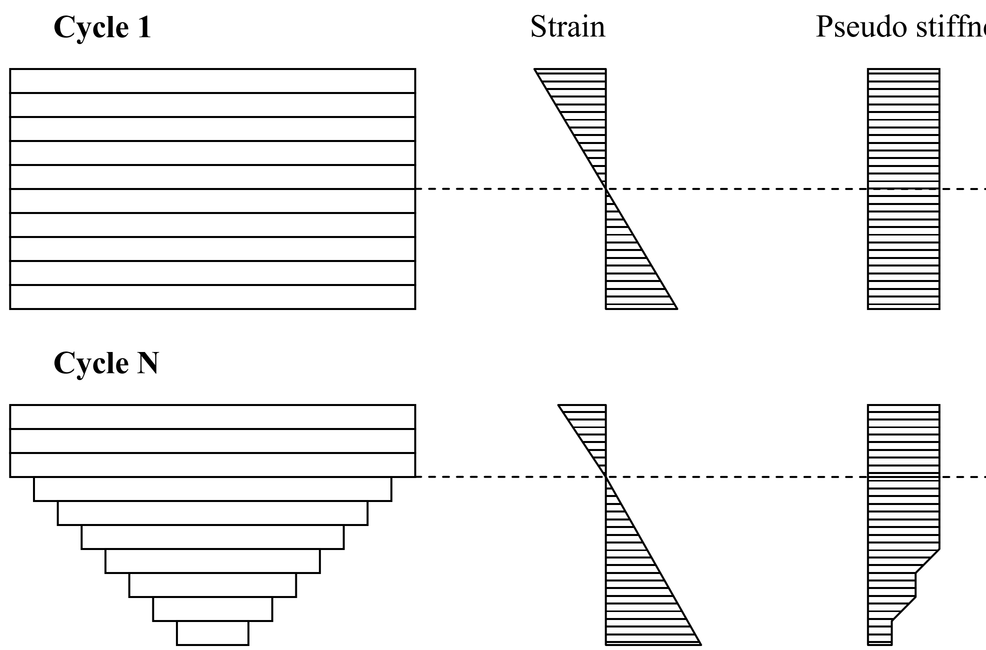

Figure 6.41. Beam fatigue test simulation process.

For each layer, when the pseudo stiffness touches the failure envelope, as described in Section 6.7.3, its effective width is assumed zero for the rest of the analysis. For the entire beam structure, failure is defined by the 50% stiffness reduction criterion, of which the stiffness ratio at cycle N is calculated using Equation (6.56).

$$S(N) = \frac{I_N}{I_{ini}} \quad (6.56)$$

where I_{ini} and I_N are moments of inertia at the 50th and at the Nth loading cycle, respectively.

Figure 6.42 shows an example of the beam fatigue simulation results.

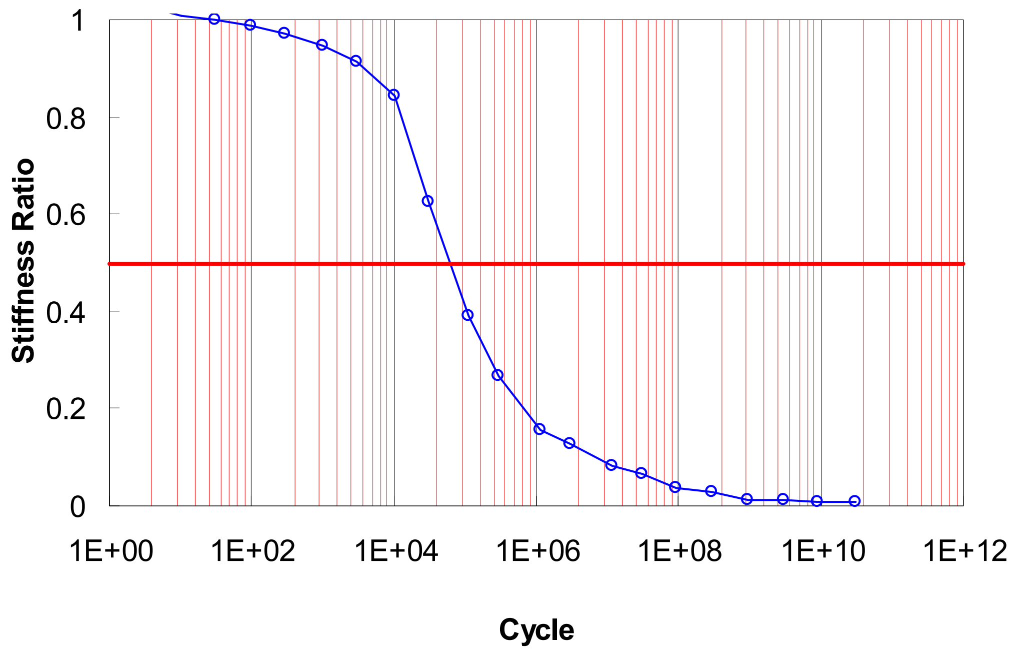

Figure 6.42. Example of beam fatigue simulation results.

Similar to the process used for the direct tension fatigue simulation, beam fatigue tests subjected to different strain levels were simulated to give different fatigue lives. Those results were then fitted by the empirical model. Figure 6.43 and Figure 6.44 show the simulation results at 5°C, 19°C and 27°C. Table 6.7 summarizes the regression coefficients for the empirical model.

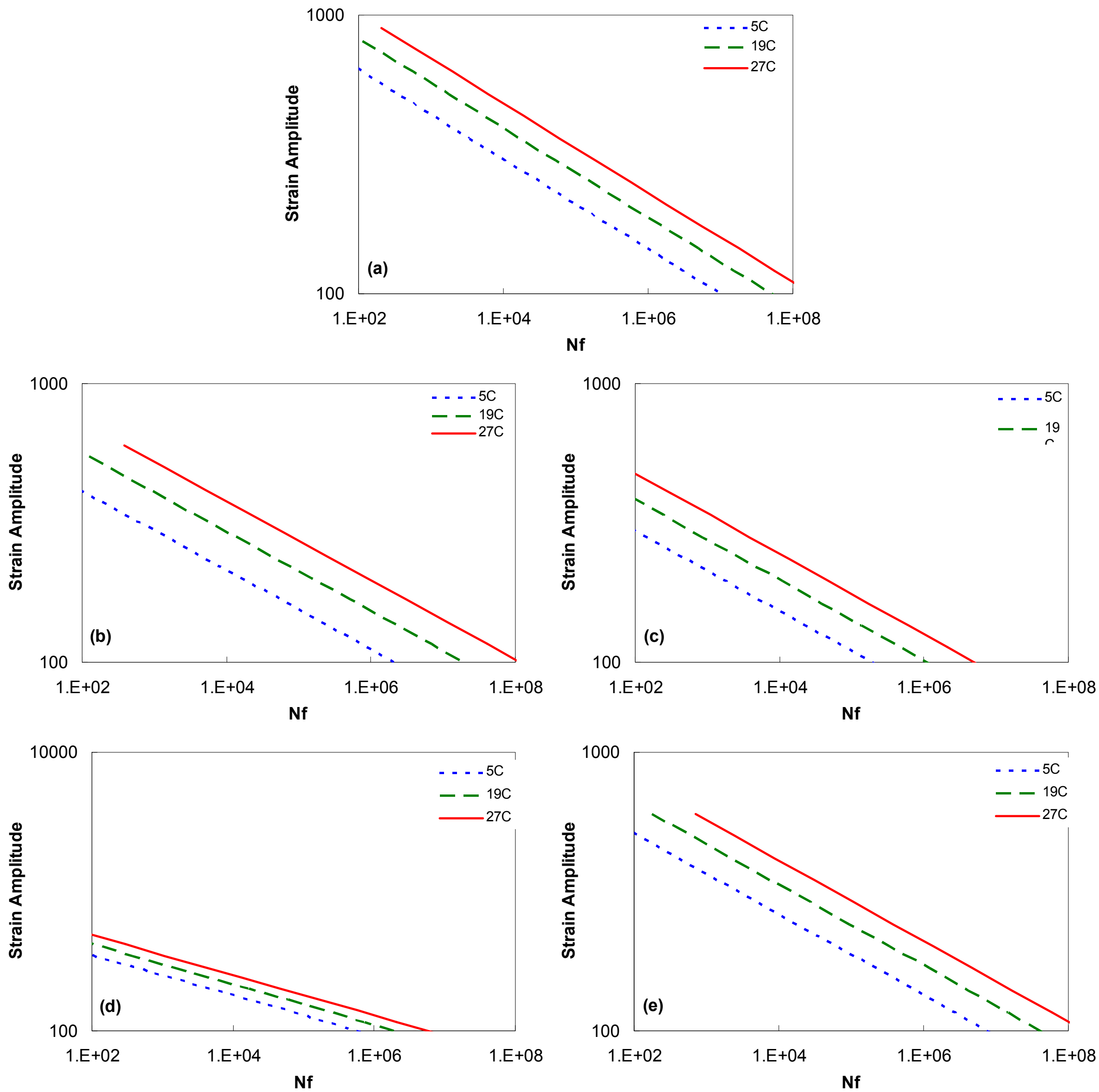

Figure 6.43. Beam fatigue test simulation results for: (a) S9.5C; (b) S9.5B; (c) I19.0C; (d) B25.0B; and (e) RS9.5C mixtures.

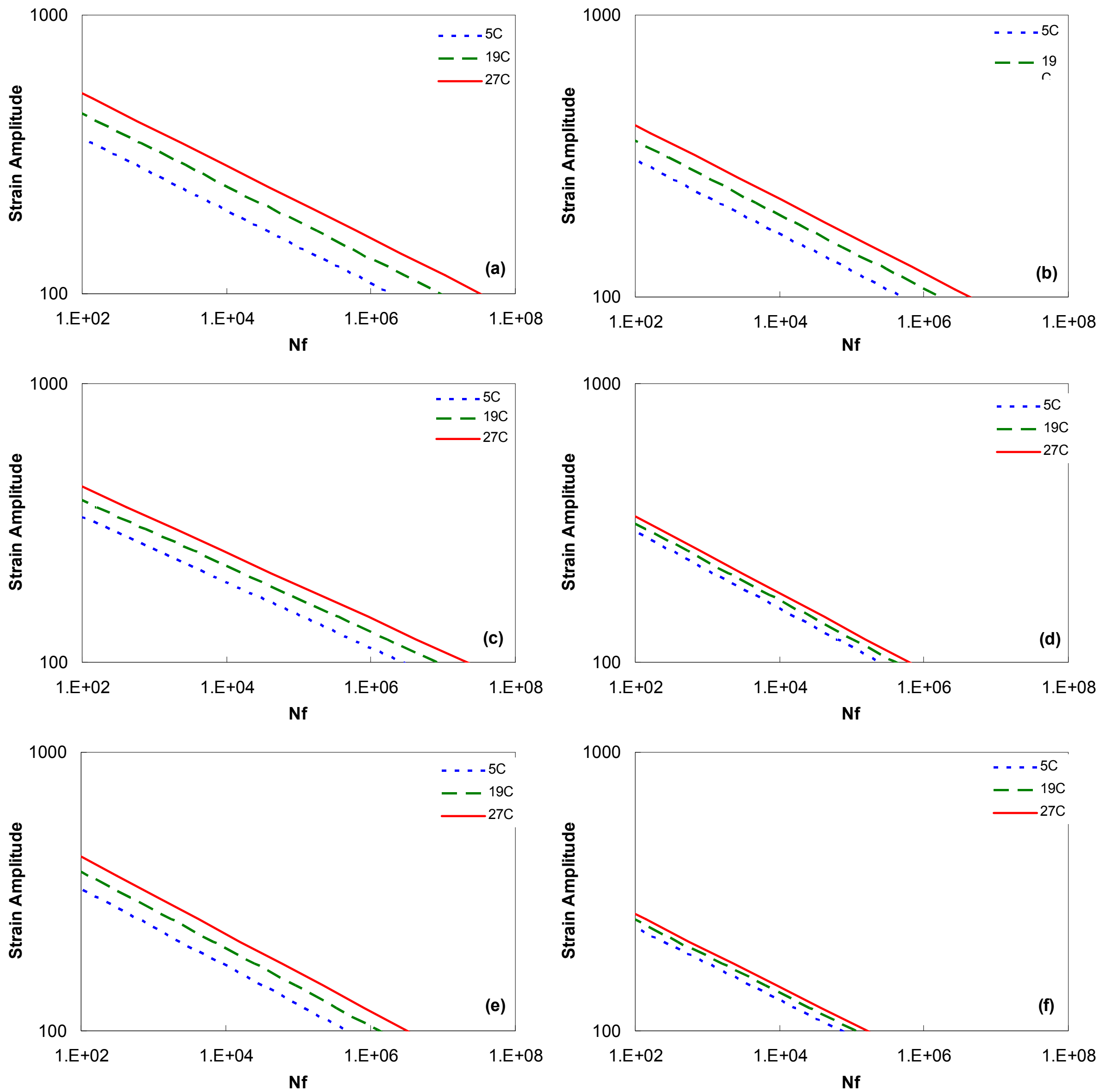

Figure 6.44. Beam fatigue test simulation results for: (a) S12.5C; (b) I19.0B; (c) RS12.5C; (d) RI19.0B; (e) RI19.0C; and (f) RB25.0B mixtures.

Table 6.7. Summary of Regression Coefficients for the Empirical Model as Obtained from Beam Fatigue Simulations

mixture	k_1	k_2	k_3
S9.5B	1.83E+00	7.056	-3.096
S9.5C	6.96E-01	6.235	-2.481
RS9.5C	1.19E-02	6.914	-2.609
S12.5C	1.06E-07	7.688	-2.43
RS12.5C	1.69E-13	8.454	-2.002
I19.0B	2.65E-12	7.609	-1.829
RI19.0B	5.45E-18	7.231	-0.859
I19.0C	2.71E-04	6.916	-2.595
RI19.0C	1.87E-11	7.203	-1.691
B25.0B	1.06E-09	6.919	-1.784
RB25.0B	1.01E-20	7.675	-0.807

Also, similar to the process that was used for the direct tension fatigue simulations, comparisons of the fatigue performance between different mixtures at three different temperatures (5°C, 19°C and 27°C) were made, as shown in Figure 6.45, Figure 6.46, and Figure 6.47, respectively. The results are consistent with those obtained from the direct tension fatigue simulation; i.e., a mixture's fatigue resistance decreases as the NMAS increases, and non-RAP mixtures exhibit better fatigue performance than RAP mixtures.

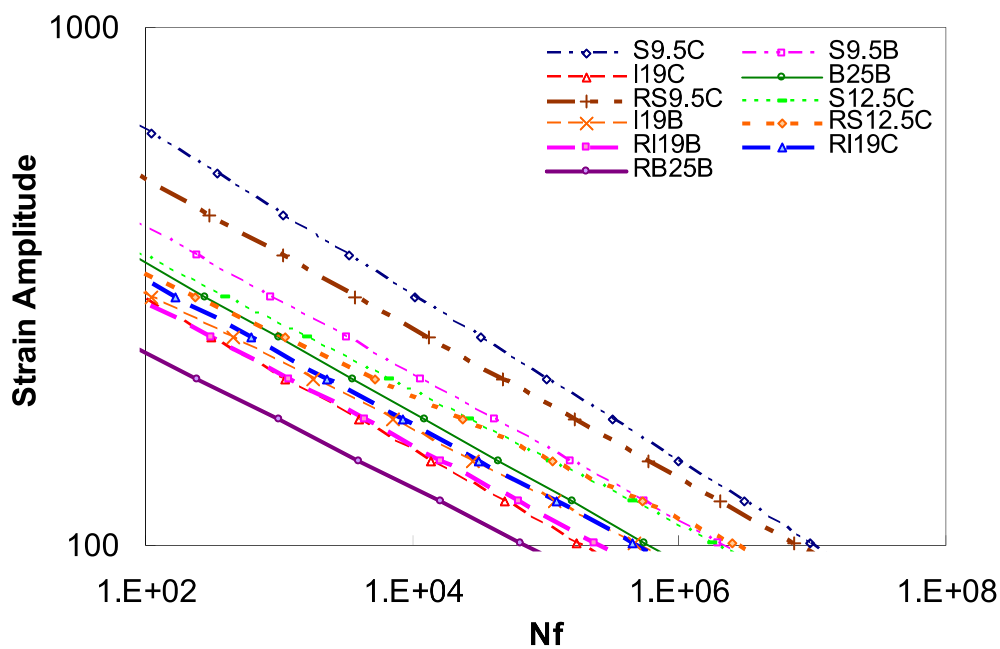

Figure 6.45. 5°C beam fatigue test simulations for all mixtures.

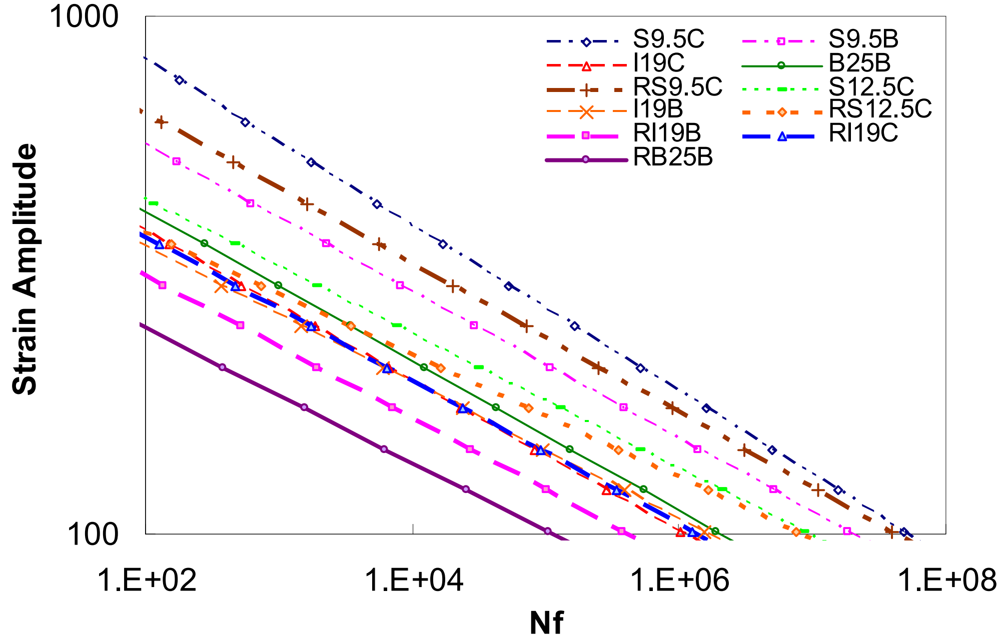

Figure 6.46. 19°C beam fatigue test simulations for all mixtures.

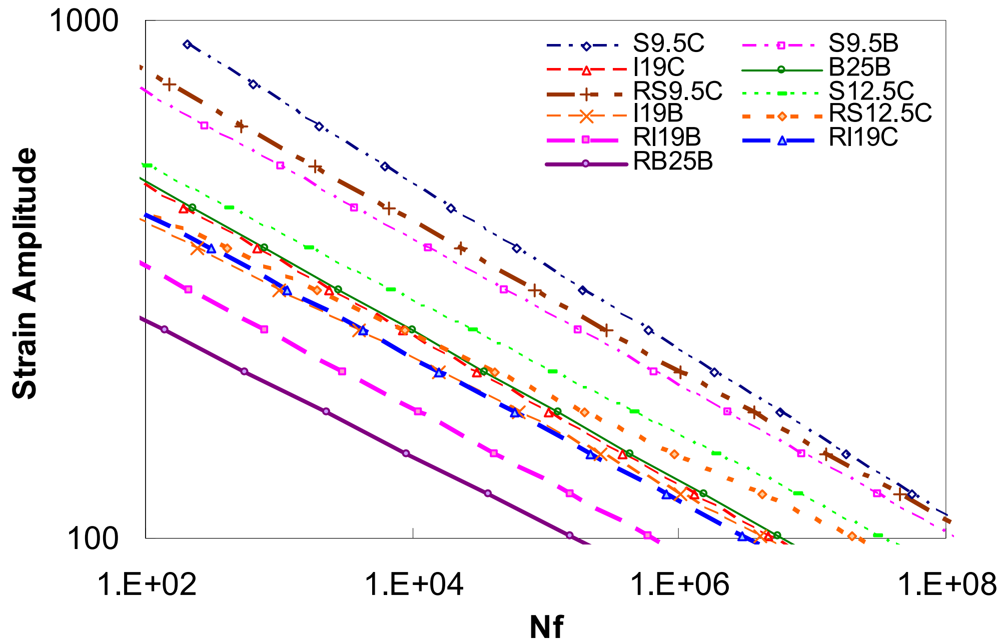

Figure 6.47. 27°C beam fatigue test simulations for all mixtures.

It is found that the slopes of the fatigue envelopes for the different mixtures are quite close to each other for both the direct tension and beam fatigue tests. By comparing the positions of those straight lines, it is simple to rank the fatigue life of the different mixtures under the same loading condition. The fatigue performance rankings obtained from both the direct tension and beam fatigue simulations are summarized in Table 6.8. The findings suggest that the two simulation approaches provide close mixture performance rankings under different test conditions.

Table 6.8. Summary of Fatigue Performance Rankings

Mixture	Fatigue Resistance Ranking from Direct Tension Fatigue Simulation			Fatigue Resistance Ranking from Beam Fatigue Test Simulation		
	5°C	19°C	27°C	5°C	19°C	27°C
S9.5C	2	1	1	1	1	1
S9.5B	3	3	3	3	3	3
I19C	8	7	6	10	7	7
B25B	5	6	5	6	6	5
RS9.5C	1	2	2	2	2	2
S12.5C	4	4	4	4	4	4
I19B	9	8	8	8	8	8
RS12.5C	6	5	7	5	5	6
RI19B	10	10	10	9	10	10
RI19C	7	9	9	7	9	9
RB25B	11	11	11	11	11	11

6.8 Conclusions and Future Research Recommendations

In this fatigue study, a simplified form of the VECD model has been derived that is capable of utilizing cyclic fatigue test data at multiple temperatures and strain magnitudes. The advantage of this simplified model over the rigorous model is that it can characterize HMA's fatigue performance quickly using cyclic data without computations at each time step. This advantage is extremely important for the newly released AMPT equipment that has a load level limitation for performing constant rate tension tests. The model was verified by characterizing the 12 most commonly used asphalt concrete mixtures in North Carolina. The results show that the model can be applied to predict the fatigue life of asphalt concrete under cyclic loading at multiple temperatures and strain levels. The model can also be applied to simulate both strain-controlled direct tension cyclic tests and beam fatigue tests. In addition, fatigue model coefficients were determined for the MEPDG calibration effort.

However, there is room for improvement. For example, the failure criterion incorporated in the prediction of fatigue life is empirical and contains certain shortcomings. A more theoretically-based failure criterion is needed to improve the accuracy of the fatigue performance prediction. The simulated direct tension and beam fatigue results that use the simplified VECD model have not yet been verified by real experiments. The relationship between the simulated results and experimental results would be a valuable research topic for the future.

CHAPTER 7 CHARACTERIZATION OF NORTH CAROLINA TRAFFIC FOR THE MEPDG

7.1 Introduction

Distress in flexible pavements can be classified under two categories: nonload-associated distress and load-associated distress. Hanson et al. (2009) relate the cause of nonload-associated distress in asphalt concrete pavements to age hardening of the asphalt matrix, which begins during construction and continues throughout the pavement service life. Transverse cracking is a good example of a nonload-associated distress that appears at approximately a right angle to the pavement center line. These transverse cracks (also called thermal cracks) usually are associated with shrinkage due to very low temperatures. Load-associated distresses, such as rutting and fatigue cracking, usually occur because of repeated heavy vehicle wheel loads (truck traffic). Worth mentioning is that North Carolina highways do not suffer as significantly from nonload-associated distress; rather, fatigue cracking and, to a lesser extent, rutting are the two distresses responsible for pavement failures in North Carolina.

Because of the negative effect of traffic on the service life of pavement structures, the developers of the MEPDG put significant effort into considering various traffic factors in the pavement design process. In the MEPDG, the traffic parameters required for pavement design have increased in type and complexity compared to those required by the current 1993 AASHTO pavement design guide. For example, prior to the MEPDG, traffic loading was handled through the concept of *equivalent single axle load* (ESAL). The ESAL is a “standard” or “equivalent” 18-kip single axle that was developed from the AASHO road test to simplify the process of estimating the magnitude and number of load repetitions applied to a pavement structure. In the MEPDG, however, traffic loads are handled through a more complicated process called *axle load spectra* in which all traffic loads are analyzed based on vehicle class, axle type, and axle load. This change from ESALs to axle load spectra and other changes led to the need for more detailed traffic parameters to be considered for the MEPDG. These parameters include, for example, vehicle class distribution, number of axles per vehicle class, axle load data measured from WIM sites, and more.

The goal of this chapter is three-fold: 1) to present the new traffic parameters that have been introduced into the MEPDG and to explain the role of each of these parameters; 2) to discuss ways that MEPDG software was used to help develop these various traffic parameters based on their effects on pavement performance; and 3) to present the final results of the North Carolina local traffic characterization project by Stone et al. (2010) under NCDOT Project No. HWY-2008-11.

Furthermore, the research team has developed the *North Carolina MEPDG User Reference Guide*, a copy of which can be found in Appendix H of this report. The *North Carolina MEPDG User Reference Guide* includes complete step-by-step instructions to populate the various materials and traffic inputs required by the MEPDG and to execute the MEPDG.

7.2 A Comprehensive List of Traffic Input Parameters Required by the MEPDG

In comparison to the different versions of the AASHTO design guide, the MEPDG offers users control over many traffic parameters that were never considered directly in any version of the AASHTO design guide. Table 7.1 is a comprehensive list of the input traffic parameters required by the MEPDG.

For many of the traffic parameters listed in Table 7.1, the MEPDG offers users some built-in national average default values. Some of these national default values, such as those for tire pressure, axle spacing and dual tire spacing, can be used by almost all state highway agencies because they are generally not dependent on location or traffic stream characteristics. Other factors, however, can be dependent on local traffic characteristics, and hence, characterization of such traffic parameters to reflect local traffic becomes an important task that each state highway agency should undertake. Depending on the level of detail available for each of these parameters, the MEPDG offers different hierarchical data input levels. For large projects, such as interstate highways and major arterials, it is usually important to provide traffic information at the highest level of detail available. In general, the more accurate the data, the higher the design reliability effectively will be. Section 7.3 explains the hierarchical traffic data input levels available in the MEPDG.

Table 7.1. Traffic Input Parameters Required by the MEPDG

General Traffic Inputs	Initial two-way average annual daily truck traffic (AADTT)
	Number of lanes in design direction
	Percentage of trucks in design direction
	Percentage of trucks in design lane
	Operational speed
	Mean wheel location (inches from lane marking)
	Traffic wander standard deviation
	Design lane width
	Average axle width
	Dual tire spacing
	Tire pressure
	Tandem axle spacing
	Tridem axle spacing
	Quad axle spacing
	Average steering axle spacing (steering to first driving axle)
	Percentage of trucks in each steering axle spacing category (short,
Axle Load Distribution Factors (ALDF)	
Number of Different Axle Types per Truck Class (APT)	
Traffic Volume Adjustment Factors	Monthly adjustment factors (MAF)
	Vehicle class distribution (VCD)
	Hourly distribution factors (HDF)
Options Available for Traffic Growth Consideration	1- No growth
	2- Linear
	3- Compound (default is 4%)
	4- Class-specific

7.3 Hierarchical Traffic Data Input Levels

The MEPDG offers users the flexibility of selecting different levels of sophistication and detail for many of the required traffic inputs. The MEPDG offers three hierarchical traffic data input levels (Levels 1 through 3). These levels indicate how well the pavement designer can estimate future truck traffic characteristics for the roadway being designed (NCHRP, 2004a). The selected level of input detail typically is governed by two factors: the resources available to collect detailed traffic data that are required for accurate future traffic characteristics prediction, and the size and functional importance of the project. Users can choose from the following three hierarchical input levels:

- Level 1 requires site-specific traffic data that are measured at or near the road segment or the site under study. These data include weight and volume data. This level requires very good knowledge of the traffic history at that particular site and requires good knowledge about future traffic at that site, i.e., traffic forecasting. Level 1 is the most accurate level of input because it considers actual traffic factors at the site.
- Level 2 relies mainly on accurate measurements of truck volume and the percentage of trucks at or near the site under study. However, weight data normally are obtained by taking the average of similar data types at neighboring sites. Furthermore, this level requires a good understanding of the daily and seasonal variations of traffic volume at the site.
- Level 3 requires the least amount of traffic knowledge about the site under study. Nonetheless, it requires that some data, e.g., volume data and percentage of trucks data, be measured at the site. Weight data for Level 3 are estimated using either predicative equations and/or statewide or regional averages. Table 7.1 lists the traffic parameters required by the MEPDG.

7.4 Traffic Volume Adjustment Factors

The MEPDG offers a unique and rational way of handling traffic volume changes and traffic growth. Monthly and hourly volume changes are considered through monthly adjustment factors (MAF) and hourly distribution factors (HDF), respectively. The vehicle class distribution factors (VCD) distribute the total volume into volumes for each vehicle class. The MEPDG offers the flexibility of entering a different traffic growth rate for each vehicle class. In addition, the MEPDG offers three options/functions for growth occurrence (if any): no growth, linear growth, and compound growth. At this point, it is vital to know the available vehicle classes and which of these vehicle classes are considered by the MEPDG. Figure 7.1 shows the FHWA vehicle classification scheme F report.

The FHWA scheme F classifies all vehicle types into 13 vehicle classes. Out of these 13 vehicle classes, the MEPDG considers classes 4 through 13 only. Vehicles classified under classes 1 through 3 are believed to affect the pavement very little, and hence, they are ignored in damage calculations.

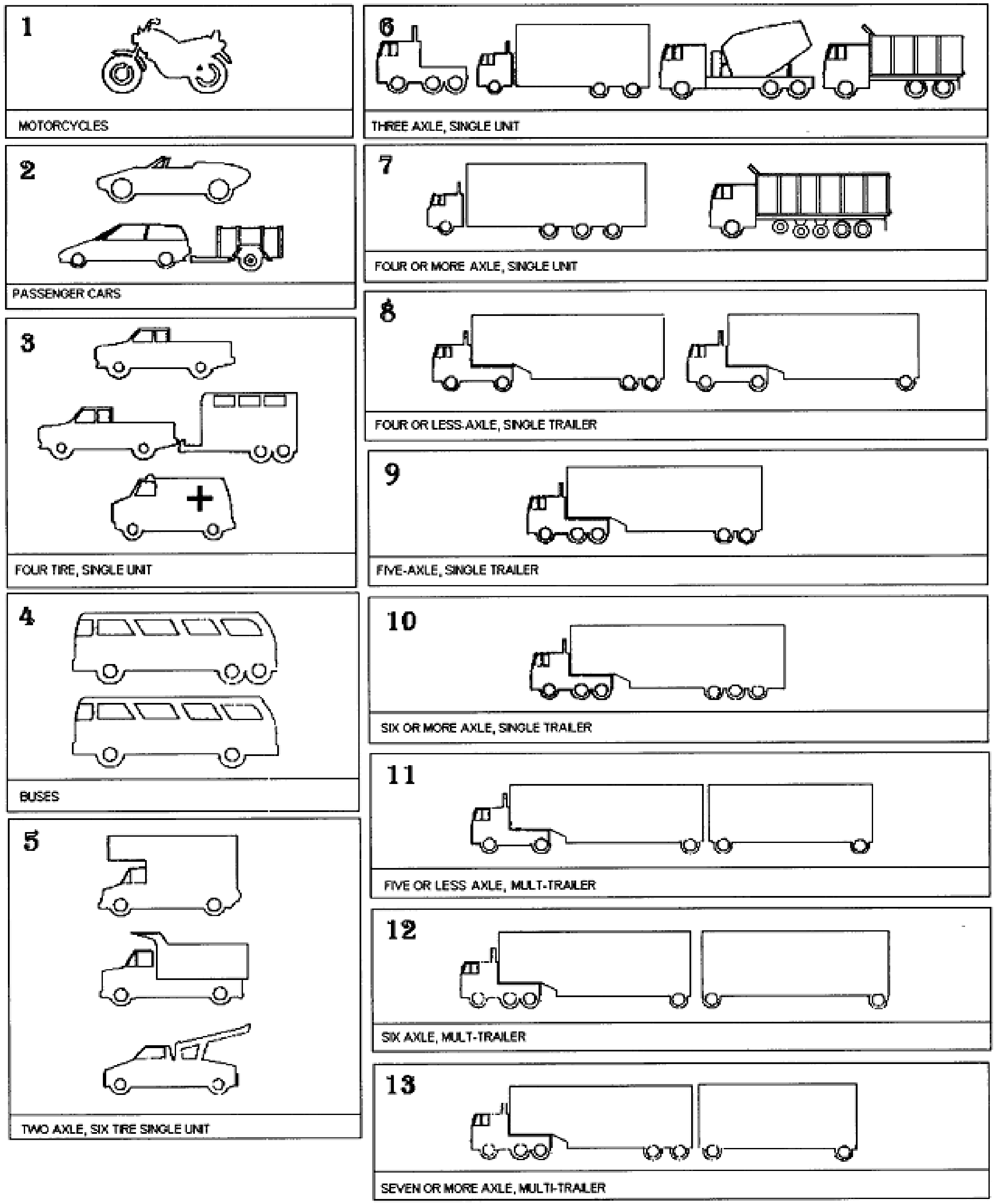

Figure 7.1. FHWA vehicle classification scheme F report (courtesy of the FHWA).

The following subsections provide more information regarding the available traffic volume adjustment factors and explain the functionality of each of these factors.

7.4.1 Monthly Adjustment Factors (MAF)

Monthly adjustment factors (MAF) represent the distribution of the annual truck traffic volume of every truck class within each month of the year. MAF depend on many factors, including the location of the road segment, i.e., whether it is urban or rural, adjacent land use, and climate. Figure 7.2 shows a MAF window captured from the MEPDG

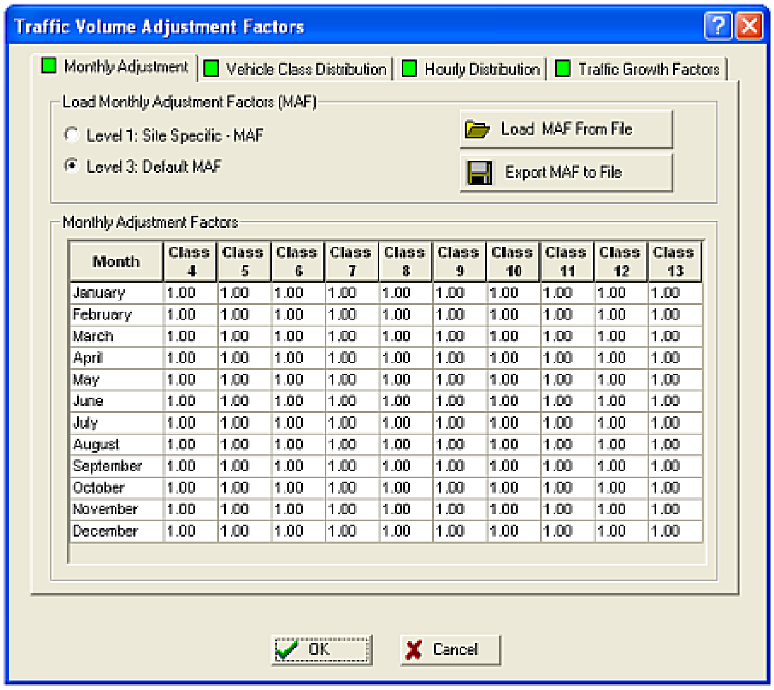

Figure 7.2. A screen capture of the MEPDG monthly adjustment factors (MAF) window.

For local MAF characterization, an assumption is made that different vehicle classes have the same MAF. In other words, after loading the local MAF file into the MEPDG, the image shown in Figure 7.2 will appear with columns that contain cells with similar numbers. Figure 7.2 shows the national MAF table with the number one (1.00) appearing in all fields; i.e., the proportion of traffic from the different truck classes do not depend on season.

In a damage-based sensitivity study performed by Stone et al. (2010), different MAF clusters were found to have similar effects on flexible pavement performance, considering sensitivity criteria developed in cooperation with the NCDOT. Therefore, Stone et al. recommended that statewide average MAF data be used for the design of flexible pavements. Final recommended MAF data are presented in a subsequent section of this chapter.

7.4.2 Vehicle Class Distribution Factors (VCD)

Vehicle class distribution (VCD) factors represent the proportion of each truck class type within the total truck traffic. Figure 7.3 shows a screen capture of the VCD window in the MEPDG.

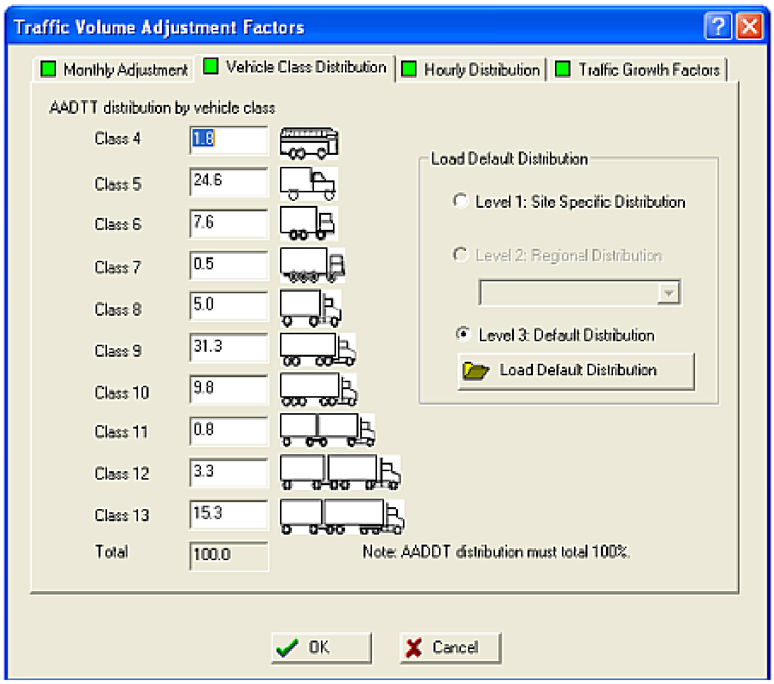

Figure 7.3. A screen capture of the MEPDG vehicle class distribution (VCD) factors window.

The MEPDG offers 17 truck traffic classification (TTC) schemes that can be selected based on the road segment functional classification. These schemes were derived from national data obtained from the LTPP program. When considering national VCD data, the MEPDG offers six highway functional classes from which to choose: principal arterials – interstate and defense; principal arterials – other; and minor arterials, major collectors, minor collectors, and local routes and streets. Upon selection of one of these five classes, the MEPDG recommends a certain TTC.

Figure 7.4 shows a screen capture from the MEPDG of the available truck traffic classification schemes in addition to the available highways functional classes. Stone et al. (2009) performed VCD characterization for local North Carolina traffic. Note that the aforementioned default classes and TTC groups were not used in the characterization effort. Decision trees developed by Stone et al. (2010) will accept the input from 48-hour counts taken at the project location to recommend a certain set of VCD factors to be used for that project location. Decision trees and final VCD clusters, as recommended by Stone et al. (2010) are presented in a subsequent section of this chapter.

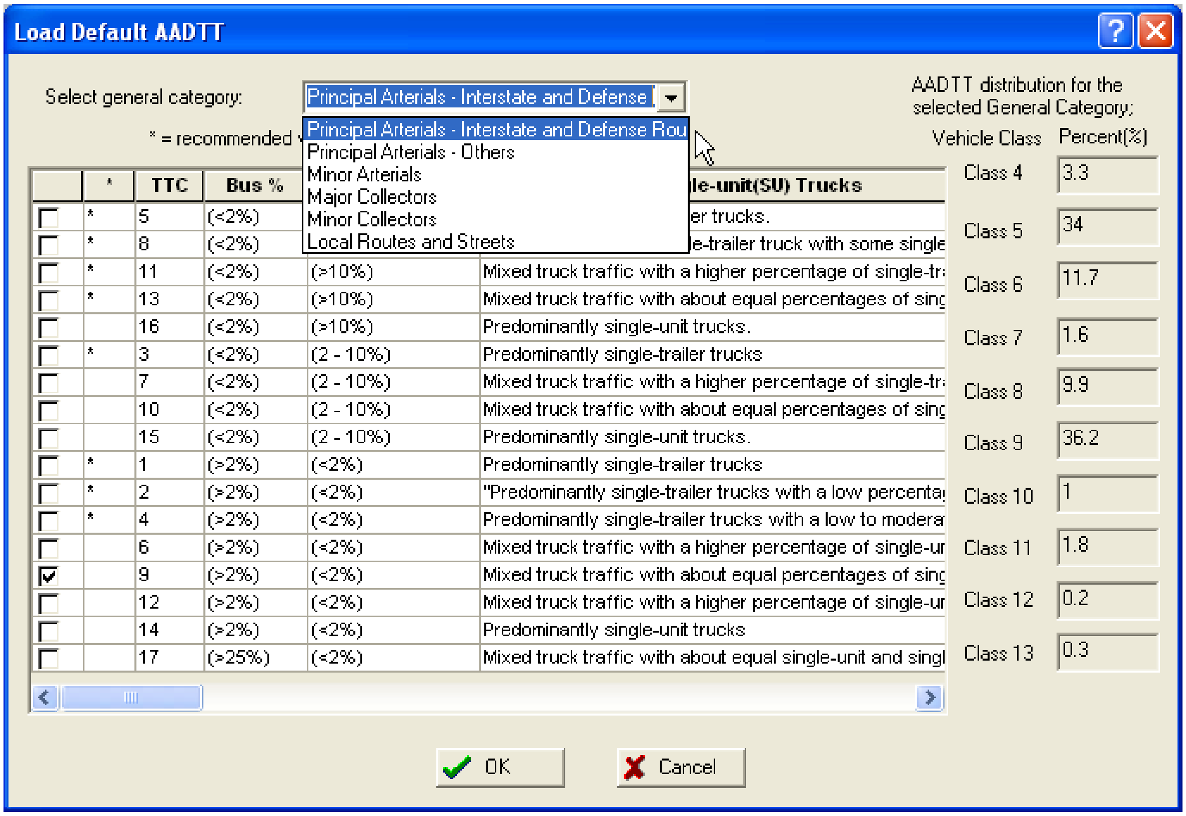

Figure 7.4. A screen capture of the available truck traffic classification (TTC) schemes window in the MEPDG.

7.4.3 Hourly Distribution Factors (HDF)

The hourly distribution factors (HDF) represent the proportion of the average annual daily truck traffic (AADTT) within each hour of the day. For local characterization of HDF, a single statewide HDF set of values was recommended by Stone et al. (2009) for all pavement design projects. Stone et al. made their recommendations based on sensitivity analysis results that show that different HDF inputs result in similar predicted pavement performance, based on sensitivity criteria developed in cooperation with the NCDOT. Figure 7.5 shows a window capture of the HDF in the MEPDG.

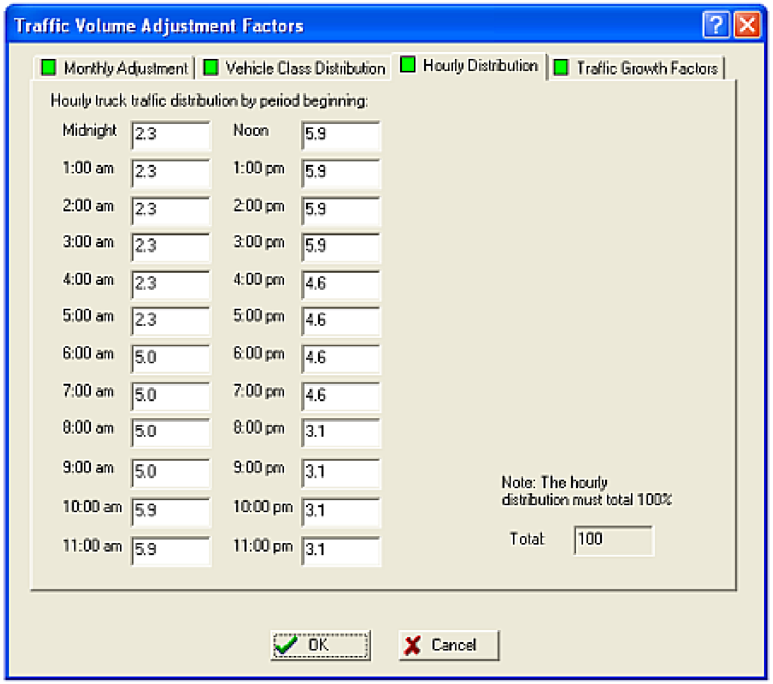

Figure 7.5. A screen capture of the MEPDG hourly distribution factors (HDF) window.

7.4.4 Traffic Growth Functions and Growth Rates

The MEPDG offers users three options for traffic growth: no growth, linear growth, and compound growth. In addition, the MEPDG offers the flexibility of entering different growth functions and growth rates for different vehicle classes if desired. Figure 7.6 shows a screen capture of the traffic growth factors window in the MEPDG when the vehicle class-specific traffic growth option is selected.

The accuracy of traffic volume forecasts plays a crucial role in the success of any pavement design. As mentioned earlier, North Carolina's highways fail mainly under load-associated distresses that are caused by truck traffic. Hence, an underestimation of the future truck traffic can result in the design of a pavement that will fail sooner than desired. On the other hand, an overestimation of the future truck traffic can result in an overdesign that would cost much more than is actually required. It is obvious that future traffic forecasts must be as accurate as possible to save money, but at the same time, design pavements must serve their intended design life. Traffic forecasters must provide the growth rates and functions to pavement designers to input in the MEPDG. Depending on the availability of the data, the growth rates and functions could be single representative values or they could be class-specific values.

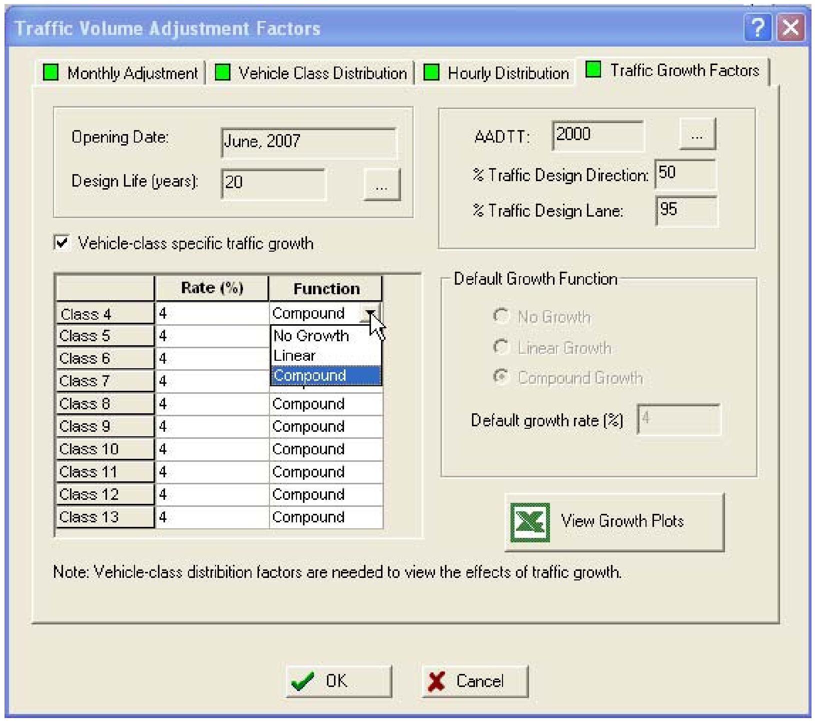

Figure 7.6. A screen capture of the traffic vehicle class-specific growth factors window.

7.5 Axle Load Distribution Factors (ALDF)

Axle load distribution factors (ALDF) represent the percentage of the total number of truck axle repetitions within each load interval (which varies with axle type) for each axle type. The MEPDG considers four types of axles: single, tandem, tridem, and quad. Load intervals range from 3,000 pounds to 40,000 pounds at 1,000 intervals for a single axle, from 6,000 pounds to 80,000 pounds at 2,000 intervals for tandem axles, and from 12,000 pounds to 102,000 pounds at 3,000 intervals for tridem and quad axles (NCHRP, 2004c). Figure 7.7 shows a screen capture of the ALDF window in the MEPDG.

ALDF constitute a major change from the current 1993 AASHTO pavement design guide that requires only the total number of 18-kip ESALs as input. For the local ALDF characterization work performed by Stone et al. (2010), weight data obtained from 44 WIM stations across North Carolina were used to generate unique clusters for the different axle types. Furthermore, Stone et al. produced a decision tree that helps the NCDOT designers select the most representative ALDF cluster for a certain project based on classification data obtained from 48-hour counts. Final ALDF clusters and decision trees are presented in a subsequent section of this chapter.

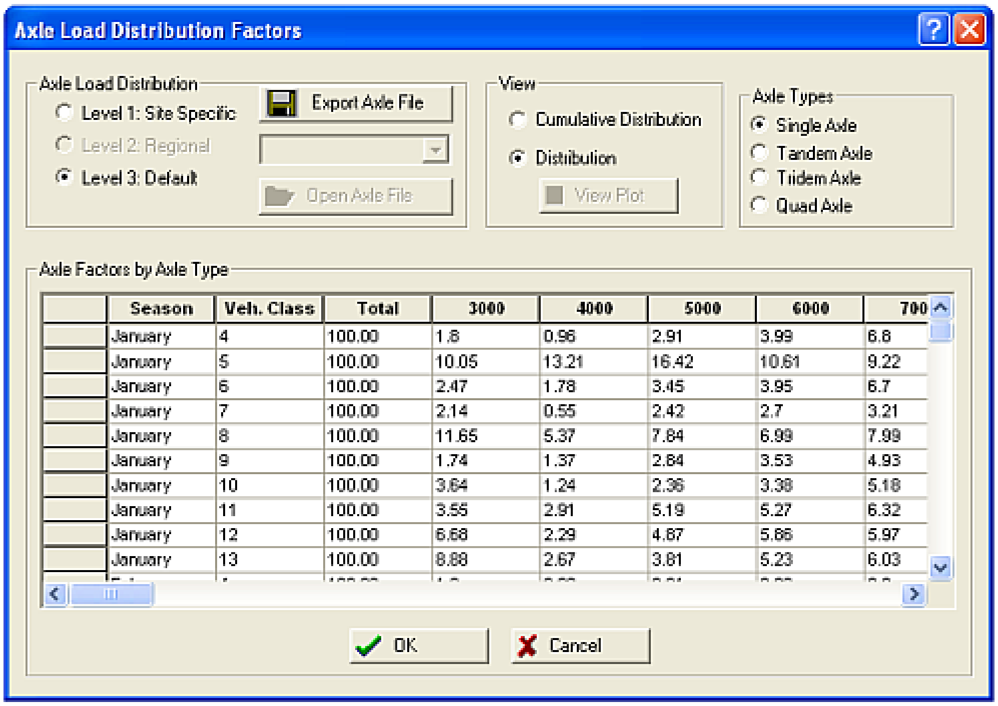

Figure 7.7. A screen capture of the MEPDG axle load distribution factors (ALDF) window.

7.6 Role of Each Traffic Parameter in the Overall Analysis Process

Prior to introducing ways that the pavement damage concept is used to guide the local traffic characterization process, it is beneficial to present an overview of the role of different traffic parameters in the overall framework of the MEPDG Figure 7.8 is a flow chart showing, among other components, the role of each traffic parameter in the analysis flow. The flow chart shown in Figure 7.8 can be summarized in the following steps:

1) When multiplied by the AADTT, the *directional distribution factor* gives the percentage of trucks in the design direction.
2) The *lane distribution factor* further reduces the truck traffic to reflect only the percentage of trucks in the design lane.
3) *Vehicle class distribution* (VCD) *factors* distribute the total number of trucks in the design lane, obtained from Step 2, over the available FHWA vehicle classes 4 through 13.
4) The *monthly adjustment factors* (MAF) redistribute the truck traffic calculated from Step 3 to reflect monthly changes in the truck classes.
5) The *hourly distribution factors* (HDF) modify the percentage of each vehicle class to reflect changes in their volume every hour of the day.
6) As this point in the procedure, the number of truck types is known for every month and every day of the year.
7) For each truck class, the *number of axles per truck* (APT) *factors* calculate the number of each axle type from all truck classes considered so far.

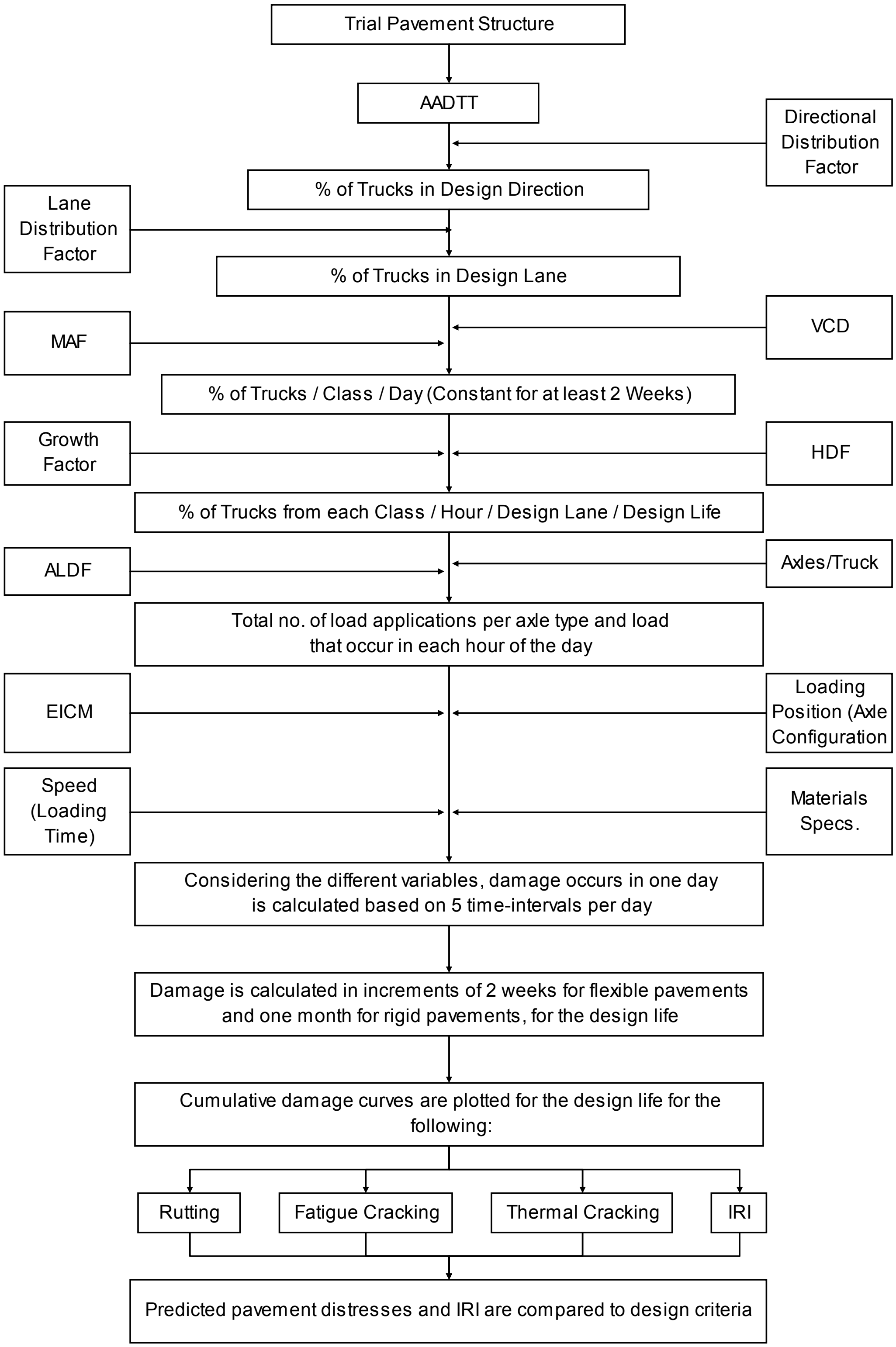

Figure 7.8. Role of traffic parameters in the MEPDG structural analysis.

8) The *axle load distribution factors* (ALDF) contain information about the weight of each axle type.
9) Thus far, the information available provides the total number of load applications per axle type/load combination for each hour of the day.
10) The *structural response model* now considers the material properties, after modifications from the EICM, to account for changes in moisture and temperature profiles, and calculates the critical responses caused by each load application by knowing the loading time (speed) and loading position (axle configuration).
11) Once the critical responses are calculated, *performance prediction models* within the MEPDG predict the damage for the different distress types.
12) *Transfer functions* within the MEPDG convert different types of damage to equivalent distresses and rideability in a form similar to that monitored in the field.
13) Predicted pavement performance is then compared to the design criteria determined at the beginning of the analysis. A design that meets all criteria of the state highway agency becomes a candidate structure.
14) *Life cycle cost analysis* (LCCA) is performed on various trial designs that satisfy the agency performance criteria. The most cost effective design is selected.

The subsequent sections present a comprehensive picture of the traffic characterization elements and discuss in detail two damage-based concepts that were developed to guide the development of traffic parameters for use by NCDOT engineers in the MEPDG.

7.7 North Carolina Traffic Characterization Elements

Figure 7.9 is a flow chart showing the different phases of the traffic characterization process that was adopted by Stone et al. (2010). The purpose of this Section 7.7 is to explain the six phases in this characterization process and to focus on the two tasks in which damage-based concepts were used to guide the development of local traffic parameters for North Carolina. The following paragraphs shed light on each phase by explaining the major work completed and the output.

- Phase 1

  In this phase, one year of volume and weight data were provided by the Traffic Survey Unit (TSU) at the NCDOT. The data were collected by the NCDOT from 44 WIM sites located throughout the three distinct regions (mountains, piedmont, and coast) of North Carolina. The data are comprehensive in terms of location and highway functional classification. The highway functional classifications cover interstates, US routes, NC routes, and local roads. WIM data typically are supplied in the form of W-cards for weight data, and C-cards for classification or volume data. Out of the 44 WIM sites, 19 are located at LTPP sites, and the rest are located at non-LTPP sites.

- Phase 2

  In this phase, all the provided traffic data had undergone comprehensive quality control procedures, performed by Ramachandran et al. (2011), prior to being considered in the traffic characterization work. Comprehensive quality control rules were created to ensure the elimination of anomalies and inconsistent data. WIM data are always prone to different types of quality issues that could arise from sensors dependability on temperature and moisture fluctuations (White et al., 2006). The issues with sensors differ based on their type. As with everything else, each sensor type has its own advantages and disadvantages.

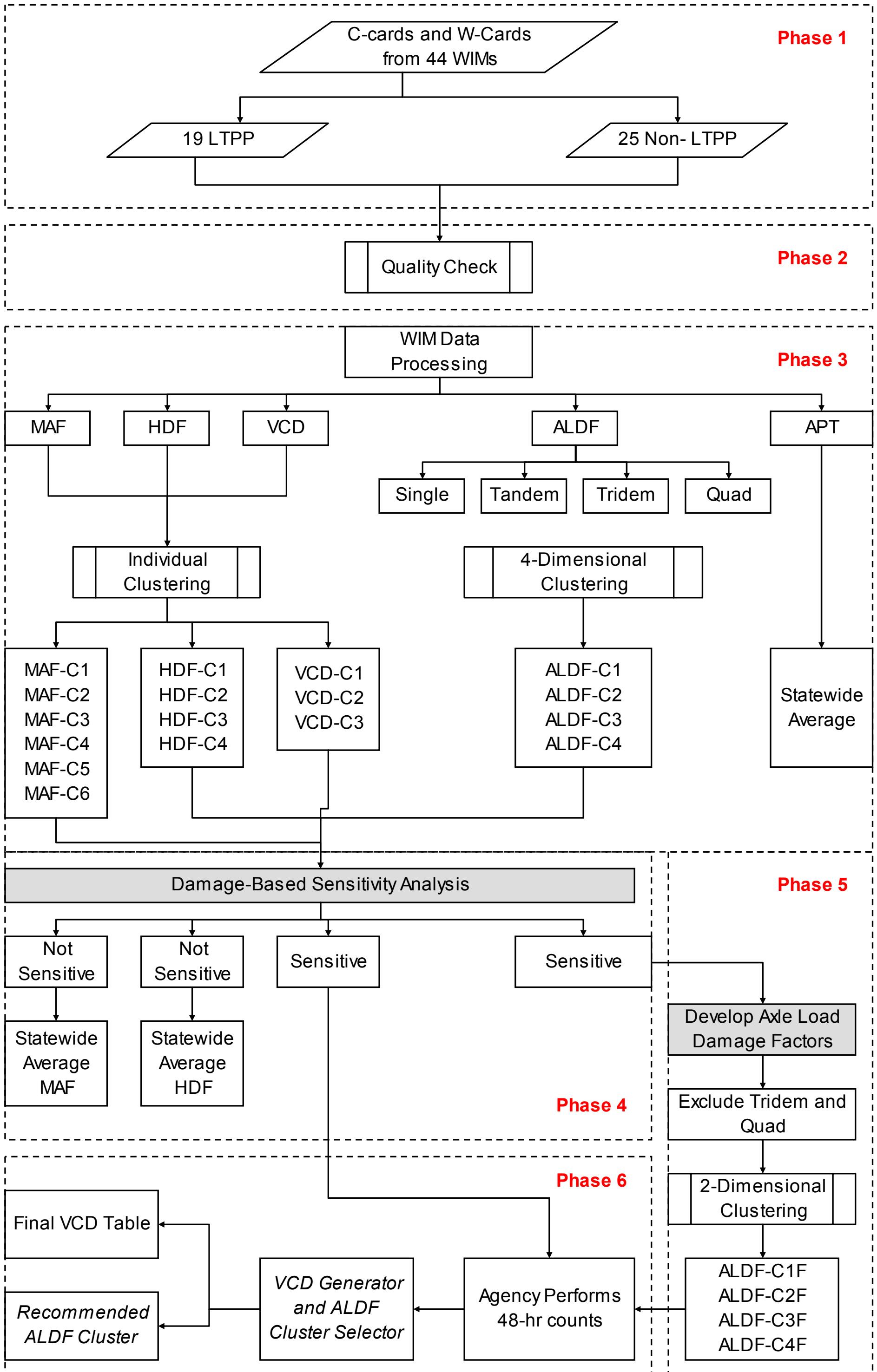

Figure 7.9. Comprehensive flowchart for the traffic characterization approach.

- Phase 3

  During this phase, Stone et al. (2010) analyzed the quality-controlled data from Phase 2 and generated the following traffic parameters for each of the 44 WIM sites: monthly adjustment factors (MAF), hourly distribution factors (HDF), vehicle class distribution factors (VCD), axle load distribution factors (ALDF), and number of axles per truck (APT). Two types of clustering techniques were then applied to group the WIM sites with respect to their similarities in one or more of the aforementioned five traffic parameters. Two types of clustering techniques were applied for this purpose: 1) individual clustering was applied to the MAF, HDF, and VCD data; and 2) four-dimensional clustering was applied to the four axle types of the ALDF. As for the APT, the statewide average was recommended for all pavement designs because this parameter is associated only with the type and axle configurations of heavy vehicles in North Carolina, which does not vary much from one location to another within the state. The results of clustering analysis suggest six clusters or groups for the MAF; i.e., the 44 WIM sites are distributed over six groups that each contains WIM sites with similar MAF data. Four clusters were suggested for the HDF, three for the VCD, and four clusters were suggested as a result of four-dimensional clustering for the ALDF. Details regarding the various clustering analysis techniques can be found in Section 7.7.2.1.

- Phase 4

  This phase is where the damage concept is first introduced in the traffic characterization process. Damage-based sensitivity analysis was performed to check the sensitivity of the predicted pavement performance to changes in each of the four traffic parameters. This step was performed to discern if the different clusters obtained from Phase 3 for the different parameters could be fully or partially combined into fewer clusters. The combination of the different clusters simplifies the design process in terms of the selection of the proper cluster for a certain project. In other words, it is simpler to select from a smaller number of options. The output from Phase 4 suggests that pavement performance is insensitive to changes in MAF clusters, insensitive to changes in HDF clusters, but sensitive to changes in VCD and ALDF clusters. As a result, Stone et al. recommended that statewide averages could be used for MAF and HDF, whereas procedures must be developed to address the effect of VCD and ALDF parameters, which were found to be sensitive. Further information regarding the damage-based sensitivity analysis is presented and discussed in a subsequent subsection.

- Phase 5

  During this phase, the other damage-based concept, i.e., *axle load damage factors*, was introduced. The purpose of this work was to guide the development of ALDF clusters based on the effect of different axle type/load combinations on pavement performance. The results obtained from this phase suggest that tridem and quad axles in addition to some single and tandem axles from the ALDF clustering process should be excluded. As a result, Stone et al. (2010) performed two-dimensional clustering analysis on the remaining single and tandem axles and concluded that there are four final ALDF clusters, as shown in Phase 5 of Figure 7.9. Details regarding the development of damage factors and the results are presented in a subsequent subsection.

- Phase 6

  Phase 6 is the final element in the characterization process. Stone et al. (2010) developed methods that use 48-hour classification data to generate a VCD table and that guide designers to the proper ALDF cluster that should be used for a certain project. Furthermore, Stone et al. (2010) developed a Microsoft Excel-based tool called the *VCD Generator and ALDF Cluster Selector* to simplify the generation of the VCD data and recommend the most appropriate ALDF cluster. The tool is simple to use as it requires users to enter only 48-hour classification counts, and then generates the VCD data and recommends the best ALDF to use. A screen capture of this tool is shown in Figure 7.10, and details can be found elsewhere (Stone et al., 2010).

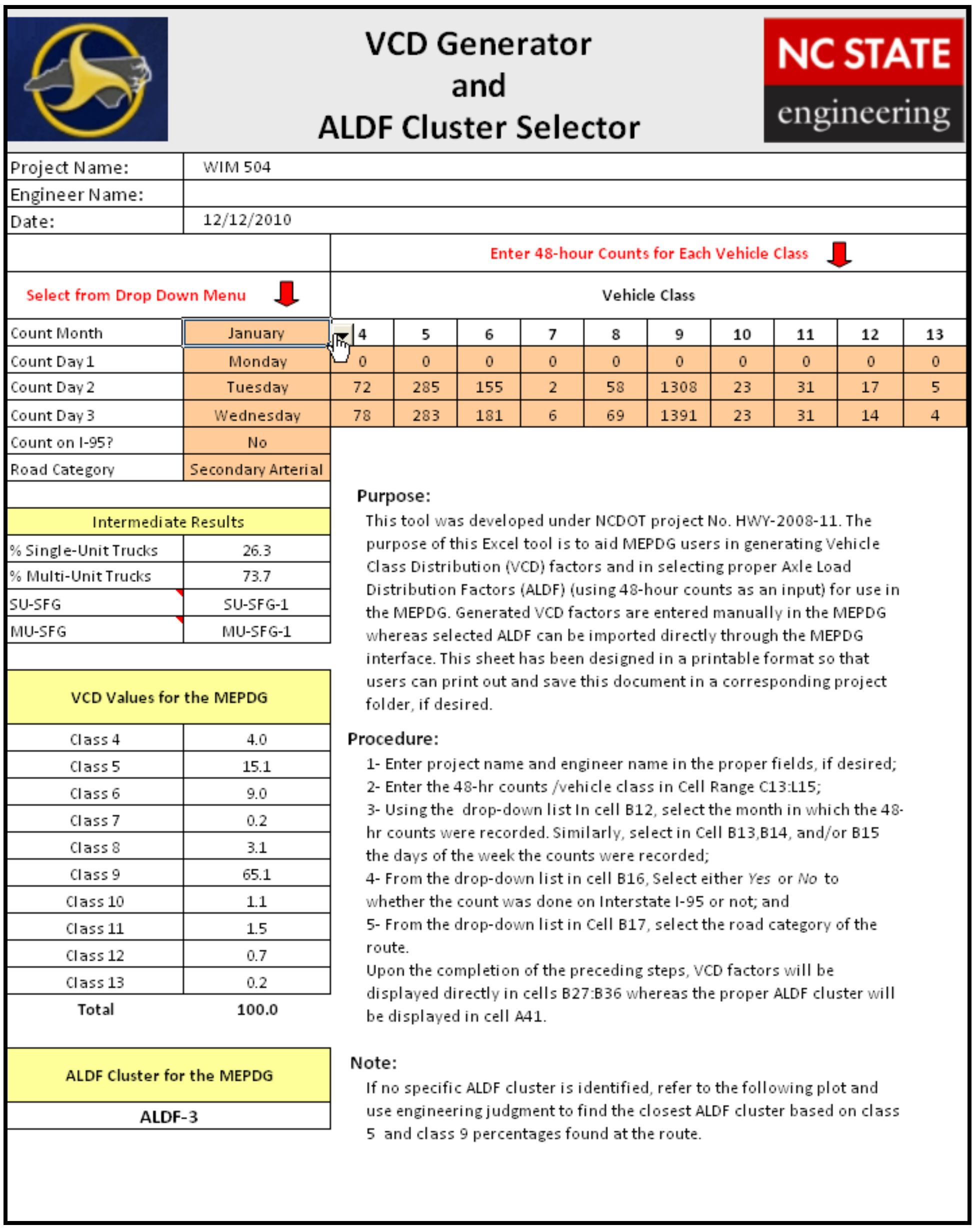

VCD Generator and ALDF Cluster Selector

NC STATE engineering

Project Name:	WIM 504
Engineer Name:	
Date:	12/12/2010

Enter 48-hour Counts for Each Vehicle Class

Select from Drop Down Menu

		Vehicle Class									
Count Month	January	4	5	6	7	8	9	10	11	12	13
Count Day 1	Monday	0	0	0	0	0	0	0	0	0	0
Count Day 2	Tuesday	72	285	155	2	58	1308	23	31	17	5
Count Day 3	Wednesday	78	283	181	6	69	1391	23	31	14	4
Count on I-95?	No										
Road Category	Secondary Arterial										

Intermediate Results

% Single-Unit Trucks	26.3
% Multi-Unit Trucks	73.7
SU-SFG	SU-SFG-1
MU-SFG	MU-SFG-1

VCD Values for the MEPDG

Class 4	4.0
Class 5	15.1
Class 6	9.0
Class 7	0.2
Class 8	3.1
Class 9	65.1
Class 10	1.1
Class 11	1.5
Class 12	0.7
Class 13	0.2
Total	**100.0**

ALDF Cluster for the MEPDG

ALDF-3

Purpose:

This tool was developed under NCDOT project No. HWY-2008-11. The purpose of this Excel tool is to aid MEPDG users in generating Vehicle Class Distribution (VCD) factors and in selecting proper Axle Load Distribution Factors (ALDF) (using 48-hour counts as an input) for use in the MEPDG. Generated VCD factors are entered manually in the MEPDG whereas selected ALDF can be imported directly through the MEPDG interface. This sheet has been designed in a printable format so that users can print out and save this document in a corresponding project folder, if desired.

Procedure:

1- Enter project name and engineer name in the proper fields, if desired;
2- Enter the 48-hr counts /vehicle class in Cell Range C13:L15;
3- Using the drop-down list In cell B12, select the month in which the 48-hr counts were recorded. Similarly, select in Cell B13,B14, and/or B15 the days of the week the counts were recorded;
4- From the drop-down list in cell B16, Select either *Yes* or *No* to whether the count was done on Interstate I-95 or not; and
5- From the drop-down list in Cell B17, select the road category of the route.
Upon the completion of the preceding steps, VCD factors will be displayed directly in cells B27:B36 whereas the proper ALDF cluster will be displayed in cell A41.

Note:

If no specific ALDF cluster is identified, refer to the following plot and use engineering judgment to find the closest ALDF cluster based on class 5 and class 9 percentages found at the route.

Figure 7.10. A screen capture of the *VCD Generator and ALDF Cluster Selector* tool.

7.7.1 Damage-Based Sensitivity Analysis

7.7.1.1 Background

The sensitivity study has three goals: 1) to determine ways that different clusters for different traffic parameters affect the predicted performance of flexible and rigid pavements in the MEPDG, i.e., to check the sensitivity of pavement-predicted distresses to different traffic parameter clusters; 2) to simplify the design process by attempting to aggregate the clusters; and 3) to develop axle load factor clusters that are based on the effect of different axle type/load combinations on pavement performance. It is worth mentioning that the ALDF and VCD are the only two traffic parameters for which clusters are selected based on traffic data collected from 48-hour classification counts performed at or near the project location (Stone et al., 2010). The selection of appropriate ALDF and VCD clusters for a certain project location will be based on three decision trees that were developed by Stone et al. (2010). In the following sections, the focus is on flexible pavements because they are within the scope of this research.

7.7.1.2 Sensitivity Criteria

The sensitivity criteria provide threshold values for each of the performance measures. These threshold values are the basis for determining if different clusters of different traffic parameters, i.e., HDF, MAF, VCD, and ALDF, result in different predicted performance. This information is necessary to attempt the aggregation of different clusters from the same traffic factors, if possible, to simplify the pavement design process.

Considering the precision of MEPDG-predicted performance and the best available precision with which NCDOT survey teams can measure the distresses of flexible and rigid pavements in the field, the research team, in cooperation with the NCDOT Pavement Management Unit (PMU), has developed sensitivity criteria that were used for all damage-based sensitivity work conducted under NCDOT Project No. HWY-2008-11. The final sensitivity criteria for flexible and jointed plain concrete pavement (JPCP) are shown in Table 7.2. Because of their high construction cost and unsatisfactory experience, continuously reinforced concrete pavements (CRCP) have been discontinued for use in North Carolina, and hence, are excluded from the criteria table (Table 7.2).

Table 7.2. NCDOT Sensitivity Criteria for Flexible and JPCP Pavements

Pavement Type	Performance Measure	Measure Unit	Failure Point (Maintenance Trigger)	Sensitivity	
				Percentage of Failure Point	Threshold
Asphalt Concrete	IRI	inch/mile	140	10	14
	Total rutting	inch	0.5	20	0.1
	Alligator	percentage of	10	10	1
	Longitudinal	feet/mile	2640 (50% of	10	264
JPCP	IRI	inch/mile	140	10	14
	Faulting	inch	0.5	20	0.1
	Slabs cracked	percentage	10	20	3

7.7.1.3 Damage-Based Sensitivity Analysis

The damage-based sensitivity analysis was performed using the MEPDG for all the simulations. Ten flexible LTPP pavements were included in the analysis. The pavement structure at each WIM site was entered in the MEPDG, and default values for all pavement materials were used. As for traffic information, site-specific traffic data were entered for each of the sites. To evaluate the sensitivity of each traffic parameter, and using MAF as an example here, all traffic information for a specific site remains unchanged, whereas the MAF information is changed between runs. For example, Phase 3 in Figure 7.9 shows six MAF clusters that result from individual clustering analysis; therefore, MEPDG simulations for each of the 10 flexible pavement structures are executed, six runs per site, to evaluate the sensitivity of the MAF. A similar approach was followed for each of the other three traffic parameters.

7.7.1.4 Sensitivity Analysis Results

Figure 7.11 and Figure 7.12 present the maximum *differences* in predicted HDF and MAF inflexible pavements when different clusters are used. Similarly, Figure 7.13 and Figure 7.14 present the maximum *differences* in predicted VCD and ALDF.
The interpretation of Figure 7.12 is presented in the following paragraph. The interpretations of all the other figures follow the same logic.

Figure 7.12 suggests that all MAF clusters (a total of six clusters), when individually implemented in the MEPDG, would result in a total rut depth and international roughness index (IRI) such that the clusters would be considered to be similar to each other. This observation is based on the threshold values shown in Table 7.2 and presented as solid lines in all the sensitivity figures. In other words, the maximum difference between predicted total rut depth and the IRI when any two MAF clusters are used is found to be below the threshold value of 0.1 inch and 14 inches/mile, respectively. On the other hand, the differences between predicted alligator cracking and longitudinal cracking were found to be larger than the threshold values presented in Table 7.2. At least two MAF clusters result in significant differences in predicted alligator cracking and longitudinal cracking.

While developing the sensitivity criteria in cooperation with the NCDOT, it was decided that the criteria should consider not only the maximum differences in predicted distresses using any two traffic parameter clusters, but also the amount of predicted distresses at a particular site. Recall from Table 7.2 that alligator cracking has a threshold value of 1% of lane area and a maintenance trigger point of 10% of lane area. For example, the average predicted alligator cracking from all MAF clusters at site 520 was found to be 25.7% of the lane area, compared to only 1.6% at site 506. Furthermore, the maximum *difference* in predicted alligator cracking due to any two MAF clusters at site 520 was found to be 1.7% of the lane area (which makes site 520 fail the criteria shown in Table 7.2) compared to 0.2% only for site 506, which makes it pass the criteria shown in Table 7.2.

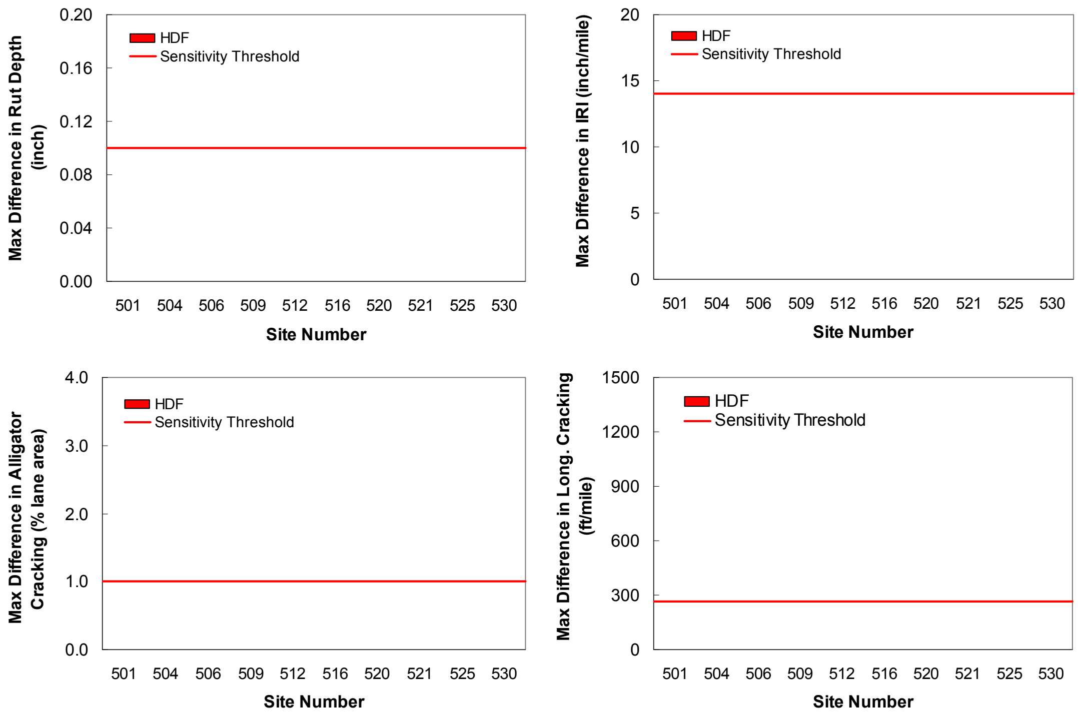

Figure 7.11. Sensitivity analysis results of HDF for flexible pavements.

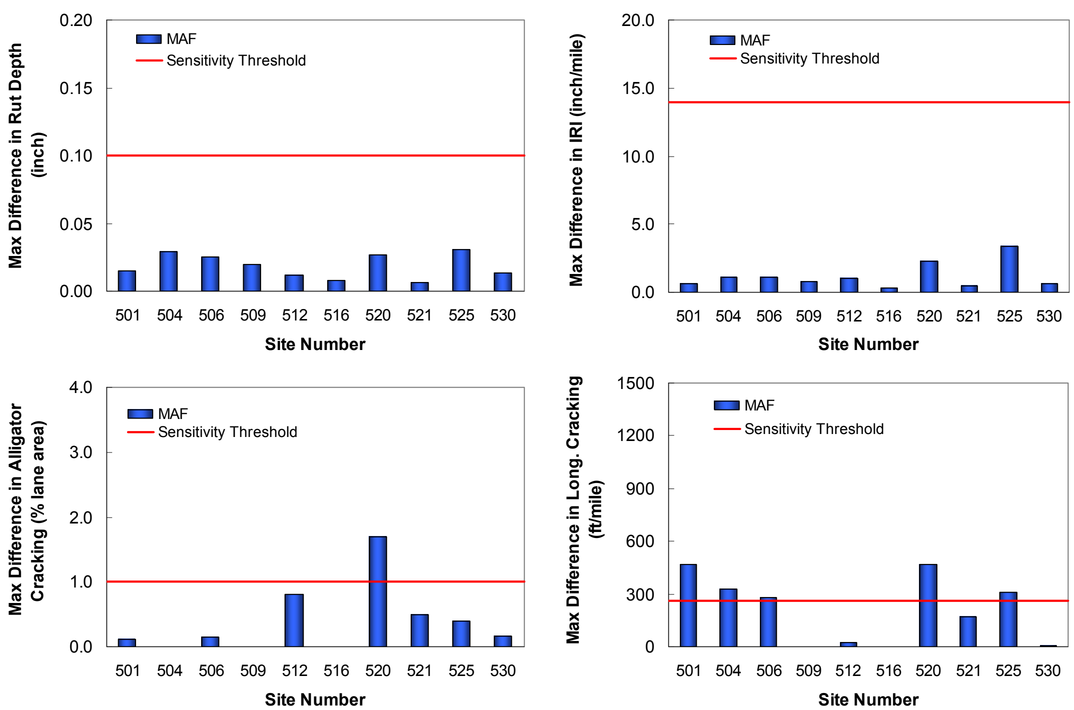

Figure 7.12. Sensitivity analysis results of MAF for flexible pavements.

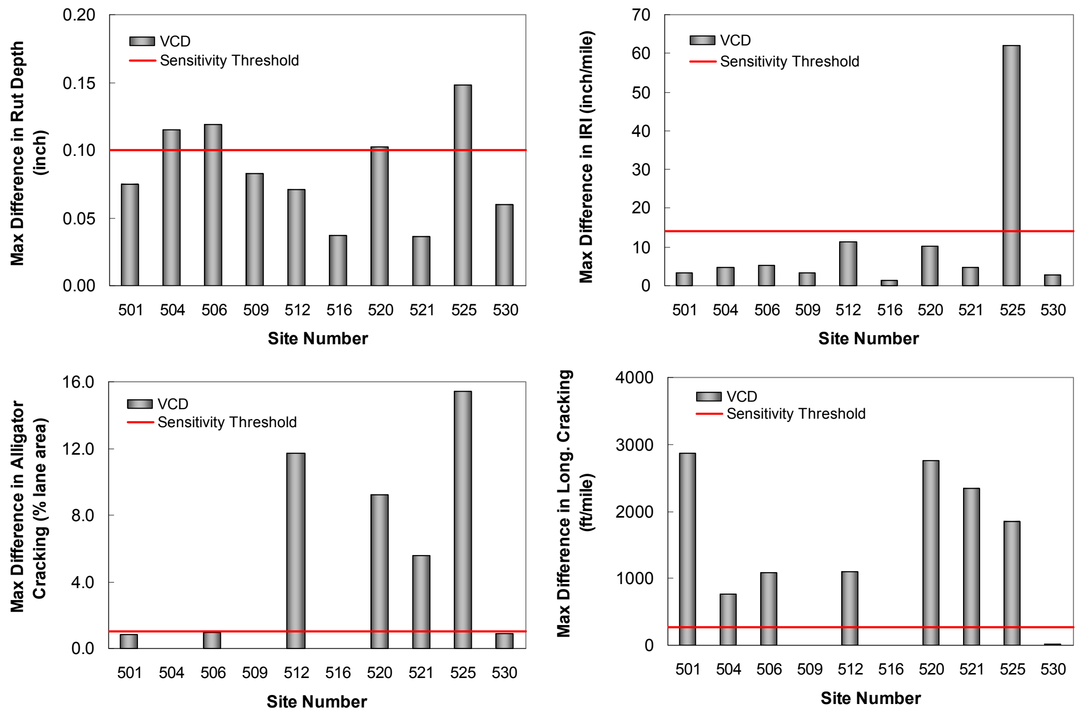

Figure 7.13. Sensitivity analysis results of VCD for flexible pavements.

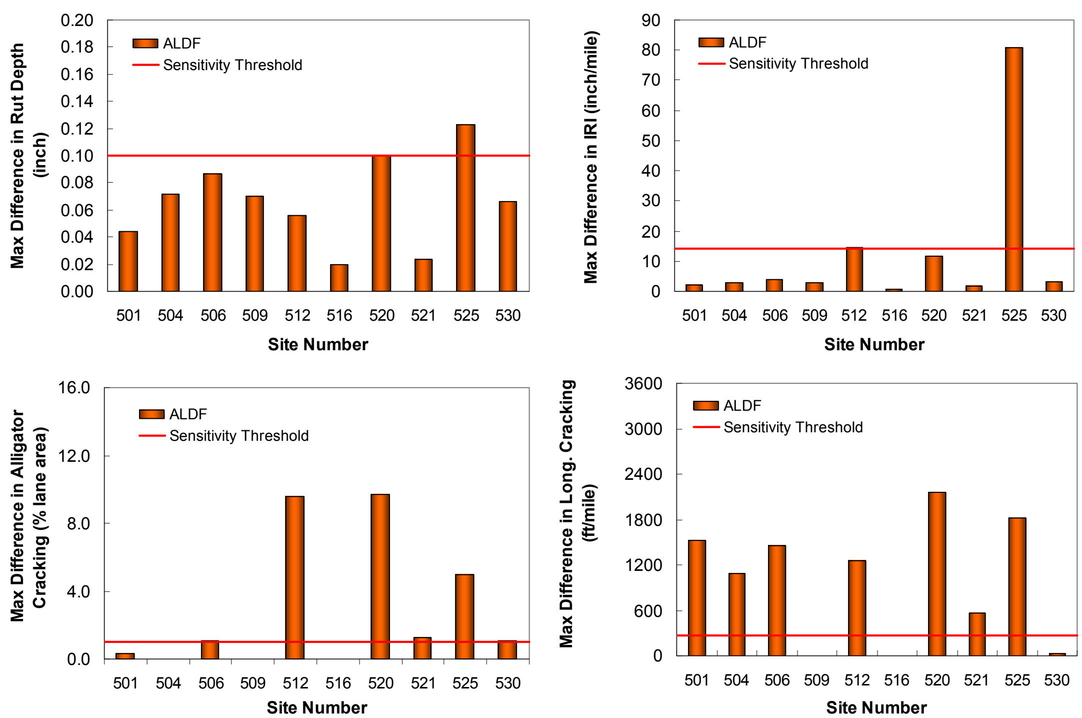

Figure 7.14. Sensitivity analysis results of ALDF for flexible pavements.

It is generally agreed that the higher the predicted distress values (27.5% at site 520), the larger the expected differences between these distresses (1.7% at site 520). To account for this fact regarding expected differences, the research team agreed with the NCDOT that the sensitivity criteria presented in Table 7.2 could be modified to account for the predicted distresses at a particular site. A value of 10% has been adopted for this tolerance. In other words, the alligator cracking sensitivity criterion at site 520 can be modified from its original value of 1.0%, as shown in Table 7.2, to become approximately 2.6% (that is 27.5% x 10%). The alligator cracking criterion at site 506 stays at 1.0% because 10% of the average predicted alligator cracking (1.6%) is already less than the unmodified 1.0% criterion. Using the updated criteria, it can be concluded that all MAF clusters would result in predicted alligator cracking values that are insignificantly different from each other.

Table 7.3 summarizes the sensitivity results of flexible pavements to different traffic parameters. A check mark (√) indicates sensitivity, whereas an (×) indicates insensitivity to the sensitivity criteria shown in Table 7.2.

Table 7.3. Sensitivity of Flexible Pavements to Different Traffic Parameters

	Flexible Pavement			
	Total Rut Depth (in.)	Alligator Cracking (%)	Longitudinal Cracking (ft/mile)	IRI (in./mile)
HDF	×	×	×	×
MAF	×	×	✓	×
VCD	✓	✓	✓	✓
ALF	✓	✓	✓	✓

Table 7.3 suggests that using different HDF clusters for a particular design project in the MEPDG results in predicted distresses that are not significantly different in flexible pavements. When distress predictions were compared for different MAF clusters, it was found that with the exception of longitudinal cracking in flexible pavements, all other predicted distresses are not significantly different.

The performance prediction model for longitudinal cracking that is embedded in MEPDG Version 0.9 has problems, and therefore, has been omitted from sensitivity results. In Version 0.9 of the MEPDG, which is the version used exclusively by Stone et al. (2010) for all their sensitivity runs, it is assumed that the number of cycles to failure (N_f) fatigue model can be used for alligator cracking as well as longitudinal cracking. This assumption is based on another assumption that the longitudinal cracking transfer function can handle the error inherent in the first assumption. Realizing that the number of cycles to failure fatigue model currently embedded in the MEPDG was developed based on critical strain criteria, and knowing that longitudinal cracking is affected mainly by thermal distress and aging of the surface layers, it is clear to the research team that the longitudinal cracking predictions obtained from the MEPDG are inaccurate; hence, these predictions are excluded from the sensitivity study.

Moreover, Table 7.3 suggests that different VCD clusters and different ALDF clusters all result in predicted performance that is significantly different for all four performance measures, i.e., total rut depth, alligator cracking, longitudinal cracking, and the IRI. Therefore, the decision was made by Stone et al. to average the four HDF clusters (shown in Phase 3 from Figure 7.9) and use statewide HDF for all flexible pavement designs. Similarly, Stone et al. suggested that the six MAF clusters (shown in Phase 3 from Figure 7.9) be averaged into a single statewide MAF cluster that can be used for all flexible pavement designs. Based on the results of this damage-based sensitivity analysis study, Stone et al. recommended methods to obtain VCD and ALDF data based on 48-hour classification counts at or near the project location. Details can be found elsewhere (Stone et al., 2010).

7.7.2 Clustering Analysis to Guide the Development of ALDF

This section has two main objectives: first, to define clustering analysis and discuss its vital role as a tool that can be applied when developing ALDF input for use in the MEPDG, and second, to present a step-by-step procedure for developing a damaged-based guide that can be followed to develop North Carolina ALDF clusters for use in the MEPDG. The following subsection (7.7.2.1) defines the clustering process and introduces some of the advantages of such process.

7.7.2.1 Definition and Advantage of Clustering Analysis

Clustering analysis is a technique that is used to group objects or observations into sub-groups (clusters) based on similarities or dissimilarities of a single or multiple variables (dimensions) measured for each case. Several clustering approaches are reported in the literature and include hierarchical, partitional, and subspace clustering. The hierarchical clustering technique offers two algorithms, agglomerative and divisive. The agglomerative algorithms start by considering small elements as separate clusters and proceed by grouping them into successively bigger clusters. Divisive algorithms, by contrast, start by considering all elements as one group and proceed by dividing them into successively smaller clusters based on similarities.

The clustering results presented in this section are borrowed from a unique clustering analysis technique that has been applied for the first time to ALDF data using a multidimensional hierarchical-agglomerative approach (Sayyady et al., 2010). As mentioned earlier under Section 7.7, a four-dimensional clustering analysis technique is proposed in which single, tandem, tridem, and quad axles form the four dimensions. Multidimensional clustering has an advantage over one-dimensional clustering in that it considers multiple dimensions simultaneously, thus accounting for any interactions among different axle types, preserving the identity of each of the dimensions, and facilitating a meaningful interpretation of the clustering analysis results. This section shows in detail the ways that damage factors were developed and used with clustering analysis to guide the development of North Carolina ALDF clusters that are presented in Phase 5 of Figure 7.9.

7.7.2.2 Preliminary Results of Four-Dimensional Clustering and Problem Definition

7.7.2.2.1 Preliminary Results

The ALDF data collected from all 44 WIM sites were clustered by Sayyady et al. (2010) based on the four dimensions of single, tandem, tridem, and quad axles, which are the clusters shown in Phase 3 of Figure 7.9. Figure 7.15 shows the results of the four-dimensional clustering analysis in the form of a normalized frequency versus axle load plot. Figure 7.15 shows four ALDF clusters for each axle type. Each cluster curve represents the average ALDF data for the WIM sites that fall into that cluster.

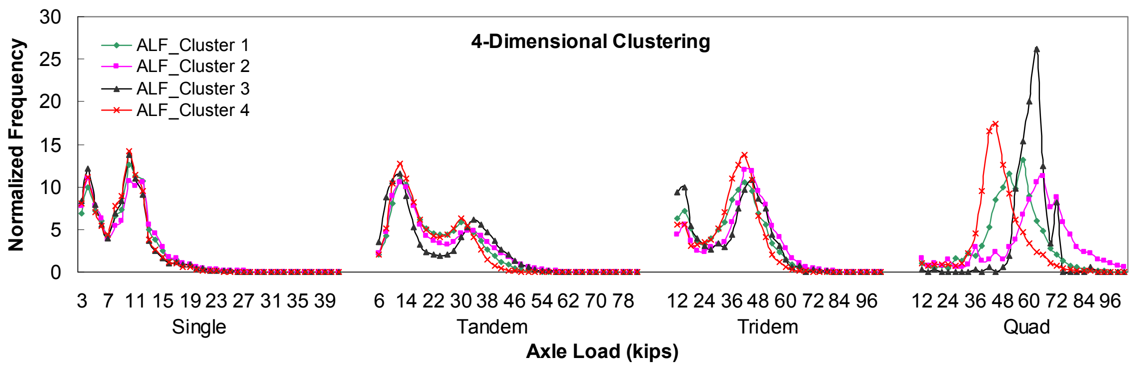

Figure 7.15. Results of four-dimensional ALDF clustering analysis.

7.7.2.2.2 Problem Definition and Proposed Solution

Figure 7.15 clearly shows that quad and tridem axles have a larger variability among the clusters than single and tandem axles. In general, the clustering process is affected by two factors: frequency and variability. In this case, large variability is an indication that the clustering process and, hence, all four resulting ALDF clusters, are governed by the tridem and quad axles. This finding is not acceptable because instances of the use of tridem and quad axles are infrequent in actual traffic streams (Sayyady et al., 2010). However, before a decision based on low frequency can be made to include or exclude tridem and quad ALDF data from ALDF clustering, the effects of these two axle types on pavement performance need to be investigated. Considering the cumulative damage principle implemented in the MEPDG, the effect of any axle type/load combination on pavement performance depends on two factors: frequency and damage caused by a single pass. Therefore, the first step in refining the four-dimensional clustering procedure and deciding whether tridem and quad axles should or should not be included in the ALDF clustering analysis is to carry out a study on ALDF to evaluate the effect of different axle type/load combinations on pavement performance. Knowing which axle type/load combinations cause the most damage to the pavement is vital in making such a decision. The next Section 7.7.2.3 explains in detail the procedure that was followed in this study for calculating ALDF using the MEPDG.

7.7.2.3 Development of Axle Load Damage Factors

7.7.2.3.1 Background and Definition

The ALDF table in the MEPDG provides information about the four axle types (single, tandem, tridem, and quad) and associated loads to calculate critical pavement responses, i.e., stresses, strains, and deflections, which are used to predict pavement performance. For the single axle, 39 axle load bins (groups) range from 3 kips to 41 kips. For the tandem axle, 39 load bins range from 6 kips to 82 kips. For each of the tridem and quad axles, 31 load bins have loads ranging from 12 kips to 102 kips.

A damage factor (DF) for any axle type/load combination is defined as the ratio of the fatigue damage caused by that axle type/load combination to the fatigue damage caused by a standard 18-kip ESAL. Equation (7.1) presents the definition of *damage factor*. This study summarizes the development of damage factors for flexible pavements. There are two reasons that only flexible pavements are considered: 1) flexible pavements contribute about 90% of the total road network in North Carolina; and 2) rigid pavements are found to be insensitive to ALDF input variations for North Carolina traffic (Sayyady et al., 2009).

$$DF_{ij} = \frac{D_{f,ij}}{D_{ESAL}} \qquad (7.1)$$

where

DF_{ij} = damage factor for axle type i and axle load j;

i = axle type (single, tandem, tridem, or quad);

$$j \quad = \quad \text{axle load} \quad = \begin{bmatrix} \text{single} & = & \text{3 kip, 4, 5, ...} & \text{41 kip} \\ \text{tandem} & = & \text{6 kip, 8, 10, ...} & \text{82 kip} \\ \text{tridem} & = & \text{12 kip, 15, 18, ...} & \text{102 kip} \\ \text{quad} & = & \text{12 kip, 15, 18, ...} & \text{102 kip} \end{bmatrix}$$

$D_{f,ij}$ = bottom-up fatigue damage caused by axle i and axle load j; and

D_{ESAL} = bottom-up fatigue damage caused by an 18-kip ESAL.

7.7.2.3.2 Significance of Axle Load Damage Factors

Damage factors play a vital role in linking pavement performance to truck axle loading and geometry. In this work, damage factors were developed and used with clustering analysis to guide the development of ALDF clusters for use in the MEPDG. Damage factors ultimately modify the percentages of the various axle type/load combinations in order to reflect their contribution to pavement damage. In this study, axle type/load combinations that cause the most damage to pavements are given more weight than those combinations that have a small effect on pavement performance. Furthermore, frequency and damage factors, both of which depend on axle type, are considered together in identifying their effects on pavement performance. The damage factors presented in this section are based on bottom-up fatigue damage as the reference criterion. Fatigue damage was selected for the reference criterion in cooperation with the NCDOT, because fatigue is the major cause of pavement failure in North Carolina.

7.7.2.3.3 Approach for Developing Damage Factors

As mentioned earlier, 44 pavement sections are included in this study. Only 36 of the sections are flexible pavements, and 8 are rigid pavements. Because the analysis in this research specifically targets flexible pavements, the 8 available rigid pavements were converted to equivalent flexible pavements using their site-specific traffic, environmental, and location information. The NCDOT's current pavement design method was used for this conversion. The conversion was made using a Microsoft Excel tool similar to the one currently used by the NCDOT for the design of flexible and rigid pavements. The major inputs required by the Microsoft Excel tool are: initial year ADT, percentage of duals and percentage of truck tractor semi-trailers (TTST), design life, number of lanes per direction, the directional distribution factor, lane distribution factor, terminal serviceability index (SI), rural versus urban, TTST factors, and the CBR of the subgrade soils. Once all of these parameters are entered, the Microsoft Excel tool calculates multiple flexible pavement designs from which the most feasible design can be selected.

The proposed development of the ALDF is a two-step process. The first step calls for executing the MEPDG for each axle type/load combination (140 total) and for each available pavement section (44 total), and recording the predicted fatigue damage at the end of the design life. The second step calls for normalizing the fatigue damage predicted for each of the axle type/load combinations with respect to the fatigue damage predicted using an 18-kip ESAL. In order for this approach to be implemented, some of the traffic inputs within the MEPDG must be adjusted to force the MEPDG to apply only a certain axle type/load combination throughout the design life. This process is repeated for each of the combinations, i.e., 140 times. Section 7.7.2.3.4 explains the process in details.

7.7.2.3.4 Traffic Input Adjustments within the MEPDG

The four traffic inputs required by the MEPDG that must be adjusted in order for the MEPDG to apply a certain axle type/load combination on a pavement structure are the AADTT, VCD factors, APT, and ALDF. The following steps provide an example of the way this adjustment procedure works using a 12-kip tandem axle for 500 initial passes with a 4% annual compound growth rate. Note that although some of the numbers entered are not realistic, the final output fulfills the intended goal. An example of unrealistic numbers is using 100% for the class 9 contribution in the VCD table; the traffic here consists only of class 9 vehicles.

1) To force the MEPDG to consider an initial number of 500 trucks, Figure 7.16 suggests that users should enter the number 1000 in the AADTT field, 2 in the number of lanes in the design direction field, 50 in the percentage of trucks in

design direction field, and 100 in the percentage of trucks in design lane field. This array of numbers yields 500 trucks.

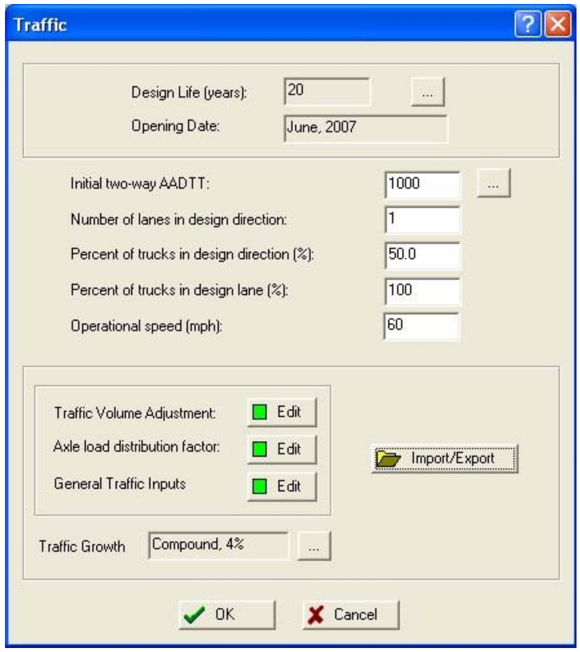

Figure 7.16. Adjustments made to AADTT and general inputs for damage factors study.

2) To distribute the AADTT by vehicle class, i.e., FHWA vehicle classes 4 through 13, users can select any of the vehicle classes so that the selected class contributes 100% to the overall truck traffic. Figure 7.17 shows an example where the MEPDG considers 500 class 9 vehicles as the only traffic.

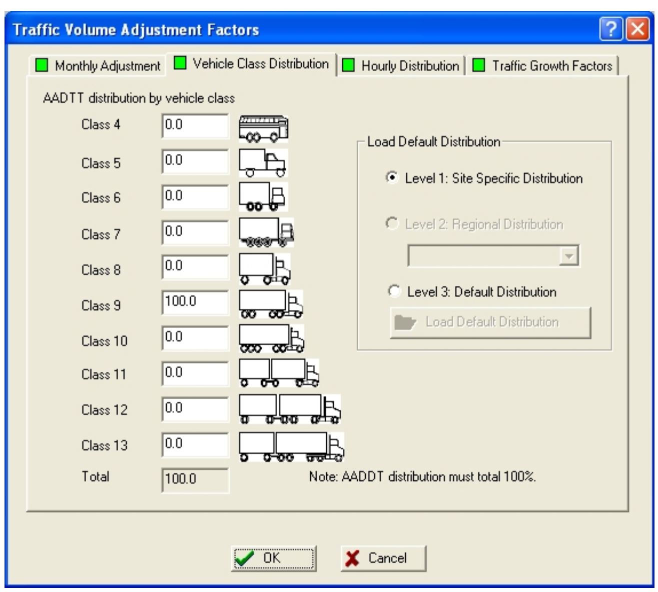

Figure 7.17. Adjustments made to VCD for damage factors study.

3) To calculate the total number of each axle type applied to the pavement, the MEPDG allows users to enter the number of each type of axle for each vehicle class. Figure 7.18 is a screen capture of the APT table. In this table, each vehicle class from 4 through 13 is shown to have only one axle from each axle type. For example, vehicle class 4 is shown to have one single, one tandem, one tridem and one quad axle, which is applicable to all vehicle classes. Again, one axle from each axle type is not realistic for some of the vehicle classes; however, the numbers are assumed as part of the overall process to achieve the aforementioned goal. Now, the total number of axles that can be applied on the pavement is 2,000, that is, 500 single axles, 500 tandem axles, 500 tridem axles and 500 quad axles.

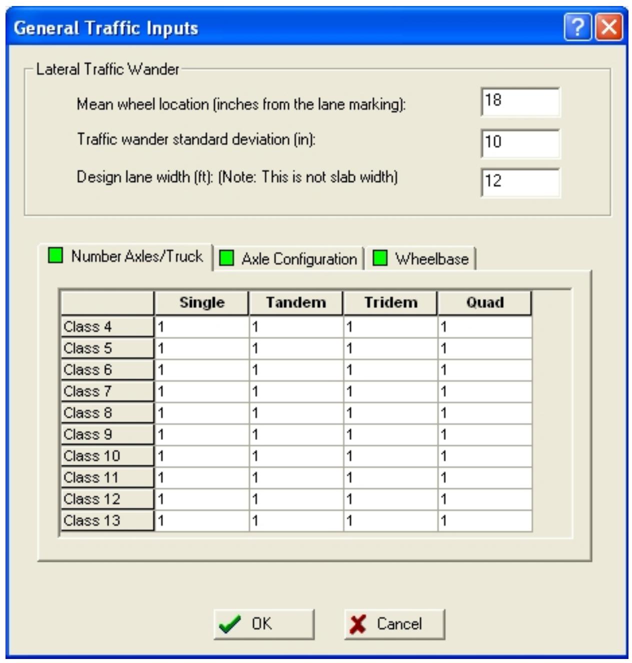

Figure 7.18. Adjustments made to APT for damage factors study.

4) To ensure that only 500 of the 12-kip tandem axles are applied to the pavement, users must consult the ALDF table, a screen capture of which is shown in Figure 7.19. The numbers in the ALDF table represent the contribution of a certain axle type/load combination from a certain vehicle class in a certain month. For example, the highlighted field in Figure 7.19 indicates that for each day in the month of January, the contribution of class 5 vehicles to the total number of tandem axles for all vehicles is determined only through the 12-kip axles. However, Figure 7.17 shows no presence of class 5 vehicles, indicating that class 5 vehicles do not contribute to any of the applied axle types despite what Figure 7.19 shows. On the other hand, class 9 vehicles contribute 500 of the 12-kip tandem axles. To ensure that class 9 vehicles contribute only tandem axles, all fields in the single, tridem, and quad axle tables are populated with the number zero, indicating that even class 9 makes zero contribution to any axle type other than tandem.

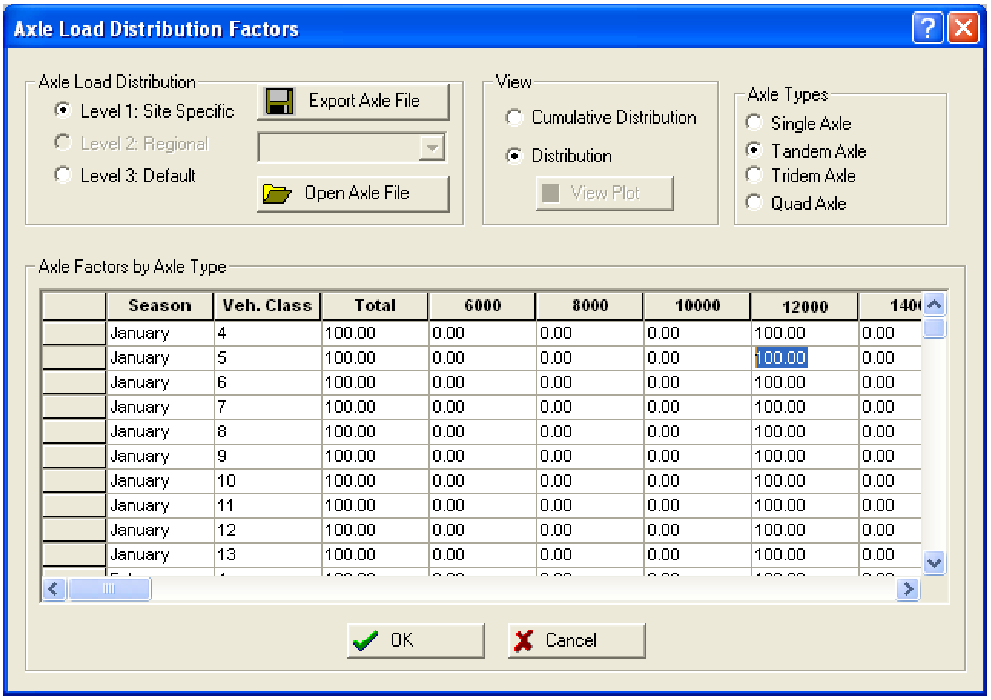

Figure 7.19. Adjustments made to ALDF for damage factors study.

At this point, information gleaned from Steps 1 through 4 suggests that any desired axle type/load combination can be achieved through changes to the ALDF table, whereas all other traffic inputs, i.e., the AADTT, VCD, and APT, remain unchanged. The procedure above was applied 140 times for one of the WIM sites and 27 times for each of the other 43 WIM sites included in this study.

7.7.2.3.5 Full versus Partial Factorial

In order to consider the aforementioned full factorial analysis, the MEPDG must be executed 6,160 times, that is, 44 pavement sections times 140 axle loads. The execution and analysis of 6,160 runs requires a substantial amount of time and effort. Therefore, the research team adopted an alternative approach that reduces the required number of MEPDG runs. In the alternative approach, the MEPDG is executed 1,301 times. The alternative approach calls for executing the MEPDG for a full factorial, i.e., 140 axle loads, for one pavement section only. Results are then used to develop a regression model. Once a good-fitting model is developed, the MEPDG is executed for a partial factorial, i.e., 27 axle loads, and the model can be used to interpolate fatigue damage that corresponds to the other axle loads. Axle loads included in the partial factorial are: 3, 9, 18, 27, 36, and 41 kips for the single axle; 6, 18, 30, 42, 54, 66, and 82 kips for the tandem axle; and 12, 27, 42, 57, 72, 87, and 102 kips for the tridem and quad axles.

7.7.2.3.6 Analysis Results of MEPDG Runs

Analysis results suggest that a bilinear function in the log-log space is a suitable model that accurately explains the fatigue damage development with increasing axle loads. Table 7.4 summarizes the statistics for the slope and intercept for linear functions that represent light axle loads (3 kips to 9 kips for the single axle, 6 kips to 18 kips for the tandem axle, 12 kips to 27 kips for the tridem and quad axles) and heavy axle loads (10 kips to 41 kips for the single axle, 19 kips to 82 kips for the tandem axle, and 28 kips to 102 kips for the tridem and quad axles).

Figure 7.20 (a) shows an example of predicted fatigue damage at WIM site 525 for the partial factorial, i.e., for the 27 axle type/load combinations. Figure 7.20 (b) shows that the proposed bilinear function fits the predicted fatigue data well with a coefficient of determination of 1.0. In addition to the 27 fatigue damage values obtained through the MEPDG runs, Figure 7.20 (c) contains 113 fatigue damage values that were interpolated using bilinear functions whose coefficients were determined from the 27 fatigue damage values obtained from the MEPDG runs. For pavement sections at each WIM site, there are four different bilinear functions, one for each axle type.

Table 7.4. Statistics of the Slope and Intercept for Linear Functions Representing Light and Heavy Axles

Light Axle Weights								
Axle Type	Single		Tandem		Tridem		Quad	
Valid Load Range	3 kips - 9 kips		6 kips - 18 kips		12 kips - 27 kips		12 kips - 27 kips	
Statistics	Slope	Intercept	Slope	Intercept	Slope	Intercept	Slope	Intercept
Avg.	6.25	-7.20	6.24	-8.94	6.25	-7.20	6.24	-8.94
Min.	6.24	-7.20	6.23	-9.12	6.24	-7.20	6.23	-9.12
Max.	6.25	-7.20	6.24	-8.62	6.25	-7.20	6.24	-8.62
Std. Dev.	0.001	0.001	0.002	0.143	0.001	0.001	0.002	0.143
% Std. Dev. From Avg.	0.02	0.02	0.03	1.59	0.02	0.02	0.03	1.59
Heavy Axle Weights								
Axle Type	Single		Tandem		Tridem		Quad	
Valid Load Range	10 kips - 41 kips		19 kips - 82 kips		28 kips - 102 kips		28 kips - 102 kips	
Statistics	Slope	Intercept	Slope	Intercept	Slope	Intercept	Slope	Intercept
Avg.	4.07	-5.11	4.06	-6.21	4.07	-5.11	4.06	-6.21
Min.	4.06	-5.12	4.06	-6.39	4.06	-5.12	4.06	-6.39
Max.	4.07	-5.11	4.07	-5.89	4.07	-5.11	4.07	-5.89
Std. Dev.	0.001	0.001	0.001	0.143	0.001	0.001	0.001	0.143
% Std. Dev. From Avg.	0.03	0.03	0.03	2.30	0.03	0.03	0.03	2.30

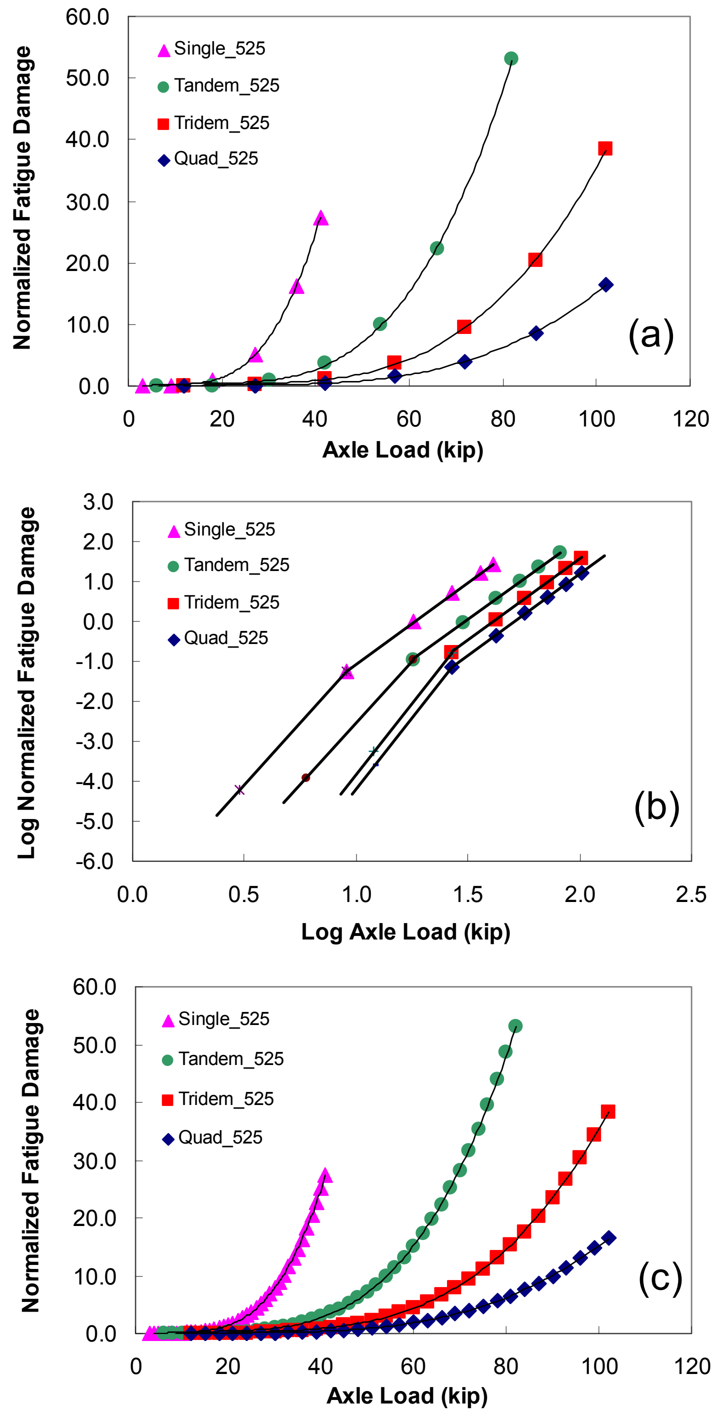

Figure 7.20. Damage factors from site 525: (a) partial results of actual MEPDG runs; (b) bilinear fitting functions; and (c) complete results of damage factors.

Equation (7.2) is a group of linear functions representing heavy axle loads for each axle type. Similarly, Equation (7.3) shows a group of linear functions that represent light axle loads for each axle type. The coefficients of these linear functions are the average slope and intercept values presented in Table 7.4. For any axle type/load combination, Equations (7.2) and (7.3) can be consulted for calculating the damage factor for that combination.

$$\begin{bmatrix} \log(DF_{SH}) & = & -5.11+4.07\log(L_1), & L_1 = 10kips-41kips \\ \log(DF_{TH}) & = & -6.21+4.06\log(L_2), & L_2 = 19kips-82kips \\ \log(DF_{TrH}) & = & -6.75+4.07\log(L_3), & L_3 = 28kips-102kips \\ \log(DF_{QH}) & = & -7.13+4.07\log(L_4), & L_4 = 28kips-102kips \end{bmatrix} \qquad (7.2)$$

where

DF_{SH} = damage factor single heavy load,
DF_{TH} = damage factor tandem heavy load,
DF_{TrH} = damage factor tridem heavy load, and
DF_{QH} = damage factor quad heavy load,

$$\begin{bmatrix} \log(DF_{SL}) & = & -7.20+6.25\log(L_1), & L_1 = 3kips-9kips \\ \log(DF_{TL}) & = & -8.94+6.24\log(L_2), & L_2 = 6kips-18kips \\ \log(DF_{TrL}) & = & -11.01+7.05\log(L_3), & L_3 = 12kips-27kips \\ \log(DF_{QL}) & = & -11.39+7.05\log(L_4), & L_4 = 12kips-27kips \end{bmatrix} \qquad (7.3)$$

where

DF_{SL} = damage factor single light load,
DF_{TL} = damage factor tandem light load,
DF_{TrL} = damage factor tridem light load, and
DF_{QL} = damage factor quad light load.

7.7.2.3.7 Discussion of Results

Table 7.5 is an example summary of damage factors developed for the pavement structure at WIM site 525. The highlighted field in Table 7.5 suggests that a single pass of a 40-kip tandem axle will cause 191% more fatigue damage to the pavement than a single pass of an 18-kip single axle. Figure 7.21 shows averaged damage factors developed using data from all 44 WIM sites and normalized based on the 18-kip ESAL.

Figure 7.21 and Table 7.5 both suggest that damage factors increase with an increasing axle load. This finding is expected because heavy loads on the same axle type will develop large stresses in the pavement structure and, hence, have a larger damage potential than light loads. Figure 7.21 and Table 7.5 also suggest that for the same axle load, damage factors decrease as the number of axles increases, e.g., from single to quad axle. This finding also makes sense because when the same load is distributed over multiple axles, each axle will support a smaller amount of load and, hence, will develop smaller stresses and less damage than it would with fewer axles. Because each of the 44 pavement sites included in this study has different pavement structures and environmental conditions, the developed damage factors are site-dependent; i.e., each site has unique axle load damage factors.

Table 7.5. Example Summary of Damage Factors Developed for WIM Site 525

Axle Type							
Single		Tandem		Tridem		Quad	
Load (Kip)	DF	Load (Kip)	DF	Load (Kip)	DF	Load (Kip)	DF
3	0.00	**6**	0.00	**12**	0.00	**12**	0.00
4	0.00	**8**	0.00	**15**	0.00	**15**	0.00
5	0.00	**10**	0.00	**18**	0.01	**18**	0.00
6	0.00	**12**	0.01	**21**	0.03	**21**	0.01
7	0.01	**14**	0.02	**24**	0.07	**24**	0.03
8	0.03	**16**	0.05	**27**	0.17	**27**	0.07
9	0.06	**18**	0.11	**30**	0.27	**30**	0.11
10	0.09	**20**	0.17	**33**	0.39	**33**	0.17
11	0.13	**22**	0.26	**36**	0.56	**36**	0.24
12	0.19	**24**	0.36	**39**	0.77	**39**	0.33
13	0.26	**26**	0.51	**42**	1.06	**42**	0.45
14	0.35	**28**	0.68	**45**	1.38	**45**	0.59
15	0.47	**30**	0.92	**48**	1.80	**48**	0.77
16	0.61	**32**	1.17	**51**	2.31	**51**	0.99
17	0.77	**34**	1.50	**54**	2.91	**54**	1.25
18	1.00	**36**	1.90	**57**	3.67	**57**	1.58
19	1.22	**38**	2.36	**60**	4.47	**60**	1.91
20	1.50	**40**	**2.91**	**63**	5.45	**63**	2.34
21	1.83	**42**	3.60	**66**	6.59	**66**	2.82
22	2.21	**44**	4.28	**69**	7.90	**69**	3.38
23	2.65	**46**	5.13	**72**	9.44	**72**	4.04
24	3.15	**48**	6.10	**75**	11.10	**75**	4.75
25	3.71	**50**	7.20	**78**	13.02	**78**	5.58
26	4.36	**52**	8.45	**81**	15.19	**81**	6.50
27	5.13	**54**	9.90	**84**	17.62	**84**	7.54
28	5.89	**56**	11.42	**87**	20.29	**87**	8.66
29	6.79	**58**	13.17	**90**	23.33	**90**	9.99
30	7.79	**60**	15.11	**93**	26.67	**93**	11.41
31	8.91	**62**	17.26	**96**	30.35	**96**	12.99
32	10.13	**64**	19.64	**99**	34.41	**99**	14.72
33	11.48	**66**	22.21	**102**	38.37	**102**	16.44
34	12.96	**68**	25.13				
35	14.59	**70**	28.27				
36	16.25	**72**	31.70				
37	18.28	**74**	35.43				
38	20.38	**76**	39.48				
39	22.65	**78**	43.88				
40	25.10	**80**	48.63				
41	27.40	**82**	52.98				

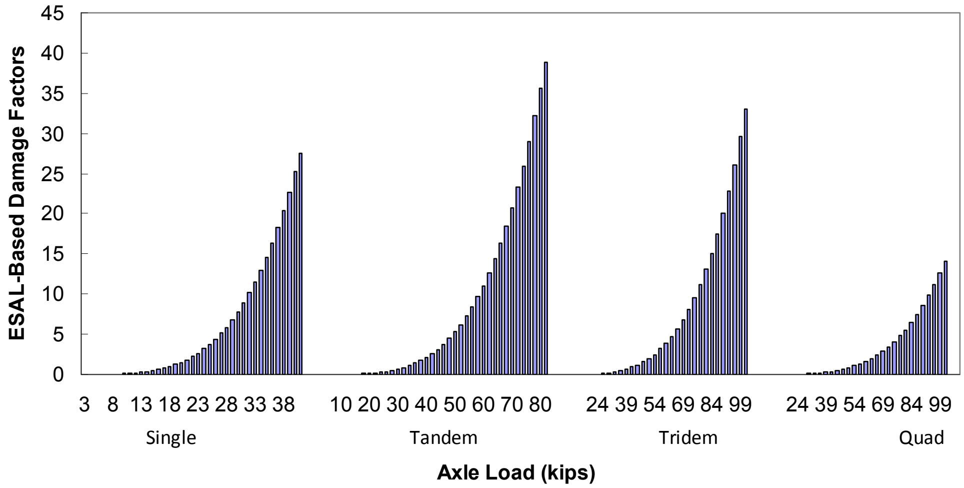

Figure 7.21. ESAL-based damage factors developed using the MEPDG.

7.7.2.3.8 Refinement of Four-Dimensional Clustering to Two-Dimensional Clustering

Results of the damage factors study presented earlier reveal that for the same axle load, tridem and quad axles actually cause less fatigue damage to the pavement than single and tandem axles. This finding indirectly suggests that it is inappropriate for tridem and quad axles to control ALDF clustering, as explained by Figure 7.15. However, before a decision was made to exclude tridem and quad axles from ALDF clustering, it was important to consider their damage effects and frequency together. Figure 7.22 shows the average frequency distribution of different axle types in North Carolina.

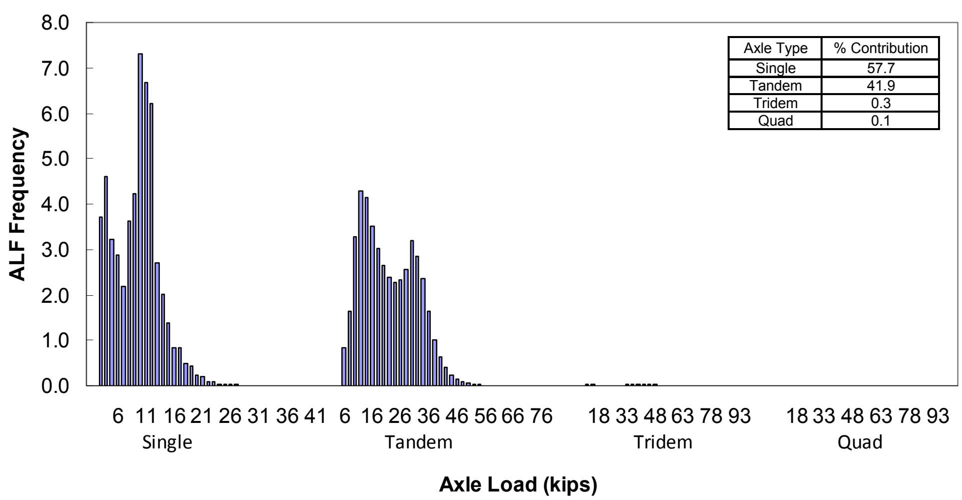

Figure 7.22. Average frequency of single, tandem, tridem, and quad axles from 44 WIMs.

Figure 7.22 shows that the contribution of tridem and quad axles is only 0.3% and 0.1%, respectively. The major contribution to damage comes from single axles (57.7%), followed by tandem axles (41.9%). Again, the research team does not yet recommend making the decision to include or exclude tridem and quad axles from the ALDF clustering process until the effects of these two axle types on pavement performance have been investigated.

To consider the effects of frequency and damage together, Stone et al. (2010) developed two rules, referred to as *Rule 1* and *Rule 2*. Rule 1 was developed to help discern whether a certain axle type/load combination should be included or excluded from ALDF clustering. The proposed rule depends on two factors: 1) the damage factors developed earlier, and 2) the frequency of the different axle type/load combinations. Rule 1 states: If the combined effect of damage factors and frequency for a certain axle type/load combination is less than 1% (normalized DF x frequency), this combination can be excluded from ALDF clustering. The 1% threshold was selected based on engineering judgment and in consideration of the actual predicted fatigue damage for each of the combinations.

Figure 7.23 shows the average combined effect of damage factors and frequency for all 44 WIM sites included in this study. Figure 7.23 also shows the 1% threshold line, below which axle type/load combinations should be excluded from the ALDF clustering process.

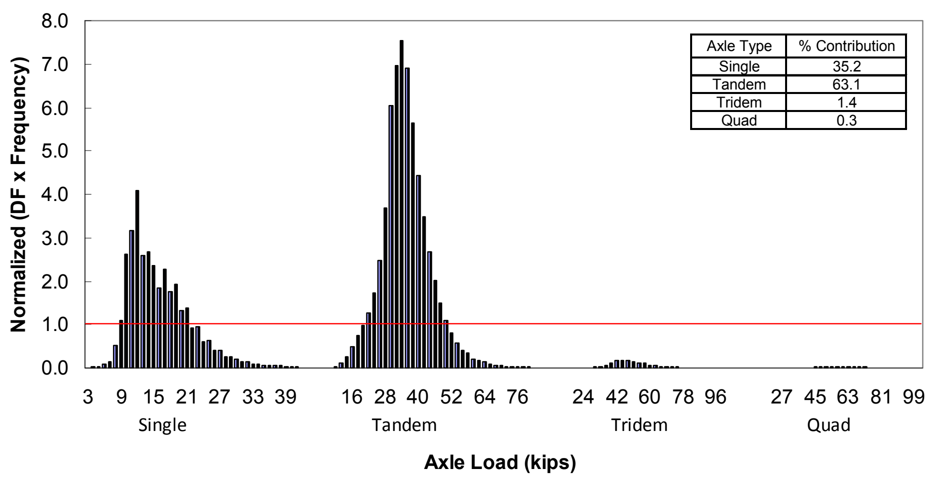

Figure 7.23. Combined effects of damage factors and frequency for different axle type/load combinations.

When Rule 1 is applied, Figure 7.23 suggests that all tridem and quad axles should be excluded from the ALDF clustering process. In addition, Figure 7.23 suggests that all the light single and tandem axles should be excluded, which includes single axles weighing 8 kips or less and tandem axles weighing 20 kips or less. However, due to the major role that these light axles with high frequencies play in defining the identity of the clusters (Stone et al., 2010), it is believed that these combinations should remain in the ALDF clustering process. These light single and tandem axles were found to help tremendously in identifying highway functional classifications and other factors that help to create decision trees for selecting proper ALDF clusters for a specific project (Sayyady et al., 2010).

Rule 2 was developed to avoid excluding light single and tandem axles from ALDF clustering. Rule 2 states: If the frequency, i.e., the contribution, of a certain axle type/load combination is less than 1% normalized frequency, this combination can be excluded from ALDF clustering.

Furthermore, Stone et al. (2010) recommended that Rule 1 and Rule 2 should both be applied before a particular axle type/load combination is selected for elimination. When both rules were applied to North Carolina ALDF data, only the following axle type/load combinations were kept: single axles weighing 3 kips through 21 kips and tandem axles weighing 6 kips through 50 kips. Using the remaining single and tandem axle type/load combinations, a two-dimensional clustering analysis was carried out, and the results are presented in Figure 7.24.

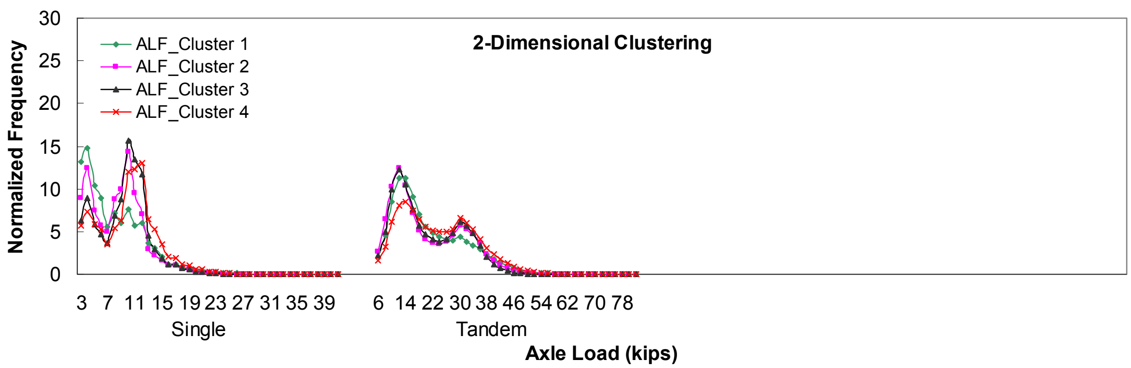

Figure 7.24. Final results of two-dimensional ALDF clustering analysis.

The results in Figure 7.24 suggest four clusters for each axle type. Note that tridem and quad axles, in addition to some of the heavier single and tandem axles, have been excluded from ALDF clustering after applying the two aforementioned rules (Sayyady et al., 2010). The most important observation to be made from Figure 7.24 is that the variations in single and tandem axles are much better delineated into different clusters than in Figure 7.15 that shows all four axle types included in the clustering analysis. ALDF clusters one through four are considered the final clusters that represent ALDF data in North Carolina. These four clusters are included in the final decision tree for ALDF selection, which is presented elsewhere (Sayyady et al., 2010).

CHAPTER 8 LOCAL CALIBRATION OF THE MEPDG FLEXIBLE PAVEMENT PERFORMANCE PREDICTION MODELS

8.1 Introduction

This chapter discusses the local calibration process of the performance prediction models currently embedded in MEPDG Version 1.1. The scope of this local calibration effort includes permanent deformation and alligator cracking distresses, both of which occur in flexible pavements. This chapter first presents the MEPDG overall design process and then introduces important terminology related to the MEPDG calibration. Some background information regarding the NCHRP 1-40B project (NCHRP, 2009) and its recommended local calibration steps are presented. Two different approaches for local calibration work have been evaluated under this research. The first approach, hereafter called 'Approach I', calls for executing the MEPDG numerous times using a large factorial of β_{r2} and β_{r3} for rutting and β_{f2} and β_{f3} for alligator cracking, and then using Microsoft Excel Solver to optimize the rest of the local calibration coefficients that correspond to the β_{r2} and β_{r3} or β_{f2} and β_{f3} combinations that give the smallest sum of squared error (SSE) between the predicted and measured distresses. The second approach, hereafter called 'Approach II', optimizes all the model coefficients simultaneously using the genetic algorithm (GA) optimization technique within the MATLAB® environment. The following sections explain in detail the implementation steps for each of the two approaches, present their calibration and validation results, and discuss the selection process of the final local calibration factors.

8.2 Overview of the MEPDG Analysis and Design Process

Figure 8.1 is a flow chart showing the MEPDG overall design and analysis process. It is important to recognize early in this chapter that MEPDG Version 1.1 is an analysis tool rather than a design tool. That is, the MEPDG requires the designer to start with a trial structural design, and then the software predicts the pavement distresses as they develop over the pavement service life.

Figure 8.1 suggests that traffic, layer materials, and location must be entered by the designer along with a proposed trial design. The pavement response models employ traffic, structural, and environmental data to compute critical pavement responses (i.e., stress, strain, and deflections). Pavement distress prediction models employ the computed critical responses to estimate the damage in the pavement structure. Transfer functions are then used to predict field performance. If a trial design satisfies the design criteria set by the agency, the trial design undergoes life cycle cost analysis (LCCA) to determine the feasibility of the design. Constructability is also checked. If the trial design passes all these checks, it becomes a candidate design structure.

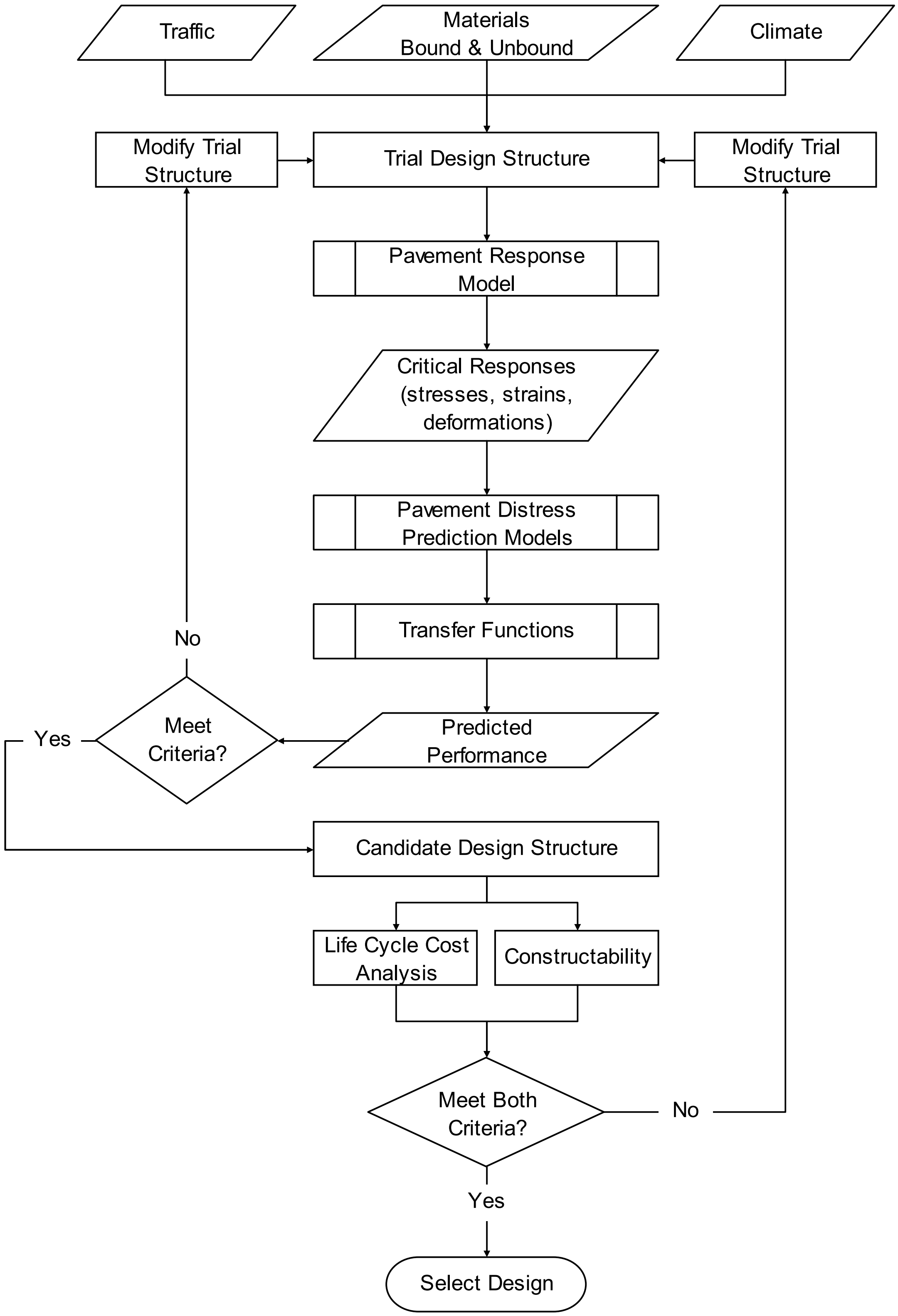

Figure 8.1. Flowchart showing an overview of the MEPDG analysis/design process.

8.3 MEPDG Calibration Terminology

This section provides definitions and explanations of some of the important calibration-related terms, some of which are used repeatedly throughout this chapter.

8.3.1 Reliability

Even though the MEPDG adopts mechanistic concepts that provide a more accurate and realistic methodology for pavement design compared to empirically-based design concepts, multiple sources of uncertainties associated with the design process remain, such as the prediction of traffic volume for years to come, construction practices, and materials, to name only a few. For this reason, the concept of *reliability* has been incorporated into the MEPDG. Reliability can be defined as the probability that the performance predicted by the MEPDG software will not exceed the design reliability criteria set by the designer for a specific performance measure at the end of the design life. The designer can design for a desired level of reliability for each distress type, and for smoothness. This reliability concept is available for use with flexible and rigid pavement designs. In general, the more important the project, the higher the desired design reliability is likely to be. This maxim explains the reason that state highway agencies generally use the level of traffic volume or truck traffic (which is normally associated with the importance of the project) as the parameter for design reliability (NCHRP, 2004b).

8.3.2 Model Verification

To simplify the definition of *verification*, the terms *conceptual model* and *simulation model* (or so-called *operational model*) should be defined first. A conceptual model is a model that reflects real-world situations. In the MEPDG, conceptual models include the performance prediction models that were developed based on mechanistic-empirical concepts to reflect real-world performance. However, because of excessive computational time, complexity issues, and other application difficulties, these models were simplified and programmed into software. These simplified models are referred to as *simulation models*. The verification process, therefore, is defined as a process to determine whether the simulation models can accurately simulate real-world performance. Verification can be carried out by executing the MEPDG using site-specific or typical materials, structural, traffic, and climatic data, and then comparing the predicted distress with the observed distress. Models are successfully verified if the predicted performance measures are found to be reasonably close to the observed or measured performance measures.

8.3.3 Model Calibration

In the MEPDG, the designer has the option to enter performance model calibration factors that reflect changes in predicted distress caused by state-specific data, including but not limited to, traffic, materials, and climatic data. These calibration factors are necessary to compensate for performance model simplifications and limitations (NCHRP, 2009). *Calibration* is defined as the process through which the *bias* (or so-called; residual error), and the standard error of the estimate (S_e) are both minimized. In simple terms, bias is a representation of the differences between predicted and field-measured performance. Within the scope of calibration, bias is defined as a systematic error that causes the model to overpredict or under predicts field performance. Note that bias itself is not the objective function in the optimization process. Instead, the sum of squared errors (SSE) between predicted and measured distresses is the objective function. In contrast with the bias term, the SSE term does not differentiate between overprediction and underprediction because the differences between predicted and measured distresses become positive when squared. It is usually expected for the bias to decrease when the *Total SSE* decreases, this is however not always true.

Mathematically, the S_e is the standard deviation of the residual error. The S_e can be seen as a measure of the dispersion of data points around the line of equality (LOE) between predicted and field-measured performance values. According to Von Quintus (NCHRP, 2009), four major sources of error contribute to the S_e. The first source is attributed to measurement errors associated with distress or smoothness measurements in the field. The second source of error is an input error, which is related to the underestimation or overestimation of certain input parameters required by the MEPDG. An example is entering an inaccurate estimation of the subgrade modulus. The third source of error is related to deficiencies in the prediction models themselves. The fourth source of error has been referred to as *pure error*. This type of error stems from the assumption that if two road sections are identical, then distresses measured from both sections should be identical. This assumption is known to be invalid due to differences in construction practices and variables encountered in the field.

8.3.4 Ratio of the Standard Deviation of the Residual Error (S_e) to the Standard Deviation of the Measured Performance (S_y): (S_e/S_y)

To better interpret the reason for calculating the ratio S_e/S_y, it is first necessary to define each of these two terms. S_e, defined earlier as the standard deviation of the residual error, measures the dispersion around the LOE between predicted and measured performance. S_y is defined as the standard deviation of the measured performance. Hence, as a ratio, S_e/S_y compares the variability in the predicted performance to that of the measured performance. A ratio that is greater than one indicates that the variability in the residual error between predicted and measured performance is larger than that in the measured data. A ratio that is smaller than one indicates that the variability in the predicted residual error is smaller than that in the measured data. It is obvious that a ratio smaller than one is always preferable.

8.3.5 Model Validation

Model validation utilizes a new set of measured performance data to check if the calibrated performance models can predict field performance with the same accuracy when using field data employed in the calibration process. A model is said to be validated successfully if the bias and S_e determined using the independent field data are reasonably close to those determined using the calibration data.

8.3.6 Hierarchical Materials Data Input Levels

The MEPDG offers the designer three hierarchical materials data input levels: Level 1, Level 2, and Level 3. This flexibility enables the designer to match the level of effort with the importance of the project under design.

- Level 1 reflects the designer's excellent knowledge of a given parameter. Level 1 input parameters are measured either directly from the site or near the site under study, or determined through laboratory testing.
- Level 2 reflects medium-level knowledge about the data for the site under study. Level 2 parameters are either determined from statewide averages or estimated from other known parameters through statistical correlations and relationships.
- Level 3 reflects the least amount of knowledge the designer needs to have about these inputs for the site under study. Level 3 input parameters are either substituted for MEPDG default values or estimated from regional averages.

In this research work, Level 2 inputs were used for asphalt concrete mixtures and for subgrade materials. Level 1 could not be applied for the asphalt concrete input because Level 1 requires characterization of the actual materials that were used in construction, which were unavailable for this research work. Similarity, Level 1 could not be applied for the subgrade layer input because the subgrade data that were used in the calibration were obtained from the NCHRP 9-23A database, as discussed in Chapter 4 and not from testing the actual subgrade materials at the project location. As for the unbound base materials, national default values were used because local unbound materials were not characterized as part of this research work; hence, Level 3 input was applied for the unbound base materials.

Table 8.1 summarizes the data required for each of the three input levels for asphalt concrete layers.

Table 8.1. Asphalt Concrete Data Requirements for the Three Levels of Input

<table>
<tr><th>Analysis Level</th><th>Data Required for HMA Mixtures</th></tr>
<tr><td>Level 1</td><td>Dynamic modulus. Min. 3 temp. and 3 frequencies, Max. 8 temp. and 6 frequencies</td></tr>
<tr><td rowspan="4">Level 2</td><td>Cumulative % retained on 3/4" sieve</td></tr>
<tr><td>Cumulative % retained on 3/8" sieve</td></tr>
<tr><td>Cumulative % retained on #4 sieve</td></tr>
<tr><td>% passing # 200 sieve</td></tr>
<tr><td>Level 3</td><td>Similar to Level 2</td></tr>
<tr><td>Analysis Level</td><td>Data Required for Binder</td></tr>
<tr><td rowspan="7">Level 1</td><td>Shear modulus and phase angle for RTFO binder and at angular frequency of 10 radians/sec. Min. 3 temp. or;</td></tr>
<tr><td>Temperature (°F) at softening point = 13000 P, and</td></tr>
<tr><td>absolute viscosity (P) at 140°F, and</td></tr>
<tr><td>kinematic viscosity (CS) at 275°F, and</td></tr>
<tr><td>Specific gravity at 77°F</td></tr>
<tr><td>Penetration / optional</td></tr>
<tr><td>Brookfield viscosity / optional</td></tr>
<tr><td>Level 2</td><td>Similar to Level 1</td></tr>
<tr><td rowspan="3">Level 3</td><td>Superpave binder grading, or</td></tr>
<tr><td>viscosity grade, or</td></tr>
<tr><td>penetration grade</td></tr>
<tr><td>Analysis Level</td><td>General Data Required for HMA Layer</td></tr>
<tr><td rowspan="7">All Levels (default values could be used)</td><td>Reference temperature (°F)</td></tr>
<tr><td>As-built effective binder content (%)</td></tr>
<tr><td>As-built air voids (%)</td></tr>
<tr><td>As-built total unit weight (pcf)</td></tr>
<tr><td>Poisson's ratio</td></tr>
<tr><td>Thermal conductivity of asphalt (BTU/hr-ft-F°)</td></tr>
<tr><td>Heat capacity of asphalt (BTU/lb-ft)</td></tr>
</table>

8.4 Local Calibration Procedure, as Recommended by NCHRP 1-40B

The following sections provide a brief background of the NCHRP 1-40B project and its local calibration recommended procedure for local traffic, climatic, and materials data.

8.4.1 Background

Based on the recommendations of the NCHRP 1-37A project team (NCHRP, 2004b), in order for distress prediction models to be fully applicable for local materials, construction practices, and environmental conditions, they should be calibrated using data obtained locally. Until 2004, no documentation was available to provide agencies with guidance to perform local calibration. So, in 2005, NCHRP 1-40B project, "Local Calibration Guidance for the Recommended Guide for Mechanistic-Empirical Design of New and Rehabilitated Pavement Structures" was awarded to Applied Research Associates, Inc. One of the main objectives of the NCHRP 1-40B project was to prepare a detailed and practical guide for highway agencies to employ in their local or regional calibration efforts of the performance prediction models in the MEPDG. Among the final documents prepared for this project is the "Recommended Practice for Local Calibration of the M-E Pavement Design Guide" (NCHRP, 2009). This final document suggests a step-by-step calibration procedure that is presented in Section 8.4.2.

8.4.2 Application of the NCHRP 1-40B Calibration Procedure to NC Conditions

Before the suggested local calibration steps are presented, it is important to mention that the local calibration process deals only with the calibration coefficients and exponents of the performance models. The local calibration process does not deal with the supporting mathematical models that are employed by the performance prediction models within the MEPDG. Examples of the supporting models are structural response models, the enhanced integrated climatic model (EICM), and time-dependent material property models. These supporting models are, in fact, statistical models themselves that are assumed to be an accurate representation of real-world conditions. The recommended local calibration procedure, as presented in the NCHRP 1-40B project, is summarized in the following sections. For further details, readers are referred to NCHRP, 2009.

8.4.2.1 Selection of a Hierarchical Input Level for Each Input Parameter

It is recommended that the hierarchical input level to be used in the local calibration process is consistent with the design procedure that will be recommended for NCDOT personnel to follow. Because the laboratory testing program within this research work does not include any of the actual materials that were built, no true input Level 1 exists for any of the layer materials, as mentioned earlier. The hot mix asphalt (HMA) material properties, including binder and mixture, are considered Level 2 inputs. Similarly, the base and subgrade materials are Level 3 and Level 2 inputs, respectively. Traffic information, on the other hand, is Level 1 input because such information was available for most of the calibration/validation sections. As mentioned earlier, the scope of this calibration/validation work covers only rutting and alligator cracking distresses that occur in flexible pavements. The NCHRP-1-40B panel recommends that a minimum of 20 test sections should be available for rutting calibration and a minimum of 30 sections for alligator cracking calibration. The following 8.4.2.2 presents the selection process for the number of sections chosen for the local calibration and validation processes.

8.4.2.2 Selection of Calibration/Validation Sections

The NCHRP 1-40B panel offers several recommendations regarding the selection of road sections to be used for calibration/validation work, as follows.

- Calibration sections must be selected with the fewest number of structural layers and materials to reduce the amount of materials input required by the MEPDG.
- In the calibration process, sections should be included that have non-traditional mix types, such as polymer-modified asphalt, stone matrix asphalt and treated base layers. Within this recommendation, asphalt and cement-treated base layers are considered in the local calibration effort.
- Calibration sections with overlay history should be included in the calibration/validation process, simply because the MEPDG is used also for rehabilitation design and should be able to accommodate such conditions.
- Calibration/validation sections should have at least ten years of distress data to ensure that all time-dependent material properties and the occurrence of distress are taken into account in the determination of any bias and standard error of the estimate.

Figure 8.2 is a flow chart that illustrates the available long-term pavement performance (LTPP) and NCDOT pavement management system (PMS) flexible and rigid pavement sections. Figure 8.2 shows that North Carolina has a total of 27 LTPP sites: 9 rigid pavement sites and 18 flexible pavement sites. The 18 flexible sites have a total of 28 test sections, each 500 feet long. The 28 sections are divided further into 12 special pavement study (SPS) sections and 16 general pavement study (GPS) sections. Only 6 of the 12 SPS sections are core sections, i.e., new construction, versus 6 agency-supplied sections that were not included in the calibration work because very few data were available for these sections. Furthermore, Figure 8.2 indicates the availability of 24 PMS flexible pavement sections from the NCDOT. Twelve of these sections were let in 1993 and 12 were let in 1999. Note that the asphalt concrete mixtures for the sections that were let in 1993 were designed using the traditional Marshall mix design method, whereas those that were let in 1999 were designed using the Superpave mix design method.

As mentioned earlier, the total number of sections available for the calibration and validation studies is 46 sections: 6 SPS sites, 16 GPS sites, and 24 non-LTPP sites. Because the LTPP sites had more complete distress and materials information available than the other sites, the research team decided to use all LTPP sites for calibration and use the 24 non-LTPP sites for validation. Some of the LTPP sections and many of the NCDOT sections were found to lack data, however, so MEPDG defaults and engineering judgment were used to populate the missing data.

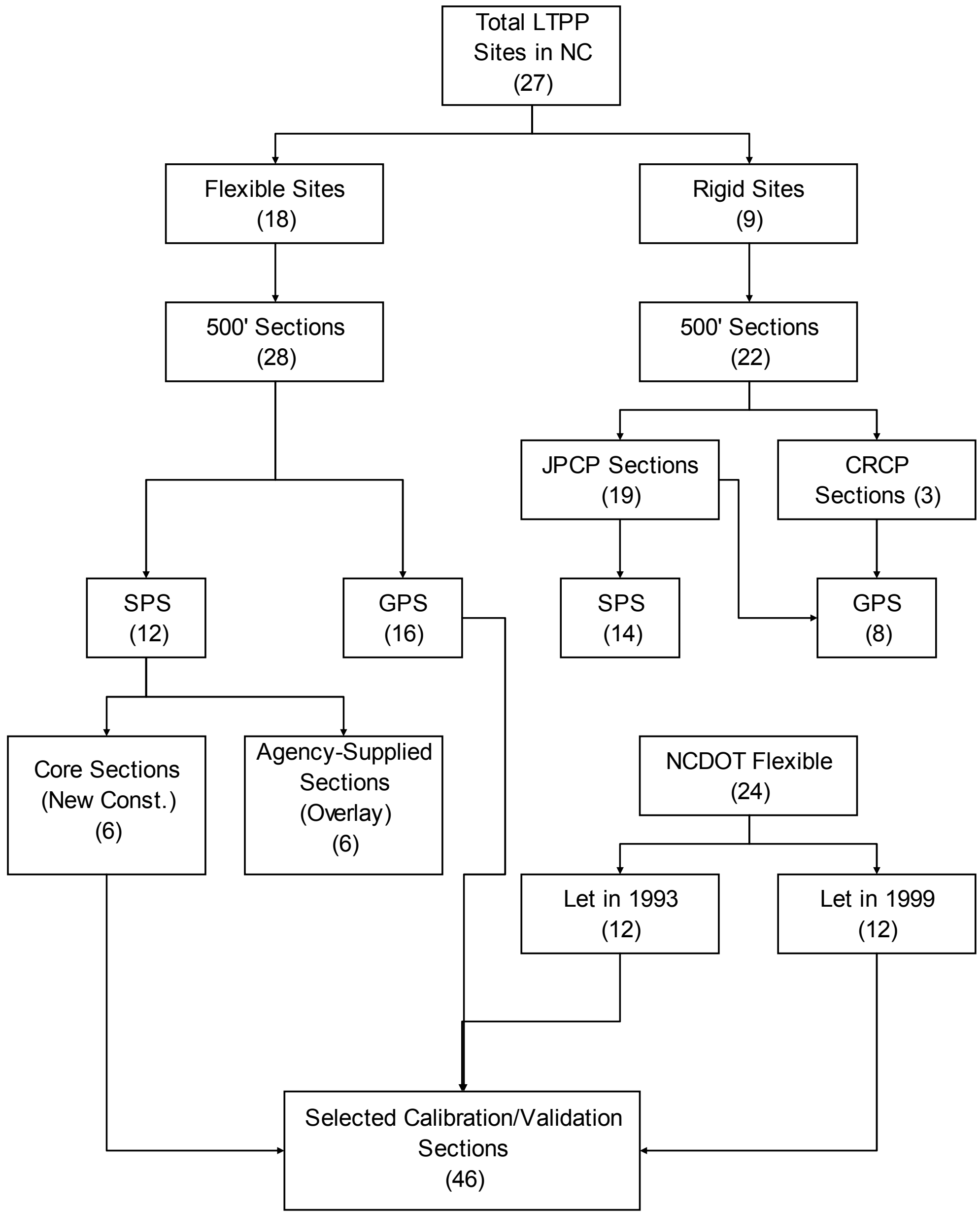

Figure 8.2. Calibration/validation sections available for local calibration in North Carolina.

8.4.2.3 Extraction and Evaluation of Distress and Project Data

The extraction of structural, materials, traffic, and performance data is a vital step for successful calibration and validation work. Due to the variations in construction practices and distress measurement methods, it became important in this research effort to convert, as necessary, the obtained data so that they adhered to the same standards followed by the MEPDG development team for calibrating the performance prediction models currently embedded in the MEPDG. All data for the LTPP sections were extracted from the LTPP standard data release 24.0 of January 2010. These extracted data are summarized in Appendix A.

In addition, pavement performance ratings for the 24 PMS sections were acquired from the NCDOT. The NCDOT pavement condition survey manual (NCDOT, 2006) was consulted in order to understand the performance ratings given for alligator cracking and rutting. During the study, several issues were identified that had to be resolved. One issue was the need to convert the NCDOT performance ratings to a format similar to that reported in the LTPP database, which coincidentally is the same format used to calibrate the MEPDG performance prediction models. This conversion was necessary because the LTPP program and the NCDOT use different distress measurement techniques. The LTPP program measures alligator cracking by directly measuring the area affected in the lane, whereas the NCDOT measures it by assigning a rating based on the length of the cracked section.

The following points provide background about the protocol used by NCDOT concerning alligator cracking distress identification and measurement.

- Alligator cracking is measured in the outer wheel path of the most distressed lane. It is observed that 90% of the time, the most distressed lane is the outer lane.
- If the outer wheel path is cracked continuously, the section is rated as 100%, even if the inner wheel path exhibits some cracks. Thus, there is no way to quantify the cracking in the inner wheel path.
- Starting in 2002, measurements of edge cracking (caused by the movement of soil beneath the pavement due to insufficient lateral support) were combined with those of alligator cracking (caused by repeated traffic loading). Thus, there is no way to quantify or separate one type of cracking from the other.
- The performance ratings do not indicate the extent to which each lane of a two-lane roadway (in an undivided case) contributes to the rating. For example, a rating of 8 for a section may mean: 4 (one lane of a two-lane roadway) + 4 (the other lane), or 5 + 3, or any other combination that makes eight.

The following sections explain the process used to convert the NCDOT ratings for alligator cracking and rutting to a format equivalent to that used by the LTPP program.

8.4.2.3.1 Conversion of NCDOT Alligator Cracking Rating to Equivalent MEPDG Format

The NCDOT distress survey effort covers the following performance measures for flexible pavements: alligator cracking, transverse cracking, rutting, raveling, oxidation, bleeding, ride quality and patching. Only alligator cracking is rated for both extent and severity, with the percentage of the total section recorded as *none*, *light*, *moderate*, or *severe* alligator cracking for each segment.

According to the NCDOT pavement condition survey manual (NCDOT, 2006), a *low* rating for alligator cracking corresponds to longitudinal disconnected hairline cracks about 1/8 inch wide running parallel to each other. A *moderate* rating refers to longitudinal cracks in one or both wheel paths or where the edge of the pavement forms an alligator pattern. In such circumstances, cracks may be lightly spalled and are about 1/4 inch wide. *Severe* alligator cracking refers to cracks that have progressed so that pieces of the pavement appear loose with severely spalled edges. Potholes may also develop. Severe cracks are between 3/8 and 1/2 inch or wider.

In a study by Corley-Lay et al. (2010), LTPP-monitored distresses were compared with NCDOT-monitored distresses for 23 LTPP flexible pavement sites in North Carolina. Large differences were found in the monitored distresses; these differences are due mainly to differences in monitoring methods. Because of the very large surveyed road network, NCDOT personnel recorded instances of alligator cracking using the windshield survey method. This approach alone introduced numerous errors. Hence, a method was needed to convert alligator cracking ratings as measured by the NCDOT to equivalent alligator cracking as defined in the LTPP database.

Corley-Lay et al. (2010) made several assumptions in order to compare the NCDOT data collected for segments of variable lengths, which generally were anywhere between 0.5 and 2.0+ miles long, with LTPP surveyed sections that are 500 feet long. Their major assumption was that the distresses within the long NCDOT segments are proportional to those in the 500 feet subsections of the LTPP sites. That is, if 20% of a long section exhibits severe alligator cracking, it was assumed that 20% of the LTPP section also has severe alligator cracking. In reality, however, such an assumption is far from correct. The 500 feet of a LTPP section is such a small percentage of a two-mile NCDOT section that even if it were 100% severe alligator cracking, it would not reach the threshold for 10% severe alligator cracking, unless the alligator cracking was present beyond the LTPP section. Having no data to justify that the LTPP sites were either worse or better than the surrounding roadway in terms of alligator cracking, Corley-Lay et al. accepted this assumption and understood its limitations.

Corley-Lay et al. made another assumption in order to convert a percentage of the extent of cracking to an area measurement. As an initial assumption, they assumed that low severity alligator cracking was 1.5 feet in width, moderate severity alligator cracking was 2 feet in width, and severe alligator cracking was 2.5 feet in width. Then, acknowledging that the actual length of cracking could vary between 500 feet and 1000 feet for 100% cracking, the lowest value was used. Based on these assumptions and using a basic conversion factor, the area of cracking was calculated in square meters for each NCDOT distress survey for each of the 23 LTPP surveyed sections.

A comparison of the LTPP survey results with the NCDOT alligator cracking measurements indicates that the NCDOT survey methods understate the distress. When the data were combined, a low degree of correlation was found. In order to optimize the relationship between NCDOT alligator cracking and LTPP alligator cracking, a calibration factor was applied to each term, as shown in Equation (8.1).

$$Total\ Fatigue\ Cracking = X_1(low, m^2) + X_2(Moderate, m^2) + X_3(Severe, m^2) \tag{8.1}$$

The values of X_1, X_2 and X_3 were varied to minimize the sum of the squared differences between the LTPP alligator cracking and NCDOT alligator cracking. The optimized values of X_1, X_2 and X_3 are:

X_1 = 5.9

X_2 = 1.7

X_3 = 13.9

Knowing the alligator cracking rating as determined by the NCDOT, the total alligator cracking area that is equivalent to that determined from the LTPP method could be calculated. Alligator cracking ratings from all 24 PMS sites were converted to LTPP equivalent alligator cracking values so that they could be used for the validation portion of the calibration effort.

8.4.2.3.2 Conversion of NCDOT Rutting Ratings to Equivalent MEPDG Format

According to the NCDOT pavement condition survey manual (NCDOT, 2006), the NCDOT has four ratings for rutting distress: *none*, *light*, *moderate*, and *severe*. *Light* refers to ruts that are 1/4 inch to less than 1/2 inch deep, *moderate* indicates ruts that are 1/2 inch to less than 1 inch deep, and *severe* indicates ruts that are deeper than 1 inch.

According to Corley-Lay et al. (2010), NCDOT personnel were instructed to take at least one physical reading each day during the survey period. These values were not recorded, however, and were for “self calibration” only. Comparing the NCDOT pavement condition rutting levels with the LTPP measured values, which are based on results from three different measuring methods for rutting, several observations could be made. First, the LTPP method of taking several repeated measurements and using the average makes it highly unlikely that a value of zero rut depth would be recorded. For all the data sets, Corley-Lay et al. reported not a single occurrence of zero rut depth in the LTPP sets used in this evaluation. In contrast, the NCDOT recorded 52 ratings of *none*. Another observation is that the NCDOT sites showed little rutting, which is consistent with agency observation as per Corley-Lay.

Because the subjective ratings of light, medium, and severe rutting cannot be used for calibration purposes, these ratings were converted to numerical values that correspond to the smaller number in the range definitions. For example, for light ratings (0.25 in. to 0.5 in.), a representative value of 0.25 inch was used. For moderate ratings (0.5 in. to 1 in.), a representative value of 0.5 inch was used. Because rutting is not a major distress in North Carolina, none of the sections exhibited severe rutting; hence, no conversion was needed.

8.4.2.3.3 Conversion of Field Asphalt Concrete Layer Materials to Equivalent Superpave Mixtures

In order to perform Level 2 calibration using material-specific performance prediction model coefficients and stiffness measures developed for the twelve most commonly used asphalt concrete mixtures in North Carolina, it was necessary to develop a method to convert each of the layer materials found in a field calibration section to an equivalent Superpave mixture, i.e., to match each HMA layer from the field with one of the twelve asphalt concrete mixtures being tested in this research work. This need arose from the fact that the LTPP and the 1993 PMS calibration and validation sites have asphalt concrete mixtures that were designed using the Marshall mix design method, which is quite different from the current Superpave mix design method. The 1999 PMS mixtures, on the other hand, were developed using the Superpave mix design method, and therefore, matching the field layer mix types from the 1999 PMS mixtures with one of the twelve mixtures was a simple task. The proposed matching process is based on the following three factors:

- Mix aggregate gradations for four sieve sizes, specifically, the percentage retained on a 3/4-inch sieve, 3/8-inch sieve, and # 4 sieve, and the percentage passing a # 200 sieve.
- Binder grade.
- Reclaimed asphalt pavement (RAP).

To match field asphalt concrete layers to one of the twelve most commonly used asphalt concrete materials that were characterized in the lab, the following procedure was followed:

1) The first step is to find the nominal maximum aggregate size (NMAS) of aggregate for every asphalt concrete layer for each of the calibration/validation sections by matching the percentage retained or the percentage passing information to the averages shown in Table 8.2. Table 8.2 was constructed to show the average percentage of retained or passing aggregate for the aforementioned four sieve sizes using the twelve mixtures used in this research. For example, a field mixture that has gradation measures of 0, 3, 26, and 5.5 is identified as a 9.5 NMAS mixture according to Table 8.2.
2) Once the NMAS for each asphalt concrete layer of the calibration/validation sections is identified, the binder grade that was used in the field for that mixture is utilized to refine the selection within the same NMAS table. For example, if the binder grade for the mixture in the example given in Step 1 is found to be a PG 70-22 or equivalent asphalt binder, the mixture will be a "C" mixture. Recall that NCDOT asphalt mixture designation rules are presented under Section 2.2. The options now are reduced to S9.5C and RS9.5C. In other words, the binder grade in this example determines whether the mixture will be a "B" mixture or a "C" mixture.
3) For older sections that were constructed with mixtures designed using the Marshall mix design method and viscosity-based binder grading, the viscosity-based binder grades must be converted to equivalent Superpave binder grades. To do so, the AC-20 viscosity binder grade is considered equivalent to a PG 64-22 Superpave performance grade, and the AC-40 viscosity binder grade is considered equivalent to a PG 70-22 Superpave performance grade. In North Carolina, AC-20 is the binder grade that has been used in most projects.
4) The field mixtures are checked for the presence of RAP. If the example mixture given is Step 1 contains a RAP portion, the mixture will best match the RS9.5C Superpave mixture; if not, it will be matched with the S9.5C mixture. When asphalt

binder data are unavailable in the LTPP or PMS sections, mixtures are assumed to have a PG 64-22 Superpave binder.

Table 8.2. Average Aggregate Gradation Measures for the Twelve Most Commonly Used Mixtures in North Carolina

Sieve Size	S9.5B	S9.5C	RS9.5B	RS9.5C	Average
% Retained on 3/4"	0.0	0.0	0.0	0.0	0.0
% Retained on 3/8"	4.0	3.0	4.0	3.0	3.5
% Retained on # 4	34.0	32.0	25.0	21.0	28.0
% Passing # 200	5.8	6.0	5.7	7.2	6.2

Sieve Size	S12.5C	RS12.5C	Average
% Retained on 3/4"	0.0	0.0	0.0
% Retained on 3/8"	11.0	11.0	11.0
% Retained on # 4	34.0	28.0	31.0
% Passing # 200	4.8	4.7	4.8

Sieve Size	I19B	I19C	RI19B	RI19C	Average
% Retained on 3/4"	1.0	2.0	1.0	3.0	1.8
% Retained on 3/8"	27.0	22.0	24.0	25.0	24.5
% Retained on # 4	50.0	49.0	48.0	61.0	52.0
% Passing # 200	4.5	5.1	5.0	5.0	4.9

Sieve Size	B25B	RB25B	Average
% Retained on 3/4"	17.0	18.0	17.5
% Retained on 3/8"	36.0	32.0	34.0
% Retained on # 4	54.0	52.0	53.0
% Passing # 200	4.0	4.4	4.2

5) Table 8.3 is consulted in circumstances where aggregate gradation data are unavailable, but the Marshall mixture designation is available, when field mixtures are identified as "D" mixtures, or when the field Superpave mixtures for the 1999 PMS sites do not directly match any of the characterized twelve mixtures. Table 8.3 was developed based on engineering knowledge and feedback from the Materials and Tests Unit at NCDOT. If a pavement design requires the use of any of the mixture types in Table 8.3 designers must use the corresponding equivalent mixture because that mixture was the mixture used in the calibration process. In other words, the effect of using an equivalent mixture type rather than the desired mixture will be smeared in the local calibration factors.

Table 8.3. Asphalt Concrete Mixture Conversion List

Mix Type	Equivalent Superpave
I-1	S9.5B
I-2	S9.5B
HDS	S9.5C or S12.5C
HDB	I19.0C
H	I19.0B
HB	B25.0B
ATB[1]	B25.0B
SF9.5A	S9.5B
S12.5D	S12.5C
I19.0D	I19.0C
B25.0C	B25.0B
B37.5C	B25.0B
B25.0	B25.0B
B37.5	B25.0B

[1]Asphalt-Treated Based.

8.4.2.4 Conducting Field and Forensic Investigations

In the context of flexible pavement distresses, forensic investigations that include trench cuts, cores, and test pits normally are conducted for two reasons: 1) to find the contribution of different layers to the total rut depth measured at the surface of the pavement, and 2) to distinguish between top-down cracking (or so-called longitudinal cracking) and bottom-up cracking (or so-called alligator cracking). Due to the large number of sections selected for the calibration/validation process, and also due to time and budget limitations, forensic investigations were not conducted in this research work.

8.5 Verification and Paper-Based Calibration Results using Level 3 Materials Data

In an early stage of this research project, national default calibration coefficients for the rutting and alligator cracking models were used to verify whether or not the global coefficients could capture the development of rutting and alligator cracking distresses found in North Carolina pavements. In addition, the MEPDG rutting and alligator cracking models were calibrated for local conditions using Level 3 materials input. This effort was undertaken as preliminary work for Level 1 calibration (explained in detail in upcoming sections). The results of this Level 3 verification and calibration, referred to also as *paper-based calibration*, were published in a Transportation Research Board paper in 2008. (A copy of this paper can be found as Appendix F of this final report.) Note that the paper-based calibration used an older version of the MEPDG (Version 1) and fewer performance data, as were available at that time. The Level 1 calibration, on the other hand, used the latest LTPP and PMS data that were available at the end of 2010. Due to the differences in resources, MEPDG version, and other differences, the results from the paper-based calibration, which were valid at the time, cannot be compared to the Level 1 calibration results presented in the following sections.

8.6 Local Calibration Procedure for Rutting and Alligator Cracking Prediction Models in the MEPDG

8.6.1 Background and Assumptions

The following sections present two approaches that were evaluated under this research work to calibrate the rutting and alligator cracking prediction models currently embedded in MEPDG Version 1.1. The first approach, hereafter called 'Approach I-R' for rutting and 'Approach I-F' for fatigue cracking, employs the MEPDG and Microsoft Excel Solver to find the local calibration factors that minimize the SSE between the measured and predicted distresses. The second approach, hereafter called 'Approach II-R' for rutting and 'Approach II-F' for fatigue cracking, employs a GA optimization technique within the MATLAB® environment to find the local calibration factors that minimize the SSE through a true optimization of all calibration factors simultaneously.

The organization of the following sections is as follows: first, the procedure, calibration, and validation results are presented for Approach I-R and Approach I-F; second, the procedure, calibration and validation results of Approach II-R and Approach II-F are presented and discussed. Finally, the two approaches are compared, and the recommended approach is selected. Recommended local calibration factors for implementation are summarized at the end of the chapter.

One of the major differences between rutting predictions and alligator cracking predictions in the MEPDG is that rutting predictions have no separate transfer function to relate MEPDG rut depth predictions to field measured rut depth. In other words, the MEPDG directly predicts rut depth in bound and unbound layers, and the predicted rut depth is expected to relate to field measurements. In other words, the MEPDG considers only a single model for each material type that users must calibrate; one model for HMA rut depth predictions, another for unbound base materials and a third for predicting the rut depth in subgrade layers. The three models have been previously presented and are presented again under Equation (8.2), Equation (8.3), and Equation (8.4) respectively. For alligator cracking, however, two models must be calibrated before a good prediction can be achieved: 1) the number of cycles to failure (N_f) model, and 2) the transfer function that converts damage to field alligator cracking.

Prior to presenting the two calibration approaches and their results, it is vital to list the following necessary assumptions that were made with respect to rutting models calibration, as follows.

1) Because no forensic studies were performed on any of the pavement sections involved in this research work, it was assumed that the contribution of each of the layers to the total rut depth measured at the pavement surface for a certain pavement

section is similar to that predicted by the MEPDG for the same section. The research team appreciates that this assumption could introduce errors. However, in the absence of the actual measured rut depth of each layer in the pavement sections, making this assumption was the only available option to estimate the contribution of each layer to total rut depth.

2) The rutting model calibration effort was performed under the assumption that the upcoming version of the MEPDG will allow users to enter material-specific rutting model coefficients for different HMA layers. This option is currently unavailable in MEPDG Version 1.1. With an increase in the use of full-depth flexible pavement design by the NCDOT, the research team felt that this assumption was necessary to account for the different rutting performances of different asphalt concrete mixtures.
3) Unbound base and sub-base materials as well as subgrade materials were not characterized as part of this project; hence, their national default *k* values were used in the calibration process. In other words, only local calibration coefficients, i.e., β_{gb} and β_{sg}, were calibrated for the unbound materials. In the MEPDG, cement-treated base (CTB) materials are treated as materials that do not rut; hence, no local calibration was required for such materials. In the calibration effort, asphalt-treated base (ATB) materials were treated as B25.0B asphalt mixtures and, therefore, were calibrated as part of the HMA rutting model calibration effort.

8.6.2 Hybrid MEPDG Version for Local Calibration

As mentioned in the second assumption above, the current MEPDG Version 1.1 does not offer the option for users to enter material-specific rutting model coefficients for different asphalt concrete mixtures. Therefore, the research team investigated this issue and, in consultation with Mr. Gregg Larson from Applied Research Associates (the developers of the MEPDG software), developed a hybrid version of the MEPDG that uses MEPDG version 1.1 as the basic platform, along with an execution file that considers multiple layers from MEPDG Version 9-30A. The hybrid version requires users to create some text files in the project directory manually and to follow a certain procedure. The procedure is explained in the *MEPDG NC User Reference Manual* presented in Appendix H.

8.6.3 Rutting Models Calibration-Approach I-R

8.6.3.1 Introduction

Rutting calibration Approach I-R is a two-step process. First, the MEPDG is executed many times using a large factorial of β_{r2} and β_{r3}, shown in Table 8.4, and second, Microsoft Excel Solver is used to optimize for the β_{r1}, β_{gb}, and β_{sg} coefficients that correspond to the β_{r2} and β_{r3} combination that is found to yield the smallest SSE between measured and predicted total rut depth. The factorial shown in Table 8.4 was developed rationally based on a wide range of possible calibration factors. Worth mentioning is that Microsoft Excel Solver uses the generalized reduced gradient (GRG) method to find the minimum SSE between predicted and measured total rut depth.

Table 8.4. Complete List of β_{r2} and β_{r3} Combinations Used in Approach I-R Calibration

No.	β_{r2}	β_{r3}	No.	β_{r2}	β_{r3}	No.	β_{r2}	β_{r3}	No.	β_{r2}	β_{r3}
1	0.1	0.2	29	0.4	1.8	57	1.0	1.4	85	1.6	1.0
2	0.1	0.4	30	0.4	2.0	58	1.0	1.6	86	1.6	1.2
3	0.1	0.6	31	0.6	0.2	59	1.0	1.8	87	1.6	1.4
4	0.1	0.8	32	0.6	0.4	60	1.0	2.0	88	1.6	1.6
5	0.1	1.0	33	0.6	0.6	61	1.2	0.2	89	1.6	1.8
6	0.1	1.2	34	0.6	0.8	62	1.2	0.4	90	1.6	2.0
7	0.1	1.4	35	0.6	1.0	63	1.2	0.6	91	1.8	0.2
8	0.1	1.6	36	0.6	1.2	64	1.2	0.8	92	1.8	0.4
9	0.1	1.8	37	0.6	1.4	65	1.2	1.0	93	1.8	0.6
10	0.1	2.0	38	0.6	1.6	66	1.2	1.2	94	1.8	0.8
11	0.2	0.2	39	0.6	1.8	67	1.2	1.4	95	1.8	1.0
12	0.2	0.4	40	0.6	2.0	68	1.2	1.6	96	1.8	1.2
13	0.2	0.6	41	0.8	0.2	69	1.2	1.8	97	1.8	1.4
14	0.2	0.8	42	0.8	0.4	70	1.2	2.0	98	1.8	1.6
15	0.2	1.0	43	0.8	0.6	71	1.4	0.2	99	1.8	1.8
16	0.2	1.2	44	0.8	0.8	72	1.4	0.4	100	1.8	2.0
17	0.2	1.4	45	0.8	1.0	73	1.4	0.6	101	2.0	0.2
18	0.2	1.6	46	0.8	1.2	74	1.4	0.8	102	2.0	0.4
19	0.2	1.8	47	0.8	1.4	75	1.4	1.0	103	2.0	0.6
20	0.2	2.0	48	0.8	1.6	76	1.4	1.2	104	2.0	0.8
21	0.4	0.2	49	0.8	1.8	77	1.4	1.4	105	2.0	1.0
22	0.4	0.4	50	0.8	2.0	78	1.4	1.6	106	2.0	1.2
23	0.4	0.6	51	1.0	0.2	79	1.4	1.8	107	2.0	1.4
24	0.4	0.8	52	1.0	0.4	80	1.4	2.0	108	2.0	1.6
25	0.4	1.0	53	1.0	0.6	81	1.6	0.2	109	2.0	1.8
26	0.4	1.2	54	1.0	0.8	82	1.6	0.4	110	2.0	2.0
27	0.4	1.4	55	1.0	1.0	83	1.6	0.6			
28	0.4	1.6	56	1.0	1.2	84	1.6	0.8			

8.6.3.2 Calibration Steps

Figure 8.3 summarizes the two major steps required for calibrating the rutting models under Approach I-R. The following subsections discuss these two steps.

8.6.3.2.1 Step 1: Replace Default *k* Values with Material-Specific *k* Values.

Step 1 in Figure 8.3 indicates that, for each calibration section, different material-specific *k* values (reported in Table 5.13) are entered for the different layers in the hybrid version of the MEPDG. Material-specific *k* values replace the national default *k* values, and all beta values (the local calibration coefficients) remain equal to one. For a section with three HMA layers, nine *k* values are required to be entered. Note that the MEPDG accepts a maximum of four asphalt concrete layers.

8.6.3.2.2 Step 2: Find Beta Values that Minimize the Sum of Squared Errors (SSE) for Total Rut Depth.

The goal of Step 2 in Figure 8.3 is to find the best values of five coefficients, shown in Equations (8.2), (8.3), and (8.4), which together minimize the bias and the standard error of estimate, S_e, as explained under Section 8.3.3. The five coefficients, or so-called *model calibration factors*, are: β_{r1}, β_{r2}, β_{r3}, β_{gb}, and β_{sg}.

$$\frac{\varepsilon_p}{\varepsilon_r} = K_z * \beta_{r1} * 10^{kr1} T^{\beta_{r2} * k_{r2}} N^{\beta_{r3} * k_{r3}} \quad (8.2)$$

$$\delta_a(N) = \beta_{gb}\, k_1\, \varepsilon_v h \left(\frac{\varepsilon_o}{\varepsilon_r}\right)\left(e^{-\left(\frac{\rho}{N}\right)^{\beta}}\right) \quad (8.3)$$

$$\delta_a(N) = \beta_{sg}\, k_1\, \varepsilon_v h \left(\frac{\varepsilon_o}{\varepsilon_r}\right)\left(e^{-\left(\frac{\rho}{N}\right)^{\beta}}\right) \quad (8.4)$$

When inspecting the models shown above under Step 2, it is obvious that three of the five calibration factors are *direct multipliers*. These three calibration factors are β_{r1}, β_{gb}, and β_{sg}. These direct multipliers suggest that the rut predictions from the models are linearly proportional to the calibration factors. For example, if β_{r1} increases in value from 1 to 10, the predicted permanent strain of the asphalt layer will increase 10 times. The same analogy applies to β_{gb} and β_{sg}. This observation suggests that β_{r1}, β_{gb}, and β_{sg} can be calibrated outside of the MEPDG, i.e., they can be optimized to reduce the bias and standard error using the Microsoft Excel Solver numerical optimization routine.

On the other hand, the remaining two calibration factors, β_{r2} and β_{r3}, are not direct multipliers and cannot be optimized outside of the MEPDG. They represent the effect of temperature and number of loading cycles on the permanent deformation of asphalt concrete layers, respectively. In other words, the effect of β_{r2} and β_{r3} on predicted asphalt concrete rut depth must be estimated by executing the MEPDG numerous times for different combinations of β_{r2} and β_{r3} and, finally, selecting the combination that gives the smallest *Total SSE* between measured and predicted total rut depth. Worth mentioning is that temperature and the number of loading cycles have a nonlinear effect on predicted performance within the MEPDG, and users will find it difficult to simulate the work performed by the EICM and the traffic modules outside the MEPDG.

The process of finding the most appropriate beta values for the HMA rutting model (β_{r1}, β_{r2}, and β_{r3}) and for the unbound material rutting models (β_{gb} and β_{sg}) is as follows:

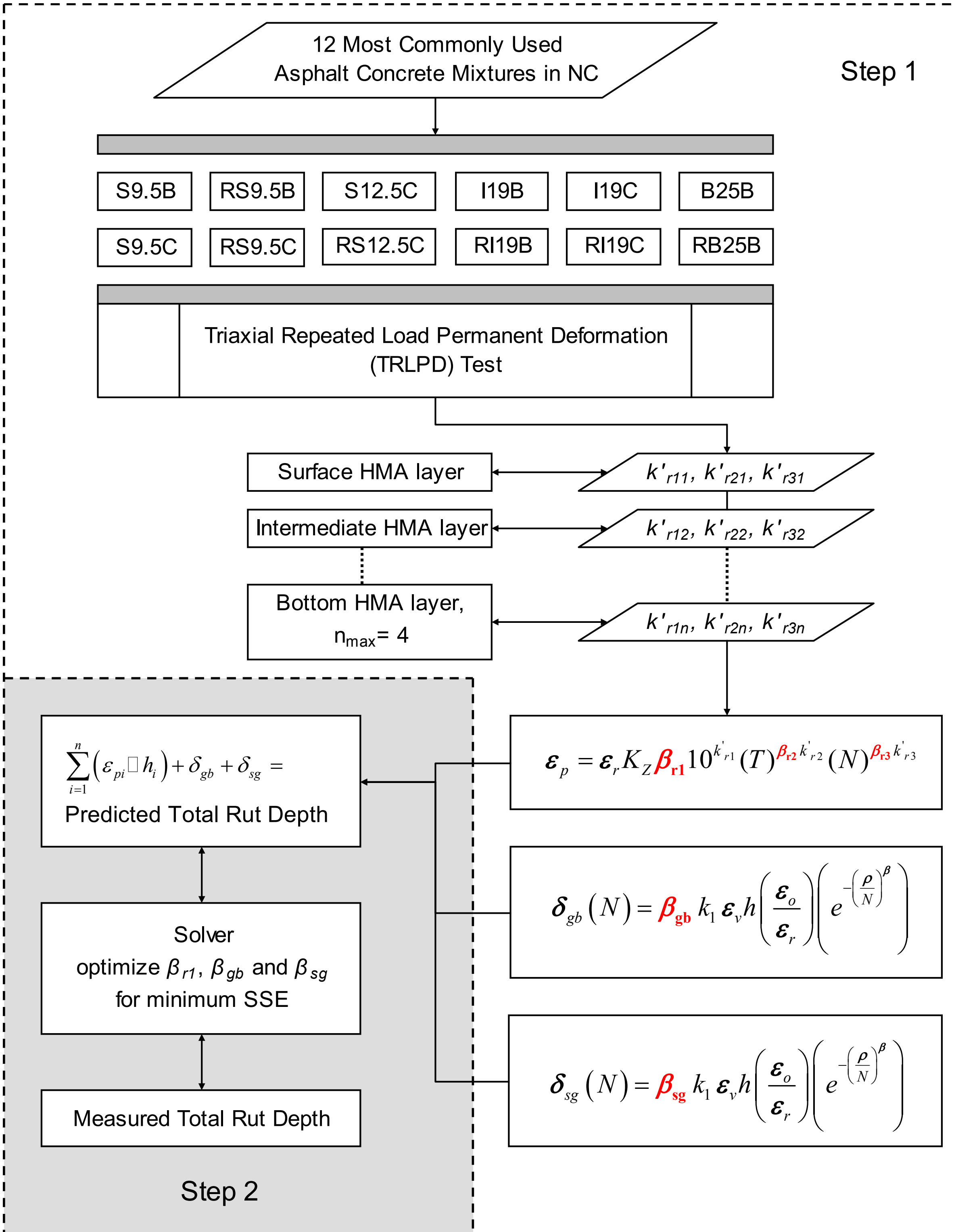

Figure 8.3. Flowchart showing the major steps for calibrating the rutting models under Approach I-R.

1) A large factorial of β_{r2} and β_{r3} combinations is first selected, as shown in Table 8.4.The values of β_{r2} and β_{r3} were selected initially to cover a wide range of values from 0.2 up to 2.0 in 0.2 increments. This large range was selected based on engineering judgment and considering the differences between the material-specific *k* values that were developed under this project and the national default *k* values.
2) Using the material-specific *k* values (denoted in Figure 8.3 by a prime (k') to differentiate them from default *k* values) for each layer in each of the 41 pavement structures (including the 24 LTPP sites illustrated in Figure 8.2 and their rehabilitated sections), the MEPDG was executed a total of 4,510 times. That is, 110 β_{r2} and β_{r3} combinations x 41 pavement structures = 4,510. For each of the 4,510 runs, the predicted rut depth values for the asphalt layer, base layer, and subgrade were extracted from MEPDG output files at the age that corresponds to the available rutting distress survey data for each of the sections.
3) The 2010 LTPP database contains a total of 235 rut depth data points for all 41 pavement sections included in this calibration work. The best combination of β_{r2} and β_{r3} is the combination that results in the minimum SSE between the predicted and measured total rut depth values (*SSE-Total*). The Microsoft Excel Solver numerical optimization routine was used to find the values of β_{r1}, β_{gb}, and β_{sg} for each combination of β_{r2} and β_{r3}. Solver was executed 110 times. Each time, i.e., for each combination of β_{r2} and β_{r3}, the values of β_{r1}, β_{gb}, and β_{sg} were optimized to minimize the *Total SSE*.

Figure 8.4 shows a three-dimensional (3D) surface for the *Total SSE* between the predicted and measured total rut depth values.

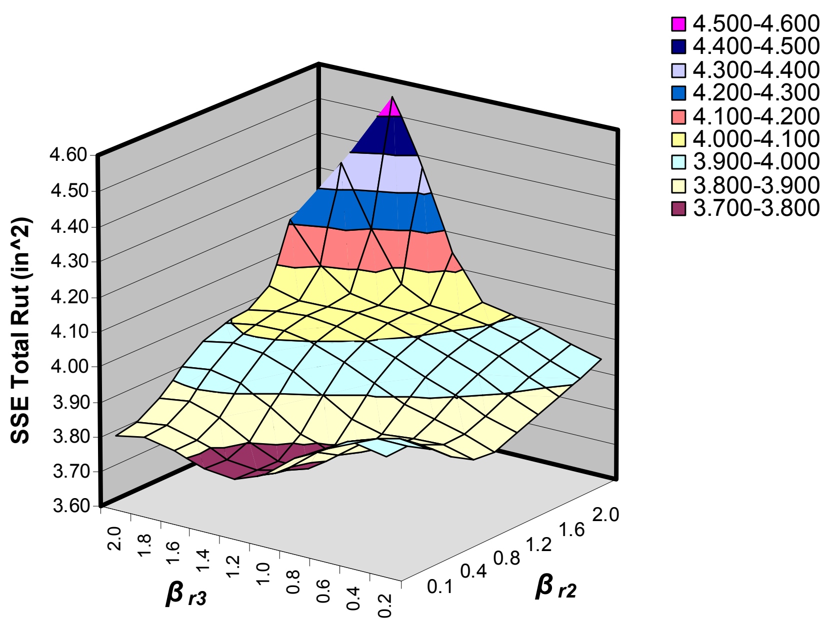

Figure 8.4. 3D surface of *Total SSE* between predicted and measured total rut depth values for 110 combinations of β_{r2} and β_{r3}.

Figure 8.4 suggests that the error increases for high combinations of β_{r2} and β_{r3} and then decreases for in-between values and increases again for very small β_{r2} and β_{r3} combinations. This trend suggests that a specific combination (or combinations) exists that, when used, results in the minimum *Total SSE*. Section 8.6.9.1 presents a more meaningful form of *Total SSE* value. The new form describes the mean rut error per single total rut depth measurement. This information is obtained by taking the square root of *Total SSE* and dividing it by the total number of field measurements, i.e. 235 points.

8.6.3.3 Adjusting LTPP Total Rut Depth Values for North Carolina Sections

When the total rut data reported in the 2010 LTPP database were investigated for the local calibration sections, unexpected trends were found among measurements taken on different survey dates. It is reasonable to expect that rut depth measurements will only increase with time, provided that no overlay or some kind of major rehabilitation work is performed. However, it was found that the total rut depth values decreased and increased for some of the local calibration sections that had not undergone any overlay or major rehabilitation work. Therefore, all the surveyed total rut data were plotted, anomalies were discarded, and exponential functions were found to capture the rutting progression trend for all the sections. Many of the LTPP total rut data points were left unmodified, but in cases where a reversal trend was found, the functions were used to adjust the measured data. All the graphs and the data obtained before and after adjustments can be found in Appendix A.

8.6.3.4 Preliminary Local Calibration Factors for the HMA, Base and Subgrade Rutting Prediction Models based on Approach I-R

Table 8.5 summarizes the permanent deformation local calibration factors as found based on Approach I-R. Out of all 110 combinations of β_{r2} and β_{r3} shown in Table 8.4, the shaded combination number 27, i.e., $\beta_{r2} = 0.4$ and $\beta_{r3} = 1.4$, was found to give the smallest *Total SSE* between the predicted and measured total rut depth values. Note that the numbers presented in Table 8.5 must be used as a group and never individually. The following Section 8.6.3.5 presents the calibration statistics when the calibration factors in Table 8.5 are used.

Table 8.5. Preliminary Local Calibration Factors for HMA and Unbound Rutting Prediction Models using Approach I-R

Parameter	Value
β_{r1}	13.100
β_{r2}	0.400
β_{r3}	1.400
β_{gb}	0.303
β_{sg}	1.102

8.6.3.5 Predicted vs. Measured Rutting Statistics Before and After Calibration – Approach I-R

Table 8.6 is a summary of the rutting distress statistical parameters before and after calibration. The null hypothesis is that the average bias, or so-called *residual error*, between the predicted and measured rut depth values is zero at the 95% confidence level selected for this study. Note that *bias* here is nothing but the difference between the mean measured total rut depth and the mean predicted total rut depth. . Equation (8.5) shows the null hypothesis.

Table 8.6. Summary of Rutting Distress Statistical Parameters Before and After Calibration using Approach I-R

Distress Type	Calibration	*Total SSE*	Bias	S_e	S_e/S_y	R^2	Hypothesis; *Ho: ∑(Meas.-Pred.) = 0*
Total Rut	National	4.110	-0.031	0.129	1.027	Poor	Reject; p = 0.000
	Approach I-R	3.803	-0.041	0.121	0.961	Poor	Reject; p = 0.000
AC Rut*	National	0.826	-0.017	0.057	1.005	Poor	Reject; p = 0.000
	Approach I-R	0.731	-0.020	0.052	1.019	Poor	Reject; p = 0.000
Base Rut*	National	0.212	-0.004	0.030	0.845	0.16	Accept; p = 0.058
	Approach I-R	0.037	-0.003	0.012	0.810	Poor	Reject; p = 0.001
Subgrade Rut*	National	1.127	-0.010	0.069	0.695	0.39	Reject; p = 0.022
	Approach I-R	1.534	-0.019	0.079	0.715	0.31	Reject; p = 0.000

*Estimated using similar % contribution of the layer rut depth as predicted by the MEPDG.

$$H_o : \sum_{i=1}^{n} \left(Rut_{measured} - Rut_{predicted} \right)_i = 0 \quad \text{.......(8.5)}$$

where n is the number of measured total rut depth data points (= 235).

Table 8.6 indicates that the calibration reduces the *Total SSE* for total rut, AC rut, and base rut values but increases the *Total SSE* for subgrade rut values. Recall that only the total rut depth was measured since no forensic investigations have been performed. Hence, all statistics related to AC rut, base rut, and subgrade rut are developed using estimated rut depth in these layer using similar percent contributions of different layer types as predicted by the MEPDG. Table 8.6 also shows that the calibration slightly reduces the standard error of the estimate (S_e) for total rut, AC rut, and base rut depth values but not the subgrade rut depth values. The calibration also reduces the standard error ratio (S_e/S_y) for the total rut depth and for the base rut values. A reduction in the standard error of the estimate term (S_e) indicates less dispersion for the predicted versus measured data points around the LOE. A smaller S_e/S_y ratio indicates that the variation between predicted rut depth values is smaller compared to the variation in the field-measured rut depth values. Other than these slight improvements, Table 8.6 suggests that the calibration process using model coefficients derived from Approach I-R does not improve the statistics compared to the national default values. In fact, Table 8.6 suggests that the nationally calibrated models are able to capture the performance better than the calibrated models from Approach I-R, especially for the base and subgrade layers. Furthermore, Table 8.6 suggests that the null hypothesis, i.e., no significant differences exist between the measured and predicted rut depth, was rejected at 95% confidence level for rut depths from all layers except the base layer, in which the null hypothesis was only accepted based on the default coefficients, i.e., before calibration. Figure 8.5, Figure 8.6, Figure 8.7, and Figure 8.8 show predicted versus measured rut depth values for the total, asphalt concrete, base, and subgrade layers before and after calibration using Approach I-R factors.

Two possible reasons may explain why the calibration process based on Approach I-R does not improve the calibration statistics. First, recall that due to the lack of information with regard to the contribution of different layers to total rut depth, the goal of the optimization was to reduce the *Total SSE* between measured and predicted total rut depth values only. In this case, it is reasonable to expect that, at least, the *Total SSE* for the total rut predictions will improve after calibration, which did happen, as shown in Table 8.6. As mentioned earlier, an improvement in *Total SSE* usually is associated with improvement in other calibration statistics. However, the only other statistics that improved were the S_e and S_e/S_y. On the other hand, bias slightly increased. The second reason that the statistics after calibration did not improve may be due to the coarseness of the factorial shown in Table 8.4. Recall from Equation (8.2) that the β_{r2} and β_{r3} are exponents, which makes small changes in these two factors affect the overall predicted rut depth. A finer mesh could possibly improve the calibration statistics by finding a more appropriate combination of β_{r2} and β_{r3}.

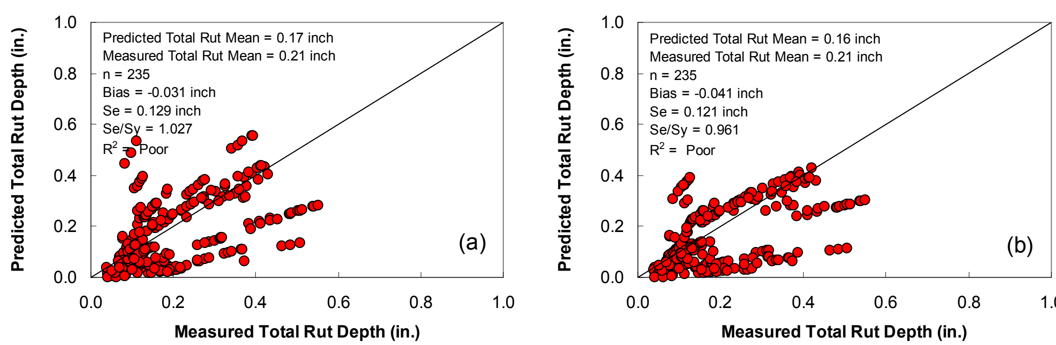

Figure 8.5. Total rut: (a) before calibration; and (b) after calibration using Approach I-R.

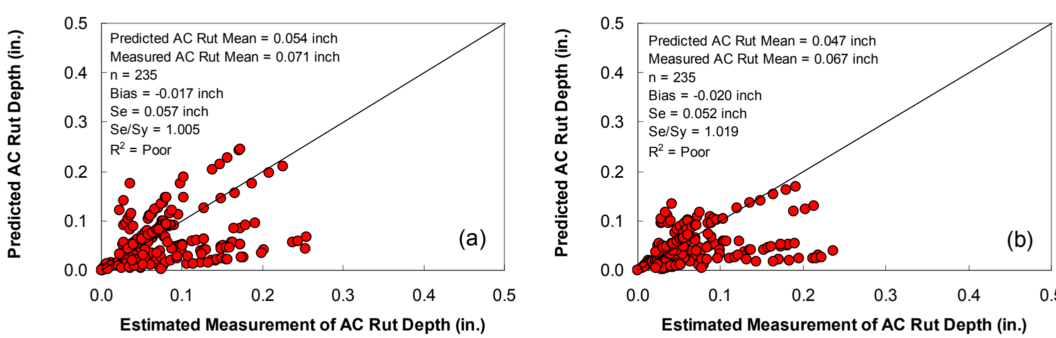

Figure 8.6. Estimated measurement of AC rut depth: (a) before calibration; and (b) after calibration using Approach I-R.

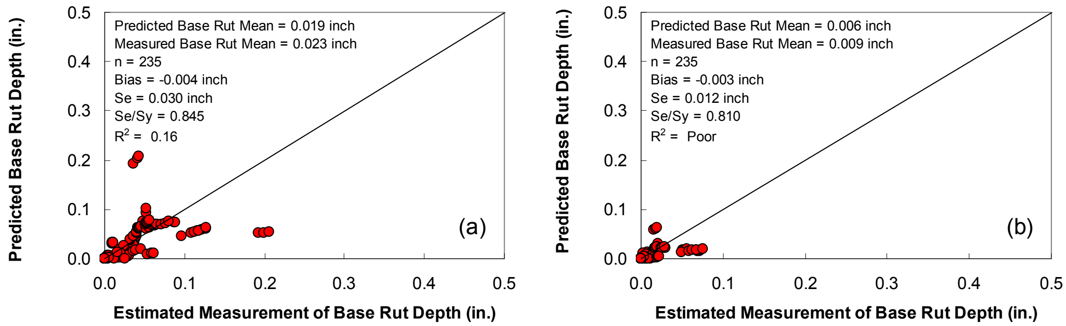

Figure 8.7. Estimated measurement of base rut depth: (a) before calibration; and (b) after calibration using Approach I-R.

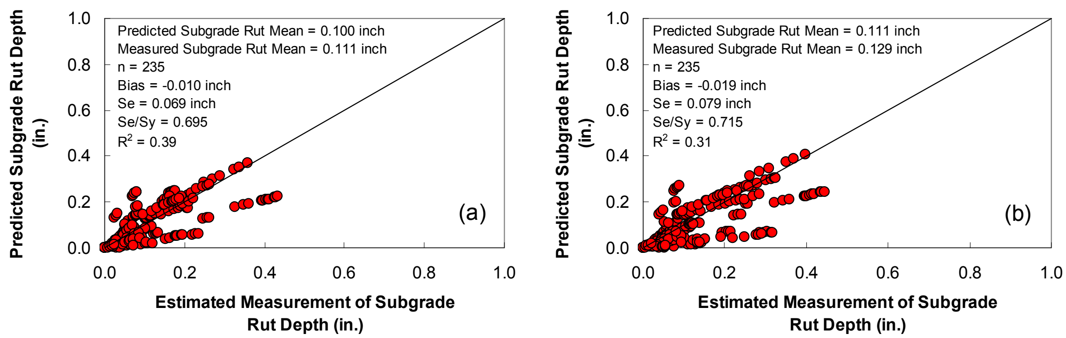

Figure 8.8. Estimated measurement of subgrade rut depth: (a) before calibration; and (b) after calibration using Approach I-R.

Table 8.7 summarizes rut depth values before and after calibration using Approach I-R.

Table 8.7. Predicted Mean Rut Depth Before and After Calibration using Approach I-R

Rut Source	Measured	National Calibration	After Calibration Approach I-R
Total	0.205	0.174	0.164
AC	Not Measured	0.054*	0.047*
Base		0.019*	0.006*
Subgrade		0.100*	0.111*

*Estimated using similar % contribution of the layer rut depth as predicted by the MEPDG.

Table 8.7 shows that the calibration effort results in slightly smaller predicted mean rut depth values, except for the subgrade layer, for which the calibration results in a slight increase of 0.01 inches in predicted rut depth. The total rut depth predicted using the MEPDG default *k* values and calibration factors is 0.17 inches compared to 0.16 inches after using material-specific *k* values and local calibration factors from Approach I-R.

8.6.4 Alligator Cracking Model and Transfer Function Calibration - Approach I-F

8.6.4.1 Introduction

To save effort and time, the same hybrid version of the MEPDG that was used to calibrate the rutting model was used also to calibrate the alligator cracking models. This savings in time and effort comes from the fact that alligator cracking predictions can be extracted from the same Microsoft Excel files where rutting predictions are found. In other words, both alligator cracking and rutting predictions can be obtained from the same MEPDG runs instead of having to execute the MEPDG twice. Note that for alligator cracking calibration, MEPDG Version 1.1 could be used without any modifications instead of the hybrid version, because the modifications are related to rutting inputs rather than to alligator cracking inputs. For the alligator cracking calibration, the performance of only the bottom asphalt concrete layer was considered, because alligator cracking initiates at the bottom of the asphalt layer and propagates upward. Figure 8.9 is a flow chart showing the two major steps that were developed to calibrate the number of cycles to failure (N_f) model and the transfer function for alligator cracking. The following section discusses these steps in detail.

8.6.4.2 Calibration Steps

8.6.4.2.1 Step 1: Replace Fatigue Default *k* Values with Material-Specific *k* Values

Similar to the first step in calibrating the rutting models, the first step in calibrating the alligator cracking model and transfer function is to populate the N_f model with the material-specific *k* values (reported in Table 6.6) that correspond to the bottom asphalt concrete layer for each pavement section. This process is illustrated in Step 1, shown in Figure 8.9.

Note that the dynamic modulus ($|E^*|$) values are not entered directly in the N_f model as it appears in Figure 8.9; rather, they are entered separately for each asphalt concrete layer in a separate input screen, as explained in the *North Carolina MEPDG User Reference Guide* found in Appendix H. Once the N_f is calculated, the MEPDG utilizes Miner's law to calculate the percentage of fatigue damage using the N_f as an input. The percentage of damage is then used by the transfer function to predict alligator cracking as a percentage of lane area. Note that in Figure 8.9, the *k* values are denoted as (k') to differentiate them from the national default *k* values.

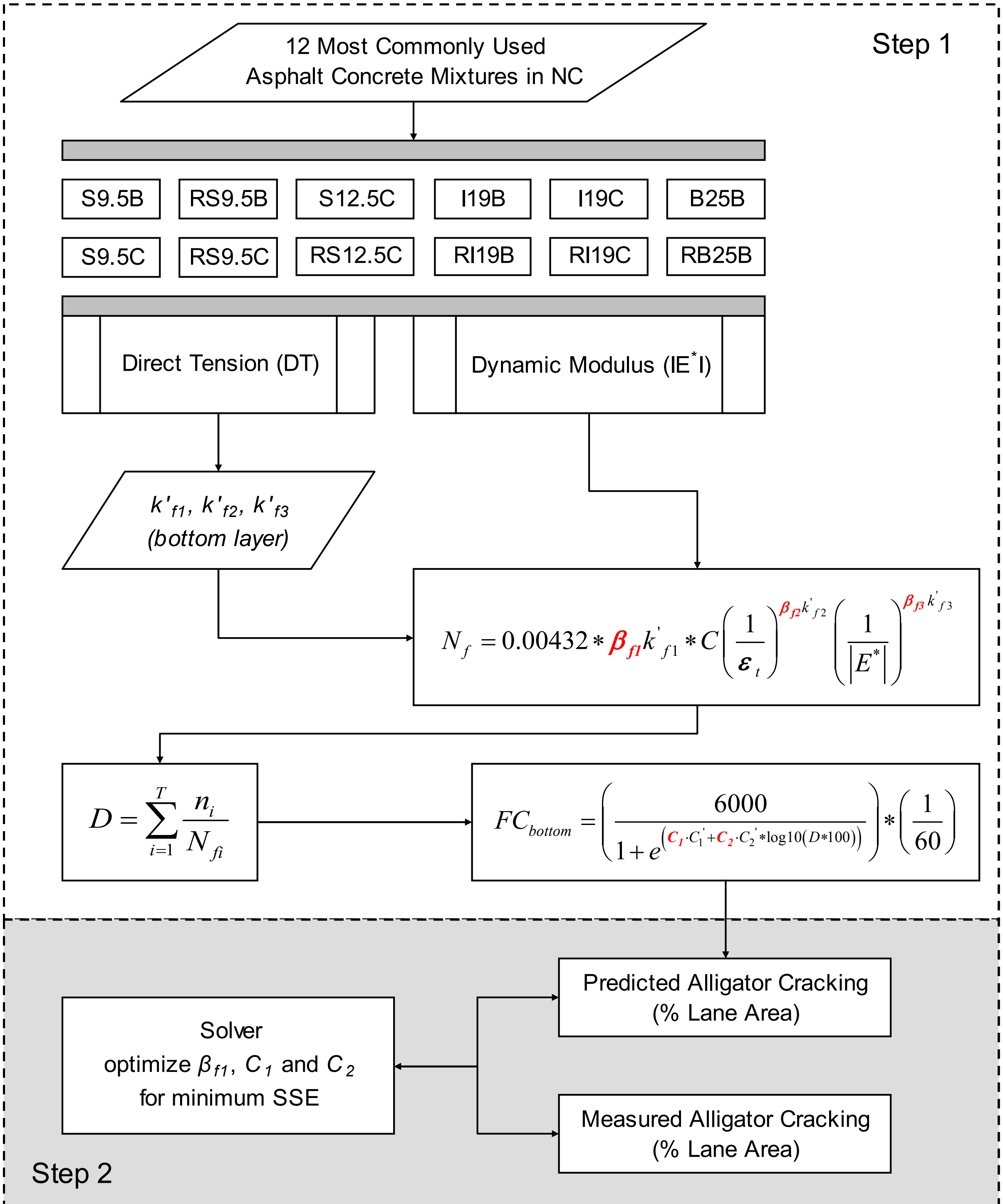

Figure 8.9. Flowchart showing the major steps for calibrating the fatigue cracking model and transfer function under Approach I-F.

8.6.4.2.2 Step 2: Find Beta and C Values that Minimize the Sum of Squared Errors (SSE) between the Predicted and Measured Alligator Cracking.

As mentioned earlier, alligator cracking in the MEPDG is predicted using two models: 1) the N_f model, from which fatigue damage is calculated, and 2) a transfer function that converts damage to bottom-up fatigue cracking ($F.C._{BU}$) as a percentage of lane area. The N_f model, the transfer function, and Miner's law that converts the N_f to damage, are shown in Equation (8.6), Equation (8.7), and Equation (8.8), respectively. Note that for alligator cracking, five calibration coefficients must be calibrated: β_{f1}, β_{f2}, and β_{f3} from the N_f model, and C_1 and C_2 from the transfer function.

$$N_f = 0.00432 * C * \beta_{f1} * k_{f1} * \left(\frac{1}{\varepsilon_t}\right)^{\beta_{f2} * k_{f2}} \left(\frac{1}{|E^*|}\right)^{\beta_{f3} * k_{f3}} \quad \text{...(8.6)}$$

where

$$C = 10^M$$

$$M = 4.84\left(\frac{V_b}{V_a + V_b} - 0.69\right)$$

$$F.C._{BU} = \left(\frac{6000}{1 + e^{(C_1 * C_1' + C_2 * C_2' * \log_{10}(\% Damage))}}\right) * \left(\frac{1}{60}\right) \quad \text{..(8.7)}$$

where

$$C_1' = -2C_2'$$

$$C_2' = -2.40874 - 39.748 * (1 + h_{ac})^{-2.856}$$

$$D = \sum_{i=1}^{T} \frac{n_i}{N_{fi}} \quad \text{...(8.8)}$$

By inspecting Equation (8.6) and Equation (8.7), the following points are concluded:

- From Equation (8.6), it can be seen that β_{f1} is a direct multiplier. That is, if the value of β_{f1} is changed from 1 to 10, for example, the number of loading cycles to failure (N_f) will increase 10 times. This phenomenon indicates that β_{f1} can be calibrated using the Microsoft Excel Solver optimization routine outside the MEPDG.
- From Equations (8.6) and (8.8), it can be seen that β_{f1} is inversely related to the percentage of fatigue damage. For example, if the value of β_{f1} changes from 1 to 0.5, the damage value will double.
- The values of C_1 and C_2 in Equation (8.7) should be equal to each other in order to maintain the sigmoidal function assumption, which is that 50% of alligator cracking

occurs at 100% fatigue damage (NCHRP, 2004d). This information reduces the number of calibration factors to four (β_{f1}, β_{f2}, β_{f3}, and $C_1 = C_2$).

- Whenever the MEPDG is executed, the Excel output files contain the percentage of predicted damage (% Damage), which is an input to the transfer function, as shown in Equation (8.7). Therefore, fatigue damage can be calculated outside the MEPDG using Equation (8.7) and the output from Equation (8.8).

Based on the information presented above, the alligator cracking coefficients were calibrated using the following procedure.

1) The N_f model in the MEPDG was populated with material-specific k values that correspond to the bottom asphalt layer for each pavement section.
2) The MEPDG was then executed many times using a large factorial of β_{r2} and β_{r3} shown in Table 8.8. The factorial shown in Table 8.8 was rationally developed based on a wide range of possible calibration factors.
3) For all 41 LTPP sections, the MEPDG was executed 7,667 times, i.e., 187 β_{f2} and β_{f3} combinations x 41 pavement structures = 7,667. For each of the 7,667 runs, predicted percentage of fatigue damage values were extracted from MEPDG output files at the age that corresponds to the available fatigue distress survey data for each of the pavement sections.
4) The 2010 LTPP database contains 124 alligator cracking data points (expressed as percentage of lane area) for 35 out of the 41 pavement sections included in this calibration work. To find the best combination of β_{f2} and β_{f3}, i.e., the combination that results in the minimum SSE between predicted and measured alligator cracking values, the Microsoft Solver numerical optimization routine is used to find the values of β_{f1} and C_1. Recall that $C_1 = C_2$ for each combination of β_{f2} and β_{f3}. Microsoft Excel Solver was executed 187 times. Each time, i.e., for each combination of β_{f2} and β_{f3}, the values of β_{f1} and C_1 were optimized to minimize the SSE.

Figure 8.10 shows a 3D surface for the SSE between the predicted and measured alligator cracking values.

Table 8.8. Complete List of β_{f2}, and β_{f3} Sets Used in the Calibration Process

No.	β_{f2}	β_{f3}
1	0.1	0.1
2	0.1	0.2
3	0.1	0.4
4	0.1	0.6
5	0.1	0.8
6	0.1	1.0
7	0.1	1.2
8	0.1	1.4
9	0.1	1.6
10	0.1	1.8
11	0.1	2.0
12	0.2	0.1
13	0.2	0.2
14	0.2	0.4
15	0.2	0.6
16	0.2	0.8
17	0.2	1.0
18	0.2	1.2
19	0.2	1.4
20	0.2	1.6
21	0.2	1.8
22	0.2	2.0
23	0.4	0.1
24	0.4	0.2
25	0.4	0.4
26	0.4	0.6
27	0.4	0.8
28	0.4	1.0
29	0.4	1.2
30	0.4	1.4
31	0.4	1.6
32	0.4	1.8
33	0.4	2.0
34	0.6	0.1
35	0.6	0.2
36	0.6	0.4
37	0.6	0.6
38	0.6	0.8
39	0.6	1.0
40	0.6	1.2
41	0.6	1.4
42	0.6	1.6
43	0.6	1.8
44	0.6	2.0
45	0.8	0.1
46	0.8	0.2
47	0.8	0.4
48	0.8	0.6
49	0.8	0.8
50	0.8	1.0
51	0.8	1.2
52	0.8	1.4
53	0.8	1.6
54	0.8	1.8
55	0.8	2.0
56	1.0	0.1
57	1.0	0.2
58	1.0	0.4
59	1.0	0.6
60	1.0	0.8
61	1.0	1.0
62	1.0	1.2
63	1.0	1.4
64	1.0	1.6
65	1.0	1.8
66	1.0	2.0
67	1.2	0.1
68	1.2	0.2
69	1.2	0.4
70	1.2	0.6
71	1.2	0.8
72	1.2	1.0
73	1.2	1.2
74	1.2	1.4
75	1.2	1.6
76	1.2	1.8
77	1.2	2.0
78	1.4	0.1
79	1.4	0.2
80	1.4	0.4
81	1.4	0.6
82	1.4	0.8
83	1.4	1.0
84	1.4	1.2
85	1.4	1.4
86	1.4	1.6
87	1.4	1.8
88	1.4	2.0
89	1.6	0.1
90	1.6	0.2
91	1.6	0.4
92	1.6	0.6
93	1.6	0.8
94	1.6	1.0
95	1.6	1.2
96	1.6	1.4
97	1.6	1.6
98	1.6	1.8
99	1.6	2.0
100	1.8	0.1
101	1.8	0.2
102	1.8	0.4
103	1.8	0.6
104	1.8	0.8
105	1.8	1.0
106	1.8	1.2
107	1.8	1.4
108	1.8	1.6
109	1.8	1.8
110	1.8	2.0
111	2.0	0.1
112	2.0	0.2
113	2.0	0.4
114	2.0	0.6
115	2.0	0.8
116	2.0	1.0
117	2.0	1.2
118	2.0	1.4
119	2.0	1.6
120	2.0	1.8
121	2.0	2.0
122	0.1	0.08
123	0.2	0.08
124	0.4	0.08
125	0.6	0.08
126	0.8	0.08
127	1.0	0.08
128	1.2	0.08
129	1.4	0.08
130	1.6	0.08
131	1.8	0.08
132	2.0	0.08
133	0.1	0.06
134	0.2	0.06
135	0.4	0.06
136	0.6	0.06
137	0.8	0.06
138	1.0	0.06
139	1.2	0.06
140	1.4	0.06
141	1.6	0.06
142	1.8	0.06
143	2.0	0.06
144	0.1	0.04
145	0.2	0.04
146	0.4	0.04
147	0.6	0.04
148	0.8	0.04
149	1.0	0.04
150	1.2	0.04
151	1.4	0.04
152	1.6	0.04
153	1.8	0.04
154	2.0	0.04
155	0.1	0.02
156	0.2	0.02
157	0.4	0.02
158	0.6	0.02
159	0.8	0.02
160	1.0	0.02
161	1.2	0.02
162	1.4	0.02
163	1.6	0.02
164	1.8	0.02
165	2.0	0.02
166	0.1	0.008
167	0.2	0.008
168	0.4	0.008
169	0.6	0.008
170	0.8	0.008
171	1.0	0.008
172	1.2	0.008
173	1.4	0.008
174	1.6	0.008
175	1.8	0.008
176	2.0	0.008
177	0.1	0.004
178	0.2	0.004
179	0.4	0.004
180	0.6	0.004
181	0.8	0.004
182	1.0	0.004
183	1.2	0.004
184	1.4	0.004
185	1.6	0.004
186	1.8	0.004
187	2.0	0.004

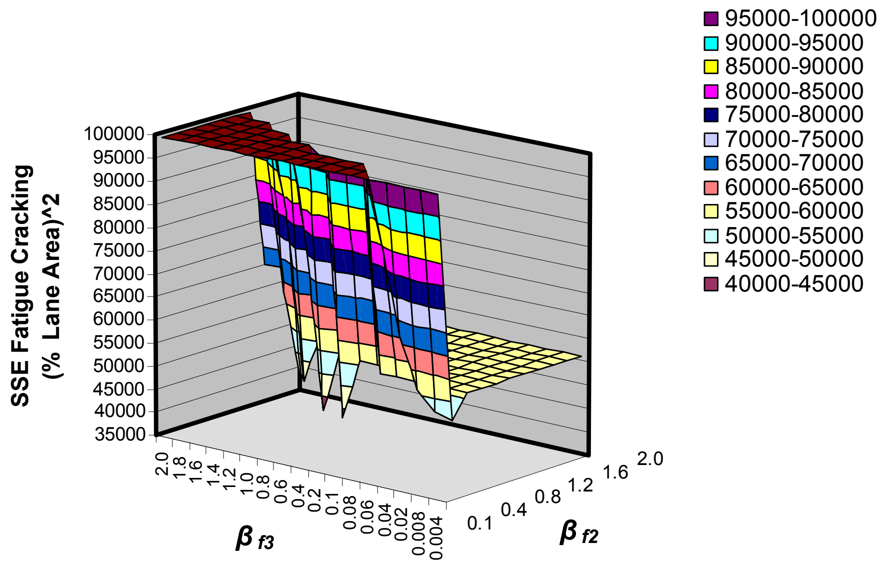

Figure 8.10. 3D surface of SSE between predicted and measured alligator cracking values for 187 combinations of β_{f2} and β_{f3}.

The error surface clearly shows that only a few combinations of β_{f2} and β_{f3} result in low SSE values, indicated by sharp pointed surfaces, as shown in Figure 8.10, whereas many of the other combinations share either a slightly larger SSE or a much larger SSE. Section 8.6.9.1 presents a more meaningful form of *Total SSE* value. The new form describes the mean alligator cracking percent error per single measurement. This information is obtained by taking the square root of *Total SSE* and dividing it by the total number of observed alligator cracking field measurements, i.e. 124 points.

8.6.4.3 Preliminary Alligator Cracking Model and Transfer Function Local Calibration Factors based on Approach I-F

Out of all 187 combinations of β_{f2} and β_{f3} shown in Table 8.8, the shaded combination number 49, i.e., $\beta_{f2} = 0.8$ and $\beta_{f3} = 0.8$, was found to give the smallest SSE between the predicted and measured alligator cracking values. Along with that best combination, the optimized values for B_{f1} and C_1 are shown in Table 8.9. Note that the numbers presented in Table 8.9 must all be used as a group and never individually.

Table 8.9. Preliminary Local Calibration Factors for Alligator Cracking Prediction Models using Approach I-F

Parameter	Value
β_{f1}	3.878
β_{f2}	0.800
β_{f3}	0.800
C_1	0.245
C_2	0.245

8.6.4.4 Predicted vs. Measured Alligator Cracking Statistics Before and After Calibration – Approach I-R

Table 8.10 is a summary of the alligator cracking statistical distress parameters before and after calibration. The null hypothesis is that the average bias, or so-called *residual error*, between the predicted and measured alligator cracking values is zero. A 95% confidence level was selected for this study. The null hypothesis is shown in Equation (8.9).

$$H_o : \sum_{i=1}^{n} \left(Alligator_{measured} - Alligator_{predicted} \right)_i = 0 \quad (8.9)$$

Table 8.10. Summary of Alligator Cracking Statistical Parameters Before and After Calibration using Approach I-F

Distress Type	Calibration	*Total SSE*	Bias	S_e	S_e/S_y	R^2	Hypothesis; *Ho: ∑(Meas.-Pred.) = 0*
Alligator Cracking	National	56412	-11.034	19.498	1.022	Poor	Reject; p = 0.000
	Approach I-F	41764	-4.836	19.852	1.041	Poor	Reject; p = 0.008

Table 8.10 suggests that the *Total SSE* decreases significantly as a result of the calibration effort. Table 8.10 also suggests that bias decreases significantly after the calibration. On the other hand, the standard error of the estimate (S_e) does not show any improvement after the calibration. Furthermore, Table 8.10 suggests that the null hypothesis displayed in Equation (8.9) has been rejected at the 95% confidence level despite the improvement in the p-value. In other words, the differences between the measured and predicted alligator cracking values are still significant even after the calibration. Table 8.11 is a summary of the predicted alligator cracking mean before and after the calibration.

Table 8.11. Predicted and Measured Alligator Cracking Means, Before and After Calibration using Approach I-F

Calibration	Predicted Mean for Alligator Cracking (% Lane Area)	Measured Mean for Alligator Cracking (% Lane Area)
National	0.456	11.490
Approach I-F	6.654	

It is clear from Table 8.11 that Approach I-F significantly improves the predicted alligator cracking percentage. Before calibration, the predicted alligator cracking was about 0.5% of the lane area, whereas after calibration, the percentage increased to about 6.7% of the lane area. In North Carolina, fatigue cracking is the major distress responsible for the failure of flexible pavement, so the calibration effort has improved the prediction, but the improvement, as indicated in Table 8.10, is not statistically sufficient to accept the hypothesis that the measured alligator cracking is similar to the predicted alligator cracking at 95% confidence level.

Figure 8.11 (a) and (b) show predicted versus measured alligator cracking before and after the calibration, respectively. Figure 8.11 (b) again suggests that the calibration has improved the alligator cracking predictions, yet the improvement is not enough.

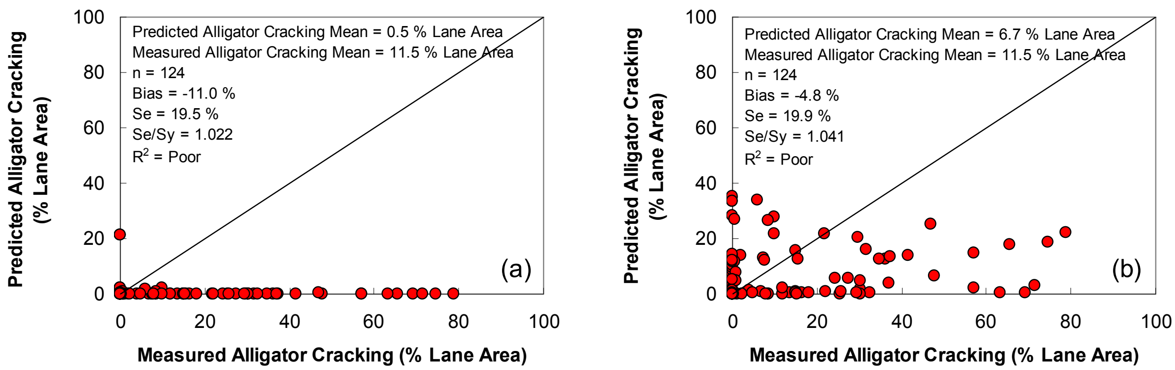

Figure 8.11. Alligator cracking calibration results: (a) before calibration; and (b) after calibration using Approach I-F.

Figure 8.11 suggests that some of the LTPP sections show large percentages, up to 80 percent, of measured alligator cracking. This observation initially triggered a concern about the validity of the measured alligator cracking data at LTPP sections, since agencies do not normally allow their pavements to reach this level of distress without performing some kind of maintenance. However, a closer inspection of the LTPP data revealed that the LTPP distress survey teams record three levels of alligator cracking severity; low, moderate, and high. The measured alligator cracking reported in this work is the sum of alligator cracking of all three levels of severity. Similar approach was followed by the NCHRP 9-37A research team in the national calibration effort (NCHRP, 2004b). In addition, it was found that the low severity cracking is the major contributor to the large recorded alligator cracking percentages. In fact, there were only few records of high severity alligator cracks in all sections combined. This might explains why agencies did not perform any maintenance on these highly cracked pavements.

Figure 8.12 shows that 96 out of 124 surveyed alligator cracking measurements lie in the zero to 20 percent bin, and only 11 readings were recorded for alligator cracking of 40 percent lane area or higher.

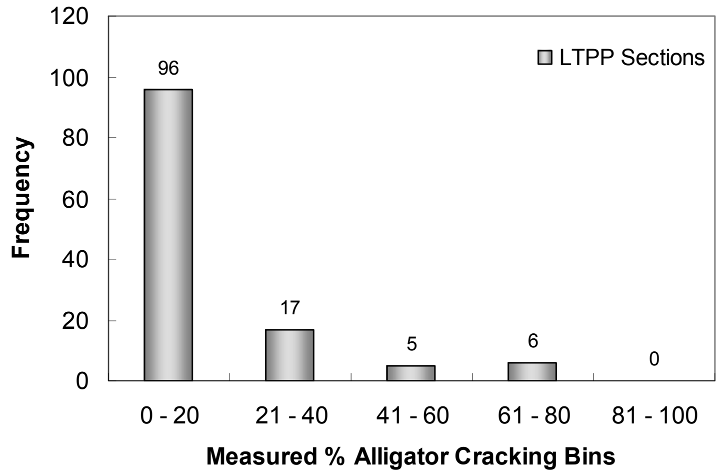

Figure 8.12. Histogram for the distribution of measured percent alligator cracking at the LTPP sections.

8.6.5 Validation of Rutting and Alligator Cracking Calibrated Models for Approach I

This section presents the validation results of the local calibration factors developed under Approach I. Originally, 24 PMS pavement sections were available for validation, as shown earlier in Figure 8.2 12 of which were let in 1993 and 12 in 1999. However, distress data could not be located for seven of the sections, leaving 15 PMS sections only for validation. For some of the sites, separate distress data sets were acquired for different travel directions, i.e., northbound versus southbound or eastbound versus westbound. Including the distress data for all directions, 25 sets of distress data were used in the validation for both the 1993 and 1999 sections. Recently, the 2010 distress data were collected from the NCDOT PMU and were used in the validation work to complement the data from 2008 and earlier. The next sections present the validation results for rutting and alligator cracking.

8.6.5.1 Validation Results for Approach I-R Rutting Local Calibration Factors

Table 8.12 is a summary of the statistical parameters for rut depth predictions obtained from validation runs compared to those determined earlier from Approach I-R calibration runs. Table 8.13 shows a comparison of the mean total rut depth predicted from validation runs compared to those determined from Approach I-R calibration runs.

Due to the large differences between the measured and predicted rut depth values, Table 8.12 shows that the validation statistics are, in general, worse than the calibration statistics mainly for total rut depth and subgrade layers. On the other hand, Table 8.12 shows that the standard error of the estimate (S_e) and the S_e/S_y term both increased slightly especially for the total rut, AC rut, and base rut values. In addition, Table 8.12 suggests that the hypothesis that measured rut is equal to predicted rut for validation sections has been rejected, indicating that significant differences exist between predicted and measured rut depth values for validation sections.

Table 8.12. Comparison of Rutting Statistical Parameters between Approach I-R Calibration and Validation

Distress Type	Analysis	Bias	S_e	S_e/S_y	R^2	Hypothesis; *Ho: ∑(Meas.-Pred.) = 0*
Total Rut	Calibration	-0.041	0.121	0.961	Poor	Reject; p = 0.000
	Validation	0.265	0.150	1.827	Poor	Reject; p = 0.000
AC Rut*	Calibration	-0.020	0.052	1.019	Poor	Reject; p = 0.000
	Validation	0.088	0.052	1.287	Poor	Reject; p = 0.000
Base Rut*	Calibration	-0.003	0.012	0.810	Poor	Reject; p = 0.001
	Validation	0.004	0.011	1.071	Poor	Reject; p = 0.000
Subgrade Rut*	Calibration	-0.019	0.079	0.715	0.31	Reject; p = 0.000
	Validation	0.172	0.130	3.759	Poor	Reject; p = 0.000

*Estimated using similar % contribution of the layer rut depth as predicted by the MEPDG.

Table 8.13 suggests that NCDOT personnel have underestimated, on average, the rut depth predicted by the MEPDG using local calibration factors and material-specific *k* values. It could be argued that the predicted total rut depth value is very large. However, Table 8.13 clearly shows that for the LTPP sections in North Carolina, the mean total rut depth is 0.205 inch. Therefore, it is unlikely that the predicted total rut depth overestimates the measured rut depth for the PMS sections. Recall that NCDOT personnel gave subjective ratings of none, light, medium, or severe for the different ranges of rut depth and that a conversion method was developed to convert the subjective ratings to rut depth values.

Table 8.13. Comparison of Predicted Total Rut Depth between Approach I-R Calibration and Validation

Analysis	Predicted Mean Total Rut Depth (inch)	Measured Mean Total Rut Depth (inch)
Calibration (LTPP Sections)	0.164	0.205
Validation (PMS Sections)	0.292	0.028

Figure 8.13 (a), (b), (c), and (d) show predicted versus measured total rut depth, asphalt concrete (AC) rut depth, base, and subgrade rut depth values, respectively.

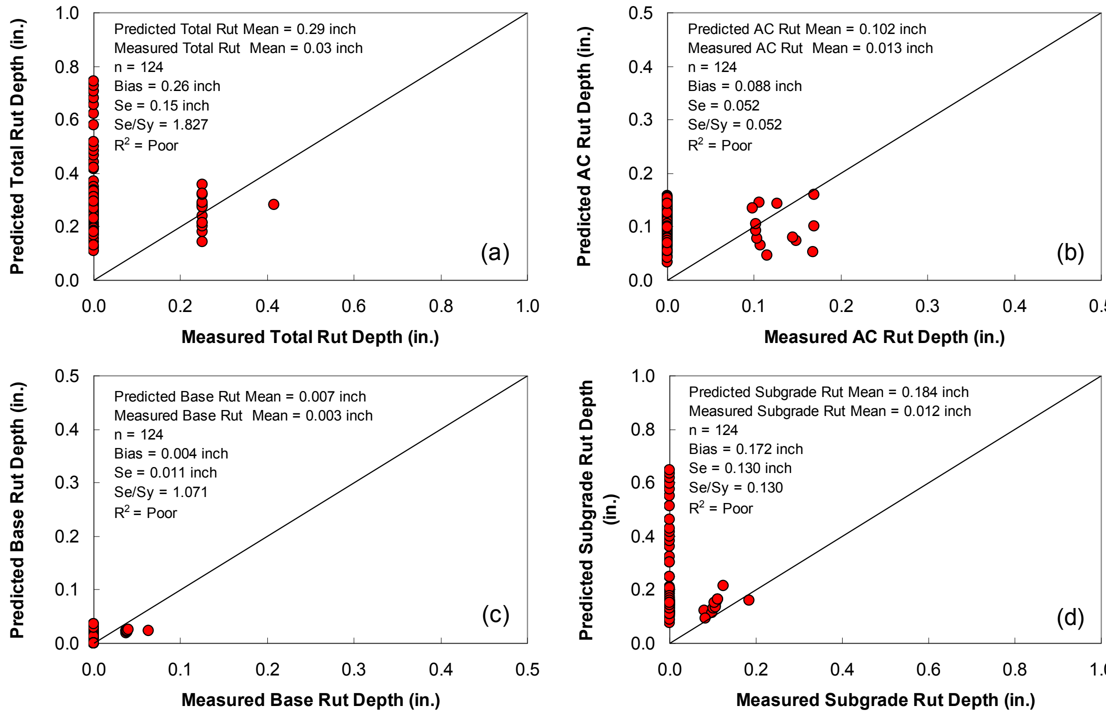

Figure 8.13. Predicted vs. measured rut depth after validation work using Approach I-R: (a) total rut; (b) estimated AC rut; (c) estimated base rut; and (d) estimated subgrade rut.

Figure 8.13 (a) clearly shows that the MEPDG, in general, overpredicts total rut depth. However, several cases are seen where the predicted total rut depth matches very well with the measured rut depth. Figure 8.13 (b) indicates that the MEPDG predicts the asphalt concrete rut depth better than total rut depth for validation sections using calibration factors developed from Approach I-R. In general, the MEPDG overpredicts the asphalt concrete rut depth, mainly because the asphalt concrete rut depth is calculated as a percentage of the total rut depth, which is overpredicted at the outset by the MEPDG.

Figure 8.13 (c) and Figure 8.13 (d) show that some of the predicted base and subgrade rut depth values are in agreement with the measured subgrade rut depth values; but, in general, the trend is clear that the MEPDG overpredicts both of these rut measurements for the PMS sections. Several recommendations are presented in Chapter 9 to improve the match between MEPDG-predicted distresses versus measured distresses in general.

8.6.5.2 Validation Results for Approach I-F Alligator Cracking Local Calibration Factors

Table 8.14 is a summary of the statistical parameters for alligator cracking predictions obtained from validation runs compared to those determined earlier from Approach I-F calibration runs. Table 8.15 compares the mean alligator cracking predictions determined from validation runs with those determined from calibration runs. Before discussing these two tables, it should be remembered that all the calibration runs were performed on LTPP sections, which, in general, have reliable materials, traffic, and distress information compared to all the validation runs performed on NCDOT PMS sections for which less accurate information was available and various distress survey techniques were used, as explained earlier in this chapter under Section 8.4.2.3

Table 8.14 suggests that even though the hypothesis, i.e. that measured and predicted alligator cracking distresses for validation sections are equal, has been rejected, Table 8.14 nonetheless shows that the p-value, bias, and *Se* improve over the calibration numbers. The S_e/S_y ratio, however , is slightly larger.

Table 8.14. Comparison of Alligator Cracking Statistical Parameters between Approach I-F Calibration and Validation

Distress Type	Analysis	Bias	S_e	S_e/S_y	R^2	Hypothesis; *Ho:* $\sum$*(Meas.-Pred.) = 0*
Alligator Cracking	Calibration	-4.836	19.852	1.041	Poor	Reject; p = 0.008
	Validation	2.064	10.602	1.750	Poor	Reject; p = 0.032

Table 8.15. Comparison of Predicted Alligator Cracking between Approach I-F Calibration and Validation

Analysis	Predicted Mean Alligator Cracking (% Lane Area)	Measured Mean Alligator Cracking (% Lane Area)
Calibration (LTPP Sections)	6.654	11.490
Validation (PMS Sections)	5.293	3.230

Table 8.15 shows that the mean predicted alligator cracking value for the PMS validation sections (5.3% of lane area) is about 2.1% higher than the mean measured alligator cracking (3.2% of lane area). Table 8.15 indicates that the MEPDG calibrated models, using factors developed from Approach I-F, underpredict the measured alligator cracking percentages for the LTPP sections but overpredicts the alligator cracking percentage for the PMS validation sections.

Table 8.15 shows that the mean measured alligator cracking values obtained from the PMS sections constitute only 3.2% of the lane area compared to those measured from the LTPP sections (11.5% of lane area). Recall that the alligator cracking distress estimated by NCDOT personnel is based on a windshield survey, so less accurate numbers are expected. In fact, it might be safe to say that more alligator cracking would have been captured if the surveyors could have been closer to the pavement surface instead of trying to observe the distress from within a vehicle. Thus, the undesirable survey technique may be the reason that LTPP-measured distress values are higher on average than the PMS-measured values.

Also, note that the alligator cracking measured from the PMS sections could have been much less if the relationship that was developed by Corley-Lay et al. (2010) for converting NCDOT alligator cracking to equivalent LTPP alligator cracking had not been used. In other words, the relationship developed by Corley-Lay et al. certainly helped by increasing the measured alligator cracking values to numbers that make more sense.

Figure 8.14 is a graph showing predicted versus measured alligator cracking after validation work on the PMS sections. Figure 8.14 emphasizes the fact that, on average, the alligator cracking measurements taken by the NCDOT are much lower than those predicted by the MEPDG using local calibration factors developed from Approach I-F. Some measurements were captured or predicted correctly, but these measurements are few.

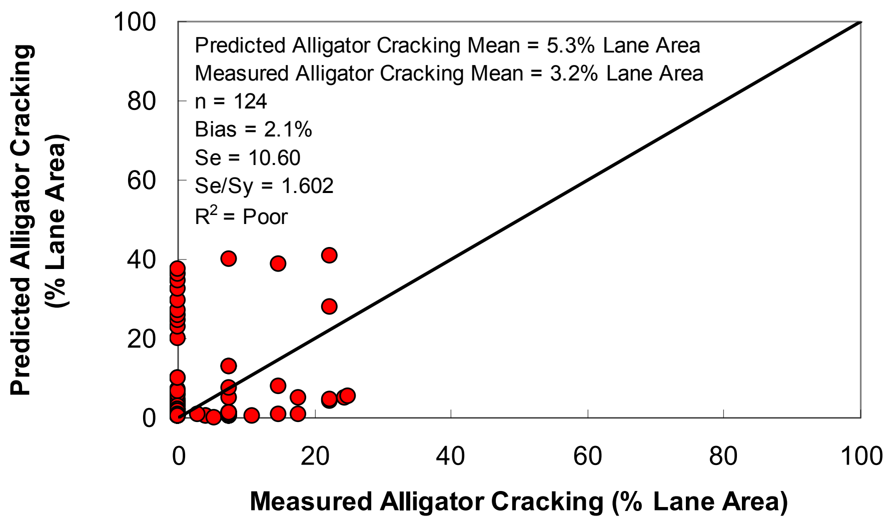

Figure 8.14. Predicted vs. measured alligator cracking values after validation work using Approach I-F.

8.6.6 Rutting Models Calibration-Approach II-R

8.6.6.1 Introduction

Approach II-R is an advanced approach that employs the GA optimization technique to find the global or a stable minimum total SSE between predicted and measured total rut depth values through a true optimization of all five rutting model parameters, β_{r1}, β_{r2}, β_{r3}, β_{gb}, and β_{sg} simultaneously. Recall that the ultimate goal is to find a single set of beta values that results in the smallest bias and standard error between the predicted and measured total rut depth values from all sections grouped. Hence, the procedure does not look to reduce the bias and standard error at a single site. Because β_{r2} and β_{r3} cannot be optimized outside of the MEPDG, Approach II-R employs the computer routine within the MEPDG that does the distress prediction work. This computer routine is called Apads.exe. For Apads.exe to predict pavement performance, it requires the following inputs: traffic over the design life of the pavement, critical pavement responses, bound and unbound material properties, and weather data including changes in temperature, and moisture profiles and depth of water table below ground level. For a specific location, these inputs do not change; hence, the MEPDG can be executed only once for each site pavement section to generate all of these inputs. The distress models' calibration factors can then be optimized outside of the MEPDG using the GA technique. The steps followed in Approach II-R are summarized below.

8.6.6.2 Calibration Steps

Figure 8.15 is a flow chart showing the steps followed in calibrating the rutting prediction models' coefficients. The detailed steps are as follows:

1) For bound and unbound rutting models calibration work, 41 pavement sections were considered for which rut depth survey data were available. For each of these sections, the MEPDG was executed once to generate processed traffic files, climatic files, critical responses (i.e. stresses, strains and deflections), and other input files that are required by Apads.exe to run. After the MEPDG runs were completed for all sections, a copy of Apads.exe file was saved in each section directory.
2) For each pavement section, material-specific *k* values for each HMA layer (up to a maximum of four layers allowed by the MEPDG) and the HMA rutting model calibrating coefficients, i.e., β_{r1}, β_{r2}, and β_{r3}, were extracted from the four text files shown in Figure 8.15. For example, the text file that contains information for the first HMA layer is called 930_CALIBRATION_LAYER1.csv, and so forth. Each of these text files must be created manually and entered in the project directory. Apads.exe looks into the project directory for the coefficients and extracts them from these files.
3) For the unbound materials rutting prediction models, the national default *k* values were left untouched because local unbound materials were not characterized as part of this research work. However, the local calibration factors for the unbound materials, i.e., β_{gb}, and β_{sg}, were imported by Apads.exe from the CalibrationFactor.dat file, which is a text file that is generated automatically as a result of executing the MEPDG.
4) In addition to material-specific *k* values for the HMA layers, national *k* values for the unbound layers, and the five local calibration coefficients, β_{r1}, β_{r2}, β_{r3}, β_{gb}, and β_{sg}, a text file must be created in a MATLAB®-readable format and must contain the measured total rut depth values for each section at the different available distress survey dates. The text file must be saved in the main directory where the MATLAB® script and all section directories exist. By the end of this step, MATLAB® is ready to run, and the following steps explain how MATLAB® finds the optimized values of β_{r1}, β_{r2}, β_{r3}, β_{gb}, and β_{sg} that minimize the bias between the predicted and measured total rut depth values.
5) MATLAB® first calls the Apads.exe file for the first section and executes it. As a result of its execution, Apads.exe generates a file called ".rut" that contains the total predicted rut depth values for the section.

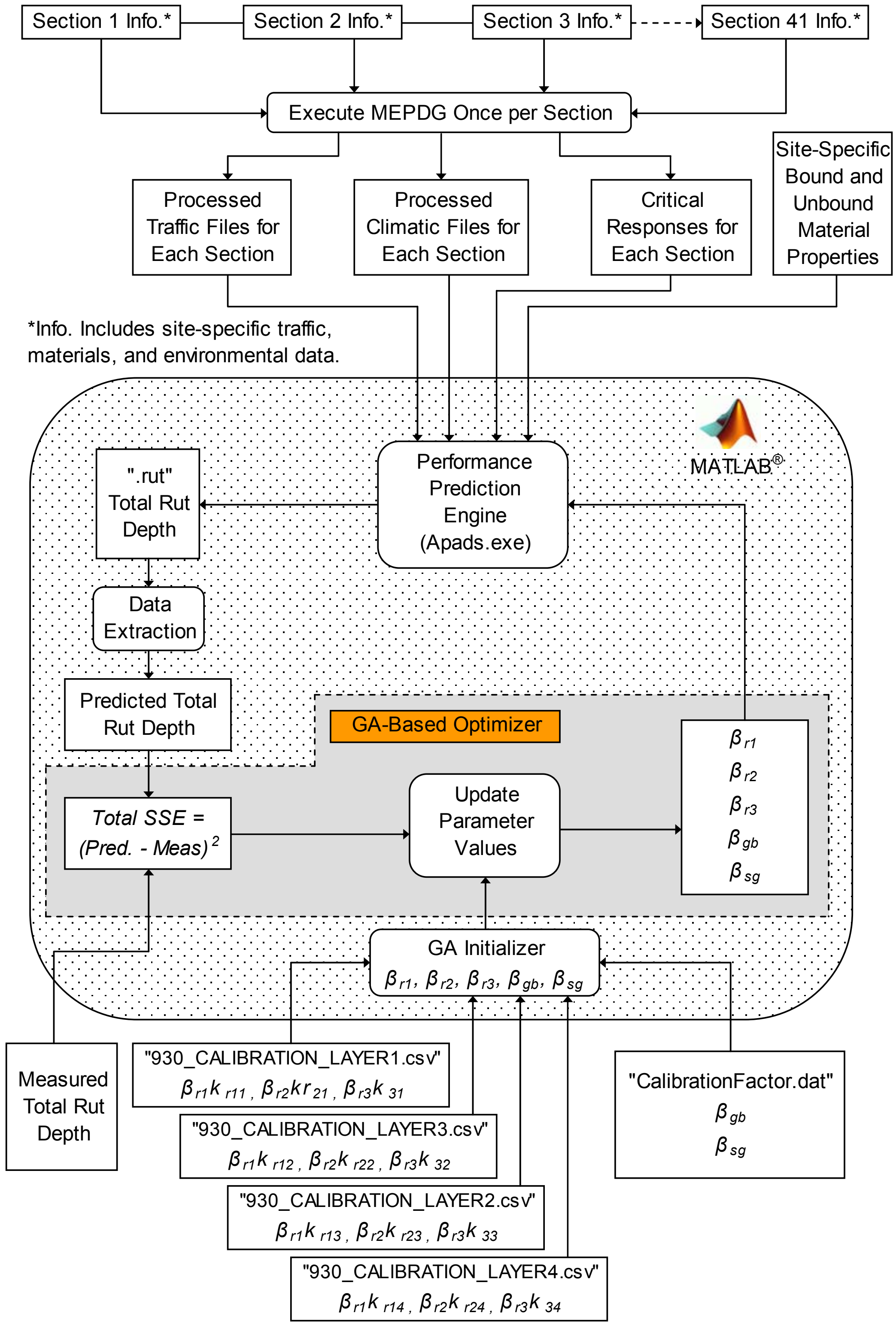

Figure 8.15. Optimization steps of rutting model coefficients using Approach II-R.

6) MATLAB® script reads the ".rut" file and extracts only certain predicted total rut depth values that correspond to the measured rut depth values previously saved in a file inside the section directory, as explained in Step 4.
7) Knowing the measured total rut depth from Step 4 and the corresponding predicted total rut depth, MATLAB® script calculates the SSE between the two values.
8) Steps 5 through 7 are repeated for all 41 sections. Once SSE values are available for all 41 sections, MATLAB® script sums the SSE from all sections to calculate the *Total SSE*. The *Total SSE* is then forwarded to the GA module within MATLAB®.
9) Based on the calculated *Total SSE*, the GA generates new values for β_{r1}, β_{r2} and β_{r3}, and a MATLAB® script writes these new values to the text files of type ".csv" defined in Step 2. Similarly, MATLAB® script writes the new values of β_{gb}, and β_{sg} to the "CalibrationFactor.dat" file.
10) Steps 5 through 9 are repeated until the change in the *Total SSE* becomes minimal. Because of the nature of the optimization problem and the time-consuming runs, the halting criterion was based mainly on changes in *Total SSE* as well as changes in the values of the calibration coefficients. Engineering judgment was used to stop the simulations after approximately five weeks of run time.

8.6.6.2.1 Background on Genetic Algorithm Function and Some Related Options in MATLAB®

MATLAB® is a powerful numerical computing program that allows the implementation of algorithms and interfacing with programs written in different languages. One of the tool boxes available in MATLAB® is the optimization toolbox using the genetic algorithm (GA) optimization technique. The GA can be implemented in MATLAB® either through a dedicated interface that can be opened using the 'optimtool' command, or through the command line using the 'gaoptimset' command. The latter was adopted in this research work due to the complex nature of the optimization problem, in the sense that the MATLAB® script is required to call and execute the executable function "Apads.exe". The GA optimization technique was selected for the 5-parameter true optimization with the hope of obtaining the global minimum value for the fitting function, i.e., *Total SSE* between the predicted and measured total rut depth values. Below are few terms that are often mentioned in the GA optimization field:

1) Individual: Refers to any possible solution. For rutting, individual refers to any possible set of beta values that can reduce bias between the total measured and total predicted rut depth values.
2) Population: Refers to a group of individuals (possible solutions).
3) Absolute boundaries: Defines the absolute lower and upper boundaries (LB and UB) in which the values of the optimized parameters should fall.
4) Options: Refers to the options available for the 'gaoptimset' function. There are 33 different available options in MATLAB®. One of the main options used in this optimization work is 'PopInitRange'. This option allows the user to enter an initial range for each of the five parameters, β_{r1}, β_{r2}, β_{r3}, β_{gb}, and β_{sg}. The values used to construct the ranges for each of the five local calibration factors are those best values obtained from rutting optimization Approach I-R. For the absolute lower and upper

boundaries, values were selected to cover the range of values found in the literature for each of the local calibration parameters and based on engineering knowledge about a possible ranges. Another option that was used in the “PopulationSize” option defines the number of possible solutions (individuals) in each generation.

The GA optimization process in MATLAB® is typically started after defining an initial range and absolute boundaries for each of the coefficients, as shown in Figure 8.16. A computer then is allowed to run until a maximum defined number of generations is reached or until the change over time in the fitting function (*Total SSE*) reaches a certain desired value. Due to the fact that the MATLAB® script is required to run Apads.exe, as shown in Figure 8.15, and considering that this process consumes about seven hours for one iteration, and because Apads.exe is not available for Unix operating systems, i.e., it cannot be run in parallel computing, the following approach was developed to make use of multiple computers to expedite the optimization process.

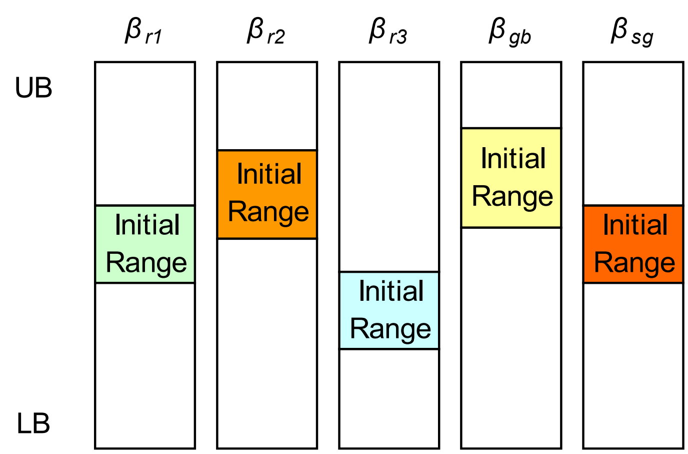

Figure 8.16 Example of initial range and absolute boundaries setup for rutting optimization – Approach II-R.

To make use of multiple computers, the absolute range for each of the calibration coefficients was divided into multiple zones. For each of these zones, the initial boundaries option was bypassed and only the absolute lower boundaries (LB) and absolute upper boundaries (UB) were defined. The zone selection for each of the calibration coefficients is based in part on the rutting optimization experience from Approach I-R and on results from some initial GA runs. The progress of the optimization process within each zone was monitored individually throughout the optimization process. The zone that yields the smallest *Total SSE* is the zone of focus. Four computers (Dual core 3.33GHz, 8GB of RAM, 64-Bit) were used for the rutting optimization study. The computers were allowed to run for approximately 32 days until the change in *Total SSE* and corresponding calibration factors became acceptable, based on different runs. Again, the change in *Total SSE* was monitored continuously throughout the optimization by plotting the data of the *Total SSE* with time.

8.6.6.3 Results and Analysis of the Rutting Models GA Optimization Runs

Figure 8.17 shows a trend that emerged by aggregating all the optimization results from the four computers and sorting their fitting function values in a descending order.

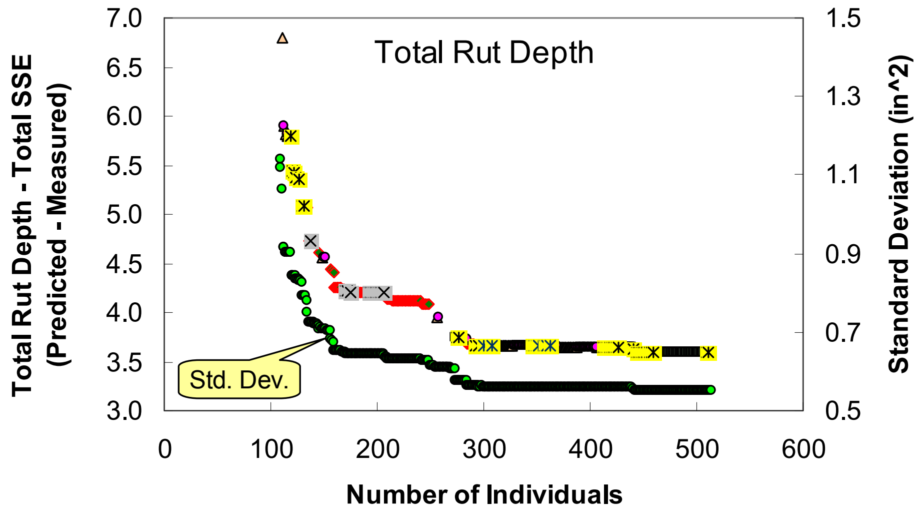

Figure 8.17. Change in total rut depth fitting function with number of individuals.

Figure 8.17 was constructed for two purposes: first, to show that a large number of optimization runs were able at some point to reach the neighborhood of the minimum value of the fitting function; and second, to show that those runs do not all stem from one iteration. The different symbols in Figure 8.17 refer to optimization runs from different computers, i.e., different optimization ranges and/or different optimization options in MATLAB®. Also, note that some of the optimization run results are excluded from Figure 8.17 because the ranges selected for these runs yielded very large *Total SSE* that, if plotted, would have distorted the actual data range of interest. Section 8.6.9.1 presents *Total SSE* value as the mean rut error per single total rut depth measurement. This information is obtained by taking the square root of *Total SSE* and dividing it by the total number of field measurements, i.e. 235 points.

Figure 8.17 also shows the standard deviation that corresponds to each of the individuals (iterations). The standard deviation curve shows that the SSE variation amongst the 41 sites for each iteration drops as the fitting function (*Total SSE*) becomes smaller. This information suggests that the solution is robust because the fitting function value is the summation of the SSE from each of the 41 sites. So, a similar value for *Total SSE* could be achieved either by having two sites with a moderate SSE or one section with a low SSE and another with a high SSE as an example. The lower standard deviation means that the optimized parameters are working well for all 41 sections and not only for some.

Figure 8.18 shows the results of the actual optimization convergence from the four optimization runs that yielded rational fitting function values.

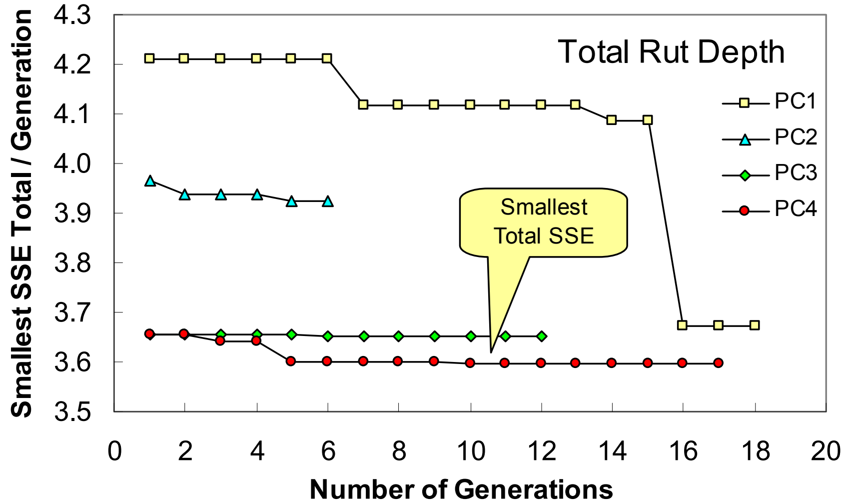

Figure 8.18. Total rut depth optimization progression from different GA runs.

As mentioned earlier, results for some of the optimization runs are excluded because they yielded very large and irrational *Total SSE* values. Note that for rutting optimization, a population size of six individuals was used. That is, each generation shown in Figure 8.18 is comprised of six individuals or iterations. In Figure 8.18, each data point refers to the individual that yielded the smallest *Total SSE* in its generation. In other words, the trends shown in Figure 8.18 show the improvement in *Total SSE* from one generation to the next as the optimization convergence takes place.

Figure 8.18 shows that depending on the initial values and/or the optimization function selected options, convergence takes anywhere between 1 and 11 generations or more to show any improvement, i.e., any drop in the fitting function value. For example, Figure 8.18 shows that PC1 went through about six generations (6 generations x 6 individuals/gen. x 7 hours ≈ 11 days) to find a better fitting function value and another seven generations to find another, and so on. Figure 8.18 also suggests that it takes about 16 generations for PC1 to reach the neighborhood of the lower fitting function value that was reached by PC3 and PC3 in a shorter period of time.

The optimization runs were halted after about 18 generations (32 days) when the changes in total fitting function and corresponding rutting calibration coefficients became acceptable based on data from three different runs, as shown in Figure 8.18. It is important to realize that the GA optimization technique is usually a very time-consuming process that can take months and even years of runs. The optimizing results in this work were achieved within a much shorter period of time mainly due to the fact that the initial ranges were already established from Approach I-R and also because the absolute lower and upper boundaries were approximated from the literature and engineering judgment. The use of multiple computers also expedited the optimization process.

8.6.6.4 Preliminary Local Calibration Factors for the HMA, Base and Subgrade Rutting Prediction Models based on Approach II-R

Table 8.16 is a summary of the rutting local calibration coefficients for bound and unbound materials based on Approach II-R. A detailed comparison between the local calibration factors from this approach and Approach I-R is presented in a subsequent section of this chapter.

Table 8.16 Preliminary Local Calibration Factors for HMA and Unbound Rutting Prediction Models using Approach II-R

Parameter	Value
β_{r1}	0.94750
β_{r2}	0.86217
β_{r3}	1.35392
β_{gb}	0.53767
β_{sg}	1.50000

8.6.6.5 Predicted vs. Measured Rutting Statistics Before and After Calibration - Approach II-R

Table 8.17 is a summary of the rutting distress statistical parameters before and after Approach II-R calibration . The null hypothesis is that the average bias, or so-called *residual error*, between the predicted and measured rut depth values is zero at the 95% confidence level. Bias represents the difference between the mean measured rut depth and the mean predicted rut depth.

Table 8.17. Summary of Rutting Distress Statistical Parameters Before and After Calibration using Approach II-R

Distress Type	Calibration	*Total SSE*	Bias	S_e	S_e/S_y	R^2	Hypothesis; *Ho: ∑(Meas.-Pred.) = 0*
Total Rut	National	4.110	-0.031	0.129	1.027	Poor	Reject; p = 0.000
	Approach II-R	3.604	-0.021	0.122	0.975	0.15	Reject; p = 0.008
AC Rut*	National	0.826	-0.017	0.057	1.005	Poor	Reject; p = 0.000
	Approach II-R	0.262	-0.011	0.032	0.921	Poor	Reject; p = 0.000
Base Rut*	National	0.212	-0.004	0.030	0.845	0.16	Accept; p = 0.058
	Approach II-R	0.060	-0.001	0.016	0.808	0.19	Accept; p = 0.450
Subgrade Rut*	National	1.127	-0.010	0.069	0.695	0.39	Reject; p = 0.022
	Approach II-R	2.370	-0.010	0.100	0.815	0.37	Accept; p = 0.135

*Estimated using similar % contribution of the layer rut depth as predicted by the MEPDG.

Table 8.17 suggests that the *Total SSE*, bias, standard error of the estimate (S_e), and the standard error ratio (S_e/S_y) all improved for the total rut, AC rut, and base layer rut as a result of using calibration factors developed from Approach II-R. Recall that a small value of S_e/S_y is always preferred because a small ratio indicates that the calibration effort is beneficial in reducing the variability among predicted rut depth values compared to the variability that exists among corresponding measured rut depth values. As for the subgrade rut predictions, bias did not change despite an increase in *Total SSE* for the subgrade layer Table 8.16 also suggests that the standard error of the estimate between the measured and predicted subgrade rut depth values increases slightly as a result of using local calibration factors, indicating a slightly high dispersion around the LOE.

Despite the improvement in rut predictions following the Approach II-R calibration, Table 8.17 indicates that the null hypothesis, i.e., that no significant difference exists between the measured and predicted rut depth values, was rejected for total rut and for AC rut at 95% confidence level. On the other hand, Table 8.17 shows that the null hypothesis was accepted for the base rut and for subgrade rut, indicating that differences between the measured and predicted rut depth values for these two layers are insignificant. Despite the slight increase in standard error for the subgrade rut due to calibration, Table 8.17 suggests that the calibration process causes the null hypothesis to be accepted, indicating no significant differences between the predicted and measured subgrade rut depth values. As for the base layer, Table 8.17 indicates that the null hypothesis was accepted before and after calibration, indicating that no significant differences exist between the predicted and measured base layer rut depth.

Figure 8.19, Figure 8.20, Figure 8.21, and Figure 8.22 show predicted versus measured rut depth values for the total, asphalt concrete, base, and subgrade layers before and after calibration using Approach II-R. Despite the fact that Figure 8.22 shows that the default calibration factors can predict the subgrade rutting, the null hypothesis, as seen in Table 8.17 was rejected at 95% confidence level. The rejection indicates that significant differences exist between the predicted and measured subgrade rut depth values. Despite the fact that Figure 8.22 (b) shows a large variability in the measured versus predicted subgrade rut depth values, the null hypothesis was accepted, as shown in Table 8.17, indicating that no significant differences exist between the measured and predicted subgrade rut depth values.

Table 8.18 summarizes the mean rut depth values for different layers before and after Approach II-R calibration. Table 8.18 shows an improvement in the mean predicted total rut depth value after calibration with a mean of 0.184 inch compared to the measured mean of 0.205 inch. The mean predicted total rut depth before calibration is 0.174 inch.

Table 8.18. Predicted Mean Rut Depth Before and After Calibration using Approach II-R

Rut Source	Measured	Before Local Calibration	After Calibration Approach II-R
Total	0.205	0.174	0.184
AC	Not Measured	0.054*	0.011*
Base		0.019*	0.010*
Subgrade		0.100*	0.163*

*Estimated using similar % contribution of the layer rut depth as predicted by the MEPDG.

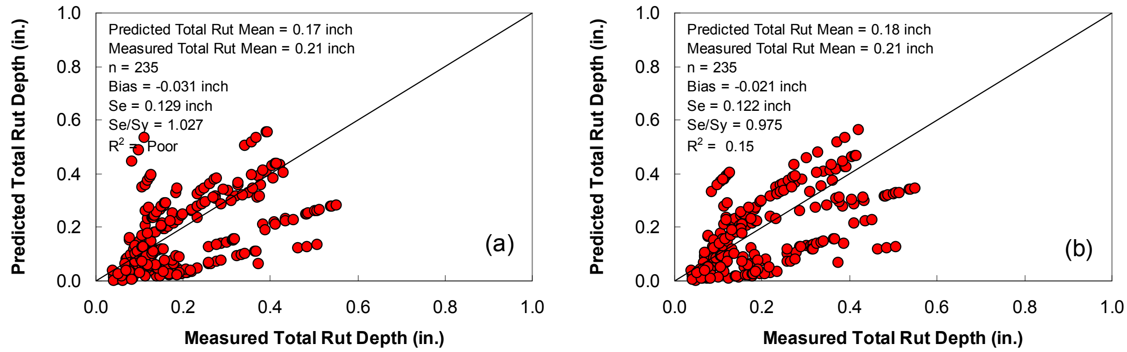

Figure 8.19. Total rut depth: (a) before calibration; and (b) after calibration using Approach II-R.

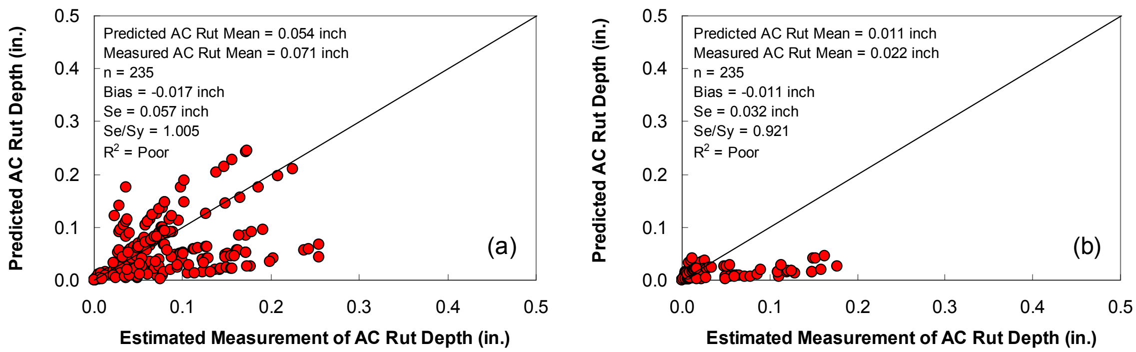

Figure 8.20. Estimated measurement of AC rut depth: (a) before calibration; and (b) after calibration using Approach II-R.

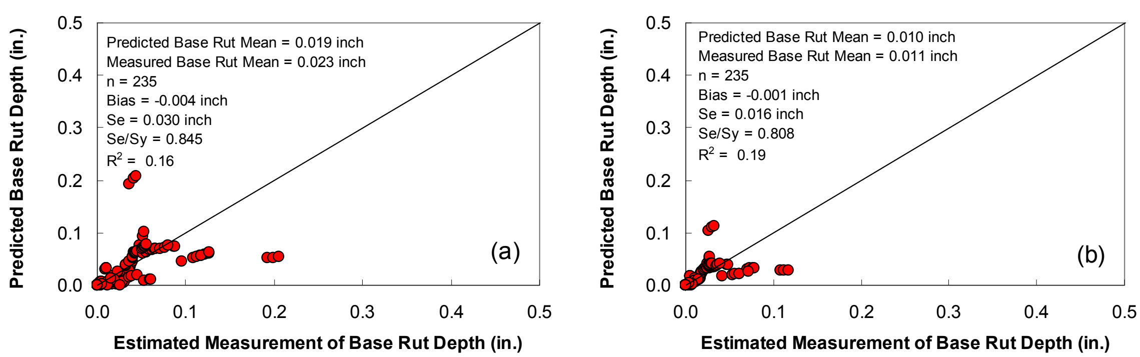

Figure 8.21. Estimated measurement of base rut depth: (a) before calibration; and (b) after calibration using Approach II-R.

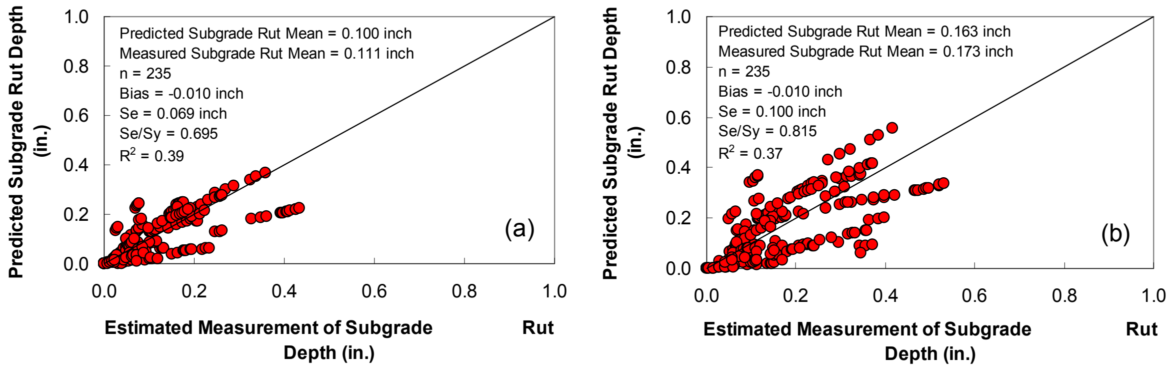

Figure 8.22. Estimated measurement of subgrade rut depth: (a) before calibration; and (b) after calibration using Approach II-R.

8.6.7 Alligator Cracking Model and Transfer Function Calibration - Approach II-F

8.6.7.1 Introduction

The alligator cracking model and transfer function GA calibration approach is similar in concept to the rutting calibration Approach II-R. In the alligator cracking context, GA optimization is a true simultaneous optimization of all four fatigue model parameters: β_{f1}, β_{f2}, β_{f3}, C_1=C_2. Similar to the rutting optimization procedure, the goal here is to find a single set of beta and C values that results in the smallest bias between predicted and measured alligator cracking from all sections grouped. Hence, the procedure does not look to reduce the bias at a single site. Because β_{f2} and β_{f3} cannot be optimized outside of the MEPDG, Approach II-F also employs Apads.exe to simulate runs from the command line rather than having to execute full runs of the MEPDG, which wastes time and effort because the traffic, weather, and other data that do not change for a certain site would have to be reprocessed. Recall that Apads.exe requires the following inputs to run successfully: traffic over the design life of the pavement, critical pavement responses, bound and unbound material properties, and weather data, including changes in temperature and moisture profiles and depth of water table below ground level. Because these inputs do not change for a specific location, the MEPDG can be executed only once per pavement section to generate all of these inputs. The number of cycles to failure (N_f) model and transfer function calibration factors then can be optimized outside of the MEPDG using the GA technique. The steps followed in Approach II-F are summarized in the following section.

8.6.7.2 Calibration Steps

Figure 8.23 is a flow chart that shows the logic behind the MATLAB® script that was developed to optimize all fatigue prediction model coefficients simultaneously. The detailed steps are as follows.

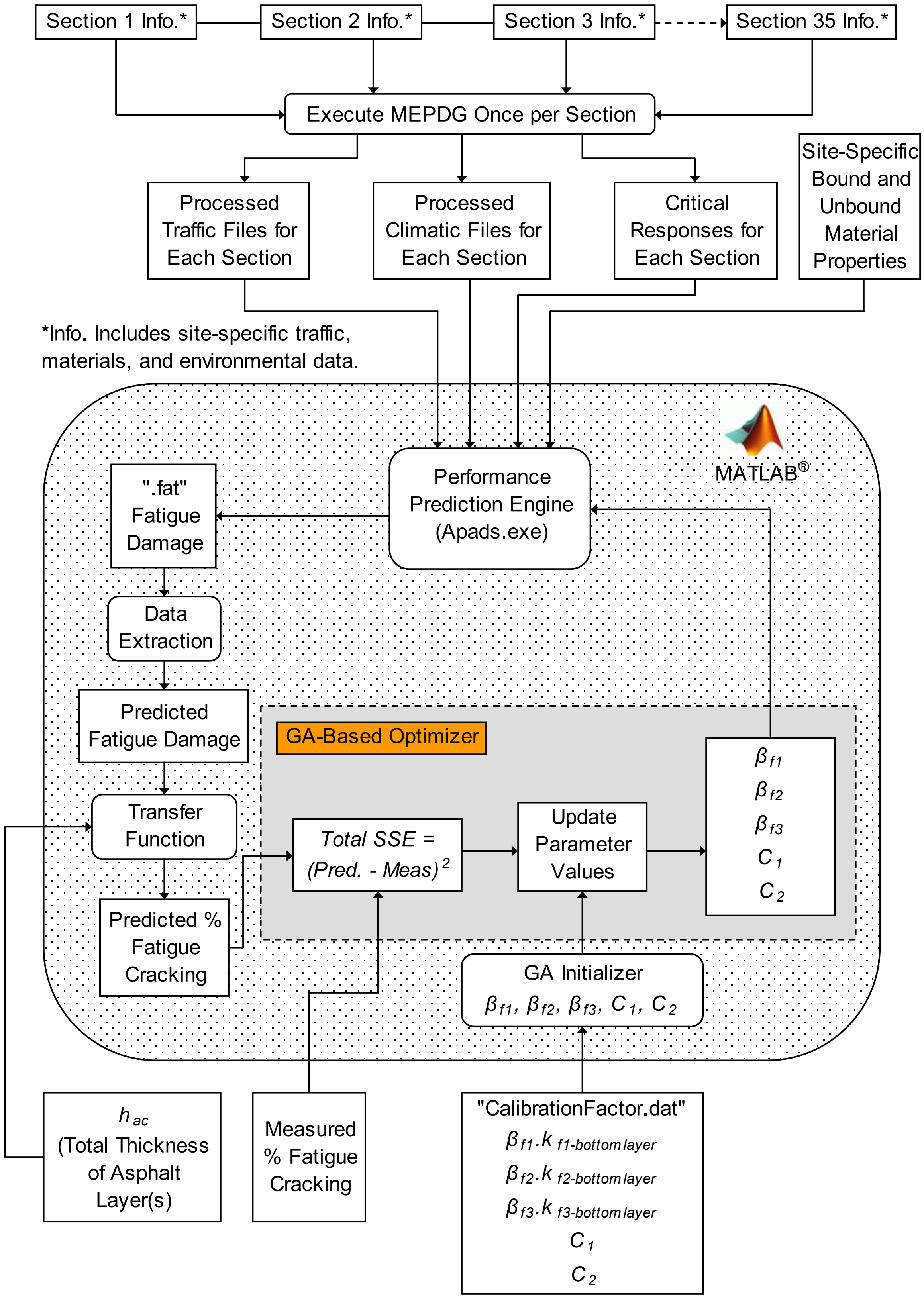

Figure 8.23. Optimization steps of fatigue models' coefficients using Approach II-F.

1) Among all 41 available LTPP calibration sections, only 35 sections had surveyed alligator cracking data available. For each of these sections, the MEPDG was executed once to generate processed traffic files, climatic files, critical responses (i.e. stresses, strains and deflections), and other input files that are required by Apads.exe to run. After the MEPDG runs were completed for all sections, a copy of Apads.exe file was saved in each section directory. The process of saving the Apads.exe file in each section directory is required for MATLAB® script to simulate the MEPDG runs and predict pavement performance outside the MEPDG.
2) As a result of executing the MEPDG for each section, as explained in Step 1, a file called 'CalibrationFactor.dat' was generated automatically and saved in each section directory. In addition to material-specific fatigue model *k* values for the bottom HMA layer, the CalibrationFactor.dat file contains all fatigue model and transfer function coefficients that need to be calibrated, i.e., β_{f1}, β_{f2}, β_{f3}, and C_1=C_2. Note that for fatigue optimization work, only one set of material-specific *k* values is required; the set corresponds to the bottom HMA layer. This requirement is in contrast to that for rutting optimization where separate material-specific *k* values are required for each HMA layer.
3) A text file in a MATLAB®-readable format that contains the measured fatigue cracking data for each survey date in addition to the total thickness of HMA layer(s) (h_{ac}) data for each of the 35 pavement sections is created. The text file must be saved in the main directory where the MATLAB® script and all section directories exist. By the end of this step, MATLAB® is ready to run. The following steps explain how MATLAB® finds the optimized values of β_{f1}, β_{f2}, β_{f3} and C_1=C_2 that minimize the bias between the predicted and measured alligator cracking percentages.
4) MATLAB® first calls the Apads.exe file for the first section and executes it. As a result, a file called ".fat" is generated. The ".fat" file contains the total predicted fatigue damage values for the site. Note that it is not fatigue damage that is measured in the field; rather, fatigue cracking is measured in the field.
5) MATLAB® script reads the ".fat" file and extracts only the predicted fatigue damage values that correspond to the measured fatigue cracking values previously saved in a text file inside the section directory, as explained in Step 3.
6) Knowing the predicted fatigue damage and the total thickness of the asphalt layer(s) (h_{ac}), MATLAB® script calculates the predicted fatigue cracking percentage.
7) Knowing the measured fatigue cracking percentage from Step 3 and the corresponding predicted fatigue cracking percentage, MATLAB® script calculates the SSE between the measured and predicted fatigue cracking percentages.
8) Steps 4 through 7 are repeated for all 35 sections. Once the SSE values are available for all 35 sections, the MATLAB® script sums the SSE values from all the sections to calculate the *Total SSE*. The *Total SSE* is then forwarded to the GA module within MATLAB®.
9) Based on the calculated *Total SSE*, the GA generates new values for β_{f1}, β_{f2} β_{f3}, and C_1=C_2, and a MATLAB® script writes these new values to the 'CalibrationFactor.dat' file.
10) Steps 4 through 9 are repeated until the change in the *Total SSE* (or so-called fitting function) becomes minimal. Because of the nature of the optimization problem and

the time-consuming runs, the halting criterion is based mainly on changes in the *Total SSE* as well as changes in the values of the calibration coefficients. Based on engineering judgment and experience, the simulations were halted after approximately seven weeks of run time.

Because of a similar extended optimization run-time issue encountered in the rutting model calibration case, the fatigue cracking GA optimization process also utilized multiple computers to expedite finding a global or at least a stable minimum *Total SSE*. The fatigue optimization process in MATLAB® is typically started after defining an initial range and absolute boundaries for each of the coefficients, as shown in Figure 8.24.

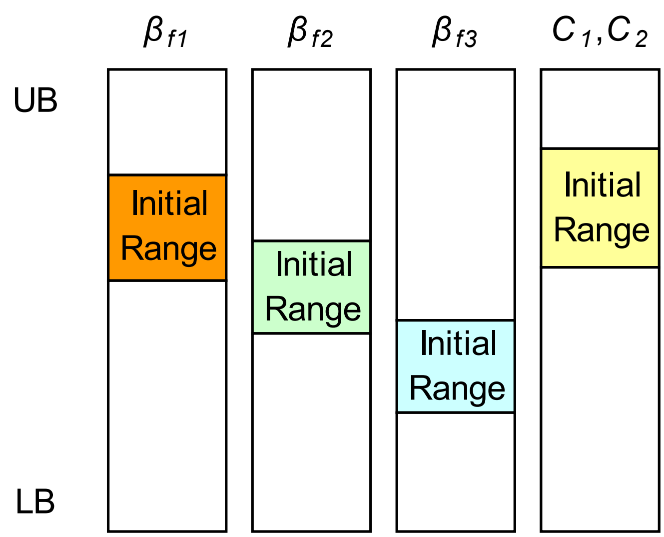

Figure 8.24. Example of initial range and absolute boundaries setup for alligator cracking optimization – Approach II-F.

The absolute range for each of the four local calibration coefficients was divided into multiple zones. For each of these zones, the initials boundaries option was bypassed, and only the absolute lower boundaries (LB) and upper boundaries (UB) were defined.

The zone selection for each of the calibration coefficients was based in part on the fatigue optimization results from Approach I-F and on results from some GA initial runs. The progress of the optimization process within each zone was monitored individually throughout the optimization process. The zone that yielded the smallest *Total SSE* was the zone of focus. Considering the fact that it takes MATLAB® about six hours to finish one iteration for all 35 sections, five computers (Dual core 3.33GHz, 8GB of RAM, 64-Bit) were used for the fatigue optimization study. Computers were allowed to run for about 37 days until the change in *Total SSE* and corresponding parameters became acceptable. Again, the change in *Total SSE* was monitored continuously throughout the optimization process by plotting the data of the *Total SSE* with time.

8.6.7.3 Results and Analysis of the Alligator Cracking Model and Transfer Function GA Optimization Runs

Figure 8.25 shows a trend that developed through aggregating the alligator cracking optimization run results from the five computers and sorting their fitting function values in a descending order. Similar to the rutting optimization case, Figure 8.25 is constructed for two purposes: first, to show that a large number of optimization runs were able at some point to reach the neighborhood of the minimum value of the fitting function; and second, to show that those runs do not all stem from one iteration. The different symbols in Figure 8.25 refer to the different optimization runs from different computers, i.e., different optimization ranges and/or different optimization options in MATLAB®. Some of the optimization initial run results and, in some cases, complete runs, as is the case for rutting, are excluded from Figure 8.25 because the ranges selected for these runs yielded very large *Total SSE* values that, if plotted, would have distorted the actual data range of interest.

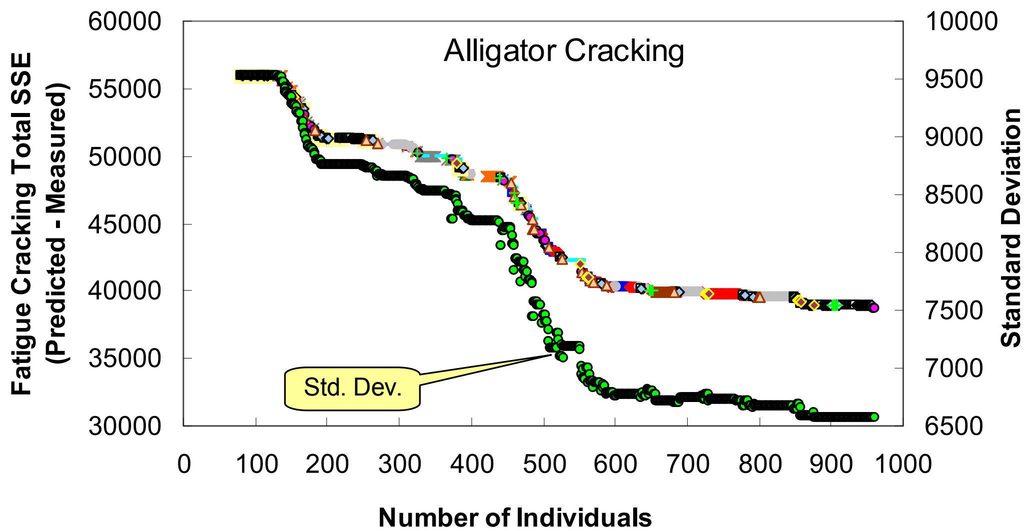

Figure 8.25. Change in total alligator cracking fitting function with number of individuals.

Figure 8.25 displays the standard deviation trend that corresponds to each iteration. The standard deviation curve shows that the SSE variation amongst the 35 sites for each iteration decreases as the fitting function (*Total SSE*) decreases. This information again suggests that the solution attained is robust. Recall that the fitting function value is the summation of the SSE from each of the 35 sites. So, a similar value for *Total SSE* could be achieved in different ways. For example, section A could have an SSE value of 50 versus an SSE of 100 for section B, in which case the *Total SSE* is 150 and indicates larger variability compared to section C with a SSE of 70 and section D with a SSE of 80 that still yields the same *Total SSE*. A lower standard deviation indicates that the optimized parameters are reasonable in reducing the differences between predicted and measured percentages of alligator cracking for all 35 sections. Section 8.6.9.1 presents a more meaningful form of *Total SSE* value. The new form describes the mean alligator cracking percent error per single measurement. This information is obtained by taking the square root of *Total SSE* and dividing it by the total number of observed alligator cracking field measurements, i.e. 124 points.

Figure 8.26 shows the results of the actual optimization convergence from nine optimization runs that yielded rational fitting function values when compared to those obtained from Approach I-F.

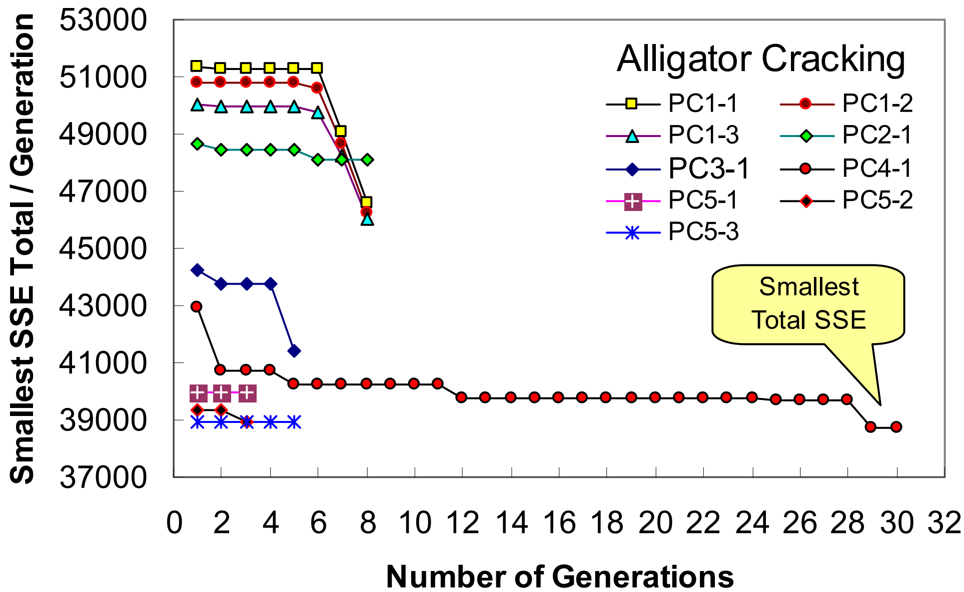

Figure 8.26. Total alligator cracking optimization progression from different GA runs.

As mentioned earlier, initial results for some of the optimization runs are excluded because they yielded very large and irrational *Total SSE* values. For alligator cracking optimization, a population size of five individuals was used compared to six for the rutting optimization. So, each generation shown in Figure 8.26 is comprised of five individuals. In Figure 8.26, each data point refers to the individual that yields the smallest *Total SSE* in its generation. In other words, the trends shown in Figure 8.26 show the improvement in *Total SSE* from one generation to the next as the optimization convergence progresses. Figure 8.26 shows that, in general, an improvement in the fitting function values were noticeable immediately after the first generation in some cases. Figure 8.26 shows that PC2-1, PC3-1 and PC4-1 all improved the fitting function immediately after the first generation. Other runs, such as PC1-2, take about six generations to improve the fitting function value.

Figure 8.26 also suggests that it takes about 28 generations (35 days) for PC4-1 to reach the neighborhood of the fitting function values that was reached by PC5-2 and PC5-3 and then two more generations (2.5 days) to achieve the best fitting function value. Again, the time depends on the starting initial values for each of the parameters and on the selected optimization function options in the GA.

In summary, the optimization runs were halted after about 30 generations (37.5 days) when the changes in total fitting function and corresponding rutting calibration coefficients became acceptable based on data from four different runs, as shown in Figure 8.26. The optimizing results in this work were achieved within a much shorter period of time because the initial ranges were already established from Approach I-F and also because the absolute lower and upper boundaries were approximated based on the literature and engineering judgment. The use of five computers also expedited the optimization process.

8.6.7.4 Preliminary Alligator Cracking Model and Transfer Function Local Calibration Factors based on Approach II-F

Table 8.19 is a summary of the alligator cracking model and transfer function local calibration factors based on Approach II-F. A detailed comparison between the local calibration factors obtained from this approach versus those obtained from Approach I-F is presented in a subsequent section of this chapter.

Table 8.19. Preliminary Local Calibration Factors for Alligator Cracking Model and Transfer Function using Approach II-F

Parameter	Value
β_{f1}	3.50000
β_{f2}	0.72364
β_{f3}	0.60000
C_1	0.24377
C_2	0.24377

8.6.7.5 Predicted vs. Measured Alligator Cracking Statistics Before and After Calibration – Approach II-F

Table 8.20 is a summary of the alligator cracking statistical distress parameters before and after Approach II-F calibration. The null hypothesis is that the average bias, or so-called residual error, between the predicted and measured alligator cracking values is zero at 95% confidence level.

Table 8.20. Summary of Alligator Cracking Statistical Parameters Before and After Calibration using Approach II-F

Distress Type	Calibration	*Total SSE*	Bias	S_e	S_e/S_y	R^2	Hypothesis; *Ho: ∑(Meas.-Pred.) = 0*
Alligator Cracking	National	56412	-11.034	19.498	1.022	Poor	Reject; p = 0.000
	Approach II-F	38752	-5.153	17.111	0.949	Poor	Reject; p = 0.001

Table 8.20 suggests that the *Total SSE*, bias, standard error of the estimate (S_e), the standard error ratio (S_e/S_y), and the p-value are all improved after calibration. Despite the improvement in the after-calibration statistics, Table 8.20 suggests that the null hypothesis was rejected at the 95% confidence level, indicating that the differences between the measured and predicted alligator cracking values are still significant even after calibration.

Table 8.21 is a summary of the predicted alligator cracking mean before and after calibration using Approach II-F.

Table 8.21. Predicted and Measured Alligator Cracking Means, Before and After Calibration using Approach II-F

Calibration	Predicted Mean Alligator Cracking (% Lane Area)	Measured Mean Alligator Cracking (% Lane Area)
National	0.456	11.490
Approach II-F	6.246	

It is clear from Table 8.21 that the calibration significantly improved the predicted alligator cracking percentage. Before calibration, the predicted alligator cracking is about 0.5% of the lane area, whereas after calibration, the percentage increases to about 6.3% of the lane area. In North Carolina, fatigue cracking is the major distress responsible for the failure of flexible pavement, so the calibration effort has improved the prediction, but the improvement, as indicated in Table 8.20, is not statistically sufficient to accept the hypothesis that the measured alligator cracking is not significantly different from the predicted alligator cracking at 95% confidence level.

Figure 8.27 (a) and (b) show predicted versus measured alligator cracking values before and after Approach II-F calibration, respectively. Figure 8.27 (b) again suggests that calibration improves the alligator cracking predictions, yet the improvement is not enough to accept the null hypothesis at 95% confidence level.

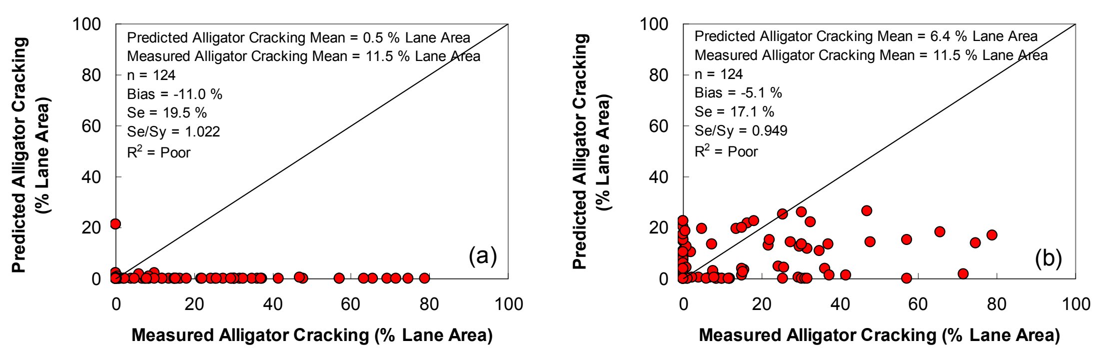

Figure 8.27. Alligator cracking calibration results: (a) before calibration; and (b) after calibration using Approach II-F.

8.6.8 Validation of Rutting and Alligator Cracking Calibrated Models for Approach II

This section presents the validation results of the rutting and alligator cracking local calibration factors developed under Approach II-R and Approach II-F, using the same NCDOT PMS sections that were used to validate the Approach I calibration factors.

8.6.8.1 Validation Results for Approach II-R Rutting Local Calibration Factors

Table 8.22 is a summary of the statistical parameters for rut depth predictions obtained from validation runs compared to those determined earlier from Approach II-R calibration runs.

Table 8.22. Comparison of Rutting Statistical Parameters between Approach II-R Calibration and Validation

Distress Type	Approach II-R	Bias	S_e	S_e/S_y	R^2	Hypothesis; *Ho: ∑(Meas.-Pred.) = 0*
Total Rut	Calibration	-0.021	0.122	0.975	0.15	Reject; p = 0.008
	Validation	0.248	0.190	2.317	Poor	Reject; p = 0.000
AC Rut*	Calibration	-0.011	0.032	0.921	Poor	Reject; p = 0.000
	Validation	0.012	0.006	1.225	Poor	Reject; p = 0.000
Base Rut*	Calibration	-0.001	0.016	0.808	0.19	Accept; p = 0.450
	Validation	0.009	0.017	1.570	Poor	Reject; p = 0.000
Subgrade Rut*	Calibration	0.010	0.100	0.815	0.37	Accept; p = 0.135
	Validation	0.227	0.187	2.710	Poor	Reject; p = 0.000

*Estimated using similar % contribution of different layers as predicted by the MEPDG.

Due to the large differences between the mean measured and predicted rut depth values for the PMS sections, Table 8.22 shows that the validation statistics are, in general, worse than the calibration statistics for rut depth in all layers. In addition, the hypothesis that measured total rut depth is equal to predicted total rut depth is rejected for the validation sections at 95% confidence level. The bias also increases for total rut depth and rut depth in the subgrade layer, whereas the standard error (S_e) increases for the total rut, base rut, and subgrade rut values but decreases significantly for the asphalt layer rut values.

Figure 8.28 (a), (b), (c), and (d) show predicted versus measured total, asphalt concrete, base, and subgrade rut depth values, respectively. Figure 8.28 (a) suggests that the MEPDG, in general, overpredicts total rut depth (0.28 inches predicted versus 0.03 inches measured). However, several cases in Figure 8.28 (a) suggest that predicted total rut depth matches very well with the measured rut depth. Figure 8.28 (b) indicates that the MEPDG still overpredicts the rut depth in the asphalt layers, but the overprediction is much less than that shown for total asphalt rut depth. Furthermore, Figure 8.28 (b) shows that the predicted rut depth in the asphalt layers is generally very small, 0.013 inches on average. Figure 8.28 (b) also indicates that several asphalt concrete rut depth measurements agree well with their predicted counterparts. Nevertheless, in general the MEPDG overpredicts the asphalt concrete rut depth, mainly because the asphalt concrete rut depth is calculated as a percentage of the total rut depth, which is overpredicted by the MEPDG initially. Alternatively, it is more likely that the measured rut depth is lower than the actual depth of the pavements at the time of the survey.

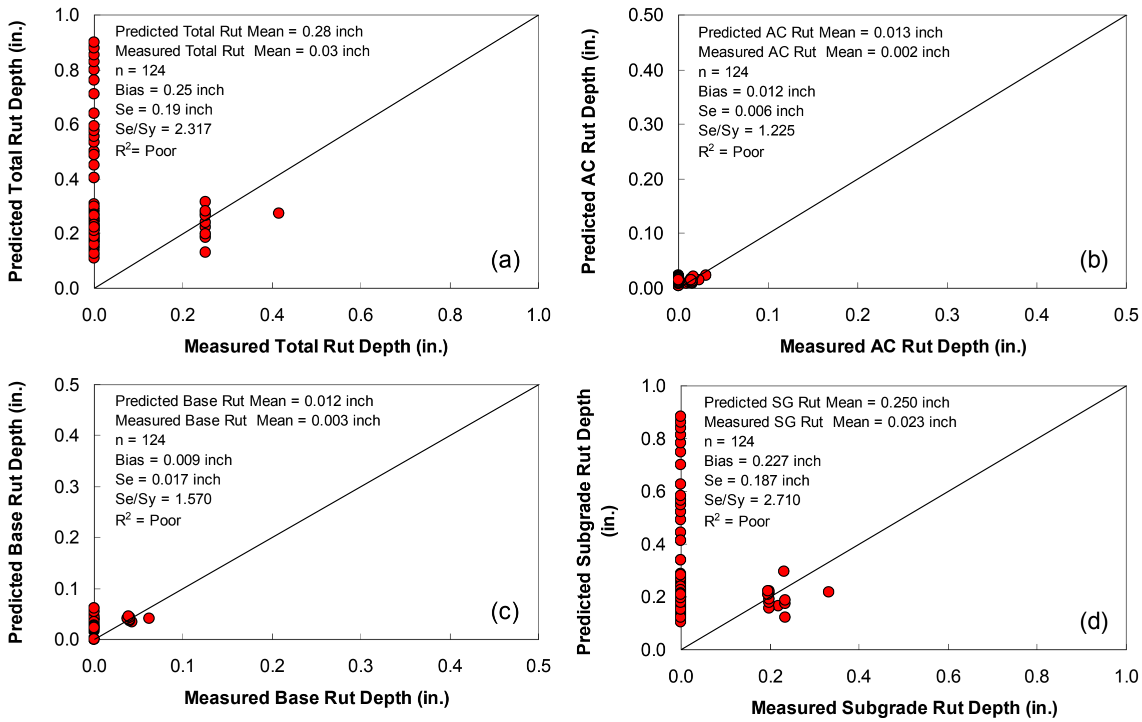

Figure 8.28. Predicted vs. measured rut depth after validation work using Approach II-R: (a) total rut; (b) estimated AC rut; (c) estimated base rut; and (d) estimated subgrade rut.

Figure 8.28 (c) shows that the MEPDG predictions for the base layer rut depth values are on average higher than the mean measured values (0.012 inches predicted compared to 0.003 inches measured). The research team recognizes that the presented numbers are very small and impractical because they are much smaller than the smallest resolution that can be measured in the field. However, the numbers are presented to give perspective on the differences between the predicted and measured rut depth values.

Figure 8.28 (d) shows that calibration Approach II-R contributes significantly to the total rut depth of the subgrade layer of about 89%. Without forensic studies, it is difficult to judge whether this finding is true or not. In general, the trend is clear that the MEPDG overpredicts rut depth measurements for the PMS sections. Several recommendations are presented in Chapter 9 to improve the match between MEPDG-predicted distresses versus measured distresses in general. Table 8.23 shows a comparison of the mean total rut depth predicted from validation runs with the values determined from Approach II-R calibration runs.

Table 8.23. Comparison of Predicted Total Rut Depth between Approach II-R Calibration and Validation

Analysis	Predicted Mean Total Rut Depth (inch)	Measured Mean Total Rut Depth (inch)
Calibration (LTPP Sections)	0.184	0.205
Validation (PMS Sections)	0.276	0.028

Table 8.23 indicates that NCDOT personnel underestimate, on average, the rut depth predicted by the MEPDG using local calibration factors and material specific *k* values. It could be argued that the predicted total rut depth value is very large. However, Table 8.23 clearly shows that for the LTPP sections in North Carolina, the mean total rut depth is 0.205 inch. Therefore, it is unlikely that the predicted total rut depth overestimates the measured rut depth for the PMS sections. Recall that NCDOT personnel gave subjective ratings of none, light, medium, or severe for the different ranges of rut depth.

8.6.8.2 Validation Results for Approach II-F Alligator Cracking Local Calibration Factors

Table 8.24 is a summary of the statistical parameters for alligator cracking predictions obtained from validation runs compared to those determined earlier from Approach II-F calibration runs. Recall that Approach II-F calibration runs were performed on LTPP sections, which, in general, have very reliable materials, traffic, and distress information, compared to all the validation runs performed on NCDOT PMS sections for which less accurate information was available and various distress survey techniques were used, as explained earlier under Section 8.4.2.3.1.

Table 8.24. Comparison of Alligator Cracking Statistical Parameters between Approach II-F Calibration and Validation

Distress Type	Analysis	Bias	S_e	S_e/S_y	R^2	Hypothesis; *Ho: ∑(Meas.-Pred.) = 0*
Alligator Cracking	Calibration	-5.153	17.111	0.949	Poor	Reject; p = 0.001
	Validation	1.973	10.239	1.690	Poor	Reject; p = 0.034

Recall that the goal of the validation work is to determine whether the improvement in performance through the calibration effort can be translated into performance prediction improvement for sections not used in the calibration; i.e., PMS sections. Table 8.24 suggests that this goal has been achieved. The bias, standard error of the estimate (S_e) and p-value not only matched those from the calibration effort, but they were improved even further. Despite the improvement in the validation statistics, Table 8.24 shows that the null hypothesis was rejected, indicating that significant differences between the predicted and measured alligator cracking values for the PMS sections still exist. Table 8.25 shows a comparison of the mean alligator cracking predictions determined from the validation runs in comparison to those determined from the calibration runs.

Table 8.25. Comparison of Predicted Alligator Cracking between Approach II-F Calibration and Validation

Analysis	Predicted Mean Alligator Cracking (% Lane Area)	Measured Mean Alligator Cracking (% Lane Area)
Calibration (LTPP Sections)	6.246	11.490
Validation (PMS Sections)	5.202	3.230

Table 8.25 suggests that the alligator cracking validation results for Approach II-F are similar to those of Approach I-F. The calibrated alligator cracking models that use Approach II-F underpredict the LTPP-measured alligator cracking by about 5.5% and overpredict the PMS measured alligator cracking by about 2.0 percent. Realizing that the alligator cracking distress is the main cause of flexible pavement failure in North Carolina, and knowing that the LTPP distress survey methods are more accurate that the windshield survey method exercised by the NCDOT, it can be concluded from Table 8.25 that the measured alligator cracking for NC PMS sections, especially when compared to the 11.5% alligator cracking measured at LTPP sections, is underestimated. Therefore, the predicted alligator cracking of 5.2% is a more realistic number when compared to the measured mean of 3.2 percent. Also note that the aforementioned alligator cracking conversion relationship developed by Corley-Lay et al. (2010) certainly had helped minimize the differences between the measured and predicted alligator cracking values for the validation sections, using the alligator cracking prediction models that were calibrated using Approach II-F.

Figure 8.29 is a graph showing predicted versus measured alligator cracking after validation work for the PMS sections. Figure 8.29 suggests that, on average, the alligator cracking measurements taken by the NCDOT are much lower than those predicted by the MEPDG using local calibration factors developed from Approach II-F. Figure 8.29 shows that few alligator cracking measurements were captured or predicted correctly.

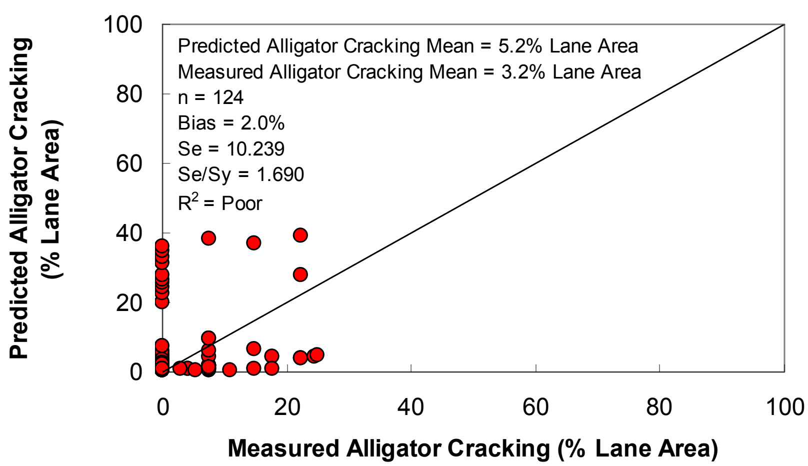

Figure 8.29. Predicted vs. measured alligator cracking values after validation work using Approach II-F.

8.6.9 Comparison between Approach I and Approach II and the Final Selection

The purpose of this section is to summarize, side by side, the calibration and validation results obtained from Approach I and Approach II in order to select the final rutting and alligator cracking local calibration coefficients based on the better approach.

8.6.9.1 Comparison of Calibration Results

Table 8.26 is a summary of the rutting and alligator cracking local calibration factors developed from Approach I and Approach II. On the rutting side, Table 8.26 suggests that Approach I-R and II-R both give close β_{r3} values but differ in the other four factors. Recall that the β_{r3} factor accounts for the effect of loading cycles or traffic volume. The higher β_{r3} is, the more effect of traffic on increasing the rut depth. Table 8.26 indicates that the β_{r1} obtained from Approach I-R it is much higher than from Approach II-R (13.1 compared to 0.95). With constant βr_2 and βr_3, the higher β_{r1} indicates larger ruts in the HMA layer. Also, note that the effect of the β_{r2} and β_{r3} parameters on the predicted HMA rut depth is exponential, because they are exponents in the HMA rut prediction model.

Table 8.26. Comparison between Local Calibration Factors from Approach I and II

Distress Type	Parameter	Approach I	Approach II
Rutting	β_{r1}	13.1000	0.94750
	β_{r2}	0.40000	0.86217
	β_{r3}	1.40000	1.35392
	β_{gb}	0.30300	0.53767
	β_{sg}	1.10200	1.50000
Alligator Cracking	β_{f1}	3.87800	3.50000
	β_{f2}	0.80000	0.72364
	β_{f3}	0.80000	0.60000
	C_1	0.24500	0.24377
	C_2	0.24500	0.24377

With regard to the alligator cracking local calibration factors, Table 8.26 indicates smaller differences between factors developed from Approach I-F versus those developed from Approach II-F. Table 8.26 shows that the differences in calibration factors between the two approaches are slightly higher for β_{f1} and β_{f3} compared to the other three factors.

Figure 8.30 (a) compares predicted versus measured total rut depth values for default calibration values, calibration factors from Approach I-R, and for calibration factors from Approach II-R. Recall that default values refer to default *k* values and default beta values that are equal to one. As for Approaches I-R and II-R, material-specific *k* values were used along with the local calibration factors presented in Table 8.26.

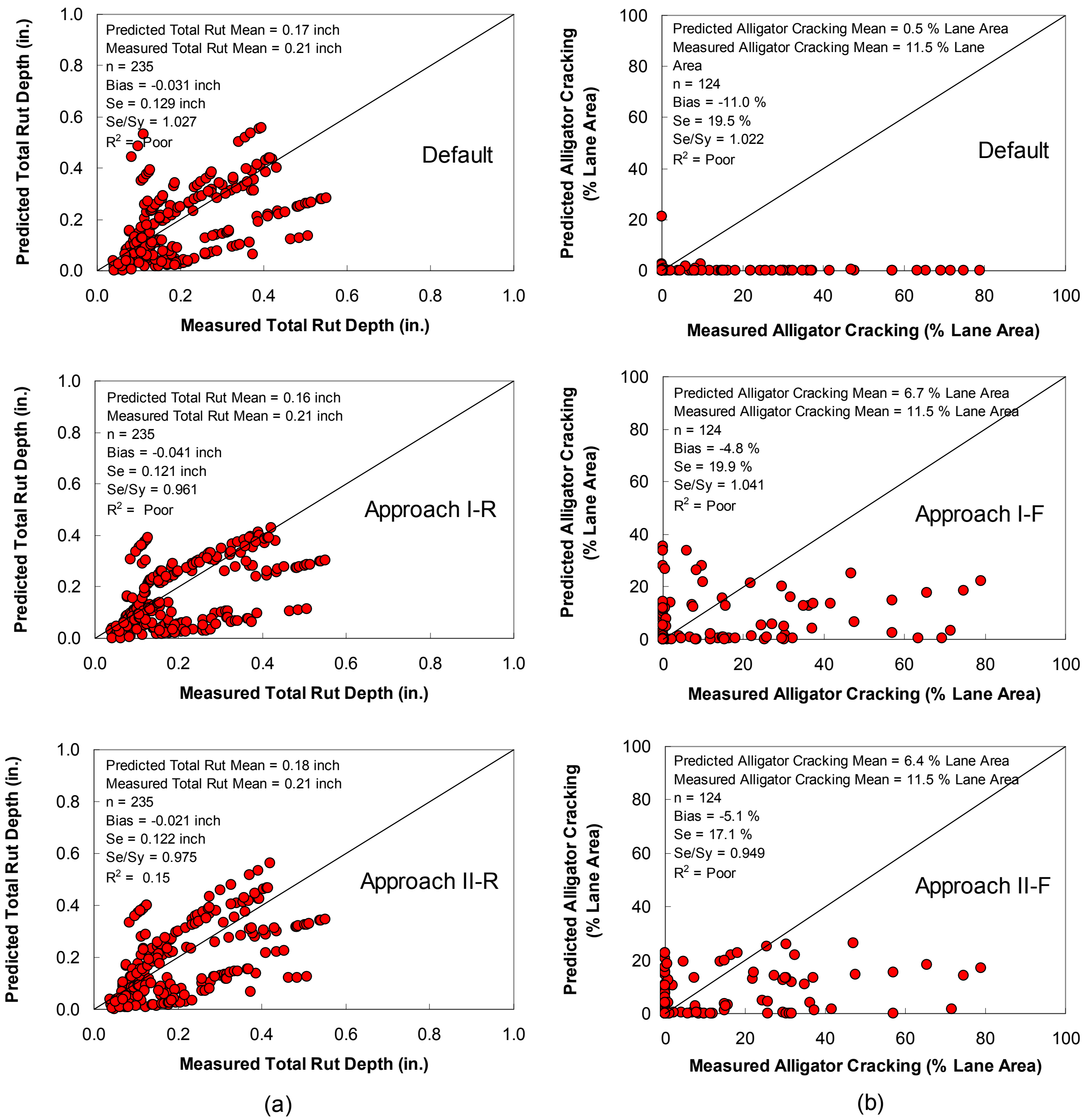

Figure 8.30. Comparison between calibration results from Approach I and Approach II: (a) predicted vs. measured total rut depth; and (b) predicted vs. measured alligator cracking.

Figure 8.30 (a) clearly shows that Approach I-R and Approach II-R both reduce the scatter around the LOE. However, Figure 8.30 (a) suggests that the data points in the Approach II-R plot are better distributed around the LOE compared to those in the Approach I-R plot. The actual statistics are presented and discussed in the next section.

Recall that the optimization fitting function in both approaches is the total rut depth; hence, only the total rut depth comparison is consulted, especially given that no forensic investigations were performed to determine the contribution of each pavement layer to the total rut depth that is measured at the surface.

As for the alligator cracking predictions, Figure 8.30 (b) shows clearly that the default values underpredict alligator cracking, whereas Approach I-F and Approach II-F both improve the predictions with Approach II-F doing a better job in reducing the scatter around the LOE. Table 8.27 is a summary of the mean predicted rut depth and alligator cracking values from both approaches compared with the measured values as reported in the LTPP database.

Table 8.27. Comparison between Predicted and Measured Rut Depth and Alligator Cracking from Approach I and Approach II

Distress Type	Measured distress value	Mean distress value before local calibration	After Calibration Approach I	After Calibration Approach II
Total Rut (in,)	0.205	0.174	0.164	0.184
AC Rut (in.)	Not Measured	0.054*	0.047*	0.011*
Base Rut (in.)		0.019*	0.006*	0.010*
Subgrade Rut (in.)		0.100*	0.111*	0.163*
Alligator Cracking (%)	11.49	0.456	6.654	6.246

*Estimated using similar % contribution of the layer rut depth as predicted by the MEPDG.

Note that Table 8.27 also includes information about the rut depth from the HMA, base, and subgrade layers. The information is provided just to note that Approach I-R results in higher predicted HMA rut than Approach II-R, whereas Approach II-R results in higher predicted subgrade rut depth than Approach I-R. This outcome is expected because the value of the parameter β_{sg} obtained from Approach II-R is 1.5 compared to 1.102 as obtained from Approach I-R.

Table 8.27 suggests that the total rut depth value predicted by Approach II-R (0.184 inch) is closer to the LTPP-measured total rut depth value (0.205 inch) than that predicted by Approach I-R (0.164 inch). It is also interesting to observe that the total rut depth predicted before calibration is in between that predicted from Approach I-R and Approach II-R.

With regard to alligator cracking predictions, Table 8.27 shows that Approaches I-F and II-F result in similar predictions: 6.7% versus 6.3%, respectively. Both predictions are still far behind the measured distress value of 11.5% lane area. Both approaches, however, improve the predictions compared to the nationally calibrated models that underpredict measured alligator cracking.

When looking at the mean, it is vital to consider other calibration statistics before making a decision. Table 8.28 compares total rut depth and alligator cracking calibration statistics for Approach I and Approach II with those obtained using nationally calibrated models.

Table 8.28. Comparison of Approaches I and II Calibration Statistics to Default Statistics

Distress Type	Calibration	*Total SSE*	Bias	S_e	S_e/S_y	R^2	Hypothesis; *Ho: ∑(Meas.-Pred.) = 0*
Total Rut	National	4.110	-0.031	0.129	1.027	Poor	Reject; p = 0.000
	Approach I-R	3.803	-0.041	0.121	0.961	Poor	Reject; p = 0.000
	Approach II-R	3.604	-0.021	0.122	0.975	0.15	Reject; p = 0.008
AC Rut*	National	0.826	-0.017	0.057	1.005	Poor	Reject; p = 0.000
	Approach I-R	0.731	-0.020	0.052	1.019	Poor	Reject; p = 0.000
	Approach II-R	0.262	-0.011	0.032	0.921	Poor	Reject; p = 0.000
Base Rut*	National	0.212	-0.004	0.030	0.845	0.16	Accept; p = 0.058
	Approach I-R	0.037	-0.003	0.012	0.810	Poor	Reject; p = 0.001
	Approach II-R	0.060	-0.001	0.016	0.808	0.19	Accept; p = 0.450
Subgrade Rut*	National	1.127	-0.010	0.069	0.695	0.39	Reject; p = 0.022
	Approach I-R	1.534	-0.019	0.079	0.715	0.31	Reject; p = 0.000
	Approach II-R	2.370	0.010	0.100	0.815	0.37	Accept; p = 0.135
Alligator Cracking	National	56412	-11.034	19.498	1.022	Poor	Reject; p = 0.000
	Approach I-F	41764	-4.836	19.852	1.041	Poor	Reject; p = 0.008
	Approach II-F	38752	-5.153	17.111	0.949	Poor	Reject; p = 0.001

*Estimated using similar % contribution of the layer rut depth as predicted by the MEPDG.

When looking at the total rut depth statistics fields in Table 8.28 it is clear that Approach II-R is the better approach. Table 8.28 suggests that Approach II-R decreases the bias from -0.031 inches down to -0.021 inches, whereas Approach I-R increases the bias to -0.041 inches. Furthermore, Table 8.28 shows that Approach II-R improves the *Total SSE* better than Approach I-R. It is also obvious that Approach II-R improves bias, standard error of the estimate (S_e), standard error ratio (S_e/S_y), R^2, and p-value when compared to nationally calibrated models. In addition, Table 8.28 suggests that no significant differences exist between the measured and predicted AC rut depth and base rut depth when Approach II-R calibration factors are used. This finding is due to the fact that the null hypothesis was accepted at 95% confidence level. However, Table 8.28 suggests that significant differences exist between the measured and predicted rut depth values when Approach I-R calibration factors are used, indicated by the rejection of the null hypothesis at 95% confidence level.

With regard to alligator cracking, Table 8.28 indicates that the differences between Approach I-F and Approach II-F statistics are generally smaller compared to the differences found in their rutting statistics. Table 8.28 shows that Approach I-F and Approach II-F both reduce the bias almost equally by about 6% compared to the nationally calibrated models. Table 8.28 suggests that Approach II-F improves the Total SSE, standard error of the estimate (S_e), and the standard error ratio (S_e/S_y) better than Approach I-F. Moreover, Table 8.28 suggests that Approach I-F slightly increases the standard error of the estimate (S_e) when compared to the default. The null hypothesis, i.e., that predicted alligator cracking is equal to measured alligator cracking, is rejected for both approaches at 95% confidence interval.

Table 8.29 breaks down the *Total SSE* values presented under the various calibration and validation sections into simpler and more meaningful parameters that represent the mean error per each distress measurement.

Table 8.29. *Total SSE* Reported as Error per Field Measurement for Total Rut Depth and Alligator Cracking

Distress Type	Calibration	*Total SSE*	Number of measurements/ predictions (N)	Mean error per field measurement	
				Value	Measuring Unit
Total Rut	National	4.110	235	0.0086 inch	inch
	Approach I-R	3.803		0.0083 inch	
	Approach II-R	3.604		0.0081 inch	
Alligator Cracking	National	56412	124	1.92 %	% lane area
	Approach I-F	41764		1.65 %	
	Approach II-F	38752		1.59 %	

Table 8.29 converts *Total SSE* into error values by taking the square root of the *Total SSE* and dividing it by the total number of observed points, i.e., 235 for total rut and 124 for alligator cracking. Table 8.29 suggests that the nationally calibrated rutting models, Approach I-R, and Approach II-R all give very small mean error in total rut depth per rut measurement, i.e. about 0.01 inch. A mean error of about 0.01 inch is considered very low and not even measurable, when compared to the threshold value of 0.1 inch, as reported in Table 7.2. Table 8.29 shows that Approach II-R result in the lowest error per field measurements compared to the nationally calibrated and to Approach I-R results. On the other hand, Table 8.29 shows a mean error in predicting alligator cracking of about 1.6 to 2.0% lane area. Approach II-F is shown to result in the lowest mean error per field measurement of 1.59% compared to 1.65% for Approach I-F and 1.92% for the nationally calibrated models. A value of 1.59% for Approach II-F is relatively close to the alligator cracking threshold value of 1.0%, as reported in Table 7.2.

8.6.9.2 Comparison of Validation Results

Recall that the validation runs are based on NCDOT PMS sections, none of which was considered in the calibration work. Also, recall that major differences exist between the distress survey methods used by the NCDOT and those used by LTPP personnel. Every effort was made in this research work to close the gap between the two different distress survey methods by adjusting the PMS sections according to formulae that were developed and are presented in Section 8.4.2.3 of this chapter.

Figure 8.31 (a) compares the validation statistics for total rut depth as obtained from Approach I-R and Approach II-R. Similarly, Figure 8.31 (b) compares the validation statistics for alligator cracking between Approach I-F and Approach II-F.

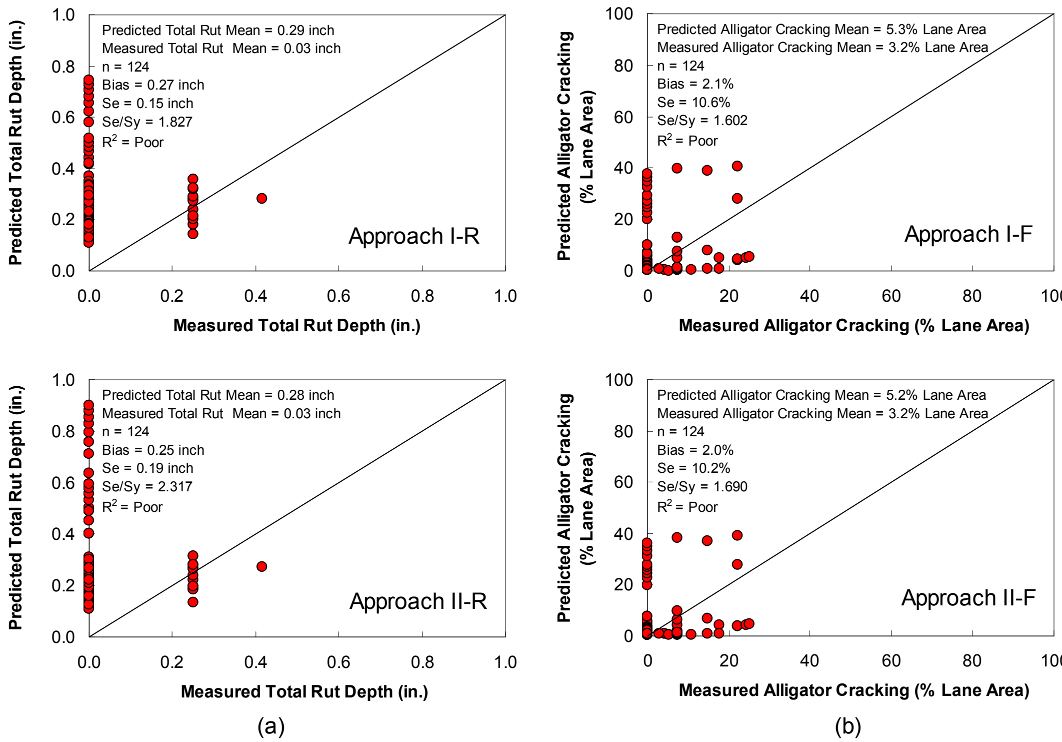

Figure 8.31. Comparison between validation results from Approach I and Approach II: (a) predicted vs. measured total rut depth; and (b) predicted vs. measured alligator cracking.

Table 8.30 is a summary of the mean predicted and measured total rut depth and alligator cracking using calibration and validation sections with local calibration factors from Approach I and Approach II. Table 8.30 also summarizes the mean measured total rut depth and alligator cracking percentages from the LTPP sections.

Because of the inaccurate windshield distress measurements recorded by NCDOT survey personnel for the PMS validation sections, i.e., approximately 0.03 inches of mean total rut depth and 3.2% of lane area mean alligator cracking, it is reasonable to expect poor validation statistics between the measured and predicted distresses, regardless of whether Approach I or Approach II calibration factors are used.

With respect to total rut depth, Table 8.30 and Figure 8.31 (a) show that Approach I-R and Approach II-R both overpredict the measured total rut depth for the PMS validation sections. Some data points in Figure 8.31 (a) suggest that Approach II-R predicts much higher total rut depth; however, these data points represent only a few incidents at one section. This latter observation is supported by the fact that the mean total rut depth obtained from Approach II-R (0.28 inch) is smaller than that from Approach I-R (0.29 inch), as shown in Table 8.30.

Table 8.30. Comparison between Mean Predicted Total Rut and Alligator Cracking from Approach I and Approach II for Validation and Calibration Sections

Approach	Analysis	Mean Total Rut Depth (inch)		Mean Alligator Cracking (% Lane Area)	
		Predicted	Measured	Predicted	Measured
Approach I	Calibration (LTPP Sections)	0.164	0.205	6.654	11.490
	Validation (PMS Sections)	0.292	0.028	5.293	3.230
Approach II	Calibration (LTPP Sections)	0.184	0.205	6.246	11.490
	Validation (PMS Sections)	0.276	0.028	5.202	3.230

For alligator cracking, the mean predicted value was again slightly better from Approach II-F than from Approach I-F. Approach II-F predictions show approximately 5.2% mean predicted alligator cracking compared to the mean measured value of 3.2% for the PMS validation sections. However, Approach I-F predicts a mean of 5.3% alligator cracking for the PMS sections. This similarity is expected because the alligator cracking calibration factors are not very different between the two approaches, as shown in Table 8.26.

Figure 8.31 (b) shows the similarity between the Approach I-F and Approach II-F predictions compared to the measured alligator cracking. Moreover, Table 8.30 is a good indicator of the inaccuracy of the NCDOT windshield distress survey method, especially when the LTPP accurate distress data are compared to NCDOT windshield survey data. This finding applies to rut depth and alligator cracking distress surveys.

Table 8.31 compares the total rut and alligator cracking calibration and validation statistics using Approach I and Approach II. Table 8.31 suggests that Approach II-R performs slightly better in reducing the bias in the validation section compared to Approach I-R but performs slightly worse in terms of reducing the standard error. Furthermore, bias predicted for the validation sections is still much higher than that predicted for the calibration sections, as shown in Table 8.31. Again, it is believed that the differences are due to the inaccurate distress measurements taken at the PMS sites. Table 8.31 also shows that the null hypothesis was rejected for total rut depth for both calibration approaches at 95% confidence level. This finding indicates that the differences between the predicted and measured total rut depth values at the validation sites are significant.

With respect to alligator cracking, Table 8.31 indicates that Approach I-F and Approach II-F reduce the bias and standard error for the validation sites, even when compared to the calibration statistics. Despite the improvement, neither approach led to the acceptance of the null hypothesis that no significant differences exist between the predicted and measured alligator cracking for the validation sections at 95% confidence level. When compared to

Approach I-F, Table 8.31 clearly shows that Approach II-F results in smaller bias, smaller standard error of the estimate (S_e), smaller standard error ratio (S_e/S_y), and larger p-values.

Table 8.31. Comparison between Total Rut and Alligator Cracking Calibration and Validation Statistics from Approach I and Approach II

Distress Type	Approach	Analysis	Bias	S_e	S_e/S_y	R^2	Hypothesis; *Ho: ∑(Meas.-Pred.) = 0*
Total Rut	Approach I-R	Calibration	-0.041	0.121	0.961	Poor	Reject; p = 0.000
		Validation	0.265	0.150	1.827	Poor	Reject; p = 0.000
	Approach II-R	Calibration	-0.021	0.122	0.975	0.15	Reject; p = 0.008
		Validation	0.248	0.190	2.317	Poor	Reject; p = 0.000
Alligator Cracking	Approach I-F	Calibration	-4.836	19.852	1.041	Poor	Reject; p = 0.008
		Validation	2.064	10.602	1.750	Poor	Reject; p = 0.032
	Approach II-F	Calibration	-5.153	17.111	0.949	Poor	Reject; p = 0.001
		Validation	1.973	10.239	1.690	Poor	Reject; p = 0.034

8.6.9.3 Rutting Local Calibration Factors Reasonableness Check

This section discusses the reasonableness of the HMA and unbound materials local calibration factors developed from Approach I-R and Approach II-R. This check could aid in the selection of the final rutting local calibration factors developed from either approach. In order for the final selection to make sense, this reasonableness check takes into account the location of the local calibration factors in the distress prediction models. Therefore, the comparisons are made for the calibration *terms* as they fit in the prediction models.

For the HMA rutting model, the three calibration terms are $\beta_{r1}.10^{kr1}$, $\beta_{r2}.\ k_{r2}$, and $\beta_{r3}.k_{r3}$. Note that β_{r1} in the first term is a multiplier, whereas the $\beta_{r2}.k_{r2}$ and $\beta_{r3}.k_{r3}$ terms are exponents. Also note that the reasonableness check is performed against the local calibration terms while considering the predicted versus measured performance relationships using the default terms. At this time, reasonableness checks cannot be checked against calibration efforts found in the literature, mainly because the calibration and validation work performed under this research considers the material-specific HMA layer *k* values that were developed as part of this research work. All the work found in the literature adopts the default *k* values. Hence, comparisons do not reflect local materials and are not appropriate.

An important reminder about rutting calibration is that forensic studies were not conducted to determine the derivation of the total rut depth at the pavement surface. Hence, the real contribution of different layers to total rut depth remains unknown.

Table 8.32 is a summary of the HMA rutting calibration terms calculated from calibration factors that were developed from Approach I-R and Approach II-R. The $\beta_{r1}.10^{kr1}$ term can be considered to be a scaling multiplier that increases or decreases the predicted HMA rut depth values but does not change the progression trend of HMA rut accumulation with time.

Table 8.32 shows that the $\beta_{r1}.10^{kr1}$ terms, as calculated from Approach I-R and Approach II-R, are larger in value than the default values. The opposite is true for $\beta_{r2}.k_{r2}$ and $\beta_{r3}.k_{r3}$ in which these two terms are lower than the default for both approaches. Lower $\beta_{r2}.k_{r2}$ values indicate that local HMA mixtures are less sensitive to temperature in general compared to national averages. Similarly, a low $\beta_{r3}.k_{r3}$ indicates that rutting accumulation in the HMA mixtures is less affected by traffic volume when compared to national averages. When the 12 mixtures are compared for Approach I-R and Approach II-R, Table 8.32 indicates that mixtures under Approach II-R have more reasonable calibration terms than the national defaults. This finding is obvious for the $\beta_{r2}.k_{r2}$ term whose values are much smaller for Approach I-R than for Approach II-R when compared to the national defaults.

Table 8.32. Reasonableness Check of HMA Rutting Local Calibration Factors Developed from Approach I and Approach II

Default / Mix ID	Approach I-R			Approach II-R		
	$\beta_{r1}.10^{kr1}$	$\beta_{r2}.k_{r2}$	$\beta_{r3}.k_{r3}$	$\beta_{r1}.10^{kr1}$	$\beta_{r2}.k_{r2}$	$\beta_{r3}.k_{r3}$
Default	4.4E-04	1.561	0.479	4.4E-04	1.561	0.479
S9.5B	7.4E-01	0.302	0.332	5.4E-02	0.651	0.321
RS9.5B	9.5E-01	0.274	0.238	6.9E-02	0.590	0.230
S9.5C	3.4E+00	0.132	0.309	2.5E-01	0.285	0.299
RS9.5C	4.9E-01	0.319	0.259	3.6E-02	0.687	0.250
S12.5C	9.6E+00	0.064	0.299	6.9E-01	0.139	0.289
RS12.5C	1.7E+00	0.156	0.343	1.2E-01	0.337	0.331
I19B	1.7E+01	0.071	0.293	1.2E+00	0.154	0.283
RI19B	8.9E+00	0.053	0.311	6.4E-01	0.115	0.301
I19C	9.9E-01	0.291	0.228	7.2E-02	0.628	0.220
RI19C	3.8E-02	0.531	0.295	2.7E-03	1.144	0.285
B25B	5.9E-01	0.294	0.333	4.3E-02	0.634	0.322
RB25B	4.0E-01	0.285	0.375	2.9E-02	0.614	0.363

Table 8.33 compares the unbound materials calibration terms from Approach I-R and Approach II-R to the default values. Table 8.33 shows that Approach I-R underestimates the rut accumulation in the unbound base layer when compared to the national average. A similar observation is made to a less extent for Approach II-R. As for the subgrade rut depth, Table 8.33 suggests that Approach I-R and Approach II-R both overestimate the rut depth in the subgrade unbound layer when compared to the default values. Approach II-R seems to overestimate the subgrade rut depth more than Approach I-R when compared to the default

values. Note that without knowledge of the contribution of the unbound layers to the total rut depth at the surface of the pavement, it is difficult to calibrate the unbound rutting models properly. In addition, it is recommended that representative local unbound materials be characterized in the lab for performance before further calibration work is performed on rut depth prediction models for unbound materials.

Table 8.33. Reasonableness Check of Unbound Materials Rutting Local Calibration Factors Developed from Approach I and Approach II

Unbound Layer Parameters	$\beta_{gb}.k_{gb}$	$\beta_{sg}.k_{sg}$
Default	2.03	1.67
Approach I-R	0.62	1.84
Approach II-R	1.09	2.51

8.6.9.4 Alligator Cracking Local Calibration Factors Reasonableness Check

This section discusses the reasonableness of the alligator cracking local calibration factors developed from Approach I-F and Approach II-F. The purpose of this reasonableness check is to help identify the most appropriate alligator cracking factors to use, that is, those developed from Approach I-F or those developed from Approach II-F. Similar to the rutting factors reasonableness check, the check for alligator cracking local calibration factors takes into account the location of these factors in the distress prediction models. Therefore, the comparisons are made for the calibration *terms* as they fit in the prediction models. For the alligator cracking number of cycles to failure (N_f) model, β_{f1}, β_{f2}, and β_{f3} are multiplied by the material-specific fatigue *k* values, i.e., k_{f1}, k_{f2}, and k_{f3}, respectively, to form the three terms of interest. Note that for the N_f model, the $\beta_{f1}.k_{f1}$ term is a multiplier, whereas the $\beta_{f2}.k_{f2}$ and $\beta_{f3}.k_{f3}$ terms are exponents. Again, the reasonableness check for alligator cracking calibration factors is compared against default values because the material-specific fatigue *k* values were used in the calibration and validation runs.

Table 8.34 summarizes the alligator cracking calibration terms, including the material-specific fatigue *k* values and beta values developed from Approach I-F and Approach II-F. The default values in Table 8.34 reflect the national default fatigue *k* values (one set for all HMA mixtures) and beta values that are equal to one. Out of the 12 most commonly used asphalt concrete mixtures in North Carolina, Table 8.34 includes only the intermediate and base HMA mixtures, each of which could potentially be the bottom layer in a pavement structure. Recall that alligator cracking is bottom-up cracking in which the crack initiates at the bottom of the pavement structure and proceeds upward; hence, only the bottom HMA layer properties are of major interest when predicting alligator cracking.

Table 8.34 indicates that the differences in the alligator cracking calibration terms are not large between Approach I-F and Approach II-F. However, both approaches result in much smaller values for the $\beta_{f1}.k_{f1}$ term compared to the default values and larger $\beta_{f2}.k_{f2}$ and $\beta_{f3}.k_{f3}$

terms compared to the default values. A smaller $\beta_{f1}.k_{f1}$ term reduces the number of fatigue cycles to failure (N_f), which means the predicted alligator cracking value will be larger. A large predicted alligator cracking value is required to counterbalance the underprediction of alligator cracking by the default model. Therefore, both approaches present reasonable $\beta_{f1}.k_{f1}$ term values that at least appear to be in the right direction.

Table 8.34. Reasonableness Check of Alligator Cracking Local Calibration Factors Developed from Approach I and Approach II

Possible Bottom Layer Type	Approach I-F			Approach II-F		
	$\beta_{f1}.k_{f1}$	$\beta_{f2}.k_{f2}$	$\beta_{f3}.k_{f3}$	$\beta_{f1}.k_{f1}$	$\beta_{f2}.k_{f2}$	$\beta_{f3}.k_{f3}$
Default	7.57E-03	3.949	1.281	7.57E-03	3.949	1.281
I19B	6.57E-10	6.472	1.908	5.93E-10	5.854	1.431
RI19B	4.77E-15	5.913	0.953	4.30E-15	5.349	0.714
I19C	7.19E-07	5.820	1.899	6.49E-07	5.265	1.424
RI19C	1.80E-09	6.087	1.701	1.62E-09	5.506	1.276
B25B	4.29E-10	6.005	1.561	3.87E-10	5.432	1.171
RB25B	1.42E-18	6.210	0.767	1.28E-18	5.617	0.575

Table 8.34 also shows that Approach I-F and Approach II-F both seem to have reasonable values for the $\beta_{f2}.k_{f2}$ and $\beta_{f3}.k_{f3}$ terms when compared to the default values. Also, note that the transfer function coefficients, C_1 and C_2, play a significant role in the amount of predicted alligator cracking. These factors are similar for Approach I-F and Approach II-F.

8.6.9.5 Final Rutting and Alligator Cracking Local Calibration Factors

Based on the calibration, validation, and reasonableness discussions, the research team decided to select the rutting model final calibration factors obtained from Approach II-R. Rutting calibration factors obtained from Approach II-R proved to improve all the statistics when compared to Approach I-R and to the nationally calibrated models, as shown in Table 8.28.

In addition, Table 8.32 suggests that the calibration factors obtained from Approach II-R are more reasonable than the default terms. The final decision to select the right set of rutting model calibration factors was simple, because the rutting model calibration factors obtained from Approach I-R seem to introduce more bias even though they reduce the standard error of the estimate (S_e) and the standard error ratio (S_e/S_y). The final rutting model local calibration factors that are recommended for implementing into the MEPDG are summarized in Table 8.35.

Table 8.35. Final Recommended Local Calibration Factors for the Rutting Prediction Models

Parameter	Recommended Value
β_{r1}	0.94750
β_{r2}	0.86217
β_{r3}	1.35392
β_{gb}	0.53767
β_{sg}	1.50000

With respect to alligator cracking, the differences in performance predictions between the factors from Approach I-F versus those from Approach II-F are not large. Calibration factors obtained from both approaches improve the predicted alligator cracking and bring their values closer to those obtained from field measurements. Calibration factors from both approaches reduced bias by almost 6% when compared to the nationally calibrated models. However, Approach II-F produces slightly smaller values for the standard error of the estimate (S_e) and the standard error ratio (S_e/S_y)m as shown in Table 8.28. Moreover, Table 8.28 shows that calibration factors obtained from Approach II-F reduce the *Total SSE* to a lower value compared to the calibration factors obtained from Approach I-F. In addition, when validation work is compared using factors from both approaches, Table 8.31 shows that Approach II-F results in smaller bias, smaller standard error of the estimate (S_e), smaller standard error ratio (S_e/S_y), and larger p-values for validation sections compared to Approach I-F. Based on the presented information, the research team decided to select the final alligator cracking local calibration factors that are based on Approach II-F. These factors are summarized in Table 8.36.

Table 8.36. Final Recommended Local Calibration Factors for the Alligator Cracking Prediction Models

Parameter	Recommended Value
β_{f1}	3.50000
β_{f2}	0.72364
β_{f3}	0.60000
C_1	0.24377
C_2	0.24377

CHAPTER 9 CONCLUSIONS AND RECOMMENDATIONS

This chapter summarizes the conclusions of this research work and presents recommendations by the research team for future projects and improvements that are necessary for the successful implementation of the MEPDG.

9.1 Conclusions

The following conclusions are drawn from this study:

- When the MEPDG national default rutting calibration values are used, the total rut depth predictions and HMA rut depth predictions are found to be significantly different from the measured total rut depth and the estimated measurements of HMA rut depth for the LTPP calibration sections at 95% confidence level. The MEPDG default calibration factors are found to underpredict the total rut depth and HMA rut depth. On the other hand, predicted unbound base and subgrade rut depth values are found to be insignificantly different from the estimated measurements at 95% confidence level when national model coefficients are used.
- When the MEPDG national default calibration values are used in the alligator cracking N_f model and transfer function, the predicted alligator cracking value is significantly different from the measured alligator cracking value (about 0.5% lane area predicted versus about 11.5% lane area measured) at the 95% confidence level. National default calibration factors significantly underestimate the mean measured alligator cracking in the LTPP sections.
- Despite the accuracy of the LTPP distress survey techniques, the measured total rut depth was found to vary irrationally for some LTPP sites. It is reasonable to expect that the total rut depth will only increase with time, provided that no maintenance or rehabilitation work is performed. Some total rut depth measurements were found to decrease with time and then increase again without any maintenance work.
- Realizing the significant differences between the distress survey methods followed by LTPP and the NCDOT personnel, the decision was made in this research work to use only LTPP sections for calibration and use PMS sections for validation. The research team realized early that the PMS validation sections may not be the best representation for checking the improvements expected from the calibration effort; however, the decision was made in an effort to obtain adequate local calibration factors for future implementation.
- The current distress survey techniques followed by the NCDOT are windshield-based and yield subjective ratings for the total rut depth and alligator cracking distresses. Every effort was made to convert subjective rut depth and alligator cracking ratings to equivalent LTPP ratings. The conversion model developed by Corley-Lay et al. (2010) to convert the NCDOT subjective ratings of alligator cracking to equivalent LTPP alligator cracking values seems to improve, i.e., increase, the alligator cracking measurements for the PMS sections.
- For the subgrade soil characterization, a GIS-based methodology was developed for NCDOT engineers to accurately superimpose road sections of interest on the

NCHRP 9-23A soil maps and find the corresponding alphanumeric soil unit code required to extract related soil information. The proposed methodology uses ESRI's ArcGIS® 9.2 software (ESRI, 2010) and soil shape files downloaded from the website of the Natural Resources Conservation Service (NRCS) of the United States Department of Agriculture.

- Material-specific HMA rutting and fatigue cracking model coefficients were successfully developed for the twelve most commonly used HMA mixtures in North Carolina using data obtained from the triaxial repeated load permanent deformation test (TRLPD) and the direct tension cyclic test, respectively. A total of twelve sets of *k* values were developed, one for each HMA mixture type.
- A damage-based approach was developed and successfully used to aid in characterizing local traffic data for use in the MEPDG. The developed approach considers the effect of different traffic input parameters on pavement performance. Heavy tandem axles were found to cause the largest fatigue damage compared to a similar axle weights from other axle types.
- Two approaches were evaluated for re-calibrating the rutting and alligator cracking models for local conditions and materials. Approach I uses the generalized reduced gradient (GRG) method, whereas Approach II uses the genetic algorithm (GA) optimization technique. Approach II was found to result in statistically better total rut depth and alligator cracking predictions.
- The local calibration of the MEPDG rutting models, using HMA material-specific *k* values, can significantly reduce bias and standard error between the predicted and measured rut depth values for all layer types, except for the subgrade. The mean total rut depth after calibration is about 0.18 inch compared to the measured mean total rut depth of 0.20 inch. However, the improvements in predicted versus measured statistics are not enough to accept the null hypothesis that the predicted and measured total rut depth values are equal at 95% confidence level.
- The local calibration of the MEPDG using HMA material-specific *k* values can reduce alligator cracking bias from about -11.0% lane area to about -5.2% lane area and also improves the mean predicted alligator cracking percentage from about 0.5% to about 6.3% lane area, which is much closer to the mean measured alligator cracking of 11.5% lane area. However, this improvement is not enough to accept the null hypothesis that the measured alligator cracking percentage is equal to the predicted alligator cracking percentage at the 95% confidence level.
- When local calibration factors are used in the MEPDG to predict alligator cracking in the PMS validation sections, the results suggest that both bias and standard error decrease. In this work, bias decreased from about -5.2% lane area to about 2.0% lane area, and the standard error decreased from 17.1% lane area to 10.2% lane area. However, the differences between the predicted and measured alligator cracking values are still significant at the 95% confidence level. One reason for this significant difference is that the mean measured alligator cracking in the PMS sections was lower than expected (only 3.23% lane area). This lower-than-expected outcome is supported by the fact that the mean measured alligator cracking is about 11.5% of the lane area for the LTPP sections, as determined in the calibration effort. For PMS sections, the predicted alligator cracking, after calibration, is 5.2% compared to the measured value of 3.2% lane area.

- The validation check for rutting reveals that the MEPDG, using local calibration factors, overpredicts the total rut depth for PMS sections, i.e., 0.28 inch mean predicted versus 0.03 inch mean measured, causing a significant difference between the measured and predicted rut depth values at the 95% confidence level. The research team believes that the major factor for such difference is that the mean measured total rut depth value of 0.03 inch, as determined from the windshield survey, is unrealistic. Other factors include errors in converting the total rut depth subjective ratings of light, medium, and severe into a numerical value of total rut depth. Another factor that could have contributed to the difference is the errors in matching field HMA mixture types to the twelve most commonly used mixtures in North Carolina as explained in the next point.
- In the calibration and validation work, it is assumed that the matching process (based on NMAS, binder grade, and RAP content) is accurate between the field asphalt concrete mixtures and the 12 mixtures that were characterized as part of this research work. The research team appreciates the fact that this assumption is not necessarily accurate, especially when Marshall-based mixtures are matched. However, the assumption stems from the decision that the calibration process should be oriented towards future projects and not towards trying to capture older mixtures and construction practices. Note that the local calibration factors developed under this project include the effects of making this assumption.

9.2 Recommendations

The following recommendations are made based on the outcomes of this research work:

- Acknowledging that only granite aggregates were used in all 12 asphalt concrete mixtures that are characterized in this research work, the research team recommends that HMA mixtures with limestone aggregate should be characterized to reflect asphalt mixtures produced in the coastal region of North Carolina, where limestone aggregate is prevalent. Aggregate characteristics, including strength, surface texture, and shape have a large effect on HMA performance.
- The twelve HMA mixtures performance database developed in this research uses one mixture per mix type e.g., one S9.5B mixture opposed to two or three S9.5B mixtures that use different aggregate sources and different binder source or grade. As a result, the local calibration factors are based on the performance of these mixtures. A wider range of mixtures needs to be tested and included in the database to balance the database, e.g., low gyration mixtures for permanent deformation evaluation. It is vital that the rutting and alligator cracking model coefficients, i.e. k values, be of good representations to the different HMA mixture designations.
- It is critical to understand that the LTPP sections utilized in the local calibration effort do not cover the use of all 12 asphalt mixtures that are characterized in this research work, as a result of the matching process. Therefore, more calibration sections that use more of the 12 mixtures should be included in the future, if possible, to fine-tune the calibration coefficients.

- Because only a few of the LTPP calibration sections include reclaimed asphalt pavement (RAP), and because the use of RAP is increasing, it is recommended that more sections with RAP be included in future refinements of the local calibration factors.
- Reliable distress data are crucial for successful calibration. Realizing that it is not easy for the NCDOT to survey its large network of roads, which extends over 65,000 miles, using detailed procedures such as those followed by the LTPP program, the NCDOT should nonetheless follow the LTPP Distress Identification Manual (FHWA, 2003) to complete distress surveys, at least for the sections selected for future calibration purposes. Use of this manual will ensure consistency in the MEPDG predictions.
- For each new project, whenever possible, subgrade soils should be sampled at the project location and tested in the lab for resilient modulus, index properties, and soil water characteristic curve (SWCC) parameters. The NCHRP 9-23A soils data can be used to populate the subgrade soils data in situations where detailed coring and test results are unavailable, such as for low volume roadways, relatively short bridge projects, and projects where widening is relatively narrow. The NCHRP 9-23A soils data also can be used for preliminary designs.
- It is recommended that the most commonly used unbound base and sub-base materials be characterized in the lab. Populating the MEPDG with accurate subgrade, base, and sub-base information enhances the probability of better predictions.
- It is recommended to begin a field and forensic (trenches and cores) investigation to check for the reasonableness of the MEPDG assumptions in assigning the observed surface permanent deformations to each pavement layer and also to differentiate between bottom-up alligator cracks and top-down longitudinal cracks.
- For future fine-tuning or recalibration efforts, it is recommended that the NCDOT PMU start building a database for each of the projects that they construct from now on. The database should contain the information required by the MEPDG for asphalt layers, asphalt binders, unbound and bound base layers, subgrade soils, and some as-built volumetrics for asphalt layers, including *in situ* air voids immediately after construction, measured effective binder content by volume, and total unit weight.
- Realizing that LTPP data are not perfect, agencies are encouraged to look in depth for any anomalies and modify/correct them as necessary using the approach described in this report or any other proper approach.

REFERENCES

AASHTO T 321 (2008). "Standard Method of Test for Determining the Fatigue Life of Compacted Hot-Mix Asphalt (HMA) Subjected to Repeated Flexural Bending." American Association of State Highway and Transportation Officials, Washington, DC.

AASHTO TP 62 (2004). "Standard Method of Test for Determining Dynamic Modulus of Hot-Mix Asphalt Concrete Mixtures." American Association of State Highway and Transportation Officials, Washington, DC.

AASHTO-a (1990). "Standard Methods of Sampling Aggregates." American Association of State Highway and Transportation Officials, Washington, DC.

AAT (2004). "Asphalt Concrete Mixture Performance Testing and Analysis: Western Research Institute Test Sections, Interstate 15, Clark County, Nevada." Advanced Asphalt Technologies, LLC. Sterling, VA.

ARA, Inc. ERES Consultants Division (2004). "Background, Scope and Overview in Design Guide: Part 1/Chapter 1." National Cooperative Highway Research Program, NCHRP 1-37A, Transportation Research Board, Washington, DC.

ARA, Inc. ERES Consultants Division (2004). "Design Inputs/Environmental Effects in Design Guide: Part 2/Chapter 3." National Cooperative Highway Research Program, NCHRP 1-37A, Transportation Research Board, Washington, DC.

Asphalt Institute (1991). "Thickness Design, Asphalt Pavement for highways and streets." Manual Series No. 1 (MS-1) Lexington, Kentucky.

ASTM D 6307-98 (1998). "Standard Test Method for Asphalt Content of Hot Mix Asphalt by Ignition Method." American Society for Testing and Materials, West Conshohocken, PA.

ASTM C-136-06 (2006). "Standard Test Method for sieve Analysis of Fine and Coarse Aggregates.". American Society for Testing and Materials, West Conshohocken, PA.

Barbour, S. L. (1998). "The Soil–Water Characteristic Curve: a Historical Perspective." 19^{th} Canadian Geotechnical Colloquium, Canadian Geotechnical Journal 35 (5), pp 873–894.

Beyer, H. Hawth's Analysis Tools for ArcGIS. http://www.spatialecology.com/htools/download.php. Accessed June 24, 2010.

Chehab, G., Y. R. Kim, R. A. Schapery, M. Witczack, R. Bonaquist (2002). “Time-Temperature Superposition Principle for Asphalt Concrete Mixtures with Growing Damage in Tension State.” Journal of Association of Asphalt Paving Technologists, Vol. 71, pp: 559-593.

Chehab, G., Y.R. Kim, R.A. Schapery, M. Witczack, R. Bonaquist (2003). “Characterization of Asphalt Concrete in Uniaxial Tension Using a Viscoelastoplastic Model.” Journal of Association of Asphalt Paving Technologists, Vol. 72, pp: 315-355.

Christensen, D.W. and R. Bonaquist (2005). “Practical Application of Continuum Damage Theory to Fatigue Phenomena in Asphalt Concrete Mixtures.” Journal of the Association of Asphalt Paving Technologists, Vol. 74, pp: 963-1002.

Corely-Lay J., Jadoun F. M., Mastin J. N., and Kim Y. R. (2010). “Comparison of Flexible Pavement Distresses Monitored by North Carolina Department of Transportation and Long-Term Pavement Performance Program.” Transportation Research Record, No. 2153, pp: 91-96. National Research Council, Transportation Research Board, Washington, DC.

Daniel, J.S. and Y. R. Kim (2002). “Development of a Simplified Fatigue Test and Analysis Procedure Using a Viscoelastic Continuum Damage Model.” Journal of Association of Asphalt Paving Technologists, Vol. 71, pp: 619-650.

ESRI® Geographic Information System Software. ArcGIS Desktop Help 9.2. Georeferencing a Raster Dataset. http://webhelp.esri.com/arcgisdesktop/9.2/index.cfm?TopicName=Georeferencing_a_raster_dataset. Accessed June 23, 2010.

Federal Highway Administration (FHWA) (2003). “Distress Identification Manual for Long Term Pavement Performance Program.” (Fourth Revised Edition), Publication No. FHWA-RD-03-031, Washington, DC.

Fredlund,, D. G. and A. Xing. (1994). “Equations for the Soil-Water Characteristic Curve.” Canadian Geotechnical Journal 31 (4), pp 521-532.

Gibson Nelson, M. Emin Kutay, Dan Keramat, and Jack Youtcheff (2009). “Multiaxial Strain Response of Asphalt Concrete Measured During Flow Number Performance Test”. Journal of the Association of Asphalt Paving Technologists. In press.

Gibson Nelson, and C.W. Schwartz (2006). “Three-dimensional Viscoplastic Characterization of Asphalt Concrete Utilizing Perzyna and HiSS Methodologies”. Proceedings of the 10th International Conference on Asphalt Pavement, Quebec City, Canada, Vol. I, pp. 205-214

Hanson D.I., King G., Buncher M., Duval J., Blankenship P., Anderson M. (2009). “Techniques for Prevention and Remediation of Non-Load Related Distresses on HMA Airport Pavements (Phase I). Airport Asphalt Pavement Technology Program (AAPTP) Project 05-07. Federal Aviation Administration (FAA). Washington D.C.

Kaloush K.E. (2001). “Simple Performance Test for Permanent Deformation of Asphalt Mixtures”. Ph.D. Dissertation. Arizona State University, Arizona.

Kim, Y. R. (2006). “Local Calibration of the MEPDG for Flexible Pavement Design.” A research proposal submitted to North Carolina Department of Transportation, Raleigh, NC.

Kim, Y. R., and D. N. Little (1990). “One-Dimensional Constitutive Modeling of Asphalt Concrete." ASCE Journal of Engineering Mechanics, Vol. 116, No. 4, pp. 751-772.
Lee, H. J. and Kim Y. R. (1998a). “A Uniaxial Viscoelastic Constitutive Model for Asphalt Concrete under Cyclic Loading.” ASCE Journal of Engineering Mechanics, Vol. 124, No. 1, pp: 32-40.

Kutay, M.E., N. Gibson, and J. Youtcheff (2008). “Conventional and Viscoelastic Continuum Damage (VECD) Based Fatigue Analysis of Polymer Modified Asphalt Pavements.” Journal of Association of Asphalt Paving Technologists, Vol. 77. In Press.

Lee, H.J. and Kim Y.R.(1998a). “A Uniaxial Viscoelastic Constitutive Model for Asphalt Concrete under Cyclic Loading.” ASCE Journal of Engineering Mechanics, Vol. 124, No. 1, pp: 32-40.

Lee, H. J. and Y. R. Kim Y. R. (1998b). “A Viscoelastic Continuum Damage Model of Asphalt Concrete with Healing.” ASCE Journal of Engineering Mechanics, Vol. 124, No. 11, pp: 1224-1232.

LTPP (2010). "Standard Data Release V.24.0". Federal Highway Administration (FHWA), Long Term Pavement Performance customer support center, Mclean, VA.

Monismith, C. L., Epps, J. A., and Finn, F. N. (1985). "Improved asphalt mix design." Journal of Association of Asphalt Paving Technologists, Vol. 54, pp: 347–391.

Muthadi (2007). "Local Calibration of the MEPDG for Flexible Pavement Design". Masters Thesis, North Carolina State University, Raleigh, North Carolina.

Muthadi, N. R. and Kim Y. R. (2008). "Local Calibration of the MEPDG for Flexible Pavement Design." Transportation Research Record, Vol. 2087, pp: 131-141, National Research Council, Transportation Research Board, Washington, DC.

NCDOT (2006). "Pavement Condition Survey Manual.". Pavement Management Unit (PMU), North Carolina Department of Transportation, Raleigh, North Carolina.

NCDOT (2008). "2008 HMA/QMS Manual". Section 7.4.4, North Carolina Department of Transportation, Raleigh, NC. http://www.ncdot.org/doh/Operations/dp_chief_eng/constructionunit/paveconst/Asphalt_Mgmt/qms_manual/2008/default.html

NCHRP (2002). "Simple Performance Test for Superpave Mix Design". NCHRP 9-19, Report No. 465. National Cooperative Highway Research Program, Washington, DC.

NCHRP (2003). "Simple Performance Tester for Superpave Mix Design: First-Article Development and Evaluation". NCHRP 9-29, Report No. 513. National Cooperative Highway Research Program, Washington, DC.

NCHRP (2004a). "Guide for Mechanistic Empirical Design of New and Rehabilitated Pavement Structures". NCHRP 1-37A, Final Report, Part 1, Introduction. National Cooperative Highway Research Program, Washington, DC.

NCHRP (2004b). "Guide for Mechanistic Empirical Design of New and Rehabilitated Pavement Structures". NCHRP 1-37A, Final Report, Part 3. National Cooperative Highway Research Program. Washington, DC.

NCHRP (2005). "Use of the M-E Pavement Design Guide. Demonstration to Optimize or Maximize Structural and Mixture Design." Draft document submitted by Applied Research Associate, Inc. as part of NCHRP 1-40B project to the National Cooperative Highway Research Program, Washington, DC.

NCHRP (2007a). Mechanistic-Empirical Pavement Design Guide Software, Version 1.0. National Cooperative Highway Research Program, Washington, DC.

NCHRP (2007b). "Calibration of Rutting Models for HMA Structural and Mix Design." NCHRP 9-30A, second quarterly progress report. National Cooperative Highway Research Program, Washington, DC.

NCHRP (2009). "Local Calibration Guidance for the Recommended Guide for Mechanistic-Empirical Design of New and Rehabilitated Pavement Structures." NCHRP 1-40B, Final Report, National Cooperative Highway Research Program, Washington, DC.

Prowel and Brown (2007). "Superpave Mix Design. Verifying Gyration Level in the Ndesign Table". NCHRP Report No. 573, National Cooperative Highway Research Program, Washington, DC.

Ramachandran, A., Taylor, K. L, Stone, J. R, and Sajjadi. S. (2011). "NCDOT Quality Control Methods for Weigh in Motion Data." Public Works Management and Policy, Volume 16, Issue 1, 2011, pp 3-19. National Research Council, Transportation Research Board, Washington, DC.

Reese, R. (1997). "Properties of aged asphalt binder related to Asphalt Concrete Fatigue Life." Journal of the Association of Asphalt Paving Technologists, Vol. 66, pp. 604-632.

Reese, R. (1997). "Properties of Aged Asphalt Binder Related to Asphalt Concrete Fatigue Life." Journal of the Association of Asphalt Paving Technologists, Vol. 66, pp: 604-632.

Sayyady, F., Stone ,J. R., Taylor, K. L.., Jadoun ,F. M. and Kim, Y. R (2009). "Clustering Analysis to Characterize Mechanistic-Empirical Pavement Design Guide Traffic Data in North Carolina." Transportation Research Record, No. 2160, pp: 118-127. National Research Council, Transportation Research Board, Washington, DC.

Sayyady, F., Stone ,J. R., Jadoun, F. M. and Kim, Y. R (2010). "Multi-dimensional Clustering to Characterize Axle Load Distribution for MEPDG in North Carolina.". In press, Journal of Transportation Research Board, National Research Council, Washington, DC.

Schapery, R.A.(1981). "On Viscoelastic Deformation and Failure Behavior of Composite Materials with Distributed Flaws." Advances in Aerospace Structures and Materials, AD-01, ASME, New York, pp. 5-20.

Schapery, R.A. (1984). "Correspondence principles and a Generalized J-integral for Large Deformation and Fracture Analysis of Viscoelastic Media." Int. J. Fract., Vol. 25, pp: 195-223.

Schapery, R.A. (1990). "A Theory of Mechanical Behavior of Elastic Media with Growing Damage and Other Changes in Structure" J. Mech. Phys. Solids, Vol. 38, pp: 215-253.

Solaimanian, M., Bonaquist, R. F., and Tandon, V. (2007). "Improved Conditioning and Testing Procedures for HMA Moisture Susceptibility." NCHRP Report 589, Transportation Research Board, Washington, DC.

Sousa J. B., Craus J., and Monismith C. L. (1991). "Summary Report on Permanent Deformation in Asphalt Concrete". Strategic Highway Research Program (SHRP) Report No. SHRP-A/IR-91-104. National Research Council. Washington, D.C.

Stone, J. R., Kim, Y. R., List, G. F., Rasdorf, W., Sayyady, F., Jadoun, F. M., and Ramachandran, A. N.. (2010). "Development of Traffic Data Input Resources for the Mechanistic Empirical-Pavement Design Process." Final Report for Project No. HWY-2008-11, under review by the North Carolina Department of Transportation, Raleigh, NC.

Strategic Highway Research Program (SHRP) (1994). "Fatigue response of asphalt-aggregate mixes." SHRP-A-404, National Research Council, Washington, D.C.

Tayebali, A. T., J. A. Deacon, and C. L. Monismith (1995). "Development and Evaluation of Surrogate Fatigue Models for SHRP A-003A Abridged Mix Design Procedure," Journal of the Association of Asphalt Paving Technologists, Vol. 64, pp: 340-364.

Underwood, B. S., Y. R. Kim, and M. N. Guddati (2006). “Characterization and Performance Prediction of ALF Mixtures Using a Viscoelastoplastic Continuum Damage Model.” Journal of Association of Asphalt Paving Technologists, Vol. 75, pp: 577-636.

Underwood, B.S., Y.R. Kim, and M.N. Guddati. (2009). “Improved Calculation Method of Damage Parameter in Viscoelastic Continuum Damage Model,” International Journal of Pavement Engineering. Under Review.

Underwood B.S., Kim Y. R., Savadatti S., Thirunavukkarasu , and Guddati M. N (2009). “Response and Fatigue Performance Modeling of ALF Pavements Using 3-D Finite Element Analysis and a Simplified Viscoelastic Continuum Damage Model.” Journal of the Association of Asphalt Paving Technologists. In Press.

United States Department of Agriculture (USDA) (2010). National Resources Conservation Service (NRCS), Geospatial Data Gateway. http://datagateway.nrcs.usda.gov/GDGOrder.aspx?order=QuickState. Accessed June 23 2010.

White, R., Song, J., Haas, C., and Middleton, D. (2006). “Evaluation of Quartz Piezoelectric Weigh-in-Motion Sensors.” Transportation Research Record, Vol. 1945, pp: 109-117. National Research Council, Washington, DC.

Zapata, C. E. (2010). “A National Catalog of Subgrade Soil Water Characteristic Curve (SWCC) Default Input and Selected Soil Properties for Use with the MEPDG.” NCHRP 9-23A, final Report. National Cooperative Highway Research Program, Washington, DC.

APPENDICES

Appendix A   Local Calibration Sites Database

Appendix A1 Summary of Structural Information for Calibration and Validation Sections*

Site ID	Layer Type	Layer Thickness (inch)	Equivalent Superpave Mix/ NCHRP 9-23 Soil Unit Code	Volumetric Properties as Built		
				% Effective Binder Content (V_{be})	% Air Voids (V_a)	Total Unit Weight (pcf)
370801	AC1	1.6	S9.5B	11.4	7.0	137.0
	AC2	2.2	I19B	7.3	7.3	135.3
	Crushed Gravel	8.7	Crushed Gravel			
	Subgrade	inf.	Z78			
370802	AC1	1.8	S9.5B	10.3	8.1	135.9
	AC2	2.4	I19B	6.5	8.1	134.8
	AC3	2.7	B25B	3.3	10.2	132.9
	Crushed Gravel	11.5	Crushed Gravel			
	Subgrade	inf.	Z78			
370859	AC1	1.4	S9.5B	9.7	8.7	135.0
	Crushed Gravel	6.8	Crushed Gravel			
	Subgrade	inf.	Z78			
370901	AC1	2.6	S9.5B	11.9	6.3	148.0
	AC2	2.8	I19C	11.4	5.0	147.9
	ATB	3.4	B25B	10.8	5.0	143.2
	Subgrade	7.0	Lime Stab.			
		inf.	Z95			
370902	AC1	2.7	S9.5B	9.6	5.2	146.3
	AC2	2.6	I19C	9.1	3.7	147.9
	ATB	3.2	B25B	10.2	5.4	143.2
	Subgrade	7.0	Lime Stab.			
		inf.	Z95			
370903	AC1	2.4	S9.5C	9.2	5.3	145.6
	AC2	2.9	I19D	10.1	3.8	147.9
	ATB	3.4	B25B	10.3	5.5	143.2
	Subgrade	7.0	Lime Stab.			
		inf.	Z95			

Appendix A1 (Continued)

371006-CN1	AC1-FC	1.0	S9.5C	12.2	17.0	124.9
	AC2	2.0	S9.5C	5.4	6.5	143.6
	AC3	6.5	B25B	9.3	5.2	145.7
	Crushed Gravel	9.4	Crushed Gravel			
	Subgrade	inf.	AA2			
371006-CN3	AC1-RAP	1.4	RS9.5B	12.1	7.4	140.1
	AC2-RAP	2.2	RS9.5B	10.8	9.3	138.2
	AC3	1.0	S9.5C	5.4	6.5	143.6
	AC4	6.5	B25B	9.3	5.2	145.7
	Crushed Gravel	9.4	Crushed Gravel			
	Subgrade	inf.	AA2			
371024-CN1	AC1-FC	1.0	S9.5C	12.2	17.0	124.9
	AC2	3.8	I19C	9.9	7.5	149.8
	Crushed Gravel	12.0	Crushed Gravel			
	Subgrade	54.0	AB4			
371024-CN2	AC1	2.3	S9.5B	15.5	10.3	148.3
	AC2	4.2	I19B	12.1	5.7	153.5
	AC3	2.8	I19C	9.9	4.6	149.8
	Crushed Gravel	12.0	Crushed Gravel			
	Subgrade	54.0	AB4			
371028-CN1	AC1	1.6	S9.5C	12.1	4.9	143.1
	ATB	8.2	B25B	11.0	6.7	146.0
	Subgrade	inf.	Z81			
371028-CN2	AC1	1.6	S9.5C	12.1	7.6	139.7
	AC2	2.6	S9.5C	12.1	11.0	146.3
	ATB	8.2	B25B	9.3	6.2	143.2
	Subgrade	inf.	Z81			
371030-CN1	AC1	4.0	I19C	10.5	7.6	142.0
	ATB	4.7	B25B	10.2	6.5	145.8
	Subgrade	inf.	Z76			

Appendix A1 (Continued)

371040-CN1	AC1-FC	1.0	S9.5C	12.2	17.0	124.9
	AC2	2.0	S9.5C	12.1	9.3	142.6
	AC3	2.6	I19C	9.9	6.0	148.3
	Soil-Agg.-Mix	14.4	A-1-a			
	Subgrade	inf.	AB4			
371040-CN2	AC1	1.9	S9.5B	11.1	9.1	143.5
	AC2-FC	1.0	S9.5C	12.2	17.0	124.9
	AC3	2.0	S9.5C	12.1	9.3	142.6
	AC4	2.6	I19C	9.9	6.0	148.3
	Soil-Agg.-Mix	14.4	A-1-a			
	Subgrade	inf.	AB4			
371352-CN1	AC1-FC	1.0	S9.5C	12.2	17.0	124.9
	AC2	2.2	I19C	9.9	6.5	154.9
	AC3	3.4	S12.5C	12.1	5.5	144.8
	Crushed Stone	6.0	Crushed Stone			
	Subgrade	inf.	Z97			
371352-CN2	AC1	2.0	S9.5B	13.0	9.1	143.6
	AC2	1.4	I19C	9.9	6.5	154.9
	AC3	3.4	S12.5C	12.1	5.5	144.8
	Crushed Stone	6.0	Crushed Stone			
	Subgrade	inf.	Z97			
371352-CN3	AC1-RAP	1.5	RS9.5C	12.1	7.6	145.6
	AC2-RAP	1.4	RS9.5C	12.1	8.4	144.6
	AC3	2.0	S9.5B	13.0	9.1	143.6
	AC4	1.4	I19C	9.9	6.5	154.9
	AC5	3.4	S12.5C	12.1	5.5	144.8
	Crushed Stone	6.0	Crushed Stone			
	Subgrade	inf.	Z97			
371645-CN1	AC1	1.9	I19C	8.2	8.0	146.0
	AC2	6.0	S12.5C	9.4	6.5	148.6
	Subgrade	8.2	Cement Stab.			150
		inf.	Z93			

Appendix A1 (Continued)

371645-CN3	AC1	1.6	S9.5C	12.1	5.5	147.0
	AC2	1.9	I19C	8.2	8.0	146.0
	AC3	6.0	S12.5C	9.4	6.5	148.6
	Subgrade	8.2	Cement Stab.			150.0
		inf.	Z93			
371801-CN1	AC1	2.0	S9.5C	12.1	10.5	143.4
	AC2	5.2	I19C	9.9	7.0	145.7
	Soil-Agg.-Mix	12.0	A-1-a			
	Subgrade	inf.	Z69			
371801-CN2	AC1	1.6	S9.5B	12.7	9.5	143.0
	AC2-RAP	2.8	RI19C	9.9	4.1	152.4
	AC3	5.2	I19C	9.9	7.0	145.7
	Soil-Agg.-Mix	12.0	A-1-a			
	Subgrade	inf.	Z69			
371802-CN1	AC1	2.2	S9.5C	14.1	8.7	140.6
	AC2	2.2	I19C	5.9	6.2	144.4
	Crushed Gravel	8.2	Crushed Gravel			
	Subgrade	inf.	AA6			
371802-CN3	AC1	1.0	S9.5B	13.1	8.1	139.0
	AC2	2.2	S9.5C	18.2	4.6	140.6
	AC3	2.2	I19C	5.9	6.2	144.4
	Crushed Gravel	8.2	Crushed Gravel			
	Subgrade	inf.	AA6			
371803-CN1	AC1-FC	1.0	S9.5C	12.2	17.0	124.9
	AC2	2.1	S9.5C	12.1	12.1	138.0
	AC3	2.5	I19C	9.9	5.3	154.2
	Soil-Agg.-Mix	12.6	A-1-b			
	Subgrade	42.0	AC2			
371803-CN2	AC1	1.0	S9.5B	13.8	7.0	150.3
	AC2	2.4	S9.5B	10.8	4.7	153.4
	AC3	1.0	S9.5C	12.1	12.1	138.0
	AC4	2.5	I19C	9.9	5.3	154.2
	Soil-Agg.-Mix	12.6	A-1-b			
	Subgrade	42.0	AC2			

Appendix A1 (Continued)

371803-CN3	AC1	1.5	S9.5C	12.1	5.5	153.4
	AC2	1.0	S9.5B	13.8	7.0	150.3
	AC3	2.4	S9.5B	10.8	4.7	153.4
	AC4	1.0	S9.5C	12.1	12.1	138.0
	AC5	2.5	I19C	9.9	5.3	154.2
	Soil-Agg.-Mix	12.6	A-1-b			
	Subgrade	42.0	AC2			
371814-CN1	AC1	2.4	S9.5C	12.1	8.8	149.1
	AC2	2.7	I19C	9.9	7.5	150.9
	Soil-Agg.-Mix	13.5	A-1-a			
	Subgrade	168.0	Z69			
371814-CN2	AC1-RAP	1.8	RS9.5C	12.1	4.7	155.7
	AC2	1.4	I19C	9.9	6.6	161.6
	AC3	1.7	S12.5C	12.1	6.3	151.2
	AC4	1.0	S9.5C	12.1	8.8	149.1
	AC5	2.7	I19C	9.9	7.5	150.9
	Soil-Agg.-Mix	13.5	A-1-a			
	Subgrade	168.0	Z69			
371817-CN1	AC1	2.1	S9.5B	14.8	7.2	145.6
	AC2	2.5	I19C	11.3	8.5	149.5
	Soil-Agg.-Mix	12.0	A-1-a			
	Subgrade	inf.	AA2			
371817-CN4	AC1-RAP	1.3	RS12.5C	12.1	8.4	144.2
	AC2	2.1	S9.5B	14.8	7.2	145.6
	AC3	2.5	I19C	11.3	8.5	149.5
	Soil-Agg.-Mix	12.0	A-1-a			
	Subgrade	inf.	AA2			
371817-CN5	AC1	1.5	S9.5C	12.1	7.6	148.1
	AC2	3.2	S9.5C	12.1	7.6	148.1
	AC3-RAP	1.3	RS12.5C	12.1	8.4	144.2
	AC4	2.1	S9.5B	14.8	7.2	145.6
	AC5	2.5	I19C	11.3	8.5	149.5
	Soil-Agg.-Mix	12.0	A-1-a			
	Subgrade	inf.	AA2			

Appendix A1 (Continued)

371992-CN1	AC1	2.4	S9.5B	11.8	9.6	148.0
	Crushed Stone #303	12.0	Crushed Stone			
	Soil-Agg.-Mix	24.0	A-1-a			
	Subgrade	inf.	Z97			
371992-CN2	AC1-RAP	2.3	RS9.5C	12.1	7.6	153.4
	AC2-RAP	1.5	RS12.5C	12.1	2.7	157.9
	AC3-RAP	2.6	RS9.5C	12.1	5.7	150.5
	AC4	1.9	S9.5C	12.1	7.6	150.6
	AC5	2.4	S9.5B	11.8	9.6	148.0
	Crushed Stone #303	12.0	Crushed Stone			
	Soil-Agg.-Mix	24.0	A-1-a			
	Subgrade	inf.	Z97			
372819-CN1	AC1-FC	1.0	S9.5C	12.2	17.0	124.9
	AC2	2.0	S9.5B	12.1	12.0	144.1
	AC3	2.1	I19B	12.6	12.3	135.2
	CTB	8.2	Cement Stab.			
	Soil-Agg. Mix	8.8	A-1-b			
	Subgrade	inf.	AA5			
372819-CN2	AC1-RAP	1.5	RS12.5C	12.1	5.0	145.5
	AC2-FC	1.0	S9.5C	12.2	17.0	124.9
	AC3	2.0	S9.5B	12.1	12.0	144.1
	AC4	2.1	I19B	12.6	12.3	135.2
	CTB	8.2	Cement Stab.			
	Soil-Agg. Mix	8.8	A-1-b			
	Subgrade	inf.	AA5			

Appendix A1 (Continued)

372819-CN3	AC1	1.6	S9.5C	12.1	7.6	147.5
	AC2	1.4	S9.5C	12.1	7.6	144.1
	AC3-RAP	1.5	RS9.5C	12.1	7.6	151.8
	AC4-FC	1.0	S9.5C	12.2	17.0	124.9
	AC5	2.0	S9.5B	12.1	12.0	144.1
	AC6	2.1	I19B	12.6	12.3	135.2
	CTB	8.2	Cement Stab.			
	Soil-Agg. Mix	8.8	A-1-b			
	Subgrade	inf.	AA5			
372824-CN1	AC1	1.9	S12.5C	13.0	7.3	143.1
	AC2	2.8	I19C	11.4	5.9	147.3
	CTB	6.0	Cement Stab.			150
	Subgrade	inf.	AA0			
372824-CN2	AC1-RAP	2.2	RS9.5C	12.1	9.0	150.4
	AC2	1.9	S12.5C	13.0	7.3	143.1
	AC3	2.8	I19C	11.4	5.9	147.3
	CTB	6.0	Cement Stab.			
	Subgrade	inf.	AA0			
372824-CN3	AC1	2.0	S9.5C	12.1	7.6	148.6
	AC2-RAP	2.2	RS9.5C	12.1	7.6	150.4
	AC3	1.9	S12.5C	13.0	7.3	143.1
	AC4	2.8	I19C	11.4	5.9	147.3
	CTB	6.0	Cement Stab.			
	Subgrade	inf.	AA0			
372825-CN1	AC1	2.4	S9.5B	12.6	8.2	154.0
	AC2	2.2	I19C	12.7	5.6	155.3
	CTB	7.5	Cement Stab.			
	Subgrade	inf.	AA7			
R-2000BB	HDS	2.5	S9.5C	12.1	7.6	145.6
	HDB	3.5	I19.0C	9.9	6.5	147.9
	HB	4.5	B25.0B	9.3	6.2	143.2
	CTB	8.0	Cement Stab.			
	Subgrade	8.0	Z96			150.0

Appendix A1 (Continued)

U-77LA	HDS	2.5	S9.5C	12.1	7.6	145.6
	HDB	3.5	I19.0C	9.9	6.5	147.9
	HB	3.0	B25.0B	9.3	6.2	143.2
	CTB	8.0	Cement Stab.			
	Subgrade	inf.	Z96			
R-2318B	HDS	2.5	S9.5C	12.1	7.6	145.6
	HDB	3.5	I19.0C	9.9	6.5	147.9
	ABC	8.0	Crushed Stone			
	Subgrade	8.0	Lime Stab.			
		inf.	Z95			
U-508CB	HDS	2.5	S9.5C	12.1	7.6	145.6
	HDB	2.5	I19.0C	9.9	6.5	147.9
	HB	3.0	B25.0B	9.3	6.2	143.2
	Subgrade	inf.	Z72			
U-2413B	HDS	2.5	S9.5C	12.1	7.6	145.6
	HDB	3.0	I19.0C	9.9	6.5	147.9
	HB	3.0	B25.0B	9.3	6.2	143.2
	Subgrade	8.0	Lime Stab.			
		inf.	AA6			
U-508CA	HDS	2.5	S9.5C	12.1	7.6	145.6
	HDB	2.5	I19.0C	9.9	6.5	147.9
	HB	3.0	B25.0B	9.3	6.2	143.2
	Subgrade	inf.	AC7			
R-1017AC	HDS	2.5	S9.5C	12.1	7.6	145.6
	HDB	2.5	I19.0C	9.9	6.5	147.9
	HB	3.0	B25.0B	9.3	6.2	143.2
	Subgrade	7.0	Cement Stab.			
		inf.	AA2			
R-2232A	HDS	2.5	S9.5C	12.1	7.6	145.6
	HDB	2.5	I19.0C	9.9	6.5	147.9
	HB	3.5	B25.0B	9.3	6.2	143.2
	CTB	8.0	Cement Stab.			
	Subgrade	inf.	Z95			

Appendix A1 (Continued)

R-2232B	HDS	2.5	S9.5C	12.1	7.6	145.6
	HDB	2.5	I19.0C	9.9	6.5	147.9
	HB	3.5	B25.0B	9.3	6.2	143.2
	CTB	8.0	Cement Stab.			
	Subgrade	inf.	AA3			
R-2211BA	HDS	2.5	S9.5C	12.1	7.6	145.6
	HDB	3.5	I19.0C	9.9	6.5	147.9
	ABC	8.0	Crushed Stone			
	Subgrade	inf.	Z87			
R-519	HDS	2.5	S9.5C	12.1	7.6	145.6
	HDB	2.5	I19.0C	9.9	6.5	147.9
	HB	3.0	B25.0B	9.3	6.2	143.2
	SG	7.0	Cement Stab.			150.0
	Subgrade	inf.	AA2			
R-85AD	HDS	2.5	S9.5C	12.1	7.6	145.6
	HDB	3.5	I19.0C	9.9	6.5	147.9
	HB	5.5	B25.0B	9.3	6.2	143.2
	Subgrade	7.0	Soil-Cement			
		inf.	AA2			
R-2120AA						
	S12.5C	2.8	S12.5C	12.1	7.6	145.6
	I19C	3.5	I19.0C	9.9	6.5	147.9
	ABC	9.8	Crushed Stone			
	Subgrade	7.0	Cement Stab.			
		inf.	AA2			
R-2120AB	SP12.5C	2.4	S12.5C	12.1	7.6	145.6
	SP19.0	3.5	I19.0C	9.9	6.5	147.9
	ABC	9.8	Crushed Stone			
	Subgrade	8.0	Lime Stab.			
		inf.	AA2			

Appendix A1 (Continued)

R-2123AC	S12.5C	3.0	S12.5C	12.1	7.6	145.6
	I19C	2.6	I19.0C	9.9	6.5	147.9
	B25C	3.1	B25.0B	9.3	6.2	143.2
	ABC	8.0	Crushed Stone			
	Subgrade	8.0	Lime Stab.			
		inf.	AA2			
R-2123BB	S12.5D	2.8	S12.5C	12.1	7.6	145.6
	I19D	2.8	I19.0C	9.9	6.5	147.9
	B25.0	3.9	B25.0B	9.3	6.2	143.2
	ABC	7.9	Crushed Stone			
	Subgrade	8.0	Lime Stab.			
		inf.	AA2			
R-2123CC	S12.5C	2.5	S12.5C	12.1	7.6	145.6
	I19C	3.5	I19.0C	9.9	6.5	147.9
	B25.0	5.5	B25.0B	9.3	6.2	143.2
	ABC	8.0	Crushed Stone			
	Subgrade	8.0	Lime Stab.			
		inf.	AA7			
R-2219AC	S12.5C	2.5	S12.5C	12.1	7.6	145.6
	I19C	2.5	I19.0C	9.9	6.5	147.9
	B25.0	3.0	B25.0B	9.3	6.2	143.2
	ABC	8.0	Crushed Stone			
	Subgrade	8.0	Lime Stab.			
		inf.	AA0			
R-2217B	S12.5C	2.8	S12.5C	12.1	7.6	145.6
	I19C	2.2	I19.0C	9.9	6.5	147.9
	B25.0	10.8	B25.0B	9.3	6.2	143.2
	Subgrade	8.0	Lime Stab.			
		inf.	Z97			

Appendix A1 (Continued)

R-1023AB	S9.5C	2.4	S9.5C	12.1	7.6	145.6
	I19C	3.5	I19.0C	9.9	6.5	147.9
	ABC	7.9	Crushed Stone			
	Subgrade	7.0	Cement Stab.			
		inf.	Z72			
R-1023B	S9.5C	2.4	S9.5C	12.1	7.6	145.6
	I19C	3.5	I19.0C	9.9	6.5	147.9
	ABC	7.9	Crushed Stone			
	Subgrade	7.0	Cement Stab.			
		inf.	Z72			
R-2000EA	S12.5D	2.4	S12.5C	12.1	7.6	145.6
	I19D	3.5	I19.0C	9.9	6.5	147.9
	B25.0	4.3	B25.0B	9.3	6.2	143.2
	CTABC	7.9	CTABC			
	Subgrade	8.0	Lime Stab.			
		inf.	AA2			
R-2000EB	S12.5D	2.4	S12.5C	12.1	7.6	145.6
	I19D	3.5	I19.0C	9.9	6.5	147.9
	B25.0	4.3	B25.0B	9.3	6.2	143.2
	CTB	7.9	Cement Stab.			
	Subgrade	8.0	Lime Stab.			
		inf.	AA2			
R-2001C	S12.5C	2.5	S12.5C	12.1	7.6	145.6
	I19C	1.8	I19.0C	9.9	6.5	147.9
	B25.0	3.0	B25.0B	9.3	6.2	143.2
	ABC	8.0	Crushed Stone			
	Subgrade	8.0	Lime Stab.			
		inf.	Z88			

* Legend

CN1 = Construction Number 1

AC1 = Asphalt Concrete Layer 1

AC1-FC = Friction-Course Asphalt Concrete

ATB = Asphalt Treated Base

CTB = Cement Treated Base

Appendix A2 Summary of Traffic Information as entered in the MEPDG for Calibration and Validation Sections

Site ID	Traffic Opening Date	Design Life (years)	Initial 2-way AADTT	Number of lanes in design direction	% of Trucks in design direction	% of Trucks in design lane	Speed (mph)	Traffic Growth function / rate (%)
370801	10/30/1997	20	5	2	40	50	50	C / 58.5
370802	10/30/1997	20	5	2	40	50	50	C / 58.5
370859	10/30/1997	20	5	2	40	50	50	C / 58.5
370901	10/30/1996	20	1055	2	50	100	60	C / 4.1
370902	10/30/1996	20	1055	2	50	100	60	C / 4.1
370903	10/30/1996	20	1055	2	50	100	60	C / 4.1
371006-CN1	7/1/1982	30	2987	2	50	100	70	C / 2.9
371006-CN3	10/9/1994	20	4208	2	50	100	70	C / 2.9
371024-CN1	11/1/1980	30	100	2	46	100	50	C / 7.5
371024-CN2	11/10/1992	20	217	2	50	100	50	C / 7.5
371028-CN1	5/1/1982	28	152	2	50	100	60	C / 7.6
371028-CN2	9/2/2002	20	657	2	50	100	60	C / 7.6
371030-CN1	12/1/1984	26	236	2	50	100	60	C / 7.2
371040-CN1	9/1/1978	20	50	2	40	50	60	C / 12.8
371040-CN2	6/21/1995	20	153	2	50	100	60	C / 12.8
371352-CN1	7/1/1980	30	272	2	50	100	60	C / 4.7
371352-CN2	10/30/1989	21	411	2	50	100	60	C / 4.7
371352-CN3	7/11/2003	20	780	2	50	100	60	C / 4.7
371645-CN1	10/1/1986	25	757	2	50	100	60	C / 2.8
371645-CN3	5/16/2000	20	1117	2	50	100	60	C / 2.8
371801-CN1	5/1/1974	35	4485	2	50	100	70	C / 0.2
371801-CN2	9/20/1996	20	4656	2	50	100	70	C / 0.2
371802-CN1	10/1/1985	25	290	2	50	100	60	C / 5.7
371802-CN3	5/1/1996	20	536	2	50	100	60	C / 5.7

Appendix A2 (Continued)

371803-CN1	12/1/1977	33	756	2	50	100	60	C / 1.0
371803-CN2	8/1/1990	20	860	2	50	100	60	C / 1.0
371803-CN3	5/2/2000	20	950	2	50	100	60	C / 1.0
371814-CN1	9/1/1970	40	131	2	50	100	60	C / 5.7
371814-CN2	7/18/2000	20	689	2	50	100	60	C / 5.7
371817-CN1	12/1/1983	27	117	2	50	100	60	C / 11.3
371817-CN4	11/19/1995	20	421	2	50	100	60	C / 11.3
371817-CN5	10/8/2002	20	888	2	50	100	60	C / 11.3
371992-CN1	2/1/1990	20	1300	2	50	100	60	C / 2.3
371992-CN2	9/2/1996	20	1493	2	50	100	60	C / 2.3
372819-CN1	8/1/1981	30	552	2	50	100	60	C / 6.4
372819-CN2	9/18/1992	20	1095	2	50	100	60	C / 6.4
372819-CN3	6/2/2002	20	2042	2	50	100	60	C / 6.4
372824-CN1	10/1/1983	27	717	2	50	100	60	C / 4.2
372824-CN2	9/18/1991	20	995	2	50	100	60	C / 4.2
372824-CN3	7/14/2003	20	1627	2	50	100	60	C / 4.2
372825-CN1	2/1/1987	30	335	2	50	100	60	C / 1.0
R-2000BB	2/15/1994	20	7346	3	50	80	70	L / 3.1
U-77LA	7/20/1993	20	2108	2	50	90	50	L / 2.9
R-2318B	5/17/1994	20	1696	1	50	100	60	L / 3.0
U-508CB	9/1/1993	20	1134	2	50	90	50	L / 2.9
U-508CA	9/1/1993	20	1250	2	50	90	50	L / 2.8
R-1017AC	5/18/1993	20	759	1	50	100	60	L / 2.5
R-2211BA	4/15/1997	20	830	1	50	100	50	L / 3.6
R-519	7/20/1993	20	660	2	60	90	50	L / 2.9
R-85AD	11/16/1993	20	2352	2	50	90	60	L / 3.6
R-2120AA	4/24/2002	20	1403	2	50	90	60	L / 3.1
R-2120AB	10/01/2001	20	1707	2	50	90	60	L / 2.5
R-2123AC	7/1/2003	20	6769	3	50	80	70	L / 2.9
R-2123BB	9/3/2003	20	5624	3	50	80	70	L / 2.9

Appendix A2 (Continued)

R-2123CC	8/15/2003	20	7913	3	50	80	70	L / 3.3
R-2219AC	7/23/2001	20	1634	2	50	90	60	L / 2.5
R-2217B	7/10/2002	20	1361	2	50	90	60	L / 3.0
R-1023AB	12/31/2002	20	2156	2	50	90	60	L / 3.0
R-1023B	12/20/2002	20	2156	2	50	90	60	L / 3.0
R-2000EA	8/1/2002	20	9181	3	50	80	70	L / 2.6
R-2000EB	8/23/2002	20	7460	3	50	80	70	L / 2.6
R-2001C	7/1/2001	20	1049	2	50	90	50	L / 2.9

Appendix A3 Summary of Measured Total Rut Depth for LTPP Local Calibration Sections*

LTPP Site ID	Total Rut Measured from LTPP (in.)	Survey Date	Survey Date (Days from Construction Date)	Modified Total Rut Measured (in.) **
370801	Construction Date	10/31/1997	0.0	0.000
	0.079	3/9/1998	129	0.040
	0.079	12/7/1999	767	0.074
	0.118	2/17/2000	839	0.077
	0.079	12/19/2000	1145	0.085
	0.079	12/11/2001	1502	0.094
	0.157	1/26/2002	1548	0.095
	0.079	1/21/2003	1908	0.102
	0.079	12/9/2003	2230	0.107
	0.118	1/28/2004	2280	0.108
	0.079	12/14/2004	2601	0.113
	0.118	8/23/2006	3218	0.122
	0.079	11/10/2007	3662	0.127
370802	Construction Date	10/31/1997	0.0	0.000
	0.039	3/9/1998	129	0.042
	0.079	12/7/1999	767	0.077
	0.157	2/17/2000	839	0.080
	0.079	12/19/2000	1145	0.089
	0.079	12/11/2001	1502	0.097
	0.157	1/26/2002	1548	0.098
	0.079	1/21/2003	1908	0.106
	0.079	12/9/2003	2230	0.112
	0.118	1/28/2004	2280	0.112
	0.118	12/14/2004	2601	0.118
	0.118	8/23/2006	3218	0.127
	0.118	11/10/2007	3662	0.132
370859	0.000	10/31/1997	0.0	0.000
	0.039	3/9/1998	129	0.038
	0.079	12/7/1999	767	0.070
	0.157	2/17/2000	839	0.072
	0.079	12/20/2000	1146	0.080
	0.079	12/11/2001	1502	0.088
	0.118	1/26/2002	1548	0.089

Appendix A3 (Continued)

	0.079	1/21/2003	1908	0.095
	0.079	12/9/2003	2230	0.101
	0.157	1/28/2004	2280	0.101
	0.079	12/15/2004	2602	0.106
	0.079	8/23/2006	3218	0.114
	0.079	11/10/2007	3662	0.119
370901	Construction Date	10/30/1996	0.0	0.000
	0.039	10/8/1997	343	0.077
	0.157	1/23/2001	1546	0.130
	0.118	3/14/2001	1596	0.131
	0.157	10/10/2001	1806	0.137
	0.118	1/26/2003	2279	0.149
	0.197	11/13/2003	2570	0.155
	0.157	1/29/2004	2647	0.157
	0.276	2/8/2008	4118	0.183
370902	Construction Date	10/30/1996	0.0	0.000
	0.039	10/8/1997	343	0.078
	0.157	1/23/2001	1546	0.132
	0.118	3/14/2001	1596	0.134
	0.157	10/10/2001	1806	0.140
	0.157	1/26/2003	2279	0.151
	0.197	11/13/2003	2570	0.158
	0.157	1/29/2004	2647	0.160
	0.236	2/8/2008	4118	0.186
370903	Construction Date	10/30/1996	0.0	0.000
	0.079	10/8/1997	343	0.092
	0.157	1/23/2001	1546	0.156
	0.157	3/14/2001	1596	0.158
	0.157	10/10/2001	1806	0.165
	0.157	1/26/2003	2279	0.179
	0.197	11/13/2003	2570	0.187
	0.197	1/29/2004	2647	0.189
	0.276	2/8/2008	4118	0.221

Appendix A3 (Continued)

371006-CN1	Construction Date	7/1/1982	0.0	0.000
	0.079	10/13/1989	2661	0.106
	0.079	3/19/1991	3183	0.113
	0.197	10/11/1992	3755	0.120
	0.118	4/18/1994	4309	0.125
	0.157	9/20/1994	4464	0.127
371006-CN3	Construction Date	10/9/1994	0.0	0.000
	0.157	2/8/1996	487	0.079
	0.079	3/12/1998	1250	0.110
	0.118	12/12/2000	2256	0.135
	0.118	3/14/2001	2348	0.137
	0.157	1/27/2003	3032	0.150
	0.157	8/28/2003	3245	0.154
	0.157	12/3/2007	4803	0.176
371024-CN1	Construction Date	11/1/1980	0.0	0.000
	0.354	11/3/1989	3289	0.286
	0.433	3/9/1991	3780	0.301
	0.354	4/10/1992	4178	0.312
	0.157	10/14/1992	4365	0.317
371024-CN2	Construction Date	11/10/1992	0.0	0.000
	0.236	1/31/1996	1177	0.141
	0.157	4/29/1998	1996	0.169
	0.157	3/9/2001	3041	0.196
	0.197	6/26/2002	3515	0.207
	0.197	10/9/2002	3620	0.209
	0.197	3/17/2004	4145	0.219
371028-CN1	Construction Date	5/1/1982	0.0	0.000
	0.433	10/12/1989	2721	0.384
	0.433	3/20/1991	3245	0.410
	0.512	10/10/1992	3815	0.435
	0.512	2/9/1996	5032	0.481
	0.472	4/18/1996	5101	0.484

Appendix A3 (Continued)

	0.433	8/15/1996	5220	0.488
	0.472	10/2/1997	5633	0.502
	0.551	3/17/1998	5799	0.507
	0.512	9/29/1998	5995	0.513
	0.551	1/3/2001	6822	0.538
	0.433	3/14/2001	6892	0.540
	0.512	3/22/2002	7265	0.551
371028-CN2	Construction Date	9/2/2002	0.0	0.000
	0.079	1/16/2003	136	0.049
	0.079	12/5/2007	1920	0.123
371030-CN1	Construction Date	12/1/1984	0.0	0.000
	0.276	10/12/1989	1776	0.275
	0.315	3/20/1991	2300	0.302
	0.394	10/10/1992	2870	0.327
	0.315	2/9/1996	4087	0.372
	0.394	10/9/1997	4695	0.391
	0.394	8/29/2000	5750	0.421
1040-CN1	Construction Date	9/1/1978	0.0	0.000
	0.472	11/3/1989	4081	0.465
	0.472	3/11/1991	4574	0.485
	0.512	10/15/1992	5158	0.507
371040-CN2	Construction Date	6/21/1995	0.0	0.000
	0.079	12/12/1995	174	0.074
	0.157	1/31/1996	224	0.081
	0.118	11/18/1998	1246	0.148
	0.157	2/15/2001	2066	0.177
	0.157	3/9/2001	2088	0.178
	0.197	3/25/2004	3200	0.207
	0.197	11/14/2007	4529	0.234
371352-CN1	Construction Date	7/1/1980	0.0	0.000
	0.276	3/9/1989	3173	0.276

Appendix A3 (Continued)

371352-CN2	Construction Date	10/30/1989	0.0	0.000
	0.079	3/18/1991	504	0.069
	0.118	10/15/1992	1081	0.090
	0.157	4/21/1994	1634	0.103
	0.079	2/6/1996	2290	0.116
	0.118	4/23/1998	3097	0.129
	0.197	1/24/2001	4104	0.142
	0.118	3/11/2001	4150	0.142
	0.118	10/9/2002	4727	0.149
	0.118	5/28/2003	4958	0.151
371352-CN3	Construction Date	7/11/2003	0.0	0.000
	0.079	3/23/2004	256	0.070
	0.118	11/8/2007	1581	0.132
371645-CN1	Construction Date	10/1/1986	0.0	0.000
	0.276	3/15/1989	896	0.232
	0.276	3/6/1991	1617	0.288
	0.433	10/12/1992	2203	0.322
	0.315	4/19/1994	2757	0.350
	0.433	1/29/1996	3407	0.378
	0.315	2/5/1998	4145	0.406
	0.354	2/29/2000	4899	0.431
371645-CN3	Construction Date	5/16/2000	0.0	0.000
	0.079	3/10/2001	298	0.056
	0.039	6/27/2002	772	0.077
	0.118	1/27/2003	986	0.084
	0.118	11/30/2007	2754	0.120
371801-CN1	Construction Date	5/1/1974	0.0	0.000
	0.354	3/15/1989	5432	0.341
	0.354	3/10/1991	6157	0.357
	0.394	10/14/1992	6741	0.368
	0.394	1/31/1996	7945	0.391
	0.354	7/25/1996	8121	0.394

Appendix A3 (Continued)

371801-CN2	Construction Date	9/20/1996	0.0	0.000
	0.079	4/28/1998	585	0.068
	0.079	5/18/2000	1336	0.090
	0.118	3/9/2001	1631	0.096
	0.118	10/9/2002	2210	0.107
	0.079	3/12/2003	2364	0.109
371802-CN1	Construction Date	10/1/1985	0.0	0.000
	0.315	10/13/1989	1473	0.292
	0.315	3/18/1991	1994	0.327
	0.354	10/10/1992	2566	0.358
	0.354	4/15/1994	3118	0.385
	0.394	7/18/1995	3577	0.404
	0.472	2/9/1996	3783	0.413
	0.394	4/2/1996	3836	0.415
371802-CN3	Construction Date	5/1/1996	0.0	0.000
	0.118	12/11/1996	224	0.084
	0.118	10/10/1997	527	0.114
	0.197	2/2/2000	1372	0.160
	0.118	3/14/2001	1778	0.176
	0.157	1/15/2002	2085	0.186
371803-CN1	Construction Date	12/1/1977	0.0	0.000
	0.394	11/3/1989	4355	0.370
	0.354	6/6/1990	4570	0.377
371803-CN2	Construction Date	8/1/1990	0.0	0.000
	0.157	3/9/1991	220	0.064
	0.157	10/14/1992	805	0.101
	0.236	1/31/1996	2009	0.139
	0.118	4/22/1996	2091	0.141
	0.118	4/7/1999	3171	0.163
	0.079	11/17/1999	3395	0.167
	0.118	11/14/2001	4123	0.179
	0.157	1/3/2002	4173	0.180

Appendix A3 (Continued)

371803-CN3	Construction Date	5/2/2000	0.0	0.000
	0.118	1/28/2003	1001	0.123
	0.157	1/6/2004	1344	0.136
	0.157	11/9/2007	2747	0.175
371814-CN1	Construction Date	9/1/1970	0.0	0.000
	0.236	3/13/1989	6768	0.234
	0.236	3/9/1991	7494	0.242
	0.236	10/14/1992	8079	0.249
	0.276	1/31/1996	9283	0.261
	0.276	4/1/1999	10439	0.272
	0.276	6/26/2000	10891	0.276
371814-CN2	Construction Date	7/18/2000	0.0	0.000
	0.079	10/12/2000	86	0.055
	0.118	3/9/2001	234	0.078
	0.118	10/9/2002	813	0.120
	0.118	6/7/2005	1785	0.159
	0.118	11/13/2007	2674	0.183
371817-CN1	Construction Date	12/1/1983	0.0	0.000
	0.433	10/15/1989	2145	0.310
	0.276	3/18/1991	2664	0.336
	0.315	10/18/1992	3244	0.361
371817-CN4	Construction Date	11/19/1995	0.0	0.000
	0.079	12/15/1995	26	0.043
	0.157	2/6/1996	79	0.063
	0.118	4/27/1999	1255	0.168
	0.118	3/11/2001	1939	0.196
	0.118	3/13/2002	2306	0.208
371817-CN5	Construction Date	10/8/2002	0.0	0.000
	0.079	2/5/2003	120	0.059
	0.118	2/5/2008	1946	0.156
371992-CN1	Construction Date	2/1/1990	0.0	0.000
	0.197	10/15/1992	987	0.084
	0.039	4/20/1994	1539	0.098
	0.118	2/6/1996	2196	0.111

Appendix A3 (Continued)

371992-CN2	Construction Date	9/2/1996	0.0	0.000
	0.236	4/22/1998	597	0.192
	0.315	5/16/2000	1352	0.259
	0.236	3/14/2001	1654	0.278
	0.276	1/26/2003	2337	0.316
	0.315	3/6/2003	2376	0.317
	0.354	11/29/2007	4105	0.387
372819-CN1	Construction Date	8/1/1981	0.0	0.000
	0.433	10/13/1989	2995	0.411
	0.433	3/18/1991	3516	0.436
	0.433	4/13/1992	3908	0.453
372819-CN2	Construction Date	9/18/1992	0.0	0.000
	0.118	1/13/1993	117	0.082
	0.157	2/6/1996	1236	0.191
	0.236	8/13/1997	1790	0.218
	0.276	8/30/2000	2903	0.259
	0.197	3/14/2001	3099	0.265
	0.276	3/28/2002	3478	0.276
372819-CN3	Construction Date	6/2/2002	0.0	0.000
	0.039	2/6/2003	249	0.051
	0.079	1/28/2004	605	0.069
	0.118	2/6/2008	2075	0.105
372824-CN1	Construction Date	10/1/1983	0.0	0.000
	0.118	10/13/1989	2204	0.114
	0.118	3/18/1991	2725	0.123
372824-CN2	Construction Date	9/18/1991	0.0	0.000
	0.197	10/15/1992	393	0.156
	0.276	2/6/1996	1602	0.259
	0.276	8/14/1997	2157	0.288
	0.315	12/2/1999	2997	0.325
	0.315	8/31/2000	3270	0.335
	0.354	3/14/2001	3465	0.342
	0.315	1/26/2003	4148	0.365
	0.354	3/27/2003	4208	0.367

Appendix A3 (Continued)

372824-CN3	Construction Date	7/14/2003	0.0	0.000
	0.197	3/24/2004	254	0.186
	0.354	2/7/2008	1669	0.373
372825-CN1	Construction Date	2/1/1987	0.0	0.000
	0.157	3/9/1989	767	0.120
	0.157	3/7/1991	1495	0.151
	0.197	10/15/1992	2083	0.170
	0.118	7/19/1995	3090	0.196
	0.236	1/31/1996	3286	0.200
	0.197	11/17/1998	4307	0.220
	0.236	2/14/2001	5127	0.234
	0.197	3/11/2001	5152	0.234
	0.197	10/9/2002	5729	0.243
	0.276	3/23/2004	6260	0.251
	0.354	11/7/2007	7584	0.269

*CN1 = Construction Number 1, ** See Section 8.6.3.3

Appendix A4 Summary of LTPP Total Rut Adjustment Graphs for LTPP Local Calibration Sections

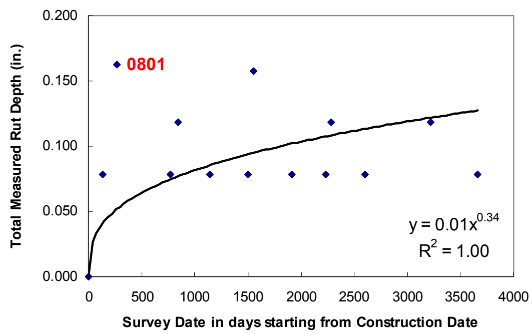

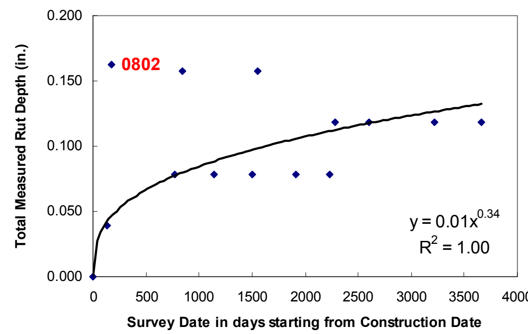

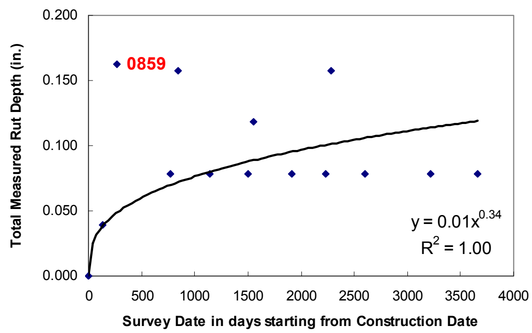

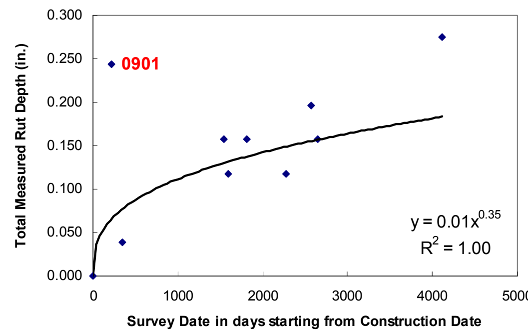

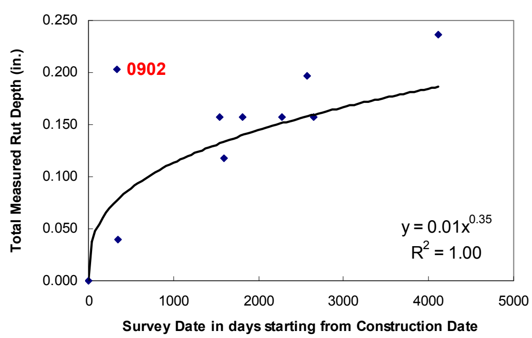

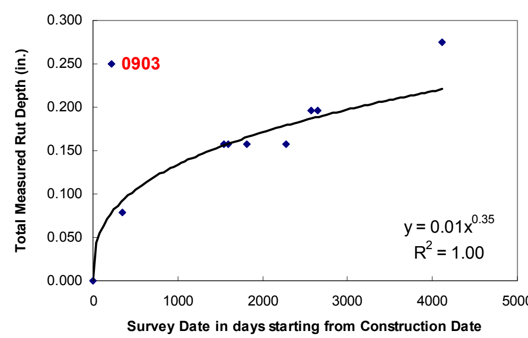

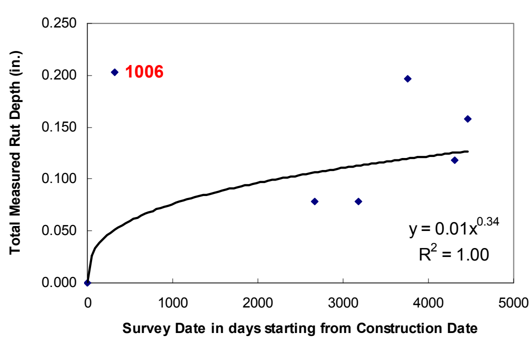

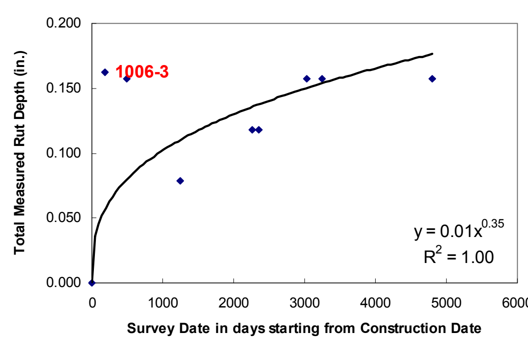

Appendix A4 (Continued)

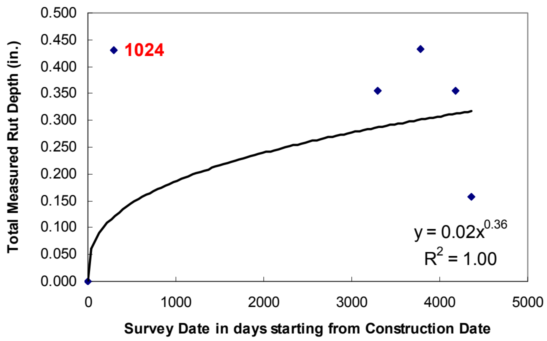

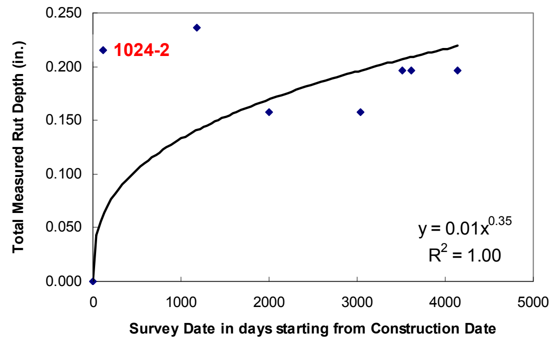

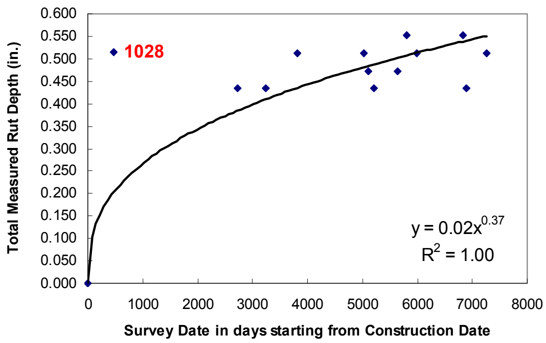

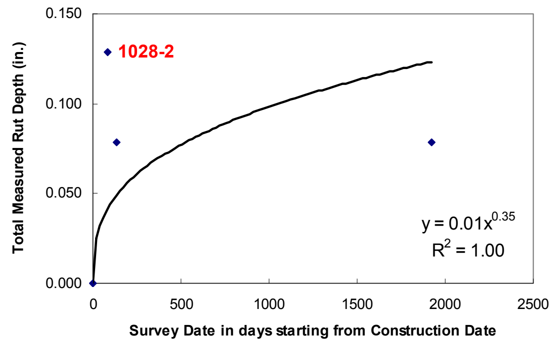

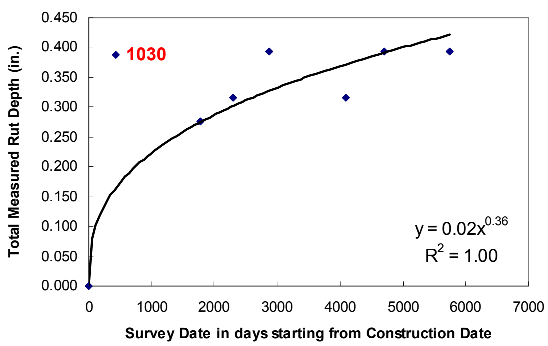

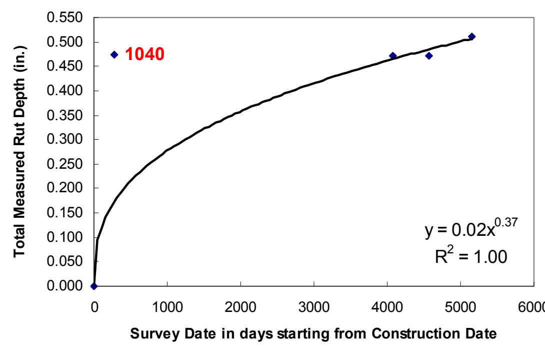

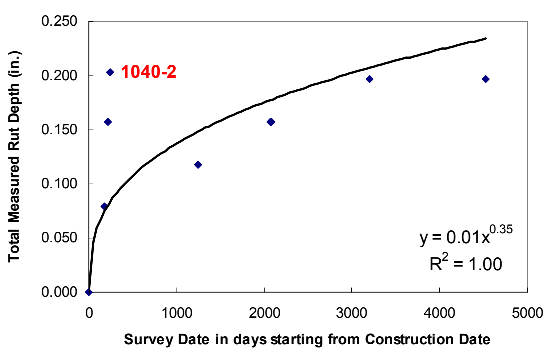

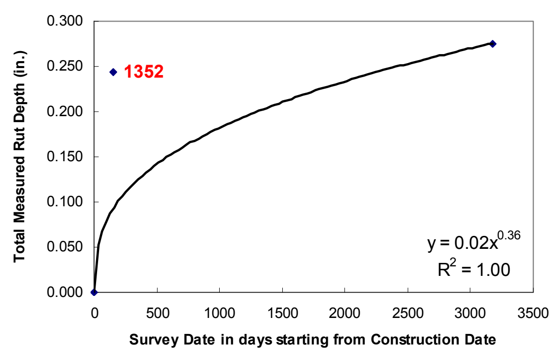

Appendix A4 (Continued)

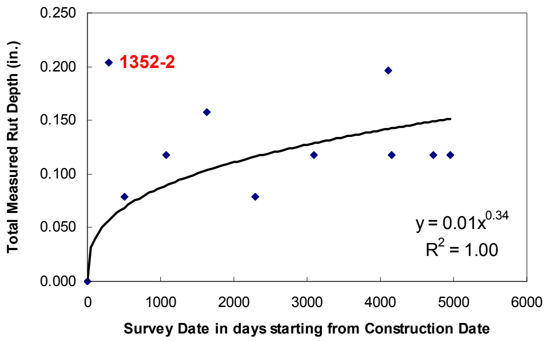

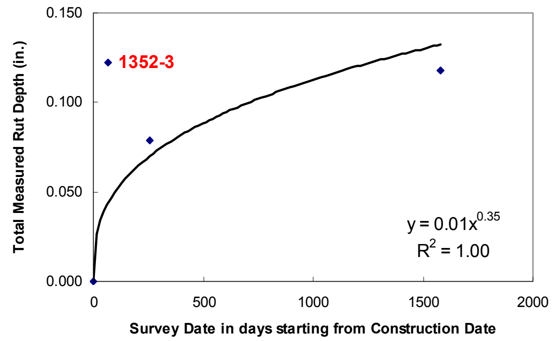

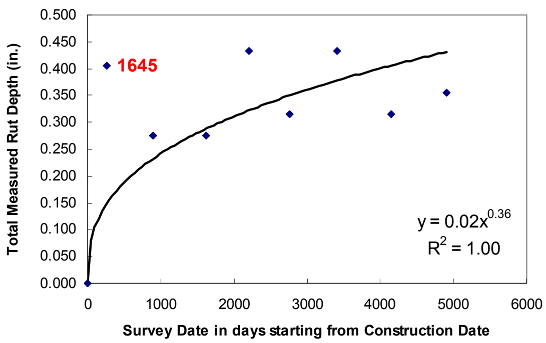

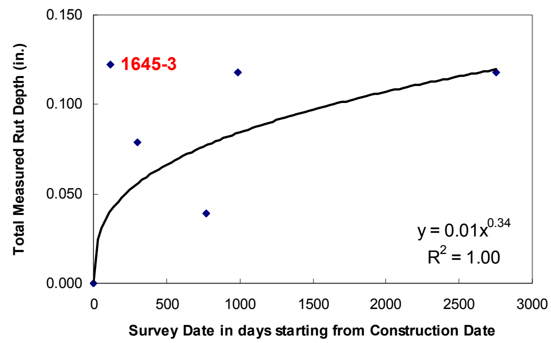

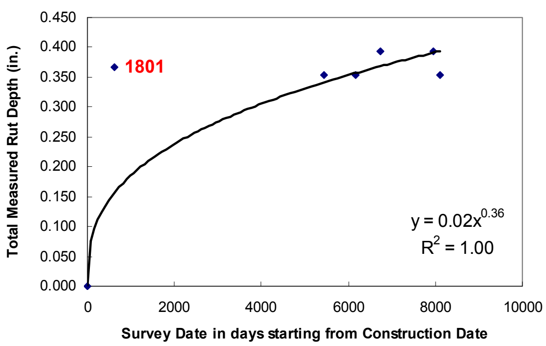

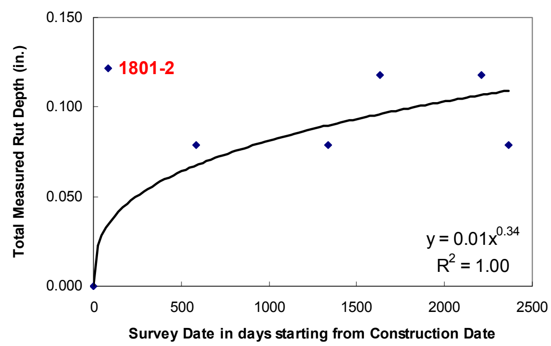

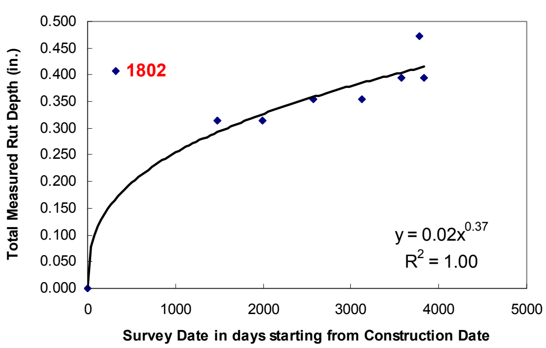

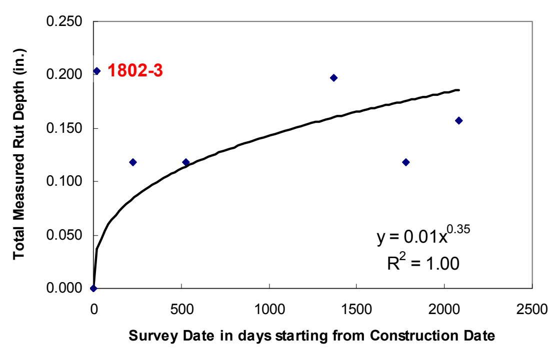

Appendix A4 (Continued)

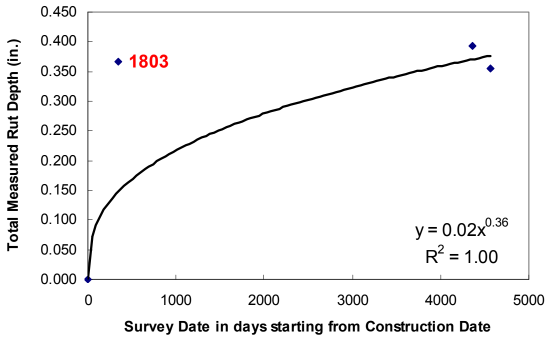

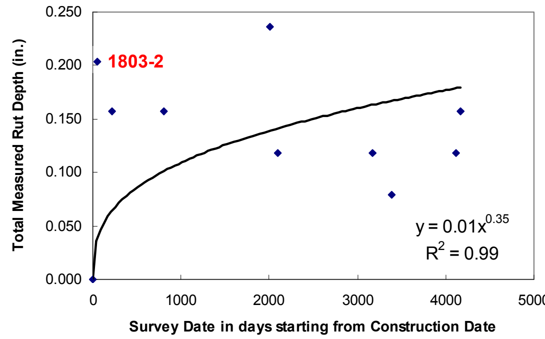

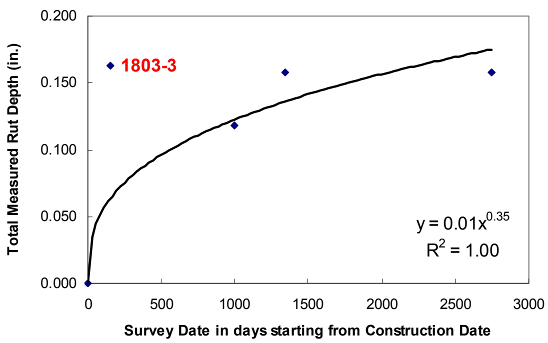

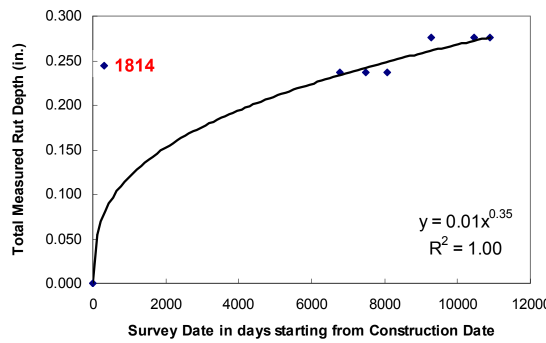

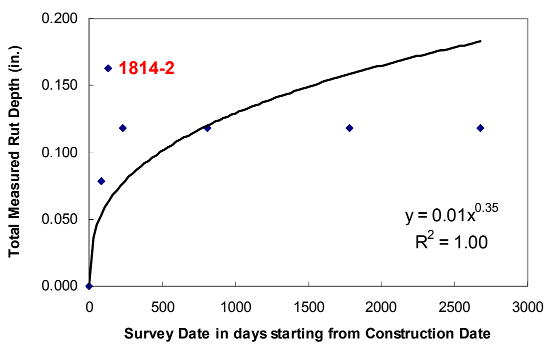

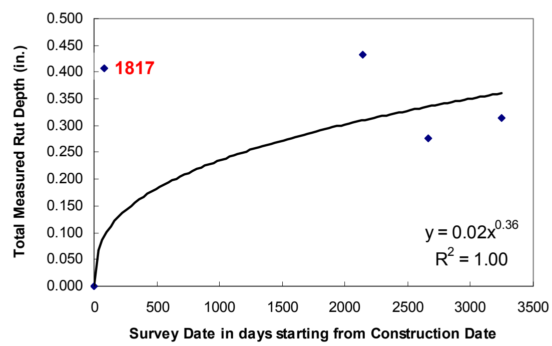

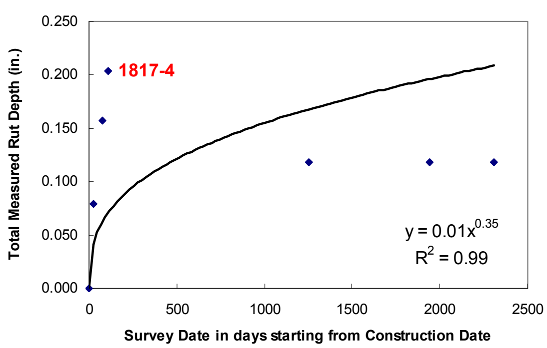

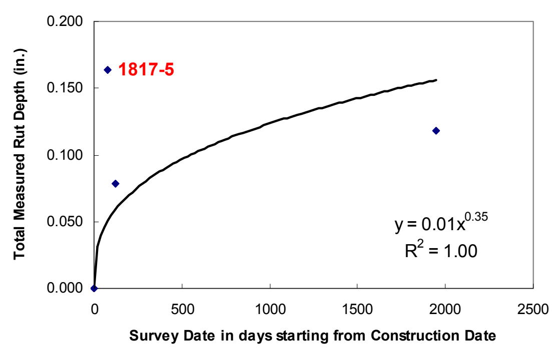

Appendix A4 (Continued)

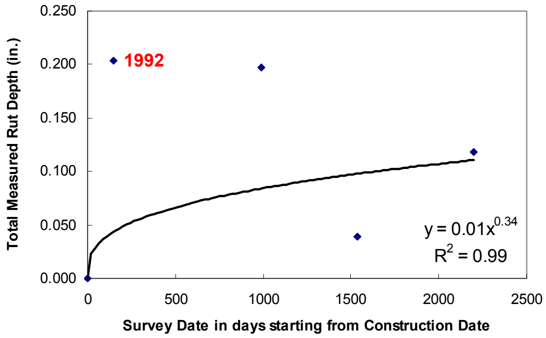

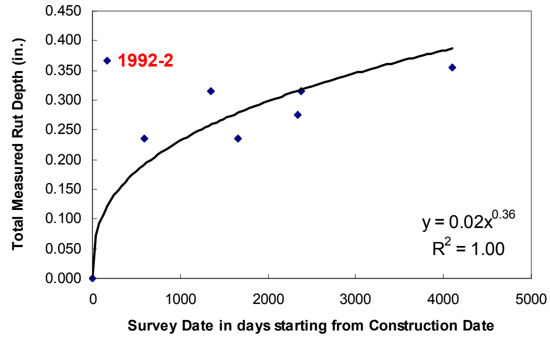

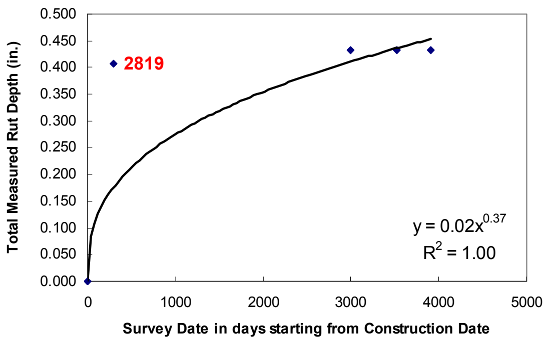

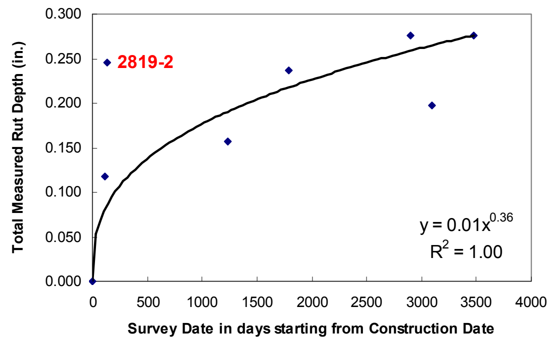

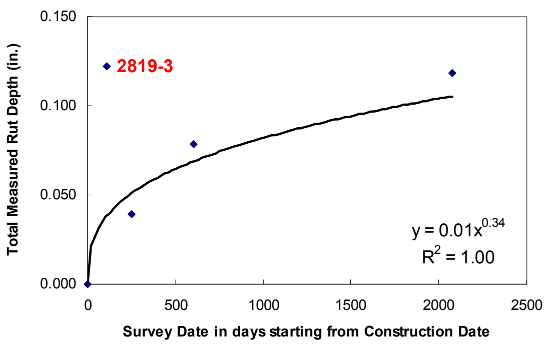

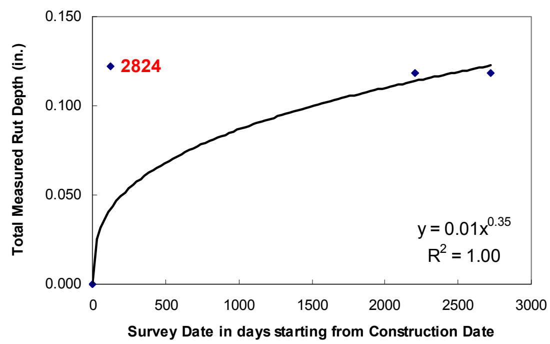

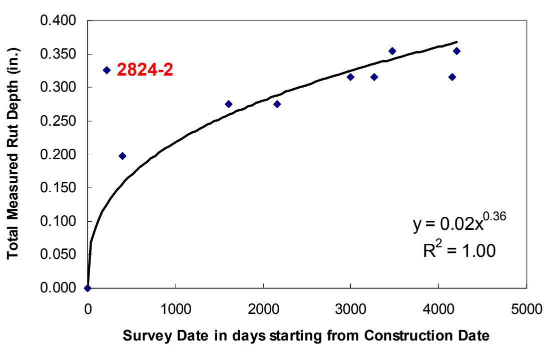

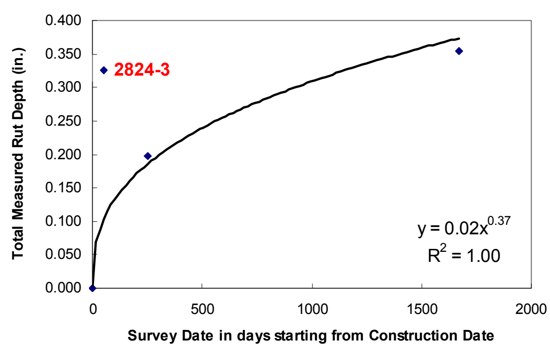

Appendix A4 (Continued)

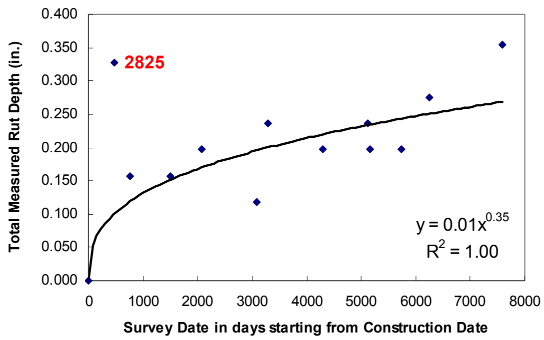

Appendix A5 Summary of Measured Alligator Cracking for LTPP Local Calibration Sections

LTPP Site ID	Survey Date	Measured Alligator Cracking (% Lane Area)	Total Thickness of Asphalt Layers (inch)
370801	3/9/1998	0.000	3.8
	12/7/1999	0.000	
	12/19/2000	0.000	
	12/11/2001	0.000	
	1/21/2003	0.000	
	12/9/2003	1.866	
	12/14/2004	31.736	
	8/23/2006	74.684	
	11/10/2007	78.935	
370802	3/9/1998	0.000	6.9
	12/7/1999	0.000	
	12/19/2000	0.000	
	12/11/2001	0.000	
	1/21/2003	0.000	
	12/9/2003	0.592	
	12/14/2004	7.391	
	8/23/2006	57.103	
	11/10/2007	65.463	
370859	3/9/1998	0.000	1.4
	12/7/1999	0.000	
	12/20/2000	0.000	
	12/11/2001	0.000	
	1/21/2003	0.000	
	12/9/2003	0.000	
	12/15/2004	0.000	
	8/23/2006	63.381	
	11/10/2007	69.302	
370901	10/8/1997	0.000	8.8
	1/23/2001	0.000	
	10/10/2001	0.000	
	11/13/2003	0.000	
	2/8/2008	6.763	

Appendix A5 (Continued)

370902	10/8/1997	0.000	8.5
	1/23/2001	0.000	
	10/10/2001	0.000	
	11/13/2003	0.000	
	2/8/2008	8.468	
370903	10/8/1997	0.000	8.7
	1/23/2001	0.000	
	10/10/2001	0.000	
	11/13/2003	0.000	
	2/8/2008	14.890	
371006	8/17/1991	0.000	9.5
	4/18/1994	0.000	
	9/20/1994	0.000	
371006-3	6/7/1995	0.000	11.1
	3/12/1998	0.000	
	12/12/2000	7.624	
	8/28/2003	15.626	
	12/3/2007	36.221	
371024	4/10/1992	34.875	4.8
371024-2	4/29/1998	37.315	9.3
	6/26/2002	41.656	
	3/17/2004	71.580	
371028	5/18/1995	0.897	9.8
	4/18/1996	29.547	
	8/15/1996	21.887	
	10/2/1997	30.265	
	3/17/1998	37.082	
	9/29/1998	30.121	
	1/3/2001	27.269	
	3/22/2002	47.630	
371028-2	1/16/2003	0.000	12.4
	12/5/2007	32.363	
371030	10/9/1997	0.000	8.7
	8/29/2000	16.379	

Appendix A5 (Continued)

371040-2	12/13/1995	0.000	7.5
	11/18/1998	0.000	
	2/15/2001	0.000	
	3/25/2004	13.652	
	11/14/2007	18.101	
371352-2	4/21/1994	0.000	6.8
	4/23/1998	8.378	
	1/24/2001	11.751	
	5/28/2003	9.777	
371352-3	3/23/2004	0.000	9.7
	11/8/2007	3.929	
371645	4/19/1994	0.000	7.9
	2/5/1998	11.769	
	2/29/2000	5.795	
371645-3	6/27/2002	0.000	9.5
	4/11/2005	0.000	
	11/30/2007	1.202	
371801	1/26/1996	0.000	7.2
	7/25/1996	0.000	
371801-2	4/28/1998	0.000	9.6
	5/18/2000	0.000	
	3/12/2003	0.000	
371802	4/15/1994	25.349	4.4
	7/18/1995	30.157	
	4/2/1996	46.895	
371802-3	12/11/1996	8.414	5.4
	10/10/1997	0.520	
	1/15/2002	57.049	
1803-2	4/22/1996	0.861	6.9
	4/7/1999	24.362	
371803-3	11/14/2001	9.831	8.4
	1/28/2003	7.947	
	11/9/2007	29.493	
371814	1/30/1996	0.556	5.1
	4/1/1999	4.664	
	6/26/2000	14.854	

Appendix A5 (Continued)

371814-2	10/12/2000	0.000	8.1
	6/7/2005	14.962	
	11/13/2007	25.762	
371817	8/30/1990	22.084	4.6
371817-4	12/15/1995	0.000	5.9
	4/27/1999	0.000	
	3/13/2002	0.000	
371817-5	2/5/2003	0.000	10.6
	2/5/2008	15.213	
371992	4/20/1994	0.000	2.4
1992-2	4/22/1998	0.000	7.2
	5/16/2000	0.000	
	3/6/2003	0.000	
	11/29/2007	2.225	
372819	4/13/1992	0.000	5.1
372819-2	8/13/1997	0.000	6.6
	8/30/2000	0.000	
	3/28/2002	0.000	
372819-3	2/6/2003	0.000	7.6
	2/6/2008	0.323	
372824-2	8/14/1997	0.000	6.9
	12/2/1999	0.000	
	8/31/2000	0.090	
	3/27/2003	1.023	
372824-3	3/24/2004	0.000	8.8
	2/7/2008	0.000	
372825	7/19/1995	11.464	4.6
	11/17/1998	25.564	
	2/14/2001	30.282	
	3/23/2004	31.197	
	11/7/2007	31.610	

Appendix A6 Summary of Measured Alligator Cracking and Total Rut Depth for PMS Validation Sections

PMS Site ID	Survey Date	Measured Alligator Cracking (% Lane Area)	Measured Total Rut (inch)
EB, R-2000BB	6/1/1997	0.00	0.000
	6/1/2000	0.00	0.000
	6/1/2001	0.00	0.000
	6/1/2002	0.00	0.000
	6/1/2003	7.40	0.000
	6/1/2004	7.40	0.000
	6/1/2005	7.40	0.000
	6/1/2006	0.00	0.000
WB, R-2000BB	6/1/1997	0.00	0.000
	6/1/1998	0.00	0.000
	6/1/2000	0.00	0.000
	6/1/2001	0.00	0.000
	6/1/2002	0.00	0.000
	6/1/2003	7.40	0.000
	6/1/2004	7.40	0.000
	6/1/2005	7.40	0.000
	6/1/2006	7.40	0.250
WB, R-2318B	1/1/1996	0.00	0.250
	1/1/1998	0.00	0.250
	1/1/2000	0.00	0.250
	1/1/2002	22.20	0.000
	1/1/2004	22.20	0.000
	1/1/2006	17.60	0.250
	1/1/2008	24.40	0.417
	1/1/2010	25.00	0.250
NB, U-508CB	1/1/1996	0.00	0.000
	1/1/1998	0.00	0.000
	1/1/2000	0.00	0.000
	1/1/2002	0.00	0.000
	1/1/2004	0.00	0.000
	1/1/2006	22.20	0.000

Appendix A6 (Continued)

SB, U-508CB	1/1/1996	0.00	0.000
	1/1/1998	0.00	0.000
	1/1/2000	0.00	0.000
	1/1/2002	0.00	0.000
	1/1/2004	0.00	0.000
	1/1/2006	14.80	0.000
	1/1/2008	7.40	0.000
	1/1/2010	22.20	0.000
NB, U-77LA	1/1/2000	0.00	0.000
	1/1/2002	4.16	0.000
	1/1/2004	7.40	0.000
	1/1/2006	7.40	0.000
	1/1/2008	14.80	0.000
	1/1/2010	17.60	0.250
SB, U-77LA	1/1/2000	0.00	0.000
	1/1/2002	4.16	0.000
	1/1/2004	7.40	0.000
	1/1/2006	7.40	0.000
EB, R-1017AC	1/1/1994	5.26	0.250
	1/1/1996	0.00	0.000
	1/1/1998	0.00	0.250
	1/1/2000	7.40	0.250
	1/1/2002	0.00	0.000
	1/1/2004	7.40	0.000
	1/1/2006	0.00	0.000
	1/1/2008	10.90	0.000
	1/1/2010	0.00	0.000
NB, R-85AD	1/1/2002	0.00	0.000
	1/1/2004	0.00	0.000
	1/1/2006	0.00	0.000
	1/1/2008	7.40	0.000
	1/1/2010	0.00	0.000
SB, R-85AD	1/1/2002	0.00	0.000
	1/1/2004	0.00	0.000
	1/1/2006	0.00	0.000

Appendix A6 (Continued)

NB, R-2120AA	1/1/2004	0.00	0.000
	1/1/2006	0.00	0.000
	1/1/2008	0.00	0.000
	1/1/2010	7.40	0.250
SB, R-2120AA	1/1/2004	0.00	0.000
	1/1/2006	0.00	0.000
NB, R-2120AB	1/1/2004	0.00	0.000
	1/1/2006	0.00	0.000
SB, R-2120AB	1/1/2004	0.00	0.000
	1/1/2006	0.00	0.000
	1/1/2008	7.40	0.000
	1/1/2010	14.80	0.250
NB-Outer, R-2123AC	6/1/2004	0.00	0.000
	6/1/2005	0.00	0.000
	6/1/2006	0.00	0.000
SB-Inner, R-2123AC	6/1/2004	0.00	0.000
	6/1/2005	0.00	0.000
	6/1/2006	0.00	0.000
NB-Outer, R-2123CC	6/1/2004	0.00	0.000
	6/1/2005	0.00	0.000
	6/1/2006	0.00	0.000
SB-Inner, R-2123CC	6/1/2004	2.80	0.000
	6/1/2005	7.40	0.000
	6/1/2006	7.40	0.000
EB, R-2219AC	1/1/2002	0.00	0.00
	1/1/2004	0.00	0.00
	1/1/2006	0.00	0.00
	1/1/2008	0.00	0.00
	1/1/2010	0.00	0.00
WB, R-2219AC	1/1/2002	0.00	0.00
	1/1/2004	0.00	0.00
	1/1/2006	0.00	0.00
EB, R-2217B	1/1/2004	0.00	0.00
	1/1/2006	0.00	0.00
	1/1/2008	0.00	0.00
	1/1/2010	0.00	0.00

Appendix A6 (Continued)

WB, R-2217B	1/1/2004	0.00	0.00
	1/1/2006	0.00	0.00
EB, R-1023B	1/1/2004	0.00	0.000
	1/1/2006	7.40	0.000
WB, R-1023B	1/1/2004	0.00	0.000
	1/1/2006	7.40	0.000
EB/Inner, R-2000EA	6/1/2003	0.00	0.000
	6/1/2004	0.00	0.000
	6/1/2005	0.00	0.000
	6/1/2006	0.00	0.000
WB/Outer, R-2000EA	6/1/2003	0.00	0.000
	6/1/2004	0.00	0.000
	6/1/2005	0.00	0.000
	6/1/2006	0.00	0.000
EB/Inner, R-2000EB	6/1/2003	0.00	0.000
	6/1/2004	0.00	0.000
	6/1/2005	0.00	0.000
	6/1/2006	0.00	0.000
WB/Outer, R-2000EB	6/1/2003	0.00	0.000
	6/1/2004	0.00	0.000
	6/1/2005	0.00	0.000
	6/1/2006	0.00	0.000

Appendix A7 Summary of Geographic Coordinates and Depth of Water Table for Calibration and Validation Sections

Section ID	Start			End			Depth of Water Table (ft)	County
	Latitude	Longitude	Elevation (ft)	Latitude	Longitude	Elevation (ft)		
371006	35.7822	-78.7490	438	35.7837	78.7491	449	18.5	Wake
371024	35.2961	-83.1801	2129	35.2948	83.1796	2135	45	Jackson
371028	36.5298	-76.3665	17	36.5285	76.3658	19	2.4	Camden
371030	36.3817	-76.3128	15	36.3807	76.3118	16	4.9	Pasquotank
371040	35.9135	-82.0626	2566	35.9146	82.0616	2571	30.0	Mitchell
371352	35.4461	-80.2291	700	35.4454	80.2277	695	26.7	Stanly
371645	34.3479	-78.6485	72	34.3482	78.6501	70	29.7	Columbus
371801	35.5926	-82.4240	2276	35.5930	82.4224	2280	24.2	Buncombe
371802	36.3162	-78.6152	496	36.3151	78.6142	495	18.0	Granville
371803	35.3895	-83.2944	1901	35.3907	83.2953	1898	22.5	Jackson
371814	35.1698	-83.3663	2042	35.1688	83.3675	2058	30.2	Macon
371817	36.0548	-80.1515	842	36.0547	80.1498	846	33.3	Forsyth
371992	35.7454	-79.4413	589	35.7446	79.4399	585	23.7	Chatham
372819	35.9344	-79.8278	802	35.9331	79.8279	795	25.3	Randolph
372824	35.7059	-79.4291	636	35.7045	79.4290	631	22.3	Chatham
372825	35.1421	-80.9167	598	35.1428	80.9182	618	7.1	Mecklenburg
370801	34.8069	-77.6639	76	34.8083	77.6637	70	184.3	Onslow
370802	34.8088	-77.6635	69	34.8101	77.6631	61	184.3	Onslow
370859	34.8115	-77.6642	62	34.8117	77.6659	64	184.3	Onslow
370901	35.5428	-79.1698	287	35.5438	79.1686	284	25.4	Lee
370902	35.5508	-79.1614	283	35.5519	79.1605	276	25.4	Lee
370903	35.5387	-79.1742	296	35.5398	79.1730	296	25.4	Lee
R2120AA	36.1196	-80.8054	1069	36.1183	80.7235	882	26.5	Yadkin
R2120AB	36.1183	-80.7235	882	36.1190	80.6626	906	28.2	Yadkin
R2123AC	35.1792	-80.6292	747	35.2167	80.6469	738	18.4	Mechlenburg
R2123BB	35.2342	-80.6534	653	35.2684	80.6703	669	18.5	Mechlenburg
R2123CC	35.2798	-80.6729	707	35.3119	80.7070	679	18.1	Mechlenburg
R2219AC	35.7296	-79.2521	460	35.7446	79.1603	510	23.8	Chatham
R2217B	35.7436	-79.5786	655	35.7336	79.4792	702	39.4	Randolph
R1023AB	35.7270	-78.0083	136	35.6764	77.9398	94	15.0	Wilson
R1023B	35.6764	-77.9398	94	35.6796	77.8453	80	11.4	Wilson
R2000EA	35.8996	-78.6208	412	35.8828	78.5904	294	88.9	Wake

Appendix A7 (Continued)

R2000EB	35.8828	-78.5904	294	35.8724	78.5634	249	99.9	Wake
R2001C	35.1537	-77.7043	91	35.2251	77.6424	75	61.2	Lenoir
R2000BB	35.8811	-78.8236	359	35.8945	78.7964	352	47.2	Wake
U77LA	36.0297	-78.9625	481	36.0170	78.9524	425	21.3	Durham
R2318B	35.7482	-78.8752	323	35.7489	78.8459	490	27.4	Wake
U508CB	35.0241	-78.8723	100	35.0037	78.8665	87	27.1	Cumberland
U2413B	36.0307	-79.9635	886	36.0472	79.9225	870	21.2	Guilford
U508CA	35.0368	-78.8827	105	35.0241	78.8723	100	27.1	Cumberland
R1017AC	35.8552	-81.0442	1057	35.8018	80.9428	965	34.7	Iredell
R2232A	36.3784	-79.9412	647	36.4600	79.9261	695	46.1	Rockingham
R2232B	36.4600	-79.9261	695	36.5323	79.9138	995	46.1	Rockingham
R2211BA	34.9639	-77.9474	121	34.9348	77.8468	79	13.0	Duplin
R519	35.2571	-81.5639	824	35.2720	81.5400	790	12.5	Cleveland
R85AD	35.5315	-81.2246	911	35.5557	81.2440	822	20.2	Lincoln

Appendix B   Dynamic Modulus (|E*|) Database

Appendix B1 Summary of Dynamic Modulus Data for Popular Asphalt Concrete Mixtures in North Carolina

Mix ID	Temp. (°F)	|E*| (psi)					
		0.1 Hz	0.5 Hz	1 Hz	5 Hz	10 Hz	25 Hz
S9.5A	14	3,179,855	3,601,671	3,763,157	4,089,808	4,210,292	4,352,114
	40	1,471,473	1,968,367	2,190,486	2,701,885	2,913,534	3,180,038
	70	324,882	539,393	660,249	1,010,286	1,189,285	1,447,937
	100	62,797	109,193	139,235	243,781	308,188	415,665
	130	19,817	30,738	37,856	63,720	80,726	111,134
S9.5B	14	2,899,388	3,299,058	3,450,426	3,753,103	3,863,378	3,992,102
	40	1,331,997	1,811,959	2,026,158	2,515,590	2,715,931	2,965,832
	70	288,772	492,081	608,736	950,779	1,126,667	1,380,661
	100	57,431	100,916	129,578	231,313	295,013	402,352
	130	19,139	29,463	36,289	61,535	78,414	108,968
S9.5C	14	3,477,881	3,841,349	3,978,499	4,253,698	4,354,765	4,473,690
	40	1,915,519	2,416,838	2,629,637	3,099,006	3,286,307	3,517,430
	70	548,155	851,110	1,009,796	1,435,346	1,637,966	1,917,046
	100	116,295	200,761	253,085	424,099	522,833	679,183
	130	32,804	53,196	66,459	113,843	144,196	196,949
S12.5B	14	3,178,414	3,586,118	3,739,780	4,046,213	4,157,675	4,287,727
	40	1,452,961	1,964,701	2,191,357	2,706,541	2,916,672	3,178,440
	70	307,341	531,349	659,089	1,030,335	1,219,596	1,491,335
	100	58,842	109,831	143,798	264,458	339,549	464,961
	130	18,682	32,139	41,344	76,329	100,049	143,076
S12.5C	14	3,340,219	3,700,879	3,837,932	4,114,968	4,217,531	4,338,902
	40	1,851,067	2,331,465	2,535,961	2,988,577	3,169,989	3,394,700
	70	561,247	849,585	1,000,516	1,405,293	1,598,028	1,863,503
	100	141,662	224,805	275,254	437,969	531,270	678,717
	130	51,511	73,340	86,887	133,214	161,962	211,080
S12.5D	14	3,739,485	4,152,910	4,313,858	4,647,005	4,773,395	4,925,452
	40	2,066,922	2,578,282	2,799,001	3,297,101	3,501,255	3,758,382
	70	641,318	955,516	1,116,352	1,542,608	1,745,059	2,025,161
	100	141,206	239,633	298,200	481,749	584,142	743,059
	130	33,509	57,493	72,870	126,352	159,616	216,050
I19.0B	14	3,516,178	3,903,750	4,045,263	4,319,631	4,416,711	4,528,028
	40	1,761,953	2,331,003	2,573,455	3,102,926	3,310,402	3,562,090
	70	398,660	678,231	836,324	1,286,905	1,510,664	1,824,379
	100	85,424	146,350	186,846	331,286	421,602	572,740
	130	33,955	49,287	59,464	97,304	122,704	168,762

Appendix B1 (Continued)

I19.0C	14	2,687,128	3,190,620	3,396,983	3,839,790	4,012,382	4,222,536
	40	1,292,943	1,756,971	1,973,450	2,494,634	2,720,108	3,012,654
	70	337,491	540,185	653,306	981,402	1,150,628	1,397,794
	100	69,380	116,300	145,516	243,427	302,122	398,769
	130	18,774	28,708	34,962	56,666	70,324	93,956
I19.0D	14	3,732,648	4,127,058	4,276,441	4,576,884	4,687,380	4,817,439
	40	2,090,704	2,622,913	2,849,303	3,350,128	3,550,608	3,798,493
	70	627,698	958,895	1,130,474	1,587,023	1,803,342	2,100,782
	100	136,257	233,058	292,170	482,360	590,704	760,845
	130	36,807	59,968	74,913	127,697	161,124	218,706
B25.0B	14	3,650,444	4,020,452	4,155,821	4,419,026	4,512,461	4,619,839
	40	1,944,851	2,505,635	2,741,078	3,251,255	3,450,356	3,691,698
	70	484,380	806,122	980,709	1,458,624	1,688,168	2,003,978
	100	94,819	172,359	223,463	401,314	509,155	684,735
	130	30,392	48,917	61,491	109,004	141,091	199,100
B25.0C	14	3,634,329	4,064,777	4,223,683	4,535,081	4,646,578	4,775,552
	40	1,751,551	2,341,438	2,598,012	3,167,991	3,394,699	3,672,163
	70	392,383	655,843	806,164	1,243,391	1,465,658	1,782,844
	100	79,950	137,614	175,094	306,900	389,089	527,423
	130	26,235	40,078	49,126	82,174	104,067	143,532
RS9.5A	14	2,652,862	2,938,077	3,043,194	3,248,638	3,321,872	3,406,206
	40	1,335,698	1,742,148	1,917,017	2,303,982	2,457,826	2,646,312
	70	323,879	525,164	636,486	950,654	1,106,696	1,326,855
	100	74,396	123,046	154,024	259,781	323,709	428,679
	130	28,873	42,180	50,680	80,856	100,284	134,453
RS9.5B	14	2,994,001	3,295,937	3,408,431	3,631,035	3,711,516	3,805,146
	40	1,631,285	2,060,809	2,243,381	2,645,422	2,805,211	3,001,505
	70	467,391	715,439	846,604	1,202,304	1,373,449	1,610,725
	100	115,248	184,433	226,695	364,161	443,673	570,244
	130	42,367	61,224	72,961	113,264	138,370	181,385
RS9.5C	14	3,076,920	3,348,575	3,447,891	3,641,252	3,710,078	3,789,381
	40	1,784,319	2,214,005	2,391,607	2,772,542	2,920,152	3,098,577
	70	542,946	826,221	972,886	1,359,879	1,540,724	1,786,023
	100	134,092	217,396	268,328	432,943	527,062	674,956
	130	48,675	71,277	85,499	134,786	165,655	218,591

Appendix B1 (Continued)

RI19.0B	14	3,295,213	3,616,694	3,735,321	3,968,100	4,051,584	4,148,228
	40	1,810,157	2,289,367	2,490,990	2,930,009	3,102,462	3,312,643
	70	518,508	804,845	956,408	1,365,502	1,560,713	1,829,143
	100	130,213	212,930	264,011	431,275	528,177	682,015
	130	49,848	73,991	89,288	142,681	176,313	234,205
RI19.0C	14	3,369,350	3,637,481	3,734,781	3,923,087	3,989,741	4,066,284
	40	2,065,381	2,513,600	2,695,550	3,080,064	3,227,100	3,403,450
	70	685,031	1,020,556	1,189,208	1,621,306	1,817,882	2,079,961
	100	169,710	279,048	344,847	552,396	667,988	845,847
	130	56,206	85,941	104,757	169,925	210,484	279,401
RB25.0B	14	3,543,504	3,834,812	3,937,512	4,130,374	4,196,413	4,270,517
	40	2,055,852	2,573,375	2,783,651	3,223,782	3,389,326	3,584,872
	70	581,526	911,190	1,086,270	1,555,770	1,776,690	2,075,807
	100	141,975	226,810	280,188	459,151	565,053	735,463
	130	57,972	79,657	93,363	141,518	172,259	226,015
RB25.0C	14	3,045,763	3,285,924	3,368,299	3,518,942	3,569,082	3,624,287
	40	1,775,014	2,238,695	2,423,937	2,803,199	2,942,207	3,103,301
	70	489,990	790,201	951,598	1,384,941	1,587,373	1,858,502
	100	121,781	198,475	247,940	417,632	519,581	684,498
	130	52,846	73,271	86,496	134,265	165,497	220,972

Appendix C Complex Shear Modulus (G*) Database

Appendix C1 Summary of Complex Shear Modulus Database for Popular Asphalt Binders in North Carolina

Binder Grade	Temperature (°F)	|G*| (Pa)	Phase Angle (degree)
PG64-22	50.0	15,600,000	36.8
	77.0	1,668,000	58.2
	104.0	144,000	68.6
	147.2	4,500	82.4
PG70-22	50.0	17,800,000	33.5
	77.0	2,175,000	54.5
	104.0	211,750	64.1
	140.0	13,700	75.5
	158.0	3,843	81.0
PG76-22	50.0	24,582,328	42.5
	66.2	6,146,101	50.3
	86.0	1,118,810	57.9
	104.0	245,433	61.5
	122.0	63,015	63.9
	140.0	19,482	63.6
	158.0	6,403	66.2
	168.8	3,529	66.7

Appendix D Permanent Deformation (Rutting) Database

Appendix D1 Summary of Mean TRLPD Test Results at 20°, 40°, and 54°C for the Most Commonly Used Asphalt Concrete Mixtures in North Carolina

(Test Conditions: 10 psi Confining Pressure, 70 psi Deviatoric Stress, 5.5 ± 0.5 % Air Voids)

S9.5B								
20°C			40°C			54°C		
Cycles	ε_p	$\varepsilon_p/\varepsilon_r$	Cycles	ε_p	$\varepsilon_p/\varepsilon_r$	Cycles	ε_p	$\varepsilon_p/\varepsilon_r$
2.4	0.000019	0.26	2.1	0.000195	0.59	2.3	0.001508	1.88
4.4	0.000028	0.43	4.1	0.000422	1.07	4.3	0.002273	2.64
9.4	0.000040	0.71	9.1	0.000796	1.92	9.3	0.003366	3.88
19.4	0.000056	0.63	19.1	0.001291	3.05	17.6	0.004381	5.15
29.4	0.000068	0.71	29.1	0.001645	3.91	29.3	0.005224	6.18
39.4	0.000077	0.77	39.1	0.001919	4.55	39.3	0.005745	6.83
49.4	0.000090	0.95	49.1	0.002148	5.06	49.3	0.006152	7.36
59.4	0.000097	0.98	59.1	0.002345	5.60	59.3	0.006491	7.79
69.4	0.000105	1.09	69.1	0.002517	6.03	69.3	0.006784	8.14
79.4	0.000112	1.18	79.2	0.002666	6.36	79.3	0.007038	8.46
89.4	0.000119	1.22	89.2	0.002801	6.68	89.3	0.007267	8.76
99.4	0.000127	1.35	99.2	0.002927	6.99	99.3	0.007472	8.99
109.4	0.000132	1.40	109.2	0.003039	7.29	109.3	0.007661	9.23
119.4	0.000136	1.42	119.2	0.003141	7.52	119.3	0.007835	9.45
129.4	0.000145	1.50	129.2	0.003234	7.66	129.3	0.007994	9.60
139.4	0.000149	1.53	139.2	0.003326	7.99	139.3	0.008144	9.79
148.5	0.000151	1.57	149.2	0.003408	8.13	148.7	0.008276	9.94
159.5	0.000156	1.59	159.2	0.003486	8.36	159.4	0.008418	10.10
169.5	0.000163	1.69	169.2	0.003559	8.52	169.4	0.008546	10.24
179.5	0.000167	1.71	179.2	0.003625	8.60	179.4	0.008662	10.34
189.5	0.000173	1.79	189.2	0.003692	8.81	189.4	0.008776	10.49
199.5	0.000178	1.88	199.2	0.003755	8.96	199.4	0.008884	10.61
209.5	0.000182	1.92	209.2	0.003814	9.05	209.4	0.008988	10.72
219.5	0.000188	1.95	219.2	0.003869	9.20	219.4	0.009086	10.81
229.5	0.000190	1.90	229.2	0.003923	9.31	229.4	0.009182	10.95

Appendix D1 – S9.5B (Continued)

239.5	0.000195	1.98	239.2	0.003976	9.45	239.4	0.009275	11.07
249.5	0.000199	2.05	249.2	0.004027	9.61	249.4	0.009363	11.16
259.5	0.000204	2.12	259.2	0.004074	9.69	259.4	0.009446	11.21
269.5	0.000204	2.05	269.2	0.004117	9.78	269.4	0.009528	11.28
279.5	0.000215	2.32	279.2	0.004161	9.85	279.1	0.009605	11.38
289.5	0.000212	2.14	289.2	0.004202	9.98	289.4	0.009684	11.47
299.5	0.000219	2.24	299.2	0.004244	10.08	299.4	0.009762	11.58
309.5	0.000219	2.23	309.2	0.004282	10.12	309.4	0.009830	11.61
319.5	0.000225	2.31	319.2	0.004322	10.28	319.4	0.009904	11.72
329.5	0.000227	2.30	329.2	0.004361	10.37	329.4	0.009971	11.78
339.5	0.000233	2.48	339.2	0.004395	10.39	339.4	0.010041	11.91
349.5	0.000236	2.47	349.2	0.004431	10.50	349.4	0.010105	11.98
359.5	0.000239	2.48	359.2	0.004465	10.57	359.4	0.010166	11.98
369.5	0.000243	2.51	369.2	0.004500	10.70	369.4	0.010229	12.09
379.5	0.000244	2.57	379.2	0.004529	10.73	379.1	0.010288	12.14
389.5	0.000249	2.55	389.2	0.004559	10.80	389.1	0.010348	12.23
399.5	0.000253	2.67	399.3	0.004594	10.90	399.1	0.010404	12.29
409.5	0.000254	2.56	409.3	0.004621	10.93	409.1	0.010459	12.31
419.5	0.000258	2.65	419.3	0.004651	10.98	419.1	0.010514	12.36
429.5	0.000262	2.74	429.3	0.004677	11.04	429.1	0.010569	12.41
439.5	0.000264	2.70	439.3	0.004702	11.04	439.1	0.010622	12.53
449.5	0.000268	2.74	449.3	0.004733	11.18	449.1	0.010673	12.57
459.5	0.000271	2.79	459.3	0.004756	11.16	459.1	0.010724	12.62
469.6	0.000274	2.85	469.3	0.004784	11.30	469.1	0.010772	12.62
479.6	0.000278	2.90	479.3	0.004807	11.31	479.1	0.010822	12.71
489.6	0.000280	2.96	489.3	0.004831	11.32	489.1	0.010870	12.76
499.6	0.000284	3.00	499.3	0.004854	11.38	499.1	0.010915	12.76
599.6	0.000310	3.21	599.3	0.005075	12.03	599.1	0.011345	13.28
699.1	0.000335	3.38	699.3	0.005252	12.30	699.2	0.011712	13.60
799.2	0.000361	3.77	799.4	0.005409	12.62	799.2	0.012034	13.89
899.2	0.000381	3.87	899.4	0.005544	12.95	899.2	0.012322	14.21

Appendix D1 – S9.5B (Continued)

999.2	0.000401	4.08	999.4	0.005665	13.19	999.3	0.012581	14.48
1099.2	0.000420	4.22	1099.5	0.005774	13.32	1099.3	0.012815	14.71
1199.3	0.000440	4.52	1199.5	0.005868	13.50	1199.3	0.013030	14.94
1299.3	0.000458	4.65	1299.5	0.005954	13.57	1299.3	0.013228	15.08
1399.3	0.000476	4.81	1399.5	0.006039	13.87	1399.4	0.013414	15.31
1499.4	0.000494	5.02	1499.6	0.006116	13.92	1499.4	0.013585	15.39
1599.4	0.000508	5.17	1599.6	0.006186	14.07	1599.4	0.013748	15.59
1699.4	0.000527	5.48	1699.6	0.006253	14.22	1699.5	0.013903	15.73
1799.4	0.000541	5.49	1799.7	0.006315	14.45	1799.5	0.014045	15.87
1899.5	0.000553	5.57	1899.7	0.006373	14.46	1899.5	0.014184	16.03
1999.5	0.000571	5.86	1999.7	0.006428	14.48	1999.6	0.014311	16.11
2099.5	0.000583	6.02	2099.7	0.006482	14.70	2099.6	0.014436	16.20
2199.6	0.000598	6.16	2199.8	0.006534	14.82	2199.6	0.014551	16.31
2299.6	0.000609	6.23	2299.8	0.006578	14.79	2299.6	0.014664	16.41
2399.6	0.000622	6.37	2399.8	0.006625	14.97	2399.7	0.014771	16.50
2499.1	0.000633	6.30	2499.4	0.006667	15.01	2498.7	0.014874	16.63
2599.7	0.000648	6.48	2599.4	0.006709	15.04	2599.7	0.014976	16.73
2699.7	0.000662	6.96	2699.4	0.006748	15.15	2699.8	0.015071	16.77
2799.7	0.000675	6.97	2799.4	0.006789	15.10	2799.8	0.015162	16.84
2899.8	0.000686	6.97	2899.5	0.006829	15.35	2899.8	0.015253	16.97
2999.8	0.000695	6.90	2999.5	0.006865	15.31	2999.8	0.015340	17.02
3099.8	0.000707	7.12	3099.5	0.006899	15.44	3099.9	0.015423	17.14
3199.9	0.000714	7.16	3199.6	0.006932	15.44	3199.9	0.015505	17.20
3299.9	0.000727	7.58	3299.6	0.006966	15.57	3299.9	0.015581	17.25
3399.4	0.000736	7.45	3399.6	0.006998	15.60	3399.3	0.015655	17.30
3499.4	0.000747	7.61	3499.2	0.007028	15.60	3499.3	0.015729	17.36
3599.5	0.000757	7.81	3599.2	0.007059	15.70	3599.4	0.015800	17.46
3699.5	0.000763	7.38	3699.2	0.007087	15.63	3699.4	0.015873	17.55
3799.5	0.000777	7.96	3799.2	0.007114	15.70	3799.4	0.015940	17.60
3899.6	0.000785	8.01	3899.3	0.007141	15.76	3899.1	0.016004	17.61
3999.6	0.000795	8.41	3999.3	0.007169	15.78	3999.1	0.016067	17.67

Appendix D1 – S9.5B (Continued)

4099.1	0.000804	7.99	4099.3	0.007197	15.91	4099.2	0.016130	17.74
4199.1	0.000813	8.16	4199.4	0.007221	15.96	4199.2	0.016192	17.83
4299.2	0.000820	8.18	4299.4	0.007243	15.93	4299.2	0.016248	17.82
4399.2	0.000831	8.64	4399.4	0.007268	16.00	4399.3	0.016306	17.90
4499.2	0.000839	8.57	4499.4	0.007289	15.96	4499.3	0.016360	17.94
4599.3	0.000846	8.74	4599.5	0.007317	16.13	4599.3	0.016416	18.02
4699.3	0.000855	8.77	4699.5	0.007337	16.03	4699.3	0.016469	17.99
4799.3	0.000863	8.84	4799.5	0.007358	16.11	4799.4	0.016523	18.08
4899.3	0.000870	8.79	4899.6	0.007381	16.16	4899.4	0.016575	18.13
4999.4	0.000878	8.58	4999.6	0.007402	16.14	4999.4	0.016625	18.19
5099.4	0.000886	8.84	5099.6	0.007423	16.19	5099.5	0.016674	18.25
5199.4	0.000894	8.91	5199.6	0.007446	16.26	5199.5	0.016722	18.25
5299.5	0.000904	9.42	5299.7	0.007466	16.35	5299.5	0.016770	18.28
5399.5	0.000911	9.21	5399.7	0.007486	16.39	5399.5	0.016815	18.30
5499.5	0.000919	9.50	5499.7	0.007503	16.25	5499.6	0.016860	18.37
5599.6	0.000927	9.38	5599.8	0.007524	16.47	5599.6	0.016906	18.41
5699.6	0.000934	9.64	5699.8	0.007545	16.46	5699.6	0.016951	18.44
5799.6	0.000941	10.05	5799.8	0.007564	16.56	5799.7	0.016993	18.49
5899.6	0.000947	9.83	5899.9	0.007584	16.54	5899.7	0.017035	18.51
5999.7	0.000953	9.58	5999.4	0.007600	16.49	5999.7	0.017076	18.53
6099.7	0.000957	9.31	6099.4	0.007616	16.53	6099.8	0.017116	18.55
6199.7	0.000965	9.72	6199.4	0.007633	16.52	6199.8	0.017159	18.60
6299.8	0.000971	9.71	6299.5	0.007651	16.47	6299.8	0.017197	18.62
6399.8	0.000980	9.86	6399.5	0.007667	16.58	6399.8	0.017239	18.73
6499.8	0.000986	10.28	6499.5	0.007685	16.63	6499.9	0.017274	18.69
6599.8	0.000992	10.09	6599.6	0.007699	16.57	6599.9	0.017312	18.74
6699.9	0.000998	10.25	6699.6	0.007716	16.56	6699.9	0.017348	18.74
6799.9	0.001006	10.41	6799.6	0.007730	16.60	6800.0	0.017385	18.76
6899.4	0.001012	10.56	6899.1	0.007746	16.55	6899.3	0.017420	18.78
6999.5	0.001014	10.15	6999.2	0.007760	16.58	6999.3	0.017457	18.87
7099.5	0.001024	10.77	7099.2	0.007775	16.62	7099.4	0.017494	18.87

Appendix D1 – S9.5B (Continued)

7199.0	0.001030	10.68	7199.2	0.007793	16.73	7198.7	0.017528	18.94
7299.5	0.001035	10.70	7299.3	0.007805	16.68	7299.1	0.017562	18.97
7399.6	0.001039	10.65	7399.3	0.007823	16.74	7399.1	0.017596	18.91
7499.1	0.001047	10.68	7499.3	0.007834	16.67	7499.2	0.017630	19.02
7599.1	0.001052	10.55	7599.3	0.007852	16.81	7599.2	0.017663	19.04
7699.2	0.001060	10.79	7699.4	0.007865	16.79	7699.2	0.017694	19.08
7799.2	0.001062	10.71	7799.4	0.007876	16.77	7799.2	0.017725	19.09
7899.2	0.001069	11.24	7899.4	0.007890	16.88	7899.3	0.017756	19.12
7999.3	0.001073	11.06	7999.5	0.007903	16.87	7999.3	0.017786	19.16
8099.3	0.001080	11.09	8099.5	0.007916	16.82	8099.3	0.017815	19.14
8199.3	0.001087	11.43	8199.5	0.007934	16.91	8199.4	0.017844	19.16
8299.3	0.001089	11.14	8299.6	0.007948	16.98	8299.4	0.017875	19.18
8399.4	0.001095	11.10	8399.6	0.007960	16.99	8399.4	0.017905	19.24
8499.4	0.001100	11.38	8499.6	0.007974	17.02	8499.5	0.017934	19.30
8599.4	0.001106	11.48	8599.6	0.007988	17.05	8599.5	0.017962	19.27
8699.5	0.001112	11.24	8699.7	0.007998	17.03	8699.5	0.017990	19.30
8799.5	0.001117	11.58	8799.7	0.008010	16.97	8799.5	0.018015	19.35
8899.5	0.001120	11.14	8899.7	0.008025	17.10	8899.6	0.018042	19.35
8999.5	0.001124	11.17	8999.8	0.008036	17.04	8999.6	0.018068	19.35
9099.6	0.001131	11.44	9099.8	0.008049	17.11	9099.6	0.018096	19.41
9199.6	0.001135	11.03	9199.8	0.008059	17.11	9199.7	0.018121	19.45
9299.6	0.001141	11.46	9299.8	0.008069	17.06	9299.7	0.018147	19.43
9399.7	0.001145	11.58	9399.9	0.008082	17.12	9399.7	0.018172	19.44
9499.7	0.001155	11.93	9499.4	0.008093	17.08	9499.7	0.018198	19.48
9599.7	0.001158	12.36	9599.4	0.008104	17.16	9599.8	0.018223	19.50
9699.7	0.001161	12.08	9699.5	0.008117	17.21	9699.8	0.018249	19.53
9799.8	0.001167	12.20	9799.5	0.008127	17.14	9799.8	0.018272	19.55
9899.8	0.001170	11.92	9899.5	0.008138	17.22	9899.9	0.018298	19.60
9999.8	0.001176	12.11	9999.5	0.008149	17.10	9999.9	0.018321	19.59
10099.9	0.001181	12.09	10099.6	0.008160	17.29	10099.9	0.018342	19.61
10199.9	0.001186	12.56	10199.6	0.008171	17.24	10200.0	0.018367	19.65

Appendix D1 – S9.5B (Continued)

10299.4	0.001190	12.45	10299.1	0.008183	17.36	10299.3	0.018389	19.68
10399.5	0.001192	12.07	10399.2	0.008194	17.38	10399.3	0.018412	19.64
10499.5	0.001202	12.63	10499.2	0.008203	17.26	10499.4	0.018436	19.73
10599.5	0.001206	12.68	10599.2	0.008213	17.32	10599.4	0.018457	19.72
10699.5	0.001207	12.42	10699.2	0.008223	17.33	10699.1	0.018478	19.73
10799.6	0.001212	12.31	10799.3	0.008231	17.17	10799.1	0.018504	19.78
10899.6	0.001216	12.42	10899.3	0.008243	17.37	10899.2	0.018526	19.80
10999.1	0.001222	12.76	10999.3	0.008252	17.33	10999.2	0.018546	19.74
11099.2	0.001224	12.83	11099.4	0.008261	17.24	11099.2	0.018569	19.81
11199.2	0.001231	12.92	11199.4	0.008270	17.39	11199.2	0.018590	19.84
11299.2	0.001233	12.60	11299.4	0.008280	17.32	11299.3	0.018612	19.90
11399.2	0.001237	12.59	11399.5	0.008290	17.43	11399.3	0.018632	19.91
11499.3	0.001241	12.69	11499.5	0.008300	17.34	11499.3	0.018652	19.92
11599.3	0.001246	13.21	11599.5	0.008310	17.52	11599.4	0.018671	19.95
11699.3	0.001251	13.44	11699.5	0.008319	17.35	11699.4	0.018687	19.96
11799.4	0.001252	12.55	11799.6	0.008329	17.39	11799.4	0.018707	19.98
11898.9	0.001258	13.20	11899.6	0.008337	17.40	11899.1	0.018724	19.95
11999.4	0.001261	12.94	11999.6	0.008347	17.42	11999.5	0.018747	19.98

S9.5C								
20°C			40°C			54°C		
Cycles	ε_p	$\varepsilon_p/\varepsilon_r$	Cycles	ε_p	$\varepsilon_p/\varepsilon_r$	Cycles	ε_p	$\varepsilon_p/\varepsilon_r$
2.0	0.000013	0.26	2.0	0.000195	0.65	2.5	0.000661	1.15
4.0	0.000018	0.34	4.0	0.000304	0.96	4.5	0.000977	1.58
7.0	0.000026	0.32	9.0	0.000501	1.50	9.5	0.001454	2.28
18.5	0.000041	0.63	18.0	0.000734	2.17	18.5	0.001943	3.05
26.5	0.000053	0.60	29.0	0.000936	2.74	29.5	0.002307	3.62
38.5	0.000064	0.70	39.0	0.001075	3.17	39.5	0.002540	3.99
47.0	0.000074	0.83	49.0	0.001186	3.49	49.5	0.002727	4.27
58.0	0.000075	0.80	59.0	0.001279	3.77	59.5	0.002883	4.51
67.0	0.000082	0.91	69.0	0.001358	3.94	69.5	0.003009	4.66

Appendix D1 – S9.5C (Continued)

76.5	0.000089	0.99	79.0	0.001430	4.16	79.5	0.003120	4.80
79.5	0.000090	0.98	89.0	0.001494	4.35	89.5	0.003225	5.00
98.5	0.000100	1.06	99.0	0.001549	4.48	99.5	0.003313	5.12
97.0	0.000098	1.04	109.0	0.001599	4.62	109.5	0.003394	5.21
111.5	0.000105	1.13	119.0	0.001648	4.79	119.5	0.003471	5.32
127.5	0.000115	1.31	129.0	0.001692	4.88	129.5	0.003543	5.44
139.0	0.000119	1.28	139.0	0.001733	5.02	139.5	0.003603	5.46
147.5	0.000120	1.27	148.1	0.001767	5.08	149.0	0.003662	5.58
147.6	0.000125	1.38	159.1	0.001805	5.20	159.5	0.003722	5.64
161.1	0.000129	1.40	169.1	0.001839	5.30	169.6	0.003776	5.73
178.1	0.000137	1.49	179.1	0.001866	5.34	179.6	0.003825	5.78
183.6	0.000140	1.56	189.1	0.001898	5.44	189.6	0.003875	5.86
195.6	0.000145	1.66	199.1	0.001926	5.51	199.6	0.003920	5.91
202.1	0.000145	1.60	209.1	0.001948	5.50	209.6	0.003963	5.94
214.1	0.000150	1.66	219.1	0.001977	5.63	219.6	0.004004	5.99
222.1	0.000152	1.65	229.1	0.001999	5.69	229.6	0.004047	6.07
229.6	0.000154	1.66	239.1	0.002020	5.71	239.6	0.004083	6.11
248.1	0.000161	1.82	249.1	0.002041	5.81	249.6	0.004118	6.12
253.6	0.000160	1.68	259.1	0.002064	5.84	259.6	0.004155	6.17
253.6	0.000160	1.68	269.1	0.002082	5.85	269.6	0.004188	6.21
278.1	0.000169	1.88	278.1	0.002101	5.97	279.1	0.004220	6.25
283.1	0.000170	1.87	289.1	0.002119	5.92	289.6	0.004254	6.28
294.1	0.000172	1.82	299.1	0.002138	5.97	299.6	0.004285	6.34
305.1	0.000177	1.93	309.1	0.002156	6.06	309.6	0.004313	6.36
312.1	0.000181	2.01	319.1	0.002170	6.04	319.6	0.004343	6.41
326.1	0.000184	2.04	329.1	0.002186	6.10	329.6	0.004369	6.42
326.1	0.000184	2.04	339.1	0.002203	6.14	339.6	0.004401	6.48
348.1	0.000189	2.08	349.1	0.002217	6.17	349.6	0.004427	6.52
358.1	0.000191	2.10	359.1	0.002232	6.19	359.6	0.004450	6.54
366.6	0.000198	2.22	369.1	0.002251	6.28	369.6	0.004476	6.58
373.1	0.000197	2.16	379.1	0.002263	6.27	379.6	0.004500	6.60

Appendix D1 – S9.5C (Continued)

387.1	0.000201	2.22	389.1	0.002273	6.28	389.6	0.004524	6.61
395.6	0.000200	2.15	399.1	0.002285	6.30	399.6	0.004547	6.64
402.6	0.000206	2.27	409.1	0.002299	6.33	409.6	0.004571	6.69
416.6	0.000207	2.27	419.1	0.002313	6.43	419.6	0.004590	6.70
427.1	0.000208	2.16	429.1	0.002326	6.45	429.6	0.004614	6.73
436.6	0.000212	2.24	439.1	0.002339	6.47	439.6	0.004634	6.72
445.1	0.000215	2.36	449.1	0.002350	6.52	449.6	0.004655	6.76
453.6	0.000218	2.46	459.1	0.002361	6.53	459.6	0.004678	6.81
464.1	0.000220	2.36	469.1	0.002372	6.54	469.6	0.004697	6.84
474.7	0.000226	2.62	479.2	0.002381	6.57	479.6	0.004715	6.85
481.7	0.000223	2.41	489.2	0.002394	6.63	489.6	0.004735	6.86
490.7	0.000226	2.42	499.2	0.002404	6.57	499.6	0.004754	6.90
593.2	0.000249	2.73	599.2	0.002495	6.86	599.7	0.004921	7.07
687.2	0.000267	2.88	699.2	0.002566	6.95	699.7	0.005069	7.24
795.2	0.000289	3.14	799.2	0.002631	7.02	799.7	0.005193	7.39
888.8	0.000307	3.37	899.3	0.002689	7.19	899.8	0.005303	7.49
988.3	0.000318	3.24	999.3	0.002744	7.41	999.8	0.005404	7.61
1086.3	0.000336	3.57	1099.3	0.002790	7.43	1099.8	0.005496	7.71
1194.4	0.000354	3.87	1199.4	0.002828	7.45	1199.9	0.005578	7.81
1286.4	0.000368	4.12	1299.4	0.002866	7.60	1299.9	0.005654	7.89
1395.4	0.000382	4.13	1399.4	0.002898	7.61	1399.4	0.005724	7.95
1496.9	0.000395	4.33	1499.5	0.002930	7.66	1499.4	0.005790	8.01
1593.5	0.000406	4.34	1599.5	0.002960	7.81	1599.5	0.005853	8.09
1689.0	0.000418	4.66	1699.5	0.002987	7.76	1699.5	0.005913	8.17
1795.5	0.000432	4.69	1799.5	0.003011	7.83	1799.5	0.005967	8.21
1899.1	0.000443	4.67	1899.6	0.003038	7.92	1899.6	0.006018	8.26
1996.1	0.000452	4.67	1999.6	0.003062	8.07	1999.6	0.006069	8.34
2093.6	0.000463	4.85	2099.6	0.003086	8.11	2099.1	0.006113	8.31
2198.2	0.000478	5.31	2199.7	0.003103	8.09	2199.1	0.006159	8.37
2280.2	0.000484	5.37	2299.7	0.003121	8.08	2299.2	0.006205	8.47
2398.7	0.000500	5.67	2399.7	0.003141	8.19	2399.2	0.006249	8.53

Appendix D1 – S9.5C (Continued)

2496.2	0.000507	5.66	2498.7	0.003157	8.12	2498.7	0.006286	8.54
2597.8	0.000511	5.18	2599.8	0.003180	8.27	2599.3	0.006325	8.57
2696.3	0.000521	5.46	2699.8	0.003196	8.24	2699.3	0.006362	8.59
2795.3	0.000531	5.61	2799.8	0.003210	8.39	2799.3	0.006399	8.65
2873.8	0.000540	5.95	2899.9	0.003220	8.24	2899.4	0.006432	8.68
2997.9	0.000549	5.94	2999.9	0.003239	8.39	2999.4	0.006468	8.76
3096.4	0.000554	5.65	3099.9	0.003251	8.40	3099.4	0.006498	8.77
3177.9	0.000565	6.27	3199.9	0.003265	8.40	3199.4	0.006529	8.81
3297.5	0.000572	6.23	3300.0	0.003275	8.39	3299.5	0.006559	8.84
3397.0	0.000580	6.09	3399.0	0.003290	8.45	3399.5	0.006586	8.83
3497.5	0.000588	6.51	3499.0	0.003301	8.45	3499.5	0.006612	8.84
3597.1	0.000595	6.52	3599.1	0.003313	8.48	3599.6	0.006644	8.90
3689.1	0.000604	6.71	3699.1	0.003325	8.52	3699.6	0.006670	8.95
3797.6	0.000608	6.57	3799.1	0.003337	8.50	3799.6	0.006698	9.00
3894.6	0.000623	7.04	3899.2	0.003351	8.58	3899.6	0.006723	8.97
3991.2	0.000624	6.73	3999.2	0.003360	8.62	3999.7	0.006747	9.01
4094.2	0.000634	7.24	4099.2	0.003371	8.61	4099.7	0.006771	9.02
4183.7	0.000636	6.98	4199.2	0.003381	8.69	4199.7	0.006795	9.07
4286.8	0.000642	7.09	4299.3	0.003393	8.68	4299.8	0.006815	9.04
4395.8	0.000651	7.14	4399.3	0.003401	8.63	4399.8	0.006840	9.10
4482.8	0.000653	7.07	4499.3	0.003412	8.75	4499.8	0.006861	9.11
4584.8	0.000660	7.22	4599.4	0.003421	8.76	4599.9	0.006880	9.10
4693.9	0.000666	7.46	4699.4	0.003430	8.75	4699.9	0.006902	9.10
4790.4	0.000675	7.83	4799.4	0.003437	8.70	4799.4	0.006925	9.14
4890.9	0.000676	7.30	4899.5	0.003448	8.67	4899.4	0.006946	9.19
4997.0	0.000681	7.43	4999.5	0.003457	8.79	4999.5	0.006966	9.23
5094.0	0.000690	7.60	5099.5	0.003464	8.77	5099.5	0.006984	9.24
5181.5	0.000694	7.77	5199.5	0.003476	8.87	5199.5	0.007001	9.24
5293.1	0.000696	7.52	5299.6	0.003482	8.85	5299.6	0.007021	9.27
5389.1	0.000701	7.60	5399.6	0.003491	8.88	5399.6	0.007039	9.29
5493.1	0.000708	7.93	5499.6	0.003498	8.84	5499.1	0.007057	9.30

Appendix D1 – S9.5C (Continued)

5596.1	0.000713	8.11	5599.7	0.003508	8.92	5599.1	0.007074	9.34
5697.7	0.000719	7.92	5699.7	0.003515	8.92	5699.2	0.007091	9.32
5780.7	0.000723	8.43	5799.7	0.003522	8.88	5799.2	0.007109	9.35
5886.7	0.000725	8.22	5899.7	0.003528	8.88	5899.2	0.007126	9.37
5999.8	0.000731	8.29	5999.8	0.003537	9.00	5999.3	0.007144	9.41
6093.3	0.000736	8.28	6099.8	0.003544	8.97	6099.3	0.007161	9.46
6199.3	0.000741	8.38	6199.8	0.003549	8.94	6199.3	0.007176	9.41
6298.8	0.000744	8.50	6299.9	0.003560	8.99	6299.3	0.007191	9.44
6390.9	0.000749	8.55	6399.9	0.003565	9.01	6399.4	0.007207	9.48
6493.4	0.000756	8.53	6499.9	0.003573	9.01	6499.4	0.007224	9.49
6594.9	0.000757	8.38	6599.9	0.003577	8.96	6599.4	0.007240	9.51
6689.5	0.000762	8.60	6700.0	0.003586	9.01	6699.5	0.007255	9.52
6797.0	0.000766	8.74	6799.0	0.003592	9.04	6799.5	0.007267	9.54
6897.5	0.000768	8.36	6899.0	0.003600	9.03	6899.5	0.007285	9.57
6975.5	0.000775	9.30	6999.1	0.003606	9.09	6999.6	0.007297	9.56
7091.1	0.000777	9.13	7099.1	0.003611	9.05	7099.6	0.007311	9.58
7189.1	0.000780	8.74	7198.1	0.003619	9.14	7199.1	0.007326	9.60
7297.1	0.000784	8.73	7299.2	0.003622	9.07	7299.6	0.007340	9.62
7398.2	0.000790	8.98	7399.2	0.003628	9.04	7399.7	0.007351	9.61
7491.7	0.000794	8.96	7499.2	0.003639	9.14	7499.7	0.007363	9.61
7594.2	0.000799	8.97	7599.2	0.003642	9.11	7599.7	0.007378	9.65
7697.8	0.000804	9.18	7699.3	0.003651	9.15	7699.8	0.007389	9.65
7798.3	0.000807	9.09	7799.3	0.003654	9.10	7799.8	0.007403	9.66
7898.8	0.000811	9.02	7899.3	0.003660	9.14	7899.8	0.007415	9.69
7979.8	0.000814	9.33	7999.4	0.003669	9.28	7999.9	0.007428	9.71
8097.4	0.000821	9.19	8099.4	0.003674	9.20	8099.9	0.007440	9.70
8193.9	0.000826	9.25	8199.4	0.003677	9.15	8199.4	0.007450	9.72
8299.4	0.000831	9.40	8299.4	0.003686	9.20	8299.4	0.007462	9.74
8385.5	0.000838	9.26	8399.5	0.003691	9.25	8399.5	0.007471	9.69
8490.0	0.000847	9.88	8499.5	0.003696	9.30	8499.5	0.007485	9.73
8593.5	0.000850	9.67	8599.5	0.003702	9.25	8599.5	0.007495	9.71

Appendix D1 – S9.5C (Continued)

8698.0	0.000855	9.87	8699.6	0.003707	9.30	8699.6	0.007505	9.72
8753.6	0.000856	9.78	8799.6	0.003709	9.23	8799.6	0.007520	9.78
8858.6	0.000863	9.48	8899.6	0.003717	9.29	8899.6	0.007528	9.74
8907.6	0.000861	9.44	8999.7	0.003722	9.34	8999.1	0.007542	9.83
8951.1	0.000861	9.23	9099.7	0.003726	9.25	9099.2	0.007552	9.80
9008.1	0.000865	9.58	9199.7	0.003732	9.28	9199.2	0.007562	9.80
9058.7	0.000866	9.47	9299.7	0.003741	9.33	9299.2	0.007575	9.84
9108.2	0.000866	9.19	9399.8	0.003745	9.31	9399.3	0.007582	9.82
9157.7	0.000867	9.48	9499.8	0.003752	9.39	9499.3	0.007591	9.82
9200.2	0.000873	9.45	9599.8	0.003757	9.37	9599.3	0.007599	9.82
9257.7	0.000873	9.34	9699.9	0.003760	9.29	9699.3	0.007611	9.87
9293.2	0.000873	9.28	9799.9	0.003769	9.40	9799.4	0.007621	9.85
9357.7	0.000877	9.64	9899.9	0.003768	9.29	9899.4	0.007630	9.86
9987.9	0.000906	9.94	9999.9	0.003773	9.30	9999.4	0.007641	9.89
10088.5	0.000908	9.93	10100.0	0.003779	9.44	10099.5	0.007649	9.87
10184.0	0.000908	9.58	10199.0	0.003781	9.35	10199.5	0.007661	9.91
10284.0	0.000916	10.76	10299.0	0.003785	9.35	10299.5	0.007670	9.94
10398.5	0.000919	10.30	10399.1	0.003789	9.33	10399.6	0.007678	9.93
10494.1	0.000924	10.08	10499.1	0.003798	9.38	10499.6	0.007685	9.90
10593.6	0.000929	10.84	10599.1	0.003804	9.49	10599.6	0.007697	9.95
10698.6	0.000928	9.75	10699.1	0.003804	9.36	10699.6	0.007705	9.95
10793.2	0.000933	10.29	10799.2	0.003812	9.45	10799.7	0.007715	9.94
10895.7	0.000937	10.51	10899.2	0.003815	9.39	10899.7	0.007725	9.95
10991.2	0.000940	10.68	10999.2	0.003822	9.47	10999.7	0.007731	9.91
11098.2	0.000947	10.52	11099.3	0.003826	9.45	11099.8	0.007743	10.00
11195.3	0.000945	10.13	11199.3	0.003829	9.44	11199.8	0.007749	9.98
11290.3	0.000951	10.40	11299.3	0.003836	9.42	11299.8	0.007759	10.00
11390.8	0.000953	10.19	11399.4	0.003841	9.52	11399.8	0.007769	10.01
11486.9	0.000956	10.01	11499.4	0.003844	9.48	11499.9	0.007778	10.03
11557.4	0.000957	9.79	11599.4	0.003846	9.46	11599.4	0.007786	10.05
11688.4	0.000967	10.32	11699.4	0.003855	9.52	11699.4	0.007795	10.08

Appendix D1 – S9.5C (Continued)

11796.4	0.000971	10.53	11799.5	0.003859	9.53	11799.5	0.007802	10.06
11895.5	0.000977	10.80	11898.5	0.003865	9.57	11899.5	0.007811	10.06
11961.5	0.000974	10.47	11999.5	0.003870	9.57	11999.5	0.007819	10.06

RS9.5C								
20°C			40°C			54°C		
Cycles	ε_p	$\varepsilon_p/\varepsilon_r$	Cycles	ε_p	$\varepsilon_p/\varepsilon_r$	Cycles	ε_p	$\varepsilon_p/\varepsilon_r$
2.5	0.000002	0.04	2.9	0.000235	0.65	2.0	0.000753	1.06
4.5	0.000008	0.16	4.9	0.000366	0.96	4.0	0.001112	1.49
9.5	0.000021	0.56	9.9	0.000599	1.54	9.0	0.001666	2.23
18.0	0.000024	0.47	19.9	0.000909	2.35	19.0	0.002290	3.12
29.5	0.000054	0.74	29.9	0.001127	2.92	29.0	0.002676	3.66
39.5	0.000061	0.89	39.9	0.001296	3.40	39.0	0.002956	4.05
49.5	0.000070	0.98	49.9	0.001427	3.67	49.0	0.003177	4.35
59.5	0.000073	1.08	59.9	0.001542	3.99	59.0	0.003353	4.57
69.5	0.000072	0.96	69.9	0.001640	4.21	69.0	0.003507	4.78
79.5	0.000076	1.03	79.9	0.001728	4.44	79.0	0.003644	4.96
89.5	0.000079	1.09	89.9	0.001803	4.61	89.0	0.003761	5.11
99.5	0.000088	1.25	99.9	0.001872	4.78	99.0	0.003870	5.27
109.5	0.000084	1.10	109.9	0.001932	4.95	109.0	0.003963	5.32
119.5	0.000091	1.38	119.9	0.001989	5.07	119.0	0.004053	5.45
129.5	0.000088	1.17	129.9	0.002045	5.23	129.0	0.004134	5.57
139.5	0.000094	1.26	139.9	0.002093	5.34	139.0	0.004204	5.62
149.0	0.000102	1.41	148.9	0.002134	5.43	149.1	0.004276	5.70
159.5	0.000097	1.29	159.9	0.002182	5.55	159.1	0.004339	5.76
169.5	0.000097	1.24	169.9	0.002220	5.64	169.1	0.004401	5.85
179.5	0.000105	1.49	179.9	0.002255	5.70	179.1	0.004461	5.92
189.5	0.000100	1.27	189.4	0.002289	5.74	189.1	0.004512	5.94
199.5	0.000108	1.40	199.4	0.002322	5.79	199.1	0.004566	6.00
209.5	0.000110	1.40	209.4	0.002355	5.89	209.1	0.004618	6.07
219.5	0.000111	1.44	219.4	0.002382	5.93	219.1	0.004662	6.11

Appendix D1 – RS9.5C (Continued)

229.5	0.000114	1.57	229.4	0.002413	6.06	229.1	0.004704	6.13
239.5	0.000113	1.40	239.4	0.002436	6.03	239.1	0.004745	6.16
249.6	0.000113	1.50	249.4	0.002463	6.10	249.1	0.004790	6.25
259.6	0.000119	1.57	259.4	0.002489	6.18	259.1	0.004826	6.23
269.6	0.000118	1.49	269.5	0.002514	6.28	269.1	0.004865	6.30
279.6	0.000121	1.69	279.5	0.002535	6.23	279.1	0.004904	6.35
289.6	0.000125	1.64	289.5	0.002560	6.31	289.1	0.004937	6.37
299.6	0.000130	1.93	299.5	0.002581	6.34	299.1	0.004971	6.39
309.6	0.000133	1.99	309.5	0.002600	6.37	309.1	0.005005	6.44
319.6	0.000130	1.61	319.5	0.002624	6.46	319.1	0.005034	6.44
329.6	0.000138	1.77	329.5	0.002640	6.45	329.1	0.005068	6.52
339.6	0.000137	1.84	339.5	0.002662	6.55	339.1	0.005095	6.50
349.6	0.000133	1.71	349.5	0.002677	6.55	349.1	0.005127	6.56
359.6	0.000136	1.94	359.5	0.002697	6.60	359.1	0.005154	6.58
369.6	0.000139	1.87	369.5	0.002714	6.68	369.1	0.005180	6.58
379.6	0.000136	1.82	379.5	0.002732	6.68	379.1	0.005208	6.63
389.6	0.000139	1.91	389.5	0.002748	6.70	389.1	0.005233	6.64
399.6	0.000138	1.67	399.5	0.002760	6.68	399.1	0.005257	6.64
409.6	0.000141	1.81	409.5	0.002778	6.77	409.1	0.005282	6.66
419.6	0.000143	1.86	419.5	0.002791	6.77	419.1	0.005304	6.70
429.6	0.000144	1.87	429.5	0.002807	6.81	429.1	0.005332	6.73
439.6	0.000143	1.79	439.5	0.002819	6.78	439.1	0.005351	6.72
449.6	0.000147	1.88	449.5	0.002832	6.82	449.1	0.005376	6.77
459.6	0.000150	2.05	459.5	0.002849	6.87	459.1	0.005399	6.78
469.6	0.000151	2.12	469.5	0.002861	6.90	469.2	0.005419	6.81
479.6	0.000147	1.90	479.5	0.002873	6.92	479.2	0.005443	6.86
489.6	0.000147	1.93	489.5	0.002884	6.92	489.2	0.005458	6.81
499.6	0.000158	2.12	499.5	0.002897	6.90	499.2	0.005480	6.87
599.7	0.000163	2.28	599.5	0.003007	7.15	599.2	0.005661	7.03
699.7	0.000181	2.50	699.1	0.003098	7.36	699.2	0.005807	7.12
799.7	0.000179	2.45	799.1	0.003174	7.45	799.2	0.005941	7.25

Appendix D1 – RS9.5C (Continued)

899.7	0.000191	2.51	899.1	0.003244	7.53	899.3	0.006059	7.39
999.8	0.000199	2.70	999.2	0.003305	7.65	999.3	0.006162	7.47
1099.8	0.000206	2.64	1099.2	0.003360	7.70	1099.3	0.006252	7.53
1199.8	0.000215	2.77	1199.2	0.003411	7.79	1199.4	0.006340	7.66
1299.9	0.000220	2.84	1299.3	0.003455	7.88	1299.4	0.006414	7.69
1399.9	0.000229	2.90	1399.3	0.003498	7.95	1399.4	0.006488	7.79
1499.9	0.000233	2.98	1499.3	0.003540	8.02	1499.5	0.006551	7.83
1599.4	0.000237	2.96	1599.3	0.003575	8.11	1599.5	0.006612	7.88
1699.5	0.000245	3.22	1699.4	0.003606	8.03	1699.5	0.006671	7.94
1799.5	0.000252	3.30	1799.4	0.003641	8.06	1799.5	0.006723	7.97
1899.5	0.000257	3.20	1899.4	0.003666	8.16	1899.6	0.006774	8.03
1999.6	0.000259	3.37	1999.5	0.003702	8.23	1999.6	0.006821	8.07
2099.1	0.000263	3.48	2099.5	0.003726	8.20	2099.6	0.006868	8.14
2199.1	0.000273	3.53	2199.5	0.003754	8.23	2199.7	0.006910	8.18
2299.2	0.000273	3.68	2299.5	0.003780	8.28	2299.7	0.006951	8.22
2399.2	0.000276	3.53	2399.6	0.003803	8.31	2399.7	0.006987	8.23
2498.7	0.000285	4.08	2498.6	0.003827	8.36	2498.7	0.007023	8.27
2599.2	0.000292	4.26	2599.6	0.003849	8.39	2599.8	0.007057	8.31
2699.3	0.000300	4.39	2699.7	0.003868	8.39	2699.8	0.007089	8.31
2799.3	0.000297	3.90	2799.7	0.003888	8.43	2799.8	0.007124	8.38
2899.3	0.000304	3.89	2899.7	0.003911	8.45	2899.9	0.007155	8.41
2999.4	0.000303	4.01	2999.8	0.003931	8.43	2999.9	0.007184	8.45
3099.4	0.000312	4.16	3099.8	0.003948	8.55	3099.9	0.007212	8.46
3199.4	0.000315	4.38	3199.8	0.003969	8.58	3200.0	0.007243	8.50
3299.4	0.000317	4.51	3299.8	0.003980	8.56	3300.0	0.007269	8.54
3399.5	0.000322	4.44	3399.9	0.004000	8.53	3399.0	0.007291	8.54
3499.5	0.000321	4.19	3499.9	0.004020	8.57	3499.0	0.007318	8.58
3599.5	0.000323	4.28	3599.4	0.004035	8.69	3599.1	0.007342	8.61
3699.6	0.000326	4.37	3699.5	0.004046	8.54	3699.1	0.007365	8.63
3799.6	0.000329	4.46	3799.5	0.004068	8.67	3799.1	0.007387	8.66
3899.6	0.000332	4.58	3899.5	0.004080	8.64	3899.2	0.007407	8.67

Appendix D1 – RS9.5C (Continued)

3999.6	0.000338	4.55	3999.5	0.004094	8.59	3999.2	0.007427	8.68
4099.7	0.000338	4.55	4099.1	0.004110	8.70	4099.2	0.007446	8.72
4199.7	0.000339	4.25	4199.1	0.004123	8.69	4199.3	0.007465	8.69
4299.7	0.000346	4.39	4299.1	0.004138	8.75	4299.3	0.007490	8.81
4399.8	0.000349	4.63	4399.2	0.004152	8.73	4399.3	0.007508	8.82
4499.8	0.000352	5.02	4499.2	0.004164	8.72	4499.3	0.007524	8.82
4599.8	0.000353	4.51	4599.2	0.004171	8.65	4599.4	0.007541	8.85
4699.8	0.000350	4.59	4699.3	0.004188	8.73	4699.4	0.007557	8.86
4799.9	0.000356	4.87	4799.3	0.004202	8.76	4799.4	0.007574	8.87
4899.9	0.000357	4.30	4899.3	0.004214	8.86	4899.5	0.007587	8.83
4999.4	0.000354	4.47	4999.3	0.004225	8.82	4999.5	0.007604	8.87
5099.5	0.000364	4.90	5099.4	0.004229	8.67	5099.5	0.007619	8.88
5199.5	0.000371	5.29	5199.4	0.004247	8.74	5199.5	0.007640	8.96
5299.5	0.000365	4.99	5299.4	0.004258	8.80	5299.6	0.007657	8.97
5399.6	0.000373	4.85	5399.5	0.004269	8.80	5399.6	0.007669	8.96
5499.1	0.000373	4.97	5499.5	0.004280	8.82	5499.6	0.007681	8.93
5599.1	0.000383	4.87	5599.5	0.004293	8.92	5599.7	0.007695	8.95
5699.1	0.000378	4.79	5699.5	0.004303	8.86	5699.7	0.007711	8.98
5799.2	0.000376	4.77	5799.6	0.004316	8.92	5799.7	0.007726	9.01
5899.2	0.000387	5.44	5899.6	0.004324	8.88	5899.8	0.007739	9.02
5999.2	0.000384	4.94	5999.6	0.004336	8.82	5999.8	0.007754	9.06
6099.3	0.000381	4.87	6099.7	0.004346	8.93	6099.8	0.007767	9.07
6199.3	0.000385	4.79	6199.7	0.004356	8.98	6199.8	0.007781	9.09
6299.3	0.000389	4.77	6299.7	0.004364	8.92	6299.9	0.007791	9.09
6399.3	0.000403	5.10	6399.8	0.004377	9.01	6399.9	0.007805	9.11
6499.4	0.000399	5.50	6499.8	0.004385	8.99	6499.9	0.007816	9.11
6599.4	0.000392	4.79	6599.8	0.004397	8.94	6600.0	0.007828	9.13
6699.4	0.000396	4.79	6699.8	0.004405	8.97	6700.0	0.007844	9.20
6799.5	0.000404	5.51	6799.9	0.004415	8.97	6799.0	0.007849	9.14
6899.5	0.000399	5.34	6899.9	0.004425	9.06	6899.0	0.007865	9.18
6999.5	0.000398	4.89	6999.4	0.004429	8.92	6999.1	0.007876	9.19

Appendix D1 – RS9.5C (Continued)

7099.5	0.000395	5.03	7099.5	0.004438	8.99	7099.1	0.007883	9.16
7199.6	0.000405	5.85	7199.5	0.004448	9.04	7199.1	0.007895	9.16
7299.6	0.000418	5.50	7299.5	0.004453	8.93	7299.2	0.007907	9.20
7399.6	0.000416	6.49	7399.6	0.004468	9.07	7399.2	0.007918	9.23
7499.7	0.000410	5.59	7499.1	0.004477	9.08	7499.2	0.007932	9.25
7599.7	0.000404	5.44	7599.1	0.004483	9.06	7599.3	0.007943	9.30
7699.7	0.000405	5.20	7699.1	0.004492	9.09	7699.3	0.007954	9.32
7799.8	0.000430	5.86	7799.2	0.004499	9.03	7799.3	0.007964	9.31
7899.8	0.000412	5.74	7899.2	0.004506	9.07	7899.3	0.007970	9.29
7999.8	0.000420	6.05	7999.2	0.004517	9.10	7999.4	0.007978	9.29
8099.8	0.000420	5.84	8099.3	0.004525	9.19	8099.4	0.007987	9.29
8199.9	0.000410	5.30	8199.3	0.004526	8.98	8199.4	0.007999	9.33
8299.9	0.000424	5.76	8299.3	0.004540	9.13	8299.5	0.008010	9.33
8399.4	0.000432	5.67	8399.3	0.004548	9.10	8399.5	0.008020	9.36
8499.5	0.000430	5.28	8499.4	0.004555	9.06	8499.5	0.008030	9.40
8599.5	0.000427	5.23	8599.4	0.004560	9.06	8599.5	0.008036	9.37
8699.5	0.000431	5.59	8699.4	0.004567	9.16	8699.6	0.008044	9.37
8799.5	0.000435	5.59	8799.5	0.004575	9.07	8799.6	0.008053	9.37
8898.6	0.000432	5.40	8899.5	0.004582	9.09	8899.6	0.008060	9.34
8999.1	0.000431	6.08	8999.5	0.004589	9.13	8999.7	0.008071	9.37
9099.1	0.000447	6.16	9099.6	0.004593	9.06	9099.7	0.008079	9.38
9199.2	0.000443	5.67	9199.6	0.004605	9.19	9199.7	0.008088	9.36
9299.2	0.000433	5.43	9299.6	0.004614	9.18	9299.8	0.008097	9.41
9399.2	0.000438	5.60	9399.6	0.004621	9.19	9399.8	0.008104	9.38
9499.2	0.000442	5.53	9499.7	0.004630	9.18	9499.8	0.008117	9.45
9599.3	0.000457	6.71	9599.7	0.004635	9.17	9599.8	0.008124	9.42
9699.3	0.000445	5.55	9699.7	0.004635	9.21	9699.9	0.008131	9.43
9799.3	0.000457	6.54	9799.8	0.004647	9.21	9799.9	0.008140	9.44
9899.4	0.000452	6.17	9899.8	0.004647	9.15	9899.9	0.008150	9.47
9999.4	0.000446	5.50	9999.8	0.004660	9.17	10000.0	0.008156	9.48
10099.4	0.000460	5.97	10099.8	0.004657	9.11	10099.5	0.008168	9.55

Appendix D1 – RS9.5C (Continued)

10199.4	0.000460	5.77	10199.9	0.004668	9.16	10199.0	0.008179	9.57
10299.5	0.000459	5.90	10299.9	0.004679	9.22	10299.1	0.008187	9.59
10399.5	0.000456	5.77	10399.4	0.004687	9.26	10399.1	0.008192	9.56
10499.5	0.000449	4.71	10499.5	0.004688	9.16	10499.1	0.008201	9.59
10599.6	0.000456	6.08	10599.5	0.004692	9.16	10599.1	0.008205	9.53
10699.6	0.000462	6.28	10699.5	0.004702	9.24	10699.2	0.008214	9.57
10799.6	0.000461	5.42	10799.5	0.004708	9.26	10799.2	0.008223	9.63
10899.6	0.000459	5.74	10899.1	0.004713	9.22	10899.2	0.008227	9.59
10999.7	0.000460	5.86	10999.1	0.004717	9.17	10999.3	0.008237	9.63
11099.2	0.000459	5.75	11099.1	0.004723	9.21	11099.3	0.008240	9.55
11199.7	0.000473	6.66	11199.2	0.004730	9.25	11199.3	0.008250	9.64
11299.8	0.000468	5.98	11299.2	0.004736	9.19	11299.3	0.008253	9.58
11399.8	0.000459	5.40	11399.2	0.004740	9.17	11399.4	0.008264	9.62
11499.8	0.000466	6.44	11499.3	0.004748	9.28	11499.4	0.008269	9.64
11599.9	0.000472	5.81	11599.3	0.004752	9.22	11599.4	0.008275	9.62
11699.9	0.000472	6.37	11699.3	0.004758	9.24	11699.5	0.008280	9.62
11799.9	0.000475	6.00	11799.3	0.004765	9.22	11799.5	0.008287	9.62
11898.9	0.000473	5.91	11898.4	0.004770	9.24	11899.5	0.008292	9.60
11999.5	0.000479	6.22	11999.4	0.004777	9.27	11999.6	0.008299	9.62

S12.5C								
20°C			40°C			54°C		
Cycles	ε_p	$\varepsilon_p/\varepsilon_r$	Cycles	ε_p	$\varepsilon_p/\varepsilon_r$	Cycles	ε_p	$\varepsilon_p/\varepsilon_r$
2.0	0.000012	0.33	2.1	0.000206	0.67	2.0	0.000936	1.47
4.0	0.000021	0.47	4.1	0.000362	1.06	4.0	0.001413	2.09
9.0	0.000030	0.74	9.1	0.000633	1.81	9.0	0.002108	3.04
19.0	0.000043	0.63	18.1	0.000961	2.72	18.0	0.002794	4.10
29.1	0.000054	0.71	29.1	0.001240	3.46	29.0	0.003294	4.94
39.1	0.000065	0.87	39.1	0.001437	4.01	39.0	0.003610	5.48
49.1	0.000069	0.88	49.1	0.001598	4.53	49.0	0.003855	5.92
59.1	0.000079	1.07	59.1	0.001731	4.86	59.0	0.004049	6.17

Appendix D1 – S12.5C (Continued)

69.1	0.000085	1.13	69.1	0.001847	5.19	69.0	0.004212	6.43
79.1	0.000090	1.18	79.1	0.001949	5.52	79.0	0.004356	6.66
89.1	0.000093	1.20	89.1	0.002039	5.74	89.0	0.004478	6.83
99.1	0.000100	1.31	99.1	0.002119	6.01	99.0	0.004591	6.99
109.1	0.000103	1.38	109.1	0.002190	6.10	109.0	0.004691	7.14
119.1	0.000107	1.41	119.1	0.002260	6.41	119.0	0.004783	7.27
129.1	0.000111	1.42	129.1	0.002317	6.49	129.0	0.004867	7.43
139.1	0.000113	1.44	139.1	0.002375	6.67	139.0	0.004947	7.52
148.6	0.000121	1.64	148.6	0.002423	6.78	148.0	0.005008	7.60
159.1	0.000123	1.62	159.1	0.002475	6.92	159.1	0.005083	7.73
169.1	0.000126	1.66	169.1	0.002518	7.00	169.1	0.005144	7.78
179.1	0.000128	1.63	179.1	0.002561	7.14	179.1	0.005203	7.90
189.1	0.000134	1.81	189.1	0.002602	7.26	189.1	0.005258	7.94
199.1	0.000135	1.75	199.2	0.002639	7.36	199.1	0.005310	8.03
209.1	0.000142	1.93	209.2	0.002675	7.45	209.1	0.005358	8.05
219.1	0.000143	1.91	219.2	0.002707	7.49	219.1	0.005408	8.17
229.1	0.000146	1.87	229.2	0.002740	7.60	229.1	0.005451	8.18
239.1	0.000149	1.94	239.2	0.002770	7.68	239.1	0.005495	8.23
249.1	0.000151	1.95	249.2	0.002799	7.77	249.1	0.005535	8.29
259.1	0.000154	2.02	259.2	0.002826	7.80	259.1	0.005572	8.33
269.1	0.000156	2.05	269.2	0.002851	7.89	269.1	0.005612	8.37
279.1	0.000163	2.27	278.7	0.002877	8.00	278.1	0.005642	8.40
289.1	0.000161	2.03	289.2	0.002902	8.01	289.1	0.005680	8.40
299.1	0.000167	2.29	299.2	0.002923	7.98	299.1	0.005716	8.50
309.1	0.000167	2.15	309.2	0.002947	8.14	309.1	0.005747	8.50
319.1	0.000171	2.31	319.2	0.002968	8.12	319.1	0.005782	8.59
329.1	0.000172	2.21	329.2	0.002987	8.18	329.1	0.005808	8.61
339.1	0.000176	2.30	339.2	0.003009	8.26	339.1	0.005841	8.62
349.2	0.000175	2.25	349.2	0.003028	8.32	349.1	0.005867	8.66
359.2	0.000178	2.26	359.2	0.003045	8.30	359.1	0.005896	8.71
369.2	0.000181	2.37	369.2	0.003066	8.41	369.1	0.005922	8.69

Appendix D1 – S12.5C (Continued)

379.2	0.000183	2.34	379.2	0.003081	8.39	379.1	0.005949	8.79
389.2	0.000186	2.40	389.2	0.003098	8.46	389.1	0.005972	8.78
399.2	0.000187	2.39	399.2	0.003115	8.48	399.1	0.005995	8.75
409.2	0.000192	2.56	409.2	0.003130	8.54	409.1	0.006020	8.82
419.2	0.000192	2.52	419.2	0.003147	8.55	419.1	0.006045	8.83
429.2	0.000194	2.52	429.2	0.003162	8.61	429.1	0.006066	8.87
439.2	0.000199	2.67	439.2	0.003175	8.59	439.1	0.006089	8.91
449.2	0.000199	2.62	449.2	0.003191	8.67	449.1	0.006112	8.94
459.2	0.000201	2.56	459.2	0.003204	8.64	459.1	0.006129	8.91
469.2	0.000203	2.69	469.2	0.003220	8.81	469.1	0.006153	8.98
479.2	0.000207	2.70	479.2	0.003233	8.80	479.2	0.006172	8.99
489.2	0.000208	2.70	489.2	0.003244	8.80	489.2	0.006193	9.02
499.2	0.000210	2.78	499.2	0.003256	8.81	499.2	0.006210	9.02
599.2	0.000227	2.96	599.3	0.003365	8.98	599.2	0.006385	9.17
699.3	0.000245	3.25	699.3	0.003456	9.19	699.2	0.006530	9.34
799.3	0.000260	3.29	799.3	0.003533	9.36	799.2	0.006654	9.41
899.3	0.000275	3.58	899.4	0.003597	9.36	899.3	0.006768	9.58
999.3	0.000288	3.68	999.4	0.003659	9.64	999.3	0.006863	9.64
1099.4	0.000304	4.00	1099.4	0.003709	9.63	1099.3	0.006955	9.78
1199.4	0.000318	4.30	1199.4	0.003753	9.63	1199.4	0.007033	9.81
1299.4	0.000326	4.13	1299.5	0.003797	9.78	1299.4	0.007109	9.91
1399.5	0.000338	4.34	1399.5	0.003832	9.79	1399.4	0.007178	9.99
1499.5	0.000347	4.37	1499.5	0.003870	9.76	1499.4	0.007238	10.01
1599.5	0.000359	4.70	1599.6	0.003905	10.01	1599.5	0.007295	10.07
1699.5	0.000370	4.97	1699.6	0.003933	9.93	1699.5	0.007353	10.16
1799.6	0.000380	5.10	1799.6	0.003960	9.90	1799.5	0.007404	10.24
1899.6	0.000389	5.03	1899.6	0.003988	9.92	1899.6	0.007454	10.22
1999.6	0.000399	5.21	1999.7	0.004013	10.06	1999.6	0.007498	10.26
2099.7	0.000409	5.61	2099.7	0.004039	10.01	2099.6	0.007543	10.33
2199.7	0.000414	5.25	2199.7	0.004062	10.16	2199.6	0.007585	10.37
2299.7	0.000422	5.51	2299.8	0.004083	10.10	2299.7	0.007624	10.38

Appendix D1 – S12.5C (Continued)

2399.8	0.000432	5.69	2399.8	0.004105	10.14	2399.7	0.007661	10.42
2499.3	0.000442	5.97	2498.3	0.004123	10.07	2497.7	0.007698	10.47
2599.8	0.000448	6.12	2599.9	0.004143	10.19	2599.8	0.007732	10.46
2699.8	0.000454	5.84	2699.9	0.004162	10.20	2699.8	0.007768	10.56
2799.9	0.000463	5.90	2799.9	0.004181	10.25	2799.8	0.007803	10.52
2899.9	0.000470	6.26	2899.4	0.004201	10.32	2899.9	0.007833	10.57
2999.9	0.000478	6.25	2999.5	0.004215	10.27	2999.9	0.007862	10.61
3100.0	0.000486	6.47	3099.5	0.004232	10.34	3099.9	0.007890	10.59
3199.5	0.000491	6.47	3199.5	0.004248	10.38	3199.9	0.007920	10.66
3299.5	0.000499	6.37	3299.6	0.004262	10.36	3300.0	0.007946	10.69
3399.0	0.000507	6.86	3399.1	0.004274	10.37	3400.0	0.007973	10.71
3499.1	0.000513	6.93	3499.1	0.004290	10.45	3499.0	0.007995	10.67
3599.1	0.000518	6.78	3599.1	0.004303	10.38	3599.1	0.008020	10.71
3699.1	0.000524	6.78	3699.2	0.004318	10.49	3699.1	0.008043	10.75
3799.2	0.000530	6.89	3799.2	0.004329	10.41	3799.1	0.008068	10.75
3899.2	0.000538	7.20	3899.2	0.004343	10.40	3899.1	0.008091	10.79
3999.2	0.000544	7.55	3999.3	0.004355	10.37	3999.2	0.008112	10.74
4099.2	0.000547	6.93	4099.3	0.004365	10.35	4099.2	0.008137	10.83
4199.3	0.000554	7.31	4199.3	0.004379	10.45	4199.2	0.008156	10.76
4299.3	0.000557	7.08	4299.3	0.004391	10.46	4299.3	0.008178	10.89
4399.3	0.000565	7.37	4399.4	0.004399	10.40	4399.3	0.008197	10.93
4499.4	0.000570	7.44	4499.4	0.004416	10.54	4499.3	0.008214	10.85
4599.4	0.000580	7.86	4599.4	0.004428	10.55	4599.3	0.008233	10.85
4699.4	0.000582	7.76	4699.5	0.004439	10.59	4699.4	0.008254	10.93
4799.5	0.000587	7.72	4799.5	0.004446	10.50	4799.4	0.008271	10.94
4899.5	0.000593	7.58	4899.5	0.004456	10.42	4899.4	0.008288	10.96
4999.5	0.000598	7.81	4999.6	0.004467	10.54	4999.5	0.008305	10.97
5099.5	0.000604	8.03	5099.6	0.004478	10.58	5099.5	0.008321	11.01
5199.6	0.000608	7.81	5199.6	0.004488	10.49	5199.5	0.008339	11.04
5299.6	0.000614	8.28	5299.6	0.004495	10.53	5299.5	0.008355	11.03
5399.6	0.000618	7.97	5399.7	0.004505	10.52	5399.6	0.008370	11.00

Appendix D1 – S12.5C (Continued)

5499.7	0.000626	8.45	5499.7	0.004517	10.55	5499.6	0.008388	11.12
5599.7	0.000629	8.29	5599.7	0.004524	10.56	5599.6	0.008402	11.06
5699.7	0.000635	8.48	5699.8	0.004536	10.65	5699.7	0.008419	11.10
5799.7	0.000642	8.75	5799.8	0.004543	10.61	5799.7	0.008434	11.08
5899.8	0.000646	8.60	5899.8	0.004552	10.56	5899.7	0.008446	11.09
5999.8	0.000649	8.56	5999.8	0.004561	10.60	5999.7	0.008461	11.07
6099.8	0.000653	8.34	6099.9	0.004570	10.67	6099.8	0.008476	11.14
6199.9	0.000659	8.59	6199.9	0.004580	10.67	6199.8	0.008490	11.16
6299.9	0.000662	8.45	6299.4	0.004587	10.67	6299.8	0.008502	11.14
6399.9	0.000667	8.71	6399.5	0.004594	10.61	6399.9	0.008519	11.15
6500.0	0.000672	8.94	6499.5	0.004604	10.72	6499.9	0.008531	11.14
6599.5	0.000674	8.66	6599.5	0.004610	10.62	6599.9	0.008545	11.15
6699.5	0.000681	8.91	6699.5	0.004614	10.59	6700.0	0.008557	11.18
6799.0	0.000682	9.00	6799.6	0.004625	10.68	6800.0	0.008568	11.11
6899.1	0.000690	9.16	6899.1	0.004634	10.73	6899.0	0.008583	11.17
6999.1	0.000691	8.99	6999.1	0.004641	10.70	6999.0	0.008591	11.14
7099.1	0.000696	9.21	7099.2	0.004647	10.65	7099.1	0.008606	11.16
7198.7	0.000702	9.47	7198.7	0.004655	10.70	7198.1	0.008616	11.18
7299.2	0.000709	9.53	7299.2	0.004663	10.70	7299.1	0.008627	11.18
7399.2	0.000708	8.92	7399.3	0.004670	10.64	7399.2	0.008641	11.23
7499.2	0.000715	9.35	7499.3	0.004677	10.72	7499.2	0.008651	11.21
7599.3	0.000718	9.63	7599.3	0.004685	10.77	7599.2	0.008660	11.23
7699.3	0.000720	9.43	7699.3	0.004691	10.69	7699.2	0.008672	11.23
7799.3	0.000725	9.06	7799.4	0.004696	10.68	7799.3	0.008684	11.24
7899.4	0.000732	9.90	7899.4	0.004706	10.75	7899.3	0.008694	11.28
7999.4	0.000733	9.48	7999.4	0.004713	10.78	7999.3	0.008706	11.32
8099.4	0.000738	9.86	8099.5	0.004718	10.82	8099.4	0.008714	11.27
8199.5	0.000741	9.49	8199.5	0.004724	10.76	8199.4	0.008722	11.27
8299.5	0.000745	9.95	8299.5	0.004732	10.74	8299.4	0.008735	11.32
8399.5	0.000749	9.83	8399.5	0.004739	10.80	8399.4	0.008743	11.33
8499.5	0.000752	9.71	8499.6	0.004744	10.77	8499.5	0.008755	11.39

Appendix D1 – S12.5C (Continued)

8599.6	0.000756	9.91	8599.6	0.004751	10.82	8599.5	0.008765	11.35
8699.6	0.000760	9.51	8699.6	0.004758	10.73	8699.5	0.008774	11.38
8799.6	0.000765	9.96	8799.7	0.004767	10.84	8799.6	0.008782	11.39
8899.7	0.000768	10.17	8899.7	0.004773	10.75	8899.6	0.008795	11.43
8999.7	0.000772	10.26	8999.7	0.004778	10.84	8999.6	0.008803	11.41
9099.7	0.000776	10.18	9099.8	0.004782	10.86	9099.6	0.008816	11.40
9199.7	0.000784	10.30	9199.8	0.004788	10.83	9199.7	0.008823	11.37
9299.8	0.000789	10.49	9299.8	0.004792	10.85	9299.7	0.008834	11.49
9399.8	0.000791	10.14	9399.8	0.004800	10.87	9399.7	0.008840	11.40
9499.8	0.000796	10.54	9499.9	0.004807	10.92	9499.8	0.008848	11.43
9599.9	0.000796	10.17	9599.9	0.004811	10.89	9599.8	0.008856	11.43
9699.9	0.000802	10.51	9699.4	0.004816	10.83	9699.8	0.008866	11.44
9799.9	0.000806	10.34	9799.5	0.004820	10.83	9799.9	0.008873	11.46
9899.9	0.000808	10.37	9899.5	0.004828	10.88	9899.9	0.008883	11.46
9999.5	0.000812	10.24	9999.5	0.004831	10.79	9999.9	0.008890	11.43
10099.5	0.000817	10.73	10099.5	0.004839	10.91	10099.9	0.008898	11.47
10199.0	0.000818	10.35	10199.6	0.004842	10.81	10200.0	0.008907	11.47
10299.1	0.000822	10.55	10299.1	0.004848	10.85	10300.0	0.008917	11.53
10399.1	0.000823	10.50	10399.1	0.004853	10.83	10399.0	0.008924	11.50
10499.1	0.000829	10.86	10499.2	0.004860	10.90	10499.1	0.008929	11.48
10599.2	0.000833	11.12	10599.2	0.004864	10.88	10599.1	0.008936	11.47
10699.2	0.000835	10.46	10699.2	0.004869	10.82	10699.1	0.008943	11.51
10799.2	0.000837	10.60	10799.2	0.004874	10.85	10799.1	0.008950	11.49
10899.2	0.000839	10.54	10899.3	0.004881	10.99	10899.2	0.008961	11.52
10999.3	0.000841	10.72	10999.3	0.004885	10.95	10999.2	0.008967	11.50
11099.3	0.000844	10.83	11099.3	0.004889	10.91	11099.2	0.008978	11.55
11199.3	0.000849	10.94	11199.4	0.004892	10.86	11199.3	0.008984	11.55
11299.4	0.000851	10.61	11299.4	0.004900	10.96	11299.3	0.008990	11.54
11399.4	0.000854	10.71	11399.4	0.004905	10.93	11399.3	0.009000	11.60
11499.4	0.000857	10.86	11499.5	0.004909	10.95	11499.3	0.009005	11.59
11599.4	0.000863	11.36	11599.5	0.004915	10.96	11599.4	0.009015	11.62

Appendix D1 – S12.5C (Continued)

11699.5	0.000865	10.87	11699.5	0.004920	10.98	11699.4	0.009020	11.61
11799.5	0.000868	11.37	11799.5	0.004925	10.99	11799.4	0.009026	11.60
11898.5	0.000871	11.17	11899.1	0.004927	10.93	11899.0	0.009034	11.62
11999.6	0.000870	10.34	11999.6	0.004931	10.93	11999.5	0.009039	11.62

I19B								
20°C			40°C			54°C		
Cycles	ε_p	$\varepsilon_p/\varepsilon_r$	Cycles	ε_p	$\varepsilon_p/\varepsilon_r$	Cycles	ε_p	$\varepsilon_p/\varepsilon_r$
2.2	0.000017	0.38	2.0	0.000329	1.09	2.1	0.000973	1.74
4.2	0.000026	0.36	4.0	0.000532	1.61	4.1	0.001691	2.62
9.2	0.000043	0.59	9.0	0.000910	2.62	9.1	0.002655	4.00
19.2	0.000067	0.91	19.0	0.001426	4.09	19.1	0.003658	5.57
29.2	0.000084	0.95	29.0	0.001793	5.08	29.1	0.004271	6.59
39.2	0.000100	1.14	39.0	0.002086	5.98	39.1	0.004710	7.23
49.2	0.000113	1.28	49.0	0.002321	6.64	49.1	0.005059	7.77
59.2	0.000123	1.31	59.0	0.002524	7.16	59.1	0.005350	8.20
69.2	0.000135	1.48	69.0	0.002701	7.70	69.1	0.005600	8.56
79.2	0.000144	1.57	79.0	0.002857	8.16	79.1	0.005820	8.95
89.2	0.000155	1.76	89.0	0.002999	8.63	89.1	0.006015	9.24
99.2	0.000159	1.71	99.0	0.003125	8.93	99.1	0.006193	9.51
109.2	0.000170	1.85	109.0	0.003240	9.32	109.1	0.006352	9.71
119.2	0.000181	2.03	119.0	0.003345	9.64	119.1	0.006502	9.98
129.2	0.000187	2.05	129.0	0.003441	9.82	129.1	0.006640	10.18
139.2	0.000195	2.12	139.0	0.003532	10.15	139.1	0.006768	10.26
149.2	0.000201	2.23	148.0	0.003607	10.28	148.6	0.006884	10.54
159.2	0.000209	2.29	159.1	0.003696	10.60	159.2	0.007005	10.69
169.2	0.000215	2.33	169.1	0.003770	10.83	169.2	0.007110	10.82
179.2	0.000222	2.44	179.1	0.003841	11.00	179.2	0.007214	10.98
189.2	0.000230	2.62	189.1	0.003907	11.20	189.2	0.007309	11.11
199.2	0.000235	2.60	199.1	0.003971	11.31	199.2	0.007406	11.31
209.2	0.000240	2.61	209.1	0.004030	11.53	209.2	0.007491	11.37

Appendix D1 – I19B (Continued)

219.2	0.000250	2.84	219.1	0.004087	11.60	219.2	0.007577	11.52
229.2	0.000253	2.80	229.1	0.004141	11.71	229.2	0.007659	11.62
239.2	0.000259	2.79	239.1	0.004193	11.85	239.2	0.007737	11.72
249.3	0.000267	3.01	249.1	0.004243	11.96	249.2	0.007813	11.88
259.3	0.000272	3.06	259.1	0.004293	12.17	259.2	0.007885	11.91
269.3	0.000277	2.99	269.1	0.004338	12.21	269.2	0.007957	12.07
279.3	0.000285	3.20	279.1	0.004383	12.30	279.2	0.008023	12.10
289.3	0.000292	3.28	289.1	0.004425	12.39	289.2	0.008091	12.26
299.3	0.000297	3.32	299.1	0.004468	12.55	299.2	0.008153	12.32
309.3	0.000303	3.47	309.1	0.004507	12.74	309.2	0.008216	12.41
319.3	0.000307	3.36	319.1	0.004547	12.73	319.2	0.008273	12.45
329.3	0.000310	3.35	329.1	0.004585	12.94	329.2	0.008334	12.58
339.3	0.000319	3.67	339.1	0.004621	13.05	339.2	0.008392	12.66
349.3	0.000321	3.54	349.1	0.004655	13.09	349.2	0.008445	12.71
359.3	0.000323	3.42	359.1	0.004690	13.25	359.2	0.008499	12.77
369.3	0.000332	3.77	369.1	0.004723	13.24	369.2	0.008549	12.80
379.3	0.000336	3.79	379.1	0.004757	13.35	379.2	0.008602	12.94
389.3	0.000340	3.83	389.1	0.004787	13.37	389.2	0.008652	12.99
399.3	0.000346	3.86	399.1	0.004818	13.46	399.2	0.008702	13.09
409.3	0.000349	3.83	409.1	0.004850	13.57	409.2	0.008749	13.11
419.3	0.000357	4.14	419.1	0.004880	13.67	419.2	0.008794	13.18
429.3	0.000358	3.84	429.1	0.004912	13.91	429.2	0.008839	13.18
439.3	0.000362	3.92	439.1	0.004935	13.65	439.2	0.008885	13.28
449.3	0.000367	4.04	449.1	0.004964	13.77	449.2	0.008931	13.38
459.3	0.000371	4.10	459.1	0.004990	13.90	459.2	0.008972	13.38
469.3	0.000377	4.25	469.1	0.005015	13.90	469.2	0.009014	13.44
479.3	0.000380	4.20	479.1	0.005042	14.06	479.2	0.009058	13.58
489.3	0.000383	4.14	489.2	0.005066	13.99	489.3	0.009098	13.61
499.3	0.000386	4.22	499.2	0.005094	14.29	499.3	0.009138	13.65
599.4	0.000423	4.61	599.2	0.005314	14.71	599.3	0.009500	14.10
699.4	0.000461	5.10	699.2	0.005497	15.10	699.3	0.009806	14.51

Appendix D1 – I19B (Continued)

799.4	0.000493	5.36	799.2	0.005657	15.44	799.3	0.010079	14.84
899.4	0.000524	5.78	899.3	0.005797	15.76	899.4	0.010323	15.19
999.5	0.000556	6.23	999.3	0.005924	16.07	999.4	0.010539	15.45
1099.5	0.000585	6.55	1099.3	0.006037	16.25	1099.4	0.010734	15.69
1199.5	0.000611	6.86	1199.4	0.006143	16.52	1199.5	0.010912	15.85
1299.6	0.000634	6.77	1299.4	0.006237	16.62	1299.5	0.011076	16.10
1399.6	0.000660	7.26	1399.4	0.006328	17.03	1399.5	0.011230	16.28
1499.6	0.000681	7.43	1499.4	0.006411	17.12	1499.5	0.011376	16.55
1599.6	0.000778	8.59	1599.5	0.006487	17.26	1599.6	0.011507	16.59
1699.7	0.000802	9.20	1699.5	0.006561	17.46	1699.6	0.011633	16.72
1799.7	0.000824	9.19	1799.5	0.006628	17.49	1799.6	0.011752	16.92
1899.7	0.000849	9.89	1899.6	0.006694	17.66	1899.7	0.011864	17.05
1999.8	0.000867	9.42	1999.6	0.006753	17.60	1999.7	0.011972	17.20
2099.8	0.000884	9.69	2099.6	0.006812	17.77	2099.7	0.012075	17.35
2199.8	0.000905	10.30	2199.7	0.006869	17.87	2199.7	0.012173	17.44
2299.8	0.000921	10.34	2299.7	0.006924	18.00	2299.8	0.012265	17.52
2399.9	0.000941	11.15	2399.7	0.006973	18.02	2399.8	0.012354	17.60
2498.9	0.000958	10.88	2498.2	0.007023	18.17	2498.8	0.012439	17.77
2599.9	0.000974	11.17	2599.8	0.007070	18.36	2599.9	0.012522	17.86
2699.5	0.000993	11.36	2699.8	0.007117	18.32	2699.9	0.012601	17.91
2799.5	0.001007	11.61	2799.8	0.007159	18.37	2799.4	0.012678	18.05
2899.5	0.001023	11.88	2899.9	0.007203	18.38	2899.5	0.012752	18.12
2999.1	0.001036	11.44	2999.9	0.007244	18.56	2999.5	0.012822	18.20
3099.1	0.001052	11.80	3099.9	0.007283	18.54	3099.5	0.012893	18.30
3199.1	0.001066	12.06	3199.9	0.007323	18.65	3199.5	0.012959	18.34
3299.1	0.001081	12.35	3300.0	0.007359	18.63	3299.6	0.013024	18.45
3399.2	0.001096	12.89	3399.5	0.007395	18.73	3399.1	0.013084	18.39
3499.2	0.001110	12.64	3499.0	0.007435	18.82	3499.1	0.013148	18.59
3599.2	0.001122	13.13	3599.1	0.007465	18.79	3599.2	0.013205	18.58
3699.3	0.001137	13.04	3699.1	0.007499	18.96	3699.2	0.013263	18.71
3799.3	0.001148	12.56	3799.1	0.007534	18.99	3799.2	0.013321	18.83

Appendix D1 – I19B (Continued)

3899.3	0.001161	13.23	3899.1	0.007567	19.20	3899.2	0.013373	18.83
3999.3	0.001174	13.81	3999.2	0.007595	19.11	3999.3	0.013425	18.93
4099.4	0.001185	13.43	4099.2	0.007624	19.06	4099.3	0.013472	18.88
4199.4	0.001198	13.68	4199.2	0.007657	19.24	4199.3	0.013523	18.94
4299.4	0.001210	13.88	4299.3	0.007685	19.22	4299.4	0.013571	19.05
4399.5	0.001221	14.09	4399.3	0.007714	19.26	4399.4	0.013618	19.08
4499.5	0.001231	13.96	4499.3	0.007740	19.38	4499.4	0.013659	19.09
4599.5	0.001242	14.42	4599.4	0.007769	19.37	4599.5	0.013706	19.24
4699.5	0.001254	14.27	4699.4	0.007798	19.46	4699.5	0.013748	19.19
4799.6	0.001263	14.26	4799.4	0.007824	19.44	4799.5	0.013793	19.34
4899.6	0.001273	14.18	4899.4	0.007851	19.53	4899.5	0.013833	19.34
4999.6	0.001285	15.15	4999.5	0.007875	19.40	4999.6	0.013874	19.37
5099.7	0.001297	15.11	5099.5	0.007899	19.47	5099.6	0.013916	19.53
5199.7	0.001307	15.09	5199.5	0.007926	19.59	5199.6	0.013953	19.48
5299.7	0.001317	15.35	5299.6	0.007950	19.63	5299.7	0.013990	19.53
5399.8	0.001325	15.25	5399.6	0.007974	19.69	5399.7	0.014029	19.62
5499.8	0.001334	15.19	5499.6	0.007997	19.62	5499.7	0.014067	19.76
5599.8	0.001343	15.00	5599.6	0.008021	19.80	5599.7	0.014102	19.76
5699.8	0.001351	14.94	5699.7	0.008041	19.74	5699.8	0.014132	19.64
5799.9	0.001365	16.36	5799.7	0.008063	19.82	5799.8	0.014168	19.79
5899.9	0.001370	15.42	5899.7	0.008086	19.95	5899.8	0.014201	19.84
5999.9	0.001377	15.44	5999.8	0.008109	19.87	5999.9	0.014233	19.87
6100.0	0.001385	15.30	6099.8	0.008129	19.83	6099.9	0.014265	19.90
6199.5	0.001396	16.83	6199.8	0.008152	19.94	6199.4	0.014298	19.98
6299.5	0.001404	16.16	6299.8	0.008174	19.93	6299.4	0.014326	19.96
6399.0	0.001412	16.62	6399.9	0.008192	19.92	6399.5	0.014359	20.06
6499.1	0.001421	15.65	6499.9	0.008212	19.86	6499.5	0.014386	20.05
6599.1	0.001430	16.53	6599.9	0.008232	19.96	6599.5	0.014415	20.02
6699.1	0.001437	17.26	6700.0	0.008252	19.96	6699.6	0.014446	20.16
6799.2	0.001446	17.38	6800.0	0.008271	19.98	6799.1	0.014473	20.18
6899.2	0.001450	16.62	6899.0	0.008290	20.10	6899.1	0.014501	20.21

Appendix D1 – I19B (Continued)

6999.2	0.001457	16.79	6999.1	0.008310	20.05	6999.1	0.014529	20.26
7099.2	0.001464	16.38	7099.1	0.008328	20.10	7099.2	0.014561	20.36
7198.8	0.001475	17.14	7198.6	0.008346	20.08	7199.2	0.014582	20.26
7299.3	0.001481	16.72	7299.1	0.008364	20.11	7299.2	0.014610	20.31
7399.3	0.001487	16.71	7399.2	0.008384	20.15	7399.3	0.014640	20.47
7499.4	0.001495	16.97	7499.2	0.008403	20.34	7499.3	0.014663	20.40
7599.4	0.001504	17.29	7599.2	0.008420	20.28	7599.3	0.014688	20.42
7699.4	0.001511	17.70	7699.3	0.008436	20.14	7699.4	0.014714	20.45
7799.5	0.001519	17.87	7799.3	0.008457	20.38	7799.4	0.014739	20.47
7899.5	0.001525	17.98	7899.3	0.008475	20.38	7899.4	0.014763	20.51
7999.5	0.001530	17.40	7999.3	0.008491	20.34	7999.4	0.014789	20.59
8099.5	0.001536	17.84	8099.4	0.008507	20.21	8099.5	0.014810	20.53
8199.6	0.001546	18.12	8199.4	0.008525	20.36	8199.5	0.014835	20.64
8299.6	0.001551	17.87	8299.4	0.008543	20.50	8299.5	0.014857	20.61
8399.6	0.001560	18.76	8399.5	0.008556	20.24	8399.6	0.014881	20.68
8499.7	0.001563	18.07	8499.5	0.008573	20.38	8499.6	0.014904	20.67
8599.7	0.001568	17.93	8599.5	0.008588	20.36	8599.6	0.014928	20.81
8699.7	0.001575	17.66	8699.6	0.008604	20.47	8699.6	0.014950	20.88
8799.7	0.001582	17.99	8799.6	0.008621	20.43	8799.7	0.014969	20.71
8899.8	0.001589	18.71	8899.6	0.008636	20.51	8899.7	0.014992	20.84
8999.8	0.001595	18.22	8999.6	0.008653	20.68	8999.7	0.015013	20.90
9099.8	0.001599	17.90	9099.7	0.008666	20.49	9099.8	0.015033	20.87
9199.9	0.001606	18.20	9199.7	0.008681	20.62	9199.8	0.015055	20.96
9299.9	0.001616	19.85	9299.7	0.008696	20.59	9299.8	0.015075	21.00
9399.9	0.001618	18.14	9399.8	0.008710	20.59	9399.9	0.015094	20.94
9499.9	0.001623	18.87	9499.8	0.008726	20.66	9499.9	0.015113	21.02
9599.5	0.001630	19.31	9599.8	0.008742	20.78	9599.9	0.015137	21.10
9699.5	0.001633	18.32	9699.8	0.008756	20.70	9699.4	0.015155	21.13
9799.5	0.001639	18.59	9799.9	0.008770	20.71	9799.5	0.015174	21.15
9899.1	0.001646	19.09	9899.9	0.008782	20.71	9899.5	0.015194	21.19
9999.1	0.001652	19.13	9999.9	0.008799	20.77	9999.5	0.015210	21.13

Appendix D1 – I19B (Continued)

10099.1	0.001657	18.97	10100.0	0.008812	20.81	10099.6	0.015228	21.16
10199.2	0.001663	19.05	10200.0	0.008825	20.77	10199.1	0.015248	21.20
10299.2	0.001665	18.31	10299.0	0.008840	20.83	10299.1	0.015267	21.28
10399.2	0.001673	19.35	10399.0	0.008852	20.83	10399.1	0.015280	21.12
10499.2	0.001681	20.49	10499.1	0.008866	20.85	10499.2	0.015302	21.32
10599.3	0.001684	19.48	10599.1	0.008879	20.80	10599.2	0.015319	21.29
10699.3	0.001689	19.72	10699.1	0.008895	20.79	10699.2	0.015336	21.34
10799.3	0.001696	20.18	10799.2	0.008907	20.76	10799.3	0.015350	21.24
10899.4	0.001699	19.52	10899.2	0.008922	20.95	10899.3	0.015370	21.33
10999.4	0.001704	19.16	10999.2	0.008935	20.93	10999.3	0.015388	21.45
11099.4	0.001709	19.87	11099.3	0.008950	20.98	11099.3	0.015401	21.28
11199.4	0.001717	20.65	11199.3	0.008962	21.02	11199.4	0.015418	21.35
11299.5	0.001719	19.75	11299.3	0.008973	20.89	11299.4	0.015435	21.43
11399.5	0.001728	20.41	11399.3	0.008987	20.89	11399.4	0.015449	21.35
11499.5	0.001731	19.69	11499.4	0.009000	21.04	11499.5	0.015467	21.47
11599.6	0.001739	20.79	11599.4	0.009009	21.07	11599.5	0.015484	21.49
11699.6	0.001746	20.93	11699.4	0.009024	21.22	11699.5	0.015501	21.58
11799.6	0.001747	20.26	11799.5	0.009036	21.22	11799.6	0.015517	21.61
11899.6	0.001749	19.13	11899.5	0.009045	21.02	11899.1	0.015533	21.62
11999.7	0.001760	21.65	11999.5	0.009059	21.07	11999.6	0.015547	21.66

RI19B								
20°C			40°C			54°C		
Cycles	ε_p	$\varepsilon_p/\varepsilon_r$	Cycles	ε_p	$\varepsilon_p/\varepsilon_r$	Cycles	ε_p	$\varepsilon_p/\varepsilon_r$
2.2	0.000010	0.27	2.3	0.000097	0.48	2.2	0.000501	1.03
4.2	0.000015	0.35	4.3	0.000184	0.81	4.2	0.000809	1.49
9.2	0.000024	0.53	9.3	0.000318	1.30	9.2	0.001261	2.22
19.2	0.000029	0.68	19.0	0.000494	1.96	18.6	0.001740	2.99
29.2	0.000039	0.62	29.3	0.000626	2.45	29.2	0.002079	3.55
39.2	0.000043	0.68	39.3	0.000723	2.81	39.2	0.002311	3.93
49.2	0.000048	0.76	49.3	0.000805	3.10	49.2	0.002498	4.22

Appendix D1 – RI19B (Continued)

59.2	0.000050	0.75	59.3	0.000876	3.35	59.2	0.002651	4.45
69.2	0.000054	0.81	69.3	0.000938	3.58	69.2	0.002783	4.63
79.2	0.000059	0.88	79.3	0.000989	3.74	79.2	0.002899	4.82
89.2	0.000065	1.06	89.3	0.001041	3.97	89.2	0.003003	5.00
99.2	0.000069	1.11	99.3	0.001086	4.10	99.2	0.003094	5.10
109.2	0.000070	1.08	109.3	0.001126	4.25	109.2	0.003181	5.25
119.2	0.000074	1.19	119.3	0.001161	4.34	119.3	0.003259	5.34
129.2	0.000077	1.27	129.3	0.001196	4.44	129.3	0.003333	5.48
139.2	0.000078	1.16	139.4	0.001231	4.57	139.3	0.003399	5.56
148.2	0.000084	1.36	149.0	0.001258	4.64	148.6	0.003463	5.71
159.2	0.000085	1.29	159.4	0.001289	4.79	159.3	0.003526	5.76
169.2	0.000088	1.41	169.4	0.001315	4.84	169.3	0.003579	5.81
179.2	0.000092	1.46	179.4	0.001339	4.89	179.3	0.003633	5.90
189.2	0.000090	1.30	189.4	0.001363	4.93	189.3	0.003680	5.95
199.2	0.000093	1.48	199.4	0.001388	5.09	199.3	0.003726	6.01
209.2	0.000097	1.51	209.4	0.001411	5.15	209.3	0.003777	6.10
219.2	0.000098	1.46	219.4	0.001432	5.19	219.3	0.003816	6.14
229.2	0.000104	1.64	229.4	0.001450	5.23	229.3	0.003856	6.20
239.3	0.000105	1.65	239.4	0.001468	5.31	239.3	0.003900	6.27
249.3	0.000105	1.66	249.4	0.001486	5.34	249.3	0.003937	6.34
259.3	0.000109	1.74	259.4	0.001505	5.45	259.3	0.003973	6.37
269.3	0.000110	1.61	269.4	0.001523	5.45	269.3	0.004009	6.43
279.3	0.000113	1.76	279.4	0.001539	5.56	279.0	0.004038	6.42
289.3	0.000116	1.74	289.4	0.001555	5.57	289.3	0.004076	6.51
299.3	0.000118	1.92	299.4	0.001572	5.68	299.3	0.004106	6.53
309.3	0.000120	1.87	309.4	0.001584	5.67	309.3	0.004138	6.60
319.3	0.000122	1.91	319.4	0.001599	5.76	319.3	0.004165	6.61
329.3	0.000123	1.86	329.4	0.001611	5.73	329.3	0.004197	6.64
339.3	0.000124	1.95	339.4	0.001625	5.78	339.3	0.004224	6.67
349.3	0.000128	2.00	349.4	0.001639	5.81	349.3	0.004252	6.72
359.3	0.000131	2.10	359.4	0.001650	5.82	359.3	0.004278	6.74

Appendix D1 – RI19B (Continued)

369.3	0.000134	2.12	369.4	0.001664	5.91	369.3	0.004306	6.80
379.3	0.000134	2.08	379.4	0.001676	5.90	379.3	0.004330	6.81
389.3	0.000134	2.08	389.4	0.001687	5.96	389.3	0.004356	6.84
399.3	0.000138	2.19	399.4	0.001697	5.95	399.3	0.004380	6.89
409.3	0.000139	2.13	409.4	0.001710	6.03	409.3	0.004405	6.90
419.3	0.000140	2.24	419.4	0.001720	6.01	419.3	0.004426	6.91
429.3	0.000141	2.22	429.4	0.001730	6.04	429.3	0.004449	6.96
439.3	0.000146	2.28	439.4	0.001742	6.14	439.4	0.004472	7.01
449.3	0.000145	2.13	449.4	0.001750	6.10	449.4	0.004493	7.02
459.3	0.000144	2.15	459.5	0.001760	6.11	459.4	0.004515	7.03
469.3	0.000147	2.19	469.5	0.001770	6.13	469.4	0.004533	7.04
479.3	0.000150	2.38	479.5	0.001780	6.23	479.4	0.004554	7.07
489.3	0.000153	2.23	489.5	0.001791	6.21	489.4	0.004575	7.13
499.3	0.000151	2.29	499.5	0.001799	6.27	499.4	0.004592	7.11
599.4	0.000167	2.62	599.5	0.001881	6.41	599.4	0.004772	7.34
699.4	0.000181	2.76	699.5	0.001950	6.62	699.4	0.004926	7.52
799.4	0.000193	2.98	799.6	0.002007	6.73	799.5	0.005060	7.68
899.4	0.000203	3.05	899.6	0.002059	6.87	899.5	0.005182	7.87
999.5	0.000215	3.44	999.6	0.002108	7.05	999.5	0.005288	7.97
1099.5	0.000224	3.49	1099.3	0.002150	7.16	1099.5	0.005386	8.09
1199.5	0.000233	3.68	1199.3	0.002184	7.15	1199.6	0.005477	8.22
1299.6	0.000243	3.81	1299.4	0.002221	7.23	1299.6	0.005554	8.29
1399.6	0.000254	3.88	1399.4	0.002252	7.27	1399.6	0.005630	8.38
1499.6	0.000259	3.83	1499.4	0.002283	7.35	1499.7	0.005701	8.46
1599.6	0.000270	4.05	1599.5	0.002310	7.40	1599.7	0.005767	8.58
1699.7	0.000279	4.35	1699.5	0.002335	7.43	1699.7	0.005825	8.63
1799.7	0.000287	4.71	1799.5	0.002362	7.51	1799.4	0.005884	8.72
1899.7	0.000292	4.64	1899.5	0.002384	7.54	1899.4	0.005936	8.76
1999.8	0.000299	4.43	1999.6	0.002404	7.52	1999.5	0.005988	8.82
2099.8	0.000309	4.78	2099.6	0.002427	7.65	2099.5	0.006036	8.89
2199.8	0.000314	4.76	2199.6	0.002448	7.66	2199.5	0.006083	8.96

Appendix D1 – RI19B (Continued)

2299.4	0.000321	4.94	2299.7	0.002468	7.68	2299.6	0.006129	9.03
2399.4	0.000329	5.10	2399.7	0.002486	7.73	2399.6	0.006172	9.07
2497.9	0.000335	5.33	2499.0	0.002507	7.79	2499.0	0.006211	9.09
2599.4	0.000342	5.47	2599.7	0.002522	7.79	2599.7	0.006252	9.17
2699.5	0.000348	5.18	2699.4	0.002538	7.75	2699.7	0.006290	9.23
2799.5	0.000354	5.44	2799.5	0.002555	7.87	2799.7	0.006326	9.27
2899.5	0.000359	5.44	2899.5	0.002570	7.87	2899.4	0.006359	9.28
2999.6	0.000364	5.66	2999.5	0.002584	7.88	2999.4	0.006393	9.37
3099.6	0.000370	5.93	3099.6	0.002598	7.95	3099.5	0.006422	9.34
3199.6	0.000375	5.70	3199.6	0.002613	7.89	3199.5	0.006454	9.41
3299.6	0.000382	6.00	3299.6	0.002625	7.95	3299.5	0.006487	9.44
3399.2	0.000385	5.92	3399.3	0.002641	8.02	3399.2	0.006514	9.46
3499.2	0.000391	5.70	3499.3	0.002653	8.02	3499.2	0.006542	9.49
3599.2	0.000395	6.21	3599.4	0.002661	7.99	3599.3	0.006569	9.55
3699.3	0.000402	6.29	3699.4	0.002678	8.12	3699.3	0.006596	9.58
3799.3	0.000407	6.64	3799.4	0.002690	8.01	3799.3	0.006621	9.58
3899.3	0.000408	6.27	3899.5	0.002702	8.03	3899.4	0.006648	9.64
3999.3	0.000416	6.51	3999.5	0.002718	8.17	3999.4	0.006673	9.67
4099.4	0.000421	6.55	4099.5	0.002724	8.11	4099.4	0.006697	9.71
4199.4	0.000422	6.66	4199.5	0.002735	8.16	4198.8	0.006720	9.72
4299.4	0.000426	6.46	4299.6	0.002743	8.11	4299.5	0.006742	9.76
4399.5	0.000433	6.77	4399.6	0.002756	8.20	4399.5	0.006766	9.82
4499.5	0.000437	7.29	4499.3	0.002765	8.20	4499.5	0.006787	9.80
4599.5	0.000440	6.83	4599.3	0.002777	8.21	4599.6	0.006807	9.86
4699.6	0.000450	6.92	4699.4	0.002787	8.29	4699.6	0.006828	9.89
4799.6	0.000450	6.94	4799.4	0.002794	8.26	4799.6	0.006849	9.90
4899.6	0.000455	7.53	4899.4	0.002805	8.30	4899.7	0.006870	9.93
4999.6	0.000459	6.97	4999.4	0.002811	8.30	4999.7	0.006889	9.95
5099.7	0.000462	7.11	5099.5	0.002820	8.29	5099.7	0.006905	9.95
5199.7	0.000466	7.47	5199.5	0.002829	8.33	5199.4	0.006925	9.97
5299.7	0.000475	7.85	5299.5	0.002836	8.33	5299.4	0.006944	10.03

Appendix D1 – RI19B (Continued)

5399.8	0.000474	7.86	5399.6	0.002844	8.29	5399.5	0.006964	10.07
5499.8	0.000477	7.22	5499.6	0.002851	8.30	5499.5	0.006979	10.05
5599.8	0.000484	7.98	5599.6	0.002859	8.34	5599.5	0.006995	10.07
5699.3	0.000489	7.53	5699.6	0.002867	8.40	5699.6	0.007014	10.10
5799.4	0.000490	7.87	5799.7	0.002876	8.37	5799.6	0.007033	10.09
5899.4	0.000491	8.04	5899.7	0.002881	8.38	5899.6	0.007049	10.16
5999.4	0.000494	7.69	5999.7	0.002890	8.48	5999.6	0.007063	10.13
6099.5	0.000500	7.74	6099.4	0.002896	8.43	6099.7	0.007080	10.16
6199.5	0.000501	7.60	6199.5	0.002904	8.50	6199.7	0.007111	10.18
6299.5	0.000506	7.95	6299.5	0.002911	8.49	6299.4	0.007127	10.17
6399.5	0.000507	7.79	6399.5	0.002919	8.47	6399.4	0.007146	10.22
6499.6	0.000515	7.88	6499.6	0.002926	8.53	6499.5	0.007163	10.26
6599.6	0.000518	8.10	6599.6	0.002934	8.55	6599.5	0.007177	10.24
6699.6	0.000518	8.05	6699.6	0.002939	8.58	6699.5	0.007195	10.32
6799.7	0.000520	8.59	6799.6	0.002945	8.52	6799.2	0.007207	10.29
6899.2	0.000525	8.18	6899.3	0.002951	8.59	6899.2	0.007225	10.34
6999.2	0.000528	8.21	6999.4	0.002955	8.51	6999.3	0.007237	10.33
7099.3	0.000530	8.63	7099.4	0.002963	8.57	7099.3	0.007252	10.30
7198.8	0.000536	8.44	7199.1	0.002971	8.58	7198.7	0.007266	10.36
7299.3	0.000536	8.34	7299.5	0.002977	8.64	7299.4	0.007280	10.37
7399.3	0.000543	8.60	7399.5	0.002980	8.52	7399.4	0.007291	10.38
7499.4	0.000547	8.81	7499.5	0.002986	8.54	7499.4	0.007306	10.42
7599.4	0.000549	8.47	7599.5	0.002992	8.57	7599.5	0.007318	10.42
7699.4	0.000549	8.85	7699.6	0.002999	8.66	7699.5	0.007331	10.44
7799.5	0.000551	8.65	7799.6	0.003004	8.65	7799.5	0.007343	10.43
7899.5	0.000552	8.93	7899.3	0.003009	8.59	7899.5	0.007357	10.48
7999.5	0.000557	8.95	7999.3	0.003015	8.72	7999.6	0.007366	10.46
8099.5	0.000565	9.29	8099.4	0.003020	8.64	8099.6	0.007381	10.53
8199.6	0.000564	8.99	8199.4	0.003026	8.70	8199.6	0.007394	10.55
8299.6	0.000566	9.11	8299.4	0.003032	8.65	8299.7	0.007407	10.57
8399.6	0.000568	9.25	8399.4	0.003035	8.66	8399.7	0.007415	10.53

Appendix D1 – RI19B (Continued)

8499.7	0.000573	8.91	8499.5	0.003041	8.69	8499.7	0.007429	10.56
8599.7	0.000576	9.24	8599.5	0.003046	8.71	8599.4	0.007439	10.57
8699.7	0.000578	8.81	8699.5	0.003053	8.73	8699.4	0.007451	10.61
8799.8	0.000577	8.87	8799.6	0.003056	8.69	8799.5	0.007465	10.60
8899.8	0.000581	8.94	8899.6	0.003062	8.69	8898.8	0.007474	10.59
8999.8	0.000586	9.79	8999.6	0.003067	8.72	8999.5	0.007484	10.63
9099.3	0.000586	9.25	9099.6	0.003071	8.72	9099.6	0.007498	10.69
9199.4	0.000588	8.90	9199.7	0.003077	8.74	9199.6	0.007508	10.70
9299.4	0.000591	9.32	9299.7	0.003079	8.64	9299.6	0.007519	10.68
9399.4	0.000596	8.96	9399.7	0.003084	8.73	9399.6	0.007527	10.67
9499.5	0.000597	9.32	9499.4	0.003088	8.75	9499.7	0.007538	10.70
9599.5	0.000601	9.97	9599.5	0.003092	8.73	9599.7	0.007549	10.72
9699.5	0.000602	9.61	9699.5	0.003098	8.81	9699.4	0.007559	10.71
9799.5	0.000609	10.13	9799.5	0.003102	8.79	9799.4	0.007570	10.73
9899.6	0.000606	9.47	9899.5	0.003108	8.80	9899.5	0.007581	10.75
9999.6	0.000608	10.19	9999.6	0.003113	8.81	9999.5	0.007590	10.75
10099.6	0.000611	9.32	10099.6	0.003115	8.76	10099.5	0.007602	10.78
10199.7	0.000612	9.35	10199.6	0.003123	8.89	10199.2	0.007613	10.83
10299.2	0.000614	9.81	10299.3	0.003125	8.79	10299.2	0.007623	10.80
10399.2	0.000620	10.06	10399.4	0.003131	8.85	10399.3	0.007632	10.85
10499.2	0.000620	10.12	10499.4	0.003136	8.92	10499.3	0.007644	10.89
10599.3	0.000621	9.67	10599.4	0.003139	8.86	10599.3	0.007652	10.85
10699.3	0.000628	10.29	10699.4	0.003143	8.84	10699.4	0.007662	10.90
10799.3	0.000626	9.90	10799.5	0.003148	8.85	10799.4	0.007673	10.92
10899.4	0.000630	10.39	10899.5	0.003153	8.89	10899.4	0.007680	10.91
10999.4	0.000630	9.79	10999.5	0.003156	8.89	10999.4	0.007690	10.90
11099.4	0.000633	10.30	11099.6	0.003161	8.92	11099.5	0.007700	10.97
11199.5	0.000635	10.32	11199.6	0.003167	8.92	11199.5	0.007710	10.97
11299.5	0.000638	10.16	11299.3	0.003171	8.93	11299.5	0.007717	10.97
11399.5	0.000639	10.19	11399.3	0.003173	8.91	11399.6	0.007728	11.01
11499.5	0.000640	10.00	11499.3	0.003176	8.87	11499.6	0.007736	11.00

11599.6	0.000644	10.27	11599.4	0.003180	8.87	11599.6	0.007742	10.93
11699.6	0.000647	10.06	11699.4	0.003188	8.96	11699.7	0.007751	10.99
11799.6	0.000646	10.44	11799.4	0.003192	8.92	11799.7	0.007759	11.00
11898.7	0.000650	10.13	11899.5	0.003196	8.97	11899.4	0.007768	11.00
11999.7	0.000650	10.20	11999.5	0.003199	8.96	11999.4	0.007779	11.05

B25B								
20°C			40°C			54°C		
Cycles	ε_p	$\varepsilon_p/\varepsilon_r$	Cycles	ε_p	$\varepsilon_p/\varepsilon_r$	Cycles	ε_p	$\varepsilon_p/\varepsilon_r$
2.7	0.000014	0.27	2.3	0.000273	0.90	2.0	0.001000	1.59
4.7	0.000020	0.59	4.3	0.000426	1.33	4.0	0.001461	2.17
9.7	0.000028	0.67	9.3	0.000715	2.09	9.0	0.002124	3.01
19.7	0.000042	0.82	19.3	0.001100	3.31	17.0	0.002737	3.80
29.7	0.000049	0.69	29.3	0.001358	3.73	29.0	0.003301	4.59
39.7	0.000057	0.81	39.3	0.001568	4.33	39.0	0.003629	5.01
49.7	0.000065	0.92	49.3	0.001738	4.80	49.0	0.003893	5.37
59.7	0.000070	1.02	59.3	0.001875	5.11	59.0	0.004112	5.69
69.7	0.000073	1.02	69.3	0.001992	5.32	69.0	0.004299	5.96
79.7	0.000076	1.01	79.3	0.002103	5.69	79.0	0.004459	6.14
89.7	0.000081	1.09	89.3	0.002200	5.94	89.0	0.004606	6.36
99.8	0.000085	1.17	99.3	0.002286	6.21	99.0	0.004732	6.52
109.8	0.000091	1.26	109.3	0.002366	6.33	109.0	0.004851	6.70
119.8	0.000092	1.29	119.3	0.002440	6.57	119.0	0.004953	6.82
129.8	0.000097	1.35	129.3	0.002498	6.62	129.0	0.005053	6.98
139.8	0.000097	1.31	139.3	0.002555	6.70	139.0	0.005145	7.09
148.8	0.000102	1.40	148.3	0.002610	6.88	149.1	0.005227	7.15
159.3	0.000108	1.48	159.4	0.002664	6.99	159.1	0.005306	7.28
169.3	0.000108	1.45	169.4	0.002709	7.15	169.1	0.005379	7.35
179.3	0.000111	1.51	179.4	0.002757	7.29	179.1	0.005453	7.46
189.3	0.000113	1.50	189.4	0.002802	7.35	189.1	0.005520	7.53
199.3	0.000121	1.78	199.4	0.002852	7.52	199.1	0.005585	7.60

Appendix D1 – B25B (Continued)

209.3	0.000117	1.56	209.4	0.002891	7.63	209.1	0.005647	7.69
219.3	0.000125	1.82	219.4	0.002923	7.60	219.1	0.005708	7.78
229.3	0.000125	1.64	229.4	0.002957	7.73	229.1	0.005768	7.89
239.3	0.000126	1.70	239.4	0.002993	7.85	239.1	0.005821	7.92
249.3	0.000130	1.87	249.4	0.003030	7.99	249.1	0.005874	8.01
259.3	0.000129	1.73	259.4	0.003058	7.84	259.1	0.005921	8.01
269.3	0.000135	1.91	269.4	0.003097	8.04	269.1	0.005972	8.05
279.3	0.000135	1.79	279.4	0.003124	8.19	278.1	0.006015	8.14
289.3	0.000141	2.01	289.4	0.003153	8.18	289.1	0.006068	8.22
299.3	0.000140	1.91	299.4	0.003177	8.20	299.1	0.006112	8.24
309.3	0.000144	2.01	309.4	0.003206	8.26	309.1	0.006154	8.29
319.3	0.000144	2.01	319.4	0.003224	8.35	319.1	0.006196	8.31
329.3	0.000147	2.01	329.4	0.003256	8.40	329.1	0.006239	8.43
339.3	0.000147	1.92	339.4	0.003275	8.29	339.1	0.006279	8.45
349.3	0.000153	2.16	349.4	0.003297	8.38	349.1	0.006315	8.51
359.3	0.000151	2.01	359.4	0.003319	8.39	359.1	0.006352	8.55
369.3	0.000156	2.18	369.4	0.003337	8.44	369.1	0.006390	8.61
379.3	0.000159	2.25	379.4	0.003360	8.52	379.1	0.006424	8.65
389.3	0.000159	2.22	389.4	0.003374	8.53	389.1	0.006460	8.68
399.3	0.000161	2.18	399.4	0.003392	8.62	399.1	0.006493	8.71
409.3	0.000162	2.22	409.4	0.003408	8.66	409.1	0.006529	8.79
419.4	0.000165	2.29	419.4	0.003425	8.70	419.1	0.006562	8.84
429.4	0.000165	2.23	429.4	0.003446	8.76	429.1	0.006594	8.86
439.4	0.000167	2.31	439.4	0.003457	8.77	439.1	0.006626	8.87
449.4	0.000166	2.17	449.4	0.003477	8.76	449.1	0.006654	8.90
459.4	0.000173	2.37	459.4	0.003493	8.78	459.1	0.006687	8.99
469.4	0.000174	2.42	469.4	0.003511	8.79	469.1	0.006715	9.03
479.4	0.000175	2.46	479.4	0.003528	8.86	479.2	0.006744	9.05
489.4	0.000178	2.47	489.4	0.003545	8.87	489.2	0.006772	9.09
499.4	0.000180	2.48	499.4	0.003567	8.99	499.2	0.006800	9.10
599.4	0.000195	2.77	599.5	0.003703	9.22	599.2	0.007047	9.39

Appendix D1 – B25B (Continued)

699.4	0.000209	2.90	699.5	0.003821	9.36	699.2	0.007258	9.69
799.5	0.000220	3.01	799.5	0.003917	9.64	799.2	0.007432	9.82
899.5	0.000234	3.17	899.6	0.003998	9.81	899.3	0.007583	9.98
999.5	0.000245	3.25	999.6	0.004058	9.78	999.3	0.007719	10.15
1099.5	0.000255	3.44	1099.6	0.004122	9.75	1099.3	0.007839	10.35
1199.6	0.000268	3.62	1199.7	0.004204	10.01	1199.4	0.007945	10.39
1299.6	0.000279	3.76	1299.7	0.004264	10.11	1299.4	0.008051	10.56
1399.6	0.000289	4.02	1399.7	0.004326	10.29	1399.4	0.008146	10.66
1499.7	0.000300	4.07	1499.2	0.004382	10.35	1499.4	0.008235	10.75
1599.7	0.000310	4.19	1599.3	0.004431	10.48	1599.5	0.008314	10.83
1699.7	0.000318	4.29	1699.3	0.004478	10.52	1699.5	0.008392	10.94
1799.3	0.000326	4.38	1799.3	0.004494	10.51	1799.5	0.008462	11.01
1899.3	0.000337	4.66	1899.4	0.004521	10.44	1899.6	0.008534	11.13
1999.3	0.000343	4.43	1999.4	0.004594	10.68	1999.6	0.008601	11.19
2099.3	0.000351	4.54	2099.4	0.004612	10.68	2099.6	0.008658	11.22
2199.4	0.000359	4.83	2199.4	0.004662	10.70	2199.7	0.008721	11.29
2299.4	0.000368	4.97	2299.5	0.004699	10.81	2299.7	0.008779	11.40
2399.4	0.000373	4.92	2399.5	0.004741	10.85	2399.7	0.008832	11.42
2499.0	0.000383	5.00	2498.5	0.004765	10.92	2498.2	0.008881	11.51
2599.5	0.000392	5.15	2599.6	0.004785	10.87	2599.8	0.008934	11.59
2699.5	0.000399	5.23	2699.6	0.004822	10.90	2699.8	0.008980	11.61
2799.5	0.000407	5.32	2799.6	0.004842	10.96	2799.8	0.009029	11.71
2899.6	0.000411	5.23	2899.6	0.004879	11.02	2899.9	0.009070	11.72
2999.6	0.000421	5.56	2999.7	0.004892	11.11	2999.9	0.009110	11.77
3099.6	0.000425	5.56	3099.7	0.004939	11.14	3099.9	0.009153	11.86
3199.7	0.000434	5.78	3199.7	0.004957	11.11	3199.9	0.009190	11.90
3299.7	0.000440	5.89	3299.8	0.004988	11.16	3300.0	0.009229	11.92
3399.7	0.000447	5.78	3399.3	0.005021	11.24	3399.0	0.009268	12.03
3499.8	0.000451	5.90	3499.3	0.005036	11.15	3499.0	0.009306	12.06
3599.3	0.000458	6.06	3599.4	0.005073	11.43	3599.1	0.009341	12.10
3699.3	0.000463	5.99	3699.4	0.005077	11.22	3699.1	0.009378	12.18

Appendix D1 – B25B (Continued)

3799.3	0.000470	6.25	3799.4	0.005104	11.31	3799.1	0.009415	12.23
3899.4	0.000472	5.89	3899.4	0.005133	11.33	3899.2	0.009447	12.28
3999.4	0.000479	6.24	3999.5	0.005164	11.47	3999.2	0.009480	12.29
4099.4	0.000485	6.34	4099.5	0.005186	11.45	4099.2	0.009514	12.37
4199.5	0.000491	6.46	4199.5	0.005333	11.80	4199.2	0.009546	12.41
4299.5	0.000496	6.73	4299.6	0.005415	12.36	4299.3	0.009576	12.44
4399.5	0.000499	6.44	4399.6	0.005417	11.98	4399.3	0.009606	12.50
4499.5	0.000501	6.26	4499.6	0.005419	12.03	4499.3	0.009637	12.53
4599.6	0.000506	6.51	4599.6	0.005404	11.92	4599.4	0.009664	12.54
4699.6	0.000515	6.78	4699.7	0.005424	12.01	4699.4	0.009691	12.60
4799.6	0.000519	6.53	4799.7	0.005422	11.97	4799.4	0.009717	12.60
4899.7	0.000525	6.84	4899.2	0.005432	11.91	4899.4	0.009747	12.67
4999.7	0.000527	6.66	4999.3	0.005457	11.98	4999.5	0.009769	12.64
5099.7	0.000535	7.00	5099.3	0.005470	11.93	5099.5	0.009797	12.71
5199.2	0.000538	6.86	5199.3	0.005483	11.95	5199.5	0.009822	12.73
5299.3	0.000545	7.02	5299.3	0.005499	12.08	5299.6	0.009844	12.78
5399.3	0.000549	7.16	5399.4	0.005514	12.06	5399.6	0.009869	12.81
5499.3	0.000552	6.99	5499.4	0.005533	12.09	5499.6	0.009894	12.87
5599.4	0.000554	6.95	5599.4	0.005544	12.06	5599.6	0.009916	12.88
5699.4	0.000559	7.04	5699.5	0.005550	12.02	5699.7	0.009940	12.91
5799.4	0.000561	7.10	5799.5	0.005578	12.43	5799.7	0.009963	12.99
5899.4	0.000567	7.51	5899.5	0.005589	12.19	5899.7	0.009984	12.99
5999.5	0.000575	7.69	5999.5	0.005599	12.13	5999.8	0.010008	13.04
6099.5	0.000578	7.19	6099.6	0.005609	12.00	6099.8	0.010030	13.05
6199.5	0.000580	7.16	6199.6	0.005623	12.07	6199.8	0.010050	13.03
6299.6	0.000585	7.27	6299.6	0.005635	12.20	6299.9	0.010072	13.05
6399.6	0.000587	7.39	6399.7	0.005644	11.96	6399.9	0.010093	13.08
6499.6	0.000592	7.52	6499.7	0.005660	12.12	6499.9	0.010116	13.11
6599.7	0.000595	7.81	6599.7	0.005683	12.26	6599.9	0.010140	13.19
6699.7	0.000596	7.58	6699.8	0.005693	12.23	6700.0	0.010159	13.20
6799.7	0.000603	7.77	6799.8	0.005706	12.32	6799.5	0.010180	13.16

Appendix D1 – B25B (Continued)

6899.7	0.000607	8.02	6899.3	0.005713	12.17	6899.0	0.010200	13.22
6999.8	0.000609	8.10	6999.3	0.005729	12.30	6999.1	0.010221	13.26
7099.3	0.000606	7.63	7099.4	0.005737	12.35	7099.1	0.010242	13.26
7199.3	0.000610	7.89	7198.9	0.005726	12.27	7198.6	0.010262	13.30
7299.4	0.000617	8.12	7299.4	0.005723	12.25	7299.1	0.010284	13.33
7399.4	0.000619	8.09	7399.5	0.005744	12.24	7399.2	0.010306	13.39
7499.4	0.000623	7.88	7499.5	0.005757	12.27	7499.2	0.010322	13.39
7599.4	0.000628	7.99	7599.5	0.005778	12.25	7599.2	0.010341	13.40
7699.5	0.000630	7.96	7699.5	0.005800	12.36	7699.3	0.010362	13.47
7799.5	0.000635	7.97	7799.6	0.005811	12.42	7799.3	0.010376	13.41
7899.5	0.000640	8.11	7899.6	0.005829	12.40	7899.3	0.010397	13.46
7999.6	0.000644	8.11	7999.6	0.005839	12.38	7999.4	0.010414	13.48
8099.6	0.000649	8.33	8099.7	0.005854	12.45	8099.4	0.010430	13.49
8199.6	0.000652	8.10	8199.7	0.005871	12.58	8199.4	0.010446	13.46
8299.6	0.000654	8.21	8299.2	0.005886	12.54	8299.4	0.010462	13.51
8399.7	0.000658	8.23	8399.2	0.005893	12.46	8399.5	0.010481	13.53
8499.7	0.000664	8.72	8499.3	0.005904	12.42	8499.5	0.010498	13.59
8599.2	0.000665	8.32	8599.3	0.005915	12.52	8599.5	0.010515	13.62
8699.3	0.000665	8.17	8699.3	0.005927	12.53	8699.6	0.010529	13.59
8799.3	0.000669	8.24	8799.4	0.005935	12.65	8799.6	0.010541	13.55
8899.3	0.000674	8.60	8899.4	0.005933	12.44	8899.6	0.010558	13.61
8999.3	0.000675	8.54	8999.4	0.005956	12.56	8999.6	0.010574	13.66
9099.4	0.000678	8.27	9099.4	0.005959	12.59	9099.7	0.010589	13.67
9199.4	0.000681	8.63	9199.5	0.005972	12.80	9199.7	0.010600	13.65
9299.4	0.000683	8.53	9299.5	0.005984	12.65	9299.7	0.010615	13.69
9399.5	0.000689	8.47	9399.5	0.005993	12.65	9399.8	0.010629	13.71
9499.5	0.000689	8.35	9499.6	0.006001	12.64	9499.8	0.010642	13.71
9599.5	0.000694	8.57	9599.6	0.006006	12.73	9599.8	0.010658	13.75
9699.6	0.000696	8.37	9699.6	0.006020	12.69	9699.8	0.010671	13.77
9799.6	0.000701	8.71	9799.7	0.006031	12.74	9799.9	0.010686	13.78
9899.6	0.000705	8.97	9899.7	0.006042	12.75	9899.9	0.010700	13.83

Appendix D1 – B25B (Continued)

9999.6	0.000705	8.94	9999.7	0.006049	12.76	9999.9	0.010711	13.77
10099.7	0.000710	8.93	10099.7	0.006060	12.85	10100.0	0.010727	13.82
10199.7	0.000712	9.11	10199.8	0.006066	12.75	10199.5	0.010740	13.86
10299.7	0.000715	8.59	10299.3	0.006077	12.89	10299.0	0.010754	13.85
10399.8	0.000719	9.08	10399.3	0.006087	12.83	10399.1	0.010766	13.88
10499.3	0.000719	8.85	10499.4	0.006096	12.91	10499.1	0.010777	13.86
10599.3	0.000722	8.74	10599.4	0.006102	12.87	10599.1	0.010792	13.92
10699.3	0.000724	9.11	10699.4	0.006102	12.73	10699.1	0.010803	13.91
10799.4	0.000728	8.98	10799.4	0.006115	12.86	10799.2	0.010816	13.93
10899.4	0.000734	9.40	10899.5	0.006124	12.96	10899.2	0.010831	13.96
10999.4	0.000736	8.91	10999.5	0.006129	12.73	10999.2	0.010842	13.95
11099.5	0.000741	9.35	11099.5	0.006141	12.88	11099.3	0.010855	14.02
11199.5	0.000742	9.24	11199.6	0.006146	13.06	11199.3	0.010867	13.99
11299.5	0.000743	9.11	11299.6	0.006155	12.86	11299.3	0.010879	13.98
11399.5	0.000743	8.53	11399.6	0.006160	12.85	11399.3	0.010896	14.04
11499.6	0.000749	9.31	11499.6	0.006171	12.89	11499.4	0.010907	14.08
11599.6	0.000753	9.20	11599.7	0.006178	12.99	11599.4	0.010918	14.05
11699.6	0.000756	9.57	11699.7	0.006190	13.02	11699.4	0.010931	14.10
11799.7	0.000759	9.67	11799.2	0.006194	12.97	11799.5	0.010944	14.10
11898.7	0.000763	9.64	11898.8	0.006198	12.91	11899.5	0.010954	14.07
11999.7	0.000771	10.04	11999.3	0.006213	13.13	11999.5	0.010967	14.17

RB25B								
20°C			40°C			54°C		
Cycles	ε_p	$\varepsilon_p/\varepsilon_r$	Cycles	ε_p	$\varepsilon_p/\varepsilon_r$	Cycles	ε_p	$\varepsilon_p/\varepsilon_r$
2.2	0.000003	0.08	2.4	0.000065	0.41	2.2	0.000469	1.09
4.3	0.000007	0.13	4.4	0.000115	0.64	3.8	0.000637	1.39
9.3	0.000014	0.42	9.4	0.000198	1.05	8.2	0.000991	2.03
18.8	0.000021	0.36	19.4	0.000309	1.62	19.2	0.001534	3.10
29.4	0.000026	0.44	29.4	0.000385	1.96	29.2	0.001832	3.67
39.4	0.000029	0.48	39.4	0.000452	2.34	39.2	0.002051	4.11

Appendix D1 – RB25B (Continued)

49.4	0.000031	0.49	49.4	0.000499	2.48	49.2	0.002224	4.46
59.4	0.000034	0.56	59.4	0.000547	2.78	59.2	0.002367	4.69
69.4	0.000039	0.65	69.4	0.000589	2.98	69.2	0.002493	4.95
79.4	0.000041	0.67	79.4	0.000622	3.11	79.2	0.002599	5.10
89.4	0.000042	0.68	89.4	0.000656	3.30	89.2	0.002698	5.30
99.4	0.000047	0.73	99.4	0.000685	3.41	99.2	0.002785	5.44
109.4	0.000047	0.77	109.4	0.000717	3.68	109.2	0.002862	5.53
119.4	0.000050	0.85	119.4	0.000738	3.64	119.2	0.002937	5.68
129.4	0.000051	0.84	129.4	0.000764	3.87	129.2	0.003004	5.78
139.4	0.000053	0.88	139.4	0.000785	3.92	139.2	0.003070	5.94
148.4	0.000056	0.90	148.9	0.000808	4.04	148.2	0.003123	6.00
159.4	0.000057	0.93	159.4	0.000829	4.04	159.2	0.003181	6.07
169.4	0.000059	0.95	169.4	0.000848	4.29	169.2	0.003235	6.18
179.4	0.000062	1.08	179.4	0.000868	4.33	179.2	0.003285	6.26
189.4	0.000069	1.29	189.4	0.000885	4.38	189.2	0.003331	6.35
199.4	0.000068	1.19	199.4	0.000900	4.41	199.2	0.003378	6.43
209.4	0.000067	1.16	209.4	0.000920	4.55	209.2	0.003419	6.46
219.4	0.000068	1.11	219.4	0.000932	4.58	219.2	0.003460	6.53
229.4	0.000071	1.22	229.4	0.000949	4.74	229.2	0.003499	6.59
239.4	0.000072	1.18	239.4	0.000961	4.75	239.3	0.003537	6.64
249.4	0.000075	1.29	249.4	0.000971	4.66	249.3	0.003573	6.72
259.4	0.000074	1.20	259.4	0.000986	4.85	259.3	0.003611	6.79
269.4	0.000072	1.15	269.4	0.001001	4.88	269.3	0.003641	6.80
279.4	0.000075	1.24	279.4	0.001012	4.94	279.3	0.003674	6.83
289.4	0.000077	1.32	289.4	0.001026	5.01	289.3	0.003707	6.90
299.4	0.000081	1.45	299.4	0.001037	5.08	299.3	0.003735	6.93
309.4	0.000079	1.31	309.4	0.001048	5.17	309.3	0.003768	7.02
319.4	0.000080	1.31	319.5	0.001058	5.11	319.3	0.003796	7.05
329.4	0.000080	1.31	329.5	0.001069	5.26	329.3	0.003821	7.06
339.4	0.000083	1.40	339.5	0.001078	5.19	339.0	0.003849	7.09
349.4	0.000083	1.36	349.5	0.001091	5.43	349.3	0.003876	7.15

Appendix D1 – RB25B (Continued)

359.5	0.000084	1.35	359.5	0.001101	5.45	359.0	0.003903	7.21
369.5	0.000087	1.53	369.5	0.001109	5.45	369.3	0.003929	7.25
379.5	0.000087	1.42	379.5	0.001115	5.37	379.3	0.003953	7.28
389.5	0.000087	1.44	389.5	0.001129	5.65	389.3	0.003977	7.32
399.5	0.000091	1.60	399.5	0.001133	5.44	399.3	0.004001	7.37
409.0	0.000090	1.53	409.5	0.001142	5.58	409.3	0.004022	7.34
419.5	0.000092	1.58	419.5	0.001153	5.63	419.3	0.004044	7.40
429.5	0.000090	1.46	429.5	0.001156	5.50	429.3	0.004068	7.44
439.5	0.000097	1.78	439.5	0.001166	5.65	439.3	0.004088	7.48
449.5	0.000093	1.54	449.5	0.001174	5.75	449.3	0.004107	7.47
459.5	0.000095	1.56	459.5	0.001183	5.71	459.3	0.004130	7.54
469.5	0.000095	1.60	469.5	0.001189	5.78	469.3	0.004151	7.57
479.5	0.000097	1.62	479.0	0.001195	5.78	479.3	0.004171	7.61
489.5	0.000098	1.65	489.5	0.001203	5.78	489.3	0.004190	7.61
499.5	0.000100	1.66	499.0	0.001214	6.06	499.3	0.004209	7.63
599.5	0.000112	1.80	599.5	0.001274	6.07	599.4	0.004385	7.88
699.6	0.000116	1.87	699.6	0.001326	6.34	699.4	0.004534	8.05
799.6	0.000125	2.01	799.6	0.001374	6.60	799.4	0.004668	8.29
899.6	0.000137	2.35	899.6	0.001416	6.76	899.4	0.004785	8.44
999.6	0.000148	2.46	999.6	0.001450	6.78	999.5	0.004893	8.63
1099.7	0.000155	2.55	1099.7	0.001485	7.10	1099.5	0.004988	8.75
1199.7	0.000160	2.62	1199.2	0.001514	7.09	1199.5	0.005077	8.85
1299.7	0.000166	2.83	1299.2	0.001542	7.19	1299.6	0.005159	8.95
1399.8	0.000172	2.81	1399.3	0.001565	7.25	1399.6	0.005235	9.03
1499.8	0.000180	3.16	1499.3	0.001588	7.37	1499.6	0.005306	9.09
1599.8	0.000184	2.88	1599.3	0.001614	7.55	1599.7	0.005377	9.28
1699.8	0.000191	3.20	1699.4	0.001630	7.48	1699.3	0.005438	9.32
1799.9	0.000199	3.41	1798.4	0.001654	7.59	1799.4	0.005499	9.39
1899.9	0.000200	3.35	1899.4	0.001671	7.58	1899.4	0.005557	9.45
1999.9	0.000207	3.35	1999.4	0.001688	7.67	1999.4	0.005612	9.50
2100.0	0.000212	3.58	2099.5	0.001705	7.80	2099.5	0.005663	9.63

Appendix D1 – RB25B (Continued)

2199.5	0.000217	3.44	2199.5	0.001724	7.90	2199.5	0.005714	9.66
2299.5	0.000227	3.73	2298.5	0.001737	7.95	2299.5	0.005760	9.69
2399.1	0.000229	3.72	2399.6	0.001756	8.10	2399.6	0.005809	9.81
2498.1	0.000233	3.80	2499.6	0.001767	7.87	2498.9	0.005849	9.80
2599.1	0.000237	3.86	2599.6	0.001779	8.01	2599.6	0.005893	9.84
2699.1	0.000242	3.66	2699.6	0.001790	8.06	2699.6	0.005934	9.90
2799.2	0.000248	3.96	2799.7	0.001803	8.09	2799.7	0.005974	10.00
2899.2	0.000256	4.22	2899.7	0.001815	8.07	2899.7	0.006012	10.02
2999.2	0.000256	4.10	2999.2	0.001826	8.15	2999.7	0.006050	10.09
3099.3	0.000263	4.29	3099.8	0.001838	8.19	3099.8	0.006085	10.08
3199.3	0.000267	4.11	3199.8	0.001851	8.41	3199.8	0.006122	10.18
3299.3	0.000269	4.14	3299.3	0.001862	8.43	3299.8	0.006154	10.20
3399.3	0.000276	4.75	3399.4	0.001873	8.22	3399.2	0.006189	10.25
3499.4	0.000276	4.10	3499.4	0.001884	8.32	3498.9	0.006218	10.26
3599.4	0.000283	4.56	3599.4	0.001895	8.51	3599.2	0.006251	10.31
3699.4	0.000290	4.68	3699.4	0.001905	8.34	3699.3	0.006281	10.39
3799.5	0.000293	4.75	3799.5	0.001913	8.25	3799.3	0.006309	10.39
3899.5	0.000307	5.87	3899.5	0.001921	8.19	3899.3	0.006340	10.46
3999.5	0.000302	4.63	3999.5	0.001930	8.36	3999.4	0.006369	10.51
4099.5	0.000306	4.94	4099.6	0.001941	8.44	4099.4	0.006396	10.53
4199.6	0.000307	4.79	4199.6	0.001949	8.32	4199.4	0.006421	10.54
4299.6	0.000311	4.90	4299.6	0.001962	8.65	4299.4	0.006446	10.55
4399.6	0.000318	4.94	4399.6	0.001972	8.62	4399.5	0.006471	10.58
4499.7	0.000320	4.90	4499.7	0.001977	8.46	4499.5	0.006499	10.69
4599.7	0.000325	5.68	4599.2	0.001985	8.34	4599.5	0.006520	10.62
4699.7	0.000327	5.41	4699.2	0.001995	8.66	4699.6	0.006550	10.74
4799.8	0.000332	5.34	4799.3	0.002002	8.79	4799.6	0.006570	10.74
4899.8	0.000335	5.19	4899.3	0.002010	8.71	4899.6	0.006595	10.81
4999.8	0.000338	5.47	4999.3	0.002020	8.69	4999.6	0.006616	10.79
5099.8	0.000340	5.17	5099.3	0.002027	8.63	5099.3	0.006640	10.85
5199.9	0.000345	5.53	5199.4	0.002033	8.48	5199.4	0.006663	10.86

Appendix D1 – RB25B (Continued)

5299.9	0.000347	5.55	5299.4	0.002046	8.83	5299.4	0.006685	10.89
5399.9	0.000351	5.57	5399.4	0.002053	8.92	5399.4	0.006704	10.91
5500.0	0.000357	5.53	5499.5	0.002058	8.68	5499.1	0.006728	11.00
5599.5	0.000355	5.53	5599.5	0.002064	8.61	5599.5	0.006749	11.03
5699.5	0.000359	5.65	5699.5	0.002076	8.80	5699.2	0.006769	11.01
5799.0	0.000363	6.22	5799.6	0.002079	8.79	5799.6	0.006789	11.08
5899.1	0.000365	5.73	5899.6	0.002085	8.93	5899.6	0.006807	11.03
5999.1	0.000369	5.85	5999.1	0.002089	8.73	5999.6	0.006825	11.02
6099.1	0.000374	5.86	6099.6	0.002101	8.98	6099.6	0.006843	11.07
6199.2	0.000373	5.82	6199.7	0.002108	9.00	6199.3	0.006864	11.16
6299.2	0.000375	6.01	6299.7	0.002115	8.93	6299.7	0.006882	11.15
6399.2	0.000378	5.60	6399.7	0.002119	8.89	6399.7	0.006900	11.17
6499.3	0.000383	6.14	6499.8	0.002126	8.85	6499.8	0.006916	11.17
6599.3	0.000381	5.81	6599.8	0.002128	8.78	6599.8	0.006934	11.23
6699.3	0.000383	5.80	6699.8	0.002141	9.02	6699.8	0.006955	11.30
6799.3	0.000390	6.34	6799.3	0.002141	8.88	6799.5	0.006969	11.27
6899.4	0.000393	6.50	6899.4	0.002146	8.84	6899.2	0.006986	11.31
6999.4	0.000398	6.79	6999.4	0.002154	8.90	6999.2	0.007001	11.31
7099.4	0.000397	6.11	7099.4	0.002164	9.01	7099.3	0.007016	11.33
7199.0	0.000400	6.24	7199.0	0.002171	9.06	7199.3	0.007036	11.41
7299.5	0.000403	6.61	7299.5	0.002175	8.93	7299.3	0.007049	11.40
7399.5	0.000408	6.60	7399.0	0.002179	8.84	7399.4	0.007064	11.41
7499.5	0.000411	6.62	7499.6	0.002185	8.85	7499.4	0.007081	11.44
7599.6	0.000413	6.85	7599.1	0.002194	9.11	7599.4	0.007093	11.41
7699.6	0.000419	7.27	7699.6	0.002201	8.98	7699.4	0.007109	11.45
7799.6	0.000420	6.91	7799.6	0.002205	9.07	7799.5	0.007124	11.48
7899.7	0.000422	7.21	7899.7	0.002208	8.94	7899.5	0.007138	11.45
7999.7	0.000424	6.73	7999.2	0.002216	8.97	7999.5	0.007154	11.56
8099.7	0.000424	6.42	8099.2	0.002223	9.00	8099.6	0.007168	11.52
8199.7	0.000426	6.49	8199.3	0.002227	8.96	8199.6	0.007184	11.60
8299.8	0.000428	6.51	8299.3	0.002235	9.03	8299.3	0.007197	11.60

Appendix D1 – RB25B (Continued)

8399.8	0.000432	7.24	8399.3	0.002240	9.21	8399.3	0.007209	11.60
8499.8	0.000432	7.02	8497.8	0.002245	8.95	8499.0	0.007224	11.63
8599.9	0.000434	6.88	8598.4	0.002252	9.01	8599.4	0.007236	11.62
8699.9	0.000437	6.82	8699.4	0.002259	9.16	8699.4	0.007249	11.64
8799.9	0.000440	6.99	8799.4	0.002260	8.95	8799.4	0.007262	11.67
8900.0	0.000443	7.56	8899.0	0.002267	9.09	8899.5	0.007274	11.68
8999.5	0.000446	7.30	8999.5	0.002272	9.14	8999.5	0.007283	11.66
9099.5	0.000447	7.10	9099.5	0.002279	9.11	9099.5	0.007299	11.72
9199.0	0.000449	7.26	9199.1	0.002284	9.13	9199.6	0.007310	11.73
9299.1	0.000452	7.61	9299.6	0.002292	9.16	9299.6	0.007319	11.70
9399.1	0.000455	7.37	9399.6	0.002295	8.93	9399.6	0.007334	11.80
9499.1	0.000453	7.60	9499.6	0.002301	9.12	9499.6	0.007345	11.77
9599.2	0.000456	7.26	9599.7	0.002310	9.21	9599.7	0.007357	11.78
9699.2	0.000458	7.36	9699.7	0.002314	9.11	9699.7	0.007370	11.84
9799.2	0.000462	7.85	9799.7	0.002321	9.19	9799.7	0.007380	11.84
9899.2	0.000463	7.80	9899.8	0.002324	9.17	9899.8	0.007392	11.86
9999.3	0.000463	7.73	9999.8	0.002329	9.19	9999.8	0.007403	11.85
10099.3	0.000464	7.31	10099.8	0.002339	9.38	10099.8	0.007415	11.86
10199.3	0.000468	7.64	10199.3	0.002339	9.12	10199.5	0.007426	11.89
10299.4	0.000467	7.70	10299.4	0.002347	9.19	10299.2	0.007439	11.93
10399.4	0.000469	7.33	10399.4	0.002346	9.02	10399.2	0.007449	11.94
10499.4	0.000472	7.59	10499.4	0.002356	9.24	10499.3	0.007459	11.94
10599.5	0.000474	7.49	10599.5	0.002359	9.18	10599.3	0.007471	11.97
10699.5	0.000476	7.79	10699.5	0.002370	9.39	10699.0	0.007481	11.97
10799.5	0.000477	7.64	10799.5	0.002371	9.03	10799.4	0.007490	11.98
10899.5	0.000479	7.87	10898.6	0.002376	9.14	10899.4	0.007502	12.01
10999.6	0.000480	7.41	10999.6	0.002383	9.40	10999.4	0.007512	12.02
11099.6	0.000484	8.06	11099.6	0.002387	9.21	11099.4	0.007522	12.03
11199.6	0.000486	8.25	11199.6	0.002394	9.24	11199.5	0.007532	12.02
11299.7	0.000487	7.88	11299.7	0.002396	9.21	11299.5	0.007543	12.09
11399.7	0.000491	7.70	11399.2	0.002400	9.20	11399.5	0.007551	12.05

Appendix D1 – RB25B (Continued)

11499.7	0.000493	8.14	11499.2	0.002409	9.27	11499.6	0.007562	12.08
11599.7	0.000493	8.13	11599.3	0.002413	9.36	11599.6	0.007573	12.11
11699.8	0.000497	8.38	11699.3	0.002419	9.23	11699.6	0.007583	12.13
11799.8	0.000500	8.06	11799.3	0.002428	9.35	11799.3	0.007591	12.13
11899.3	0.000499	7.80	11899.3	0.002433	9.44	11898.7	0.007601	12.12
11999.9	0.000499	7.10	11998.9	0.002434	9.38	11999.4	0.007613	12.20

RS9.5B								
20°C			40°C			54°C		
Cycles	ε_p	$\varepsilon_p/\varepsilon_r$	Cycles	ε_p	$\varepsilon_p/\varepsilon_r$	Cycles	ε_p	$\varepsilon_p/\varepsilon_r$
2.0	0.000007	0.10	2.4	0.000134	0.49	2.4	0.000479	0.84
4.0	0.000014	0.25	4.4	0.000212	0.73	4.4	0.000889	1.35
9.0	0.000019	0.28	9.4	0.000350	1.19	9.4	0.001464	2.17
18.0	0.000029	0.43	19.4	0.000542	1.86	18.9	0.002053	3.05
29.0	0.000043	0.60	29.4	0.000682	2.32	29.5	0.002456	3.69
39.0	0.000043	0.54	39.4	0.000791	2.67	39.5	0.002723	4.11
49.0	0.000045	0.58	49.4	0.000882	2.97	49.5	0.002928	4.40
59.0	0.000050	0.66	59.4	0.000962	3.22	59.5	0.003093	4.62
69.0	0.000055	0.68	69.4	0.001034	3.47	69.5	0.003234	4.81
79.0	0.000059	0.77	79.4	0.001091	3.62	79.5	0.003356	4.97
89.0	0.000062	0.83	89.4	0.001150	3.82	89.5	0.003463	5.12
99.0	0.000067	0.88	99.4	0.001200	4.02	99.5	0.003560	5.27
109.0	0.000071	0.91	109.4	0.001248	4.19	109.5	0.003646	5.37
119.0	0.000068	0.84	119.4	0.001289	4.33	119.5	0.003723	5.44
129.0	0.000072	0.91	129.4	0.001327	4.39	129.5	0.003794	5.53
139.0	0.000076	0.97	139.4	0.001367	4.59	139.5	0.003860	5.60
149.1	0.000078	0.98	147.9	0.001395	4.62	148.7	0.003918	5.66
159.1	0.000079	0.99	159.4	0.001432	4.76	159.5	0.003980	5.75
169.1	0.000082	1.07	169.4	0.001462	4.82	169.5	0.004035	5.80
179.1	0.000082	0.98	179.4	0.001497	5.05	179.5	0.004086	5.87
189.1	0.000087	1.09	189.4	0.001521	5.06	189.5	0.004133	5.90

Appendix D1 – RS9.5B (Continued)

199.1	0.000094	1.23	199.4	0.001545	5.12	199.5	0.004178	5.96
209.1	0.000091	1.14	209.4	0.001571	5.23	209.5	0.004222	5.99
219.1	0.000096	1.29	219.4	0.001593	5.27	219.5	0.004263	6.05
229.1	0.000097	1.24	229.4	0.001615	5.32	229.5	0.004302	6.08
239.1	0.000095	1.19	239.5	0.001637	5.39	239.5	0.004340	6.14
249.1	0.000101	1.32	249.5	0.001656	5.44	249.5	0.004377	6.17
259.1	0.000104	1.38	259.5	0.001677	5.53	259.5	0.004411	6.19
269.1	0.000100	1.25	269.5	0.001692	5.49	269.5	0.004447	6.24
277.6	0.000104	1.29	279.0	0.001712	5.59	279.0	0.004476	6.25
289.1	0.000104	1.27	289.5	0.001730	5.65	289.5	0.004509	6.29
299.1	0.000107	1.31	299.5	0.001748	5.72	299.5	0.004539	6.33
309.1	0.000109	1.40	309.5	0.001767	5.84	309.5	0.004567	6.33
319.1	0.000109	1.38	319.5	0.001779	5.84	319.5	0.004596	6.37
329.1	0.000113	1.50	329.5	0.001797	5.92	329.5	0.004623	6.40
339.1	0.000112	1.36	339.5	0.001808	5.85	339.5	0.004650	6.44
349.1	0.000117	1.49	349.5	0.001822	5.93	349.6	0.004675	6.45
359.1	0.000116	1.48	359.5	0.001839	5.97	359.6	0.004700	6.45
369.1	0.000118	1.44	369.5	0.001848	5.95	369.6	0.004727	6.52
379.1	0.000117	1.47	379.5	0.001861	6.03	379.6	0.004750	6.53
389.1	0.000122	1.60	389.5	0.001876	6.15	389.6	0.004772	6.55
399.1	0.000123	1.55	399.5	0.001891	6.22	399.6	0.004795	6.57
408.6	0.000126	1.58	409.0	0.001898	6.15	409.6	0.004816	6.58
419.1	0.000122	1.52	419.5	0.001910	6.14	419.6	0.004837	6.60
429.1	0.000123	1.51	429.5	0.001922	6.20	429.6	0.004860	6.64
439.1	0.000125	1.57	439.5	0.001935	6.26	439.6	0.004878	6.63
449.1	0.000130	1.58	449.5	0.001943	6.24	449.6	0.004901	6.67
459.1	0.000128	1.60	459.5	0.001953	6.22	459.6	0.004918	6.67
469.1	0.000132	1.65	469.5	0.001964	6.34	469.6	0.004939	6.70
479.2	0.000133	1.73	479.5	0.001974	6.35	479.6	0.004957	6.71
489.2	0.000135	1.81	489.5	0.001986	6.38	489.6	0.004975	6.73
499.2	0.000134	1.76	499.5	0.001992	6.35	499.6	0.004994	6.75

Appendix D1 – RS9.5B (Continued)

599.2	0.000148	1.93	599.6	0.002079	6.59	599.6	0.005156	6.91
699.2	0.000157	2.00	699.6	0.002143	6.79	699.7	0.005293	7.02
799.2	0.000165	2.11	799.6	0.002202	6.94	799.2	0.005413	7.16
899.3	0.000172	2.12	899.1	0.002253	7.12	899.2	0.005516	7.21
999.3	0.000181	2.27	999.2	0.002300	7.21	999.2	0.005613	7.33
1099.3	0.000188	2.35	1099.2	0.002336	7.30	1099.3	0.005698	7.40
1199.4	0.000200	2.69	1199.2	0.002370	7.35	1199.3	0.005774	7.43
1299.4	0.000202	2.57	1299.3	0.002403	7.42	1299.3	0.005845	7.50
1399.4	0.000210	2.68	1399.3	0.002430	7.46	1399.4	0.005911	7.54
1499.5	0.000215	2.79	1499.3	0.002458	7.54	1499.4	0.005975	7.62
1599.5	0.000222	2.90	1599.3	0.002483	7.64	1599.4	0.006032	7.63
1699.5	0.000228	2.93	1699.4	0.002505	7.61	1699.4	0.006086	7.69
1799.5	0.000233	3.08	1799.4	0.002526	7.60	1799.5	0.006136	7.72
1899.6	0.000238	3.02	1899.4	0.002548	7.68	1899.5	0.006185	7.75
1999.6	0.000243	3.14	1999.5	0.002566	7.78	1999.5	0.006232	7.80
2099.6	0.000248	3.23	2099.5	0.002584	7.83	2099.6	0.006273	7.81
2199.7	0.000255	3.38	2199.5	0.002601	7.83	2199.6	0.006317	7.88
2299.7	0.000259	3.44	2299.6	0.002617	7.87	2299.6	0.006358	7.92
2399.7	0.000262	3.47	2399.6	0.002636	7.85	2399.7	0.006398	7.96
2498.7	0.000265	3.53	2497.6	0.002649	7.96	2499.2	0.006436	7.98
2599.8	0.000273	3.65	2599.6	0.002665	8.08	2599.7	0.006471	8.00
2699.8	0.000282	3.79	2699.7	0.002676	8.03	2699.5	0.006507	8.08
2799.8	0.000287	3.99	2799.7	0.002690	8.10	2799.5	0.006539	8.06
2899.9	0.000288	3.87	2899.7	0.002702	8.09	2899.5	0.006571	8.11
2999.9	0.000293	4.06	2999.8	0.002712	8.07	2999.6	0.006601	8.12
3099.9	0.000296	3.86	3099.8	0.002724	8.10	3099.6	0.006631	8.15
3200.0	0.000297	3.88	3199.8	0.002736	8.13	3199.6	0.006658	8.16
3300.0	0.000302	3.87	3299.8	0.002747	8.14	3299.7	0.006688	8.18
3399.0	0.000306	4.16	3399.4	0.002757	8.18	3399.4	0.006716	8.23
3499.0	0.000308	4.08	3499.4	0.002768	8.20	3499.5	0.006743	8.22
3599.1	0.000310	4.11	3599.4	0.002777	8.24	3599.5	0.006767	8.22

Appendix D1 – RS9.5B (Continued)

3699.1	0.000315	4.07	3699.5	0.002786	8.24	3699.5	0.006794	8.28
3799.1	0.000318	4.36	3799.5	0.002793	8.27	3799.6	0.006818	8.31
3899.2	0.000318	4.29	3899.5	0.002804	8.28	3899.6	0.006844	8.36
3999.2	0.000322	4.34	3999.5	0.002812	8.30	3999.6	0.006864	8.34
4099.2	0.000325	4.25	4099.6	0.002822	8.32	4099.6	0.006884	8.34
4199.2	0.000326	4.33	4199.6	0.002831	8.39	4199.2	0.006908	8.40
4299.3	0.000331	4.57	4299.1	0.002837	8.35	4299.2	0.006930	8.40
4399.3	0.000332	4.39	4399.2	0.002846	8.36	4399.2	0.006950	8.42
4499.3	0.000336	4.51	4499.2	0.002852	8.37	4499.3	0.006973	8.45
4599.4	0.000341	4.86	4599.2	0.002861	8.43	4599.3	0.006993	8.47
4699.4	0.000341	4.74	4699.3	0.002866	8.33	4699.3	0.007011	8.46
4799.4	0.000342	4.68	4799.3	0.002873	8.39	4799.4	0.007032	8.49
4899.5	0.000344	4.73	4899.3	0.002880	8.38	4899.4	0.007050	8.51
4999.5	0.000348	4.85	4999.3	0.002886	8.41	4999.4	0.007068	8.52
5099.5	0.000346	4.75	5099.4	0.002894	8.45	5099.4	0.007085	8.54
5199.5	0.000347	4.78	5199.4	0.002900	8.49	5199.5	0.007101	8.53
5299.6	0.000350	4.82	5299.4	0.002907	8.50	5299.5	0.007119	8.56
5399.6	0.000353	4.88	5399.5	0.002913	8.47	5399.5	0.007135	8.55
5499.6	0.000356	5.05	5499.5	0.002919	8.52	5499.6	0.007152	8.59
5599.7	0.000358	4.76	5599.5	0.002926	8.56	5599.6	0.007168	8.59
5699.7	0.000359	5.03	5699.5	0.002929	8.50	5699.6	0.007184	8.60
5799.7	0.000356	4.83	5799.6	0.002937	8.56	5799.6	0.007202	8.66
5899.7	0.000360	4.99	5899.6	0.002942	8.52	5899.7	0.007216	8.65
5999.8	0.000362	4.96	5999.6	0.002952	8.67	5999.7	0.007232	8.69
6099.8	0.000364	5.23	6099.7	0.002955	8.58	6099.5	0.007246	8.67
6199.8	0.000366	5.23	6199.7	0.002959	8.61	6199.5	0.007259	8.66
6299.9	0.000368	5.28	6299.7	0.002964	8.55	6299.5	0.007276	8.70
6399.9	0.000368	5.23	6399.8	0.002971	8.65	6399.6	0.007290	8.71
6499.9	0.000366	4.95	6499.8	0.002975	8.67	6499.6	0.007307	8.75
6600.0	0.000368	5.04	6599.8	0.002979	8.63	6599.6	0.007319	8.77
6700.0	0.000369	5.16	6699.8	0.002985	8.64	6699.7	0.007332	8.76

Appendix D1 – RS9.5B (Continued)

6799.0	0.000375	5.44	6799.9	0.002987	8.63	6799.4	0.007347	8.76
6899.0	0.000373	5.24	6899.4	0.002994	8.61	6899.5	0.007358	8.77
6999.1	0.000371	4.72	6999.4	0.002997	8.63	6999.5	0.007371	8.80
7099.1	0.000377	5.32	7099.5	0.003003	8.62	7099.5	0.007385	8.80
7197.6	0.000380	5.51	7198.0	0.003004	8.71	7199.3	0.007396	8.81
7299.2	0.000379	5.23	7299.5	0.003011	8.73	7299.6	0.007410	8.81
7399.2	0.000381	5.40	7399.5	0.003012	8.65	7399.6	0.007424	8.85
7499.2	0.000383	5.55	7499.6	0.003018	8.68	7499.6	0.007435	8.85
7599.2	0.000382	5.31	7599.6	0.003023	8.72	7599.4	0.007444	8.84
7699.3	0.000381	5.25	7699.6	0.003027	8.69	7699.2	0.007457	8.86
7799.3	0.000385	5.37	7799.2	0.003031	8.72	7799.2	0.007468	8.85
7899.3	0.000384	5.32	7899.2	0.003036	8.68	7899.3	0.007479	8.87
7999.4	0.000386	5.34	7999.2	0.003036	8.67	7999.3	0.007491	8.87
8099.4	0.000389	5.62	8099.2	0.003042	8.72	8099.3	0.007502	8.91
8199.4	0.000391	5.51	8199.3	0.003047	8.73	8199.4	0.007513	8.91
8299.5	0.000393	5.48	8299.3	0.003051	8.79	8299.4	0.007523	8.92
8399.5	0.000397	5.57	8399.3	0.003056	8.80	8399.4	0.007535	8.92
8499.5	0.000399	5.36	8499.4	0.003058	8.82	8499.4	0.007546	8.95
8599.5	0.000399	5.62	8599.4	0.003062	8.80	8599.5	0.007555	8.95
8699.6	0.000398	5.34	8699.4	0.003066	8.81	8699.5	0.007567	8.97
8799.6	0.000402	5.84	8799.5	0.003070	8.83	8799.5	0.007575	8.95
8899.6	0.000405	5.91	8899.5	0.003075	8.86	8899.6	0.007586	8.96
8999.7	0.000401	5.71	8999.5	0.003082	8.90	8999.6	0.007596	8.98
9099.7	0.000401	5.67	9099.5	0.003080	8.79	9099.6	0.007605	8.98
9199.7	0.000408	6.12	9199.6	0.003084	8.85	9199.6	0.007615	8.99
9299.7	0.000405	5.88	9299.6	0.003087	8.85	9299.7	0.007625	8.98
9399.8	0.000404	5.67	9399.6	0.003090	8.85	9399.7	0.007635	9.01
9499.8	0.000410	5.64	9499.7	0.003092	8.82	9499.7	0.007647	9.06
9599.8	0.000411	5.56	9599.7	0.003098	8.90	9599.5	0.007653	9.03
9699.9	0.000413	5.96	9699.7	0.003101	8.87	9699.5	0.007664	9.05
9799.9	0.000416	6.10	9799.7	0.003103	8.82	9799.6	0.007671	9.04

Appendix D1 – RS9.5B (Continued)

9899.9	0.000414	5.78	9899.8	0.003107	8.86	9899.6	0.007682	9.07
9999.9	0.000417	6.34	9999.8	0.003111	8.82	9999.6	0.007692	9.06
10100.0	0.000417	6.06	10099.8	0.003114	8.87	10099.7	0.007699	9.08
10199.0	0.000417	5.85	10199.9	0.003116	8.88	10199.4	0.007708	9.10
10299.0	0.000422	6.49	10299.4	0.003119	8.90	10299.5	0.007715	9.08
10399.1	0.000423	6.21	10399.4	0.003123	8.95	10399.5	0.007726	9.11
10499.1	0.000427	6.42	10499.4	0.003125	8.92	10499.5	0.007733	9.11
10599.1	0.000423	5.92	10599.5	0.003132	8.92	10599.6	0.007742	9.13
10699.2	0.000424	6.05	10699.5	0.003133	8.96	10699.6	0.007752	9.13
10799.2	0.000425	5.96	10799.5	0.003138	8.91	10799.6	0.007761	9.16
10899.2	0.000426	6.10	10899.6	0.003141	8.95	10899.6	0.007767	9.15
10999.2	0.000430	6.31	10999.6	0.003143	8.95	10999.4	0.007774	9.14
11099.3	0.000429	6.07	11099.6	0.003145	8.93	11099.2	0.007782	9.15
11199.3	0.000427	5.94	11199.1	0.003152	8.97	11199.2	0.007789	9.13
11299.3	0.000428	5.85	11299.2	0.003151	8.92	11299.3	0.007799	9.17
11399.4	0.000429	6.24	11399.2	0.003158	9.06	11399.3	0.007806	9.18
11499.4	0.000429	6.10	11499.2	0.003160	9.02	11499.3	0.007815	9.21
11599.4	0.000430	6.25	11599.3	0.003160	8.98	11599.4	0.007822	9.20
11699.4	0.000433	6.22	11699.3	0.003164	9.00	11699.4	0.007830	9.20
11799.5	0.000431	5.92	11799.3	0.003168	8.99	11799.4	0.007838	9.20
11898.5	0.000434	6.51	11899.4	0.003168	9.00	11899.4	0.007845	9.22
11999.5	0.000433	6.06	11999.4	0.003170	8.98	11999.5	0.007853	9.21

RS12.5C								
20°C			40°C			54°C		
Cycles	ε_p	$\varepsilon_p/\varepsilon_r$	Cycles	ε_p	$\varepsilon_p/\varepsilon_r$	Cycles	ε_p	$\varepsilon_p/\varepsilon_r$
1.5	0.000000	0.00	2.1	0.000074	0.62	2.0	0.000338	0.82
2.6	0.000003	0.08	4.1	0.000124	0.86	4.0	0.000514	1.16
9.4	0.000009	0.21	9.1	0.000203	1.30	9.0	0.000795	1.74
18.4	0.000016	0.44	18.1	0.000293	1.82	18.3	0.001113	2.43
29.4	0.000017	0.34	29.1	0.000375	2.33	29.0	0.001340	2.94

Appendix D1 – RS12.5C (Continued)

39.5	0.000022	0.46	39.2	0.000434	2.69	39.0	0.001492	3.30
49.5	0.000028	0.65	49.2	0.000482	2.95	49.0	0.001612	3.55
59.5	0.000030	0.70	59.2	0.000526	3.24	59.0	0.001707	3.74
69.5	0.000027	0.56	69.2	0.000565	3.52	69.0	0.001787	3.89
79.5	0.000030	0.64	79.2	0.000596	3.68	79.0	0.001858	4.06
89.5	0.000033	0.71	89.2	0.000628	3.84	89.0	0.001920	4.17
99.5	0.000034	0.70	99.2	0.000655	4.03	99.0	0.001974	4.28
109.5	0.000034	0.69	109.2	0.000681	4.19	109.0	0.002023	4.38
119.5	0.000036	0.72	119.2	0.000708	4.45	119.0	0.002064	4.43
129.5	0.000040	0.81	129.2	0.000728	4.44	129.0	0.002105	4.52
139.5	0.000039	0.78	139.2	0.000750	4.65	138.7	0.002140	4.56
149.5	0.000040	0.81	149.2	0.000768	4.66	148.1	0.002171	4.63
159.5	0.000041	0.80	159.2	0.000792	4.90	159.1	0.002208	4.71
169.5	0.000044	0.88	169.2	0.000807	4.99	169.1	0.002235	4.71
179.5	0.000045	0.98	179.2	0.000822	5.02	179.1	0.002264	4.78
189.5	0.000047	0.93	189.2	0.000838	5.11	189.1	0.002290	4.83
199.5	0.000048	1.02	199.2	0.000853	5.23	199.1	0.002314	4.87
209.5	0.000046	0.94	209.2	0.000868	5.41	209.1	0.002338	4.92
219.5	0.000048	0.93	219.2	0.000881	5.40	219.1	0.002359	4.94
229.5	0.000050	1.04	229.2	0.000895	5.45	229.1	0.002379	4.96
239.5	0.000050	1.06	239.2	0.000908	5.48	239.1	0.002398	4.99
249.5	0.000050	1.02	249.2	0.000919	5.57	249.1	0.002420	5.04
259.5	0.000052	1.04	259.2	0.000934	5.73	259.1	0.002436	5.04
269.5	0.000055	1.20	269.2	0.000944	5.73	269.1	0.002455	5.10
279.5	0.000055	1.20	278.7	0.000953	5.67	278.4	0.002471	5.11
289.5	0.000059	1.19	289.2	0.000968	5.93	289.1	0.002488	5.12
299.5	0.000058	1.19	299.2	0.000978	6.02	299.1	0.002500	5.13
309.5	0.000061	1.32	309.2	0.000987	6.01	309.1	0.002517	5.16
319.5	0.000059	1.10	319.2	0.000998	6.05	319.1	0.002532	5.20
329.5	0.000062	1.30	329.2	0.001009	6.19	329.1	0.002546	5.21
339.5	0.000064	1.42	339.2	0.001015	6.17	339.1	0.002562	5.27

Appendix D1 – RS12.5C (Continued)

349.5	0.000063	1.31	349.2	0.001026	6.26	349.1	0.002571	5.23
359.6	0.000062	1.22	359.3	0.001032	6.28	359.1	0.002585	5.27
369.6	0.000063	1.23	369.3	0.001040	6.29	369.1	0.002597	5.28
379.6	0.000065	1.34	379.3	0.001050	6.35	379.1	0.002609	5.28
389.6	0.000063	1.28	389.3	0.001059	6.44	389.1	0.002619	5.30
399.6	0.000065	1.35	399.3	0.001065	6.47	399.1	0.002633	5.33
409.6	0.000063	1.34	409.3	0.001073	6.41	409.1	0.002643	5.36
419.6	0.000064	1.38	419.3	0.001081	6.58	419.1	0.002654	5.37
429.6	0.000066	1.33	429.3	0.001090	6.77	429.1	0.002664	5.38
439.6	0.000068	1.46	439.3	0.001095	6.62	439.1	0.002675	5.39
449.6	0.000068	1.43	449.3	0.001104	6.71	449.1	0.002686	5.42
459.6	0.000067	1.37	459.3	0.001111	6.71	459.1	0.002692	5.38
469.6	0.000074	1.72	469.3	0.001115	6.76	469.1	0.002704	5.43
479.6	0.000071	1.43	479.3	0.001124	6.85	479.2	0.002713	5.44
489.6	0.000069	1.41	489.3	0.001129	6.85	489.2	0.002722	5.46
499.6	0.000070	1.42	499.3	0.001135	6.81	499.2	0.002729	5.44
599.6	0.000078	1.59	599.3	0.001191	7.16	599.2	0.002810	5.58
699.7	0.000083	1.64	699.4	0.001240	7.43	699.2	0.002875	5.64
799.7	0.000090	1.72	799.4	0.001277	7.53	799.2	0.002933	5.73
899.7	0.000096	1.94	899.4	0.001315	7.88	899.3	0.002982	5.78
999.7	0.000103	2.18	999.4	0.001344	7.84	999.3	0.003026	5.83
1099.8	0.000103	2.11	1099.5	0.001373	8.14	1099.3	0.003064	5.87
1199.8	0.000108	2.30	1199.5	0.001397	8.21	1199.4	0.003099	5.90
1299.3	0.000111	2.13	1299.5	0.001421	8.31	1299.4	0.003133	5.95
1399.4	0.000115	2.33	1399.6	0.001443	8.38	1399.4	0.003164	6.00
1499.4	0.000124	2.56	1499.6	0.001464	8.50	1499.4	0.003193	6.03
1599.4	0.000125	2.58	1599.6	0.001482	8.59	1599.5	0.003218	6.05
1699.4	0.000125	2.48	1699.6	0.001497	8.54	1699.5	0.003241	6.09
1799.5	0.000131	2.49	1799.7	0.001514	8.72	1790.2	0.003266	6.13
1899.5	0.000136	2.85	1899.7	0.001532	8.87	1899.6	0.003287	6.14
1999.5	0.000140	2.81	1999.7	0.001542	8.73	1999.6	0.003306	6.14

Appendix D1 – RS12.5C (Continued)

2099.6	0.000142	2.72	2099.8	0.001558	8.74	2099.6	0.003328	6.21
2199.6	0.000149	2.97	2199.8	0.001571	8.84	2199.7	0.003349	6.23
2299.6	0.000155	3.05	2299.8	0.001582	8.66	2299.7	0.003363	6.23
2399.6	0.000155	3.14	2399.8	0.001596	8.92	2399.7	0.003382	6.26
2499.2	0.000155	3.08	2498.4	0.001606	8.99	2499.7	0.003397	6.29
2599.2	0.000161	3.42	2599.4	0.001619	8.94	2599.8	0.003413	6.33
2699.2	0.000162	3.28	2699.4	0.001629	8.94	2699.8	0.003428	6.32
2799.3	0.000166	3.30	2799.5	0.001639	9.17	2799.8	0.003443	6.35
2899.3	0.000168	3.43	2899.5	0.001650	9.24	2899.9	0.003457	6.36
2999.3	0.000170	3.25	2999.5	0.001658	9.33	2999.9	0.003471	6.36
3099.4	0.000176	3.48	3099.5	0.001669	9.18	3099.9	0.003486	6.40
3199.4	0.000179	3.69	3199.6	0.001679	9.31	3199.9	0.003499	6.42
3299.4	0.000182	3.91	3299.6	0.001688	9.27	3300.0	0.003509	6.41
3399.4	0.000184	3.61	3399.1	0.001699	9.25	3399.7	0.003524	6.44
3499.5	0.000188	3.70	3499.2	0.001707	9.42	3499.0	0.003535	6.46
3599.5	0.000190	3.69	3599.2	0.001716	9.39	3599.1	0.003547	6.47
3699.5	0.000188	3.47	3699.2	0.001725	9.35	3699.1	0.003558	6.47
3799.6	0.000194	3.88	3799.3	0.001732	9.32	3799.1	0.003569	6.49
3899.6	0.000199	4.46	3899.3	0.001739	9.43	3899.1	0.003578	6.47
3999.6	0.000202	4.07	3999.3	0.001749	9.35	3999.2	0.003589	6.50
4099.6	0.000203	4.06	4099.3	0.001760	9.76	4099.2	0.003599	6.52
4199.7	0.000206	4.05	4199.4	0.001764	9.48	4199.2	0.003610	6.52
4299.7	0.000210	4.50	4299.4	0.001772	9.52	4299.3	0.003620	6.56
4399.7	0.000207	4.20	4399.4	0.001780	9.40	4399.3	0.003631	6.55
4499.8	0.000212	4.47	4499.5	0.001787	9.58	4499.3	0.003641	6.59
4599.8	0.000213	4.19	4599.5	0.001795	9.62	4599.4	0.003648	6.57
4699.8	0.000217	4.60	4699.5	0.001802	9.64	4699.4	0.003659	6.59
4799.3	0.000219	4.64	4799.5	0.001803	9.57	4799.4	0.003668	6.63
4899.4	0.000221	4.52	4899.6	0.001807	9.41	4899.4	0.003677	6.62
4999.4	0.000221	4.44	4999.6	0.001817	9.71	4999.5	0.003684	6.66
5099.4	0.000224	4.57	5099.6	0.001822	9.62	5099.5	0.003692	6.65

Appendix D1 – RS12.5C (Continued)

5199.5	0.000228	4.53	5199.7	0.001826	9.53	5199.5	0.003700	6.63
5299.5	0.000227	4.39	5299.7	0.001836	9.73	5299.6	0.003708	6.65
5399.5	0.000227	4.15	5399.7	0.001841	9.43	5399.6	0.003716	6.63
5499.6	0.000232	4.61	5499.7	0.001848	9.54	5499.6	0.003723	6.66
5599.6	0.000233	4.80	5599.8	0.001854	9.55	5599.6	0.003731	6.68
5699.6	0.000236	4.66	5699.8	0.001856	9.53	5699.7	0.003739	6.68
5799.6	0.000246	5.27	5799.8	0.001863	9.70	5799.7	0.003746	6.70
5899.7	0.000245	4.90	5899.9	0.001869	9.64	5899.7	0.003753	6.69
5999.2	0.000242	4.77	5999.4	0.001877	9.78	5999.8	0.003761	6.71
6099.2	0.000244	4.71	6099.4	0.001879	9.63	6099.8	0.003769	6.74
6199.3	0.000252	5.27	6199.5	0.001885	9.76	6199.8	0.003775	6.72
6299.3	0.000249	4.94	6299.5	0.001892	9.72	6299.9	0.003782	6.73
6399.3	0.000253	5.45	6399.5	0.001896	9.77	6399.9	0.003790	6.74
6499.3	0.000251	4.78	6499.5	0.001900	9.63	6499.9	0.003795	6.72
6599.4	0.000256	5.46	6599.6	0.001906	9.70	6599.9	0.003803	6.76
6699.4	0.000254	4.92	6699.6	0.001914	9.84	6700.0	0.003809	6.75
6799.4	0.000258	5.20	6799.6	0.001915	9.60	6799.7	0.003818	6.81
6899.5	0.000260	5.50	6899.2	0.001923	9.86	6899.0	0.003822	6.76
6999.5	0.000263	5.48	6999.2	0.001929	9.79	6999.1	0.003828	6.77
7099.5	0.000263	5.22	7099.2	0.001932	9.67	7099.1	0.003834	6.77
7199.6	0.000264	5.31	7198.2	0.001939	9.86	7198.4	0.003839	6.79
7299.6	0.000267	5.08	7299.3	0.001943	9.76	7299.1	0.003846	6.79
7399.6	0.000271	5.27	7399.3	0.001946	9.63	7399.2	0.003855	6.83
7499.6	0.000274	5.28	7499.3	0.001953	9.76	7499.2	0.003856	6.77
7599.7	0.000273	5.37	7599.4	0.001957	9.75	7599.2	0.003864	6.81
7699.7	0.000276	5.55	7699.4	0.001962	9.77	7699.3	0.003870	6.82
7799.7	0.000280	5.86	7799.4	0.001966	9.73	7799.3	0.003875	6.84
7899.8	0.000277	5.34	7899.4	0.001971	9.81	7899.3	0.003883	6.88
7999.8	0.000282	5.67	7999.5	0.001971	9.69	7999.3	0.003887	6.85
8099.8	0.000283	5.70	8099.5	0.001979	9.80	8099.4	0.003892	6.85
8199.3	0.000285	6.05	8199.5	0.001982	9.86	8199.4	0.003896	6.84

Appendix D1 – RS12.5C (Continued)

8299.4	0.000286	6.11	8299.6	0.001989	9.80	8299.4	0.003902	6.84
8399.4	0.000292	6.55	8399.6	0.001991	9.70	8399.5	0.003908	6.89
8499.4	0.000289	5.83	8499.6	0.001997	9.81	8499.5	0.003909	6.87
8599.5	0.000291	5.70	8599.7	0.002001	9.83	8599.5	0.003916	6.86
8699.5	0.000294	5.82	8699.7	0.002009	10.03	8699.6	0.003922	6.87
8799.5	0.000293	5.64	8799.7	0.002008	9.76	8799.6	0.003925	6.86
8899.5	0.000293	5.71	8899.7	0.002015	9.90	8899.6	0.003932	6.90
8999.6	0.000296	6.01	8999.8	0.002020	9.85	8999.6	0.003937	6.91
9099.6	0.000303	5.92	9099.8	0.002024	9.87	9099.7	0.003942	6.90
9199.6	0.000299	6.18	9199.8	0.002029	9.88	9199.7	0.003948	6.89
9299.7	0.000298	5.66	9299.9	0.002031	9.67	9299.7	0.003951	6.90
9399.2	0.000303	6.70	9399.4	0.002038	9.99	9399.8	0.003952	6.87
9499.2	0.000305	6.56	9499.4	0.002042	10.00	9499.8	0.003961	6.93
9599.3	0.000301	5.75	9599.4	0.002046	9.81	9599.8	0.003966	6.92
9699.3	0.000306	6.14	9699.5	0.002050	9.76	9699.8	0.003970	6.92
9799.3	0.000308	6.03	9799.5	0.002054	9.86	9799.9	0.003973	6.94
9899.3	0.000307	5.76	9899.5	0.002058	9.88	9899.9	0.003976	6.92
9999.4	0.000308	5.97	9999.6	0.002064	9.89	9999.9	0.003982	6.91
10099.4	0.000310	5.78	10099.6	0.002067	9.84	10100.0	0.003987	6.94
10199.4	0.000312	6.40	10199.6	0.002070	9.78	10199.7	0.003991	6.97
10299.5	0.000312	6.20	10299.2	0.002076	9.99	10299.0	0.003995	6.93
10399.5	0.000312	6.02	10399.2	0.002080	10.00	10399.1	0.004000	6.95
10499.5	0.000314	6.28	10499.2	0.002082	9.79	10499.1	0.004004	6.96
10599.5	0.000319	6.45	10599.2	0.002088	9.94	10599.1	0.004007	6.97
10699.6	0.000314	5.87	10699.3	0.002092	10.06	10699.1	0.004010	6.93
10799.6	0.000321	6.90	10799.3	0.002096	9.94	10799.2	0.004015	6.96
10899.6	0.000320	6.11	10899.3	0.002100	9.86	10899.2	0.004018	6.94
10999.7	0.000324	7.06	10999.4	0.002106	10.07	10999.2	0.004025	6.99
11099.7	0.000320	6.45	11099.4	0.002107	9.88	11099.3	0.004027	6.95
11199.7	0.000323	6.21	11199.4	0.002109	9.85	11199.3	0.004033	7.01
11299.8	0.000327	6.57	11299.4	0.002116	10.12	11299.3	0.004032	6.95

Appendix D1 – RS12.5C (Continued)

11399.8	0.000325	6.43	11399.5	0.002120	9.86	11399.3	0.004038	6.96
11499.8	0.000326	6.37	11499.5	0.002126	10.05	11499.4	0.004042	6.98
11599.3	0.000328	6.65	11599.5	0.002131	9.87	11599.4	0.004048	7.01
11699.4	0.000328	6.42	11699.6	0.002136	10.01	11699.4	0.004052	7.01
11799.4	0.000331	6.46	11799.6	0.002136	9.81	11799.5	0.004056	7.00
11898.9	0.000334	6.30	11898.6	0.002142	9.89	11899.2	0.004058	7.02
11999.5	0.000335	6.92	11999.6	0.002146	9.91	11999.5	0.004061	7.05

I19C								
20°C			40°C			54°C		
Cycles	ε_p	$\varepsilon_p/\varepsilon_r$	Cycles	ε_p	$\varepsilon_p/\varepsilon_r$	Cycles	ε_p	$\varepsilon_p/\varepsilon_r$
2.2	0.000004	0.10	2.5	0.000194	0.68	2.0	0.000787	1.18
3.9	0.000015	0.32	4.5	0.000348	1.05	4.0	0.001163	1.64
8.9	0.000029	0.55	9.5	0.000610	1.80	9.0	0.001712	2.34
18.9	0.000041	0.93	19.5	0.000946	2.66	19.0	0.002330	3.22
29.4	0.000049	0.70	29.5	0.001189	3.32	29.0	0.002716	3.80
39.4	0.000053	0.75	39.5	0.001369	3.80	39.0	0.002998	4.21
49.4	0.000061	0.88	49.6	0.001524	4.28	49.0	0.003225	4.57
59.4	0.000069	1.03	59.6	0.001645	4.57	59.0	0.003411	4.83
69.4	0.000075	1.04	69.6	0.001755	4.85	69.0	0.003577	5.10
79.5	0.000078	1.12	79.1	0.001849	5.17	79.0	0.003716	5.27
89.5	0.000081	1.13	89.1	0.001934	5.34	89.0	0.003838	5.42
99.5	0.000086	1.21	99.1	0.002013	5.63	99.0	0.003949	5.55
109.5	0.000090	1.26	109.1	0.002083	5.78	109.0	0.004059	5.74
119.5	0.000094	1.39	119.1	0.002149	5.95	119.0	0.004155	5.89
129.5	0.000096	1.33	129.1	0.002207	6.09	129.0	0.004240	5.97
139.5	0.000101	1.50	139.1	0.002262	6.27	139.0	0.004325	6.08
149.5	0.000102	1.47	149.1	0.002314	6.39	148.0	0.004393	6.15
159.5	0.000107	1.59	159.1	0.002361	6.49	159.1	0.004475	6.28
169.5	0.000108	1.51	169.1	0.002404	6.55	169.1	0.004546	6.34
179.5	0.000113	1.67	179.1	0.002446	6.66	179.1	0.004607	6.43

Appendix D1 – I19C (Continued)

189.5	0.000116	1.64	189.1	0.002491	6.82	189.1	0.004670	6.53
199.5	0.000119	1.70	199.1	0.002524	6.90	199.1	0.004731	6.59
209.5	0.000120	1.75	209.1	0.002562	6.97	209.1	0.004788	6.67
219.5	0.000122	1.72	219.1	0.002594	7.05	219.1	0.004849	6.81
229.5	0.000123	1.72	229.1	0.002626	7.15	229.1	0.004896	6.80
239.5	0.000127	1.80	239.1	0.002654	7.14	239.1	0.004948	6.86
249.5	0.000130	1.87	249.1	0.002685	7.29	249.1	0.004989	6.88
259.5	0.000134	1.97	259.1	0.002716	7.34	259.1	0.005041	6.97
269.5	0.000133	1.94	269.1	0.002742	7.42	269.1	0.005087	7.02
279.5	0.000137	2.00	279.1	0.002765	7.44	279.1	0.005126	7.02
289.5	0.000137	1.97	289.1	0.002791	7.51	289.1	0.005174	7.15
299.0	0.000138	1.96	299.1	0.002814	7.52	299.1	0.005216	7.15
309.5	0.000143	2.16	309.1	0.002839	7.63	309.1	0.005249	7.16
319.5	0.000143	1.98	319.1	0.002863	7.71	319.1	0.005286	7.20
329.5	0.000146	2.13	329.1	0.002880	7.63	329.1	0.005321	7.25
339.5	0.000148	2.14	339.1	0.002903	7.77	339.1	0.005350	7.31
349.5	0.000149	2.16	349.1	0.002924	7.77	349.1	0.005387	7.39
359.5	0.000150	2.17	359.1	0.002942	7.77	359.1	0.005420	7.39
369.5	0.000154	2.20	369.2	0.002961	7.90	369.1	0.005461	7.48
379.5	0.000154	2.24	379.2	0.002979	7.84	379.1	0.005488	7.48
389.5	0.000155	2.20	389.2	0.002995	7.89	389.1	0.005520	7.50
399.6	0.000160	2.42	399.2	0.003011	7.87	399.1	0.005557	7.60
409.6	0.000160	2.34	409.2	0.003030	7.98	409.1	0.005577	7.53
419.6	0.000162	2.29	419.2	0.003046	8.02	419.1	0.005606	7.58
429.6	0.000165	2.34	429.2	0.003060	7.97	429.1	0.005638	7.70
439.1	0.000166	2.37	439.2	0.003081	8.23	439.1	0.005662	7.64
449.6	0.000167	2.45	449.2	0.003092	8.07	449.1	0.005695	7.81
459.6	0.000168	2.42	459.2	0.003107	8.17	459.1	0.005711	7.68
469.6	0.000172	2.55	469.2	0.003123	8.27	469.1	0.005740	7.70
479.6	0.000169	2.39	479.2	0.003135	8.18	479.2	0.005765	7.81
489.6	0.000174	2.62	489.2	0.003151	8.23	489.2	0.005788	7.76

Appendix D1 – I19C (Continued)

499.6	0.000176	2.62	499.2	0.003161	8.19	499.2	0.005815	7.87
599.6	0.000189	2.70	599.2	0.003280	8.42	599.2	0.006037	8.14
699.6	0.000200	2.87	699.2	0.003379	8.73	699.2	0.006232	8.30
799.7	0.000211	3.06	799.3	0.003461	8.79	799.2	0.006378	8.34
899.7	0.000219	3.05	899.3	0.003533	8.87	899.3	0.006533	8.62
999.2	0.000230	3.34	999.3	0.003599	9.01	999.3	0.006651	8.65
1099.8	0.000236	3.20	1099.4	0.003656	9.07	1099.3	0.006788	8.77
1199.8	0.000250	3.58	1199.4	0.003709	9.21	1199.4	0.006891	9.12
1299.8	0.000259	3.78	1299.4	0.003757	9.22	1299.4	0.006959	8.95
1399.8	0.000265	3.94	1399.5	0.003802	9.34	1399.4	0.007056	9.08
1499.9	0.000273	3.89	1499.5	0.003840	9.41	1499.5	0.007131	9.19
1599.4	0.000273	3.85	1599.5	0.003877	9.41	1599.5	0.007216	9.12
1699.4	0.000282	4.15	1699.5	0.003913	9.47	1699.5	0.007286	9.31
1799.0	0.000290	4.17	1799.6	0.003946	9.47	1799.5	0.007361	9.36
1899.5	0.000293	4.30	1899.6	0.003976	9.51	1899.6	0.007424	9.29
1999.5	0.000298	4.43	1999.6	0.004003	9.45	1999.6	0.007489	9.35
2099.5	0.000307	4.77	2099.7	0.004035	9.65	2099.6	0.007537	9.48
2199.6	0.000308	4.48	2199.7	0.004061	9.70	2199.7	0.007592	9.61
2299.6	0.000312	4.50	2299.7	0.004085	9.64	2299.7	0.007646	9.67
2399.1	0.000319	4.67	2399.7	0.004111	9.72	2399.7	0.007685	9.46
2499.2	0.000321	4.69	2499.3	0.004134	9.73	2498.2	0.007749	9.79
2599.2	0.000327	4.77	2599.8	0.004152	9.71	2599.8	0.007806	9.68
2699.2	0.000329	4.67	2699.8	0.004176	9.87	2699.8	0.007842	9.90
2799.3	0.000333	4.66	2799.9	0.004195	9.83	2799.8	0.007892	9.84
2899.3	0.000338	4.97	2899.9	0.004216	9.81	2899.9	0.007943	9.90
2999.3	0.000340	4.87	2999.9	0.004239	9.94	2999.9	0.007974	9.85
3099.3	0.000345	4.98	3099.4	0.004259	9.95	3099.9	0.008035	10.12
3199.4	0.000348	5.06	3199.5	0.004280	9.99	3200.0	0.008059	10.04
3299.4	0.000354	5.14	3299.5	0.004300	9.93	3300.0	0.008100	9.91
3399.4	0.000356	5.17	3399.5	0.004313	9.91	3399.0	0.008131	9.91
3499.5	0.000356	4.97	3499.1	0.004335	10.01	3499.0	0.008183	10.17

Appendix D1 – I19C (Continued)

3599.5	0.000362	5.31	3599.1	0.004350	10.06	3599.1	0.008203	10.00
3699.5	0.000366	5.34	3699.1	0.004365	10.04	3699.1	0.008243	10.15
3799.5	0.000369	5.57	3799.2	0.004383	10.06	3799.1	0.008295	10.26
3899.6	0.000372	5.40	3899.2	0.004399	10.02	3899.2	0.008308	10.29
3999.6	0.000375	5.84	3999.2	0.004416	10.01	3999.2	0.008336	10.44
4099.6	0.000376	5.85	4099.2	0.004422	10.12	4099.2	0.008360	10.25
4199.7	0.000377	5.48	4199.3	0.004441	10.12	4199.2	0.008398	10.29
4299.7	0.000381	5.68	4299.3	0.004461	10.19	4299.3	0.008428	10.36
4399.7	0.000381	5.68	4399.3	0.004471	10.14	4399.3	0.008474	10.48
4499.8	0.000387	5.88	4499.4	0.004483	10.12	4499.3	0.008500	10.39
4599.8	0.000389	5.83	4599.4	0.004495	10.19	4599.4	0.008492	10.38
4699.8	0.000390	5.59	4699.4	0.004508	10.16	4699.4	0.008540	10.42
4799.8	0.000391	5.72	4799.4	0.004524	10.16	4799.4	0.008597	10.56
4899.9	0.000394	5.95	4899.5	0.004538	10.09	4899.4	0.008585	10.34
4999.4	0.000397	5.74	4999.5	0.004551	10.19	4999.5	0.008619	10.63
5099.4	0.000400	6.00	5099.5	0.004565	10.28	5099.5	0.008641	10.55
5199.5	0.000400	5.90	5199.6	0.004576	10.26	5199.5	0.008665	10.56
5299.5	0.000401	5.70	5299.6	0.004590	10.36	5299.6	0.008703	10.75
5399.5	0.000404	6.06	5399.6	0.004598	10.29	5399.6	0.008726	10.90
5499.5	0.000409	6.34	5499.6	0.004613	10.28	5499.6	0.008742	10.38
5599.6	0.000408	5.94	5599.7	0.004625	10.35	5599.7	0.008765	10.50
5699.6	0.000412	6.36	5699.7	0.004637	10.35	5699.7	0.008783	10.52
5799.1	0.000414	6.34	5799.7	0.004647	10.31	5799.7	0.008796	10.57
5899.2	0.000415	6.08	5899.8	0.004660	10.46	5899.7	0.008817	10.55
5999.2	0.000417	6.31	5999.8	0.004671	10.45	5999.8	0.008889	10.78
6099.2	0.000417	6.29	6099.8	0.004683	10.41	6099.8	0.008884	10.71
6199.3	0.000421	6.33	6199.8	0.004692	10.36	6199.8	0.008871	10.67
6299.3	0.000422	6.25	6299.9	0.004705	10.40	6299.9	0.008889	10.76
6399.3	0.000422	6.27	6399.9	0.004714	10.36	6399.9	0.008905	10.75
6499.3	0.000424	6.38	6499.9	0.004730	10.52	6499.9	0.008935	10.84
6599.4	0.000425	6.30	6599.5	0.004737	10.39	6599.9	0.008945	10.78

Appendix D1 – I19C (Continued)

6699.4	0.000428	6.39	6699.5	0.004749	10.41	6700.0	0.008955	10.72
6799.4	0.000431	6.67	6799.5	0.004755	10.36	6799.5	0.008967	10.74
6899.5	0.000430	6.46	6899.6	0.004766	10.45	6899.0	0.008991	10.80
6999.5	0.000431	6.27	6999.1	0.004775	10.53	6999.1	0.009003	10.81
7099.5	0.000433	6.40	7099.1	0.004780	10.41	7099.1	0.009018	10.82
7199.5	0.000437	6.45	7199.1	0.004795	10.42	7198.6	0.009039	10.82
7299.6	0.000440	6.59	7299.2	0.004809	10.50	7299.2	0.009058	10.86
7399.6	0.000436	6.27	7399.2	0.004814	10.45	7399.2	0.009079	10.84
7499.6	0.000437	6.35	7499.2	0.004829	10.60	7499.2	0.009100	10.87
7599.7	0.000441	6.44	7599.3	0.004833	10.56	7599.2	0.009115	10.91
7699.7	0.000443	6.49	7699.3	0.004843	10.55	7699.3	0.009126	10.85
7799.7	0.000446	6.75	7799.3	0.004852	10.57	7799.3	0.009145	10.94
7899.8	0.000448	6.97	7899.3	0.004861	10.58	7899.3	0.009163	11.00
7999.8	0.000445	6.13	7999.4	0.004869	10.50	7999.4	0.009169	10.97
8099.8	0.000448	6.84	8099.4	0.004879	10.59	8099.4	0.009184	11.00
8199.8	0.000451	6.44	8199.4	0.004889	10.54	8199.4	0.009198	10.85
8299.9	0.000454	6.78	8299.5	0.004895	10.54	8299.4	0.009213	11.03
8399.4	0.000453	6.75	8399.5	0.004902	10.57	8399.5	0.009237	11.11
8498.9	0.000455	6.88	8499.5	0.004911	10.49	8499.5	0.009255	11.12
8599.5	0.000455	6.78	8599.5	0.004920	10.56	8599.5	0.009257	10.99
8699.5	0.000456	7.06	8699.6	0.004931	10.65	8699.6	0.009284	11.15
8799.5	0.000455	6.65	8799.6	0.004939	10.63	8799.6	0.009300	11.09
8899.5	0.000459	7.18	8899.6	0.004946	10.57	8899.6	0.009302	11.12
8999.6	0.000463	7.66	8999.7	0.004955	10.64	8999.7	0.009314	11.07
9099.6	0.000460	7.05	9099.7	0.004962	10.55	9099.7	0.009335	11.07
9199.1	0.000458	6.87	9199.7	0.004971	10.62	9199.7	0.009356	11.26
9299.2	0.000462	6.87	9299.7	0.004979	10.63	9299.7	0.009366	11.15
9399.2	0.000462	6.70	9399.8	0.004988	10.67	9399.8	0.009389	11.26
9499.2	0.000463	7.05	9499.8	0.004992	10.67	9499.8	0.009384	11.20
9599.2	0.000461	6.72	9599.8	0.004998	10.59	9599.8	0.009397	11.27
9699.3	0.000464	6.77	9699.9	0.005007	10.72	9699.9	0.009403	11.15

Appendix D1 – I19C (Continued)

9799.3	0.000464	6.97	9799.9	0.005011	10.64	9799.9	0.009423	11.21
9899.3	0.000470	7.08	9899.9	0.005023	10.79	9899.9	0.009432	11.26
9999.4	0.000468	6.70	9999.5	0.005027	10.75	9999.9	0.009447	11.17
10099.4	0.000472	7.44	10099.5	0.005035	10.76	10100.0	0.009462	11.23
10199.4	0.000473	6.98	10199.5	0.005040	10.70	10199.5	0.009468	11.20
10299.5	0.000473	7.09	10299.5	0.005047	10.69	10299.0	0.009481	11.33
10399.5	0.000478	7.52	10399.1	0.005052	10.70	10399.1	0.009497	11.41
10499.5	0.000472	6.82	10499.1	0.005060	10.74	10499.1	0.009492	11.24
10599.5	0.000473	7.08	10599.1	0.005067	10.76	10599.1	0.009512	11.40
10699.6	0.000476	7.18	10699.2	0.005073	10.72	10699.1	0.009524	11.27
10799.6	0.000477	7.04	10799.2	0.005083	10.79	10799.2	0.009544	11.42
10899.6	0.000479	7.56	10899.2	0.005088	10.85	10899.2	0.009546	11.34
10999.7	0.000476	7.30	10999.2	0.005095	10.84	10999.2	0.009556	11.33
11099.7	0.000478	7.26	11099.3	0.005100	10.88	11099.3	0.009572	11.38
11199.7	0.000479	7.13	11199.3	0.005103	10.72	11199.3	0.009579	11.36
11299.7	0.000482	7.71	11299.3	0.005113	10.91	11299.3	0.009595	11.48
11399.8	0.000485	8.05	11399.4	0.005119	10.81	11399.4	0.009608	11.40
11499.8	0.000485	7.58	11499.4	0.005122	10.82	11499.4	0.009609	11.35
11599.8	0.000481	7.22	11599.4	0.005132	10.93	11599.4	0.009626	11.44
11699.9	0.000483	7.44	11699.4	0.005135	10.83	11699.4	0.009633	11.45
11799.4	0.000482	7.10	11799.5	0.005140	10.88	11799.5	0.009650	11.49
11899.4	0.000486	7.70	11899.5	0.005146	10.88	11899.5	0.009652	11.41
11999.5	0.000488	7.59	11999.5	0.005154	10.93	11999.5	0.009656	11.38

RI19C								
20°C			40°C			54°C		
Cycles	ε_p	$\varepsilon_p/\varepsilon_r$	Cycles	ε_p	$\varepsilon_p/\varepsilon_r$	Cycles	ε_p	$\varepsilon_p/\varepsilon_r$
2.7	0.000008	0.23	2.2	0.000046	0.25	2.2	0.000527	1.12
4.7	0.000009	0.16	4.2	0.000094	0.48	4.2	0.000805	1.57
9.7	0.000016	0.31	9.2	0.000179	0.89	9.4	0.001155	2.19
18.7	0.000022	0.41	18.7	0.000294	1.40	19.4	0.001751	3.20

Appendix D1 – RI19C (Continued)

29.7	0.000025	0.44	29.3	0.000388	1.81	29.4	0.002113	3.84
39.7	0.000028	0.47	39.3	0.000468	2.19	39.4	0.002381	4.32
49.7	0.000032	0.57	49.3	0.000535	2.50	49.4	0.002589	4.69
59.7	0.000036	0.65	59.3	0.000594	2.73	59.4	0.002762	4.95
69.8	0.000039	0.70	69.3	0.000647	2.93	69.4	0.002908	5.23
79.8	0.000041	0.72	79.3	0.000700	3.21	79.4	0.003036	5.43
89.8	0.000042	0.72	89.3	0.000745	3.39	89.4	0.003148	5.61
99.8	0.000044	0.77	99.3	0.000785	3.59	99.4	0.003249	5.82
109.8	0.000049	0.90	109.3	0.000827	3.80	109.4	0.003345	6.00
119.8	0.000049	0.85	119.3	0.000862	3.93	119.4	0.003426	6.10
129.8	0.000050	0.89	129.3	0.000897	4.08	129.4	0.003506	6.25
139.8	0.000054	0.96	139.3	0.000928	4.19	139.4	0.003578	6.39
148.8	0.000054	0.97	149.3	0.000962	4.38	148.7	0.003639	6.44
159.3	0.000055	0.98	159.3	0.000989	4.44	159.4	0.003708	6.58
169.3	0.000058	1.04	169.3	0.001016	4.58	169.4	0.003767	6.68
179.3	0.000057	1.01	179.3	0.001043	4.74	179.4	0.003822	6.77
189.3	0.000059	1.07	189.3	0.001072	4.94	189.4	0.003875	6.84
199.3	0.000059	1.03	199.3	0.001094	4.93	199.4	0.003931	6.93
209.3	0.000063	1.15	209.3	0.001118	5.01	209.4	0.003978	7.07
219.3	0.000064	1.14	219.3	0.001140	5.14	219.4	0.004025	7.10
229.3	0.000064	1.15	229.3	0.001162	5.25	229.4	0.004067	7.19
239.3	0.000067	1.23	239.3	0.001182	5.32	239.4	0.004107	7.23
249.3	0.000067	1.18	249.3	0.001204	5.40	249.4	0.004145	7.24
259.3	0.000067	1.16	259.3	0.001218	5.44	259.5	0.004186	7.34
269.3	0.000069	1.21	269.3	0.001238	5.58	269.5	0.004222	7.41
278.8	0.000070	1.24	279.3	0.001254	5.54	279.5	0.004259	7.49
289.3	0.000072	1.30	289.3	0.001271	5.63	289.5	0.004295	7.58
299.3	0.000073	1.33	299.3	0.001290	5.72	299.5	0.004326	7.57
309.3	0.000074	1.33	309.3	0.001306	5.78	309.5	0.004360	7.67
319.3	0.000075	1.34	319.3	0.001321	5.90	319.5	0.004388	7.67
329.3	0.000075	1.35	329.3	0.001336	5.92	329.5	0.004418	7.72

Appendix D1 – RI19C (Continued)

339.3	0.000076	1.35	339.3	0.001350	5.95	339.5	0.004449	7.81
349.3	0.000076	1.33	349.4	0.001366	6.12	349.5	0.004476	7.80
359.3	0.000079	1.40	359.4	0.001380	6.07	359.5	0.004503	7.82
369.3	0.000079	1.39	369.4	0.001391	6.06	369.5	0.004530	7.89
379.3	0.000080	1.42	379.4	0.001405	6.14	379.5	0.004555	7.91
389.3	0.000079	1.36	389.4	0.001419	6.28	389.5	0.004581	7.96
399.4	0.000083	1.50	399.4	0.001436	6.48	399.5	0.004606	8.05
409.4	0.000081	1.40	409.4	0.001439	6.21	409.5	0.004630	8.07
419.4	0.000082	1.41	419.4	0.001455	6.37	419.5	0.004652	8.07
429.4	0.000085	1.51	429.4	0.001468	6.48	429.5	0.004677	8.17
439.4	0.000085	1.54	439.4	0.001478	6.42	439.5	0.004698	8.17
449.4	0.000086	1.53	449.4	0.001489	6.51	449.5	0.004717	8.11
459.4	0.000087	1.58	459.4	0.001498	6.49	459.5	0.004739	8.20
469.4	0.000086	1.53	469.4	0.001514	6.70	469.5	0.004759	8.23
479.4	0.000087	1.50	479.4	0.001525	6.80	479.5	0.004782	8.35
489.4	0.000089	1.57	489.4	0.001532	6.70	489.5	0.004799	8.30
499.4	0.000089	1.64	499.4	0.001542	6.74	499.5	0.004819	8.36
599.4	0.000097	1.76	599.4	0.001632	7.03	599.3	0.004993	8.59
699.4	0.000103	1.82	699.5	0.001707	7.30	699.3	0.005139	8.78
799.5	0.000109	1.94	799.5	0.001771	7.42	799.1	0.005269	8.98
899.5	0.000116	2.11	899.5	0.001834	7.93	899.4	0.005378	9.12
999.5	0.000120	2.15	999.5	0.001885	7.97	999.4	0.005478	9.32
1099.6	0.000124	2.19	1099.6	0.001928	8.12	1099.4	0.005566	9.41
1199.6	0.000129	2.27	1199.6	0.001975	8.38	1199.5	0.005647	9.50
1299.6	0.000134	2.39	1299.6	0.002010	8.38	1299.3	0.005723	9.60
1399.6	0.000139	2.55	1399.7	0.002039	8.22	1399.3	0.005790	9.61
1499.7	0.000142	2.60	1499.7	0.002077	8.51	1499.3	0.005858	9.80
1599.7	0.000147	2.65	1599.7	0.002108	8.71	1599.3	0.005918	9.84
1699.7	0.000149	2.62	1699.7	0.002141	8.98	1699.4	0.005973	9.90
1799.3	0.000153	2.74	1799.3	0.002163	8.80	1799.4	0.006028	10.01
1899.3	0.000155	2.77	1899.3	0.002191	9.10	1899.4	0.006079	10.07

Appendix D1 – RI19C (Continued)

1999.3	0.000160	2.93	1999.3	0.002218	9.19	1999.5	0.006128	10.15
2099.3	0.000162	2.94	2099.4	0.002237	8.96	2099.5	0.006171	10.16
2199.4	0.000165	2.93	2199.4	0.002259	9.14	2199.5	0.006216	10.23
2299.4	0.000170	3.12	2299.4	0.002283	9.20	2299.6	0.006259	10.28
2399.4	0.000170	3.08	2399.5	0.002304	9.47	2399.6	0.006298	10.30
2498.5	0.000173	3.15	2499.0	0.002320	9.31	2499.4	0.006336	10.33
2599.5	0.000176	3.19	2599.5	0.002336	9.14	2599.6	0.006373	10.39
2699.5	0.000177	3.16	2699.5	0.002358	9.60	2699.7	0.006412	10.50
2799.5	0.000180	3.27	2799.6	0.002377	9.59	2799.7	0.006447	10.56
2899.6	0.000182	3.30	2899.6	0.002389	9.55	2899.7	0.006478	10.51
2999.6	0.000185	3.36	2999.6	0.002407	9.49	2999.8	0.006512	10.60
3099.6	0.000187	3.34	3099.7	0.002421	9.45	3099.8	0.006543	10.60
3199.7	0.000190	3.34	3199.7	0.002439	9.57	3199.8	0.006574	10.63
3299.7	0.000193	3.49	3299.7	0.002453	9.69	3299.8	0.006603	10.72
3399.7	0.000194	3.62	3399.2	0.002470	9.79	3399.4	0.006630	10.74
3499.8	0.000199	3.70	3499.3	0.002487	9.73	3499.4	0.006659	10.76
3599.3	0.000199	3.66	3599.3	0.002505	9.94	3599.4	0.006687	10.84
3699.3	0.000201	3.66	3699.3	0.002515	9.81	3699.5	0.006713	10.85
3799.3	0.000202	3.81	3799.4	0.002522	9.66	3799.5	0.006740	10.89
3899.4	0.000204	3.63	3899.4	0.002537	9.82	3899.5	0.006762	10.95
3999.4	0.000206	3.68	3999.4	0.002553	10.02	3999.3	0.006787	10.96
4099.4	0.000208	3.71	4099.4	0.002564	10.01	4099.3	0.006807	10.94
4199.5	0.000210	3.91	4199.5	0.002578	9.98	4199.4	0.006829	10.94
4299.5	0.000211	3.73	4299.5	0.002588	10.11	4299.4	0.006855	11.04
4399.5	0.000215	3.96	4399.5	0.002601	10.14	4399.4	0.006875	11.06
4499.5	0.000216	3.93	4499.6	0.002614	10.11	4499.4	0.006894	11.03
4599.6	0.000217	3.98	4599.6	0.002624	10.19	4599.5	0.006913	11.02
4699.6	0.000221	4.19	4699.6	0.002634	10.15	4699.3	0.006936	11.14
4799.6	0.000221	4.06	4799.7	0.002646	10.15	4799.3	0.006958	11.15
4899.7	0.000224	4.22	4899.7	0.002655	10.00	4899.3	0.006973	11.16
4999.7	0.000225	4.29	4999.7	0.002666	10.12	4999.3	0.006992	11.18

Appendix D1 – RI19C (Continued)

5099.7	0.000224	3.96	5099.7	0.002676	10.20	5099.4	0.007013	11.23
5199.3	0.000227	4.22	5199.3	0.002690	10.16	5199.4	0.007028	11.21
5299.3	0.000228	4.27	5299.3	0.002699	10.27	5299.4	0.007047	11.20
5399.3	0.000230	4.35	5399.3	0.002710	10.31	5399.5	0.007063	11.24
5499.3	0.000231	4.25	5499.4	0.002717	10.21	5499.2	0.007079	11.28
5599.4	0.000231	4.17	5599.4	0.002726	10.20	5599.5	0.007097	11.28
5699.4	0.000233	4.24	5699.4	0.002739	10.23	5699.5	0.007113	11.31
5799.4	0.000235	4.37	5799.4	0.002750	10.35	5799.6	0.007130	11.36
5899.5	0.000237	4.50	5899.5	0.002760	10.54	5899.6	0.007147	11.38
5999.5	0.000237	4.39	5999.5	0.002770	10.43	5999.6	0.007163	11.35
6099.5	0.000239	4.44	6099.5	0.002776	10.29	6099.7	0.007178	11.37
6199.5	0.000240	4.47	6199.6	0.002788	10.41	6199.7	0.007194	11.43
6299.6	0.000241	4.41	6299.6	0.002796	10.45	6299.7	0.007210	11.47
6399.6	0.000242	4.51	6399.6	0.002799	10.29	6399.8	0.007224	11.46
6499.6	0.000244	4.58	6499.7	0.002814	10.47	6499.8	0.007241	11.58
6599.7	0.000245	4.57	6599.7	0.002823	10.56	6599.8	0.007256	11.54
6699.7	0.000248	4.77	6699.7	0.002831	10.43	6699.8	0.007265	11.54
6799.7	0.000249	4.72	6799.7	0.002839	10.34	6799.6	0.007277	11.49
6899.7	0.000250	4.52	6899.3	0.002852	10.60	6899.4	0.007290	11.48
6999.3	0.000250	4.67	6999.3	0.002863	10.58	6999.4	0.007312	11.64
7099.3	0.000250	4.48	7099.3	0.002872	10.63	7099.5	0.007323	11.57
7197.8	0.000252	4.70	7199.4	0.002879	10.51	7199.2	0.007339	11.63
7299.4	0.000253	4.61	7299.4	0.002884	10.55	7299.5	0.007354	11.73
7399.4	0.000256	4.84	7399.4	0.002893	10.60	7399.3	0.007366	11.67
7499.4	0.000255	4.72	7499.4	0.002904	10.57	7499.3	0.007377	11.67
7599.5	0.000257	4.74	7599.5	0.002911	10.64	7599.4	0.007387	11.64
7699.5	0.000260	4.95	7699.5	0.002919	10.79	7699.4	0.007401	11.67
7799.5	0.000260	4.76	7799.5	0.002933	10.66	7799.4	0.007415	11.68
7899.5	0.000261	4.98	7899.6	0.002936	10.54	7899.4	0.007425	11.67
7999.6	0.000261	4.80	7999.6	0.002945	10.61	7999.5	0.007437	11.70
8099.6	0.000261	4.84	8099.6	0.002951	10.51	8099.3	0.007447	11.72

Appendix D1 – RI19C (Continued)

8199.6	0.000265	5.15	8199.6	0.002965	10.84	8199.3	0.007462	11.77
8299.7	0.000263	4.86	8299.7	0.002968	10.51	8299.3	0.007471	11.78
8399.7	0.000264	4.93	8399.7	0.002979	10.75	8399.3	0.007484	11.82
8499.7	0.000266	5.06	8499.7	0.002989	10.84	8499.4	0.007496	11.77
8599.2	0.000266	4.88	8599.3	0.002995	10.67	8599.4	0.007505	11.78
8699.3	0.000268	4.94	8699.3	0.002997	10.71	8699.4	0.007515	11.83
8799.3	0.000268	4.97	8799.3	0.003006	10.68	8799.5	0.007527	11.85
8899.3	0.000270	4.94	8899.4	0.003015	10.72	8899.2	0.007538	11.88
8999.4	0.000270	4.94	8999.4	0.003020	10.64	8999.5	0.007549	11.89
9099.4	0.000272	5.00	9099.4	0.003027	10.63	9099.5	0.007558	11.86
9199.4	0.000272	5.00	9199.4	0.003034	10.54	9199.6	0.007569	11.88
9299.5	0.000274	5.20	9299.5	0.003045	10.78	9299.6	0.007585	11.98
9399.5	0.000275	5.13	9399.5	0.003049	10.72	9399.6	0.007589	11.87
9499.5	0.000276	5.27	9499.5	0.003060	10.86	9499.7	0.007600	11.91
9599.5	0.000275	4.97	9599.6	0.003067	10.94	9599.7	0.007610	11.92
9699.6	0.000277	5.24	9699.6	0.003071	10.72	9699.7	0.007623	12.06
9799.6	0.000279	5.30	9799.6	0.003080	10.87	9799.8	0.007628	11.95
9899.6	0.000279	5.20	9899.6	0.003088	10.77	9899.8	0.007637	11.93
9999.7	0.000280	5.31	9999.7	0.003097	10.89	9999.8	0.007647	11.95
10099.7	0.000280	5.14	10099.7	0.003103	10.87	10099.8	0.007658	12.03
10199.7	0.000282	5.24	10199.7	0.003112	10.92	10199.4	0.007666	12.01
10299.7	0.000281	5.25	10299.3	0.003115	10.87	10299.4	0.007676	12.04
10399.3	0.000284	5.52	10399.3	0.003121	10.71	10399.4	0.007685	12.06
10499.3	0.000282	5.26	10499.3	0.003136	10.99	10499.5	0.007692	12.01
10599.3	0.000283	5.26	10599.3	0.003139	10.78	10599.5	0.007702	12.11
10699.4	0.000286	5.55	10699.4	0.003148	10.86	10699.3	0.007712	12.08
10799.4	0.000285	5.23	10799.4	0.003154	10.90	10799.3	0.007719	12.08
10899.4	0.000286	5.32	10899.4	0.003165	11.08	10899.3	0.007727	12.07
10999.5	0.000287	5.29	10999.5	0.003169	10.93	10999.4	0.007737	12.09
11099.5	0.000288	5.38	11099.5	0.003176	10.95	11099.4	0.007743	12.07
11199.5	0.000288	5.39	11199.5	0.003183	10.83	11199.4	0.007754	12.10

Appendix D1 – RI19C (Continued)

11299.5	0.000289	5.45	11299.6	0.003193	10.96	11299.4	0.007763	12.14
11399.6	0.000291	5.59	11399.6	0.003202	11.15	11399.5	0.007772	12.14
11499.6	0.000291	5.56	11499.6	0.003207	11.05	11499.5	0.007781	12.17
11599.6	0.000292	5.48	11599.6	0.003212	10.99	11599.3	0.007788	12.14
11699.7	0.000292	5.37	11699.7	0.003221	10.98	11699.3	0.007795	12.13
11799.7	0.000294	5.66	11799.7	0.003225	11.02	11799.3	0.007804	12.20
11898.2	0.000294	5.53	11899.2	0.003235	11.09	11898.9	0.007813	12.21
11999.2	0.000296	5.67	11999.3	0.003239	10.90	11999.4	0.007821	12.20

Appendix D2 Permanent Strain and Permanent to Resilient Strain Ratio Plots from TRLPD Test for Common Asphalt Mixtures in NC

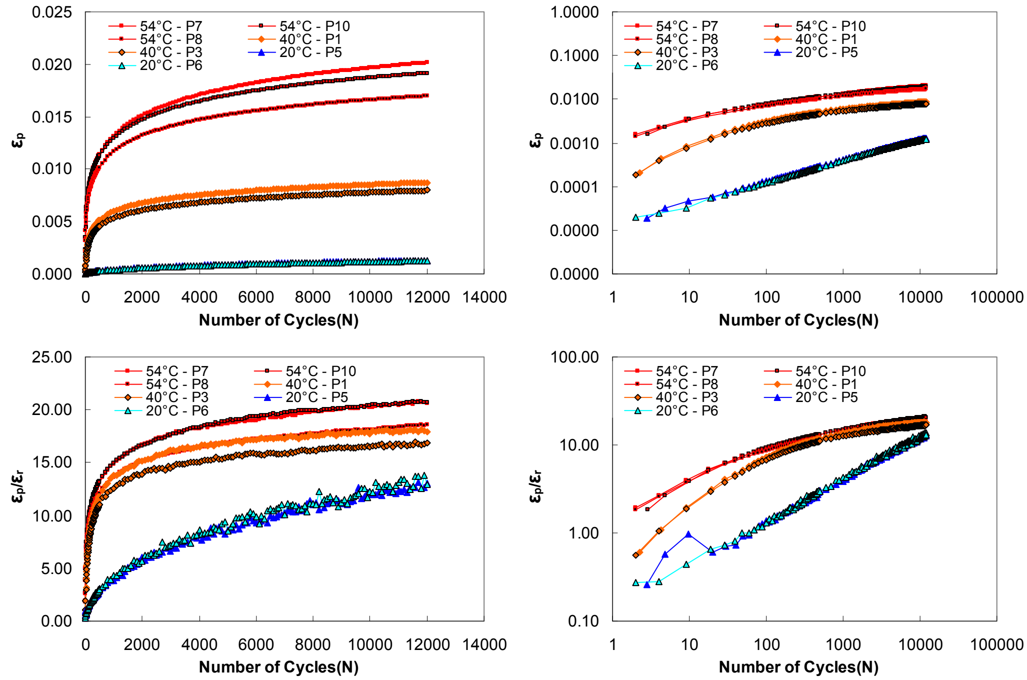

S9.5B

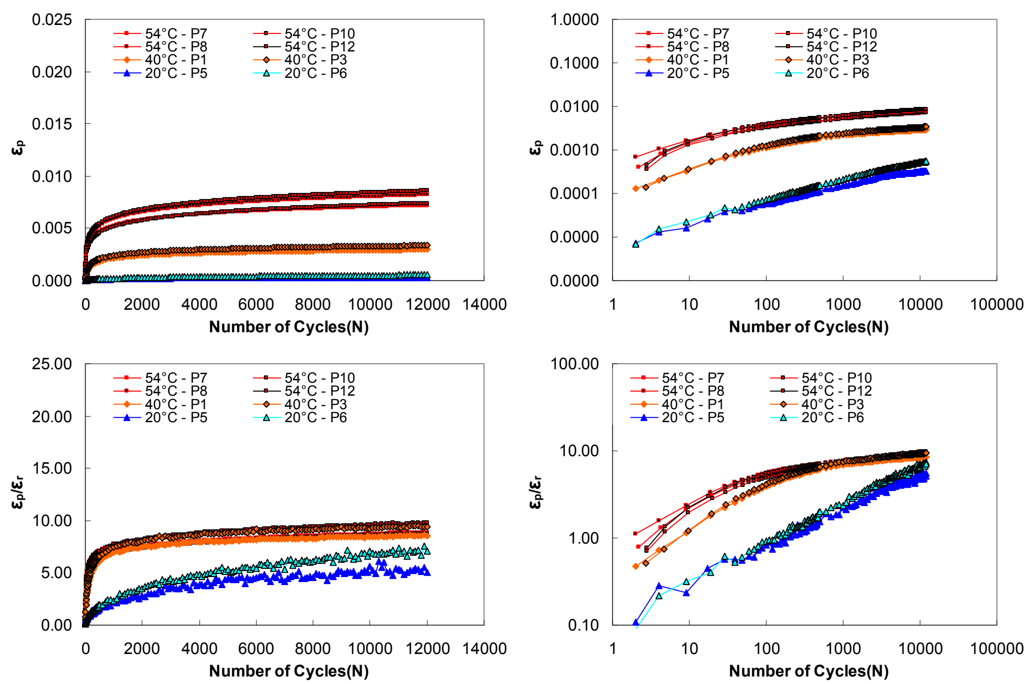

RS9.5B

Appendix D2 (Continued)

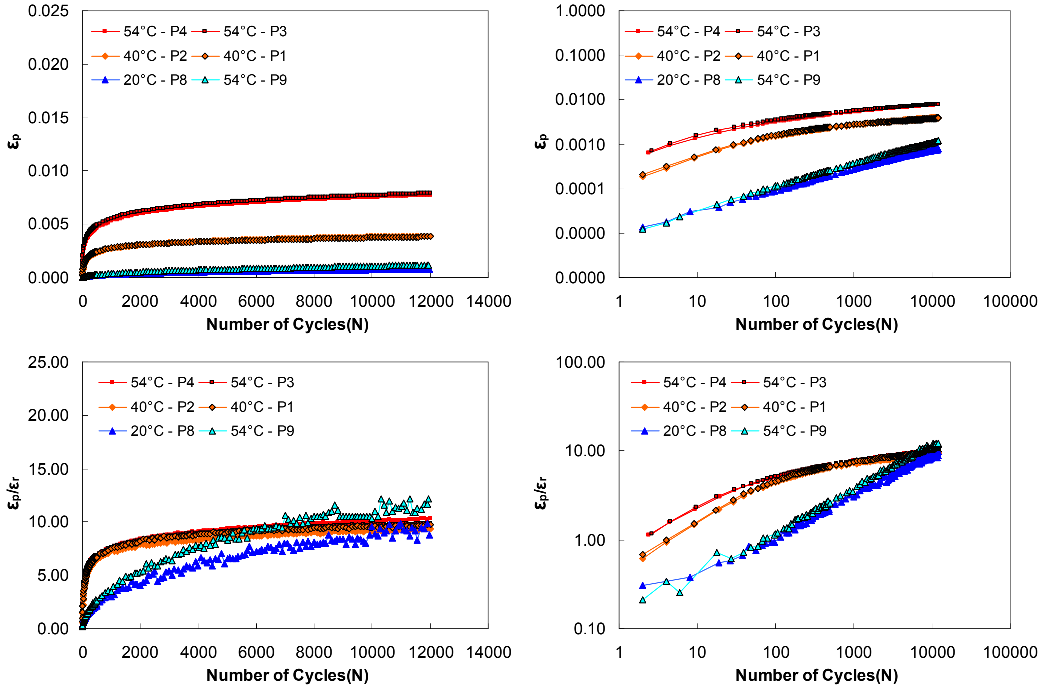

S9.5C

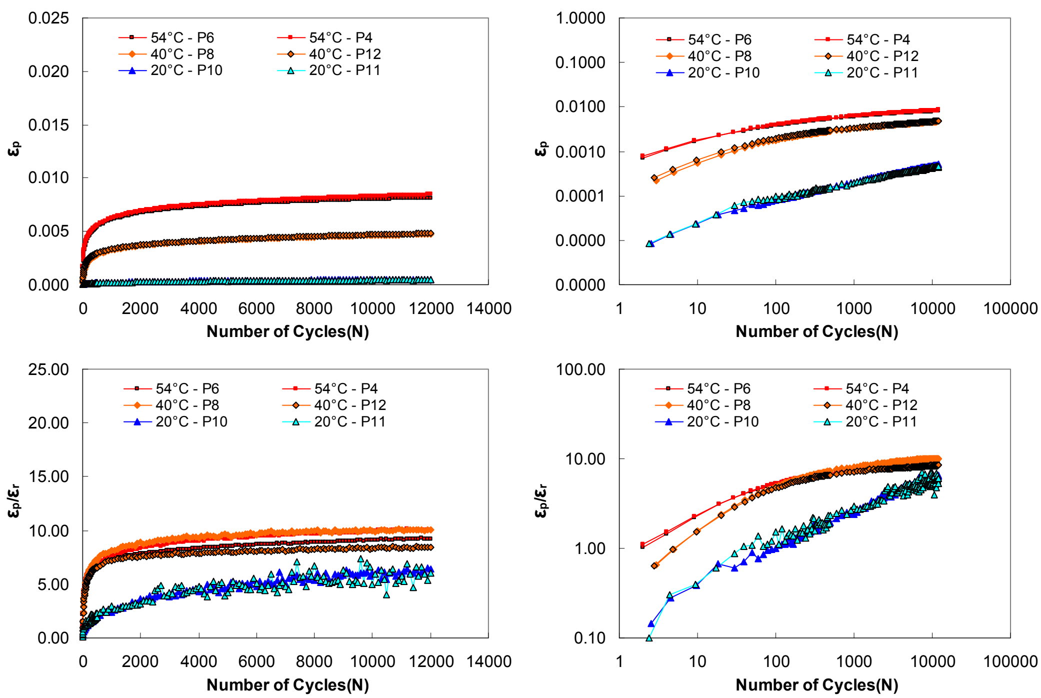

RS9.5C

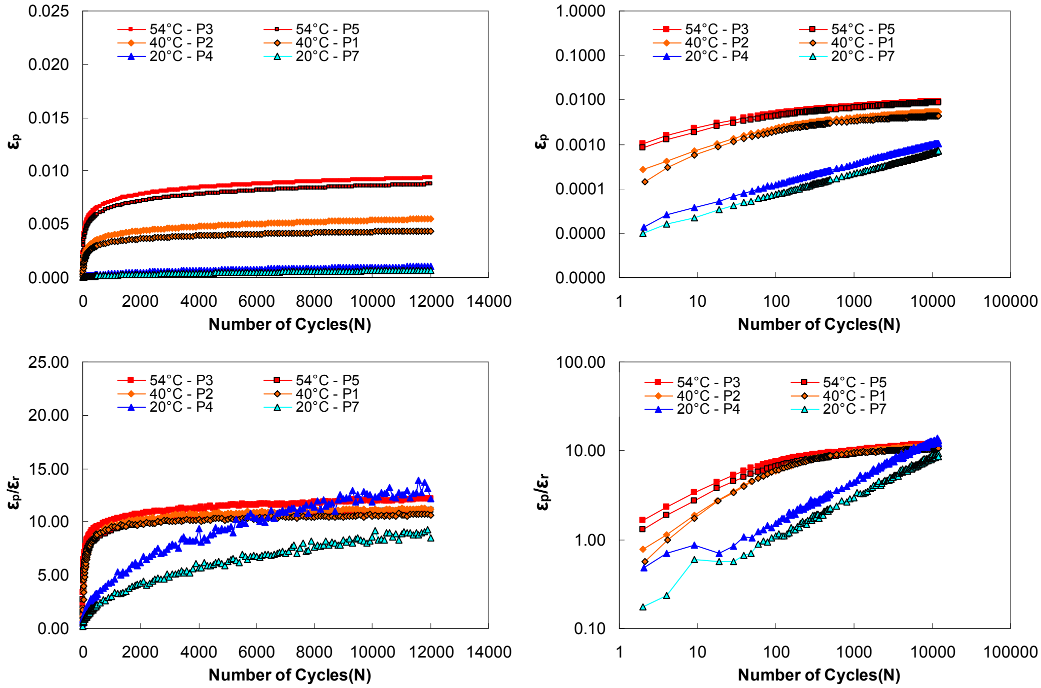

S12.5C

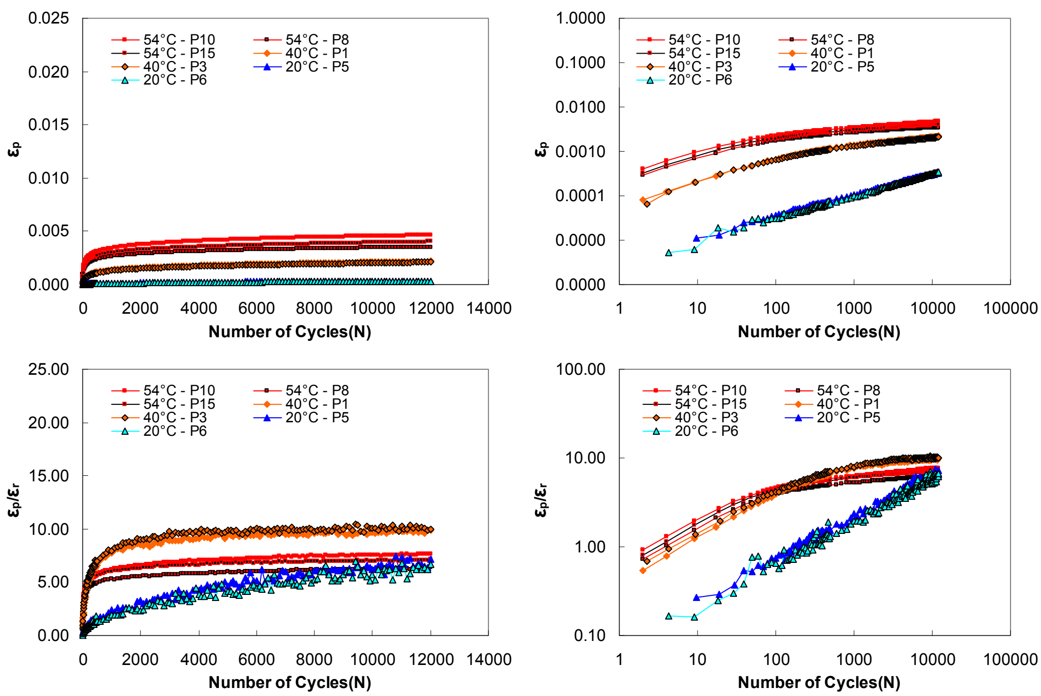

RS12.5C

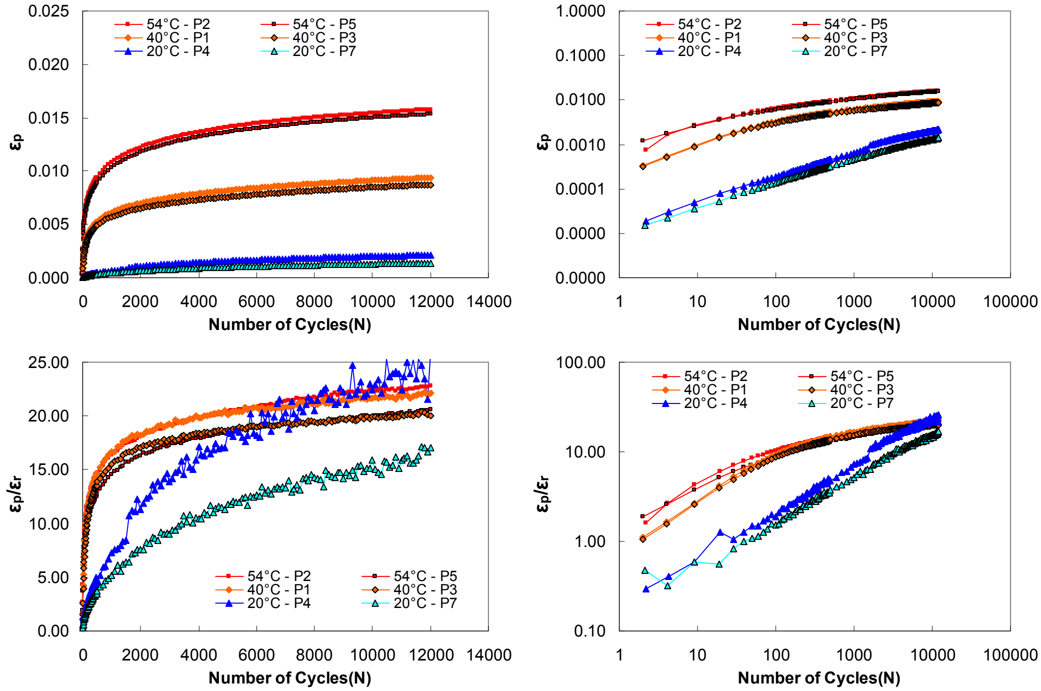

I19.0B

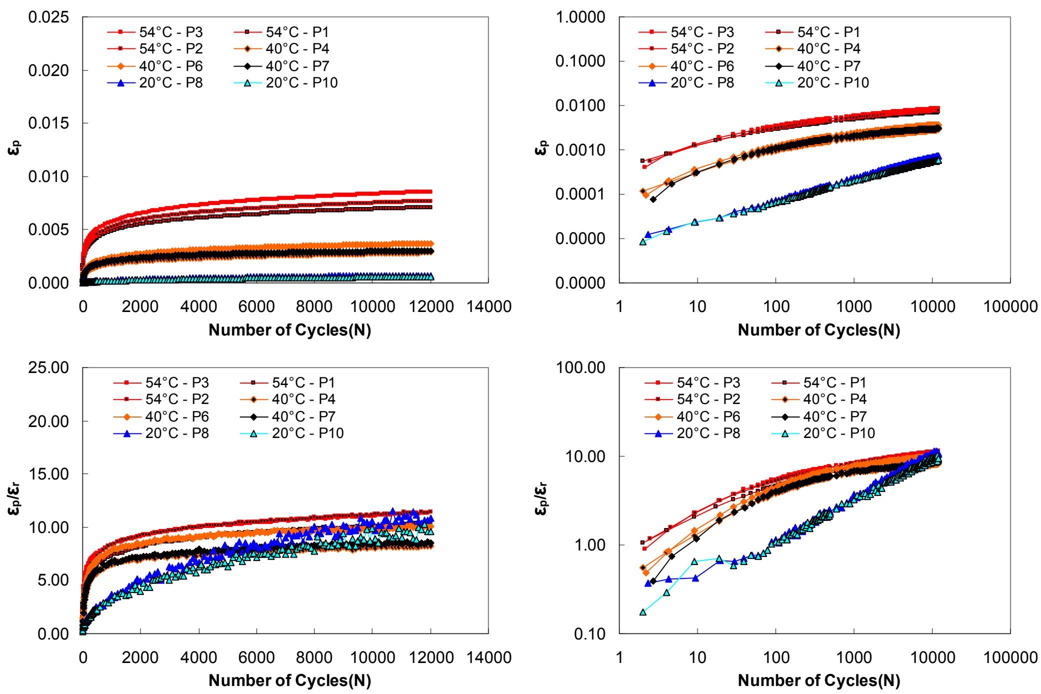

RI19.0B

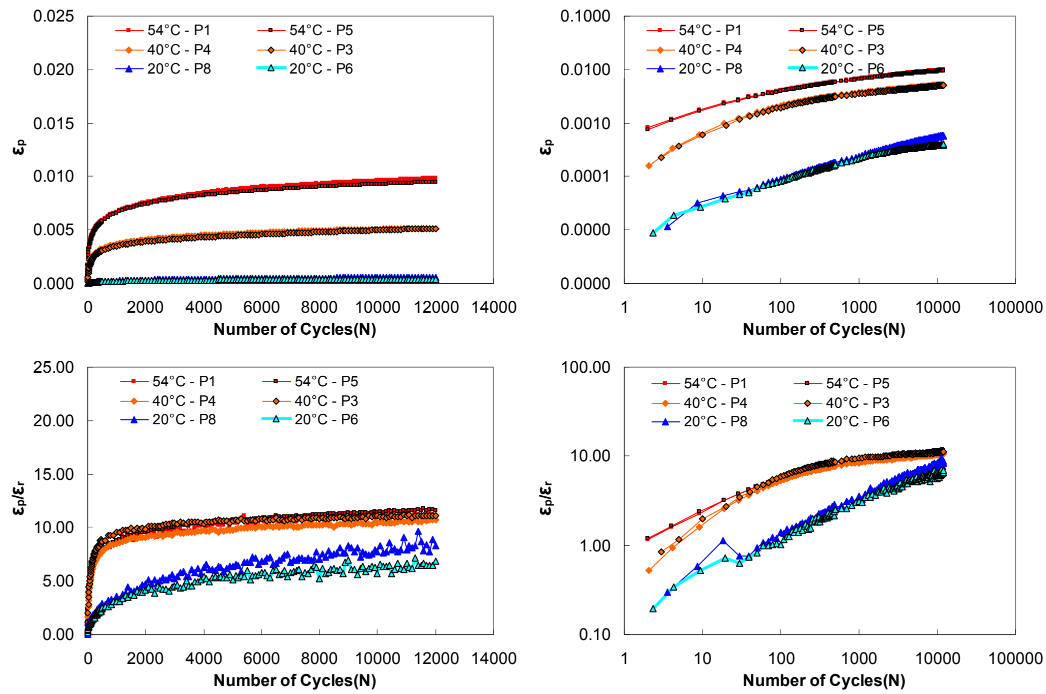

I19.0C

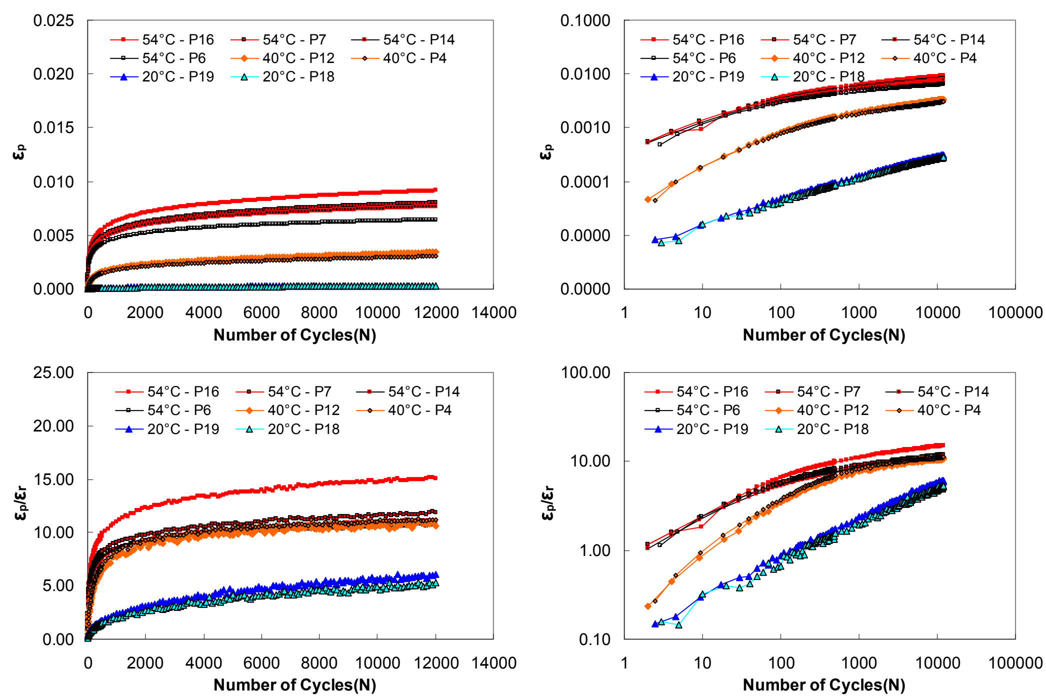

RI19.0C

Appendix D2 (Continued)

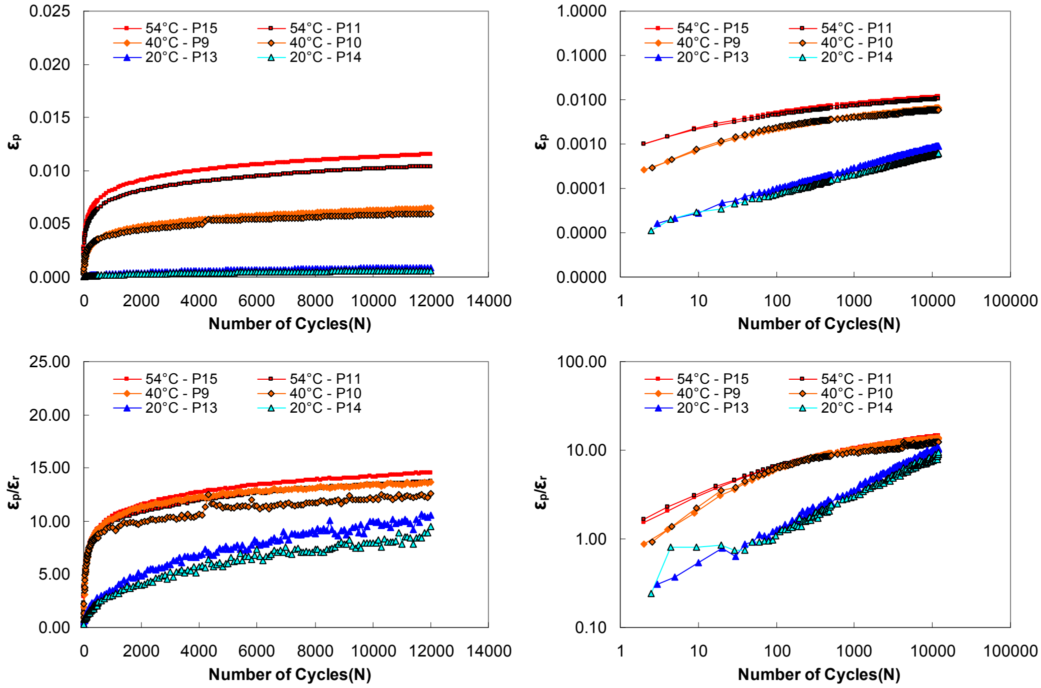

B25.0B

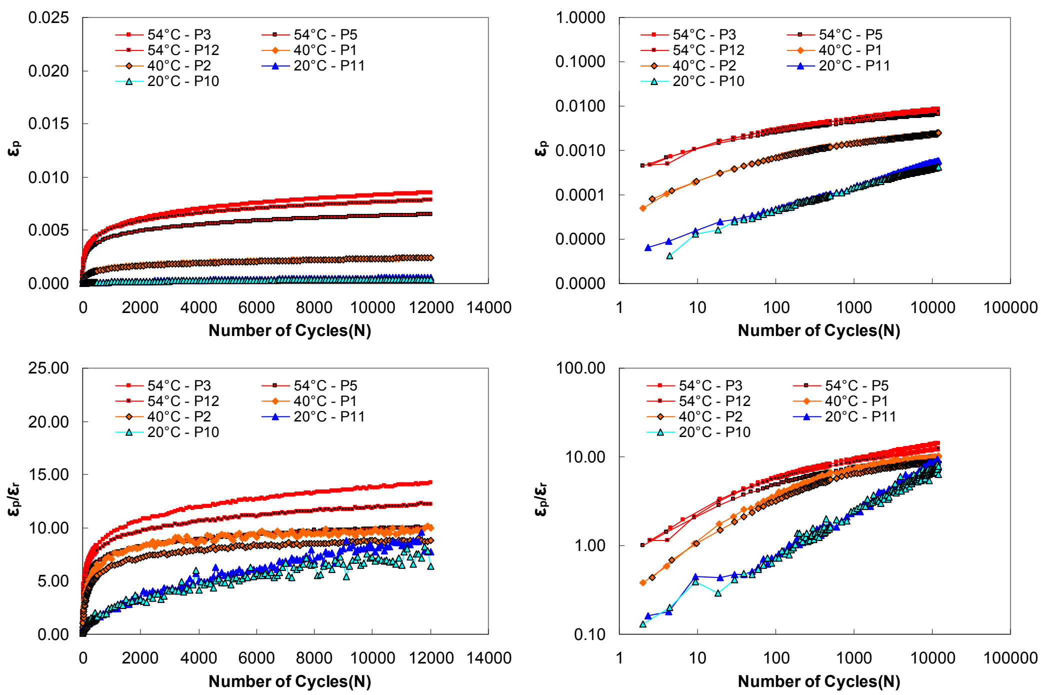

RB25.0B

Appendix D3 Predicted vs. Lab Measured Permanent Strain and Permanent to Resilient Strain Ratio for Common Asphalt Mixtures in NC

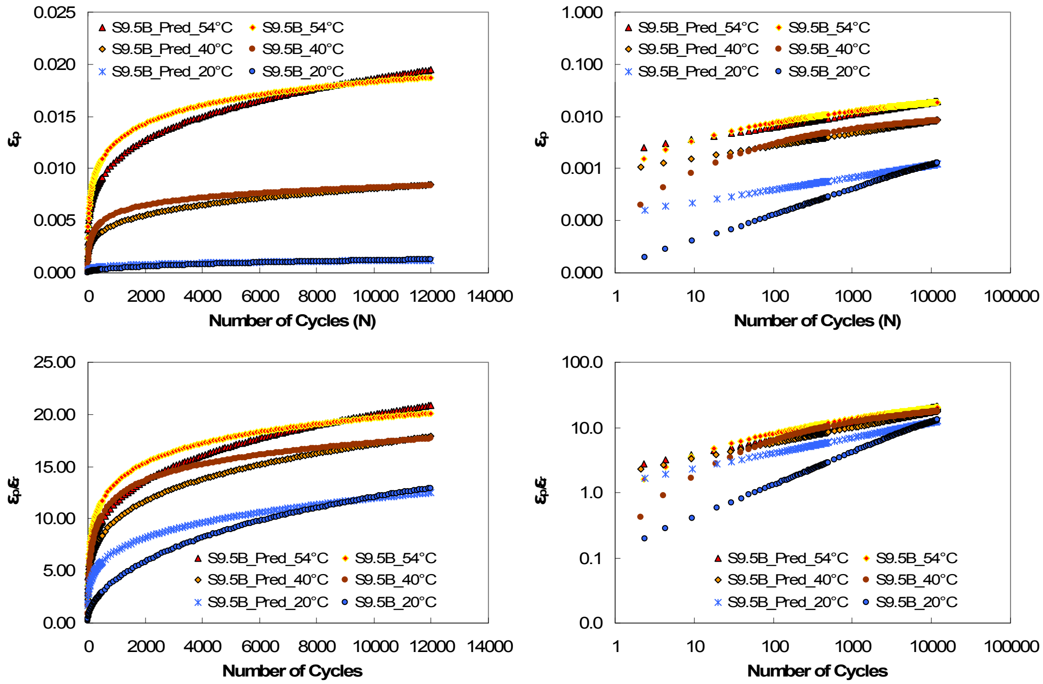

S9.5B

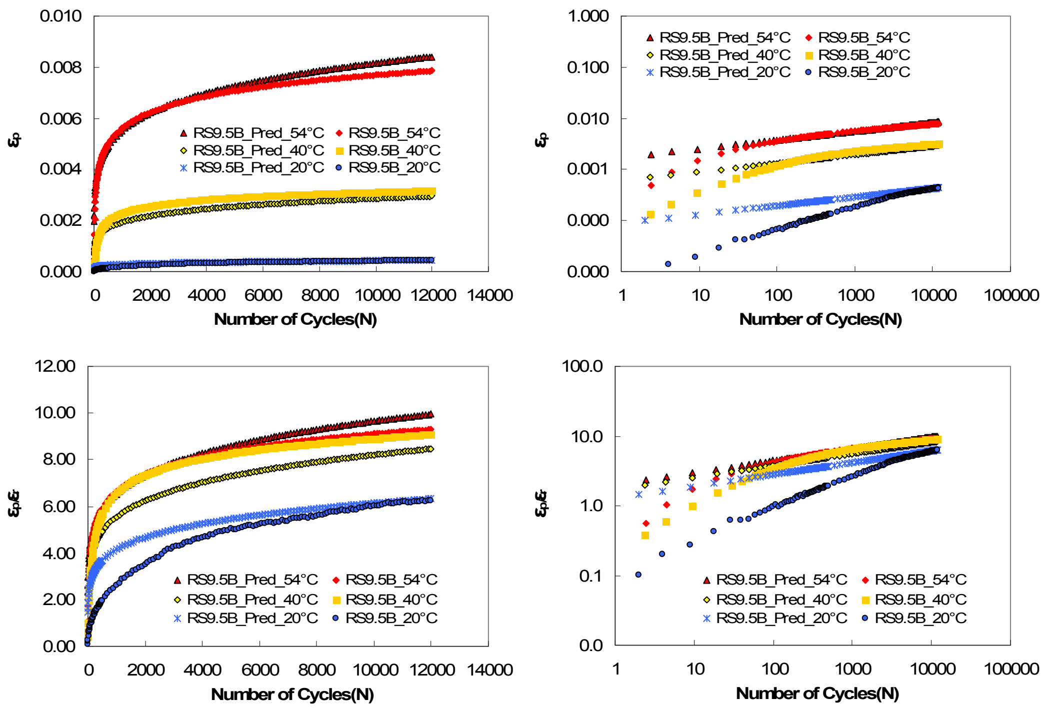

RS9.5B

Appendix D3 (Continued)

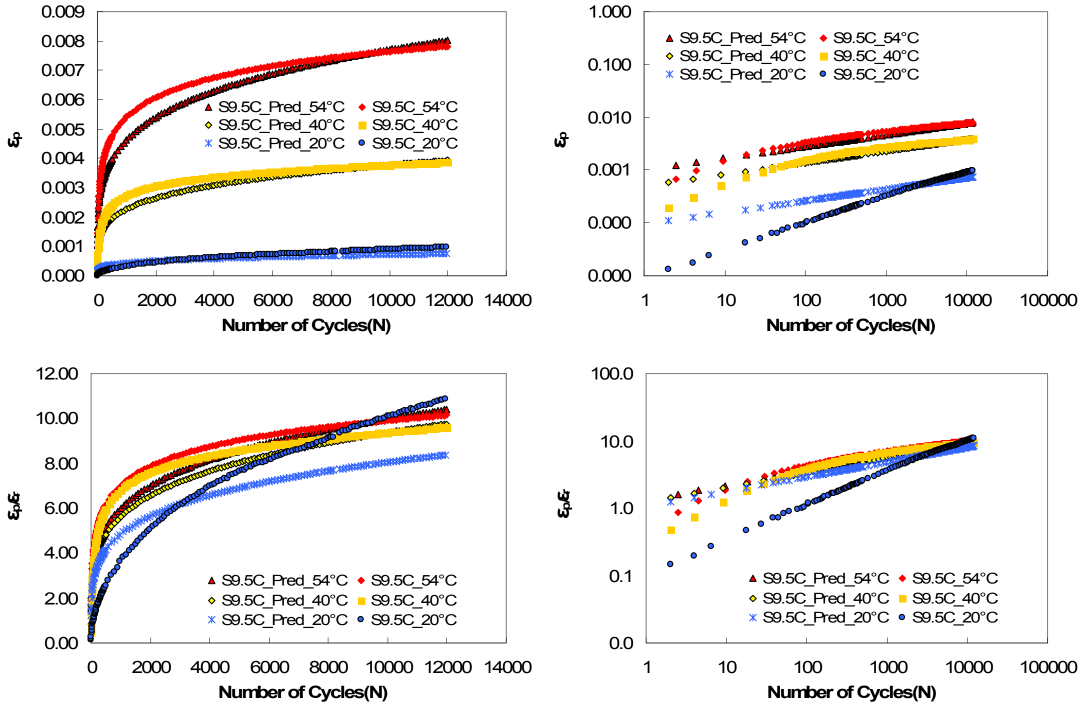

S9.5C

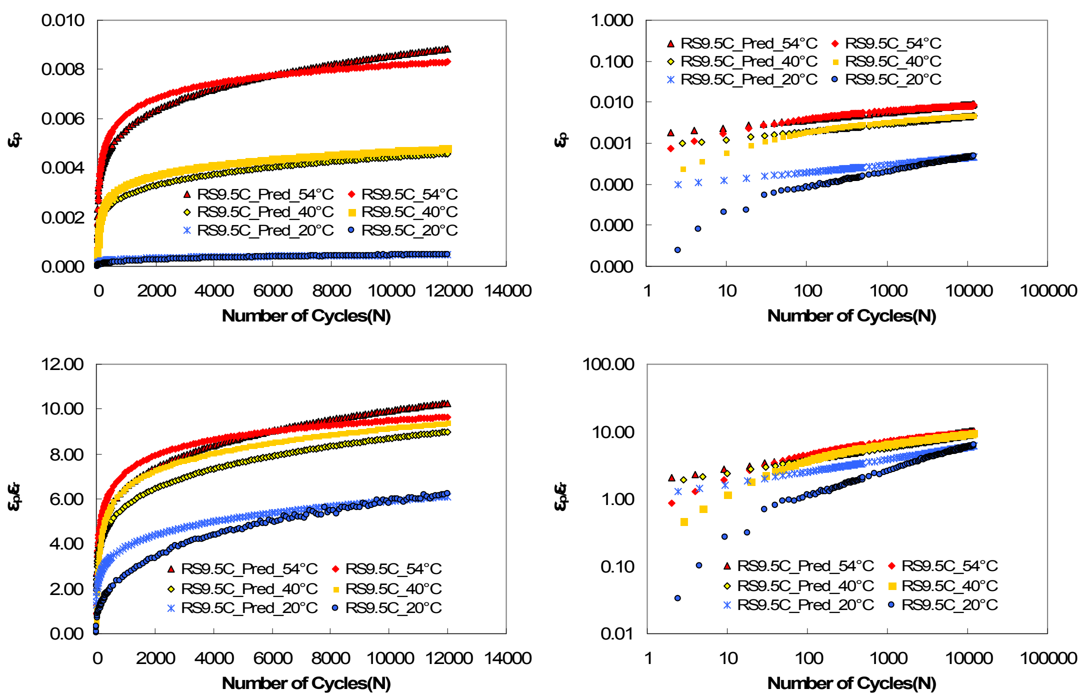

RS9.5C

Appendix D3 (Continued)

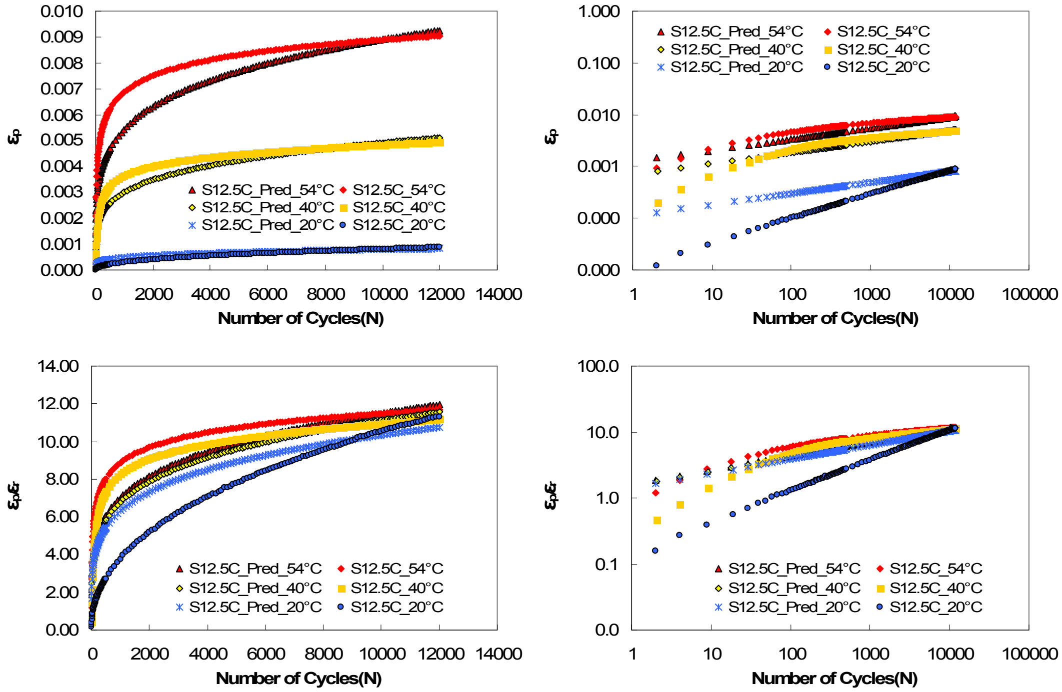

S12.5C

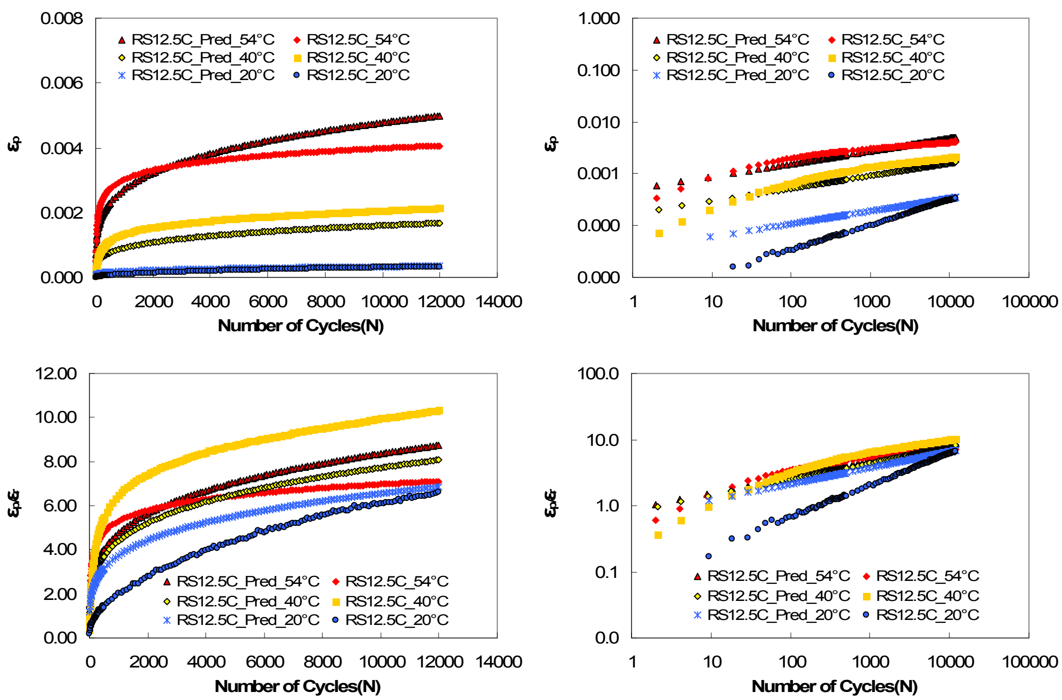

RS12.5C

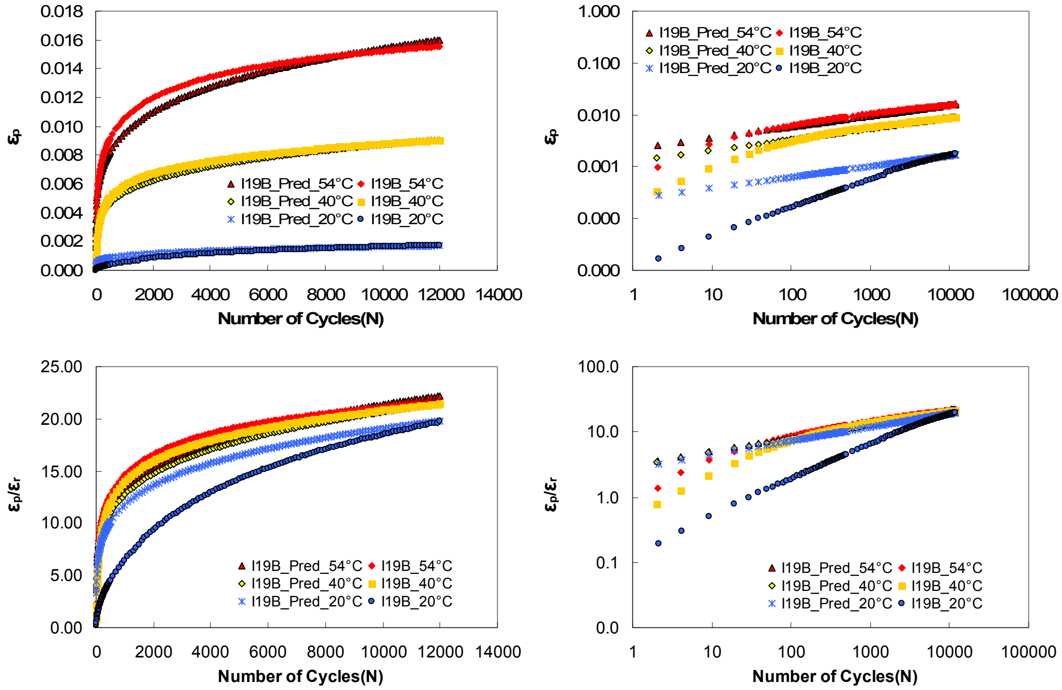
εp
εp/εr
Number of Cycles(N)
I19B_Pred_54°C
I19B_54°C
I19B_Pred_40°C
I19B_40°C
I19B_Pred_20°C
I19B_20°C

I19B

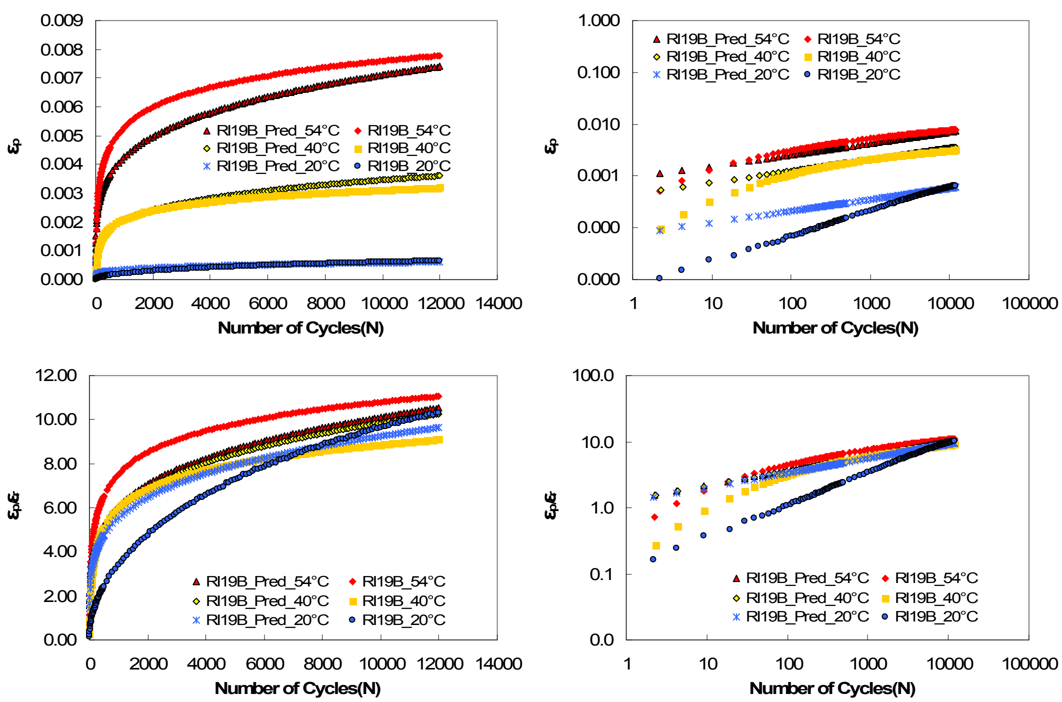
εp
εp/εr
Number of Cycles(N)
RI19B_Pred_54°C
RI19B_54°C
RI19B_Pred_40°C
RI19B_40°C
RI19B_Pred_20°C
RI19B_20°C

RI19B

Appendix D3 (Continued)

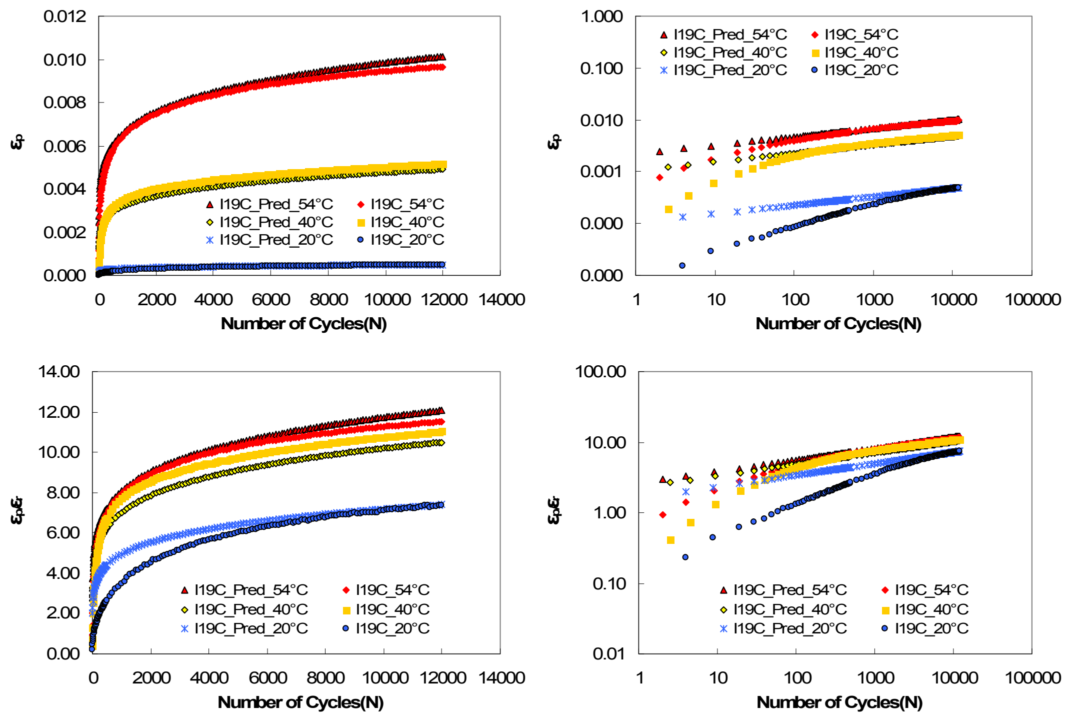

I19C

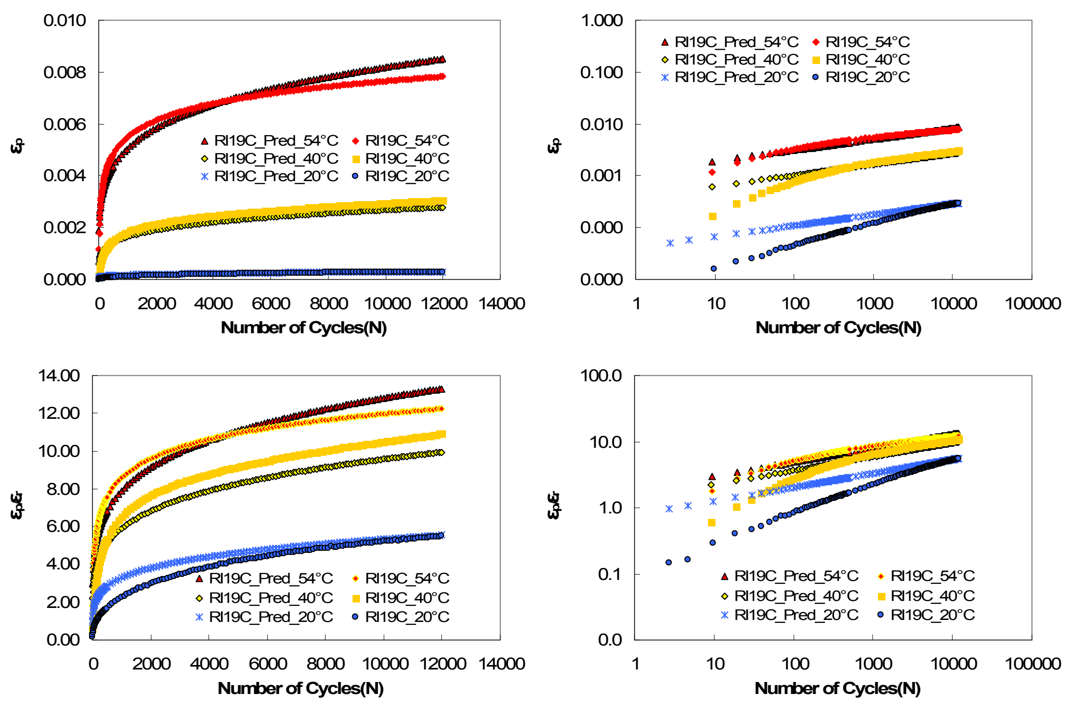

RI19C

Appendix D3 (Continued)

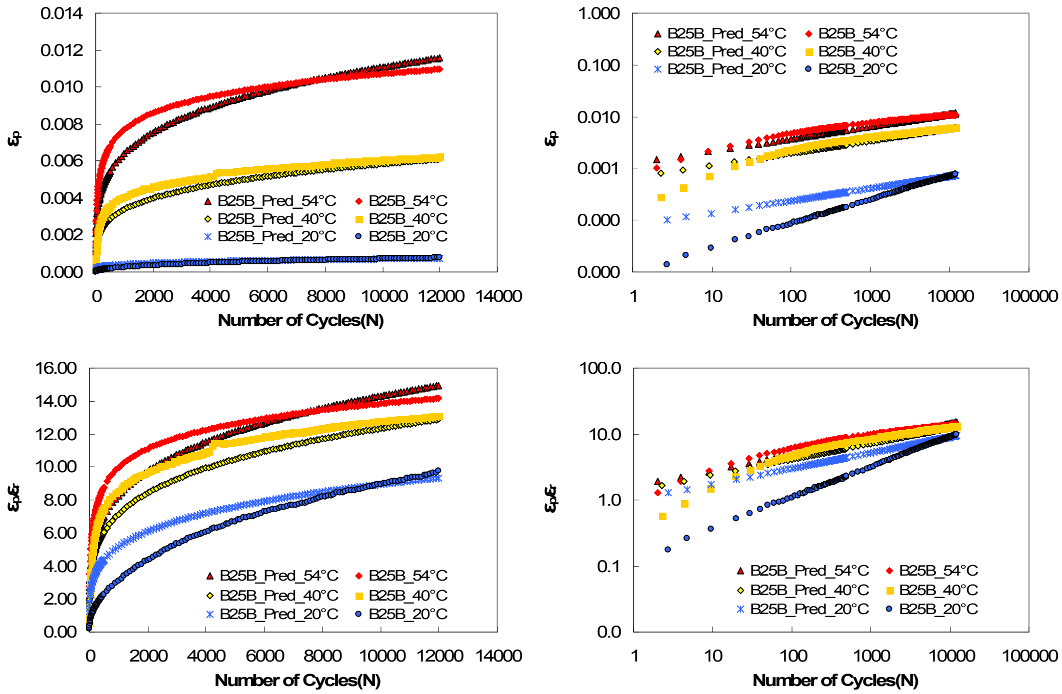

B25B

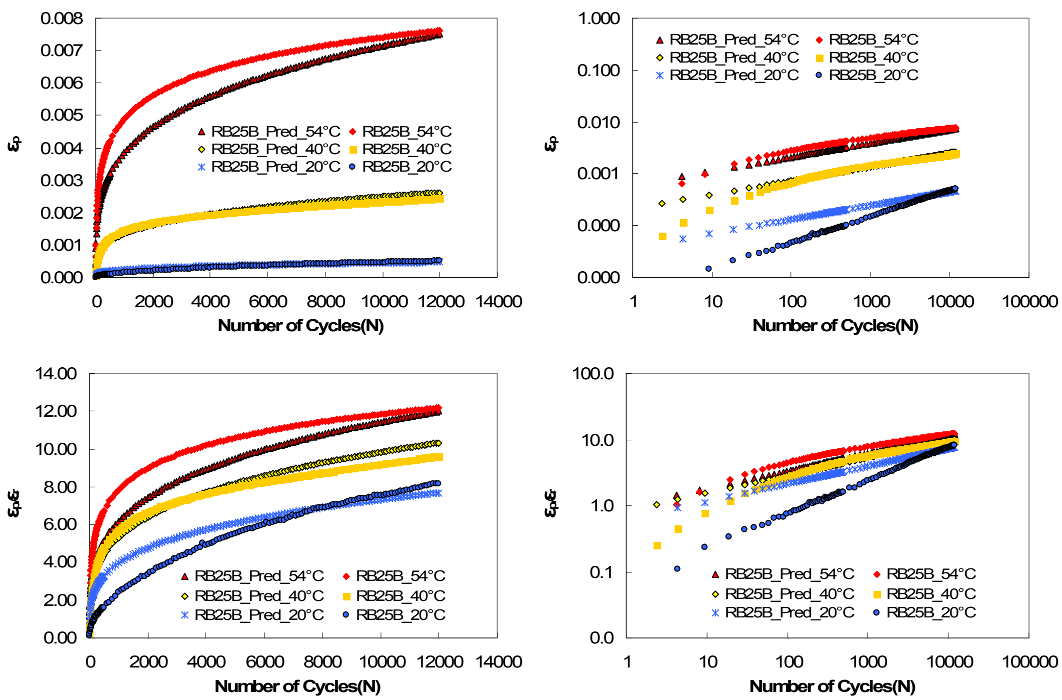

RB25B

Appendix E Fatigue Cracking Database

Appendix E1 Comparison of DMR and I Graphs From Fatigue Tests of the Most Popular Asphalt Concrete Mixtures in North Carolina

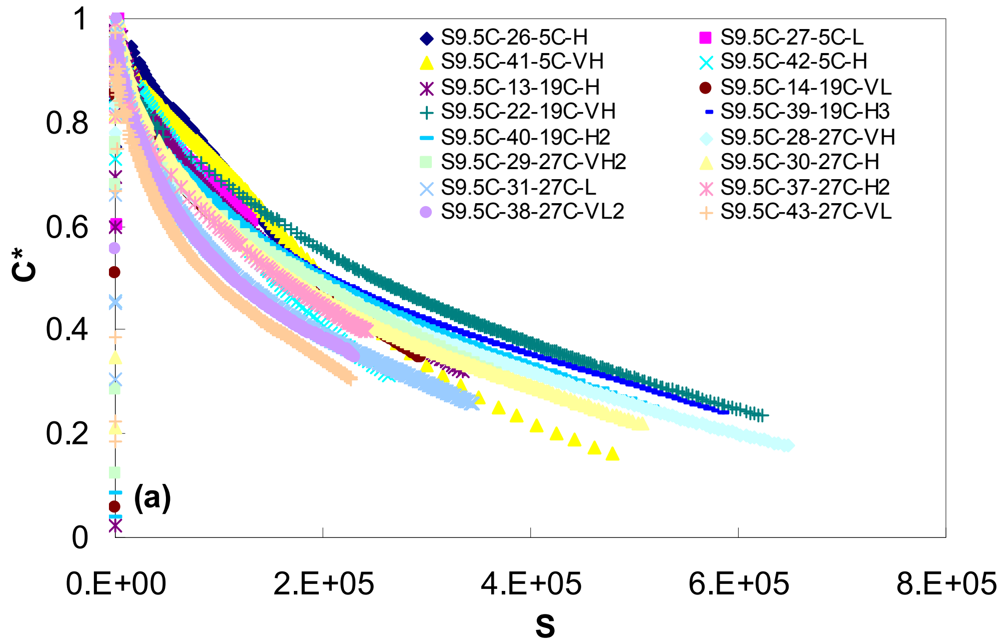

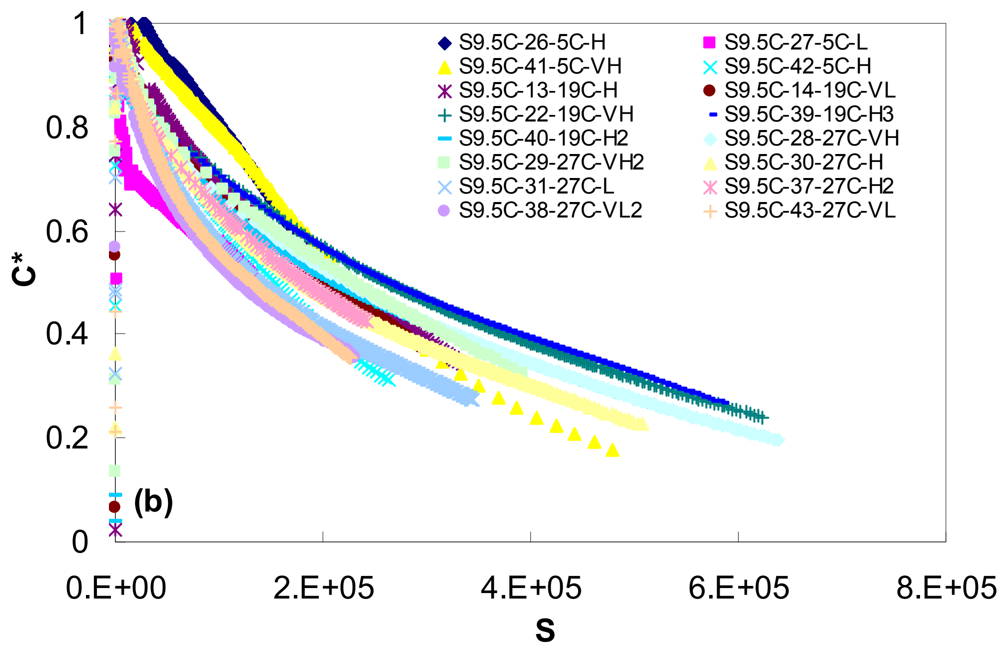

Damage curves for S9.5C mixture using (a) DMR and (b) I as specimen-to-specimen variability factor

Appendix E1 (Continued)

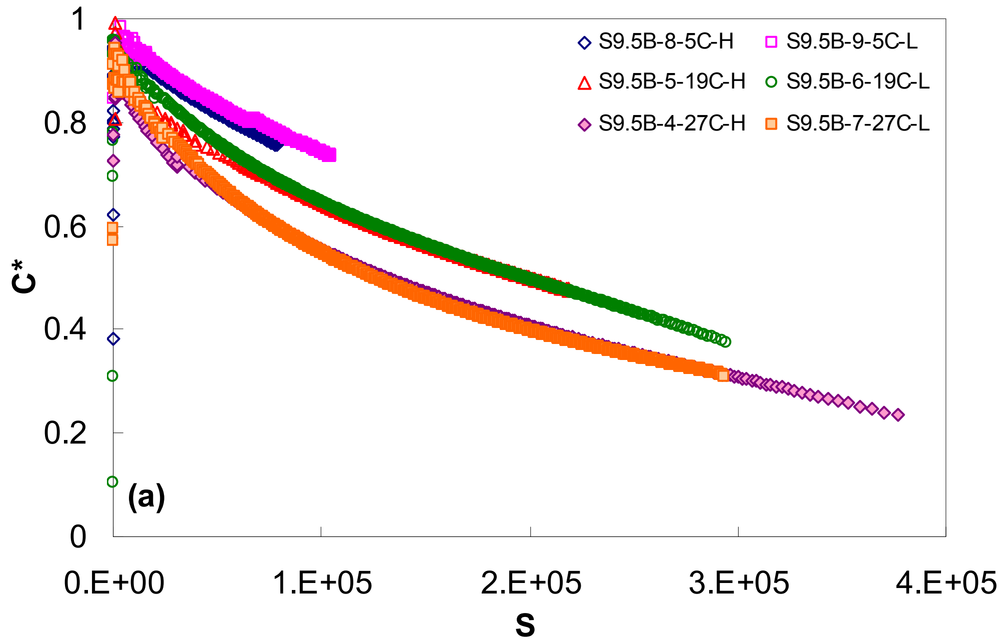

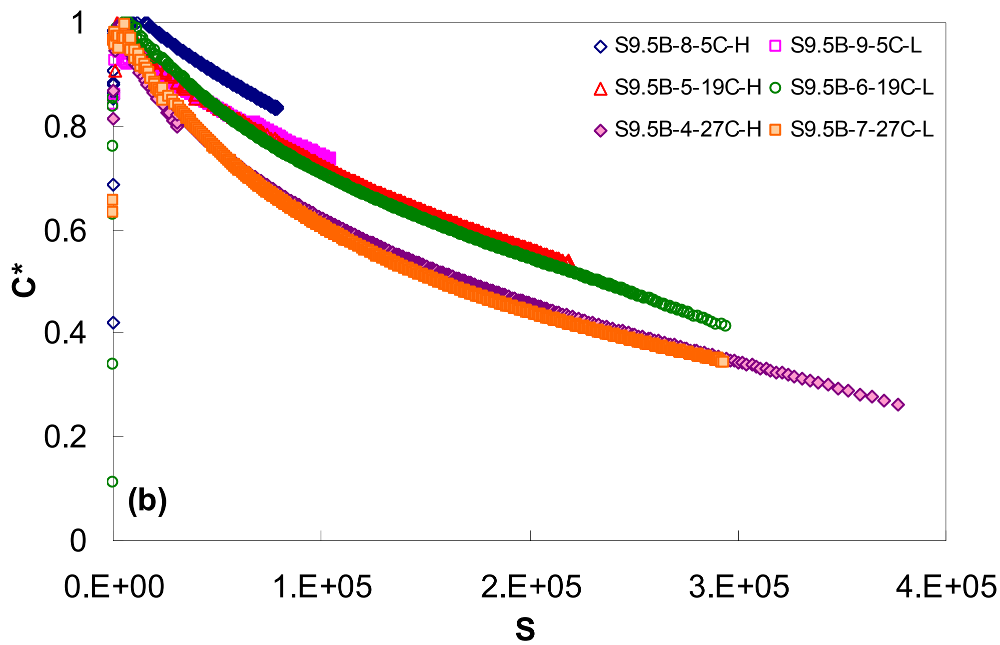

Damage curves for S9.5B mixture using (a) DMR and (b) I as specimen-to-specimen variability factor

Appendix E1 (Continued)

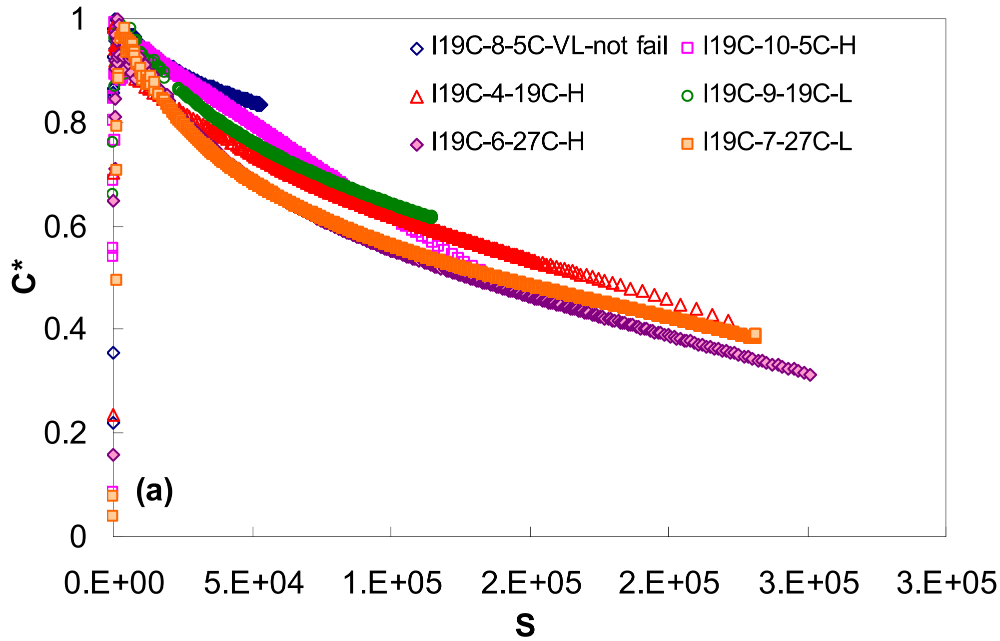

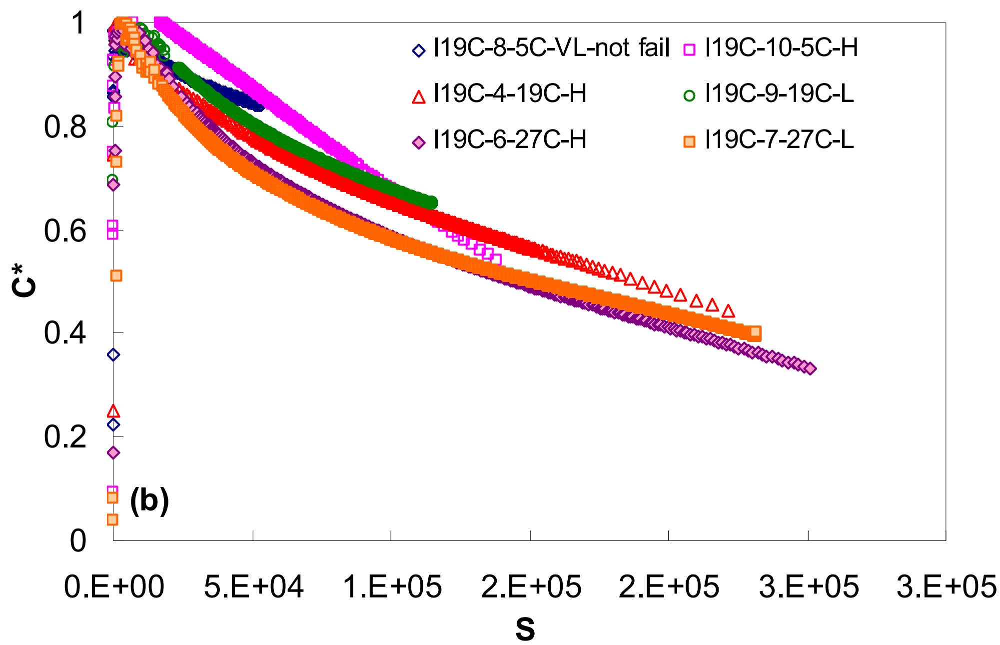

Damage curves for I19C mixture using (a) DMR and (b) I as specimen-to-specimen variability factor

Appendix E1 (Continued)

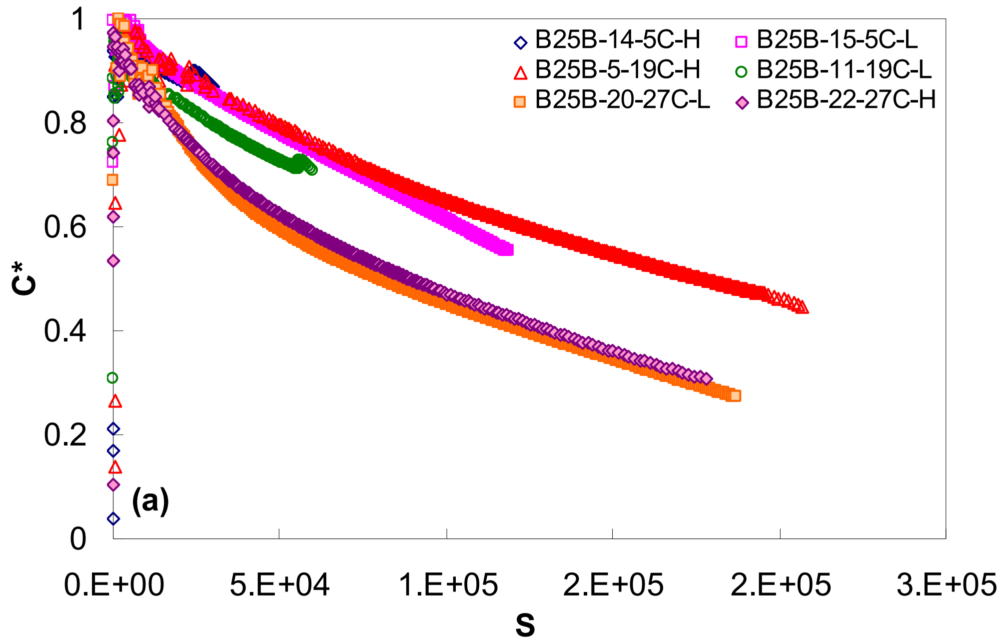

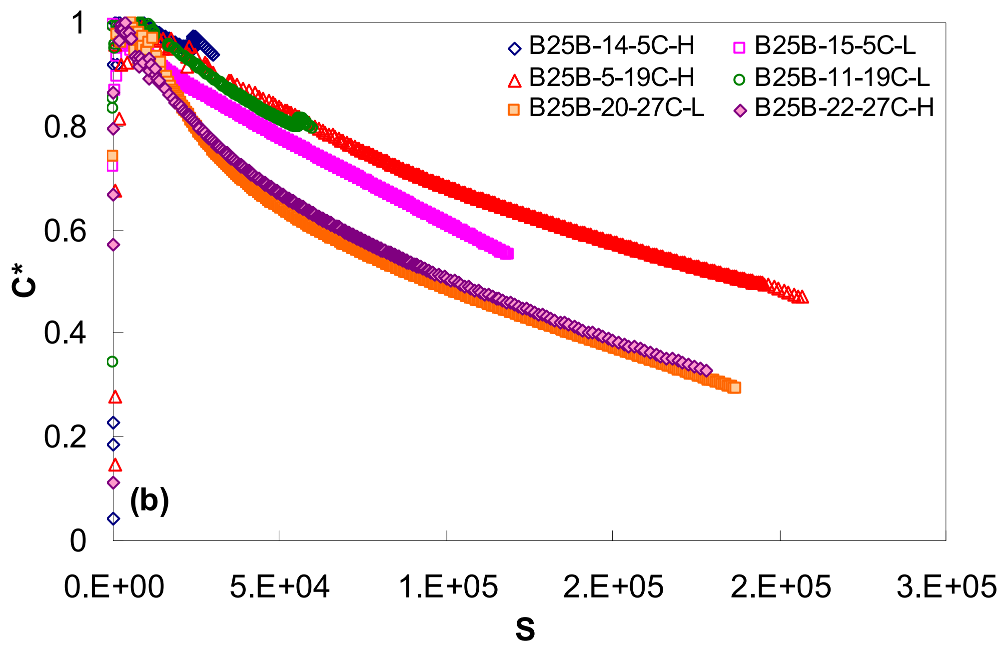

Damage curves for B25B mixture using (a) DMR and (b) I as specimen-to-specimen variability factor

Appendix E1 (Continued)

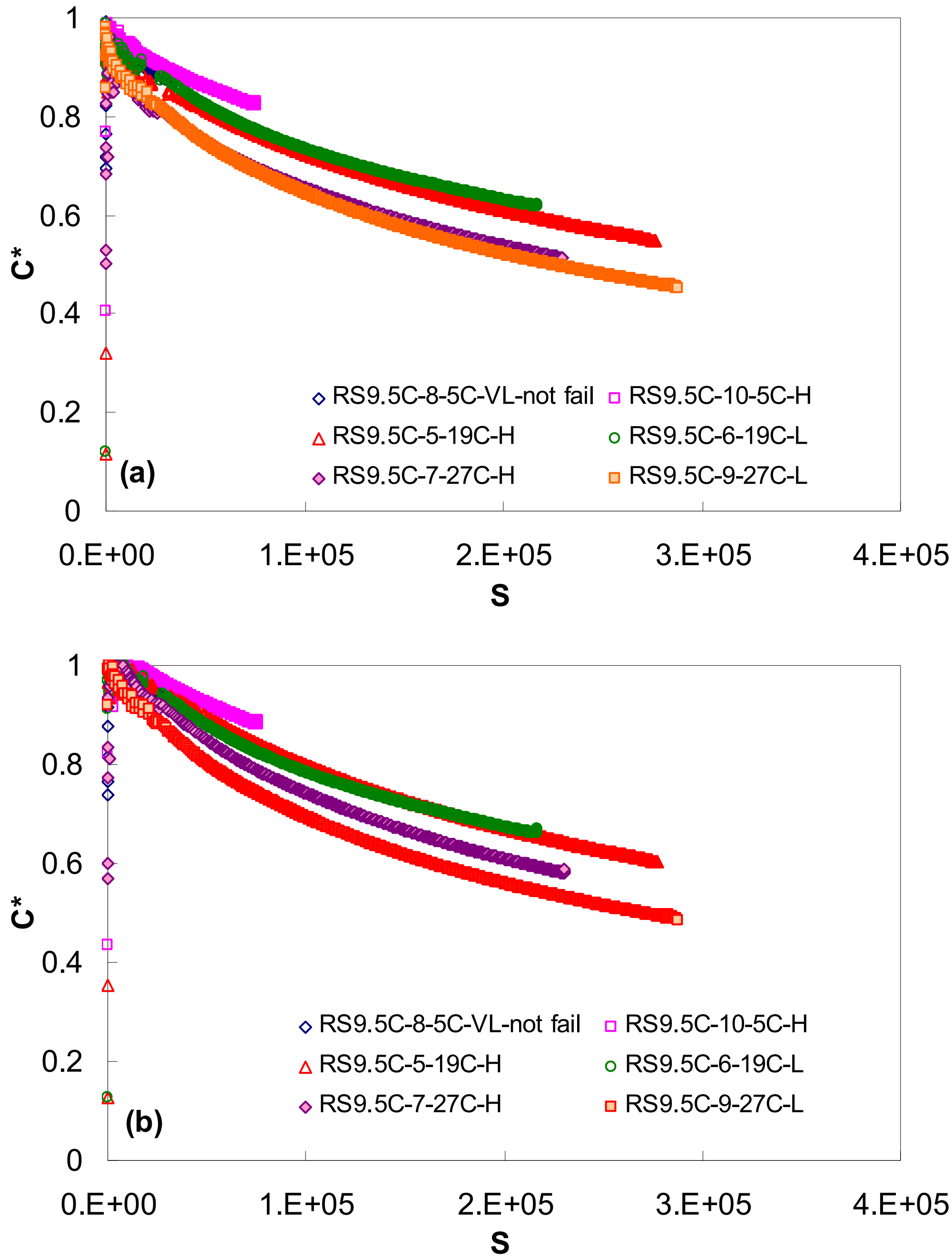

Damage curves for RS9.5C mixture using (a) DMR and (b) I as specimen-to-specimen variability factor

Appendix E1 (Continued)

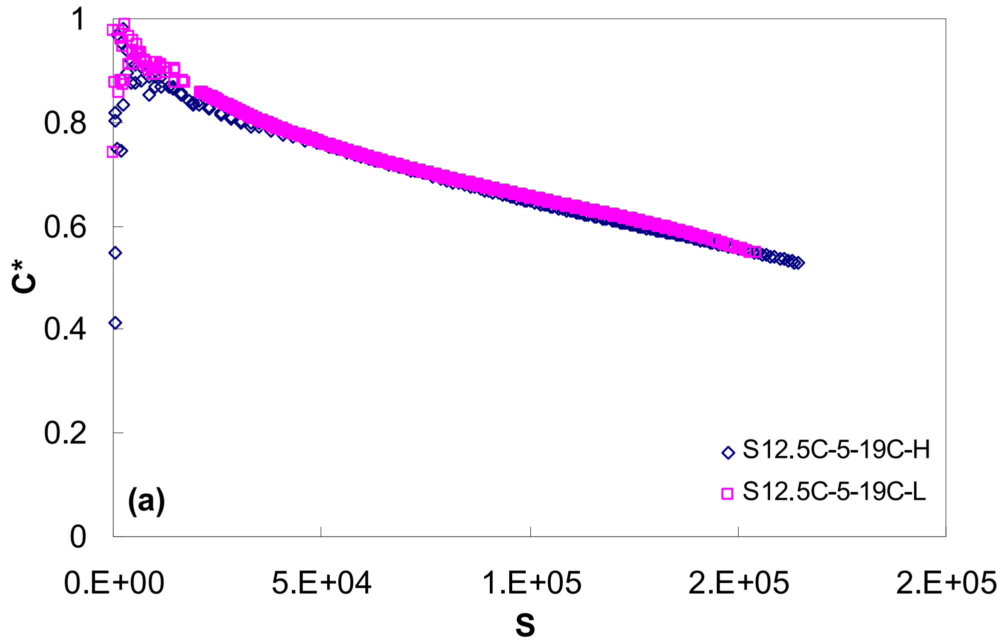

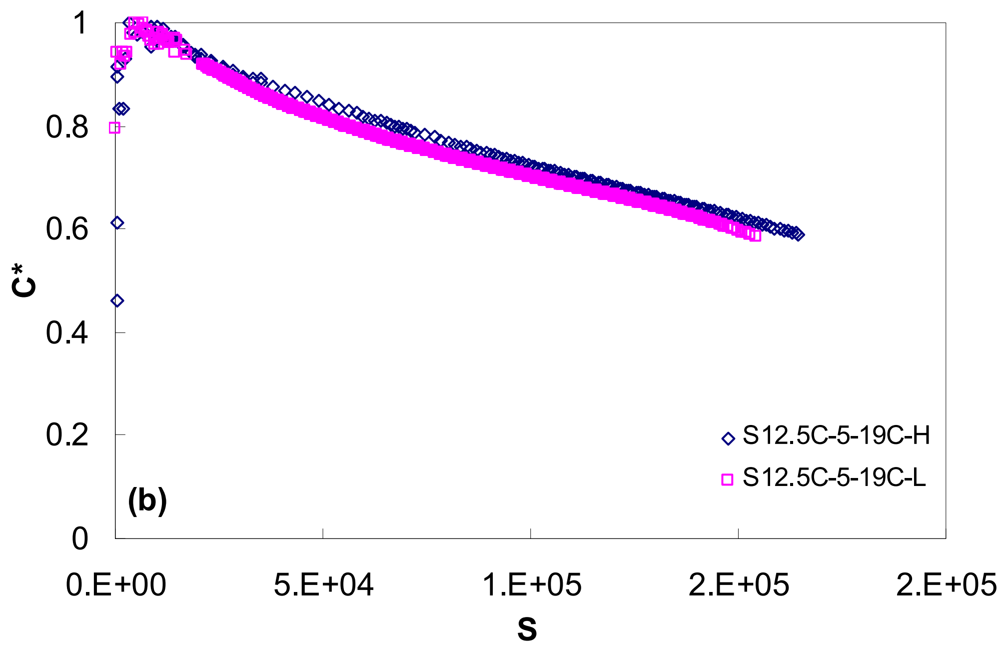

Damage curves for S12.5C mixture using (a) DMR and (b) I as specimen-to-specimen variability factor

Appendix E1 (Continued)

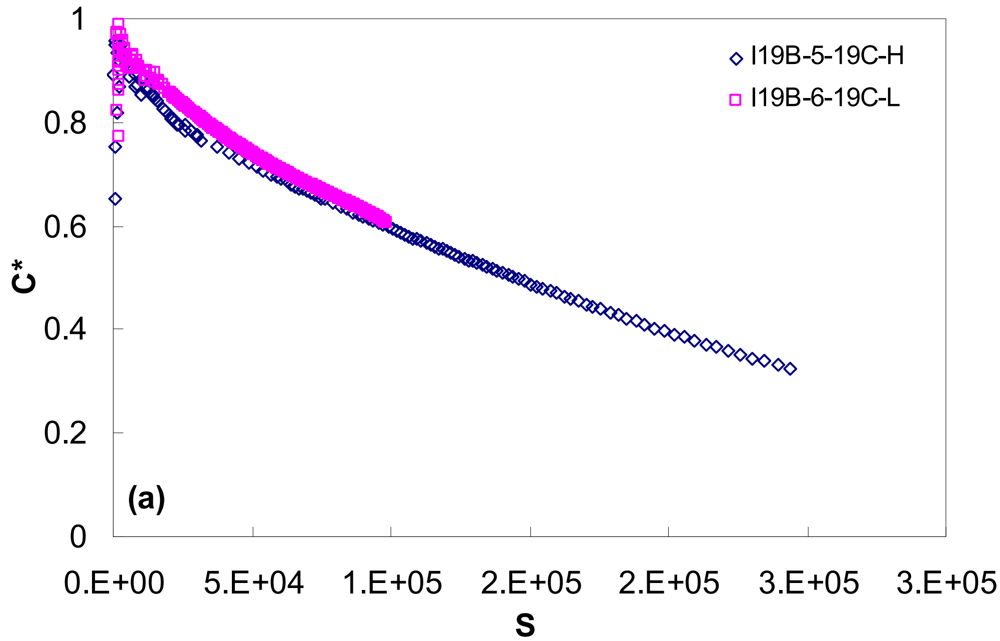

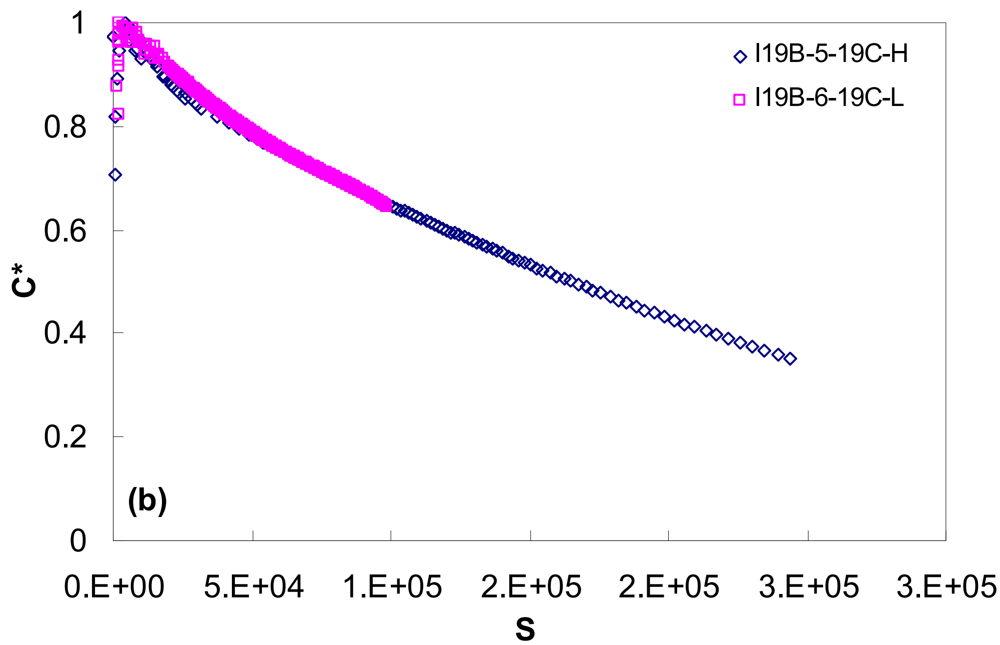

Damage curves for I19B mixture using (a) DMR and (b) I as specimen-to-specimen variability factor

Appendix E1 (Continued)

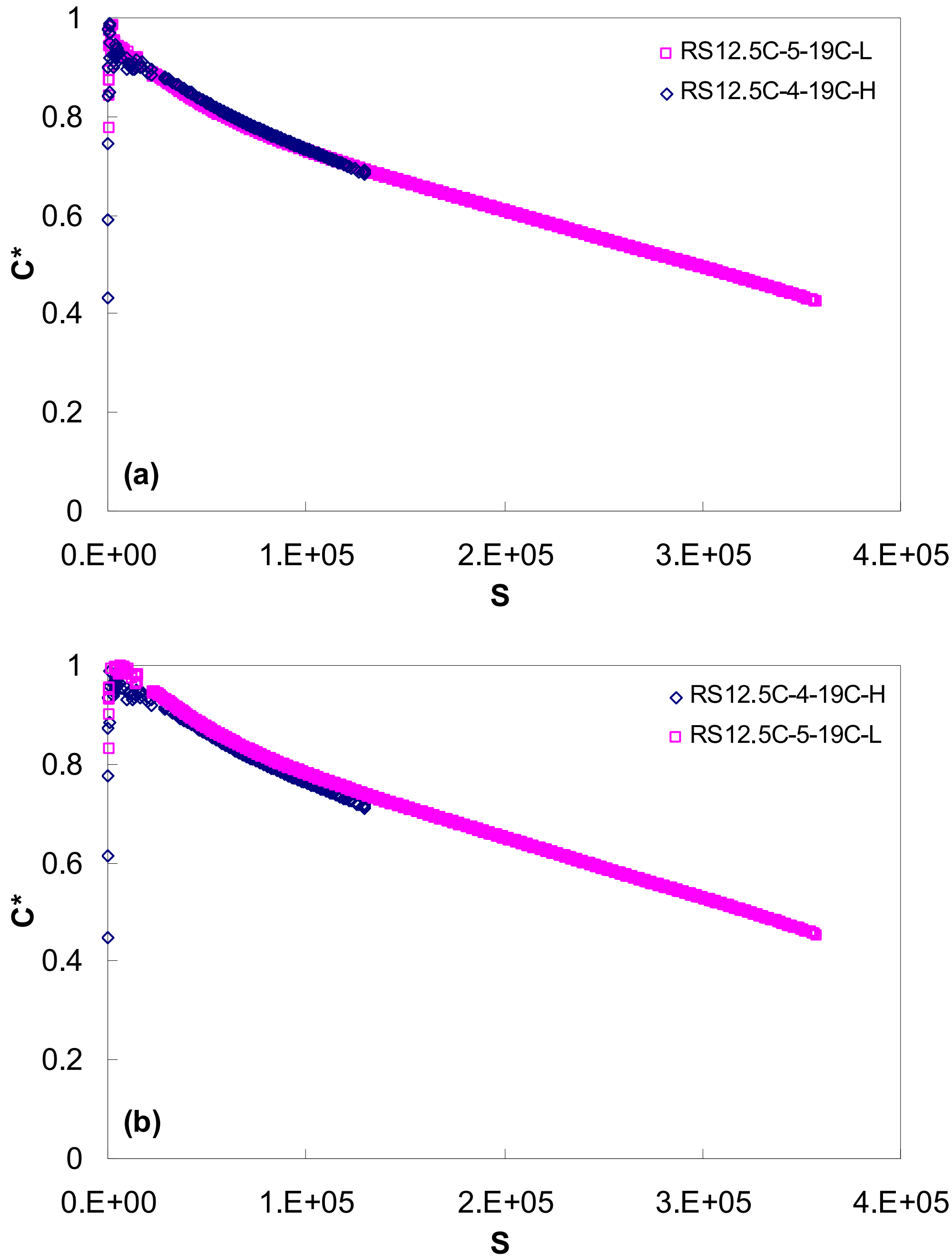

Damage curves for RS12.5C mixture using (a) DMR and (b) I as specimen-to-specimen variability factor

Appendix E1 (Continued)

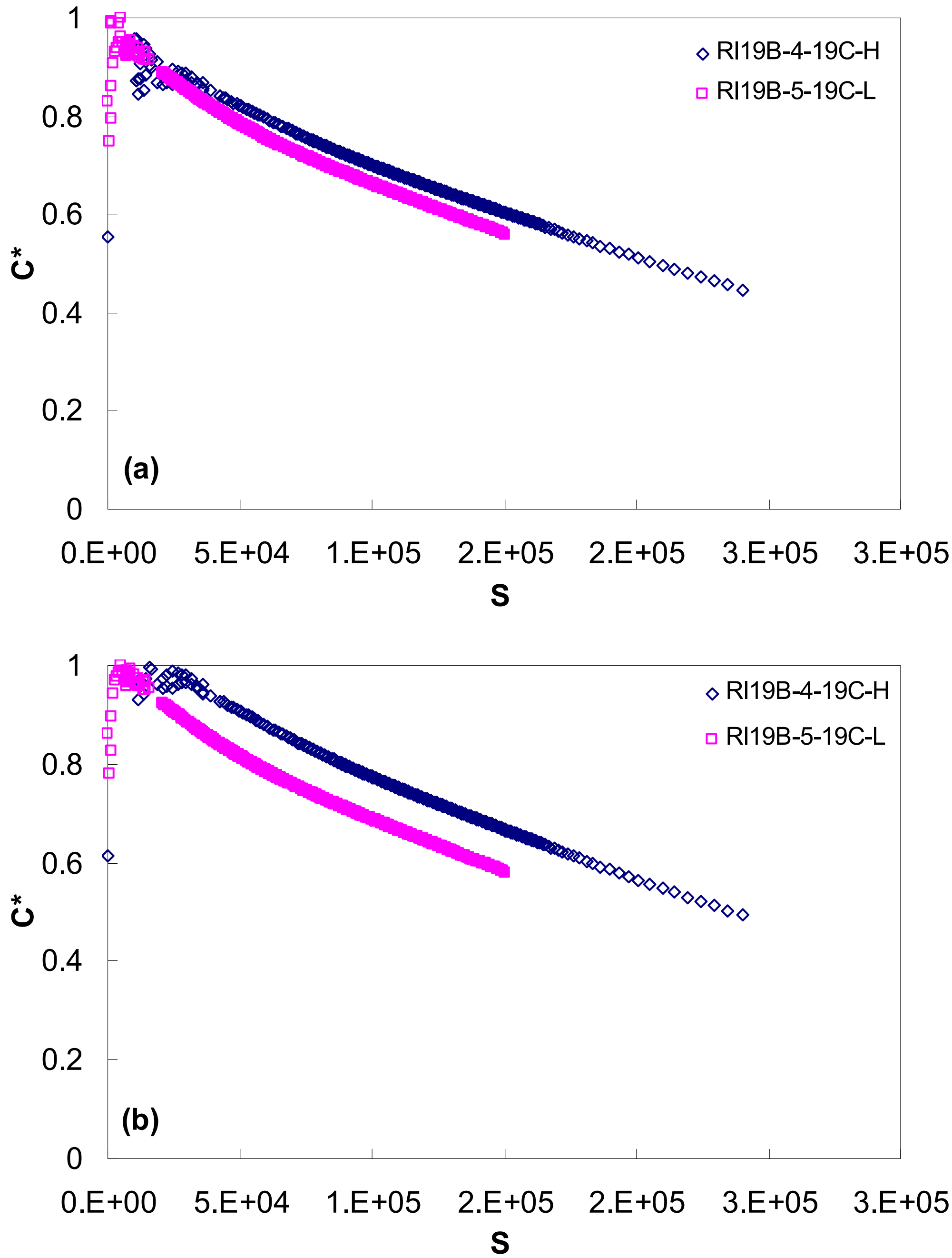

Damage curves for RI19B mixture using (a) DMR and (b) I as specimen-to-specimen variability factor

Appendix E1 (Continued)

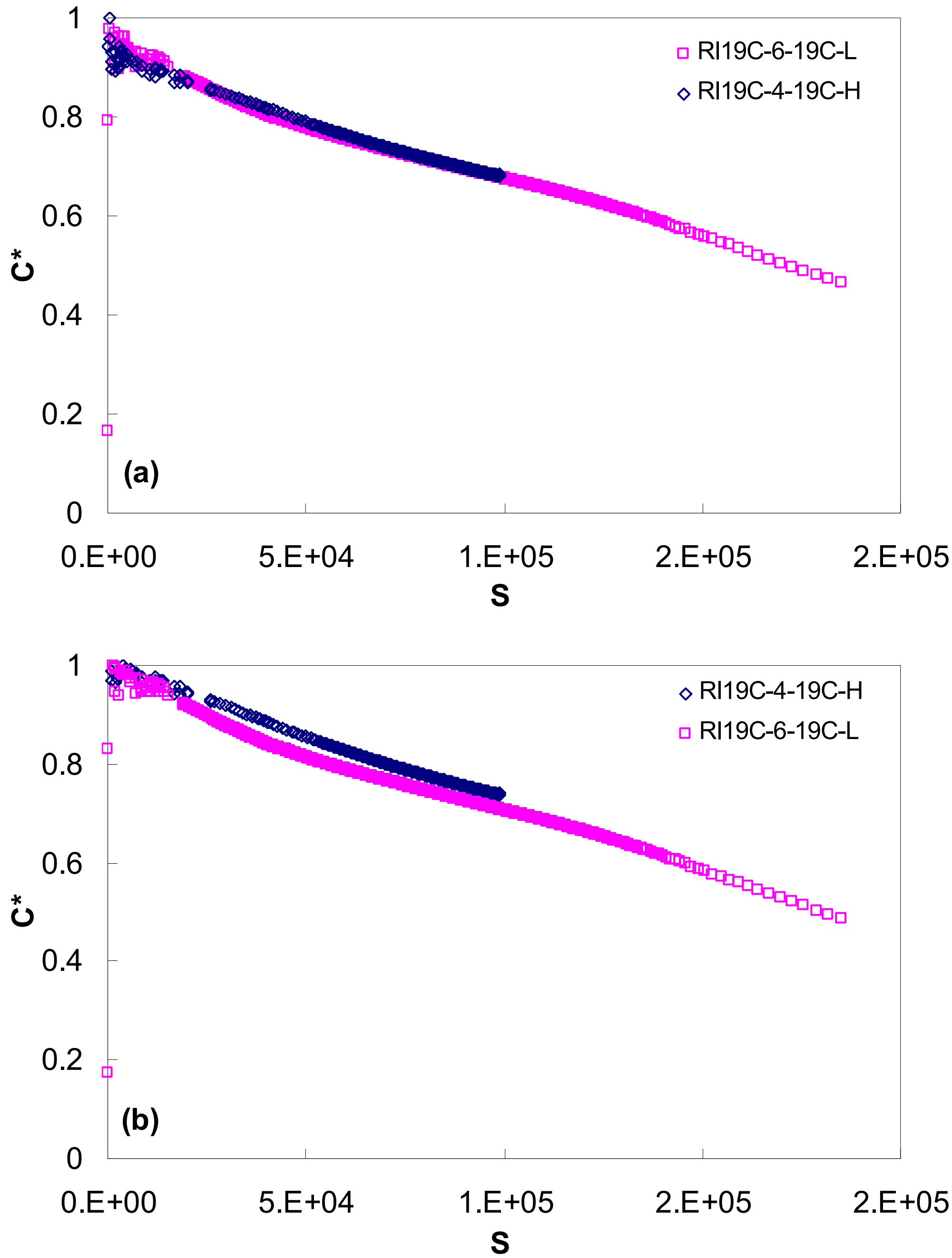

Damage curves for RI19C mixture using (a) DMR and (b) I as specimen-to-specimen variability factor

Appendix E1 (Continued)

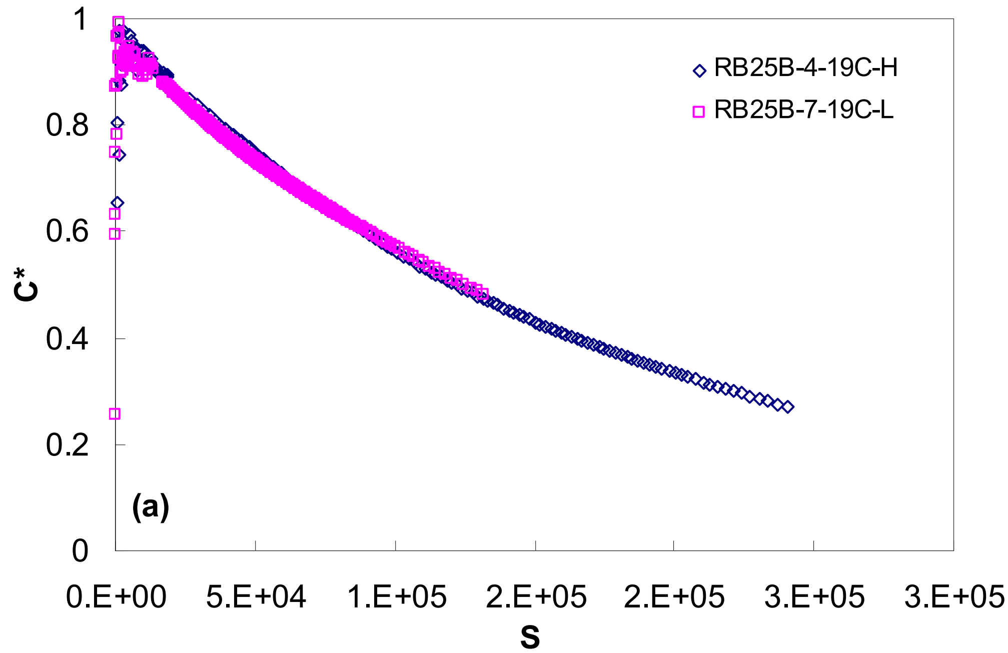

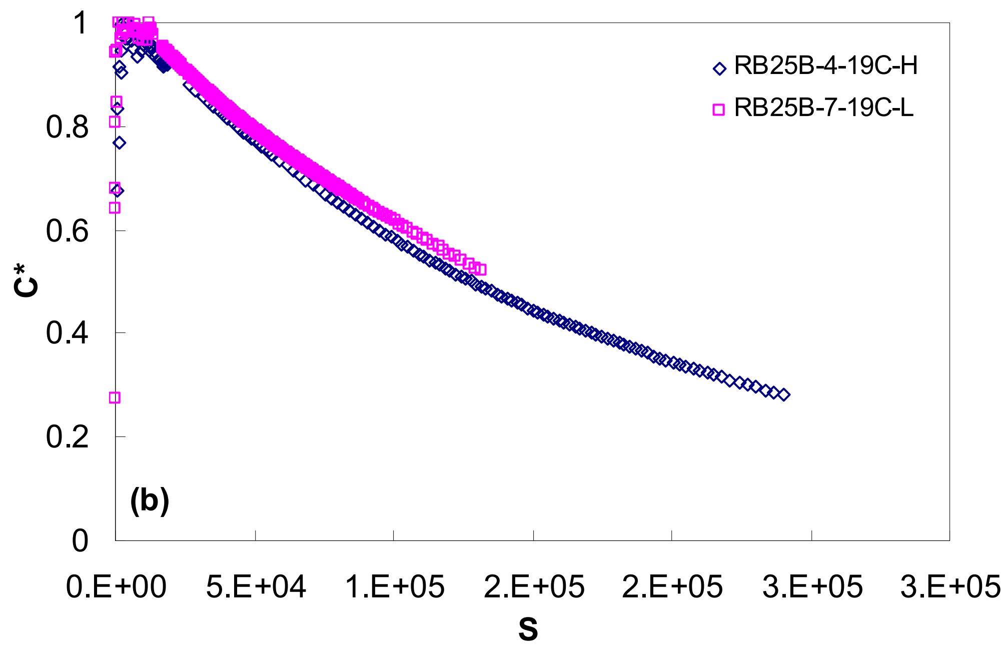

Damage curves for RB25B mixture using (a) DMR and (b) I as specimen-to-specimen variability factor

Appendix E2 Viscoelastic Damage Characterization Coefficients for Popular Asphalt Concrete Mixtures in North Carolina

Mixture	Parameters		
	C_{11}	C_{12}	α
S9.5C	0.003881	0.397445	4.126583
S9.5B	0.000900	0.518480	4.126662
I19C	0.000297	0.618120	3.637603
B25B	0.000240	0.630360	3.753415
RS9.5C	0.000687	0.517349	3.773737
S12.5C	0.000592	0.554818	3.951061
I19B	0.000348	0.611581	4.045163
RS12.5C	0.000425	0.559518	4.000179
RI19B	0.000220	0.635777	3.695799
RI19C	0.000578	0.548996	3.804381
RB25B	0.000156	0.687772	3.881082

Appendix E3 Comparison of Different Failure Definitions in Cyclic Test

Note

Although the advantage of using phase angle failure definition over the empirical 50% stiffness deduction failure definition has been stated clearly in Chapter 3, it is still interesting to examine their relationships through actual test results. The fatigue lives defined by these two methods for all mixtures are listed in

Table D. 1, and they are plotted against each other in the following graphs, together with a linear of equality. Note that those end-failure test results are not included for failure definition comparison.

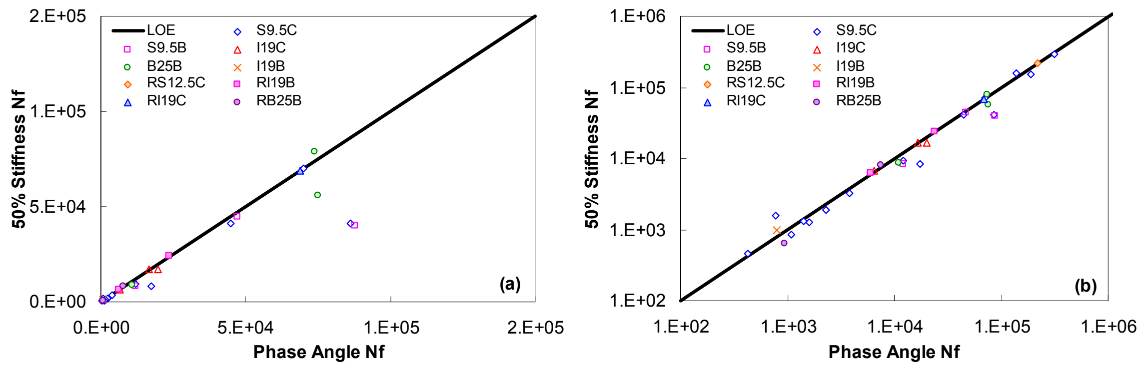

Comparison of different failure definitions: (a) arithmetic scale; (b) log scale

The Figure above shows that phase angle method tends to give a slightly longer fatigue life than the 50% stiffness method. However, in general, the differences between these two methods are quite small, usually within 25%.

Appendix E4 Experimental measured fatigue lives by two different definitions

Material	Specimen Name	N_f (phase angle)	N_f (50% Stiffness)
S9.5C	S9.5C-28	1600	1250
	S9.5C-29	420	453
	S9.5C-30	17500	8460
	S9.5C-31	86100	41223
	S9.5C-37	780	1580
	S9.5C-43	190000	149208
	S9.5C-13	45000	40927
	S9.5C-14	311000	290505
	S9.5C-22	2280	1870
	S9.5C-39	3780	3290
	S9.5C-40	12100	9350
	S9.5C-26	70000	70041
	S9.5C-27	140000	157813
	S9.5C-41	1430	1290
	S9.5C-42	1100	853
S9.5B	S9.5B-4	12100	8380
	S9.5B-6	47000	44587
	S9.5B-7	87900	40200
I19C	I19C-4	6500	6742
	I19C-6	19900	16800
	I19C-10	16600	16765
B25B	B25B-18	73800	78729
	B25B-20	75000	56022
	B25B-22	11000	8560
I19B	I19B-5	800	972
RS12.5C	RS12.5C-5	220000	217336
RI19B	RI19B-4	6000	6333
	RI19B-5	23700	23835
RI19C	RI19C-6	68900	69052
RB25B	RB25B-4	950	643
	RB25B-7	7550	8155

Appendix E5 Summary of Fatigue Test Prediction Results

Material	Specimen Name	Temperature (°C)	Failure Location	Measured N_f	Predicted N_f	Prediction Error (%)
S9.5C	S9.5C-28	26.80	middle	1600	1420	11
	S9.5C-29	26.80	middle	420	440	5
	S9.5C-30	26.80	middle	17500	16369	6
	S9.5C-31	26.60	middle	86100	103682	20
	S9.5C-37	26.95	middle	780	1190	53
	S9.5C-38	26.80	end	165000	278603	69
	S9.5C-43	27.40	middle	190000	212829	12
	S9.5C-13	19.05	middle	45000	51806	15
	S9.5C-14	19.00	middle	311000	385469	24
	S9.5C-22	18.50	middle	2280	2245	2
	S9.5C-39	18.70	middle	3780	3360	11
	S9.5C-40	18.80	middle	12100	12088	0
	S9.5C-26	5.00	middle	70000	84612	21
	S9.5C-27	4.90	middle	140000	181083	29
	S9.5C-41	4.60	middle	1430	1420	1
	S9.5C-42	5.30	middle	1100	1310	19
S9.5B	S9.5B-4	27.40	middle	12100	10400	14
	S9.5B-5	19.20	end	4570	5531	21
	S9.5B-6	19.30	middle	47000	50909	8
	S9.5B-7	27.30	middle	87900	106620	21
	S9.5B-8	5.50	end	4600	6041	31
	S9.5B-9	5.50	end	198000	257996	30
I19C	I19C-4	19.15	middle	6500	5555	15
	I19C-6	27.40	middle	19900	22880	15
	I19C-7	27.40	end	217000	113400	48
	I19C-8	5.40	N/A	>277200*	355473	N/A
	I19C-9	19.50	end	27000	31687	17
	I19C-10	5.15	middle	16600	18423	11

Appendix E5 (Continued)

B25B	B25B-5	19.10	end	4780	5176	8
	B25B-11	19.10	end	7160	12364	73
	B25B-14	5.40	end	11000	16980	54
	B25B-18	5.15	middle	73800	78020	6
	B25B-20	27.50	middle	75000	104470	39
	B25B-22	27.40	middle	11000	13812	26
RS9.5C	RS9.5C-5	19.40	end	44000	49513	13
	RS9.5C-6	19.60	end	148000	191711	30
	RS9.5C-7	27.30	end	27500	44222	61
	RS9.5C-8	5.15	N/A	>168000*	231008	N/A
	RS9.5C-9	27.35	end	79000	111266	41
	RS9.5C-10	5.35	end	41000	61350	50
S12.5C	S12.5C-4	19.20	end	1250	2140	71
	S12.5C-5	19.20	end	74100	106659	44
I19B	I19B-5	19.00	middle	800	600	25
	I19B-6	19.20	end	19000	23741	25
RS12.5C	RS12.5C-4	19.10	end	9330	12716	36
	RS12.5C-5	19.00	middle	220000	230711	5
RI19B	RI19B-4	19.45	middle	6000	6071	1
	RI19B-5	19.50	middle	23700	28732	21
RI19C	RI19C-4	19.35	end	3450	5020	46
	RI19C-6	19.20	middle	68900	85294	24
RB25B	RB25B-4	19.20	middle	950	430	55
	RB25B-7	19.20	middle	7550	7682	2

[b] Test stopped at that number of loading cycle and specimen didn't fail

Appendix F   Results of Verification and Level 3 Calibration

TRB PAPER # 08-2920

LOCAL CALIBRATION OF THE MEPDG FOR FLEXIBLE PAVEMENT DESIGN

Naresh R. Muthadi
Former Graduate Research Assistant
Department of Civil, Construction, and Environmental Engineering
North Carolina State University
Phone: (918) 704-0497
E-mail: nmuthadi@hntb.com

Y. Richard Kim, Ph.D., P.E. (Corresponding Author)
Professor
Department of Civil, Construction, and Environmental Engineering
North Carolina State University
Office: 210 Mann Hall
Phone: (919) 515-7758
Fax: (919) 515-7908
E-mail: kim@ncsu.edu

Submitted for Presentation at the 2008 TRB Annual Meeting and
Publication in the Journal of the Transportation Research Board

Word Count: 7,392 (3,892 words for text, 6 figures, and 8 tables)

March 2008

ABSTRACT

This paper presents the calibration of the Mechanistic-Empirical Pavement Design Guide (MEPDG) for flexible pavements located in North Carolina. Two distress models, permanent deformation and bottom-up fatigue cracking, were employed for this effort. A total of fifty-three pavement sections were selected from the LTPP and the NCDOT databases for the calibration and validation process. The verification runs for the LTPP sections using the parameters developed during the national calibration effort under the NCHRP (National Cooperative Highway Research Program) 1-37A project showed promising results. Microsoft Excel Solver was used to fit the predicted rut depth values to the measured values by changing the coefficients in the permanent deformation models for hot-mix asphalt (HMA) and unbound materials. In this process, the sum of the squared errors was minimized for each of the permanent deformation models separately. For the alligator cracking model, the only possibility of reducing the standard error and bias is through the transfer function. Again, Microsoft Excel Solver was used to minimize the sum of the squared errors of the measured and predicted cracking by varying the C_1 and C_2 parameters of the transfer function. The standard error for the HMA permanent deformation model as well as the alligator cracking model was found to be significantly less than the global standard error after the calibration. It was decided to keep both the models for a more robust calibration in the future that would increase the number of sections and include more detailed inputs (mostly Level 1 inputs).

Key Words: Mechanistic-Empirical, MEPDG, fatigue cracking, rutting, asphalt, LTPP, calibration

INTRODUCTION

The performance prediction equations that constitute the foundation of the 1993 AASHTO Guide for the design of pavement structures are derived from the AASHO Road Test that took place during 1958-1961 in Ottawa, Illinois. Several limitations of that test have been noted since it was first conducted, including such factors as traffic loading that was appropriate for the 1950s is now dated and ineffective, the use of a single climatic zone and a single material type for each pavement layer, and 1950s construction and drainage procedures, to name a few. The MEPDG (*1*), released by the NCHRP, is a significant improvement in pavement performance prediction methodology. The design method in the MEPDG is mechanistic because the model uses stresses and strains in a pavement system calculated from the pavement response model to predict the performance of the pavement. The empirical nature of the design method stems from the fact that the pavement performance predicted from laboratory-developed performance models is adjusted based on the observed performance in the field to reflect the differences between predicted and actual field performance.

The performance models used in the MEPDG are calibrated using limited national databases and, thus, it is necessary to calibrate these models for implementation in local settings by taking into account local materials, traffic information, and environmental conditions. A crucial step in ensuring that the calibration is commensurate with conditions in North Carolina, for example, is the sensitivity analysis. That is, the sensitivity of the final design outcome for various input parameters must consider the material, traffic and environmental conditions in North Carolina. Sensitivity analyses, along with a set of implementation guidelines, have already been developed for North Carolina (*2*) and, hence, only the calibration effort remains for the NCDOT to adopt the MEPDG. The term *calibration* here means to reduce or minimize the total error or difference between the measured and predicted distresses by varying the appropriate model coefficients. A successful validation means that the calibrated model produces robust and accurate predictions for pavement sections other than those pavements used in the calibration process.

SCOPE AND OBJECTIVES

Scope

The scope of this research includes calibration and validation of only alligator cracking and permanent deformation models for asphalt pavements. Thirty LTPP pavements (16 new flexible pavement sections and 14 rehabilitated sections) and 23 NCDOT pavement sections were obtained for use in the calibration process. The required data for the LTPP sections were obtained from the LTPP database (*3*), whereas data for the NCDOT sections were obtained from the Pavement Management Unit (structure, pavement condition survey files), Construction Unit (material and volumetric data – Job Mix Formula, i.e., JMF), Traffic Unit (AADTT, C-card and W-card data files) and the Geotechnical Unit (subgrade and ground water table depth data) of the NCDOT. The traffic data obtained from the NCDOT were processed using the TrafLoad version 1.08 software (*4*) that was developed under the NCHRP 1-39 project. The map in FIGURE 1 shows pavement sections located in three distinct geographic areas (mountain, piedmont, and coastal regions, from left to right, respectively)

Objectives

The main objective of this study is to calibrate the MEPDG for local (i.e., North Carolina) materials, conditions and policies. Once the calibration factors are determined, the reasonableness of the calibrated MEPDG procedures are checked to determine whether they are adequate and appropriate for the construction, material, climate, traffic and other conditions that are encountered within the North Carolina system. This check is accomplished by selecting a number of independent pavement sections that were not used in the local calibration effort.

DATA COLLECTION

The performance prediction models require user inputs for the following four modules: materials, traffic, environment, and pavement structure. All of the above data that are required to run the MEPDG software for the LTPP sections are available in the LTPP database. The following sections describe the data collection effort for the NCDOT pavements.

Materials

The pavement design files obtained from the Construction Unit contain structural information, i.e., layer thicknesses, HMA mix type, and subgrade type. Additionally, JMFs were obtained to determine the HMA volumetric information.

Traffic

The traffic data that are required for running the MEPDG are: Average Annual Daily Truck Traffic (AADTT) data, vehicle classification, axle load distribution, and number of axles per truck. For the NCDOT sections, the Traffic Unit has provided a list of WIM (Weigh-in-Motion) station locations on or near the project along with the necessary data (C-card and W-card) and recommendations. The raw data files (C-card and W-card) are then processed using the TrafLoad software (*4*) to obtain the vehicle classification, axle load distribution and number of axles per truck data. For projects where the WIM stations are located at the pavement sites, these data serve as Level 1 inputs to the MEPDG.

Climate

For the NCDOT sections, the latitude, longitude, and elevation data are obtained from Google Earth software using the project location data. Ground Water Table (GWT) depth values for most of the sections are provided by the NCDOT Geotechnical Unit. For those sections with missing data, the US Geological Survey (*5*) is consulted to obtain the GWT data using the latitude-longitude data.

Performance data

Performance data obtained from the Pavement Management Unit (PMU) are described using NCDOT-defined ratings (*6*). One of the major issues identified with the use of these performance data is the methodology for collecting the data. For the LTPP sections, the alligator cracking data are obtained by directly measuring the area that has undergone distress (*7*), whereas for the NCDOT sections (referred to hereafter as pavement management system (PMS) sections), a percentage of the length of the section that undergoes distress in the outer wheel path of the outer lane, or that of the most distressed lane, is given. A rating of 0-10, based on the severity of cracking for each section, is used. For example, the alligator cracking rating is given as: 7-None; 2-Low; 1-Medium; 0-Severe. Similarly for rutting, a non-numeric rating is given as None, Low, Medium, and Severe. These ratings are converted (*8*) into the MEPDG format in order to compare the measured and predicted distress values and, hence, perform the calibration.

METHODOLOGY

Literature Review

Two pre-implementation studies (*9*) involving verification and recalibration have been conducted under the NCHRP program. These studies quantify the bias and residual errors of the flexible pavement distress models included in the MEPDG. From the verification runs, it was found that the residual errors, bias and the standard errors are larger than the values reported under the national calibration effort. The results also suggest that there are systematic differences between the measured and the predicted values.

One of the studies focused on the calibration refinement of the load-related distress prediction models for flexible pavements and overlays. The HMA rut depth model was found to reasonably predict the rut depths for a diverse range of conditions. Although the standard error for the area fatigue cracking prediction model was found to be relatively large, it was also found to be a reasonable model to estimate distress for a diverse range of mixtures and structures. Hence, it is recommended that the permanent deformation model and area fatigue cracking model remain in the software, and the local calibration guide be developed accordingly.

Local Calibration Plan

The NCHRP 1-40B Draft Report (*10*) provides the necessary recommendations and guidelines to conduct the recalibration and validation efforts of the MEPDG. The local calibration process involves three important steps for calibrating the MEPDG to local conditions and materials. The first step is to perform the verification runs on the pavement sections using the calibration factors that were developed for the performance prediction models during the national calibration effort under the NCHRP 1-37A project (*1*). The second step involves the calibration of the model coefficients to eliminate the bias and reduce the standard error between the predicted and measured distresses, if any exist. Once the bias is eliminated and the standard error is within the agency acceptable level after the calibration, the final step, i.e., the validation, is performed on the models to check for the reasonableness of the performance predictions.

An experimental matrix has been developed to evaluate the effect of pavement type and local conditions and materials on the reduction of the total standard error or uncertainty. A split-sample approach is used to confirm the accuracy of the prediction models during this calibration effort. Approximately 80% of the sections were selected randomly for calibration purposes and 20% for the validation process. TABLE 1 presents the experimental matrix with all the sections classified according to pavement structure and surface layer thickness.

FIGURE 2 provides a step-by-step flow chart describing the methodology employed for this local calibration effort.

Permanent Deformation Model

For the HMA permanent deformation model, Microsoft Excel Solver is employed to fit the predicted rut depth values to the measured values by varying the coefficient k_1. Similarly, for the unbound permanent deformation model, β_{GB} and β_{SG} are varied to fit the predicted and measured granular base and subgrade values, respectively. Because trenches and cores from these pavements were unavailable, predictions rather than actual measurements were used to distribute the total rut depth measurements to each pavement layer. That is, the total rut depth measurement was distributed to each pavement layer based on the ratio of the predicted total rut depth to the predicted permanent deformation in each layer.

Fatigue (Bottom-up) Cracking Model

For the bottom-up cracking model, the only possibility that errors may occur lies in the distress transfer function (statistical model), assuming that the mathematical models (or conceptual models) are accurate simulations of real-world conditions. Hence, a fitting process using Microsoft Excel Solver again minimizes the sum of the squared errors of the predicted and measured cracking values by varying the C_1 and C_2 parameters in Equation (1). The fatigue cracking transfer function is given below:

$$FC_{bottom} = \left(\frac{6000}{1 + e^{\left(C_1 * C'_1 + C_2 * C'_2 * \log_{10}(D * 100)\right)}} \right) * \left(\frac{1}{60} \right) \qquad (1)$$

$$C_1 = 1.0$$

$$C'_1 = -2 * C'_2$$

$$C_2 = 1.0$$

$$C'_2 = -2.40874 - 39.748 * (1 + h_{ac})^{-2.856}$$

where FC_{bottom} = bottom-up fatigue cracking, % lane area, and D = bottom-up fatigue cracking.

Software

MEPDG version 1.0 (DG 2002) was used for the purposes of verification, calibration and validation. An error was found in the software in the subgrade permanent deformation national calibration factor. According to the NCHRP research results, Digest 308 (*11*), the recalibrated factor is 1.67, whereas the software presents it as 1.35. Hence, a correction was made prior to the calibration process.

DISCUSSION OF RESULTS

Verification

The verification results presented in TABLE 2 and TABLE 3 include both the new and rehabilitated LTPP pavement sections. They also show the effect of including the NCDOT sections on the standard error and the coefficient of determination of the models. The standard error obtained during the verification runs for the LTPP sections is comparable to the global standard error for both the models. It is observed that the NCDOT sections tend to increase only the sum of the squared error between the measured and predicted values. Also, it should be noted that the verification runs do not include the LTPP sections that were part of the original national calibration effort for the new and rehabilitated pavements.

From the verification results shown in FIGURE 3, it can be observed that the NCDOT measured rut depths do not match the predicted rut depths particularly well. This observation is attributed to the fact that the NCDOT rut depth measurement techniques result in a single non-numeric rating (i.e., low, medium, or severe) and, therefore, unless more objective data are collected, these measurement techniques cannot be used in the calibration or fitting process of the permanent deformation model. Thus, only the LTPP sections were used for the calibration of the permanent deformation model.

Calibration

A t-test was performed on the verification results with respect to bias as a first step in the calibration process. The hypothesis here is that no bias or significant differences exist between the measured and predicted values. A p-value greater than 0.05 (alpha) signifies that no difference exists between the measured and predicted values and, hence, the hypothesis is accepted. For the calibration of the permanent deformation models, Microsoft Excel Solver is used to reduce the bias for each layer separately. The calibrated rut depths of the individual layers are then combined for comparison to the measured total rut depth. Again, the ratio between the predicted permanent deformation in each layer and the predicted total rut depth was used in assigning the total measured surface rut depth to each layer. TABLE 4 presents the standard error and bias before and after the calibration effort of the permanent deformation model.

As a second step, a Chi-square test was performed with respect to standard error to determine if the local standard error is significantly different from the global standard error. From the results presented in TABLE 5, they are statistically the same and, hence, no further calibration to reduce the standard error was pursued during this study. FIGURE 4 shows the comparison between the measured and predicted rut depths before and after calibration for each layer. The comparisons of total rut depth before and after calibration are shown in FIGURE 5 (a) and FIGURE 5 (b) respectively.

For the alligator cracking, all the sections (both LTPP and NCDOT sections) were used in the calibration process. Again, Microsoft Excel Solver was used to minimize the sum of the squared error between measured and predicted cracking. TABLE 6 presents the standard error and bias before and after calibration. Also, a Chi-square test was performed to check if the local standard error is significantly different from the global standard error. The corresponding results shown in TABLE 5 indicate that they are statistically the same. The national re-calibrated model has a statistics of $R^2 = 0.275$ and $S_e = 5.01\%$, which includes 400 plus data points. The local calibration ($R^2 = 0.11$, S_e=3.64) of the fatigue cracking model is still considered an improvement over the verification runs ($R^2 = 0.03$, $S_e = 6.02$) considering 177 data points that also include NCDOT sections.

Even though the standard error and bias are significantly reduced after the calibration, the visual observation of FIGURE 5 (c) and FIGURE 5 (d) reveal poor prediction. One possible reason for this poor prediction that can be identified at this stage is the inclusion of NCDOT sections in the calibration process. The NCDOT measurement technique does not capture the cracking outside the outer wheel path and, hence, negligible cracking is measured most of the time. This measurement error can be eliminated in the future by following the LTPP Distress Identification Manual (*7*) to measure the distresses for the local pavement sections selected for calibration. Doing so will ensure consistency between the MEPDG predicted and measured distresses. The above reason is supported from the NCHRP 1-40B (*9*) study that the measured area fatigue cracking was found to be one of the error components that significantly increases the standard error for this prediction model, which is model independent.

TABLE 7 lists the calibration factors developed from various calibration efforts. Until further and more robust calibrations are completed using more detailed inputs and more sections, the local calibration factors will be used for the performance prediction of the sections located in North Carolina.

Validation

For the purpose of validation, the remaining 20% of the sections that were kept aside from the calibration process were used to verify the reasonableness of the final calibrated models. FIGURE 6 presents the validation results for both the models, and TABLE 8 summarizes the Chi-square test results. P-values are greater than 0.05 for both the models, indicating that there is no significant difference between the measured and predicted values. Also, the observed standard errors (0.145 in. for rut depth and 4.86% for alligator cracking, shown in TABLE 8) are higher than the local calibrated standard errors (0.109 in. for rut depth and 3.64% for alligator cracking, shown in TABLE 4 and TABLE 6, respectively), which is expected. From the Chi-square test results presented in TABLE 8, it can be deduced that the validation check is successful; therefore, the final calibrated rutting and alligator cracking models will be used until more rigorous calibration, employing an increased number of sections, is done in the future.

CONCLUSIONS

The following conclusions were made from this study:

- From the verification results, it is found that the MEPDG-predicted rut depth values match well with the measured rut depth values for the LTPP sections.
- For the alligator cracking model, the MEPDG under-predicts the percentage of cracking for most of the sections, resulting in a significant amount of bias.
- NCDOT sections are dropped from the permanent deformation calibration effort due to the NCDOT's subjective rating approach to rutting that employs a single non-numeric rating which, in turn, presents problems with the conversion to the MEPDG format.
- From the calibration efforts, it can be observed that the standard error is significantly reduced and the bias is completely eliminated. The standard error from the local

calibration effort is statistically the same as the global standard error from the national calibration effort for both the distress prediction models.

- The null hypothesis test relative to the standard error, which checks if the local calibrated standard error is significantly different from the global standard error, shows no significant difference between the errors; hence, no further calibration is pursued in this study to reduce the standard error.
- For alligator cracking, only the parameters in the transfer function (i.e., the statistical model) are varied to minimize the sum of the squared error of the measured and predicted cracking values. It is assumed that the mathematical model used to predict damage accurately models the real-world system.
- The validation check performed on both the distress prediction models using the Chi-square test shows that the validation is successful and, hence, the predictions are reasonable.
- Therefore, it was decided to keep the both the calibrated permanent deformation and alligator cracking models for performance predictions until a more robust calibration is performed with an increased number of sections.
- One of the issues identified with the calibration procedure is that the MEPDG assumptions were accepted in assigning the permanent deformation observed at the surface to each pavement layer. This assumption needs to be supported with field and forensic investigations at the site locations.
- Also, it is noted that major differences are evident between the distress measurement techniques of the NCDOT and the LTPP program. If the NCDOT adopts the LTPP standard procedure, at least for the sections to be used in the future calibration effort, a significant amount of measurement error and input error can be reduced.

The following recommendations are resulted from this study:

- It is recommended to begin a field and forensic (trenches and cores) investigation to check for the reasonableness of the MEPDG assumptions in assigning the observed surface permanent deformation to each pavement layer.
- It is recommended to increase the number of sections and include more detailed inputs (Level 1 mostly) for future calibration efforts, which will help reduce a significant amount of input error.
- It is recommended to use the LTPP Distress Identification Manual (*7*) to complete the distress surveys for the sections selected for future calibration purposes. Use of this manual will ensure consistency in the MEPDG predictions.

ACKNOWLEDGMENTS

This material is based upon work supported by the North Carolina Department of Transportation (NCDOT) under Project No. HWY-2007-07. The research team wishes to express gratitude to the NCDOT for supporting the project, providing resources to identify pavement sections and to collect all the input data.

REFERENCES

1. NCHRP. 2004a. *2002 Design Guide: Design of New and Rehabilitated Pavement Structures*. Draft Final Report NCHRP Study 1-37A. Washington DC: National Cooperative Highway Research Program (July).

2. Kim, Y. R. and N.R. Muthadi. 2006. *Implementation Plan for the New Mechanistic-Empirical Pavement Design Guide.* NCDOT Final Report No. HWY-2005-28. Raleigh, NC: NCSU.

3. FHWA. 2007. *Standard Data Release #21, Long-Term Pavement Performance Program*. McLean, VA: Federal Highway Administration (January).

4. NCHRP. 2004d. *Traffic Data Collection, Analysis, and Forecasting for Mechanistic Pavement Design*. NCHRP Project 1-39. Maryland: National Cooperative Highway Research Program, Cambridge Systematics Inc. (July).

5. USGS. *Ground Water for USA: Water Levels*. US Geological Survey. http://nwis.waterdata.usgs.gov/usa/nwis/gwlevels, accessed July 18, 2007.

6. NCDOT. 2006. *Pavement Condition Survey Manual 2006*. North Carolina Department of Transportation.

7. FHWA. 2003. *Distress Identification Manual for Long Term Pavement Performance Program*. (Fourth Revised Edition), Publication No. FHWA-RD-03-031. Washington, DC: Federal Highway Administration.

8. N. R. Muthadi. 2007. *Local Calibration of the MEPDG for Flexible Pavement Design*. Master's thesis, Department of Civil Engineering, North Carolina State University, Raleigh, NC.

9. NCHRP. 2005. *Local Calibration Guide: Design of New and Rehabilitated Pavement Structures*. Preliminary Draft Final Report. NCHRP Study 1-40B. Illinois: National Cooperative Highway Research Program (November).

10. NCHRP. 2007. *Local Calibration Guidance for the Recommended Guide for Mechanistic-Empirical Design of New and Rehabilitated Pavement Structures*. Round Rock, TX: Applied Research Associates, Inc. (April).

11. NCHRP. 2006. *Changes to the Mechanistic-Empirical Pavement Design Guide Software Through Version 0.9000*. NCHRP Research Results Digest 308, National Cooperative Highway Research Program. Washington DC: Transportation Research Board of the National Academics (September).

LIST OF TABLES

LIST OF FIGURES

TABLE 1 Experimental Matrix

Pavement Type	HMA Thickness	Mix Type	Family of Pavements					Total No. of Sections
			AC[a]-GB[b]	AC-ATB[c]	AC-Full depth	AC-CTB[d]	Rehab.	
New	Thin (<= 5 in.)	Conventional	1024,1040,1802,1803, 1817,1992	1028,1030		2819,2825		10
		PMA[e]						
		Grading						
		Drainage				2824		1
	Intermediate	Conventional	1352,1801,1814,R2120AA, R2120AB,R1023B,R1023AB,R2001C,R2318B, R2211BA			1645		11
		PMA						
		Grading						
		Drainage						
	Thick (>=8 in.)	Conventional	R2123AC,R2123BB, R2123CC,R2219AC,		R2217B,U508CB, U508CA,R1017AC,R519, R85-AD	R2000EA,R2000EB, R2000BB,U77LA, R2232A,R2232B		16
		PMA						
		Grading						
		Drainage	1006					1
Rehab.	Thin (<= 5 in.)	Conventional						
		PMA						
		Grading						
		Drainage						
	Intermediate	Conventional					1028,1040,1802, 1352,1803,1817, 2819	7
		PMA						
		Grading						
		Drainage					2824	1
	Thick (>=8 in.)	Conventional					1024,1645,1801 1814,1992	5
		PMA						
		Grading						
		Drainage					1006	1
Total No. of Sections			21	2	6	10	14	53

Note: [a]Asphalt Concrete, [b]Granular Base, [c]Asphalt-Treated Base, [d]Cement-Treated Base, [e]Polymer-Modified Asphalt

TABLE 2 Verification Runs - Summary of Statistics for the Rut Depth Predictions

Comparison of Results		AC	GB	SG	Total
Verification Runs – LTPP Sections Only (N^c=161)	Average (in.)	0.102	0.047	0.134	0.2828
	Percentage (%)	48.7	18.8	32.6	100.0
	R^2	0.197	0.545	0.653	0.340
	S_e^a *(in.)*	0.057	0.037	0.081	0.111
	SSE[b]	0.514	0.219	1.044	1.962
Verification Runs – Including NCDOT Sections (N=255)	Average (in.)	0.086	0.025	0.121	0.223
	Percentage (%)	42.8	13.0	44.2	100.0
	R^2	0.254	0.309	0.214	0.142
	S_e (in.)	0.053	0.036	0.094	0.153
	SSE	1.380	0.387	3.822	10.387
National Calibration (N=387)	Average (in.)	0.162	0.055	0.113	0.330
	Percentage (%)	46.6	16.7	36.7	100.0
	R^2	0.648	0.677	0.136	0.399
	S_e (in.)	0.063	0.023	0.045	0.121
	SSE	1.883	0.243	0.931	6.915
National Re-calibration (N=334)	R^2	0.64	0.785	0.708	0.577
	S_e *(in.)*	0.045	0.026	0.045	0.107
	S_e/S_y	0.713	0.502	0.576	0.818

Note: [a]Standard Error, [b]Sum of Squares Error, [c]Number of Data Points

TABLE 3 Verification Runs - Summary of Statistics for Alligator Cracking Predictions

Comparison of Results		Alligator Cracking
Verification Runs – LTPP Sections Only (N^c=76)	S_e^a*(%)*	10.7
	SSE[b]	8505.51
Verification Runs – Including NCDOT Sections (N=176)	S_e*(%)*	6.02
	SSE	29487.1
National Calibration (N=461)	S_e *(%)*	6.2
	SSE	17663.91
National Re-calibration (N=405)	S_e *(%)*	5.01

Note: [a]Standard Error, [b]Sum of Squares Error, [c]Number of Data Points

TABLE 4 Statistical Summary of Permanent Deformation Model Calibration Results

	AC		GB		SG		Total	
	Before	After	Before	After	Before	After	Before	After
Average (in.)	0.1178	0.1030	0.0442	0.0344	0.1551	0.1026	0.3171	0.2399
S_e^a (in.)	0.054	0.047	0.027	0.021	0.084	0.056	0.154	0.109
Bias (in.)	-0.0149	0	-0.0098	0	-0.0525	0	-0.0771	0
p-value	0.00622	0.499	0.0002	0.5>	1.6E-9	0.5 >	2.9E-7	0.499
N^b	111	111	111	111	111	111	111	111

Note: [a]Standard Error, [b]Number of Data Points

TABLE 5 Calibration Results – Null Hypothesis Test for Standard Error

Statistical Results	Permanent Deformation	Alligator Cracking
Chi-Square Statistic	112.6	92.2
Degrees of Freedom	110	176
p-value	0.42 > 0.05	0.9999 > 0.05

TABLE 6 Statistical Summary of Alligator Cracking Model Calibration Results

Statistical Results	Alligator Cracking	
	Before	After
Average (%)	1.54	5.21
R^2	0.025	0.106
S_e^a	6.02	3.64
SSE^b	6343.8	2313.7
p-value	0.00018 < 0.05	0.5 > 0.05
Bias	3.67	0
N^c	177	177

Note: [a]Standard Error, [b]Sum of Squares Error, [c]Number of Data Points

TABLE 7 Final Set of Calibration Factors

Recalibration		Calibration Factors	National Calibration	National Re-calibration	Local Calibration
Rutting	*AC*	k_1	-3.4488	-3.35412	-3.41273
		k_2	1.5606	1.5606	1.5606
		k_3	0.479244	0.479244	0.479244
	GB	β_{GB}	1.673	2.03	1.5803
	SG	β_{SG}	1.35	1.67	1.10491
Fatigue	*AC*	k_1	0.00432	0.007566	0.007566
		k_2	3.9492	3.9492	3.9492
		k_3	1.281	1.281	1.281
		C_1	1	1	0.437199
		C_2	1	1	0.150494

TABLE 8 Statistical Summary of the Validation Results

	Permanent Deformation Model	Alligator Cracking Model
S_e	0.145 in.	4.86 %
Bias	0.033 in.	-5.04 %
N	26	32
Chi-Square Statistic	36.82	5.66
Degrees of Freedom	25	31
p-value	0.0599 > 0.05	0.9999 > 0.05

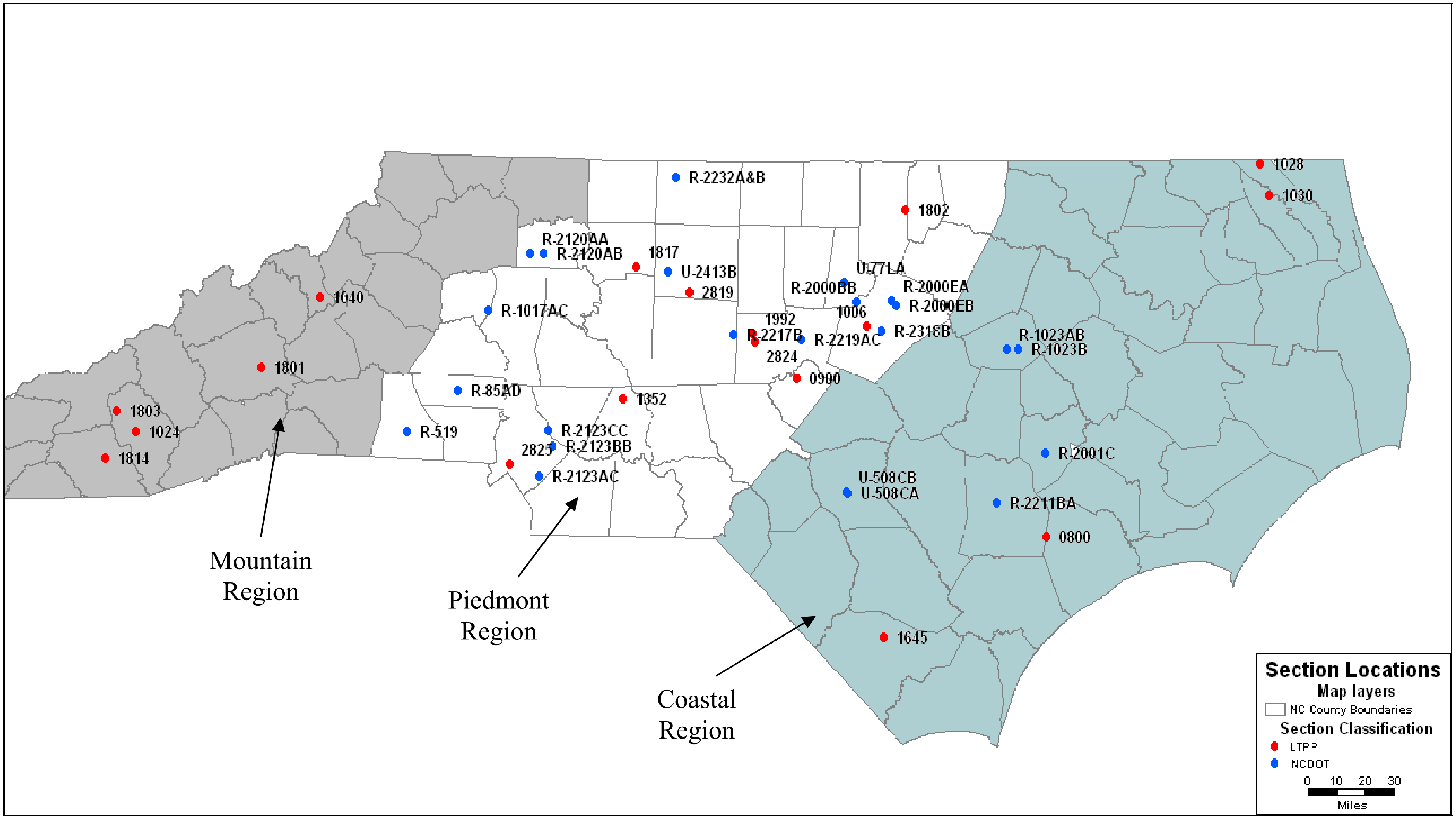

FIGURE 1 Locations of flexible pavement sections included in this study.

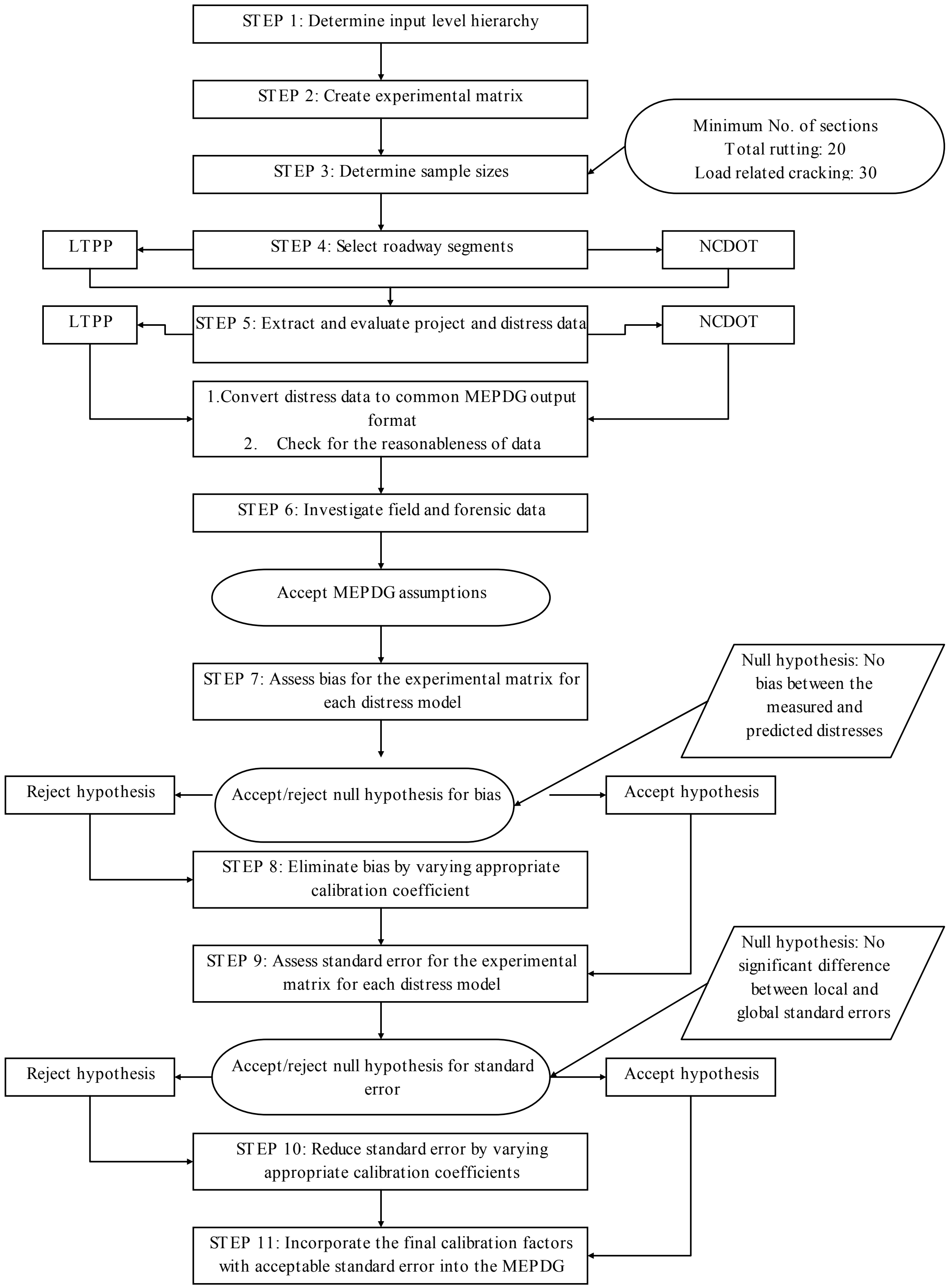

FIGURE 2 Flow chart showing the local calibration plan.

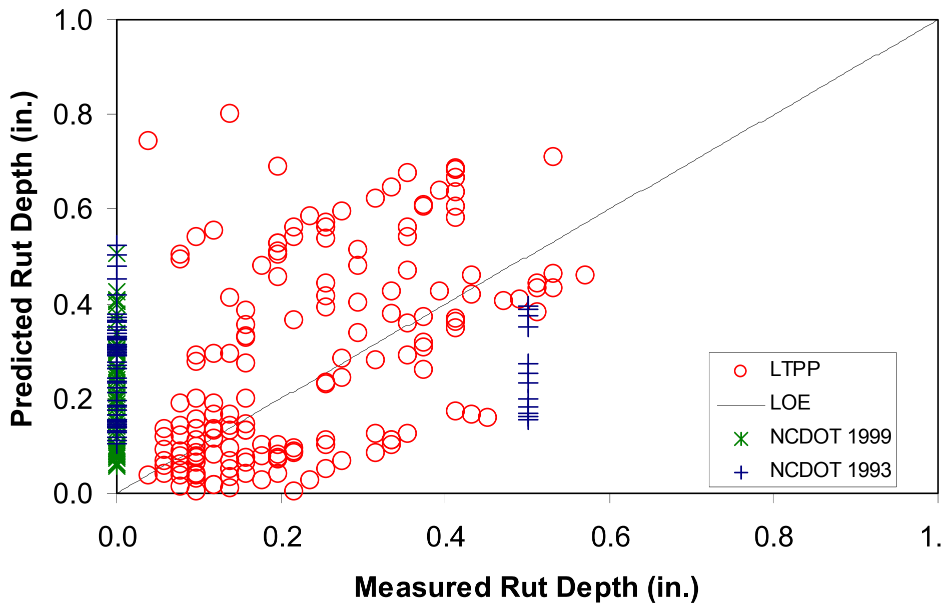

FIGURE 3 Total measured rut depth vs. predicted rut depth verification results.

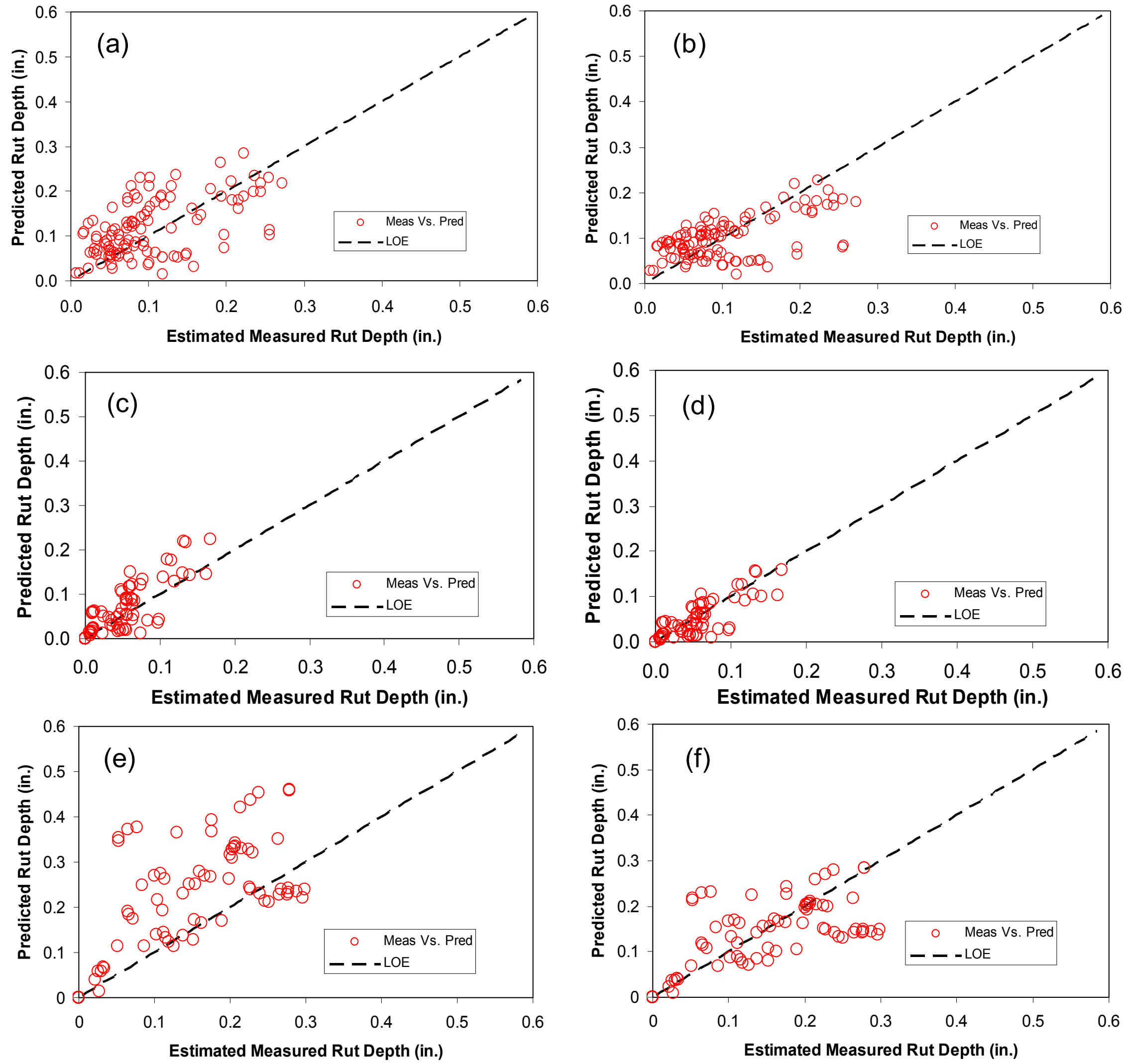

FIGURE 4 Estimated measured rut depth vs. predicted rut depth: (a) HMA before calibration; (b) HMA after calibration; (c) granular base before calibration; (d) granular base after calibration; (e) subgrade before calibration; and (f) subgrade after calibration.

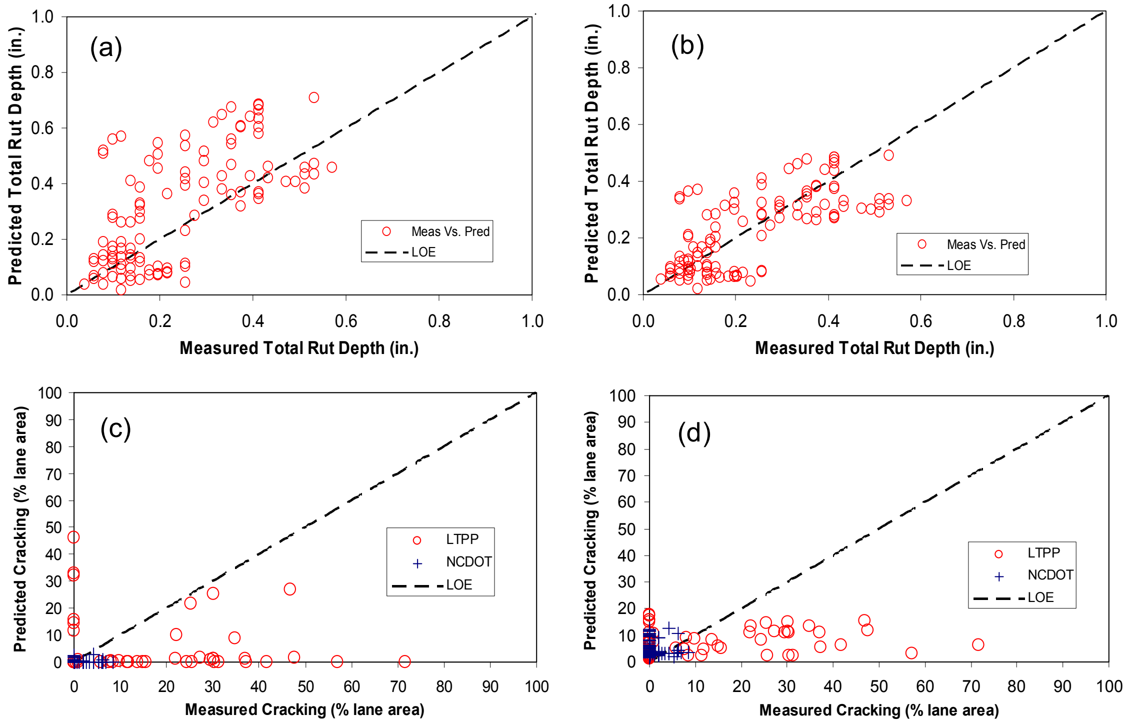

FIGURE 5 Measured vs. predicted distresses before and after calibration: (a) total rut depth before calibration; (b) total rut depth after calibration; (c) alligator cracking before calibration; and (d) alligator cracking after calibration.

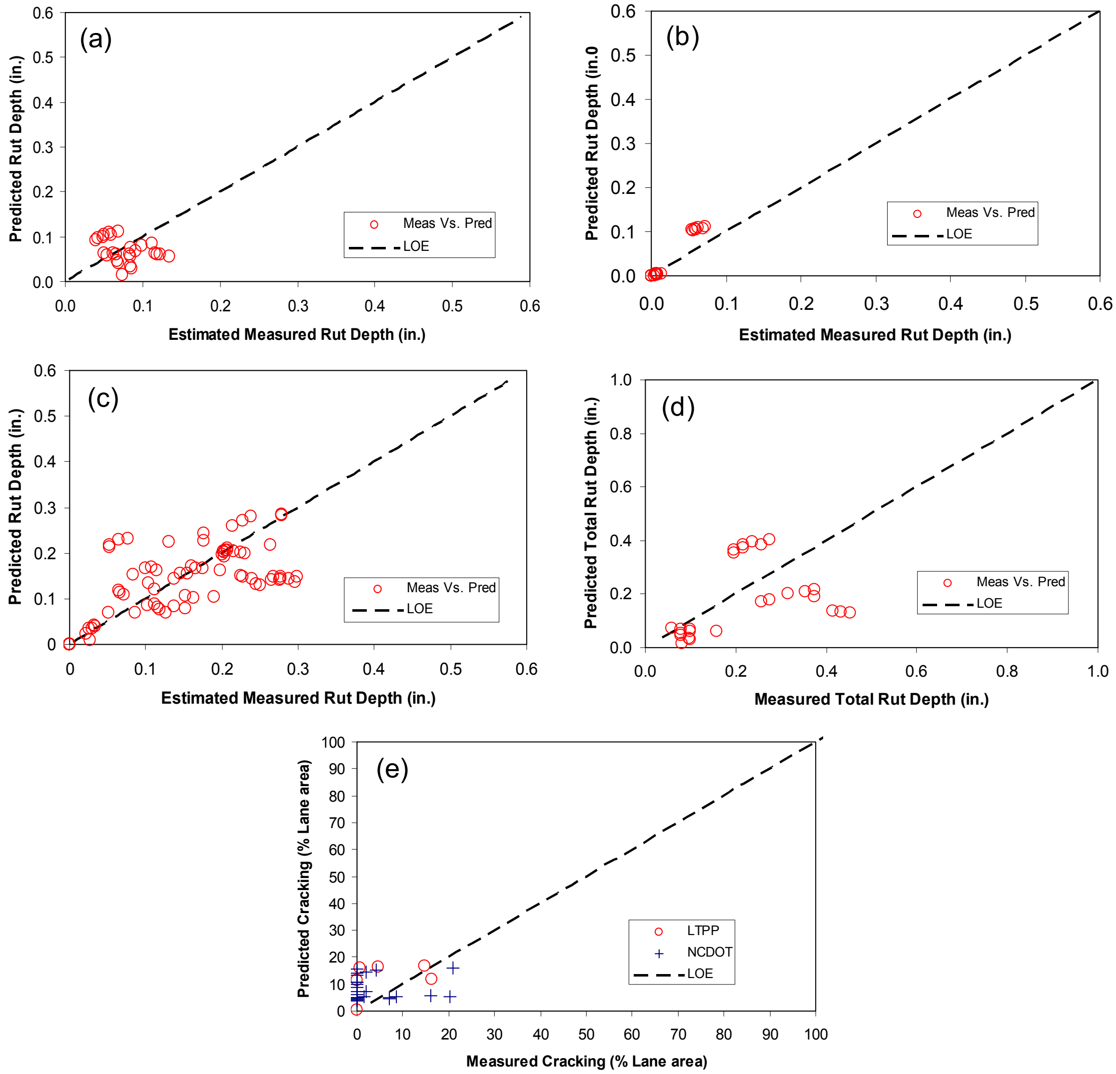

FIGURE 6 Estimated measured distresses vs. predicted distresses from validation: (a) HMA rut depth; (b) granular base rut depth; (c) subgrade rut depth; (d) total rut depth; and (e) alligator cracking.

Appendix G NC Subgrade Soils Database Extracted from NCHRP 9-23A

Enter Map Character =>>	AA0

Horizon 1 (Top)	Compacted ? Yes	Horizon 2	Compacted ? No	Horizon 3	Compacted ? No
AASHTO Classification	A-4		A-4		A-7-6
Thickness (in)	9.8		4.3		17.7
Resilient Modulus (psi)	27,829		16,315		10,184
CBR (%)	42		18		9

*Version No.	0.9	*Version No.	0.9	*Version No.	0.9
*Units	US	*Units	US	*Units	US
*Plasticity Index	3	*Plasticity Index	7.5	*Plasticity Index	17.5
*Liquid Limit	22.5	*Liquid Limit	23.5	*Liquid Limit	43
*Compacted Layer	1	*Compacted	0	*Compacted	0
*Unit Weight		*Unit Weight		*Unit Weight	
*Specific Gravity		*Specific Gravity		*Specific Gravity	
*Permeability	3.33E-01	*Permeability	1.08E-01	*Permeability	1.08E-01
*Optimum WC		*Optimum WC		*Optimum WC	
*af	1.9790	*af	8.3866	*af	5.2091
*bf	1.0410	*bf	0.8863	*bf	0.8752
*cf	0.7109	*cf	0.7145	*cf	0.3750
*df	3000.0445	*df	3000.0013	*df	3000.0368
Grain Size Dist.		Grain Size Dist.		Grain Size Dist.	
0.001mm		0.001mm		0.001mm	
0.002mm	12.5	0.002mm	22.0	0.002mm	40.0
0.020mm		0.020mm		0.020mm	
#200	36.5	#200	57.5	#200	60.0
#100		#100		#100	
#80		#80		#80	
#60		#60		#60	
#50		#50		#50	
#40	74.5	#40	88.5	#40	81.0
#30		#30		#30	
#20		#20		#20	
#16		#16		#16	
#10	90.0	#10	95.0	#10	97.5
#8		#8		#8	
#4	97.5	#4	95.0	#4	97.5
3/8"		3/8"		3/8"	
1/2"		1/2"		1/2"	
3/4"		3/4"		3/4"	
1"		1"		1"	
1 1/2"		1 1/2"		1 1/2"	
2"		2"		2"	
2 1/2"		2 1/2"		2 1/2"	
3"		3"		3"	
3 1/2"		3 1/2"		3 1/2"	

Appendix G (Continued)

Enter Map Character =>>	**AA2**

Horizon 1 (Top)	Compacted ? Yes	Horizon 2	Compacted ? No	Horizon 3	Compacted ? No
AASHTO Classification	A-4		A-4		A-7-6
Thickness (in)	7.1		3.9		39.0
Resilient Modulus (psi)	13,875		13,875		7,635
CBR (%)	14		14		6

*Version No.	0.9	*Version No.	0.9	*Version No.	0.9
*Units	US	*Units	US	*Units	US
*Plasticity Index	10	*Plasticity Index	10	*Plasticity Index	23
*Liquid Limit	28	*Liquid Limit	28	*Liquid Limit	60.5
*Compacted Layer	1	*Compacted	0	*Compacted	0
*Unit Weight		*Unit Weight		*Unit Weight	
*Specific Gravity		*Specific Gravity		*Specific Gravity	
*Permeability	1.08E-01	*Permeability	1.08E-01	*Permeability	1.08E-01
*Optimum WC		*Optimum WC		*Optimum WC	
*af	0.7296	*af	6.3600	*af	524.3522
*bf	1.0780	*bf	0.7858	*bf	0.3328
*cf	0.4064	*cf	0.6067	*cf	0.9570
*df	2990.6566	*df	3000.0052	*df	2771.0473
Grain Size Dist.		Grain Size Dist.		Grain Size Dist.	
0.001mm		0.001mm		0.001mm	
0.002mm	27.5	0.002mm	27.5	0.002mm	52.5
0.020mm		0.020mm		0.020mm	
#200	59.5	#200	59.5	#200	75.0
#100		#100		#100	
#80		#80		#80	
#60		#60		#60	
#50		#50		#50	
#40	81.5	#40	81.5	#40	86.0
#30		#30		#30	
#20		#20		#20	
#16		#16		#16	
#10	87.5	#10	87.5	#10	96.0
#8		#8		#8	
#4	87.5	#4	87.5	#4	98.5
3/8"		3/8"		3/8"	
1/2"		1/2"		1/2"	
3/4"		3/4"		3/4"	
1"		1"		1"	
1 1/2"		1 1/2"		1 1/2"	
2"		2"		2"	
2 1/2"		2 1/2"		2 1/2"	
3"		3"		3"	
3 1/2"		3 1/2"		3 1/2"	

Appendix G (Continued)

Continued…	AA0

Horizon 4	Compacted ?
	No
	A-6
	28.0
	12,985
	13

*Version No.	0.9
*Units	US
*Plasticity Index	15
*Liquid Limit	37
*Compacted Layer	0
*Unit Weight	
*Specific Gravity	
*Permeability	1.08E-01
*Optimum WC	
*af	7.0539
*bf	1.2220
*cf	0.6205
*df	3000.0051
Grain Size Dist.	
0.001mm	
0.002mm	22.5
0.020mm	
#200	45.0
#100	
#80	
#60	
#50	
#40	70.0
#30	
#20	
#16	
#10	85.0
#8	
#4	90.0
3/8"	
1/2"	
3/4"	
1"	
1 1/2"	
2"	
2 1/2"	
3"	
3 1/2"	

Appendix G (Continued)

Enter Map Character =>>	AA2

Horizon 1 (Top)	Compacted ? Yes	Horizon 2	Compacted ? No	Horizon 3	Compacted ? No
AASHTO Classification	A-4		A-4		A-7-6
Thickness (in)	7.1		3.9		39.0
Resilient Modulus (psi)	13,875		13,875		7,635
CBR (%)	14		14		6

*Version No.	0.9	*Version No.	0.9	*Version No.	0.9
*Units	US	*Units	US	*Units	US
*Plasticity Index	10	*Plasticity Index	10	*Plasticity Index	23
*Liquid Limit	28	*Liquid Limit	28	*Liquid Limit	60.5
*Compacted Layer	1	*Compacted	0	*Compacted	0
*Unit Weight		*Unit Weight		*Unit Weight	
*Specific Gravity		*Specific Gravity		*Specific Gravity	
*Permeability	1.08E-01	*Permeability	1.08E-01	*Permeability	1.08E-01
*Optimum WC		*Optimum WC		*Optimum WC	
*af	0.7296	*af	6.3600	*af	524.3522
*bf	1.0780	*bf	0.7858	*bf	0.3328
*cf	0.4064	*cf	0.6067	*cf	0.9570
*df	2990.6566	*df	3000.0052	*df	2771.0473
Grain Size Dist.		Grain Size Dist.		Grain Size Dist.	
0.001mm		0.001mm		0.001mm	
0.002mm	27.5	0.002mm	27.5	0.002mm	52.5
0.020mm		0.020mm		0.020mm	
#200	59.5	#200	59.5	#200	75.0
#100		#100		#100	
#80		#80		#80	
#60		#60		#60	
#50		#50		#50	
#40	81.5	#40	81.5	#40	86.0
#30		#30		#30	
#20		#20		#20	
#16		#16		#16	
#10	87.5	#10	87.5	#10	96.0
#8		#8		#8	
#4	87.5	#4	87.5	#4	98.5
3/8"		3/8"		3/8"	
1/2"		1/2"		1/2"	
3/4"		3/4"		3/4"	
1"		1"		1"	
1 1/2"		1 1/2"		1 1/2"	
2"		2"		2"	
2 1/2"		2 1/2"		2 1/2"	
3"		3"		3"	
3 1/2"		3 1/2"		3 1/2"	

Appendix G (Continued)

Enter Map Character =>>	**AA3**

Horizon 1 (Top)	Compacted ? Yes	Horizon 2	Compacted ? No	Horizon 3	Compacted ? No
AASHTO Classification	A-2-4		A-7-6		A-4
Thickness (in)	3.1		26.0		22.8
Resilient Modulus (psi)	28,422		8,683		15,980
CBR (%)	43		7		18

*Version No.	0.9	*Version No.	0.9	*Version No.	0.9
*Units	US	*Units	US	*Units	US
*Plasticity Index	3.5	*Plasticity Index	22	*Plasticity Index	10
*Liquid Limit	21.5	*Liquid Limit	51.5	*Liquid Limit	27.5
*Compacted Layer	1	*Compacted	0	*Compacted	0
*Unit Weight		*Unit Weight		*Unit Weight	
*Specific Gravity		*Specific Gravity		*Specific Gravity	
*Permeability	3.33E-01	*Permeability	1.08E-01	*Permeability	1.08E-01
*Optimum WC		*Optimum WC		*Optimum WC	
*af	1.4986	*af	0.2322	*af	7.0046
*bf	1.0795	*bf	1.1730	*bf	1.1424
*cf	0.7791	*cf	0.1669	*cf	0.6346
*df	3000.0266	*df	3000.2373	*df	3000.0046
Grain Size Dist.		Grain Size Dist.		Grain Size Dist.	
0.001mm		0.001mm		0.001mm	
0.002mm	14.0	0.002mm	50.0	0.002mm	22.5
0.020mm		0.020mm		0.020mm	
#200	29.0	#200	63.0	#200	45.0
#100		#100		#100	
#80		#80		#80	
#60		#60		#60	
#50		#50		#50	
#40	66.0	#40	80.0	#40	70.0
#30		#30		#30	
#20		#20		#20	
#16		#16		#16	
#10	90.0	#10	90.0	#10	85.0
#8		#8		#8	
#4	92.5	#4	90.0	#4	90.0
3/8"		3/8"		3/8"	
1/2"		1/2"		1/2"	
3/4"		3/4"		3/4"	
1"		1"		1"	
1 1/2"		1 1/2"		1 1/2"	
2"		2"		2"	
2 1/2"		2 1/2"		2 1/2"	
3"		3"		3"	
3 1/2"		3 1/2"		3 1/2"	

Appendix G (Continued)

Continued…	AA3

Horizon 4	Compacted ?
	No
	A-4
	18.1
	27,615
	41

*Version No.	0.9
*Units	US
*Plasticity Index	3
*Liquid Limit	21.5
*Compacted Layer	0
*Unit Weight	
*Specific Gravity	
*Permeability	1.08E-01
*Optimum WC	
*af	1.4040
*bf	1.0082
*cf	0.6845
*df	3000.0421
Grain Size Dist.	
0.001mm	
0.002mm	17.5
0.020mm	
#200	37.5
#100	
#80	
#60	
#50	
#40	75.0
#30	
#20	
#16	
#10	85.0
#8	
#4	90.0
3/8"	
1/2"	
3/4"	
1"	
1 1/2"	
2"	
2 1/2"	
3"	
3 1/2"	

Appendix G (Continued)

Enter Map Character =>>	**AA5**

Horizon 1 (Top)	Compacted ? Yes	Horizon 2	Compacted ? No	Horizon 3	Compacted ? No
AASHTO Classification	A-2-4		A-7-6		A-6
Thickness (in)	9.1		26.0		11.0
Resilient Modulus (psi)	29,542		8,377		11,369
CBR (%)	46		6		10

*Version No.	0.9	*Version No.	0.9	*Version No.	0.9
*Units	US	*Units	US	*Units	US
*Plasticity Index	3.5	*Plasticity Index	22.5	*Plasticity Index	15
*Liquid Limit	25	*Liquid Limit	57.5	*Liquid Limit	35
*Compacted Layer	1	*Compacted	0	*Compacted	0
*Unit Weight		*Unit Weight		*Unit Weight	
*Specific Gravity		*Specific Gravity		*Specific Gravity	
*Permeability	3.33E-01	*Permeability	1.08E-01	*Permeability	1.08E-01
*Optimum WC		*Optimum WC		*Optimum WC	
*af	2.3517	*af	2.5418	*af	1.9404
*bf	0.5683	*bf	0.8788	*bf	1.0428
*cf	0.9884	*cf	0.2887	*cf	0.4528
*df	3000.0126	*df	3000.0898	*df	2998.1987
Grain Size Dist.		Grain Size Dist.		Grain Size Dist.	
0.001mm		0.001mm		0.001mm	
0.002mm	12.5	0.002mm	47.5	0.002mm	35.0
0.020mm		0.020mm		0.020mm	
#200	25.0	#200	65.5	#200	57.5
#100		#100		#100	
#80		#80		#80	
#60		#60		#60	
#50		#50		#50	
#40	73.0	#40	82.5	#40	80.0
#30		#30		#30	
#20		#20		#20	
#16		#16		#16	
#10	90.0	#10	95.0	#10	92.5
#8		#8		#8	
#4	93.0	#4	97.5	#4	97.5
3/8"		3/8"		3/8"	
1/2"		1/2"		1/2"	
3/4"		3/4"		3/4"	
1"		1"		1"	
1 1/2"		1 1/2"		1 1/2"	
2"		2"		2"	
2 1/2"		2 1/2"		2 1/2"	
3"		3"		3"	
3 1/2"		3 1/2"		3 1/2"	

Appendix G (Continued)

Enter Map Character =>>	AA6

Horizon 1 (Top)	Compacted ? Yes	Horizon 2	Compacted ? No	Horizon 3	Compacted ? No
AASHTO Classification	A-4		A-6		A-7-6
Thickness (in)	7.9		3.1		22.0
Resilient Modulus (psi)	23,460		11,261		4,889
CBR (%)	32		10		3

*Version No.	0.9	*Version No.	0.9	*Version No.	0.9
*Units	US	*Units	US	*Units	US
*Plasticity Index	5	*Plasticity Index	13.5	*Plasticity Index	45
*Liquid Limit	22.5	*Liquid Limit	32.5	*Liquid Limit	65
*Compacted Layer	1	*Compacted	0	*Compacted	0
*Unit Weight		*Unit Weight		*Unit Weight	
*Specific Gravity		*Specific Gravity		*Specific Gravity	
*Permeability	3.33E-01	*Permeability	1.08E-01	*Permeability	1.08E-02
*Optimum WC		*Optimum WC		*Optimum WC	
*af	2.4948	*af	6.2478	*af	2.4681
*bf	0.5775	*bf	0.7801	*bf	0.9739
*cf	1.0865	*cf	0.6158	*cf	0.2970
*df	3000.0139	*df	3000.0055	*df	3000.0773
Grain Size Dist.		Grain Size Dist.		Grain Size Dist.	
0.001mm		0.001mm		0.001mm	
0.002mm	10.0	0.002mm	27.5	0.002mm	47.5
0.020mm		0.020mm		0.020mm	
#200	37.0	#200	65.0	#200	80.0
#100		#100		#100	
#80		#80		#80	
#60		#60		#60	
#50		#50		#50	
#40	72.5	#40	80.0	#40	86.5
#30		#30		#30	
#20		#20		#20	
#16		#16		#16	
#10	90.0	#10	90.0	#10	90.0
#8		#8		#8	
#4	90.0	#4	90.0	#4	92.5
3/8"		3/8"		3/8"	
1/2"		1/2"		1/2"	
3/4"		3/4"		3/4"	
1"		1"		1"	
1 1/2"		1 1/2"		1 1/2"	
2"		2"		2"	
2 1/2"		2 1/2"		2 1/2"	
3"		3"		3"	
3 1/2"		3 1/2"		3 1/2"	

Enter Map Character =>>	AA7

Horizon 1 (Top)	Compacted ? Yes	Horizon 2	Compacted ? No	Horizon 3	Compacted ? No
AASHTO Classification	A-4		A-7-6		A-7-6
Thickness (in)	7.1		16.9		3.1
Resilient Modulus (psi)	14,952		4,396		7,712
CBR (%)	16		2		6

*Version No.	0.9	*Version No.	0.9	*Version No.	0.9
*Units	US	*Units	US	*Units	US
*Plasticity Index	8.5	*Plasticity Index	57	*Plasticity Index	29.5
*Liquid Limit	31.5	*Liquid Limit	84.5	*Liquid Limit	50.5
*Compacted Layer	1	*Compacted	0	*Compacted	0
*Unit Weight		*Unit Weight		*Unit Weight	
*Specific Gravity		*Specific Gravity		*Specific Gravity	
*Permeability	1.08E-01	*Permeability	1.08E-02	*Permeability	1.08E-02
*Optimum WC		*Optimum WC		*Optimum WC	
*af	6.0437	*af	15.4512	*af	1.1333
*bf	1.1569	*bf	0.6800	*bf	1.0914
*cf	0.5902	*cf	0.3912	*cf	0.4446
*df	3000.0082	*df	2999.9283	*df	2999.1491
Grain Size Dist.		Grain Size Dist.		Grain Size Dist.	
0.001mm		0.001mm		0.001mm	
0.002mm	25.0	0.002mm	50.0	0.002mm	25.0
0.020mm		0.020mm		0.020mm	
#200	60.5	#200	75.0	#200	57.5
#100		#100		#100	
#80		#80		#80	
#60		#60		#60	
#50		#50		#50	
#40	87.5	#40	80.0	#40	82.5
#30		#30		#30	
#20		#20		#20	
#16		#16		#16	
#10	97.5	#10	80.0	#10	92.5
#8		#8		#8	
#4	99.5	#4	99.5	#4	99.0
3/8"		3/8"		3/8"	
1/2"		1/2"		1/2"	
3/4"		3/4"		3/4"	
1"		1"		1"	
1 1/2"		1 1/2"		1 1/2"	
2"		2"		2"	
2 1/2"		2 1/2"		2 1/2"	
3"		3"		3"	
3 1/2"		3 1/2"		3 1/2"	

Appendix G (Continued)

Enter Map Character =>>	AB4

Horizon 1 (Top)	Compacted ? Yes	Horizon 2	Compacted ? No	Horizon 3	Compacted ? No
AASHTO Classification	A-4		A-4		A-4
Thickness (in)	7.1		18.1		4.7
Resilient Modulus (psi)	25,934		25,421		16,098
CBR (%)	37		36		18

*Version No.	0.9	*Version No.	0.9	*Version No.	0.9
*Units	US	*Units	US	*Units	US
*Plasticity Index	3.5	*Plasticity Index	3.5	*Plasticity Index	0
*Liquid Limit	30	*Liquid Limit	30	*Liquid Limit	
*Compacted Layer	1	*Compacted	0	*Compacted	0
*Unit Weight		*Unit Weight		*Unit Weight	
*Specific Gravity		*Specific Gravity		*Specific Gravity	
*Permeability	3.33E-01	*Permeability	3.33E-01	*Permeability	3.33E-01
*Optimum WC		*Optimum WC		*Optimum WC	
*af	1.4020	*af		*af	
*bf	1.1093	*bf		*bf	
*cf	0.4142	*cf		*cf	
*df	2997.6577	*df		*df	
Grain Size Dist.		Grain Size Dist.		Grain Size Dist.	
0.001mm		0.001mm		0.001mm	
0.002mm	17.5	0.002mm	17.5	0.002mm	10.0
0.020mm		0.020mm		0.020mm	
#200	39.5	#200	42.0	#200	39.5
#100		#100		#100	
#80		#80		#80	
#60		#60		#60	
#50		#50		#50	
#40	77.5	#40	77.5	#40	75.0
#30		#30		#30	
#20		#20		#20	
#16		#16		#16	
#10	82.5	#10	87.5	#10	82.5
#8		#8		#8	
#4	85.0	#4	92.5	#4	85.0
3/8"		3/8"		3/8"	
1/2"		1/2"		1/2"	
3/4"		3/4"		3/4"	
1"		1"		1"	
1 1/2"		1 1/2"		1 1/2"	
2"		2"		2"	
2 1/2"		2 1/2"		2 1/2"	
3"		3"		3"	
3 1/2"		3 1/2"		3 1/2"	

Appendix G (Continued)

Enter Map Character =>>	**AC2**

Horizon 1 (Top)	Compacted ? Yes	Horizon 2	Compacted ? No	Horizon 3	Compacted ? No
AASHTO Classification	A-5		A-6		A-4
Thickness (in)	11.0		9.8		5.1
Resilient Modulus (psi)	19,370		11,479		19,513
CBR (%)	24		10		24

*Version No.	0.9	*Version No.	0.9	*Version No.	0.9
*Units	US	*Units	US	*Units	US
*Plasticity Index	7	*Plasticity Index	15	*Plasticity Index	6.5
*Liquid Limit	42.5	*Liquid Limit	39.5	*Liquid Limit	32.5
*Compacted Layer	1	*Compacted	0	*Compacted	0
*Unit Weight		*Unit Weight		*Unit Weight	
*Specific Gravity		*Specific Gravity		*Specific Gravity	
*Permeability	3.33E-01	*Permeability	1.08E-01	*Permeability	3.33E-01
*Optimum WC		*Optimum WC		*Optimum WC	
*af	11.6248	*af	10.3235	*af	10.6247
*bf	1.0108	*bf	0.8660	*bf	0.9500
*cf	0.7347	*cf	0.5438	*cf	0.7876
*df	2999.9997	*df	2999.9979	*df	2999.9999
Grain Size Dist.		Grain Size Dist.		Grain Size Dist.	
0.001mm		0.001mm		0.001mm	
0.002mm	11.5	0.002mm	26.5	0.002mm	17.5
0.020mm		0.020mm		0.020mm	
#200	42.5	#200	56.5	#200	45.0
#100		#100		#100	
#80		#80		#80	
#60		#60		#60	
#50		#50		#50	
#40	60.0	#40	75.0	#40	65.5
#30		#30		#30	
#20		#20		#20	
#16		#16		#16	
#10	73.0	#10	80.0	#10	77.5
#8		#8		#8	
#4	83.0	#4	87.5	#4	85.0
3/8"		3/8"		3/8"	
1/2"		1/2"		1/2"	
3/4"		3/4"		3/4"	
1"		1"		1"	
1 1/2"		1 1/2"		1 1/2"	
2"		2"		2"	
2 1/2"		2 1/2"		2 1/2"	
3"		3"		3"	
3 1/2"		3 1/2"		3 1/2"	

Appendix G (Continued)

Enter Map Character =>>	AC7

Horizon 1 (Top)	Compacted ?	Horizon 2	Compacted ?	Horizon 3	Compacted ?
	Yes		No		No
AASHTO Classification	A-3		A-3		
Thickness (in)	42.9		37.0		
Resilient Modulus (psi)	16,721		16,964		
CBR (%)	19		19		

*Version No.	0.9	*Version No.	0.9	*Version No.	0.9
*Units	US	*Units	US	*Units	US
*Plasticity Index	0	*Plasticity Index	0	*Plasticity Index	
*Liquid Limit		*Liquid Limit		*Liquid Limit	
*Compacted Layer	1	*Compacted	0	*Compacted	0
*Unit Weight		*Unit Weight		*Unit Weight	
*Specific Gravity		*Specific Gravity		*Specific Gravity	
*Permeability	1.08E+00	*Permeability	1.08E+00	*Permeability	
*Optimum WC		*Optimum WC		*Optimum WC	
*af	9.0859	*af	9.7771	*af	
*bf	6.6459	*bf	5.3560	*bf	
*cf	0.6016	*cf	0.7694	*cf	
*df	3000.0002	*df	3000.0000	*df	
Grain Size Dist.		Grain Size Dist.		Grain Size Dist.	
0.001mm		0.001mm		0.001mm	
0.002mm	5.0	0.002mm	3.5	0.002mm	
0.020mm		0.020mm		0.020mm	
#200	8.5	#200	6.5	#200	
#100		#100		#100	
#80		#80		#80	
#60		#60		#60	
#50		#50		#50	
#40	80.0	#40	75.0	#40	
#30		#30		#30	
#20		#20		#20	
#16		#16		#16	
#10	95.0	#10	95.0	#10	
#8		#8		#8	
#4	95.0	#4	95.0	#4	
3/8"		3/8"		3/8"	
1/2"		1/2"		1/2"	
3/4"		3/4"		3/4"	
1"		1"		1"	
1 1/2"		1 1/2"		1 1/2"	
2"		2"		2"	
2 1/2"		2 1/2"		2 1/2"	
3"		3"		3"	
3 1/2"		3 1/2"		3 1/2"	

Appendix G (Continued)

Enter Map Character =>>	Z69

Horizon 1 (Top)	Compacted ? Yes	Horizon 2	Compacted ? No	Horizon 3	Compacted ? No
AASHTO Classification	A-4		A-7-6		A-6
Thickness (in)	9.1		39.0		37.0
Resilient Modulus (psi)	21,768		8,723		11,768
CBR (%)	28		7		11

*Version No.	0.9	*Version No.	0.9	*Version No.	0.9
*Units	US	*Units	US	*Units	US
*Plasticity Index	5	*Plasticity Index	25	*Plasticity Index	18
*Liquid Limit	22.5	*Liquid Limit	54	*Liquid Limit	37.5
*Compacted Layer	1	*Compacted	0	*Compacted	0
*Unit Weight		*Unit Weight		*Unit Weight	
*Specific Gravity		*Specific Gravity		*Specific Gravity	
*Permeability	2.75E-01	*Permeability	1.08E-01	*Permeability	2.75E-01
*Optimum WC		*Optimum WC		*Optimum WC	
*af	6.9913	*af	3.0580	*af	5.1543
*bf	0.8169	*bf	0.8988	*bf	0.7251
*cf	0.8655	*cf	0.3197	*cf	0.5959
*df	3000.0028	*df	3000.0550	*df	3000.0093
Grain Size Dist.		Grain Size Dist.		Grain Size Dist.	
0.001mm		0.001mm		0.001mm	
0.002mm	17.5	0.002mm	45.0	0.002mm	32.5
0.020mm		0.020mm		0.020mm	
#200	45.0	#200	55.0	#200	45.0
#100		#100		#100	
#80		#80		#80	
#60		#60		#60	
#50		#50		#50	
#40	67.5	#40	60.0	#40	55.0
#30		#30		#30	
#20		#20		#20	
#16		#16		#16	
#10	87.5	#10	65.0	#10	60.0
#8		#8		#8	
#4	92.5	#4	90.0	#4	85.0
3/8"		3/8"		3/8"	
1/2"		1/2"		1/2"	
3/4"		3/4"		3/4"	
1"		1"		1"	
1 1/2"		1 1/2"		1 1/2"	
2"		2"		2"	
2 1/2"		2 1/2"		2 1/2"	
3"		3"		3"	
3 1/2"		3 1/2"		3 1/2"	

Appendix G (Continued)

Enter Map Character =>>	Z72

Horizon 1 (Top)	Compacted ? Yes	Horizon 2	Compacted ? No	Horizon 3	Compacted ? No
AASHTO Classification	A-4		A-6		A-7-6
Thickness (in)	7.1		4.7		38.2
Resilient Modulus (psi)	13,180		8,332		6,141
CBR (%)	13		6		4

*Version No.	0.9	*Version No.	0.9	*Version No.	0.9
*Units	US	*Units	US	*Units	US
*Plasticity Index	10.5	*Plasticity Index	17	*Plasticity Index	31
*Liquid Limit	27.5	*Liquid Limit	40	*Liquid Limit	57.5
*Compacted Layer	1	*Compacted	0	*Compacted	0
*Unit Weight		*Unit Weight		*Unit Weight	
*Specific Gravity		*Specific Gravity		*Specific Gravity	
*Permeability	1.08E-01	*Permeability	8.34E-01	*Permeability	8.34E-03
*Optimum WC		*Optimum WC		*Optimum WC	
*af	7.0357	*af		*af	
*bf	0.8193	*bf		*bf	
*cf	0.8520	*cf		*cf	
*df	3000.0028	*df		*df	
Grain Size Dist.		Grain Size Dist.		Grain Size Dist.	
0.001mm		0.001mm		0.001mm	
0.002mm	18.5	0.002mm	27.5	0.002mm	47.5
0.020mm		0.020mm		0.020mm	
#200	62.5	#200	87.5	#200	80.0
#100		#100		#100	
#80		#80		#80	
#60		#60		#60	
#50		#50		#50	
#40	80.0	#40	90.0	#40	92.5
#30		#30		#30	
#20		#20		#20	
#16		#16		#16	
#10	92.5	#10	92.5	#10	92.5
#8		#8		#8	
#4	97.5	#4	97.5	#4	95.0
3/8"		3/8"		3/8"	
1/2"		1/2"		1/2"	
3/4"		3/4"		3/4"	
1"		1"		1"	
1 1/2"		1 1/2"		1 1/2"	
2"		2"		2"	
2 1/2"		2 1/2"		2 1/2"	
3"		3"		3"	
3 1/2"		3 1/2"		3 1/2"	

Appendix G (Continued)

Continued…	**Z72**

Horizon 4	Compacted ? No
	A-6
	22.0
	10,184
	9

*Version No.	0.9
*Units	US
*Plasticity Index	20
*Liquid Limit	35
*Compacted Layer	0
*Unit Weight	
*Specific Gravity	
*Permeability	8.36E-01
*Optimum WC	
*af	
*bf	
*cf	
*df	
Grain Size Dist.	
0.001mm	
0.002mm	27.5
0.020mm	
#200	52.5
#100	
#80	
#60	
#50	
#40	60.0
#30	
#20	
#16	
#10	67.5
#8	
#4	70.0
3/8"	
1/2"	
3/4"	
1"	
1 1/2"	
2"	
2 1/2"	
3"	
3 1/2"	

Appendix G (Continued)

Enter Map Character =>>	Z76

Horizon 1 (Top)	Compacted ? Yes	Horizon 2	Compacted ? No	Horizon 3	Compacted ? No
AASHTO Classification	A-6		A-7-6		A-6
Thickness (in)	5.1		59.1		11.8
Resilient Modulus (psi)	10,969		7,096		10,353
CBR (%)	10		5		9

*Version No.	0.9	*Version No.	0.9	*Version No.	0.9
*Units	US	*Units	US	*Units	US
*Plasticity Index	11.5	*Plasticity Index	25.5	*Plasticity Index	17
*Liquid Limit	30	*Liquid Limit	45	*Liquid Limit	35.5
*Compacted Layer	1	*Compacted	0	*Compacted	0
*Unit Weight		*Unit Weight		*Unit Weight	
*Specific Gravity		*Specific Gravity		*Specific Gravity	
*Permeability	1.08E-01	*Permeability	1.08E-02	*Permeability	2.75E-02
*Optimum WC		*Optimum WC		*Optimum WC	
*af	5.9076	*af	12.8086	*af	0.6392
*bf	0.9922	*bf	1.1293	*bf	1.1482
*cf	0.6456	*cf	0.2516	*cf	0.3995
*df	2999.6548	*df	2999.9480	*df	2995.9483
Grain Size Dist.		Grain Size Dist.		Grain Size Dist.	
0.001mm		0.001mm		0.001mm	
0.002mm	22.5	0.002mm	47.5	0.002mm	30.0
0.020mm		0.020mm		0.020mm	
#200	80.0	#200	76.5	#200	60.0
#100		#100		#100	
#80		#80		#80	
#60		#60		#60	
#50		#50		#50	
#40	95.0	#40	95.0	#40	95.0
#30		#30		#30	
#20		#20		#20	
#16		#16		#16	
#10	99.0	#10	99.0	#10	99.0
#8		#8		#8	
#4	100.0	#4	100.0	#4	100.0
3/8"		3/8"		3/8"	
1/2"		1/2"		1/2"	
3/4"		3/4"		3/4"	
1"		1"		1"	
1 1/2"		1 1/2"		1 1/2"	
2"		2"		2"	
2 1/2"		2 1/2"		2 1/2"	
3"		3"		3"	
3 1/2"		3 1/2"		3 1/2"	

Appendix G (Continued)

Enter Map Character =>>	**Z78**

Horizon 1 (Top)	Compacted ? Yes	Horizon 2	Compacted ? No	Horizon 3	Compacted ? No
AASHTO Classification	A-3		A-4		A-2
Thickness (in)	35.8		13.0		29.1
Resilient Modulus (psi)	16,857		23,696		16,723
CBR (%)	19		32		19

*Version No.	0.9	*Version No.	0.9	*Version No.	0.9
*Units	US	*Units	US	*Units	US
*Plasticity Index	0	*Plasticity Index	5	*Plasticity Index	0
*Liquid Limit		*Liquid Limit	20	*Liquid Limit	
*Compacted Layer	1	*Compacted	0	*Compacted	0
*Unit Weight		*Unit Weight		*Unit Weight	
*Specific Gravity		*Specific Gravity		*Specific Gravity	
*Permeability	1.08E+00	*Permeability	3.33E-01	*Permeability	1.08E+00
*Optimum WC		*Optimum WC		*Optimum WC	
*af	2.1249	*af		*af	
*bf	1.0165	*bf		*bf	
*cf	1.0317	*cf		*cf	
*df	3000.0174	*df		*df	
Grain Size Dist.		Grain Size Dist.		Grain Size Dist.	
0.001mm		0.001mm		0.001mm	
0.002mm	4.0	0.002mm	17.0	0.002mm	6.0
0.020mm		0.020mm		0.020mm	
#200	12.5	#200	36.0	#200	20.0
#100		#100		#100	
#80		#80		#80	
#60		#60		#60	
#50		#50		#50	
#40	75.5	#40	80.0	#40	75.5
#30		#30		#30	
#20		#20		#20	
#16		#16		#16	
#10	100.0	#10	100.0	#10	100.0
#8		#8		#8	
#4	100.0	#4	100.0	#4	100.0
3/8"		3/8"		3/8"	
1/2"		1/2"		1/2"	
3/4"		3/4"		3/4"	
1"		1"		1"	
1 1/2"		1 1/2"		1 1/2"	
2"		2"		2"	
2 1/2"		2 1/2"		2 1/2"	
3"		3"		3"	
3 1/2"		3 1/2"		3 1/2"	

Appendix G (Continued)

Enter Map Character =>>	Z87

Horizon 1 (Top)	Compacted ? Yes	Horizon 2	Compacted ? No	Horizon 3	Compacted ? No
AASHTO Classification	A-4		A-6		A-6
Thickness (in)	11.8		28.3		21.7
Resilient Modulus (psi)	22,679		13,815		11,358
CBR (%)	30		14		10

*Version No.	0.9	*Version No.	0.9	*Version No.	0.9
*Units	US	*Units	US	*Units	US
*Plasticity Index	5	*Plasticity Index	12	*Plasticity Index	16
*Liquid Limit	25	*Liquid Limit	29	*Liquid Limit	31.5
*Compacted Layer	1	*Compacted	0	*Compacted	0
*Unit Weight		*Unit Weight		*Unit Weight	
*Specific Gravity		*Specific Gravity		*Specific Gravity	
*Permeability	3.33E-01	*Permeability	1.08E-01	*Permeability	1.08E-01
*Optimum WC		*Optimum WC		*Optimum WC	
*af	1.7528	*af	0.9247	*af	0.6651
*bf	1.0216	*bf	1.0888	*bf	1.1558
*cf	0.5707	*cf	0.3839	*cf	0.3606
*df	2999.3765	*df	3006.8559	*df	2985.6676
Grain Size Dist.		Grain Size Dist.		Grain Size Dist.	
0.001mm		0.001mm		0.001mm	
0.002mm	12.5	0.002mm	26.5	0.002mm	29.0
0.020mm		0.020mm		0.020mm	
#200	40.5	#200	50.0	#200	54.0
#100		#100		#100	
#80		#80		#80	
#60		#60		#60	
#50		#50		#50	
#40	67.5	#40	76.5	#40	79.0
#30		#30		#30	
#20		#20		#20	
#16		#16		#16	
#10	97.5	#10	97.5	#10	99.0
#8		#8		#8	
#4	100.0	#4	100.0	#4	100.0
3/8"		3/8"		3/8"	
1/2"		1/2"		1/2"	
3/4"		3/4"		3/4"	
1"		1"		1"	
1 1/2"		1 1/2"		1 1/2"	
2"		2"		2"	
2 1/2"		2 1/2"		2 1/2"	
3"		3"		3"	
3 1/2"		3 1/2"		3 1/2"	

Appendix G (Continued)

Continued…	**Z87**

Horizon 4	Compacted ?
	No
	A-4
	17.3
	15,600
	17

*Version No.	0.9
*Units	US
*Plasticity Index	10.5
*Liquid Limit	27.5
*Compacted Layer	0
*Unit Weight	
*Specific Gravity	
*Permeability	1.08E-01
*Optimum WC	
*af	0.5389
*bf	1.0694
*cf	0.3196
*df	3000.1151
Grain Size Dist.	
0.001mm	
0.002mm	30.0
0.020mm	
#200	45.0
#100	
#80	
#60	
#50	
#40	77.5
#30	
#20	
#16	
#10	97.5
#8	
#4	100.0
3/8"	
1/2"	
3/4"	
1"	
1 1/2"	
2"	
2 1/2"	
3"	
3 1/2"	

Appendix G (Continued)

Enter Map Character =>>	Z88

Horizon 1 (Top)	Compacted ?	Horizon 2	Compacted ?	Horizon 3	Compacted ?
	Yes		No		No
AASHTO Classification	A-2-4		A-4		A-6
Thickness (in)	14.2		24.0		31.9
Resilient Modulus (psi)	16,861		16,125		12,461
CBR (%)	19		18		12

*Version No.	0.9	*Version No.	0.9	*Version No.	0.9
*Units	US	*Units	US	*Units	US
*Plasticity Index	0	*Plasticity Index	9.5	*Plasticity Index	13.5
*Liquid Limit	17.5	*Liquid Limit	29	*Liquid Limit	36
*Compacted Layer	1	*Compacted	0	*Compacted	0
*Unit Weight		*Unit Weight		*Unit Weight	
*Specific Gravity		*Specific Gravity		*Specific Gravity	
*Permeability	1.08E+00	*Permeability	1.08E-01	*Permeability	1.08E-01
*Optimum WC		*Optimum WC		*Optimum WC	
*af	3.1700	*af		*af	
*bf	0.6183	*bf		*bf	
*cf	1.2966	*cf		*cf	
*df	3000.0081	*df		*df	
Grain Size Dist.		Grain Size Dist.		Grain Size Dist.	
0.001mm		0.001mm		0.001mm	
0.002mm	5.0	0.002mm	26.5	0.002mm	31.5
0.020mm		0.020mm		0.020mm	
#200	21.5	#200	46.5	#200	54.0
#100		#100		#100	
#80		#80		#80	
#60		#60		#60	
#50		#50		#50	
#40	72.5	#40	83.0	#40	81.5
#30		#30		#30	
#20		#20		#20	
#16		#16		#16	
#10	96.0	#10	95.5	#10	99.0
#8		#8		#8	
#4	97.5	#4	97.5	#4	100.0
3/8"		3/8"		3/8"	
1/2"		1/2"		1/2"	
3/4"		3/4"		3/4"	
1"		1"		1"	
1 1/2"		1 1/2"		1 1/2"	
2"		2"		2"	
2 1/2"		2 1/2"		2 1/2"	
3"		3"		3"	
3 1/2"		3 1/2"		3 1/2"	

Appendix G (Continued)

Enter Map Character =>>	Z93

Horizon 1 (Top)	Compacted ?	Horizon 2	Compacted ?	Horizon 3	Compacted ?
	Yes		No		No
AASHTO Classification	A-4		A-6		A-6
Thickness (in)	5.1		17.7		42.1
Resilient Modulus (psi)	20,438		9,868		8,850
CBR (%)	26		8		7

*Version No.	0.9	*Version No.	0.9	*Version No.	0.9
*Units	US	*Units	US	*Units	US
*Plasticity Index	3.5	*Plasticity Index	12	*Plasticity Index	14.5
*Liquid Limit	22.5	*Liquid Limit	32.5	*Liquid Limit	36.5
*Compacted Layer	1	*Compacted	0	*Compacted	0
*Unit Weight		*Unit Weight		*Unit Weight	
*Specific Gravity		*Specific Gravity		*Specific Gravity	
*Permeability	1.08E-01	*Permeability	3.33E-02	*Permeability	3.33E-02
*Optimum WC		*Optimum WC		*Optimum WC	
*af	9.8839	*af		*af	
*bf	0.9621	*bf		*bf	
*cf	0.8389	*cf		*cf	
*df	3000.0001	*df		*df	
Grain Size Dist.		Grain Size Dist.		Grain Size Dist.	
0.001mm		0.001mm		0.001mm	
0.002mm	12.5	0.002mm	26.0	0.002mm	32.5
0.020mm		0.020mm		0.020mm	
#200	75.0	#200	92.5	#200	92.5
#100		#100		#100	
#80		#80		#80	
#60		#60		#60	
#50		#50		#50	
#40	92.5	#40	92.5	#40	92.5
#30		#30		#30	
#20		#20		#20	
#16		#16		#16	
#10	100.0	#10	100.0	#10	100.0
#8		#8		#8	
#4	100.0	#4	100.0	#4	100.0
3/8"		3/8"		3/8"	
1/2"		1/2"		1/2"	
3/4"		3/4"		3/4"	
1"		1"		1"	
1 1/2"		1 1/2"		1 1/2"	
2"		2"		2"	
2 1/2"		2 1/2"		2 1/2"	
3"		3"		3"	
3 1/2"		3 1/2"		3 1/2"	

Appendix G (Continued)

Enter Map Character =>>	Z95

Horizon 1 (Top)	Compacted ? Yes	Horizon 2	Compacted ? No	Horizon 3	Compacted ? No
AASHTO Classification	A-4		A-6		A-7-6
Thickness (in)	11.8		6.3		28.7
Resilient Modulus (psi)	22,787		9,344		6,566
CBR (%)	31		8		4

*Version No.	0.9	*Version No.	0.9	*Version No.	0.9
*Units	US	*Units	US	*Units	US
*Plasticity Index	4	*Plasticity Index	16.5	*Plasticity Index	30
*Liquid Limit	25.5	*Liquid Limit	37.5	*Liquid Limit	60.5
*Compacted Layer	1	*Compacted	0	*Compacted	0
*Unit Weight		*Unit Weight		*Unit Weight	
*Specific Gravity		*Specific Gravity		*Specific Gravity	
*Permeability	3.33E-01	*Permeability	1.08E-01	*Permeability	1.08E-01
*Optimum WC		*Optimum WC		*Optimum WC	
*af	2.5746	*af	5.7084	*af	0.4687
*bf	1.0390	*bf	0.9702	*bf	1.0524
*cf	0.6782	*cf	0.4906	*cf	0.2003
*df	2998.7047	*df	2999.7616	*df	3000.1934
Grain Size Dist.		Grain Size Dist.		Grain Size Dist.	
0.001mm		0.001mm		0.001mm	
0.002mm	12.5	0.002mm	30.0	0.002mm	47.5
0.020mm		0.020mm		0.020mm	
#200	50.0	#200	74.0	#200	74.0
#100		#100		#100	
#80		#80		#80	
#60		#60		#60	
#50		#50		#50	
#40	73.5	#40	95.0	#40	90.0
#30		#30		#30	
#20		#20		#20	
#16		#16		#16	
#10	91.5	#10	97.5	#10	95.0
#8		#8		#8	
#4	96.0	#4	97.5	#4	97.5
3/8"		3/8"		3/8"	
1/2"		1/2"		1/2"	
3/4"		3/4"		3/4"	
1"		1"		1"	
1 1/2"		1 1/2"		1 1/2"	
2"		2"		2"	
2 1/2"		2 1/2"		2 1/2"	
3"		3"		3"	
3 1/2"		3 1/2"		3 1/2"	

Appendix G (Continued)

Enter Map Character =>>	Z96

Horizon 1 (Top)	Compacted ? Yes	Horizon 2	Compacted ? No	Horizon 3	Compacted ? No
AASHTO Classification	A-4		A-7-6		A-7-6
Thickness (in)	7.9		11.0		37.0
Resilient Modulus (psi)	25,934		7,570		5,411
CBR (%)	37		5		3

*Version No.	0.9	*Version No.	0.9	*Version No.	0.9
*Units	US	*Units	US	*Units	US
*Plasticity Index	3.5	*Plasticity Index	25	*Plasticity Index	37
*Liquid Limit	20	*Liquid Limit	42.5	*Liquid Limit	65
*Compacted Layer	1	*Compacted	0	*Compacted	0
*Unit Weight		*Unit Weight		*Unit Weight	
*Specific Gravity		*Specific Gravity		*Specific Gravity	
*Permeability	3.33E-01	*Permeability	3.33E-02	*Permeability	2.50E-03
*Optimum WC		*Optimum WC		*Optimum WC	
*af	2.9575	*af	10.7401	*af	0.4345
*bf	0.9721	*bf	1.0076	*bf	1.0685
*cf	0.5864	*cf	0.3878	*cf	0.2050
*df	2998.8760	*df	2999.9882	*df	3000.1521
Grain Size Dist.		Grain Size Dist.		Grain Size Dist.	
0.001mm		0.001mm		0.001mm	
0.002mm	13.5	0.002mm	27.5	0.002mm	47.5
0.020mm		0.020mm		0.020mm	
#200	39.5	#200	70.0	#200	82.5
#100		#100		#100	
#80		#80		#80	
#60		#60		#60	
#50		#50		#50	
#40	80.0	#40	90.0	#40	91.0
#30		#30		#30	
#20		#20		#20	
#16		#16		#16	
#10	97.5	#10	97.5	#10	97.5
#8		#8		#8	
#4	99.0	#4	99.0	#4	99.0
3/8"		3/8"		3/8"	
1/2"		1/2"		1/2"	
3/4"		3/4"		3/4"	
1"		1"		1"	
1 1/2"		1 1/2"		1 1/2"	
2"		2"		2"	
2 1/2"		2 1/2"		2 1/2"	
3"		3"		3"	
3 1/2"		3 1/2"		3 1/2"	

Appendix G (Continued)

Continued…	**Z96**

Horizon 4	Compacted ?
	No
	A-6
	21.3
	11,507
	11

*Version No.	0.9
*Units	US
*Plasticity Index	12.5
*Liquid Limit	37
*Compacted Layer	0
*Unit Weight	
*Specific Gravity	
*Permeability	2.50E-03
*Optimum WC	
*af	5.3805
*bf	0.8867
*cf	0.3787
*df	3000.0306
Grain Size Dist.	
0.001mm	
0.002mm	20.0
0.020mm	
#200	67.5
#100	
#80	
#60	
#50	
#40	91.5
#30	
#20	
#16	
#10	97.5
#8	
#4	99.0
3/8"	
1/2"	
3/4"	
1"	
1 1/2"	
2"	
2 1/2"	
3"	
3 1/2"	

Appendix G (Continued)

Enter Map Character =>>	Z97

Horizon 1 (Top)	Compacted ? Yes	Horizon 2	Compacted ? No	Horizon 3	Compacted ? No
AASHTO Classification	A-4		A-7-6		A-7-6
Thickness (in)	9.1		39.0		20.1
Resilient Modulus (psi)	15,980		6,556		7,860
CBR (%)	18		4		6

*Version No.	0.9	*Version No.	0.9	*Version No.	0.9
*Units	US	*Units	US	*Units	US
*Plasticity Index	6	*Plasticity Index	26.5	*Plasticity Index	22.5
*Liquid Limit	25.5	*Liquid Limit	55.5	*Liquid Limit	55.5
*Compacted Layer	1	*Compacted	0	*Compacted	0
*Unit Weight		*Unit Weight		*Unit Weight	
*Specific Gravity		*Specific Gravity		*Specific Gravity	
*Permeability	1.08E-01	*Permeability	1.08E-01	*Permeability	1.08E-01
*Optimum WC		*Optimum WC		*Optimum WC	
*af	10.2859	*af	5.3288	*af	6.2041
*bf	107.7416	*bf	0.7382	*bf	0.7778
*cf	1910.8782	*cf	0.2438	*cf	1.0053
*df	2999.9998	*df	2185.1939	*df	3000.0036
Grain Size Dist.		Grain Size Dist.		Grain Size Dist.	
0.001mm		0.001mm		0.001mm	
0.002mm	16.0	0.002mm	47.5	0.002mm	18.5
0.020mm		0.020mm		0.020mm	
#200	75.0	#200	84.0	#200	73.0
#100		#100		#100	
#80		#80		#80	
#60		#60		#60	
#50		#50		#50	
#40	89.0	#40	89.5	#40	89.5
#30		#30		#30	
#20		#20		#20	
#16		#16		#16	
#10	92.5	#10	95.0	#10	92.5
#8		#8		#8	
#4	95.0	#4	99.0	#4	95.0
3/8"		3/8"		3/8"	
1/2"		1/2"		1/2"	
3/4"		3/4"		3/4"	
1"		1"		1"	
1 1/2"		1 1/2"		1 1/2"	
2"		2"		2"	
2 1/2"		2 1/2"		2 1/2"	
3"		3"		3"	
3 1/2"		3 1/2"		3 1/2"	

Appendix H North Carolina MEPDG User Reference Guide

Local Calibration of the MEPDG for Flexible Pavement Design
Research Project No. HWY-2007-07

North Carolina MEPDG User Reference Guide

Submitted to:
North Carolina Department of Transportation

Submitted by

Y. Richard Kim, Ph.D., P.E.
Campus Box 7908
Department of Civil, Construction & Environmental Engineering
North Carolina State University
Raleigh, NC 27695-7908
Tel: 919-515-7758, Fax: 919-515-7908
E-mail: kim@ncsu.edu

Fadi M. Jadoun
Graduate Research Assistant / Ph.D. Candidate
Campus Box 7908
Department of Civil, Construction & Environmental Engineering
North Carolina State University
Raleigh, NC 27695-7908
Tel: 919-827-3877, Fax: 919-515-7908
E-mail: fmj2002@gmail.com

Department of Civil, Construction & Environmental Engineering
North Carolina State University
Raleigh, NC

May 2011

TABLE OF CONTENTS

LIST OF TABLES

LIST OF FIGURES

LIST OF ACRONYMS

Acronym	Meaning
AADTT	Annual Average Daily Truck Traffic
AASHTO	American Association of State Highway and Transportation Officials
ABC	Aggregate Base Course
AC	Asphalt Concrete
ALDF	Axle Load Distribution Factors
APT	Number of Axles per Truck
ATB	Asphalt Treated Base
AVC	Automatic Vehicle Classification
CTB	Cement Treated Base
DARWin-ME	Design, Analysis and Rehabilitation for Windows-Mechanistic Empirical
|E*|	Dynamic modulus of asphalt concrete
EICM	Enhanced Integrated Climatic Model
FHWA	Federal Highway Administration
|G*|	Dynamic shear modulus of asphalt binder
GIS	Geographic Information System
GUI	Graphical User Interface
HDF	Hourly Distribution Factors
HMA	Hot Mix Asphalt
IRI	International Roughness Index
LDF	Lane Distribution Factor
LOE	Line of Equality
M&T Unit	Materials and Tests Unit
MAF	Monthly Adjustment Factors
MEPDG	Mechanistic Empirical Pavement Design Guide
NMAS	Nominal Maximum Aggregate Size
NRCS	National Resources Conservation Service
PMS	Pavement Management Systems
PMU	Pavement Management Unit
SI	Serviceability Index
SWCC	Soil Water Characteristics Curve
TPB	Traffic Planning Branch
TSU	Traffic Survey Unit
USDA	United States Department of Agriculture
WIM	Weigh-in-Motion

CHAPTER 1 INTRODUCTION

This document describes step-by-step procedures that can be employed by pavement designers at the North Carolina Department of Transportation (NCDOT) to utilize the developed databases for local materials and performance in implementing the new AASHTO Mechanistic-Empirical Pavement Design Guide (MEPDG) (1) for designing new and rehabilitated flexible pavements in North Carolina. The asphalt materials and traffic databases were developed by North Carolina State University (NCSU) researchers under the following three projects sponsored by the NCDOT.

- HWY 2003-09: Typical Dynamic Moduli for North Carolina Asphalt Concrete Mixes
- HWY-2007-07: Local Calibration of the MEPDG for Flexible Pavement Design
- HWY-2008-11: Development of Traffic Data Input Resources for the Mechanistic Empirical-Pavement Design Process

The subgrade materials database, including an Excel-based MEPDG input generator, was developed by NCSU researchers based on data and soil maps from the NCHRP 9-23A project (2).

All procedures described in this document were developed using MEPDG version 1.1. However, due to limitations of version 1.1 in considering the properties of multiple asphalt layers in predicting total permanent deformation measured at the surface of the pavement, a hybrid version of the MEPDG was developed using both; MEPDG version 1.1 and MEPDG version 9-30A. The latter allows for entering material-specific rutting model coefficients for multiple layers. Version 9-30A was developed specifically for the NCHRP 9-30A project (3), "Calibration of Rutting Models for HMA Structural and Mix Design." A copy of MEPDG 9-30A was acquired from AASHTO to be used for research purposes only.

Units found in this document are based on the US Customary measuring system, unless otherwise noted, because it is the only available option in MEPDG version 1.1. However, some metric units are used in this document. For example, the unit used in version 1.1 for the asphalt binder shear modulus ($|G^*|$) is Pascal (Pa), a metric unit, whereas the unit used to describe the asphalt concrete dynamic modulus ($|E^*|$) is pounds per square inch (psi), which is a US Customary unit.

Version 1.1 allows for some traffic and materials input parameters to be imported directly from within the MEPDG. Other parameters, however, must be entered manually. For parameters that can be imported and are part of the database, and therefore do not change often, the research team has developed computer files that will be available to NCDOT designers in a media storage device. Detailed instructions for importing such files are presented in this document.

The scope of the local calibration effort covers only alligator cracking (or so-called bottom-up cracking) and rutting (or so-called permanent deformation) that occur in flexible pavements. The performance prediction model for longitudinal cracking that is embedded in version 1.1 of the MEPDG has problems and, therefore, is not included in the local calibration effort. In version 1.1, it is assumed that the number of cycles to failure (N_f) model can be used for alligator cracking as well as longitudinal cracking. This assumption is based on another assumption that the longitudinal cracking transfer function can handle the error inherent in the first assumption. Realizing that the N_f model currently embedded in the MEPDG was developed based on critical strain criteria, and knowing that longitudinal cracking is affected by thermal distresses and aging of the surface layers, it is clear that the longitudinal cracking predictions obtained from the MEPDG are questionable; hence, these predictions are excluded from the local calibration effort.

Users (referring in this document to person(s) running the MEPDG) are offered a choice of three hierarchical data input levels: Level 1, Level 2, and Level 3. This flexibility is available for materials as well as traffic input data. Level 1 is the most accurate and most demanding of all levels whereas Level 3 is the least accurate and least demanding data input level. This hierarchical approach offers flexibility that enables users to match the level of effort with the importance of the project under design and the available resources. For even greater flexibility, the MEPDG allows users to select different levels of input for different parameters within the same project. For example, designers can select Level 1 input for asphalt layers, Level 2 input for subgrade soils, and Level 3 input (default values) for base layer materials. Interpretation of the input levels differs for materials versus traffic data. The next section presents in detail the definitions of the input levels available for materials and traffic data.

1.1 Hierarchical Materials Data Input Levels

The MEPDG offers the following hierarchical levels of input for materials parameters:

- Level 1 input reflects the designers' high degree of knowledge of the materials in the pavement design. Level 1 input parameters are measured either directly from the site or near the site under study, or determined through laboratory testing.

- Level 2 input reflects a medium level of knowledge of the materials in the pavement design. Level 2 input parameters are determined based on state-wide averages or estimated based on known parameters through statistical correlations and relationships.

- Level 3 input reflects the least amount of knowledge about the materials in the pavement design. Level 3 input parameters are estimated based on regional values or national values, i.e., MEPDG default values.

1.2 Hierarchical Traffic Data Input Levels

The MEPDG offers the following hierarchical levels of input for traffic parameters:

- Level 1 requires site-specific traffic data that are measured at or near the road segment or the site under study. These data include weight and volume data. This level requires very good knowledge of the traffic history at that particular site and also requires good knowledge about future traffic at that site, i.e., traffic forecasts. Level 1 is the most accurate level of input because it considers actual traffic factors at the site.

- Level 2 relies mainly on accurate measurements of truck volumes and percentages at or near the site under study. However, weight data typically are obtained by taking the averages of similar data types at neighboring sites. This level also requires a good understanding of the daily and seasonal variations in traffic volume at the site.

- Level 3 requires the least amount of traffic knowledge about the site under study. However, Level 3 nonetheless requires that some data measurements, e.g., volume data and percentage of trucks, are taken at the site. Weight data for Level 3 are estimated using either predictive equations and/or state or regional averages.

1.3 General Recommendations and Issues to Consider

It is recommended, unless otherwise noted, that NCDOT pavement designers use the same level of input that was used in the local calibration effort to develop the materials and traffic databases. The different levels of input that were used in the local calibration effort are clearly presented in this document. However, because the laboratory testing program within this research tested *representative* materials, the data in the materials database is not true Level 1 input. So, although the hot mix asphalt (HMA) material properties, including binder and mixture data, should be entered as Level 1 in the MEPDG, as recommended in this document, it is important to understand that these inputs are actually Level 2 inputs unless the NCDOT tests the binder and mixture for a specific job and use the results in the MEPDG. For the base materials, Level 3 national default values were used in the local calibration effort and, therefore, are recommended for use in the design. For the subgrade soils, a combination of Level 1 and Level 2 material inputs was used in the local calibration effort, and thus is recommended for use in the design. Most of the traffic data, however, are Level 1 and Level 2 inputs because the required parameters are derived based on 48-hour counts obtained at or near the project location. For some general traffic inputs, regional values, i.e., Level 3 inputs, are recommended for all designs.

1.4 Input Parameters Required for a Trial Design

Four major input categories are required to run the MEPDG. Each category includes multiple inputs, and these inputs can change depending on the desired input level. As previously mentioned, Level 1 is the most demanding input level, and hence, users are expected to provide detailed information if they decide to use Level 1. The four major input categories are as follows.

- Project and performance reliability information.
- Traffic, vehicle, and road geometry information.
- Geographic coordinates, elevation, depth of water table and climatic information.
- Structural information.

TABLE 1.1 through TABLE 1.5 list the inputs required for each of the four main input categories for each of the three input levels.

TABLE 1.1 MEPDG Inputs Required for Project and Performance Reliability

General Information						
Input Parameter	Level 1	Level 2	Level 3 (Default)	Data Entry	Allowable Range	
Project name	√	X*	√*	O*	NA*	NA
Design life, years	√	X	√	M*	1	100
Base/subgrade construction, month and year	√	X	√	M	NA	NA
Pavement construction, month and year	√	X	√	M	NA	NA
Traffic open, month and year	√	X	√	M	NA	NA
Site/project identification						
Location	√	X	X	O	NA	NA
Project ID	√	X	X	O	NA	NA
Section ID	√	X	X	O	NA	NA
Date	√	X	X	O	NA	NA
Station/milepost format	√	X	X	O	NA	NA
Station/milepost begin	√	X	X	O	NA	NA
Station/milepost end	√	X	X	O	NA	NA
Traffic direction	√	X	X	O	NA	NA
Analysis parameters (limit and reliability)						
Initial IRI, inches/mile	√	√	√	O	0	200
Terminal IRI, inches/mile	√	√	√	O	63	1260
Longitudinal cracking, feet/mile	√	√	√	O	500	2000
Alligator cracking, percentage of lane area	√	√	√	O	0	100
Thermal fracture, feet/mile	√	√	√	O	0	10000
Chemically stabilized layer fatigue fracture, %	√	√	√	O	0	100
Permanent deformation - total pavement, inches	√	√	√	O	0	3
Permanent deformation - AC only, inches	√	√	√	O	0	3

* √ = Available Option, X = Unavailable Option, O = Optional, M = Mandatory, NA = Not Applicable.

TABLE 1.2 MEPDG Inputs Required for Traffic, Vehicle, and Road Geometry

Traffic General						
Input Parameter	Level 1	Level 2	Level 3 (Default)	Data Entry	Allowable Range	
Initial two-way AADTT	√	√*	X*	M*	100	25000
Number of lanes in design direction	√	X	√	M	1	10
Percentage of trucks in design direction	√	√	√	M	40	60
Percentage of trucks in design lane	√	√	√	M	50	100
Operational speed, mph	√	√	√	M	3	100
Mean wheel location, inches from lane marking	√	√	√	M	0	36
Traffic wander standard deviation, inches	√	√	√	M	7	13
Design lane width, feet	√	√	√	M	10	13
Average axle width, feet	√	√	√	M	8	10
Dual tire spacing, inches	√	√	√	M	0	24
Tire pressure, psi	√	√	√	M	120	120
Tandem axle spacing, inches	√	√	√	M	24	144
Tridem axle spacing, inches	√	√	√	M	24	144
Quad axle spacing, inches	√	√	√	M	24	144
Average axle spacing, inches	√	√	√	M	10	22
Percentage of trucks per category (short, medium, long)	√	√	√	M	0	100
Axle load distribution factors (ALDF)	√	√	√	M	0	100
Axles per truck (APT)	√	√	√	M	0	5
Traffic volume adjustment factors						
Monthly adjustment factors (MAF)	√	X	√	M	0	10
Vehicle class distribution factors (VCD)	√	X	√	M	0	100
Hourly distribution factors (HDF)	√	X	√	M	0	100
Traffic growth factors						
No growth	√	√	√	Select One Option	0	0
Linear (default is 4%)	√	√	√		0	10
Compound (default is 4%)	√	√	√		0	10
Class specific (default is 4%, linear or compound)	√	√	√		0	8

* √ = Available Option, X = Unavailable Option, M =Mandatory

TABLE 1.3 MEPDG Inputs Required for Defining Climatic Information at a Given Project Location

Input Parameter	Level 1	Level 2	Level 3**	Data Entry*	Allowable Range
Project longitude, degrees. minutes	√*	√	Users select a single weather station from a drop down list	M*	NA*
Project latitude, degrees. minutes	√	√		M	NA
Project elevation, feet	√	√		M	NA
Depth of water table at project location, feet	√	√		M	> 0

* √ = Available Option, M = Mandatory, NA = Not Applicable.

** Longitude, latitude, & elevation fields will be populated when a weather station is selected in Level 3.

TABLE 1.4 MEPDG Inputs Required for Asphalt Binder and Asphalt Concrete

Material	Input Level	Data Required	Allowable Range	
HMA Mixture	Level 1	Dynamic modulus, psi. min. 3 temp. and 3 frequencies, Max. 8 temperatures and 6 frequencies	NA	NA
	Levels 2 and 3	Cumulative percentage retained on 3/4" sieve	0	100
		Cumulative percentage retained on 3/8" sieve	0	100
		Cumulative percentage retained on #4 sieve	0	100
		Percentage passing # 200 sieve	0	100
	Levels 1, 2 and 3	Reference temperature (°F)	50	104
		As-built effective binder content by volume (%)	2	20
		As-built air voids (%)	0	20
		As-built total unit weight (pcf)	100	200
		Poisson's ratio	0.2	0.45
		Thermal conductivity of asphalt (BTU/hr-ft-F°)	0.5	1
		Heat capacity of asphalt (BTU/lb-ft)	0.1	0.5
Asphalt Binder	Levels 1 and 2	Option 1 Shear modulus, Pa, and phase angle for RTFO binder and at angular frequency of 10 radians/sec. min. 3 temperatures.	NA	NA
		Option 2 Temperature (°F) at softening point = 13000 P and; Absolute viscosity (P) at 140°F and; kinematic viscosity (CS) at 275°F and; Specific gravity at 77°F Penetration / optional Brookfield viscosity / optional	NA	NA
	Level 3	Superpave binder grade or; Viscosity grade or; Penetration grade	NA	NA

TABLE 1.5 MEPDG Inputs Required for Unbound Base and Subgrade Materials

Input Level			Input Category	Input Parameters
Level 1	Level 2	Level 3	Soils Gradation	Index properties are calculated within the MEPDG
			Atterberg Limits	Plasticity Index (PI)
				Liquid Limit (LL)
			Compacted Soil Properties	Max. Dry Unit Weight (pcf)
				Soils Specific Gravity, Gs
				Saturated Hydraulic Conductivity (Permeability) (ft/hr)
				Opt. Gravimetric Water Content (%)
			SWCC Parameters	(a_f, b_f, c_f, and h_r)*

* Soil Water Characteristics Curve Parameters.

Note that although some inputs do not have explicit options for the different input levels, the research team nevertheless interprets the meaning of each level. For example, the Average Annual Daily Truck Traffic (AADTT) is interpreted as Level 1 if it has been measured. A typical case would be a widening project where traffic already exists, versus an interpretation of Level 2 if data were estimated from nearby projects or from 48-hour counts, as is typical for new construction.

In addition, TABLE 1.1 through TABLE 1.5 indicate whether a particular input is mandatory for the MEPDG to run or if it is optional. For each of the inputs, where applicable, TABLE 1.1 through TABLE 1.5 list the input range allowed by the MEPDG. If users input a value that is out of the allowable range, a warning message will appear, and the font of this input will be displayed in red. For most of the input parameters, the MEPDG will still allow users to use values outside the allowable range after a warning message appears. For other parameters, however, the MEPDG requires users to input a valid value that is within the allowable range.

1.5 Overview of the MEPDG Pavement Design Procedure

Before introducing the detailed step-by-step procedure to design pavement structures using the MEPDG, it is vital for users to have an understanding of the overall design procedure. Users must realize that the MEPDG in its current form is not design software; rather, it is analysis software. Generally speaking, design software would suggest a pavement structure for a certain group of inputs, whereas analysis software requires users to start with an initial structure, which is then analyzed to predict pavement performance, which is then compared to performance criteria set by the agency. It is expected that the soon-to-be-released AASHTO MEPDG V.2.0 (or so-called DARWin-ME) will include an optimization module that facilitates the determination of the most feasible structural design that satisfies the agency's performance criteria throughout the design life of the pavement.

FIGURE 1.1 presents a flow chart that shows the sequence of the design steps, as required by the MEPDG. The first step requires users to input traffic, materials, and climatic data for the project. The second step requires users to assume a certain pavement trial design structure based on a combination of engineering knowledge, experience, and pre-MEPDG pavement design procedures. The third step involves executing the MEPDG to predict pavement performance parameters at the end of a desired design life. The predicted performance parameters are then compared to criteria set by the agency for various performance measures. If the predicted performance parameters pass the pre-set criteria, the trial design structure becomes a candidate design structure. If any of the predicted performance parameters fail the performance criteria, users should modify the first trial design structure and repeat the steps until a structure that satisfies all criteria is found.

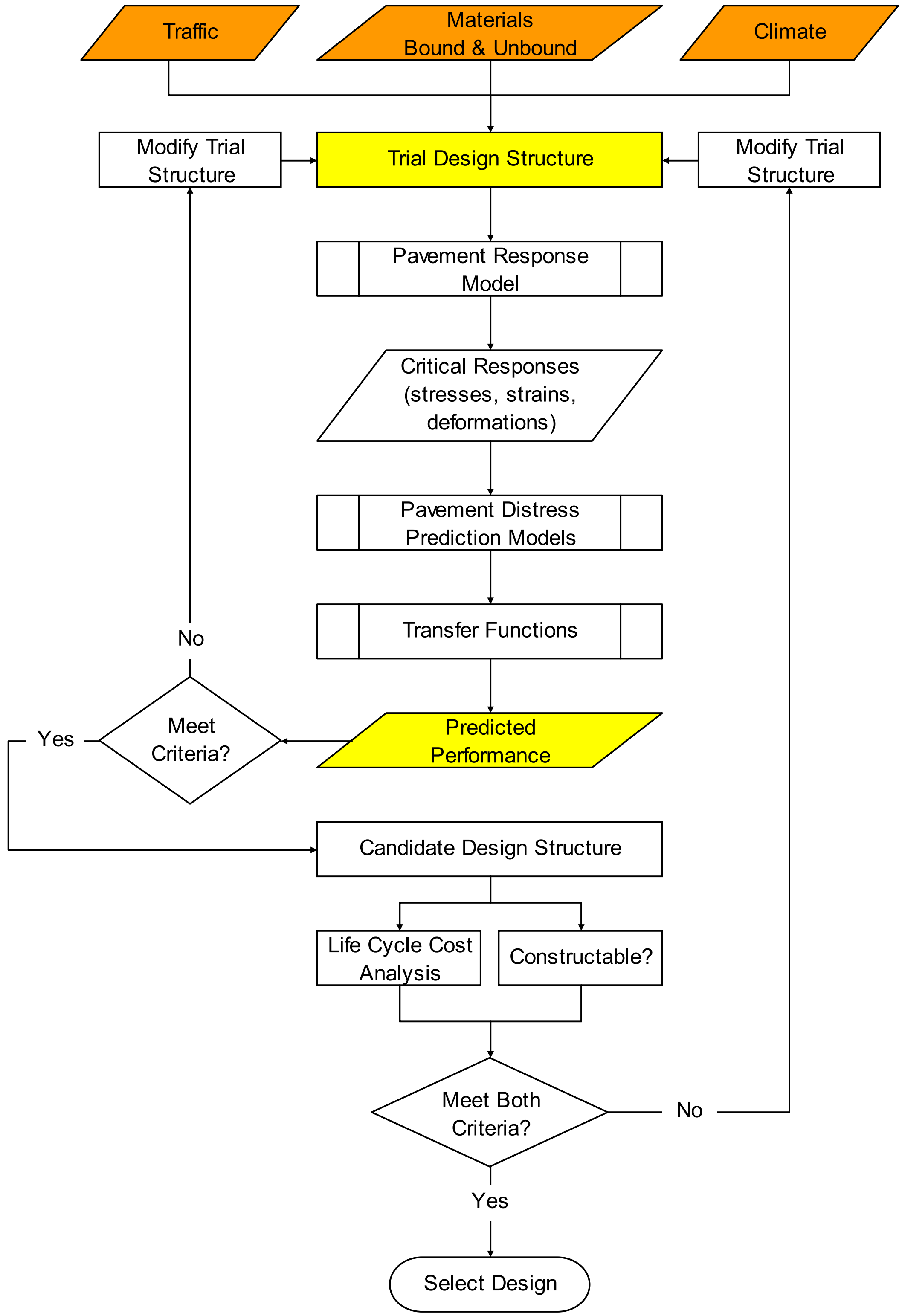

FIGURE 1.1 Overview of the MEPDG pavement design procedure.

To find the most effective pavement structure, the research team recommends that users execute the MEPDG multiple times to find multiple candidate design structures. Users can then carry out a life cycle cost analysis (LCCA) study on all candidate structures to select the most efficient design. The most efficient pavement design is that which is the most cost-effective and least expensive over the design life, yet satisfies the performance criteria set by the agency. TABLE 1.6 presents pavement performance sensitivity criteria that have been developed in cooperation with the NCDOT Pavement Management Unit (PMU) for flexible and jointed plain concrete pavements (JPCP).

TABLE 1.6 Sensitivity Criteria for Flexible and Rigid Pavement Distresses in North Carolina

Pavement Type	Performance Measure	Measuring Unit	Failure Point (Maintenance Trigger)	Sensitivity	
				% of Failure Point	Threshold
Asphalt Concrete	IRI	inch/mile	140	10	14
	Total rutting	inches	0.5	20	0.1 inch
	Alligator cracking	% lane area	10	10	1% of lane
	Longitudinal cracking is considered by NCDOT as light severity alligator cracking.	feet/mile	2,640 (50% of section length)	10	264 feet/mile
JPCP	IRI	inch/mile	140	10	14
	Faulting	inches	0.5	20	0.1 inch
	Slabs cracked	percent	15	20	3%

1.6 MEPDG Graphical User Interface

For effective and successful pavement design, users must become familiar with the MEPDG graphical user interface (GUI) and the elements that it includes. Once users click the OK button in the Create New Project window, the MEPDG GUI shown in FIGURE 1.2 appears. The MEPDG GUI is divided into six windows, as labeled in FIGURE 1.2. Windows 1, 2, and 6 are static; that is, the information displayed in these windows does not change when a project run is being executed. Windows 3 and 4, on the other hand, have a dynamic content that changes with the progression of a project run.

General project information, failure criteria, and reliability criteria are entered in Window 1. Traffic, climatic, and pavement structure information are entered in Window 2. Window 3 displays a summary of the input and output files, which changes as more output files are generated. Window 4 shows the analysis status and percentage complete during each MEPDG run. An especially useful feature of Window 4 is that it displays not only the percentage complete, but also the remaining time, which is relatively accurate. Window 5 displays general project information that gives at-a-glance information about the type of design, design life, selected climate, project construction year, traffic opening data and initial AADTT. Users who are operating multiple computers to run multiple designs simultaneously often benefit the most from the information displayed in Window 5. Window 6 displays static information about the measurement system selected, the analysis type, whether or not Excel output has been selected, and whether or not warnings have been enabled. Warnings can be disabled by selecting Expert Mode from the Tools menu. FIGURE 1.2 illustrates a screen capture of the MEPDG GUI showing different color boxes.

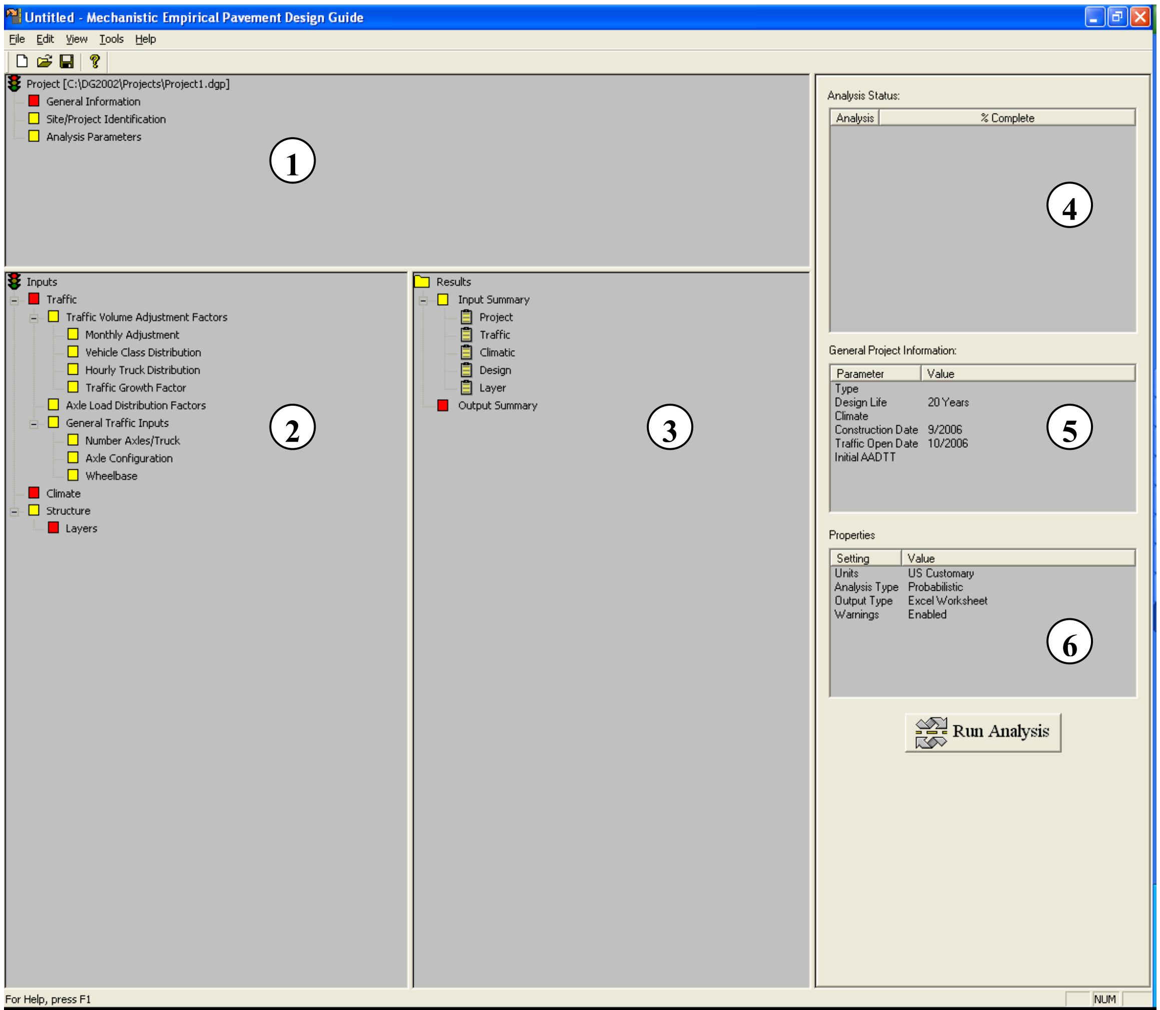

FIGURE 1.2 A screen capture of the MEPDG GUI showing the six available windows.

FIGURE 1.3 shows a closer look at Windows 1 and 2, i.e., the windows through which users input all required files, and includes explanations of the colors. For example, a red box indicates that information is missing and must be supplied by users before the MEPDG can be executed. A yellow box beside an input parameter indicates that a national default value can be used for this input. Before the MEPDG can be executed, all boxes must be green. For red boxes to change to green, users must enter the required inputs. For yellow boxes to change to green, users must at least visit these default inputs to approve them or change them if users decide to use different values.

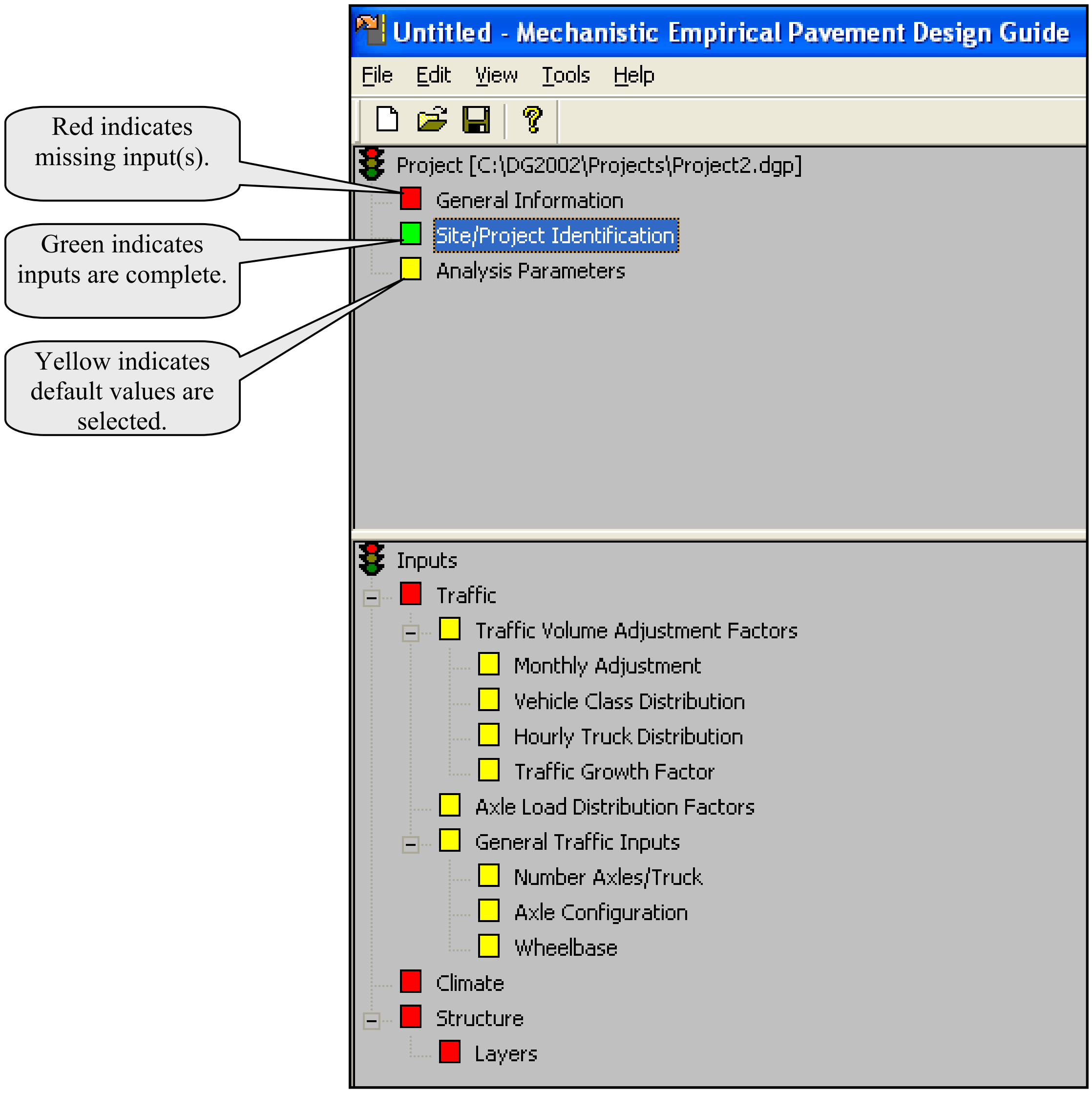

FIGURE 1.3 A screen capture for part of the MEPDG interface showing only the main input categories.

1.7 Document Organization

The inputs required to run the MEPDG are presented in detail for each of the input levels, when applicable, in Section 1.4 of this *North Carolina MEPDG User Reference Guide*. Chapters 2 through 6 provide a step-by-step procedure to help users effectively select, enter and/or import the required parameters for a specific design. To aid users in better understanding the procedure, screen captures from the MEPDG have been captured and presented for almost all the windows that users would encounter while using the software. As a reminder, all work presented in this document has been conducted using MEPDG Version 1.1. It is expected that DARWin-ME™ will have a different GUI. However, understanding the material presented in this Guide will assist users in adapting easily to the new GUI in DARWin-ME™.

Chapter 2 presents the steps that users must follow to populate the project and performance reliability data for a given design project. Because almost all required inputs are entered through the GUI, Chapter 2 also introduces the various elements of the GUI with which users should become familiar. Chapter 3 presents the detailed procedure for populating traffic, vehicle, and road geometry information. Chapter 4 guides users in determining and entering geographic coordinates, elevation, depth of water table and climatic information for a given design project. Chapter 5 provides a step-by-step procedure for populating structural information and thermal cracking information for flexible pavement design. Chapter 6 presents a detailed procedure for entering material-specific rutting and alligator cracking model *k* values and a detailed procedure for entering the local calibration factors for the rutting and alligator cracking models for flexible pavement design.

CHAPTER 2 PROJECT AND PERFORMANCE RELIABILITY

2.1 Selection of Project Name, Directory, and Measurement System

The first window that appears after selecting the New option from the File menu is the Create New Project window, shown in FIGURE 2.1. Users are prompted to type a project name and select the directory in which they want to save their project information. A directory named Projects is created automatically in the DG2002 folder upon installing the MEPDG. Typically, all project information is stored in folders within the Projects folder. The path to the directory is typically C:\DG2002\Projects, but users can select any other directory location. Users should also select a measurement system to use in their design project. At the time of writing, the only available option in MEPDG version 1.1 is the US Customary unit system. As mentioned earlier, even when the US Customary measurement system is selected, there are some parameters that nonetheless must be entered in metric units.

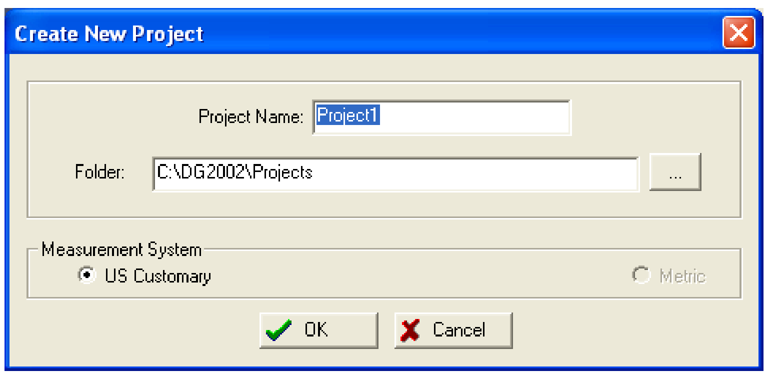

FIGURE 2.1 First window that appears when selecting a new MEPDG project.

2.2 Selecting the Type of Design and Construction and Traffic Opening Dates

In Window 1 of the GUI, double clicking General Information opens the General Information window shown in FIGURE 2.2. The General Information window is presented in FIGURE 2.2 to show the options available for different overlay designs. In the General Information window, the project name has been pre-entered from Section 2.1. Users are required to choose the desired pavement design life (or service life) in years from a drop-down menu. The General Information window requires users also to select the type of design from three categories: New Pavement, Restoration, and Overlay Design. Under the New Pavement option, users can select flexible pavement, JPCP (jointed plain concrete pavement), or CRCP (continuously reinforced concrete pavement).

[Note: in a meeting with Dr. Judith Corley-Lay and Mr. Neil Mastin from the NCDOT PMU on February 22, 2009, the research team was informed that the NCDOT is phasing out all CRCP pavements and does not intend to build CRCP pavements in North Carolina in the future.]

Note also that, as mentioned previously, the scope of this document is flexible pavement design. JPCP is not part of the local calibration project and should be investigated separately.

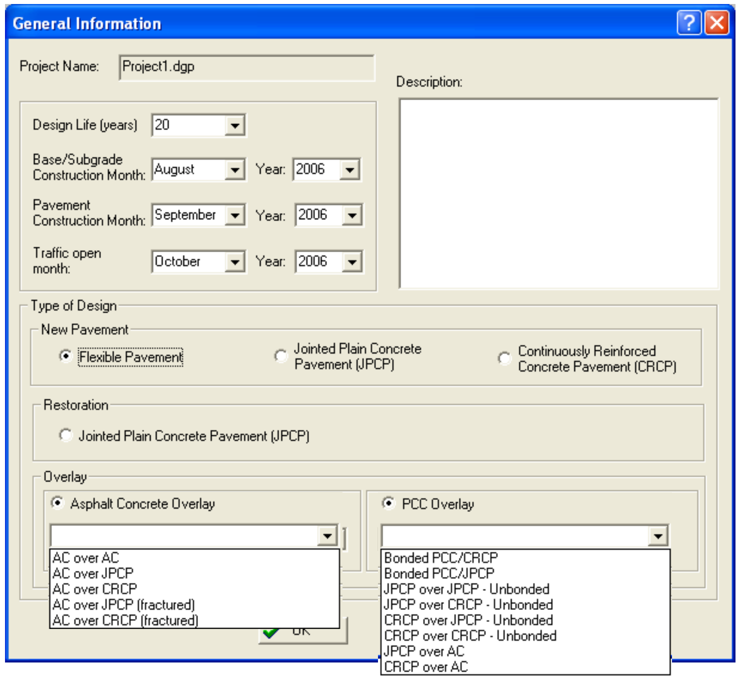

FIGURE 2.2 A screen capture of the *General Information* window in the MEPDG.

For asphalt concrete (AC) overlay design, FIGURE 2.2 shows five options: AC over AC, AC over JPCP, AC over CRCP, AC over JPCP (fractured), or AC over CRCP (fractured). For PCC (Portland cement concrete) overlay design, FIGURE 2.2 displays eight options: Bonded PCC/CRCP, Bonded PCC/JPCP, JPCP over JPCP – Unbonded, JPCP over CRCP – Unbonded, CRCP over JPCP – Unbonded, CRCP over CRCP – Unbonded, JPCP over AC, and CRCP over AC.

FIGURE 2.2 indicates also that users are required to enter construction dates and traffic opening dates. For new flexible pavement design, users must enter construction dates for both the base/subgrade layer and the asphalt layer(s). When an overlay design option is selected, users must enter construction dates for the existing pavement and for the pavement overlay. For new JPCP and CRCP pavement design, users must enter only the rigid pavement construction date. Construction dates for the different layers are required by the Enhanced Integrated Climatic Module (EICM) in the MEPDG to account for the effects of temperature and moisture profiles on unbound and bound materials. The EICM begins to calculate these effects even before the pavement is opened to traffic. At this time, the MEPDG evaluates only nonload-associated distresses. Thus, users should enter the date information as accurately as possible.

To accommodate traffic more efficiently, the NCDOT's current practice allows for partially-built sections to be opened to traffic. Partially-built sections are sections that have all the layers constructed except the surface layer (also called the wearing course). The reason for delaying construction of the surface layer is that the process of removing pavement markings causes deterioration of the final pavement surface. The NCDOT prefers that the final surface layer is paved for the project in its entirety immediately prior to opening the completed project to traffic and after permanently marking the pavement. According to Dr. Judith Corley-Lay from the PMU, the time window between opening partially-built pavement sections to traffic and the construction of the final surface layer ranges from a couple of months to several months, depending primarily on the size of the project.

The time difference between traffic opening on partially-built pavement sections and on a fully-built pavement cannot be handled in the current version of the MEPDG because users can enter only a single date for pavement construction. Therefore, considering the relative short time window between partially-built and fully-built pavements, the research team recommends that when entering the pavement construction date, users enter the date for the final completed pavement and not for the partially-built pavement sections.

2.3 Entering Project Location, Identification, Milepost, and Traffic Direction

In Window 1 of the GUI, double clicking *Site/Project Identification* opens the window shown in FIGURE 2.3.

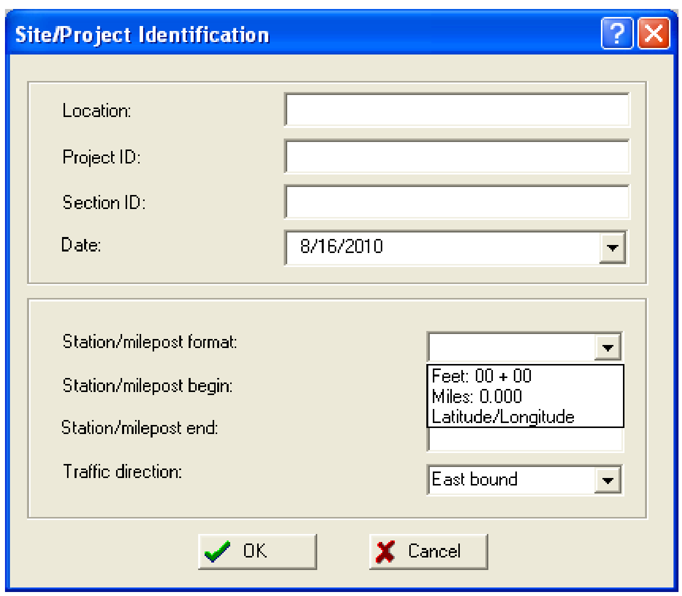

FIGURE 2.3 A screen capture of the *Site/Project Identification* window in the MEPDG.

The *Site/Project Identification* window allows users to enter the project identification number (ID), section ID, mileposts for the beginning and end of the project, and traffic direction. As per the information presented in TABLE 1.1, the information to be entered in the *Site/Project Identification* window is optional; that is, the MEPDG will accept empty fields.

2.4 Entering Limits and Reliability for Different Performance Measures

FIGURE 2.4, FIGURE 2.5, and FIGURE 2.6 are screen captures of the *Analysis Parameters* window and show the default performance limits and reliability for flexible pavements, JPCP, and CRCP, respectively.

The performance measures available will automatically change based on the selected type of design. Users can select or deselect any or all of the performance measures, as desired. In addition, users can change the initial default International Roughness Index (IRI) to reflect local construction practices. The purpose of the *Analysis Parameters* window is to give users a Pass/Fail result at the end of a MEPDG run by comparing entered performance limits to those predicted by the MEPDG. Users can choose to do this comparison manually because the MEPDG generates Excel files with all predicted distresses by default. TABLE 1.6 summarizes the failure criteria adopted by the NCDOT.

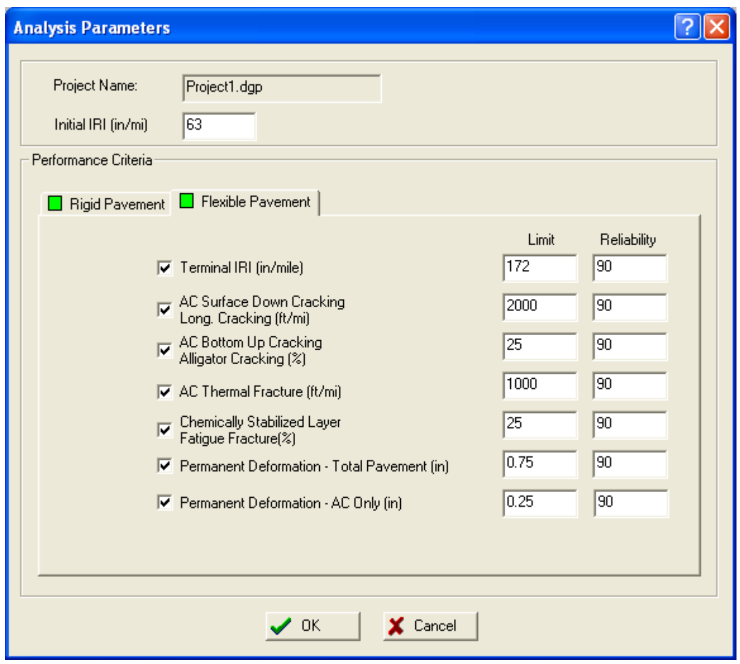

FIGURE 2.4 A screen capture of the *Analysis Parameters* window in the MEPDG: *Flexible Pavement*.

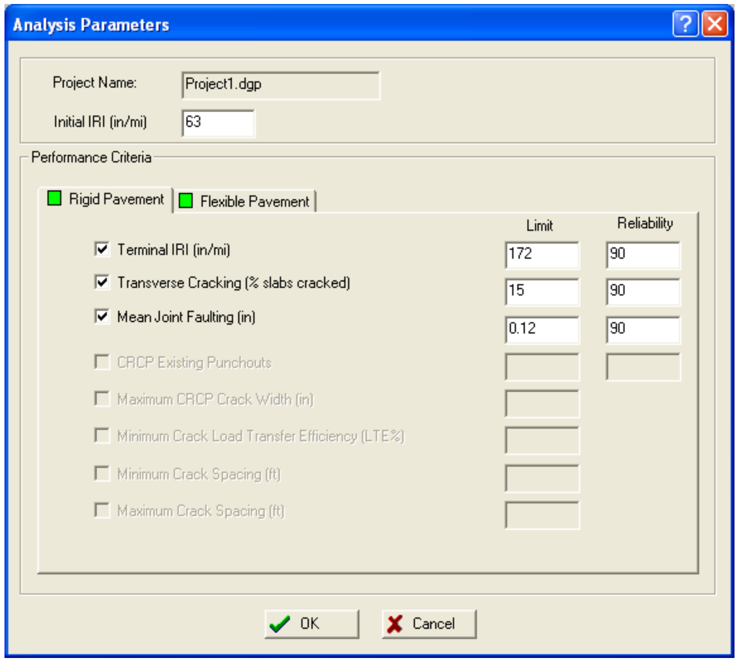

FIGURE 2.5 A screen capture of the *Analysis Parameters* window in the MEPDG: JPCP.

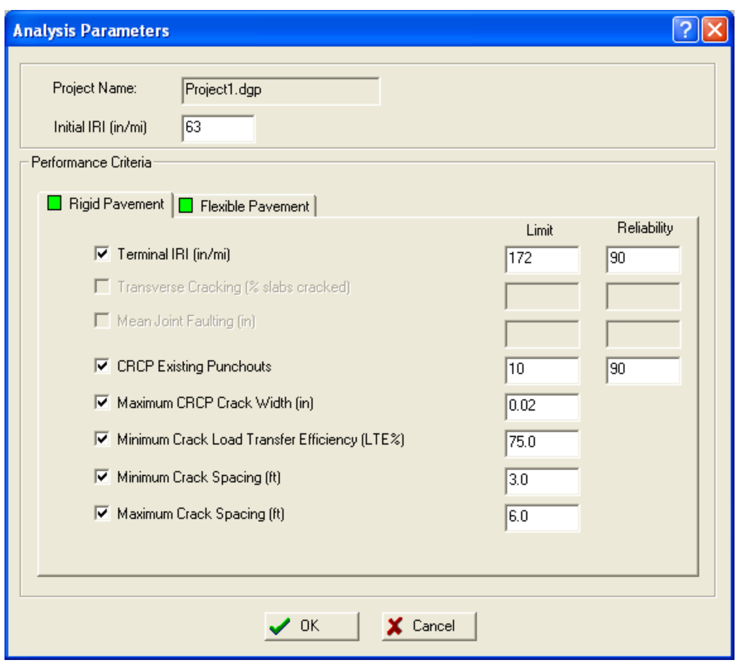

FIGURE 2.6 A screen capture of the *Analysis Parameters* window in the MEPDG: CRCP.

CHAPTER 3 TRAFFIC, VEHICLE, AND LOAD GEOMETRY

3.1 FHWA Vehicle Classification

Before presenting the design steps that involve traffic information, it is vital for users to know that the MEPDG considers in its calculations only heavy vehicles in Federal Highway Administration (FHWA) vehicle classes 4 through 13. That is, motorcycles, passenger cars, and four-tire single-unit vehicles are all excluded, so their effect on pavement performance is not included. FIGURE 3.1 shows the FHWA vehicle classification scheme F.

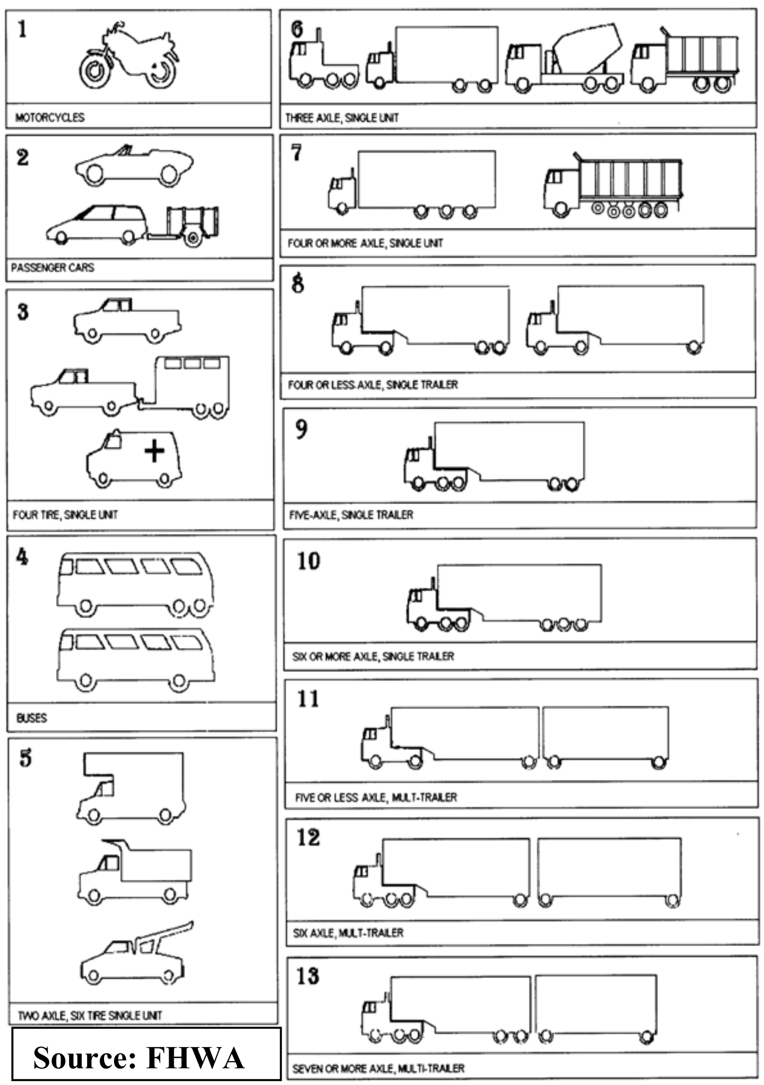

FIGURE 3.1 FHWA vehicle classification scheme F.

3.2 Truck Information and Road Geometry

In Window 2 of the GUI, double clicking *Traffic* opens the main *Traffic* window shown in FIGURE 3.2. The *Traffic* main window has links to all the traffic information needed to run the MEPDG. In addition to these links, users can directly enter values for five traffic parameters: the initial two-way AADTT, number of lanes in the design direction, percentage of trucks in the design direction, percentage of trucks in the design lane, and the vehicle operational speed.

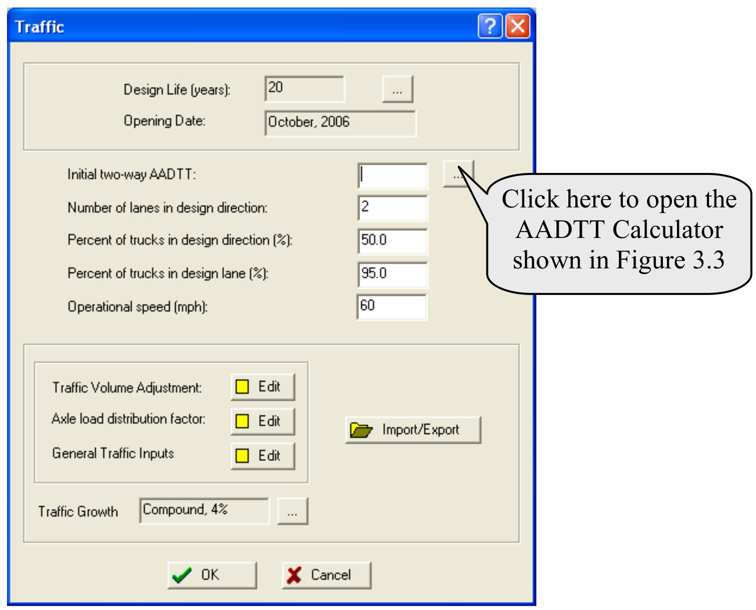

FIGURE 3.2 A screen capture of the main *Traffic* window in the MEPDG.

FIGURE 3.2 and FIGURE 3.3 show that users have the option either to enter the AADTT directly, or enter the AADT and percentage of vehicle class 4 or higher and use the *AADTT Calculator*, shown in FIGURE 3.3, to calculate the AADTT. FIGURE 3.2 also allows access to other traffic input tables including traffic volume adjustment factors, axle load distribution factors and the general traffic inputs.

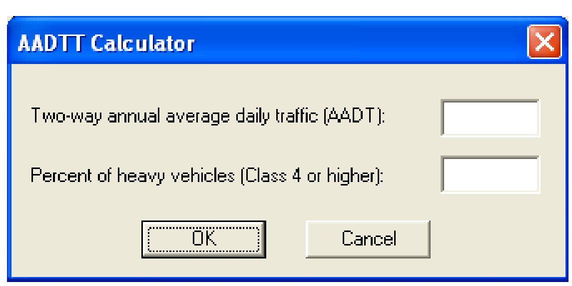

FIGURE 3.3 A screen capture of the *AADTT Calculator* window in the MEPDG.

TABLE 3.1 is a summary of the source and potential suppliers of the traffic parameters required for the *Traffic* window shown in FIGURE 3.2. In addition, TABLE 3.1 suggests alternative source(s) if local data are unavailable.

TABLE 3.1 Source and Suppliers of the Traffic Inputs Found under the Traffic Main Window*

Traffic Input	Where to Find It? / Supplier
Initial two-way AADTT, or AADT and percentage of heavy vehicles class 4 or higher	Supplied by the Traffic Survey Unit (TSU)
Number of lanes in design direction	Supplied by the Traffic Planning Branch (TPB) The MEPDG default value is 2.
Percentage of trucks in design direction	Site-specific data typically are supplied by the TPB Forecast Unit. If site-specific data are unavailable, national default values can be used. Default values must be selected based on the predominant type of vehicle that uses the roadway, as follows: • Class 4, except for local or municipal routes, use 50% • Class 4, for local or municipal routes, use 80%-100% • Classes 5, 6, 7, use 62% • Classes 8, 9, 10, use 55% • Classes 11, 12, 13, use 50% The MEPDG default value is 50%.
Percentage of trucks in design lane (Lane Distribution Factor, or LDF)	Site-specific LDFs that are determined from WIM, AVC, or vehicle count data (Level 1) or state-wide averages that are also determined from WIM, AVC, or vehicle count data (Level 2), typically are provided by the TSU. If local data are unavailable, the following national default values, which are based on Class 9 vehicles, can be used: • Single-lane roadways in one direction, use 100% • Two-lane roadways in one direction, use 90% • Three-lane roadways in one direction, use 60% • Four-lane roadways in one direction, use 45% The MEPDG default value is 95%.
Operational speed	Supplied by the PMU – Pavement Design Unit. This value can be found in the TRB Highway Capacity Manual. The MEPDG default value is 60 mph.

*National default values presented in this table were obtained from the NCHRP 1-37A documentation (4).

3.3 Traffic Volume Adjustment Factors

In Window 2 of the GUI, double clicking *Traffic Volume Adjustment Factors* opens the window shown in FIGURE 3.4. The *Traffic Volume Adjustment Factors* window allows users to account for two variables. First, users can account for changes in traffic count throughout the day and different seasons as well as changes in traffic count due to traffic growth. Second, users can control the contribution of the different vehicle classes to the total traffic, which is a critical factor given that various vehicles and axle configurations have different effects on pavement performance.

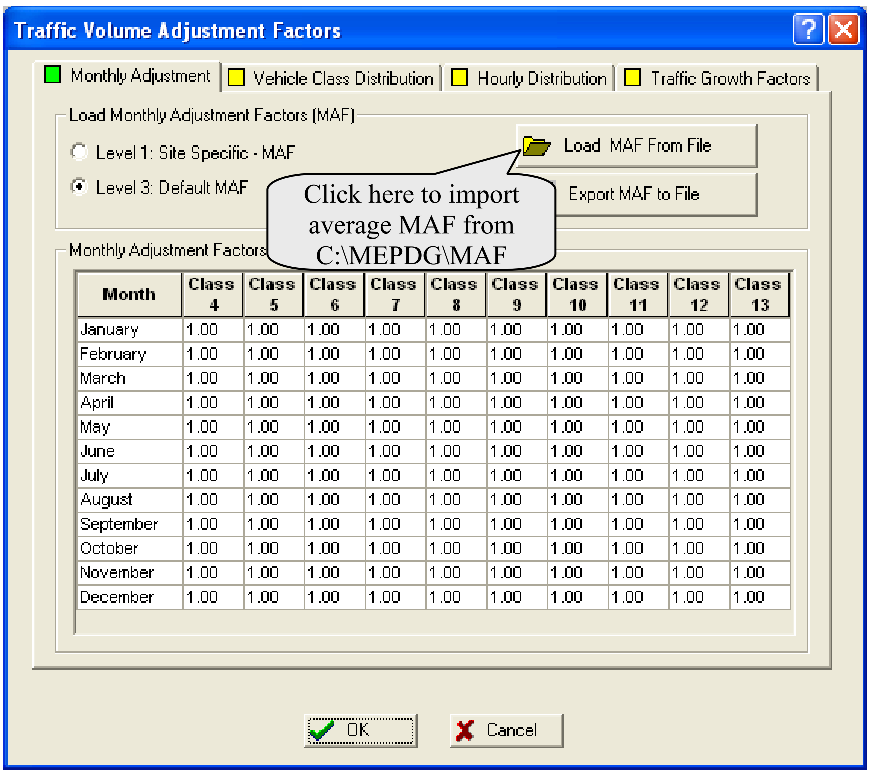

FIGURE 3.4 A screen capture of the *Traffic Volume Adjustment Factors* window in the MEPDG: *Monthly Adjustment Factors* input table.

Users can adjust the following four factors:

- Monthly adjustment factors (MAF);
- Vehicle class distribution (VCD)factors;
- Hourly distribution factors (HDF); and
- Traffic growth factor(s).

3.3.1 Monthly Adjustment Factors (MAF)

3.3.1.1 Background

Monthly adjustment factors (MAF) account for seasonal changes in traffic volume. A sensitivity analysis that utilizes more than 40 typical flexible pavement and JPCP sections in North Carolina suggests that different MAF clusters result in insignificant differences in predicted pavement performance. This finding allows state-wide averages of MAF factors to be used in the MEPDG. MAF are assumed to be similar for different vehicle classes; that is, the percentage of seasonal change in vehicle count for the different classes is similar for all the classes. FIGURE 3.4 is a screen capture of the MAF input table in the *Traffic Volume Adjustment Factors* window in the MEPDG.

3.3.1.2 Implementation

TABLE 3.2 is a summary of state-wide average MAF that are recommended for use in the MEPDG. Users have two options for entering MAF. First, users may enter the data manually through the MEPDG MAF table shown in FIGURE 3.4. Second, users may directly import a MAF file located under C:\MEPDG\MAF. To open Windows Explorer and select the MAF file, users should click the *Load MAF from File* button shown in FIGURE 3.4.

TABLE 3.2 Recommended Values for Monthly Adjustment Factors (MAF)

Month	Class 4	Class 5	Class 6	Class 7	Class 8	Class 9	Class 10	Class 11	Class 12	Class 13
January	0.91	0.91	0.91	0.91	0.91	0.91	0.91	0.91	0.91	0.91
February	0.96	0.96	0.96	0.96	0.96	0.96	0.96	0.96	0.96	0.96
March	1.01	1.01	1.01	1.01	1.01	1.01	1.01	1.01	1.01	1.01
April	1.04	1.04	1.04	1.04	1.04	1.04	1.04	1.04	1.04	1.04
May	1.03	1.03	1.03	1.03	1.03	1.03	1.03	1.03	1.03	1.03
June	1.07	1.07	1.07	1.07	1.07	1.07	1.07	1.07	1.07	1.07
July	1.00	1.00	1.00	1.00	1.00	1.00	1.00	1.00	1.00	1.00
August	1.03	1.03	1.03	1.03	1.03	1.03	1.03	1.03	1.03	1.03
September	1.01	1.01	1.01	1.01	1.01	1.01	1.01	1.01	1.01	1.01
October	1.05	1.05	1.05	1.05	1.05	1.05	1.05	1.05	1.05	1.05
November	0.97	0.97	0.97	0.97	0.97	0.97	0.97	0.97	0.97	0.97
December	0.93	0.93	0.93	0.93	0.93	0.93	0.93	0.93	0.93	0.93

3.3.2 Vehicle Class Distribution (VCD) Factors

3.3.2.1 Background

Vehicle class distribution (VCD) factors distribute heavy vehicle counts over the ten available FHWA vehicle classes 4 through 13. FIGURE 3.5 is a screen capture showing the VCD input table in the *Traffic Volume Adjustment Factors* window in the MEPDG.

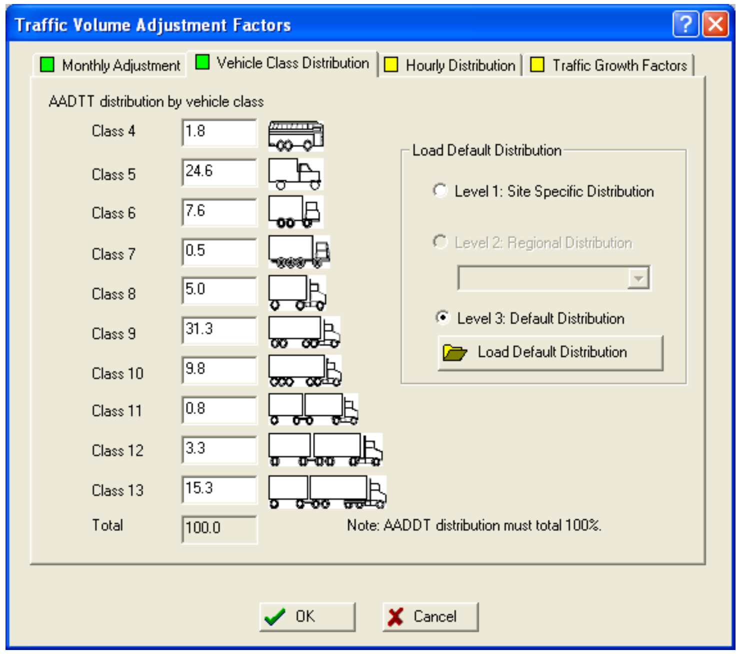

FIGURE 3.5 A screen capture of the *Traffic Volume Adjustment Factors* window in the MEPDG: *Vehicle Class Distribution* factors input table.

In contrast to MAF, VCD clusters differ significantly in their effect on pavement performance. Hence, the use of state-wide averages is not an option. A proposed methodology developed under NCDOT project HWY-22 2008-11 (5) is recommended for determining the VCD factors. The proposed methodology calls for utilizing 48-hour classification counts in conjunction with decision trees that were developed to guide the selection of seasonal factors. Seasonal factors are used to annualize the 48-hour class counts while accounting for the variation in VCD over different days of the week and different months (seasons). Two decision trees have been developed, one for single-unit (SU) vehicles (FHWA Class 4 - 7) and another for multi-unit (MU) vehicles (FHWA Class 8 - 13). FIGURE 3.6 and FIGURE 3.7 show the two decision trees that were developed for selecting the appropriate seasonal factors group for single-unit and multi-unit trucks, respectively. TABLE 3.3 and TABLE 3.4 summarize the seasonal factors developed for single-unit and multi-unit trucks, respectively.

3.3.2.2 Implementation

To facilitate the process of generating VCD factors for a selected location, the research team developed an Excel-based tool that requires few inputs. The tool integrates two decision trees, shown in FIGURE 3.6 and FIGURE 3.7, in addition to seasonal factors group data, shown in TABLE 3.3 and TABLE 3.4. Both the decision trees and seasonal factors data were developed under NCDOT project HWY-22 2008-11 (5).

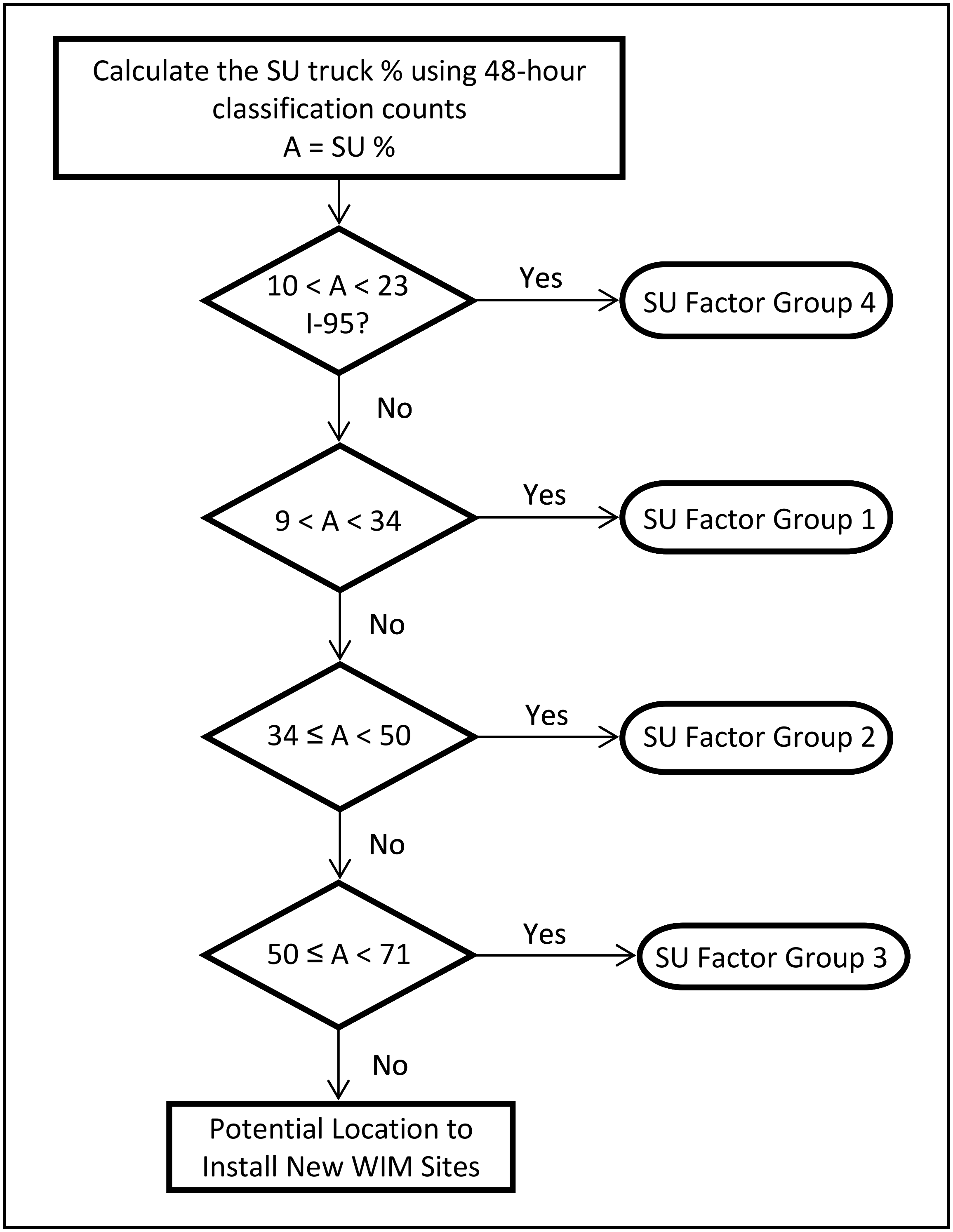

FIGURE 3.6 Decision tree to determine single-unit seasonal factors.

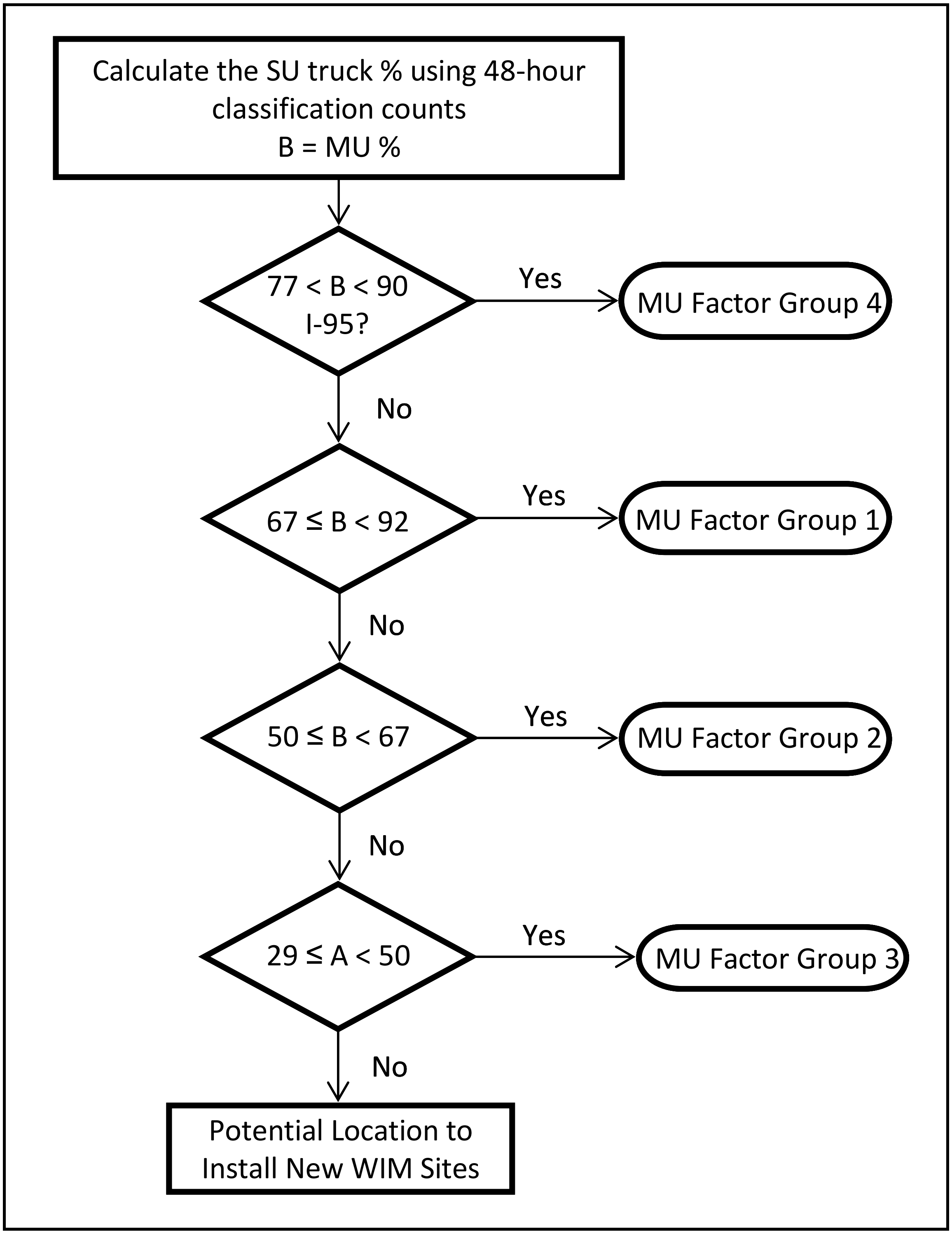

FIGURE 3.7 Decision tree to determine multi-unit seasonal factors.

TABLE 3.3 Seasonal Factors Developed for Single-Unit Trucks,
Vehicle Classes 4, 5, 6 and 7

Seasonal Factors														
Seasonal Factor Group	January							July						
	Sun	Mon	Tue	Wed	Thu	Fri	Sat	Sun	Mon	Tue	Wed	Thu	Fri	Sat
SU-SFG-1	3.03	0.91	0.87	0.87	0.83	0.87	2.05	2.13	0.81	0.82	0.81	0.78	0.79	1.61
SU-SFG-2	3.58	0.89	0.85	0.84	0.81	0.86	2.02	2.80	0.79	0.79	0.80	0.77	0.79	1.72
SU-SFG-3	3.90	0.95	0.93	0.92	0.87	0.89	2.00	3.06	0.79	0.78	0.79	0.76	0.78	1.65
SU-SFG-4	1.41	1.09	1.10	1.16	1.04	1.00	1.23	1.01	1.00	1.05	1.08	0.93	0.82	0.90
	February							August						
	Sun	Mon	Tue	Wed	Thu	Fri	Sat	Sun	Mon	Tue	Wed	Thu	Fri	Sat
SU-SFG-1	2.78	0.91	0.87	0.85	0.90	0.85	1.84	2.27	0.84	0.80	0.80	0.78	0.81	1.65
SU-SFG-2	3.19	0.94	0.84	0.84	0.89	0.83	1.80	2.71	0.84	0.81	0.79	0.78	0.80	1.69
SU-SFG-3	3.54	0.88	0.86	0.88	0.86	0.87	1.89	2.96	0.81	0.80	0.80	0.76	0.81	1.71
SU-SFG-4	1.18	0.96	1.07	1.04	1.00	0.87	1.01	1.11	1.10	1.06	1.06	0.96	0.92	1.03
	March							September						
	Sun	Mon	Tue	Wed	Thu	Fri	Sat	Sun	Mon	Tue	Wed	Thu	Fri	Sat
SU-SFG-1	2.52	0.83	0.85	0.82	0.81	0.81	1.78	2.35	0.86	0.86	0.82	0.79	0.80	1.70
SU-SFG-2	2.99	0.91	0.81	0.83	0.80	0.81	1.87	2.92	0.84	0.86	0.83	0.79	0.80	1.78
SU-SFG-3	3.44	0.82	0.83	0.85	0.81	0.81	1.87	3.07	0.87	0.83	0.83	0.79	0.78	1.74
SU-SFG-4	1.01	0.94	1.03	0.99	0.83	0.76	0.88	1.32	1.13	1.12	1.08	1.02	0.93	1.17
	April							October						
	Sun	Mon	Tue	Wed	Thu	Fri	Sat	Sun	Mon	Tue	Wed	Thu	Fri	Sat
SU-SFG-1	2.37	0.84	0.84	0.81	0.77	0.78	1.68	2.10	0.82	0.82	0.80	0.77	0.78	1.67
SU-SFG-2	2.82	0.84	0.80	0.79	0.76	0.79	1.77	2.65	0.83	0.80	0.83	0.76	0.79	1.62
SU-SFG-3	3.03	0.82	0.83	0.80	0.76	0.79	1.71	2.82	0.78	0.77	0.78	0.74	0.75	1.51
SU-SFG-4	0.99	0.96	1.03	0.96	0.85	0.78	0.85	1.11	1.01	1.05	1.00	0.99	0.90	1.11
	May							November						
	Sun	Mon	Tue	Wed	Thu	Fri	Sat	Sun	Mon	Tue	Wed	Thu	Fri	Sat
SU-SFG-1	2.33	0.83	0.81	0.78	0.76	0.76	1.73	2.34	0.83	0.82	0.83	0.80	0.80	1.68
SU-SFG-2	2.82	0.81	0.77	0.76	0.75	0.78	1.75	2.93	0.83	0.82	0.85	0.82	0.80	1.83
SU-SFG-3	3.10	0.85	0.77	0.79	0.75	0.78	1.74	3.10	0.82	0.82	0.83	0.83	0.81	1.71
SU-SFG-4	1.06	1.04	1.01	1.02	0.90	0.85	1.02	1.07	0.99	1.02	1.02	0.93	0.90	1.06
	June							December						
	Sun	Mon	Tue	Wed	Thu	Fri	Sat	Sun	Mon	Tue	Wed	Thu	Fri	Sat
SU-SFG-1	2.22	0.81	0.81	0.80	0.76	0.77	1.60	2.72	0.86	0.84	0.83	0.85	0.84	1.73
SU-SFG-2	2.79	0.82	0.77	0.79	0.75	0.79	1.73	3.12	0.84	0.82	0.81	0.80	0.80	1.68
SU-SFG-3	2.93	0.79	0.76	0.78	0.77	0.81	1.68	3.47	0.88	0.83	0.86	0.86	0.89	2.00
SU-SFG-4	1.13	1.03	1.04	0.99	0.89	0.85	0.98	1.37	1.13	1.10	1.11	0.99	0.95	1.14

TABLE 3.4 Seasonal Factors Developed for Multi-Unit Trucks, Vehicle Classes 8, 9, 10, 11, 12 and 13

Seasonal Factors														
Seasonal Factor Group	January							July						
	Sun	Mon	Tue	Wed	Thu	Fri	Sat	Sun	Mon	Tue	Wed	Thu	Fri	Sat
MU-SFG-1	3.12	0.90	0.79	0.78	0.77	0.90	2.42	2.74	0.86	0.78	0.78	0.78	0.87	2.31
MU-SFG-2	4.98	0.82	0.80	0.77	0.74	0.85	3.15	4.49	0.78	0.77	0.75	0.75	0.82	2.88
MU-SFG-3	4.53	0.96	0.85	0.86	0.82	0.94	2.63	3.61	0.82	0.78	0.78	0.73	0.81	2.13
MU-SFG-4	1.51	1.07	0.80	0.85	0.82	1.01	1.44	1.55	1.07	0.87	0.85	0.86	1.02	1.56
	February							August						
	Sun	Mon	Tue	Wed	Thu	Fri	Sat	Sun	Mon	Tue	Wed	Thu	Fri	Sat
MU-SFG-1	2.86	0.90	0.77	0.76	0.81	0.90	2.28	2.72	0.85	0.75	0.74	0.75	0.84	2.20
MU-SFG-2	4.47	0.84	0.77	0.74	0.82	0.84	3.02	4.40	0.79	0.74	0.72	0.72	0.79	2.68
MU-SFG-3	4.18	0.86	0.80	0.86	0.83	0.88	2.40	3.33	0.84	0.77	0.79	0.73	0.82	2.21
MU-SFG-4	1.48	1.05	0.79	0.76	0.85	1.01	1.43	1.60	1.09	0.81	0.82	0.86	1.04	1.59
	March							September						
	Sun	Mon	Tue	Wed	Thu	Fri	Sat	Sun	Mon	Tue	Wed	Thu	Fri	Sat
MU-SFG-1	2.75	0.85	0.76	0.76	0.76	0.86	2.27	2.84	0.84	0.78	0.75	0.74	0.84	2.16
MU-SFG-2	4.44	0.83	0.77	0.76	0.77	0.82	2.96	4.41	0.76	0.77	0.75	0.73	0.79	2.75
MU-SFG-3	3.97	0.78	0.75	0.75	0.72	0.81	2.34	3.50	0.89	0.78	0.79	0.74	0.81	2.10
MU-SFG-4	1.50	1.05	0.80	0.80	0.85	1.04	1.49	1.51	1.04	0.80	0.78	0.81	1.01	1.50
	April							October						
	Sun	Mon	Tue	Wed	Thu	Fri	Sat	Sun	Mon	Tue	Wed	Thu	Fri	Sat
MU-SFG-1	2.81	0.85	0.75	0.74	0.74	0.85	2.24	2.68	0.85	0.75	0.74	0.74	0.84	2.17
MU-SFG-2	4.50	0.78	0.74	0.75	0.74	0.81	3.05	4.28	0.77	0.73	0.74	0.73	0.80	2.77
MU-SFG-3	3.57	0.79	0.77	0.76	0.71	0.80	2.13	3.30	0.80	0.76	0.76	0.71	0.80	2.07
MU-SFG-4	1.43	1.02	0.79	0.76	0.80	1.01	1.38	1.42	1.00	0.77	0.76	0.82	0.97	1.43
	May							November						
	Sun	Mon	Tue	Wed	Thu	Fri	Sat	Sun	Mon	Tue	Wed	Thu	Fri	Sat
MU-SFG-1	2.74	0.85	0.75	0.73	0.74	0.84	2.22	2.72	0.84	0.75	0.75	0.74	0.84	2.20
MU-SFG-2	4.56	0.76	0.73	0.72	0.73	0.80	2.83	4.24	0.77	0.75	0.77	0.77	0.82	2.95
MU-SFG-3	3.70	0.84	0.74	0.76	0.72	0.78	2.18	3.51	0.82	0.78	0.78	0.76	0.82	2.34
MU-SFG-4	1.37	0.97	0.74	0.74	0.77	0.95	1.34	1.40	1.00	0.76	0.75	0.79	0.96	1.35
	June							December						
	Sun	Mon	Tue	Wed	Thu	Fri	Sat	Sun	Mon	Tue	Wed	Thu	Fri	Sat
MU-SFG-1	2.71	0.84	0.76	0.75	0.74	0.84	2.12	2.74	0.88	0.77	0.74	0.77	0.86	2.18
MU-SFG-2	4.13	0.77	0.75	0.72	0.72	0.79	2.66	4.46	0.81	0.78	0.76	0.77	0.82	2.83
MU-SFG-3	3.32	0.80	0.74	0.77	0.72	0.80	2.06	4.51	0.92	0.82	0.85	0.88	0.96	2.68
MU-SFG-4	1.44	1.02	0.76	0.75	0.80	0.97	1.38	1.37	1.02	0.74	0.75	0.81	0.98	1.37

FIGURE 3.8 is a screen capture showing the *VCD Generator & ALDF Cluster Selector* tool. This tool is also capable of selecting the most accurate axle load distribution factors (ALDF) files, as presented later in this document. The tool includes an operational procedure that is

simple to follow. Users must enter the 48-hour counts for each vehicle class 4 through 13. Users should also select the month and the days that the counts were recorded. In addition, users are required to select whether or not the project is located on Interstate I-95. Based on the entered information, the tool will automatically generate VCD factors that users should enter manually in the VCD table shown in FIGURE 3.5. The tool will also select the most representative ALDF cluster.

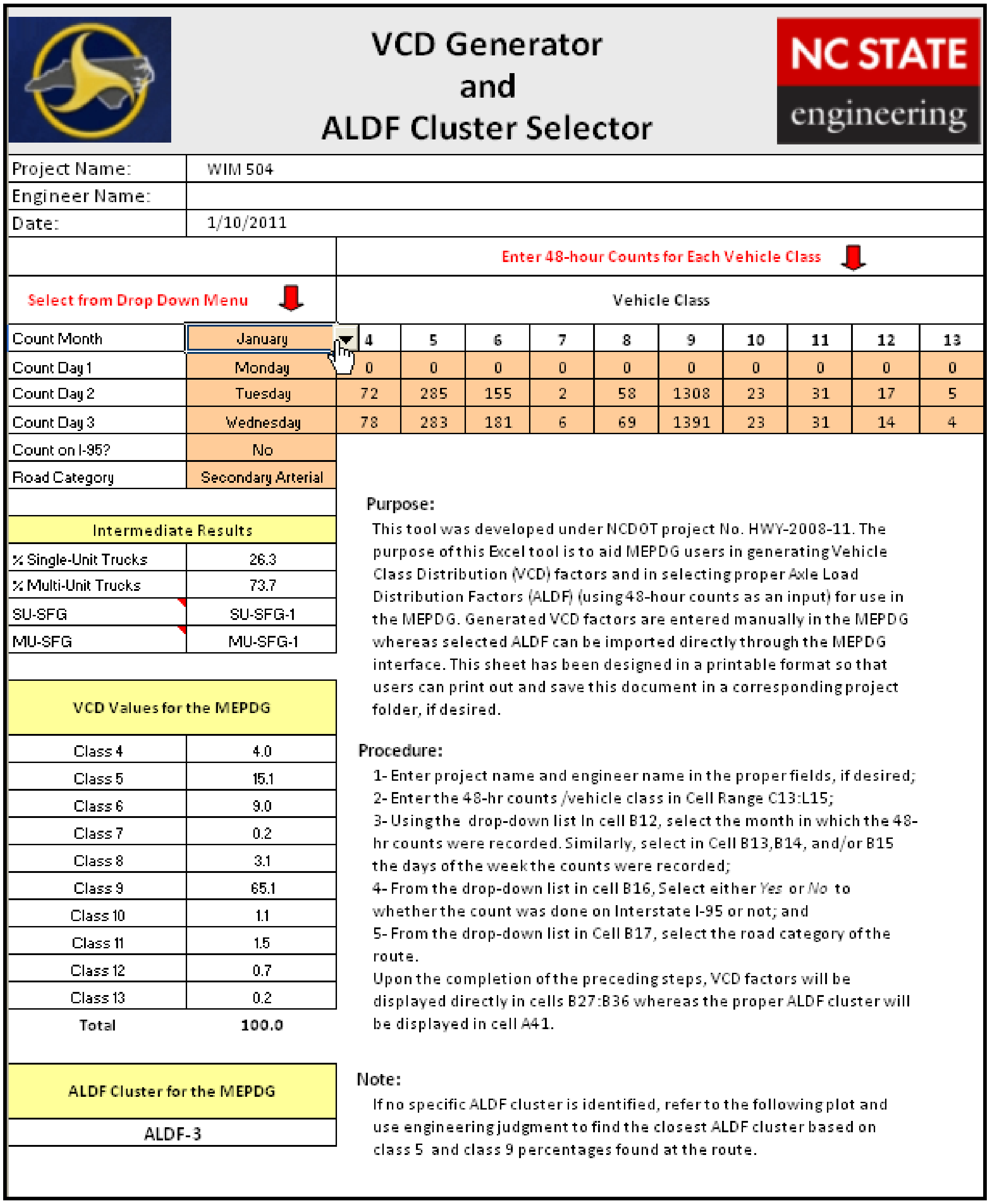

VCD Generator
and
ALDF Cluster Selector

NC STATE engineering

Project Name:	WIM 504
Engineer Name:	
Date:	1/10/2011

Enter 48-hour Counts for Each Vehicle Class

Select from Drop Down Menu

		Vehicle Class									
Count Month	January	4	5	6	7	8	9	10	11	12	13
Count Day 1	Monday	0	0	0	0	0	0	0	0	0	0
Count Day 2	Tuesday	72	285	155	2	58	1308	23	31	17	5
Count Day 3	Wednesday	78	283	181	6	69	1391	23	31	14	4
Count on I-95?	No										
Road Category	Secondary Arterial										

Intermediate Results	
% Single-Unit Trucks	26.3
% Multi-Unit Trucks	73.7
SU-SFG	SU-SFG-1
MU-SFG	MU-SFG-1

VCD Values for the MEPDG	
Class 4	4.0
Class 5	15.1
Class 6	9.0
Class 7	0.2
Class 8	3.1
Class 9	65.1
Class 10	1.1
Class 11	1.5
Class 12	0.7
Class 13	0.2
Total	**100.0**

ALDF Cluster for the MEPDG
ALDF-3

Purpose:

This tool was developed under NCDOT project No. HWY-2008-11. The purpose of this Excel tool is to aid MEPDG users in generating Vehicle Class Distribution (VCD) factors and in selecting proper Axle Load Distribution Factors (ALDF) (using 48-hour counts as an input) for use in the MEPDG. Generated VCD factors are entered manually in the MEPDG whereas selected ALDF can be imported directly through the MEPDG interface. This sheet has been designed in a printable format so that users can print out and save this document in a corresponding project folder, if desired.

Procedure:

1- Enter project name and engineer name in the proper fields, if desired;
2- Enter the 48-hr counts /vehicle class in Cell Range C13:L15;
3- Using the drop-down list In cell B12, select the month in which the 48-hr counts were recorded. Similarly, select in Cell B13,B14, and/or B15 the days of the week the counts were recorded;
4- From the drop-down list in cell B16, Select either *Yes* or *No* to whether the count was done on Interstate I-95 or not; and
5- From the drop-down list in Cell B17, select the road category of the route.
Upon the completion of the preceding steps, VCD factors will be displayed directly in cells B27:B36 whereas the proper ALDF cluster will be displayed in cell A41.

Note:

If no specific ALDF cluster is identified, refer to the following plot and use engineering judgment to find the closest ALDF cluster based on class 5 and class 9 percentages found at the route.

FIGURE 3.8 A screen capture of the *VCD Generator and ALDF Cluster Selector* tool.

3.3.3 Hourly Distribution Factors (HDF)

3.3.3.1 Background / Implementation

Hourly distribution factors (HDF) account for changes in truck distributions throughout the hour. A sensitivity analysis that utilizes 44 typical flexible pavement and JPCP sections in North Carolina suggests that different HDF clusters result in insignificant differences in predicted pavement performance. Hence, a state-wide average formula for HDF was developed and is recommended for use in the MEPDG. FIGURE 3.9 is a screen capture of the HDF input table in the MEPDG. TABLE 3.5 is a summary of state-wide averages for HDF. Users should manually replace the default HDF values shown in FIGURE 3.9 with local data shown in TABLE 3.5.

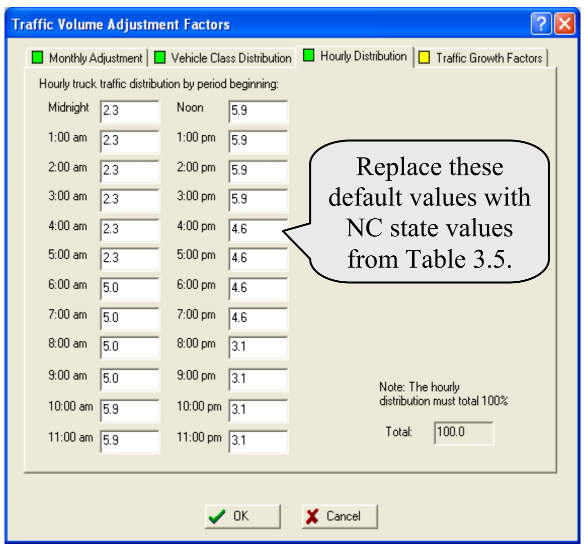

FIGURE 3.9 A screen capture of the *Traffic Volume Adjustment Factors* window in the MEPDG: *Hourly Distribution Factors* input window.

TABLE 3.5 Recommended State-Wide Averages for Hourly Truck Distribution Factors

Midnight	1.63	Noon	6.48
1:00 am	1.51	1:00 pm	6.41
2:00 am	1.64	2:00 pm	6.23
3:00 am	2.00	3:00 pm	5.87
4:00 am	2.63	4:00 pm	5.30
5:00 am	3.66	5:00 pm	4.55
6:00 am	4.65	6:00 pm	3.74
7:00 am	5.56	7:00 pm	3.15
8:00 am	6.18	8:00 pm	2.73
9:00 am	6.53	9:00 pm	2.42
10:00 am	6.66	10:00 pm	2.12
11:00 am	6.55	11:00 pm	1.79

3.3.4 Traffic Growth Factor(s)

3.3.4.1 Background

Traffic growth factors account for the growth in truck traffic over the pavement design life. The MEPDG offers three traffic growth functions for selection: no growth, linear growth, and compound growth. Additionally, users can choose to enter unique growth factors and functions for each vehicle class or for a group of different vehicle classes, if desired. FIGURE 3.10 shows a screen capture of the *Traffic Growth Functions* input window in the *Traffic Volume Adjustment Factors* window in the MEPDG.

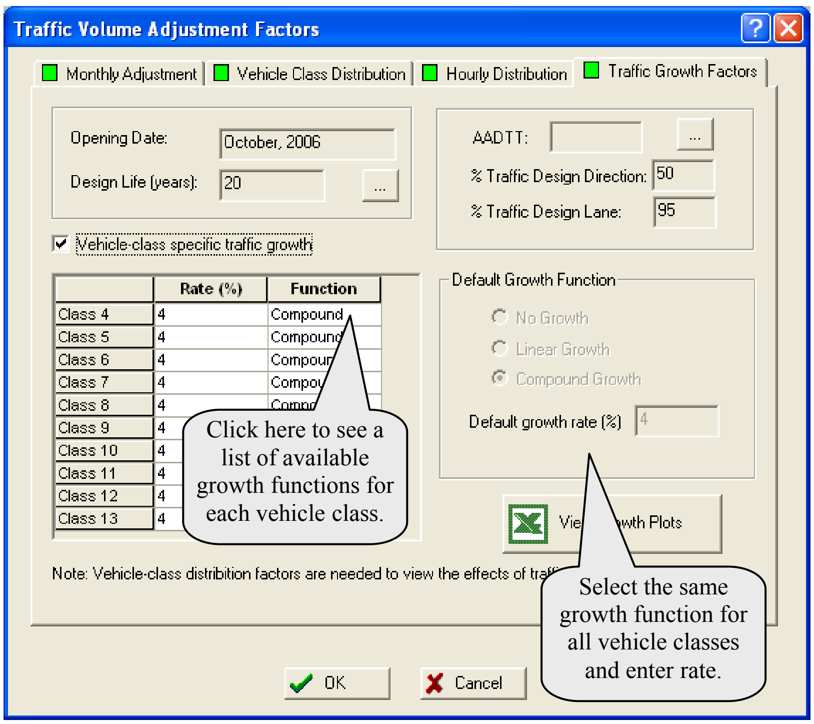

FIGURE 3.10 A screen capture of the *Traffic Volume Adjustment Factors* window in the MEPDG: *Traffic Growth Functions* input window.

3.3.4.2 Implementation

Traffic growth functions and rates typically are supplied by the Traffic Forecasting Group. If a single growth rate is assumed for all vehicle classes, users can simply activate the *Radio* button adjacent to the desired function and then enter the desired growth rate in the *Default Growth Rate* field. If users choose to enter unique growth functions and growth rates for each class or a group of vehicle classes, users can check the box adjacent to *Vehicle Class-Specific Traffic Growth,* and a window will open showing the different vehicle classes, corresponding rates and growth functions, as shown in FIGURE 3.10. Users can select the desired growth function for each of these classes from a drop-down list and overwrite the default rate of 4% with the desired rate. If users choose to have, for example, a similar growth function and rate for single-unit trucks, i.e., classes 4 through 7, they can simply enter the same rate and select the same growth function from the drop-down list for all these vehicle classes.

3.4 Axle Load Distribution Factors (ALDF)

3.4.1 Background

The axle load distribution factors (ALDF) table contains the major required traffic inputs in the MEPDG. The ALDF table provides information about different axle types and associated loads to calculate critical pavement responses, i.e., stresses, strains, and deflections, which, in turn, are used to predict pavement performance. Four axle types are considered in the ALDF table: single, tandem, tridem, and quad. For the single axle, there are 39 axle load bins (groups) that range from 3 kips to 41 kips. For the tandem axle, there are 39 load bins with loads ranging from 6 kips to 82 kips. For each of the tridem and quad axles, there are 31 load bins with loads ranging from 12 kips to 102 kips. Together, there are 140 load bins for all four axle types. The ALDF (also called *axle load spectra*) are factors that represent the distribution (in percent) of the total axle applications within each axle type-load combination. FIGURE 3.11 shows the *Axle Load Distribution Factors* window in the MEPDG.

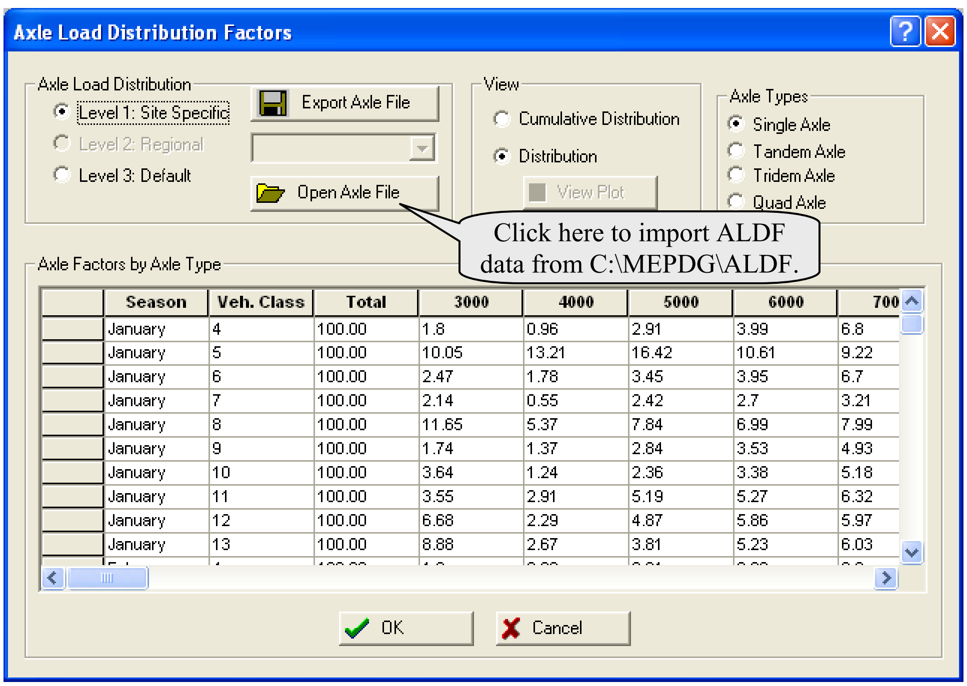

FIGURE 3.11 A screen capture of the *Axle Load Distribution Factors* table in the MEPDG.

A sensitivity analysis utilizing 44 typical flexible pavement and JPCP sections in North Carolina suggests that different ALDF clusters result in predicted performance that is significantly different for flexible pavements; hence, it became necessary to find a method to select the ALDF cluster that is most representative of traffic at the project location. The research team for NCDOT project HWY-2008-11 (5) developed a methodology that grouped all state-wide ALDF data into four different clusters: ALDF-1, ALDF-2, ALDF-3, and

ALDF-4. In addition, the team developed a decision tree, shown in FIGURE 3.12, to guide the selection of ALDF clusters.

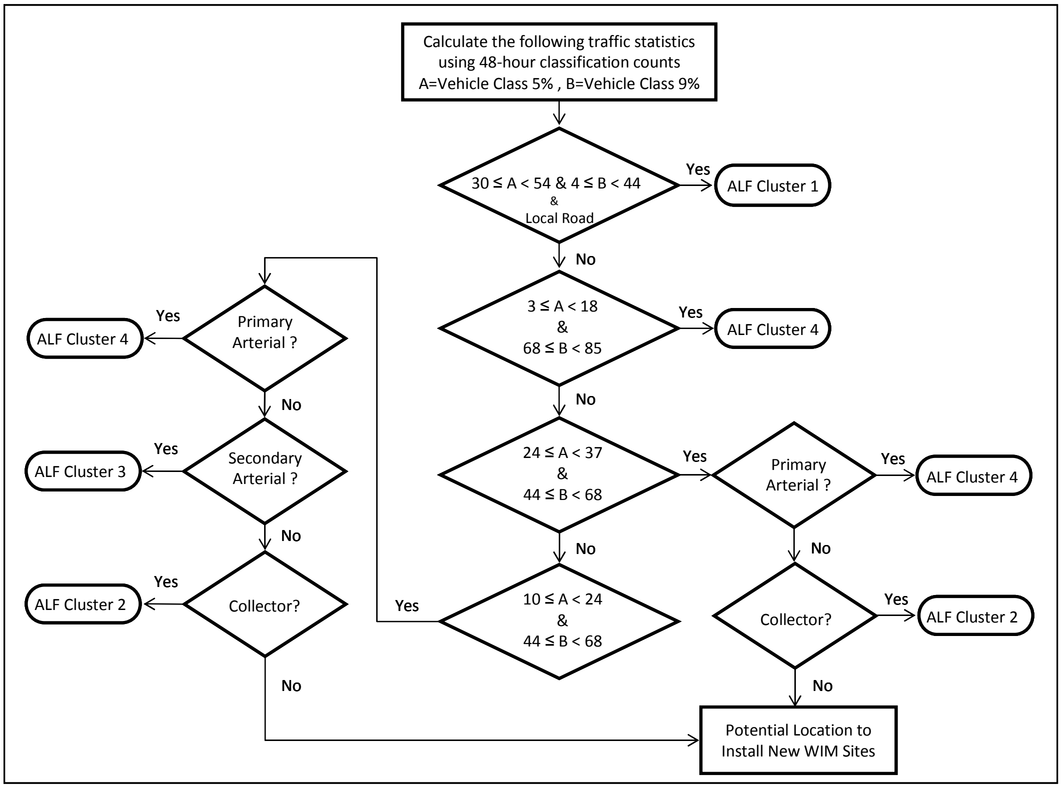

FIGURE 3.12 Decision tree for selecting ALDF, based on 48-hour class counts.

3.4.2 Implementation

To facilitate the process of entering the large amount of ALDF data required by the MEPDG, four computer files were created to represent the four ALDF clusters developed under NCDOT project No. HWY-2008-11 (5). These files are located under C:\MEPDG\ALDF. The two-step procedure for importing ALDF factors into the MEPDG is as follows:

1) For the selection of the most representative ALDF cluster based on the percentage of class 5 and class 9 vehicles obtained from 48-hour counts, the research team suggests using the same tool that was introduced under Section 3.3.2.2 for generating VCD factors. The tool, *VCD Generator & ALDF Cluster Selector* (FIGURE 3.8), integrates the ALDF decision tree shown in FIGURE 3.12 and other data to determine the most representative ALDF cluster.
2) Users can import the determined ALDF file by clicking the *Open Axle File* button, as shown in FIGURE 3.11, and can then navigate to the *C:\MEPDG\ALDF* directory to select the proper ALDF file. Note that for the *Open Axle File* button to be activated, users must first select *Level 1* from the *Axle Load Distribution Factors* window.

3.5 General Traffic Inputs

3.5.1 Background

In Window 2 of the GUI, double clicking *General Traffic Inputs* opens the window shown in FIGURE 3.13. This window has three main tabs: *Number Axles/Truck*, *Axle Configuration*, and *Wheelbase*.

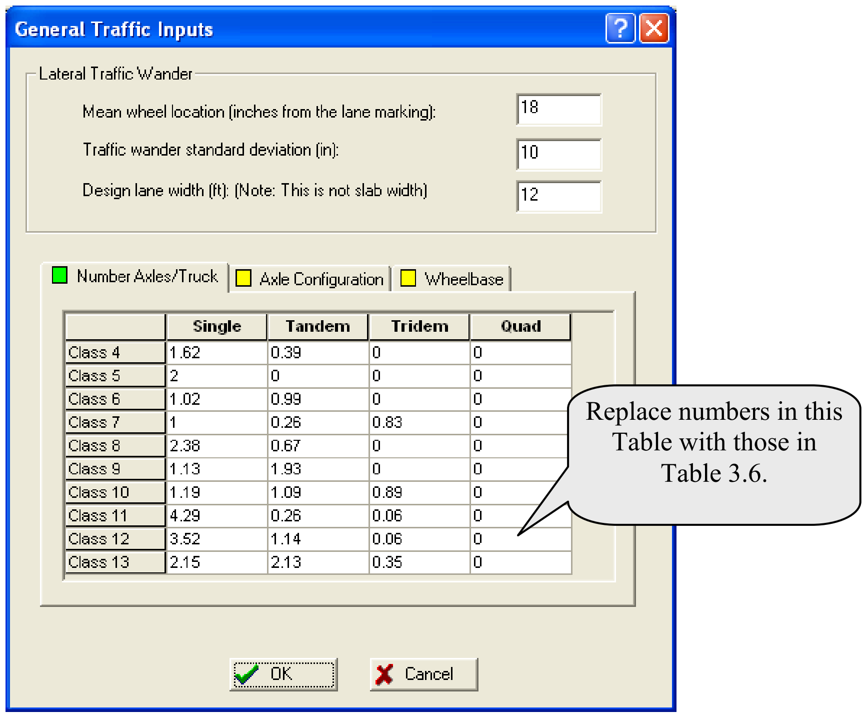

FIGURE 3.13 A screen capture of the *General Traffic Inputs* window in the MEPDG: *Number Axles/Truck* input table.

The *Number Axles/Truck* window shown in FIGURE 3.13 within the *General Traffic Inputs* window allows users to enter the number of each axle type, i.e., single, tandem, tridem, and quad, for each vehicle class. An initial assumption may be that these numbers should be integers; however, because different types of vehicles with different axle configurations might be grouped within the same class, the average number of axle types per vehicle class appears as a fraction. In this window, users can also enter the information related to lateral traffic wander, mean wheel location, traffic wander standard deviation, and the design lane width. TABLE 3.6 summarizes the state-wide averages for the *Number Axles/Truck* input based on the product of NCDOT project No. HWY-2008-11 (5) for North Carolina trucks.

TABLE 3.6 Recommended State-Wide Averages for Number of Axles per Truck (APT)

Vehicle Class	Axle Type			
	Single	Tandem	Tridem	Quad
Class 4	1.77	0.23	0.00	0.00
Class 5	2.00	0.00	0.00	0.00
Class 6	1.12	0.93	0.00	0.00
Class 7	1.12	0.19	0.79	0.00
Class 8	2.44	0.57	0.00	0.00
Class 9	1.18	1.90	0.00	0.00
Class 10	1.04	1.25	0.52	0.15
Class 11	4.87	0.01	0.00	0.00
Class 12	3.82	0.96	0.00	0.00
Class 13	1.61	1.64	0.32	0.20

The *Axle Configuration* window shown in FIGURE 3.14 within the *General Traffic Inputs* window shares the same *Lateral Traffic Wander* window found in the *Number Axles/Truck* window. However, the *Axle Configuration* window also allows users to enter information about average axle widths, dual tire spacing, tire pressure, and axle spacing for tandem, tridem and quad axles. Most of the national default inputs found in this window are recommended, with the exception of the axle spacing values.

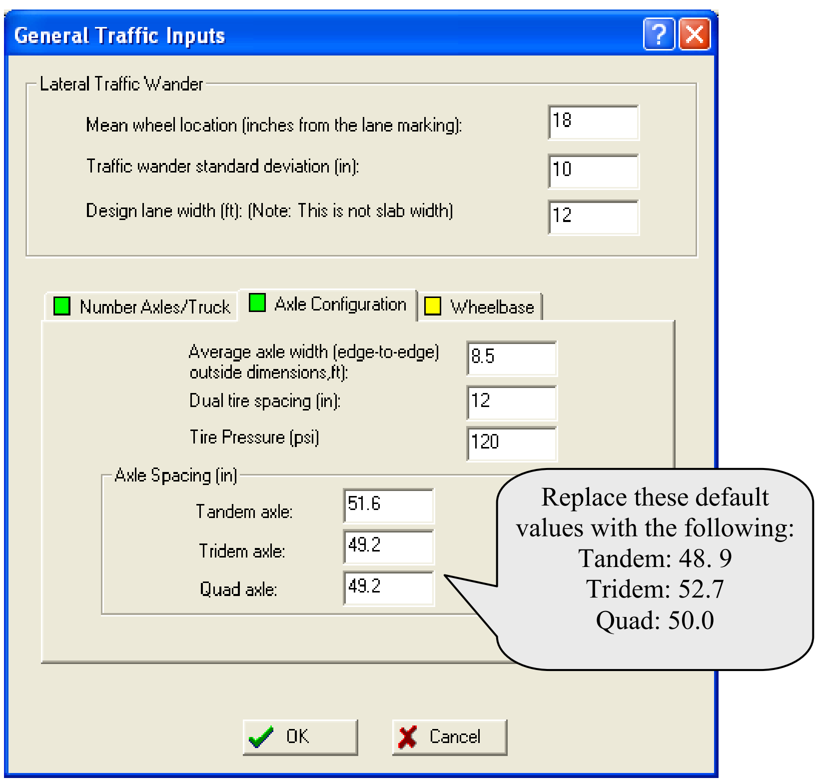

FIGURE 3.14 A screen capture of the *General Traffic Inputs* window in the MEPDG: *Axle Configuration* input window.

The *Wheelbase* window shown in FIGURE 3.15 within the *General Traffic Inputs* window shares the same *Lateral Traffic Wander* window found in the *Number Axles/Truck* window. However, in the *Wheelbase* window, users can also enter wheelbase distribution information, including average axle spacing for short, medium and long axles in addition to the percentage of trucks found in each of these axle spacing categories. This information is required for JPCP top-down cracking considerations only.

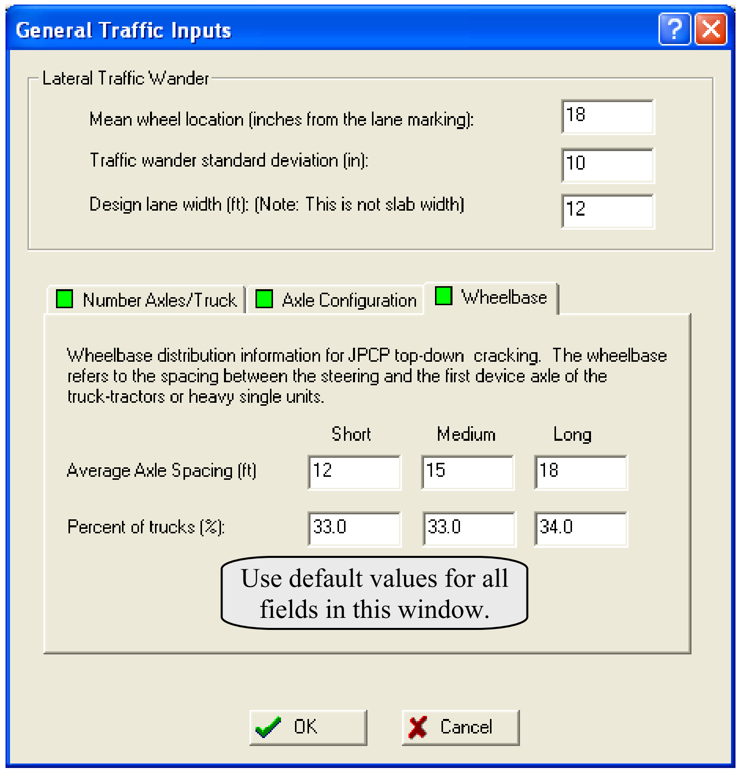

FIGURE 3.15 A screen capture of the *General Traffic Inputs* window in the MEPDG: *Wheelbase* input window.

3.5.2 Implementation

TABLE 3.6 summarizes the APT data for North Carolina local trucks. The research team recommends that data in TABLE 3.6 be used in the MEPDG for all flexible and rigid pavement design projects. Users should manually enter the information found in the table shown in FIGURE 3.13. As for the *Lateral Traffic Wander* variables, the research team recommends using national default values.

In the *Axle Configuration* window shown in FIGURE 3.14 within the *General Traffic Inputs* window, the research team recommends that all national default values stay unchanged, with the exception of axle spacing values. North Carolina values for axle spacing should be entered as follows: 48.9 inches for tandem axle, 52.7 inches for tridem axle, and 50 inches for quad axle. These dimensions, which are based on the recommendation of the NCDOT project No. HWY-2008-11 (5) research team, better represent those of local trucks compared to the national default values shown in FIGURE 3.14. These recommended dimensions were determined using data obtained from 44 WIM sites across North Carolina. As for the *Wheelbase* window shown in FIGURE 3.15, the research team recommends that all national default values be used without exceptions.

3.6 Level 1 Site-Specific Traffic Data

Level 1 traffic data, as described under section 1.2, represent site-specific volume and weight data that are measured at a WIM site located at or near the road segment or the site under study. NCDOT Project No. 2008-11 (5) dealt with 44 WIM sites. Hence, level 1 data are available for any new project to be built at or near any of these 44 WIM sites. Level 1 traffic data are available for the following traffic factors: MAF, VCD, HDF, ALDF, and APT. To facilitate the process of finding level 1 traffic data for a new project, a two-step process has been developed:

3.6.1 Step 1: Finding the Nearest WIM Site

Knowing the longitude and latitude information for any point along the new project, users can use the *Project-to-WIM Distance Finder* tool to find the approximate distance between the project and the nearest WIM site. FIGURE 3.16 is a screen capture of this tool.

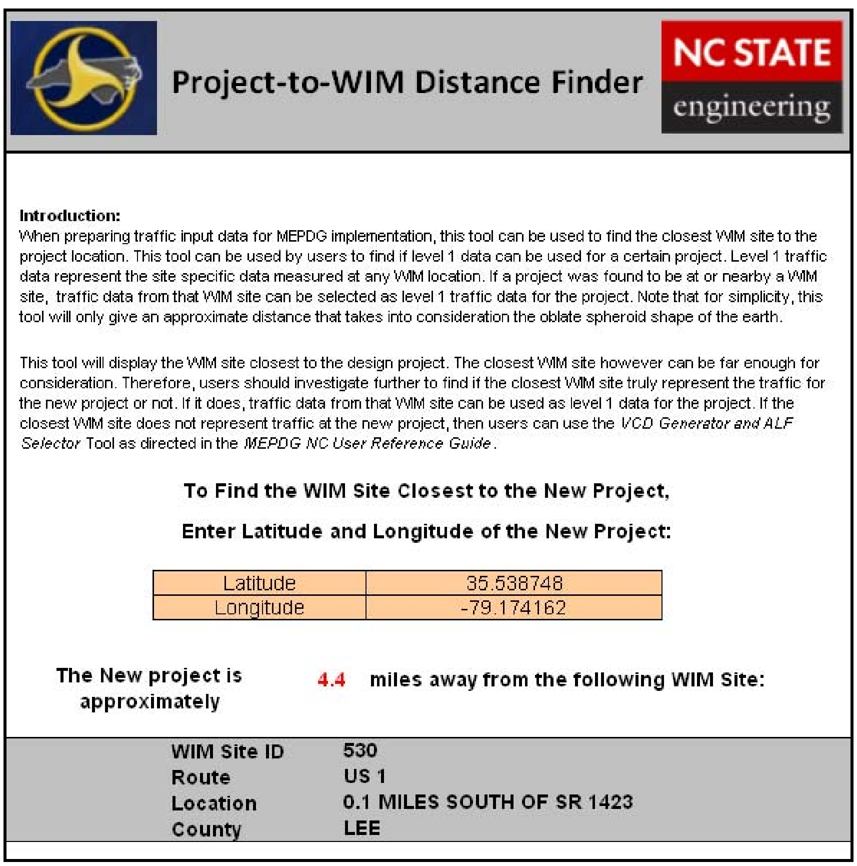

FIGURE 3.16 A screen capture of the *Project-to-WIM Distance Finder* Tool

The *Project-to-WIM Distance Finder* tool will give users quick information on the nearest WIM site including; WIM ID, Route at which the WIM is located, specific location, and the county in which the WIM site is located. Based upon the distance to the nearest WIM site, users can decide to either abandon level 1 traffic data if the nearest WIM site was found to be far from the location of the new project, or, decide to investigate more in the WIM site and evaluate whether traffic data from the nearest WIM site are representative of that at the new project location or not. If users, based on engineering experience and current practice, find that traffic data from the nearest WIM site are representative of the traffic at the new project and can be used as level 1 data, users can move on to step 2 to learn how to find and import level 1 traffic data. On the other hand, if users find that the traffic data from the nearest WIM site do not represent traffic data at the new project location; users can implement level 2 traffic data as explained under sections 3.3, 3.4, and 3.5.

3.6.2 Step 2: Finding and Entering Level 1 Traffic Data, If Applicable

3.6.2.1 Finding and Entering Level 1 MAF Data

If the nearest WIM site was found to have MAF data which represent that at the new project location, users can select the level 1 MAF file that corresponds to the nearest WIM location by clicking on the button shown in FIGURE 3.17 and navigating to *C:\MEPDG\MAF-L1* directory to select the corresponding MAF file. The *C:\MEPDG\MAF-L1* directory contains 44 MAF files, one for each WIM site.

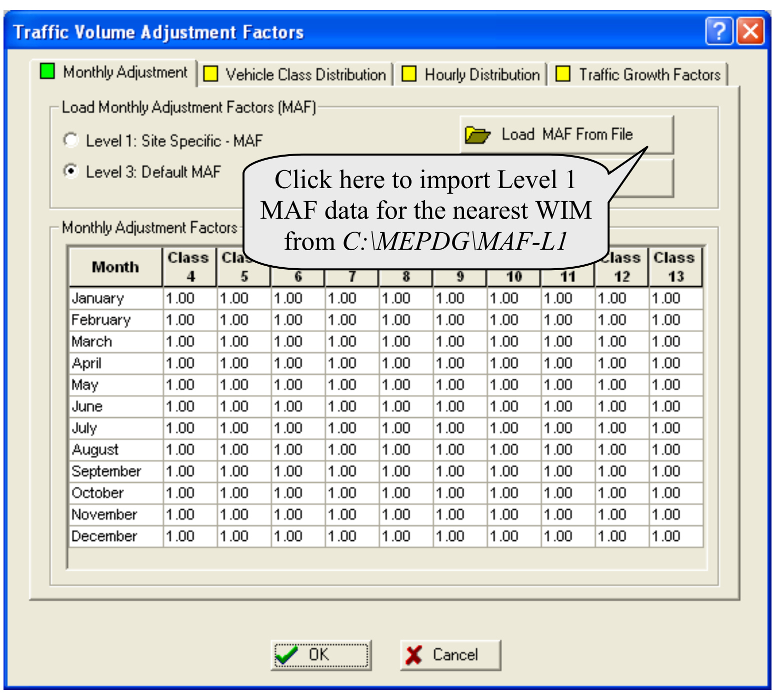

FIGURE 3.17 A screen capture of the Monthly Adjustment Factors Input table.

3.6.2.2 Finding and Entering Level 1 VCD Data

If the nearest WIM site was found to have VCD data that are of good representation to that at the new project location, users are recommended to generate level 1 VCD data for that WIM site using the *Site-Specific-Data* Excel tool developed by Stone et. al. under NCDOT Project No. HWY 2008-11(5). FIGURE 3.18 shows a partial screen capture of this tool.

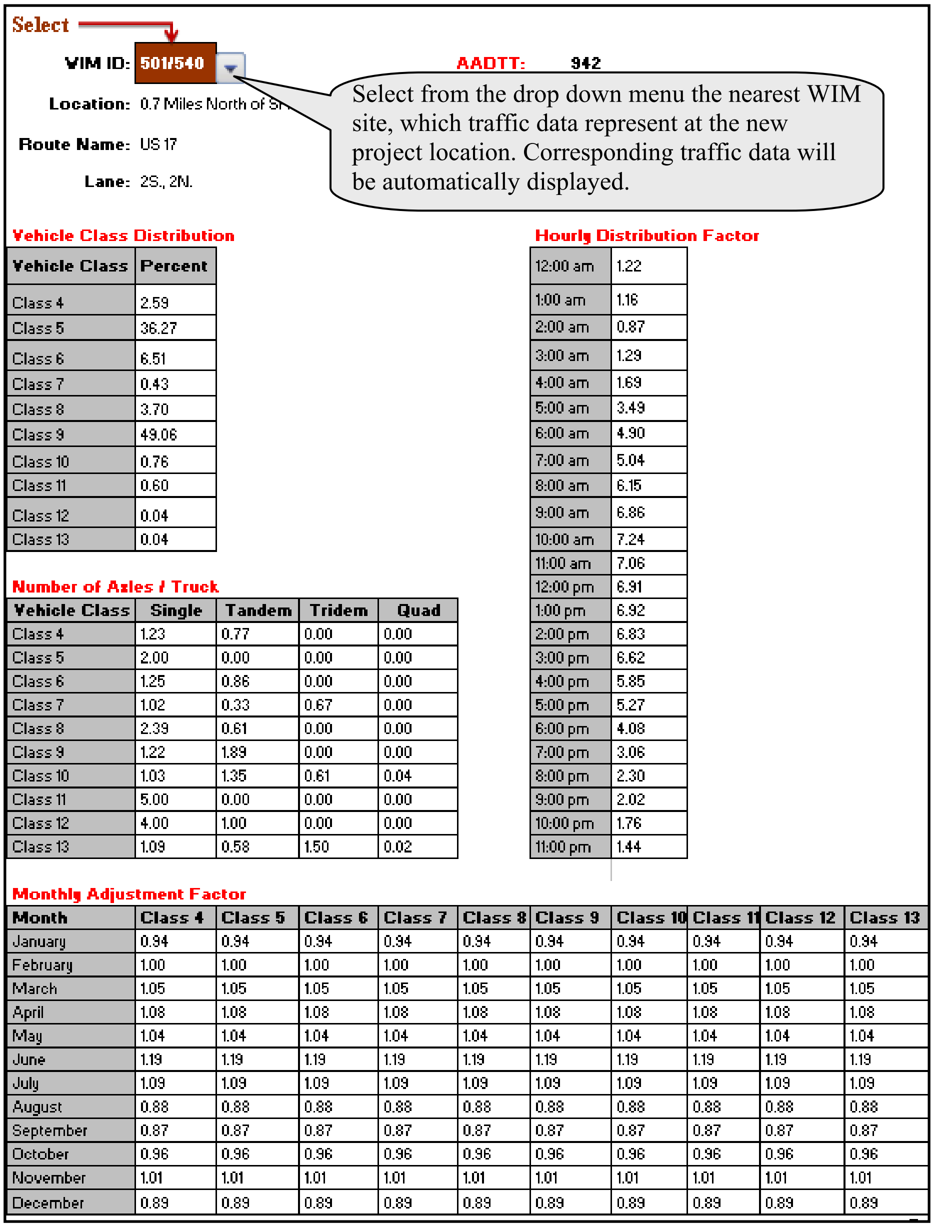

Vehicle Class Distribution

Vehicle Class	Percent
Class 4	2.59
Class 5	36.27
Class 6	6.51
Class 7	0.43
Class 8	3.70
Class 9	49.06
Class 10	0.76
Class 11	0.60
Class 12	0.04
Class 13	0.04

Hourly Distribution Factor

12:00 am	1.22
1:00 am	1.16
2:00 am	0.87
3:00 am	1.29
4:00 am	1.69
5:00 am	3.49
6:00 am	4.90
7:00 am	5.04
8:00 am	6.15
9:00 am	6.86
10:00 am	7.24
11:00 am	7.06
12:00 pm	6.91
1:00 pm	6.92
2:00 pm	6.83
3:00 pm	6.62
4:00 pm	5.85
5:00 pm	5.27
6:00 pm	4.08
7:00 pm	3.06
8:00 pm	2.30
9:00 pm	2.02
10:00 pm	1.76
11:00 pm	1.44

Number of Axles / Truck

Vehicle Class	Single	Tandem	Tridem	Quad
Class 4	1.23	0.77	0.00	0.00
Class 5	2.00	0.00	0.00	0.00
Class 6	1.25	0.86	0.00	0.00
Class 7	1.02	0.33	0.67	0.00
Class 8	2.39	0.61	0.00	0.00
Class 9	1.22	1.89	0.00	0.00
Class 10	1.03	1.35	0.61	0.04
Class 11	5.00	0.00	0.00	0.00
Class 12	4.00	1.00	0.00	0.00
Class 13	1.09	0.58	1.50	0.02

Monthly Adjustment Factor

Month	Class 4	Class 5	Class 6	Class 7	Class 8	Class 9	Class 10	Class 11	Class 12	Class 13
January	0.94	0.94	0.94	0.94	0.94	0.94	0.94	0.94	0.94	0.94
February	1.00	1.00	1.00	1.00	1.00	1.00	1.00	1.00	1.00	1.00
March	1.05	1.05	1.05	1.05	1.05	1.05	1.05	1.05	1.05	1.05
April	1.08	1.08	1.08	1.08	1.08	1.08	1.08	1.08	1.08	1.08
May	1.04	1.04	1.04	1.04	1.04	1.04	1.04	1.04	1.04	1.04
June	1.19	1.19	1.19	1.19	1.19	1.19	1.19	1.19	1.19	1.19
July	1.09	1.09	1.09	1.09	1.09	1.09	1.09	1.09	1.09	1.09
August	0.88	0.88	0.88	0.88	0.88	0.88	0.88	0.88	0.88	0.88
September	0.87	0.87	0.87	0.87	0.87	0.87	0.87	0.87	0.87	0.87
October	0.96	0.96	0.96	0.96	0.96	0.96	0.96	0.96	0.96	0.96
November	1.01	1.01	1.01	1.01	1.01	1.01	1.01	1.01	1.01	1.01
December	0.89	0.89	0.89	0.89	0.89	0.89	0.89	0.89	0.89	0.89

FIGURE 3.18 A screen capture of the Level 1 *Site-Specific Data* Excel tool.

The *Site-Specific-Data* Excel tool is located under *C:\MEPDG* directory. Double click on the *Site-Specific-Data.xls* to open the tool. Upon opening the tool, users can select the nearest

WIM Site ID from the drop down list shown in FIGURE 3.18 and VCD data, among others, will be automatically displayed. VCD data should be manually entered into the MEPDG through the VCD input table shown in FIGURE 3.19.

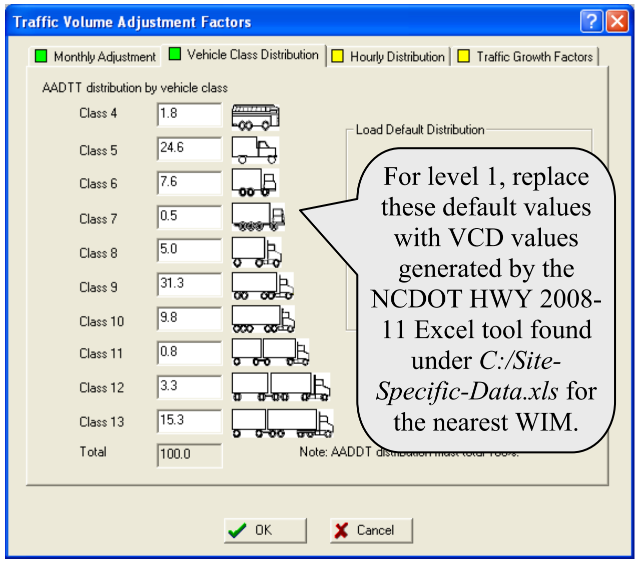

FIGURE 3.19 A screen capture of the VCD factors input table.

3.6.2.3 Finding and Entering Level 1 HDF Data

Level 1 HDF data can be found and entered in the same way as VCD data. FIGURE 3.20 is a screen capture showing the VCD factors input table within the MEPDG.

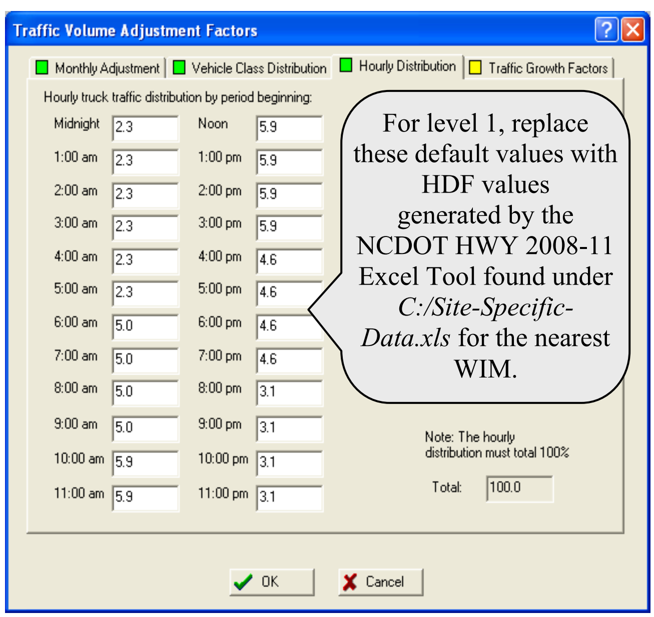

FIGURE 3.20 A screen capture of the HDF factors input table.

3.6.2.4 Finding and Entering Level 1 ALDF Data

Level 1 ALDF data can be found and imported in the same manner as level 1 MAF data. After making the decision that ALDF data from the nearest WIM site can be used to represent level 1 data at the new project location, users can click on the *Open Axle File* button shown in FIGURE 3.21 and navigate to the *C:\MEPDG\ALDF-L1* directory to select the ALDF file that corresponds to the nearest WIM site. ALDF data will be imported directly into the MEPDG. *ALDF-L1* directory contains 44 ALDF files, one for every WIM site.

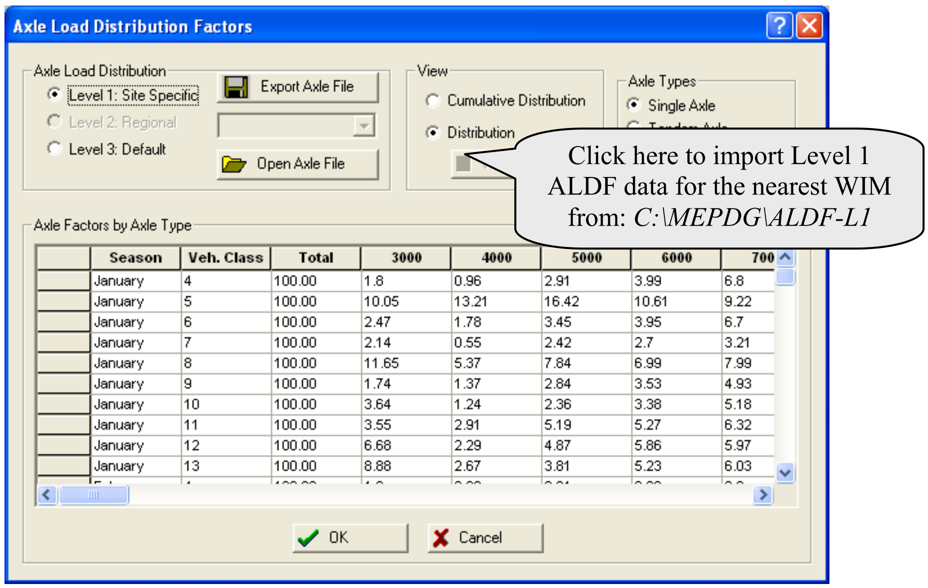

FIGURE 3.21 A screen capture of the ALDF input table.

3.6.2.5 Finding and Entering Level 1 APT Data

Level 1 APT data can be found and entered in the same manner as VCD and HDF level 1 data. It is recommended for users to use the *Site-Specific-Data* tool shown in FIGURE 3.18 to quickly generate level 1 APT data for the WIM site selected to represent traffic at the new project location. Users should enter APT data manually into the MEPDG as shown in FIGURE 3.22.

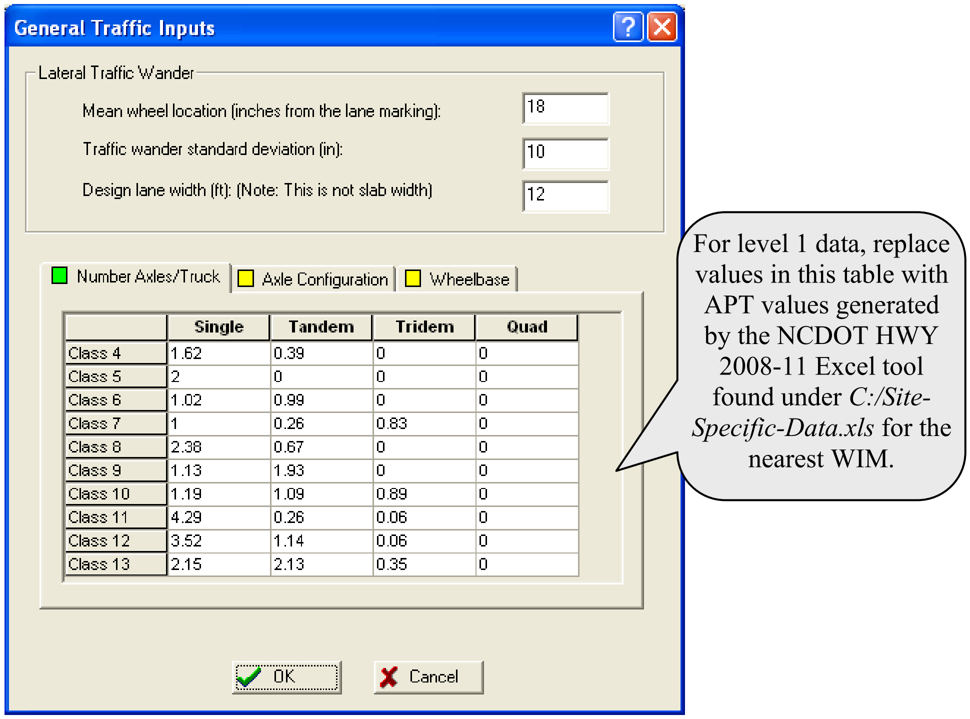

	Single	Tandem	Tridem	Quad
Class 4	1.62	0.39	0	0
Class 5	2	0	0	0
Class 6	1.02	0.99	0	0
Class 7	1	0.26	0.83	0
Class 8	2.38	0.67	0	0
Class 9	1.13	1.93	0	0
Class 10	1.19	1.09	0.89	0
Class 11	4.29	0.26	0.06	0
Class 12	3.52	1.14	0.06	0
Class 13	2.15	2.13	0.35	0

FIGURE 3.22 A screen capture of the APT input table.

CHAPTER 4 LOCATION, DEPTH OF WATER TABLE, AND CLIMATE

4.1 Climatic Data

4.1.1 Background

In Window 2 of the GUI, double clicking *Climate* opens the *Environment/Climatic* window shown in FIGURE 4.1. This window allows users to enter the geographic coordinates of the project location, average elevation above sea level, and the depth of the water table below the ground surface.

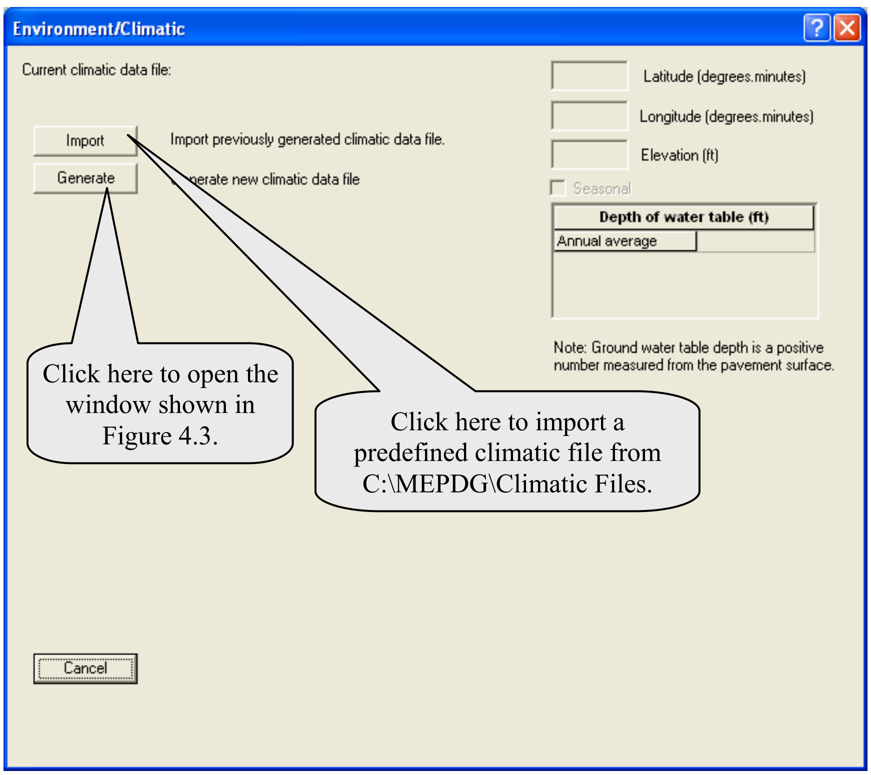

FIGURE 4.1 A screen capture of the *Environment/Climatic* input window in the MEPDG.

Users can select a single weather station or group of weather stations from which to gather information, such as air temperature, relative humidity, precipitation, wind speed, sunshine percentage, and rainfall. This information and the depth of water table information are both utilized by the EICM to account for the effect of changing temperature and moisture profiles on the performance of unbound and bound materials. Generally, the performance of unbound materials is highly affected by moisture profiles, whereas the performance of bound materials, e.g., asphalt concrete, is highly affected by temperature profiles.

The MEPDG database includes a total of 20 weather stations located in North Carolina. Details about these weather stations are summarized in TABLE 4.1. When comparing elevation data in the MEPDG database for these weather stations with elevation data obtained from Google Earth for the same weather stations, significant differences are evident. TABLE 4.1 and FIGURE 4.2 summarize and present these differences, respectively.

TABLE 4.1 Differences in Elevation between Google Earth and MEPDG Databases for NC Weather Stations

Weather Station Number	City	Latitude	Longitude	Elevation in MEPDG (ft)	Elevation from Google Earth (ft)	Difference in Elevations (ft)
3812	Asheville	35.26	-82.32	2174	1581	593
93765	Beaufort	34.44	-76.4	13	0	13
93783	Burlington	36.03	-79.29	594	577	17
93729	Cape Hatteras	35.14	-75.37	13	0	13
93785	Chapel Hill	35.56	-79.04	525	161	364
13881	Charlotte	35.13	-80.56	724	531	193
13786	Elizabeth City	36.16	-76.11	41	3	38
93740	Fayetteville	34.59	-78.53	184	23	161
53870	Gastonia	35.12	-81.1	801	649	152
13723	Greensboro	36.06	-79.56	907	629	278
3810	Hickory	35.44	-81.23	1164	884	280
13776	Lumberton	34.37	-79.04	126	68	58
93782	Maxton	34.47	-79.22	222	138	84
53872	Monroe	35.01	-80.37	692	509	183
93719	New Bern	35.04	-77.03	15	11	4
13722	Raleigh/Durham	35.52	-78.47	430	145	285
93781	Roanoke Rapids	36.26	-77.43	251	39	212
93759	Rocky Mount	35.52	-77.53	159	61	98
13748	Wilmington	34.16	-77.55	33	0	33
93807	Winston Salem	36.08	-80.13	996	854	142

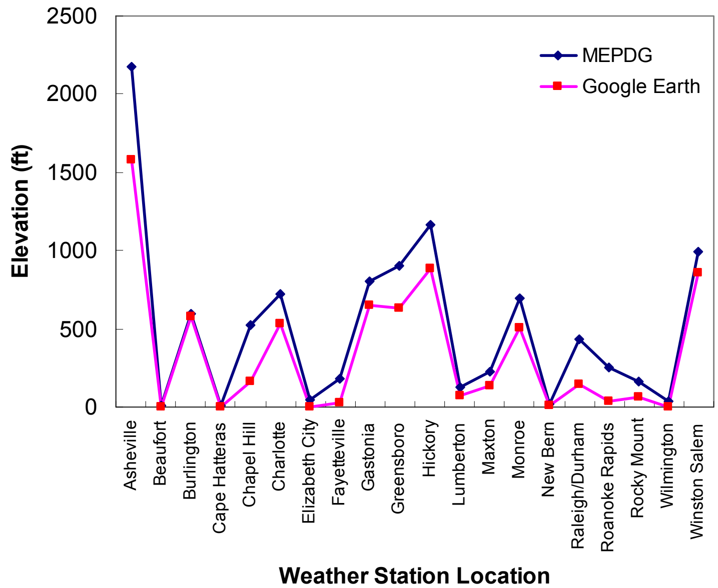

FIGURE 4.2 Comparison of weather station elevations obtained from MEPDG versus Google Earth.

Note that elevation data matter only when a weather station is selected as a representative weather station for a specific project location. If users prefer to interpolate amongst multiple weather stations, they are prompted to enter an elevation; hence, having the wrong weather station elevation in such a case does not matter. The research team has created a file with the correct elevation data and recommend its use in the MEPDG to replace the current file.

4.1.2 Implementation

4.1.2.1 Location Information

In the *Environment/Climatic* window shown in FIGURE 4.1, users have two options for defining location information that includes latitude, longitude, and elevation. The first option is to import a predetermined climatic file that has all the location information in addition to depth of water table information. This option is accessible by clicking the *Import* button shown in FIGURE 4.1. Clicking the *Import* button opens Windows Explorer through which users can navigate to the *C:\MEPDG\Climatic Files* directory and select the desired climatic input file. Note: climatic file names end with the *.ico* file extension. The second option allows users to select location information from a specific weather station or to interpolate location information from a group of weather stations that become available as soon as users enter valid longitude and latitude information for their design project. This second option is accessible by clicking the *Generate* button shown in FIGURE 4.1. Clicking the *Generate* button opens the window shown in FIGURE 4.3.

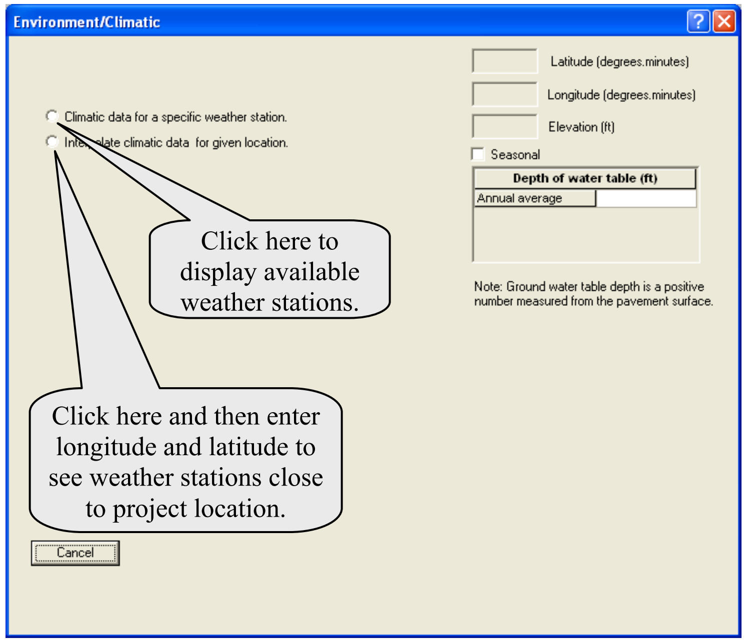

FIGURE 4.3 A screen capture of the *Environment/Climatic* input window after clicking the *Generate* button.

Selecting the *Climatic data for specific weather station* option in FIGURE 4.3 opens the *Environmental/ Climatic* window shown in FIGURE 4.4.

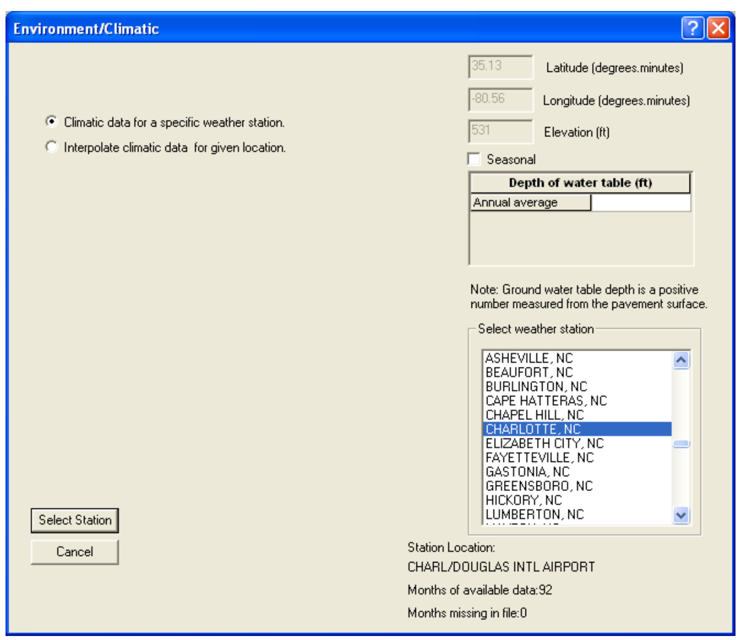

FIGURE 4.4 A screen capture of the *Environment/Climatic* window after selecting the *Climatic data for a specific weather station* option.

The *Environmental/Climatic* window shows a list of some of the available weather stations in the MEPDG database for NC. Users are advised to use this option if the project is located at or near one of the 20 available weather stations in North Carolina

Selecting the *Interpolate climatic data for a given location* option in FIGURE 4.3 opens the window shown in FIGURE 4.5, which shows the latitude, longitude, and elevation fields that appear for data entry. As soon as users enter latitude and longitude information, a list of available weather stations that are within a relatively close distance from the entered location is displayed. Users can select one or more weather stations to generate interpolated climatic input files.

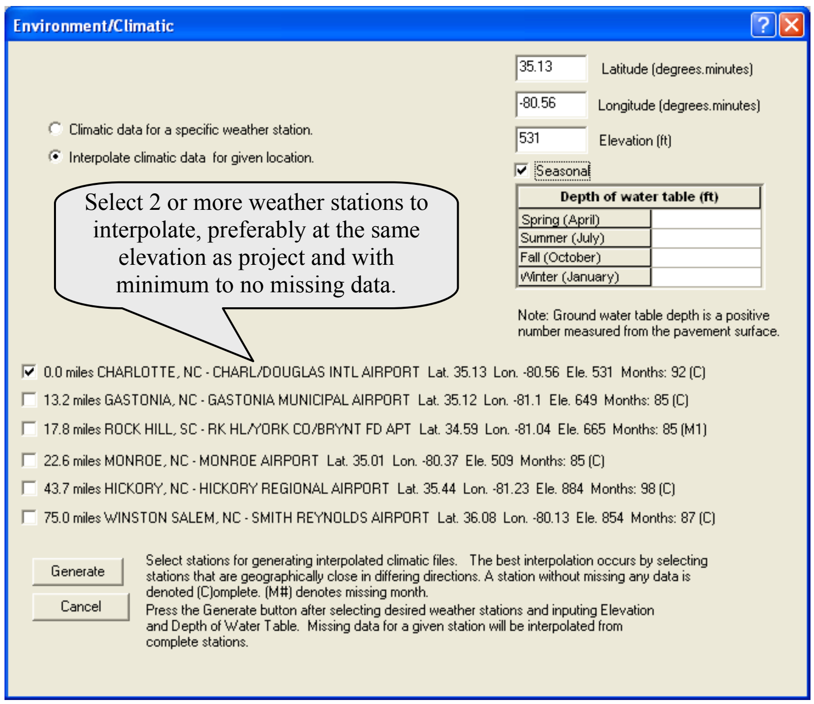

FIGURE 4.5 A screen capture of the *Environment/Climatic* window after selecting the *Interpolate climatic data for given location* option.

The selection of weather stations for interpolation purposes depends on three factors. These factors appear beside each station, as shown in FIGURE 4.5, and they are: distance from project location, elevation, and number of missing months in the climatic data. Having accurate weather station elevation data can especially help users to interpolate among weather stations that are located at approximately the same elevation as the project in question. When selecting to interpolate the climatic data, users are advised to select stations that are close to the project location, have approximately the same elevation, and have no to minimum missing files. Users must use their engineering judgment to select these stations.

4.1.2.2 Depth of Water Table Information

With the exception of the *Import previously generated climatic data file* option; users must enter the depth of water table data for the project location. Depth of water table information typically is supplied by the Geotechnical Unit. If these data are unavailable, users can find approximate depth of water table information at any location – using a tool available on the United States Geological Survey (USGS) website (6) – simply by entering longitude and latitude information. FIGURE 4.5 also shows that if the *Seasonal* box option is checked, users can enter the depth of water table for each of the four seasons: spring, summer, fall, and winter.

CHAPTER 5 STRUCTURE AND THERMAL CRACKING

5.1 HMA Design Properties

5.1.1 Background / Implementation

In Window 2 of the GUI, double clicking *HMA Design Properties* opens the window shown in FIGURE 5.1. The *HMA Design Properties* window appears only if the type of design, selected under Section 2.2, is either new flexible pavement or an overlay. The *HMA Design Properties* window allows users to select one of two *HMA E* Predictive Models*: the *NCHRP 1-37A viscosity-based model (nationally calibrated)* option or the *NCHRP 1-40D G*-based model (nationally uncalibrated)* option. Only one option is offered for the *HMA Rutting Model Coefficients* following the NCHRP 1-37A nationally calibrated model. Note: the coefficients of this rutting model have been developed for local mixes and will be presented in a separate document. Users also have the option to enter fatigue analysis endurance limits, even though the national calibration coefficients for the fatigue cracking distress model included in the MEPDG were developed based on the no endurance limit analysis. Hence, users are advised not to select an endurance limit. Lastly, if the *Overlay* design option is the type of design selected under Section 2.2, the window shown in FIGURE 5.1 will also display the option to include reflective cracking in the analysis (not shown). Users are advised to keep all options in the *HMA Design Properties* window set to national default values.

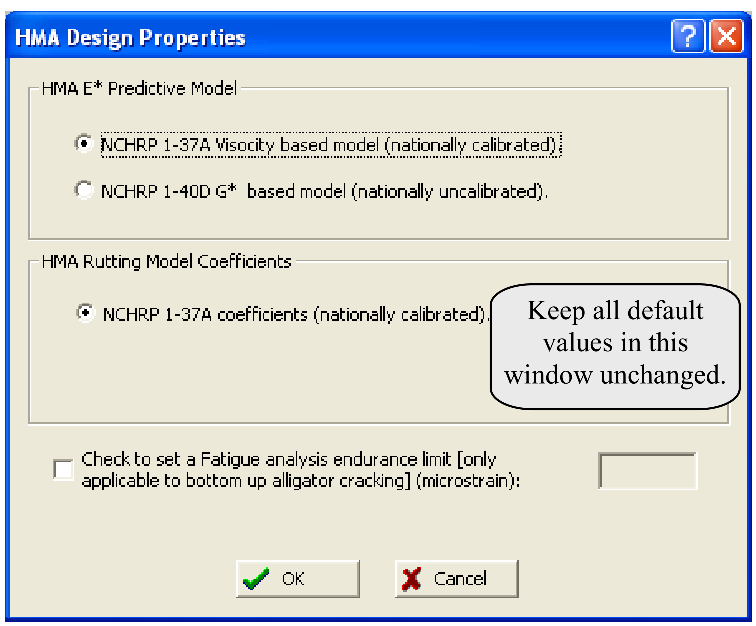

FIGURE 5.1 A screen capture of the *HMA Design Properties* window in the MEPDG.

5.2 Structure

5.2.1 Inserting, Adding, and Deleting Layers

In Window 2 of the GUI, clicking either *Structure* or *Layers* will open either the *Structure* window for new flexible pavement design, shown in FIGURE 5.2, or the *Structure* window shown in FIGURE 5.3 for AC over AC overlay design. The *Structure* window that opens for new flexible pavement design has, by default, one asphalt concrete layer pre-inserted. The window that opens for AC over AC overlay design has two pre-inserted layers, a new asphalt concrete surface layer and an old (existing) asphalt concrete layer. In addition to the asphalt layers, the *Structure* window for the AC over AC design has a *Flexible Rehabilitation* window to the right, as shown in FIGURE 5.3. Through the *Structure* window, users can insert, delete, or edit up to ten layers. In addition, users can directly modify the *Surface short-wave absorptivity* default value, if desired.

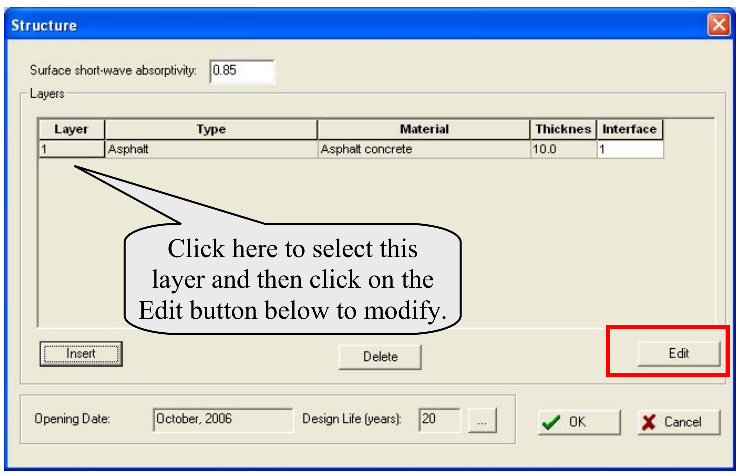

FIGURE 5.2 A screen capture of the *Structure* window for new flexible pavement design.

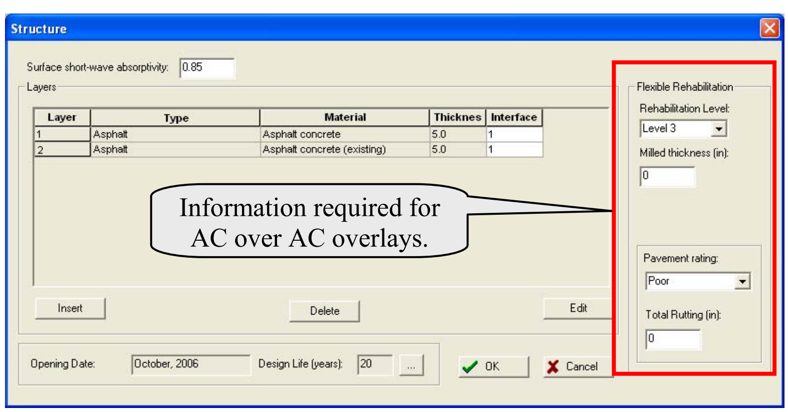

FIGURE 5.3 A screen capture of the *Structure* window for AC over AC overlay design.

Five types of layers can be added in the MEPDG: asphalt concrete, stabilized base, granular base, subgrade, and bedrock. As an example, to insert a new layer under the first layer, users would select the first layer by clicking on the number that corresponds to it, as shown in FIGURE 5.2. Users should then click the *Insert* button to open the *Insert Layer After* window from which they select the layer type to be added and related information. Details of this process are presented in subsequent sections. To edit the information of the asphalt layer as an example, users should first select the layer and then click the *Edit* button at the lower right corner of the window to open the *Asphalt Material Properties* window. Similarly, to delete a layer, users should select the layer to be deleted and then click the *Delete* button. The subsequent sections present all available layer options under each material type.

FIGURE 5.4 is a screen capture showing the *Asphalt Material Properties* window that opens once an asphalt layer selection is opened for editing. FIGURE 5.4 offers users three levels of input: Level 1, Level 2, and Level 3. Generally, each level of input requires different input parameters. Level 1 is the most demanding and most accurate input level and is used in this discussion.

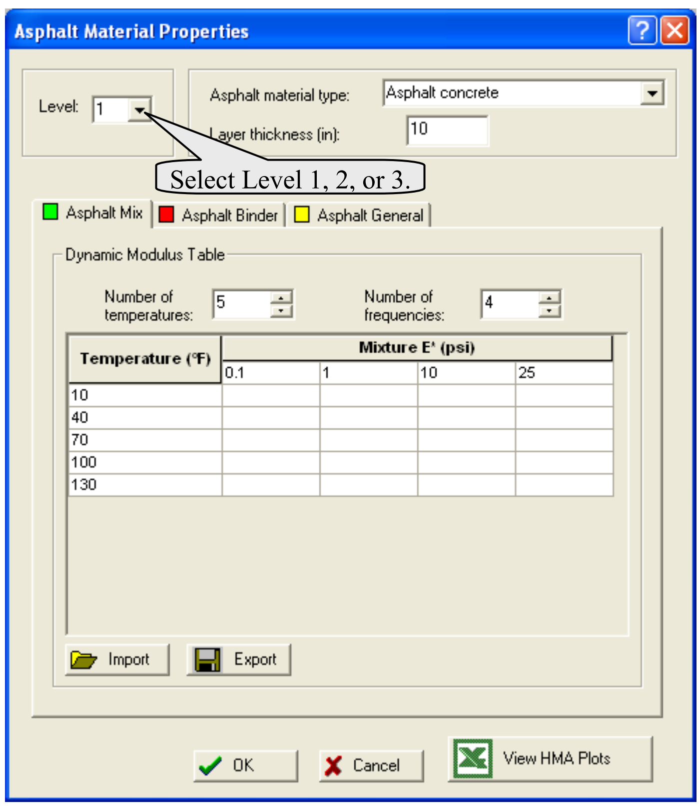

FIGURE 5.4 A screen capture of the *Asphalt Material Properties* window: *Dynamic Modulus Table* for Level 1 input.

5.2.2 Available Layer Types

As stated earlier, the MEPDG offers five types of layers from which users can select to construct a desired pavement structure: asphalt, stabilized base, granular base, subgrade, and bedrock. The MEPDG offers multiple options for each of these layer types. FIGURE 5.5 and FIGURE 5.6 are screen captures that show the options available under each layer type. Note that asphalt stabilized base layers are treated as regular *Asphalt* layers in the MEPDG.

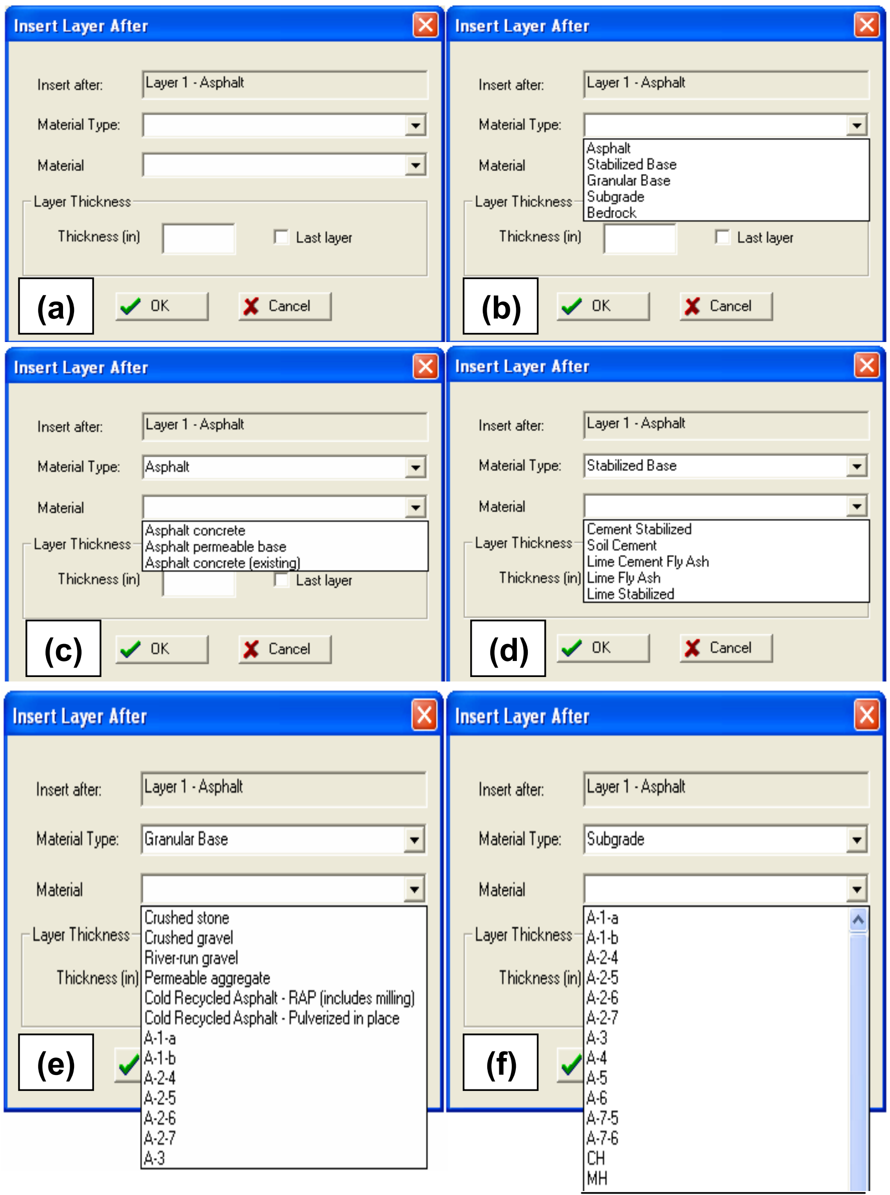

FIGURE 5.5 A screen capture of: (a) insert layer window; (b) available layer types; (c) available asphalt layer types; (d) available stabilized base types; (e) available granular base types; and (f) available subgrade types.

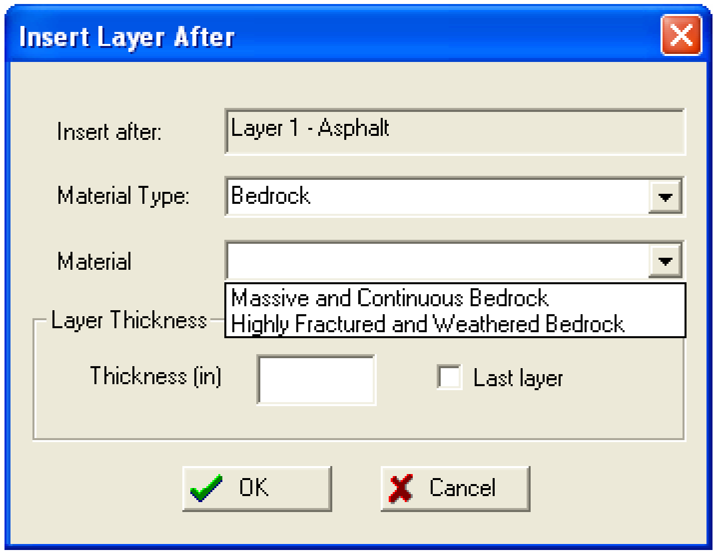

FIGURE 5.6 A screen capture showing the *Insert Layer After* window in the MEPDG: available bedrock layer options.

5.2.3 Dynamic Modulus and Complex Shear Modulus Databases

Dynamic modulus (|E*|) data were developed under NCDOT Project No. HWY 2003-09 for 18 North Carolina typical mixes with and without RAP. These mixes include: S9.5A, S9.5B, S9.5C, RS9.5A, RS9.5B, RS9.5C, S12.5B, S12.5C, S12.5D, I19B, I19C, I19D, RI19B, RI19C, B25B, B25C, RB25B, and RB25C. The dynamic modulus results are summarized in APPENDIX I. In addition, average complex shear moduli (G*) values for Superpave asphalt binder grades that are typically used in North Carolina, i.e., PG64-22, PG70-22, and PG76-22, were developed under NCDOT Project No. HWY-2007-07 and are summarized in APPENDIX II.

5.2.4 Implementation

5.2.4.1 Asphalt Layers

Inputs required for asphalt layer data in the MEPDG fall under three categories (tabs), referred to as Asphalt Mix, Asphalt Binder, and Asphalt General. The subsequent sections explain in detail how to find and enter related data.

5.2.4.1.1 Finding and Importing Level 1 Asphalt Mixture Data

The major input required by the MEPDG for the *Asphalt Mix* category is the dynamic modulus (|E*|). Dynamic modulus data for the aforementioned 18 typical North Carolina asphalt mixes have been saved into a file format (ending with ".dwn" file extension) that can be imported directly from within the MEPDG. To import dynamic modulus data for a specific mix type, users first select the *Level 1* input from the drop-down menu located in the

Asphalt Material Properties window, as shown in FIGURE 5.7, and then click the *Import* button located at the lower left corner of the window to open Windows Explorer. Users can navigate to the following directory, *C:\MEPDG\E-Star*, and select the dynamic modulus file for the appropriate mixture.

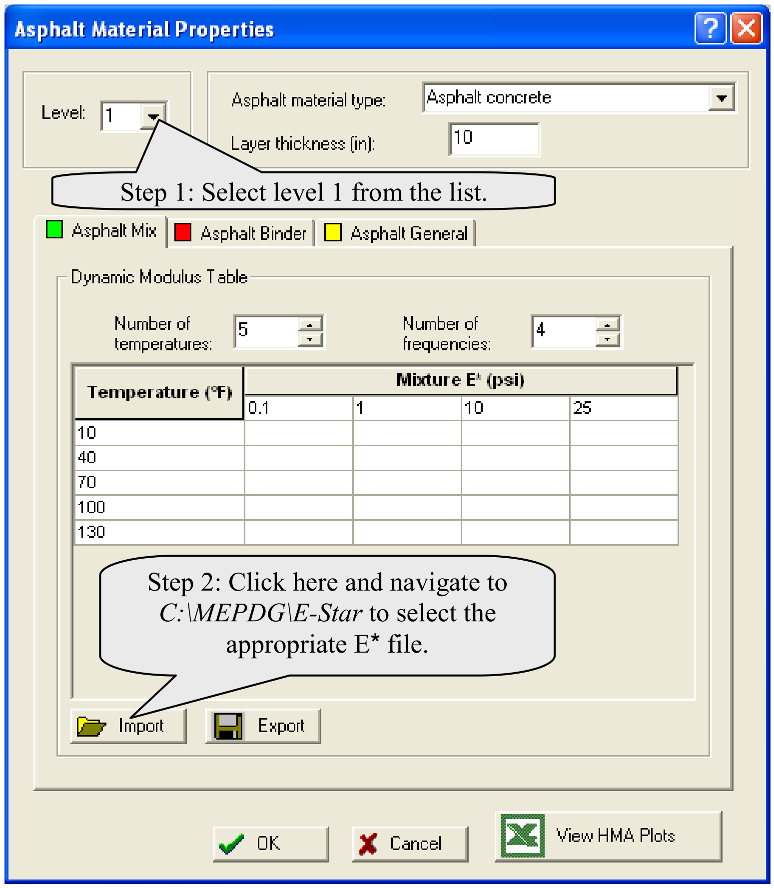

FIGURE 5.7 A screen capture showing the *Asphalt Material Properties* window: the *Dynamic Modulus Table* for Level 1 input.

5.2.4.1.2 Finding and Importing Level 1 Asphalt Binder Data

The local calibration project focused on characterizing asphalt mixtures and binders for 12 of the most representative asphalt mixtures in North Carolina. The binders used in these 12 mixtures were acquired from 9 different plants: 8 plants in North Carolina and 1 plant in South Carolina. Two binder grades, PG64-22 and PG70-22, are associated with these 12 mixtures. Additionally, four PG 76-22 binders were also acquired and tested to complete the binder database. Average dynamic shear moduli (|G*|) values were calculated for each of the grades. Averaged binder data were saved in a file format (ending with ".bif" file extension) that can be imported directly from within the MEPDG.

In the *Asphalt Materials Properties* window shown in FIGURE 5.8, users should first click the *Asphalt Binder* tab, then select *Level 1* from the drop-down menu in the upper left corner of the window, and then enter the desired Superpave binder test data. Note that although US Customary units were selected as the unit system, the dynamic shear moduli values must be entered in Pascal (Pa), i.e., a metric unit. To import the binder data, users must click the *Import* button to open Windows Explorer and then navigate to *C:\MEPDG\G-Star* to select the appropriate binder grade file.

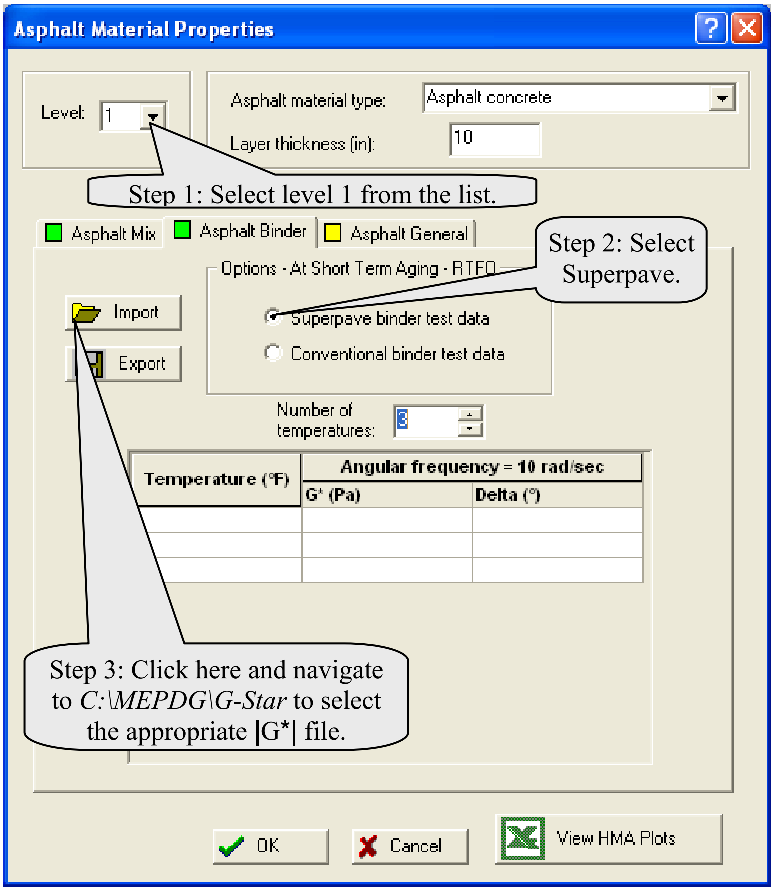

FIGURE 5.8 A screen capture of the Asphalt Material Properties window: asphalt binder shear modulus table for Level 1 input.

5.2.4.1.3 Finding and Importing Level 1 General Asphalt Data

For new and overlay asphalt concrete pavement designs, the MEPDG has default values for the different parameters required under this category. These default values are shown in FIGURE 5.9 under the *Asphalt General* tab. National default values for the *Reference Temperature*, *Poisson's Ratio*, *Thermal Conductivity* and *Asphalt Heat Capacity* entries are recommended.

As for the volumetric properties of the as-built asphalt mixtures, which are presented under the *Volumetric Properties as Built* category as *Effective binder content (%)* by volume, *Air voids (%)*, and *Total unit weight (pcf)*, no typical values have yet been developed for users to enter for various mixes. The values depend on the mix type and construction practices. The research team recommends that these values be developed by the NCDOT Materials and Tests (M&T) Unit for typical mixes used in North Carolina. For immediate implementation, users are advised to populate these inputs based on engineering experience with local asphalt mixtures.

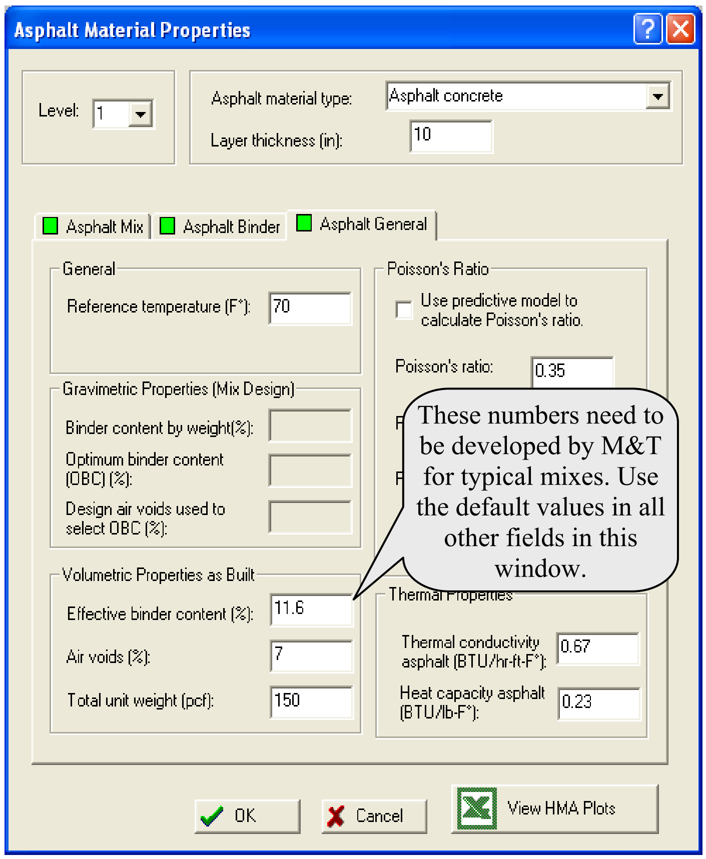

FIGURE 5.9 A screen capture of the *Asphalt Material Properties* window: *Asphalt General* parameters table for Level 1 input.

5.2.4.2 Base Materials / Background / Implementation

The MEPDG offers two main categories of base layer: the granular base and stabilized base. FIGURE 5.10 shows screen captures of the *Insert Layer After* window with a list of the available material options for each base layer category. As mentioned earlier, base layers that are treated with asphalt are not listed under either of the two base categories; rather, asphalt treated base layers are considered as asphalt layers in the MEPDG.

At the time of writing, the Geotechnical Engineering lab at the NCDOT M&T Unit does not perform any California Bearing Ratio (CBR) or resilient modulus tests on base and sub-base materials. Properties for these materials are determined by the pavement design team based on typical values and engineering experience. Until a comprehensive database is developed for typical unbound base and sub-base materials found in North Carolina, the research team recommends that national default values currently available in the MEPDG be used for all the designs. Note that to employ the default values, users should have a good idea of the base and/or sub-base material they plan to use in their design. This knowledge comes from design experience and availability of materials at or near the project location. Such prior knowledge and planning also applies to the choice of stabilized base materials for their design.

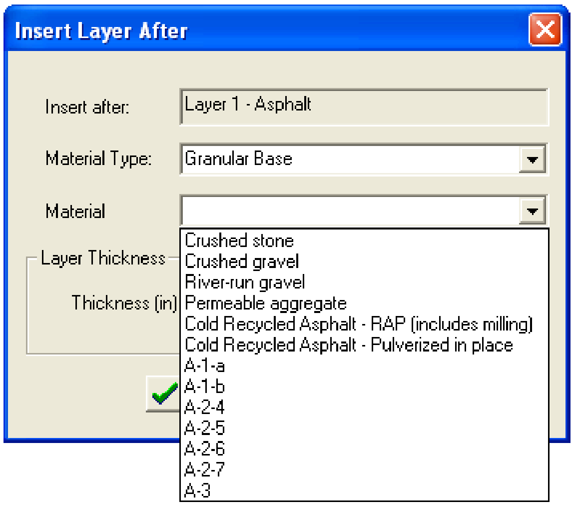

(a)

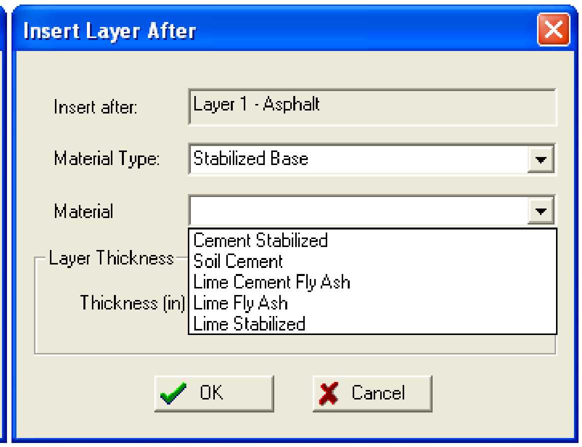

(b)

FIGURE 5.10 Screen captures of the *Insert Layer After* windows showing available material options for: (a) granular base; and (b) stabilized base.

5.2.4.2.1 Background

FIGURE 5.11 is a screen capture of the *Insert Layer After* window that shows several of the available subgrade material types. In fact, a total of 32 different material types are listed under the *Subgrade* category. FIGURE 5.12 and FIGURE 5.13 show screen captures of the Unbound Layer – Layer #2 window that present the subgrade *Strength Properties* and *EICM* input windows, respectively.

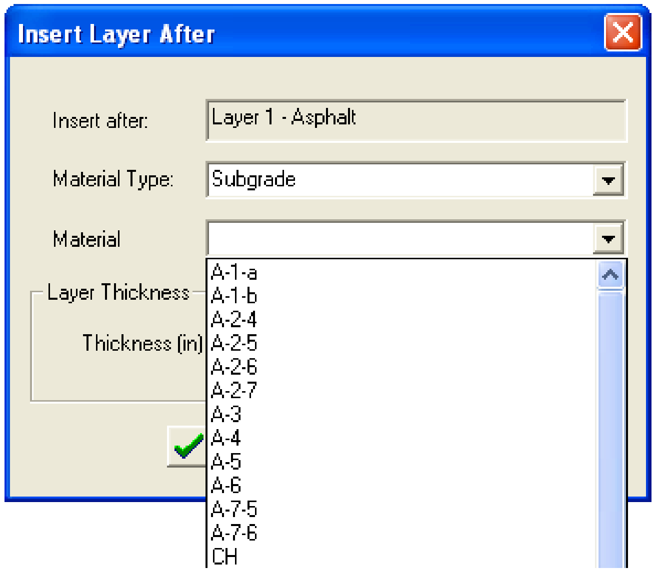

FIGURE 5.11 A screen capture of the *Insert Layer After* window: some of the *Subgrade* materials options.

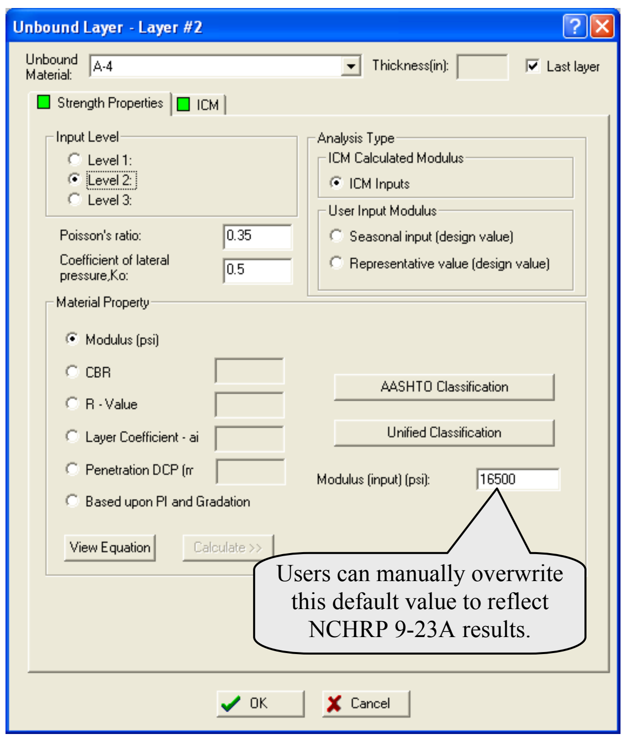

FIGURE 5.12 A screen capture of the *Insert Layer After* window: *Strength Properties* input for subgrade materials window.

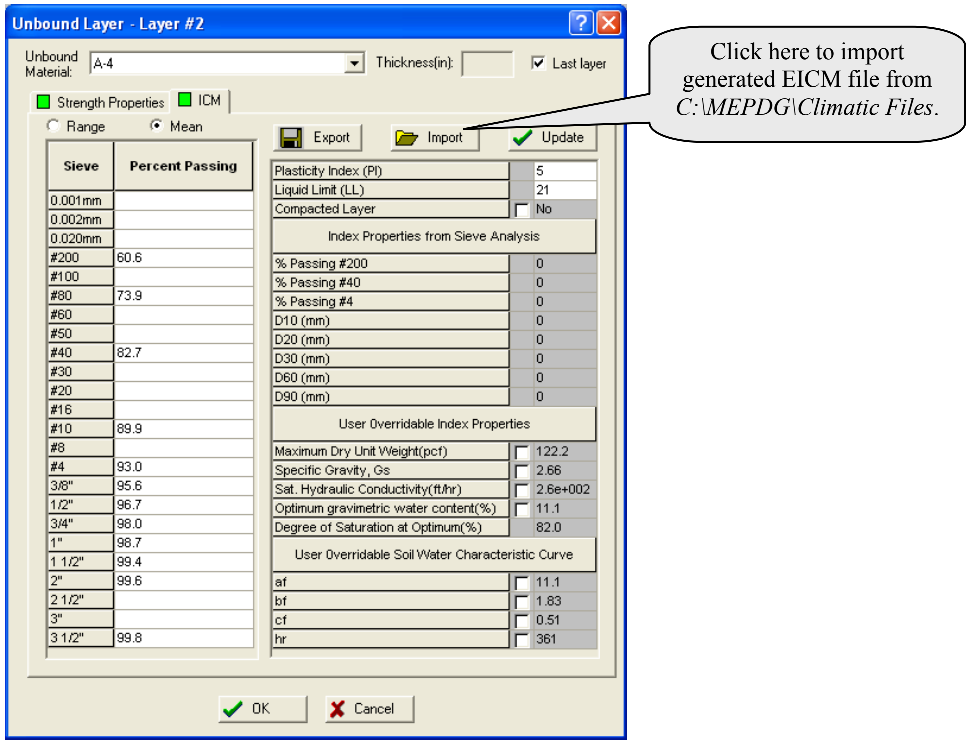

FIGURE 5.13 A screen capture of the *Unbound Layer – Layer #2* window: EICM input for subgrade materials window.

The current practice at the NCDOT for providing subgrade material information to the Pavement Design Unit (within the PMU) is as follows:

If the Geotechnical Engineering Unit at the NCDOT decides that it has a sufficient historical database and enough knowledge about the subgrade materials at the proposed location, it might decide that no field samples are required for testing and therefore would recommend a CBR value for the PMU to use in its design process. On the other hand, if the Geotechnical Engineering Unit does not have sufficient subgrade materials information for the proposed location, it will request that the Geotechnical lab at the M&T Unit conduct CBR tests on subgrade material samples acquired from the proposed project location. Based on the CBR test results and engineering judgment and experience, the Geotechnical Engineering Unit would recommend a certain CBR value(s) for the PMU to use in its design process. Note that the NCDOT does not perform any resilient modulus tests on subgrade materials in its current practice, although they have the necessary equipment to do so.

Recently, the product of the NCHRP 9-23A project (2) has become available. This product is a comprehensive nationwide soils database that includes Soil Water Characteristics Curve (SWCC) parameters and other soil properties that are required by the EICM so that it can account for changes in the moduli values of bound and unbound materials due to changes in temperature and moisture profiles within a pavement structure. The SWCC parameter represents a measure of the water-holding capacity of a given soil for different suction values. Soil suction and water content are two important parameters that control permeability, volume change, deformability and the shear strength of unsaturated soils (7). The NCHRP 9-23A product includes Geographic Information System (GIS)-based soil maps for all states. However, these maps were transformed into image files and stored as PDF documents. The main challenge in the implementation of the NCHRP 9-23A product is the absence of a method that can be used easily and reliably to superimpose any road section on a soil map and, consequently, select the most accurate soil type for that road section.

The research team has recently submitted a paper (8) for publication in the Transportation Research Board (TRB) Journal. The submitted paper presents a GIS-based methodology that can be applied to accurately superimpose any road section on NCHRP 9-23A soil maps. Moreover, a simple Excel-based Visual Basic for Application (VBA) code has been developed to generate Level 2 subgrade materials input that can be imported directly through the MEPDG interface. A copy of the submitted paper will be provided as a supplement to this *North Carolina MEPDG User Reference Guide*.

5.2.4.2.2 Implementation

To find and enter subgrade data into the MEPDG, it is recommended that users follow the procedure below. The procedure assumes that users have good knowledge of ArcMap GIS software. It is recommended that the GIS Unit be involved in this process, at least until users become familiar with the process. For more details about the procedure, users are advised to refer to the aforementioned submitted paper (8).

1) Start up ArcMap software, navigate to *C:\MEPDG\Subgrade*, and open the *Soils_Module.mxd* file. All soils unit data are stored in the *Soils_Module.mxd* file.
2) Determine the longitude and latitude for the road section to be designed. If the road section is straight and short, longitude and latitude information for the beginning and end of the section should be sufficient.
3) Using Hawth's Tools (9), a free add-in to ArcMap, convert the longitude and latitude information (points) into lines (roads) that can be displayed on the soils map.
4) Once displayed on the map, zoom in to the project location to visually determine the soils unit where the project lies. Each soils unit has an alphanumeric code that is required for the next step.
5) Using Windows Explorer, navigate to the directory *C:\MEPDG* and open the *MEPDG_Subgrade_Input_Generator.xls* file.
6) Enter the alphanumeric code obtained through Step 4 into the designated field in the *MEPDG_Subgrade_Input_Generator.xls* to display the different soils profiles available for that soils unit. In addition to the soil parameters required for Level 2 analysis, the *MEPDG_Subgrade_Input_Generator.xls* will also output the thickness, AASHTO classification, and the resilient modulus of each subgrade layer within the profile.
7) Add a subgrade layer(s) to reflect the output of the *MEPDG_Subgrade_Input_Generator.xls*. Enter the thickness of each layer.

8) For each subgrade layer(s), look in the *Strength Properties* window, shown in FIGURE 5.12, and select *Level 2*, and then overwrite the default moduli values with those values obtained from the *MEPDG_Subgrade_Input_Generator.xls*.
9) For each subgrade layers(s), look in the *EICM* window, shown in FIGURE 5.13, click the *Import* button to open Windows Explorer, and navigate to the *C:\MEPDG\Subgrade\Subgrade_Input_Files* directory to select the appropriate EICM input.
10) An example of EICM input files is: *AA0_H1.gsd*. The *H1* part of the name refers to *Horizon 1*. Therefore, if the alphanumeric code suggests a soils profile that contains more than a single subgrade layer (horizon), names may appear, such as *AA0_H2.gsd* for a second layer and *AA0_H3.gsd* for the third layer, and so on.

5.3 Thermal Cracking/ Background/Implementation

According to the AASHTO design guide, North Carolina is located in a wet freeze-thaw cycling environmental zone. However, thermal cracking on North Carolina roads has not been a major problem. Therefore, thermal cracking of local asphalt mixtures has not been characterized. FIGURE 5.14 shows a screen capture of the input table in the *Thermal Cracking* window in the MEPDG. Users are advised to use the national default values for the *Creep Compliance* data and for the coefficient of thermal contraction for all different asphalt mixtures.

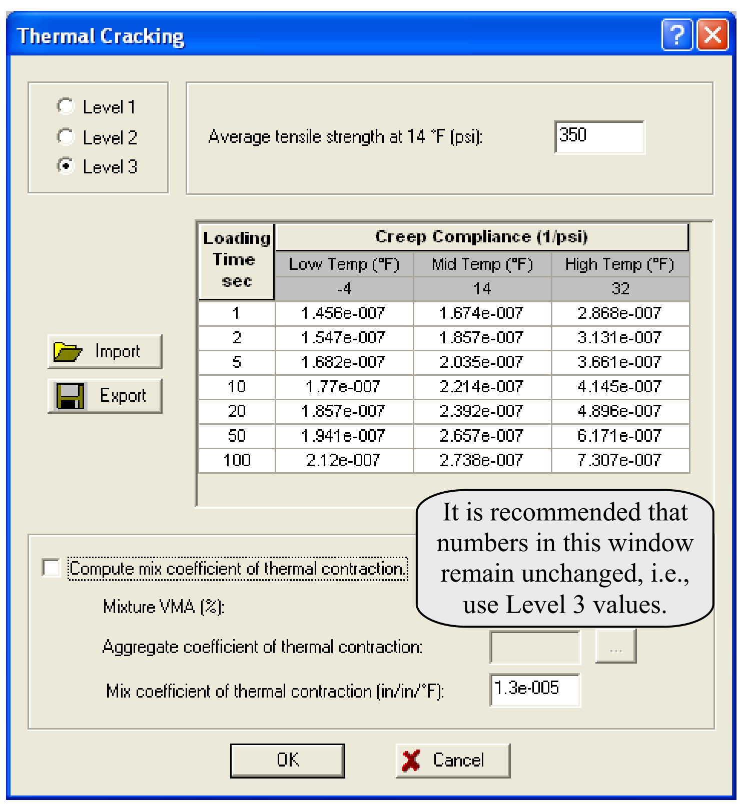

FIGURE 5.14 A screen capture of the *Thermal Cracking* input window in the MEPDG.

CHAPTER 6 MATERIAL-SPECIFIC AND LOCAL CALIBRATION FACTORS

6.1 Background

The goal of this chapter is two-fold: 1) to present the method used to develop the hybrid version of the MEPDG, as explained in Chapter 1, and 2) to explain the procedure for entering material-specific and local calibration factors for the alligator cracking and rutting models.

6.2 Developing the Hybrid Version of the MEPDG

The hybrid version of the MEPDG, shown in FIGURE 6.1, was developed to overcome the deficiencies of MEPDG Version 1.1 in accounting for different material-specific rutting coefficients for the different asphalt layers. MEPDG Version 1.1 allows users to enter only a single set of rutting material-specific *k* values for one type of asphalt mixture. In the hybrid version, executable files (Apads.exe and filteroutput.exe) are borrowed from the 9-30A version and replace those in the 1.1 version. In addition, extra text files in the CSV comma delimited format must be created and entered in the project directory for each existing asphalt layer. Recall that MEPDG Version 1.1 allows for a maximum of four asphalt layers to be entered. So, for a pavement section with three asphalt layers, for example, three CSV files are required to be created and saved in the project directory. The CSV files contain the rutting material-specific *k* values in addition to the local calibration factors, with the exception of β_{r1}, which must be entered manually, as explained in subsequent sections. As for fatigue, the MEPDG can be populated directly with the fatigue material-specific *k* values and local calibration values, as also explained in subsequent sections.

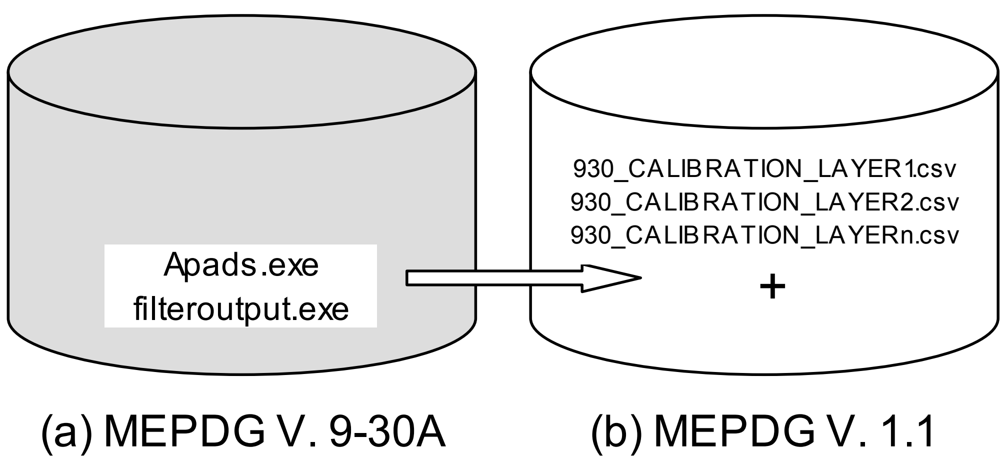

FIGURE 6.1 Changes and additions required to develop the hybrid version of the MEPDG.

6.3 Procedure for Entering Material-Specific *k* values and Local Calibration Factors

FIGURE 6.2 is a screen capture of the MEPDG graphical user interface showing how to open the calibration settings window for rutting and alligator cracking models. In the main window of the MEPDG, users can click on the *Tools* menu to open a drop-down list from which they can select either *Flexible – New* to enter the material coefficients for new flexible pavement design, or *Flexible – Rehab* to enter material coefficients for rehabilitated pavement design. The discussion below focuses on the *Flexible-New* option, but the same procedure can be applied for the *Flexible-Rehab* option.

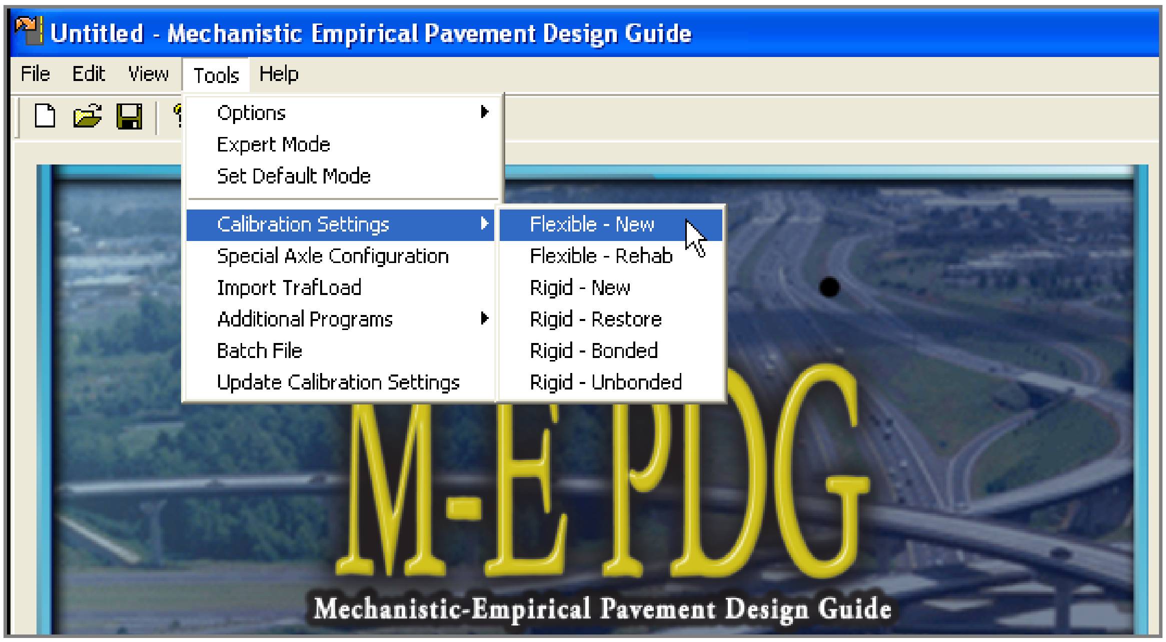

FIGURE 6.2 A screen capture of the MEPDG GUI showing how to open the calibration settings

6.3.1 Procedure for Entering the Alligator Cracking Local Calibration Coefficients

The alligator cracking distress calibration process consists of calibrating the N_f model and the transfer function, as follows.

1) Once the *Flexible-New* option is selected, as shown in FIGURE 6.2, a window with the title *Distress Model Calibration Settings – Flexible Pavement* pops up, as shown in FIGURE 6.3. Users have four analysis type options, as shown in FIGURE 6.3. The option *Typical Agency Values* should be selected so that users can replace the default *k* values with material-specific values.

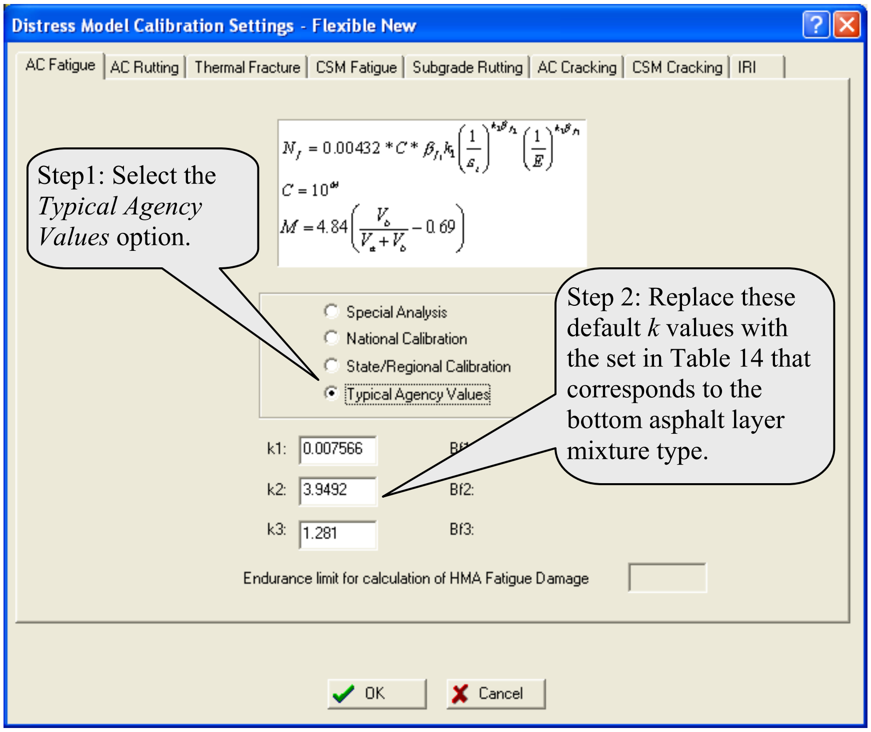

FIGURE 6.3 A screen capture of the alligator cracking calibration setting window.

2) To simplify the process of populating the material-specific *k* values and the local calibration beta values together, TABLE 6.1 was created. The numbers in TABLE 6.1 are simply the results of the multiplication of the material-specific *k* values by the corresponding beta values for each of the twelve mixtures.

TABLE 6.1 Alligator Cracking Material Specific and Local Calibration Factors Combined

Bottom Layer Mix ID	$\beta_{f1}\, k_{f1}$	$\beta_{f2}\, k_{f2}$	$\beta_{f3}\, k_{f3}$
S9.5B	2.04E+02	5.972	2.513
RS9.5B	8.25E-01	5.516	2.042
S9.5C	5.75E+07	5.972	2.983
RS9.5C	2.31E+00	5.462	2.013
S12.5C	3.26E-03	5.718	1.955
RS12.5C	2.53E-07	5.789	1.570
I19B	5.93E-10	5.854	1.431
RI19B	4.30E-15	5.349	0.714
I19C	6.49E-07	5.265	1.424
RI19C	1.62E-09	5.506	1.276
B25B	3.87E-10	5.432	1.171
RB25B	1.28E-18	5.617	0.575

3) Users should select the (β_f - k_f) set from TABLE 6.1 that corresponds to the bottom asphalt layer, because alligator cracking initiates from the bottom and propagates upward. Users can either type in the numbers manually or copy the numbers from TABLE 6.1 and paste them one at a time in the fields shown in FIGURE 6.3.

4) To populate the transfer function coefficients, users should click on the *AC Cracking* tab, shown in FIGURE 6.3, to open the transfer function window shown in FIGURE 6.4.

5) For the *AC bottom-up AC cracking* model shown on the right side of FIGURE 6.4, users should replace the default values of C_1 (bottom) and C_2 (bottom) with the local calibration factor of 0.24377 for both.

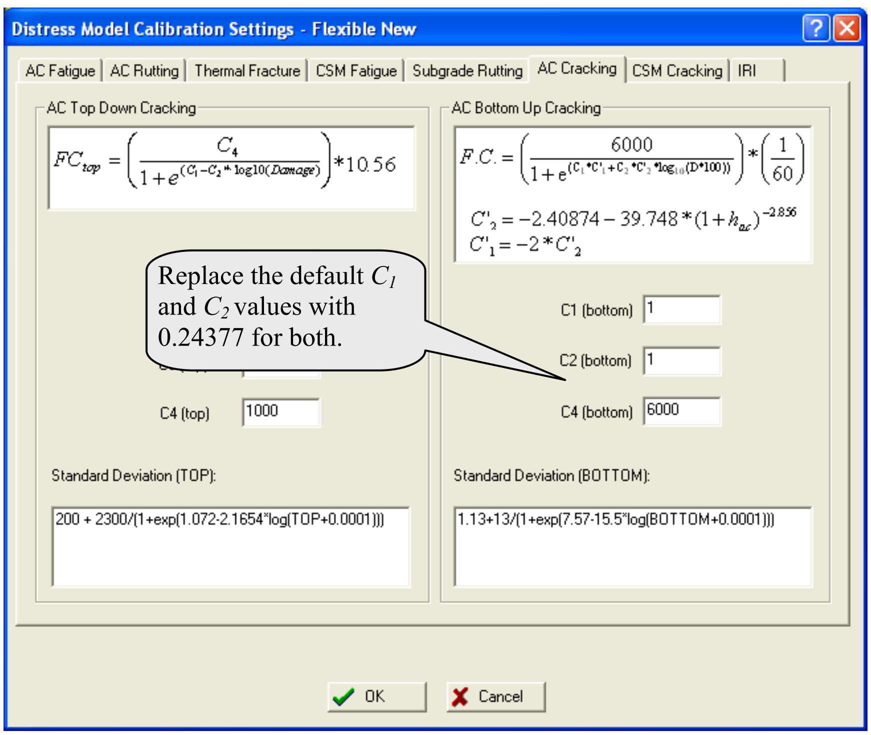

FIGURE 6.4 A screen capture of the alligator cracking transfer function calibration setting window.

6.3.2 Procedure for Entering the Rutting Model Local Calibration Coefficients

This section presents the procedure for entering the rutting model material-specific *k* values and the local calibration factors for asphalt layers and for unbound base and subgrade layers.

6.3.2.1 Asphalt Concrete

FIGURE 6.5 is a screen capture of the *Distress Model Calibration Setting* window for asphalt concrete (AC) rutting. The following steps explain the procedure for populating the AC rutting models with local calibration coefficients.

1) Select the *Typical Agency Values* analysis option, as shown in FIGURE 6.5.

2) Using Microsoft Excel, create the number of files equivalent to the number of AC layers. For example, if a pavement section has four AC layers (the maximum), users should create four Excel files (the names and content of these files are explained below).

3) Name the Excel files as follows: *930_CALIBRATION_LAYER1.csv* for the first layer, *930_CALIBRATION_LAYER2.csv* for the second layer, and so forth. Note that the only difference between the file names is the number that corresponds to the layer number. In this example, the number 1 at the end of the file name corresponds to the first (surface) layer, and number 4 corresponds to the bottom layer.

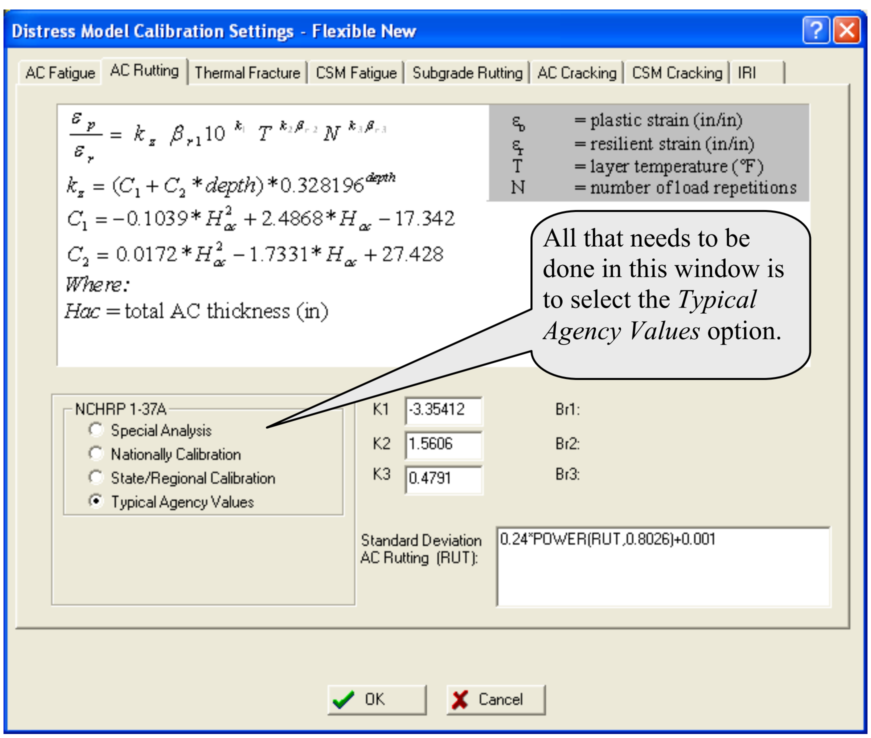

FIGURE 6.5 A screen capture of the asphalt rutting calibration setting window.

4) FIGURE 6.6 explains the content of each file. FIGURE 6.6 shows that only seven cells in each file need to be populated, as follows. Cell A0 always has a value of zero. Cells A2, A3, and A4 have the material-specific *k* values for a certain mixture,

which can be obtained from Table 6.2. In cell B2, users should enter a value of 0.9475, a value of 0.86217 in cell B3 and a value of 1.35392 in cell B4. Note that the three numbers in cells B3, B3, and B4 correspond to β_{r1}, β_{r2}, and β_{r3}, respectively. These beta values are mixture independent.

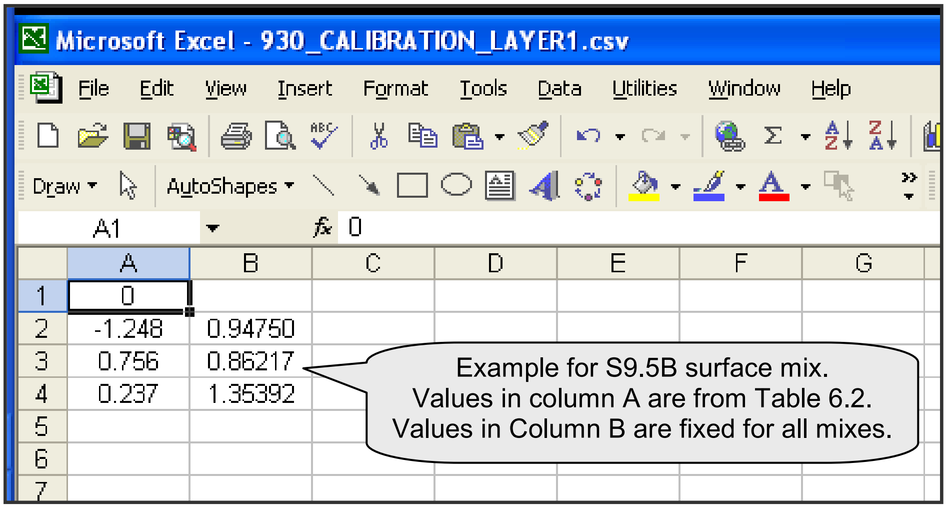

FIGURE 6.6 A screen capture of the 930_CALIBRATION_LAYER1.csv file.

TABLE 6.2 Material-Specific Rutting Coefficients for Local Mixtures

Mix ID	k'_{r1}	k'_{r2}	k'_{r3}
S9.5B	-1.248	0.756	0.237
RS9.5B	-1.141	0.684	0.170
S9.5C	-0.582	0.330	0.221
RS9.5C	-1.425	0.797	0.185
S12.5C	-0.136	0.161	0.214
RS12.5C	-0.883	0.391	0.245
I19B	0.115	0.179	0.209
RI19B	-0.168	0.134	0.222
I19C	-1.122	0.728	0.163
RI19C	-2.541	1.327	0.210
B25B	-1.347	0.735	0.238
RB25B	-1.520	0.712	0.268

5) Once the seven fields are populated, users should save each of these Microsoft Excel files with the proper names as CSV (comma delimited), as shown in FIGURE 6.7.

6) Once the correct number of CSV files are created and saved in CSV format, users should save these files (as read-only) in the project directory. It is important that these files have the correct names and that they are saved as read-only; otherwise, the predicted AC rut depth will not be correct.

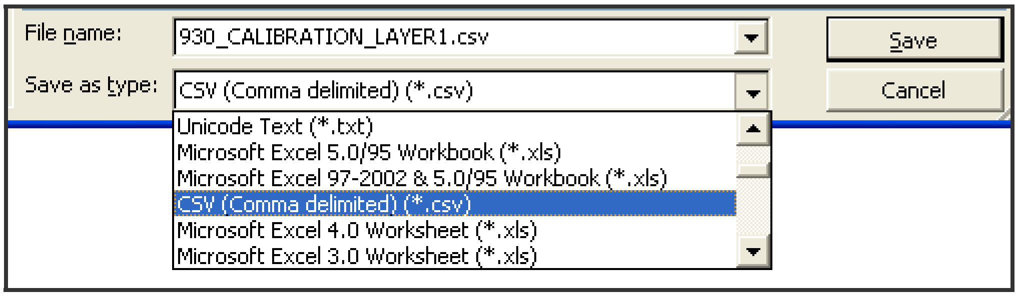

FIGURE 6.7 A screen capture showing the available "save as type" options in Microsoft Excel.

6.3.2.2 Unbound Base and Subgrade

The procedure for entering the rutting model coefficients for the unbound base and subgrade layers is as follows:

Click on the *Subgrade Rutting* tab to open the window shown in FIGURE 6.8; then select the *State/Regional Calibration* analysis option, as shown in FIGURE 6.8. As soon as the *State/Regional Calibration* option is selected, the fields for entering the beta values become available.

Note that the same rutting prediction model is used for granular (unbound base) and fine grain (subgrade) soils. The only difference is the calibration coefficients. Also note that the k values for the unbound base and sub-base have not been calibrated as part of this research work; hence, national default k values are to be used, i.e., $k = 2.03$ for the unbound base and $k = 1.67$ for the subgrade.

For local calibration beta values, enter a value of 0.53767 for the unbound base and a value of 1.5 for the subgrade. Note that these beta values can be used with any subgrade type and unbound base material.

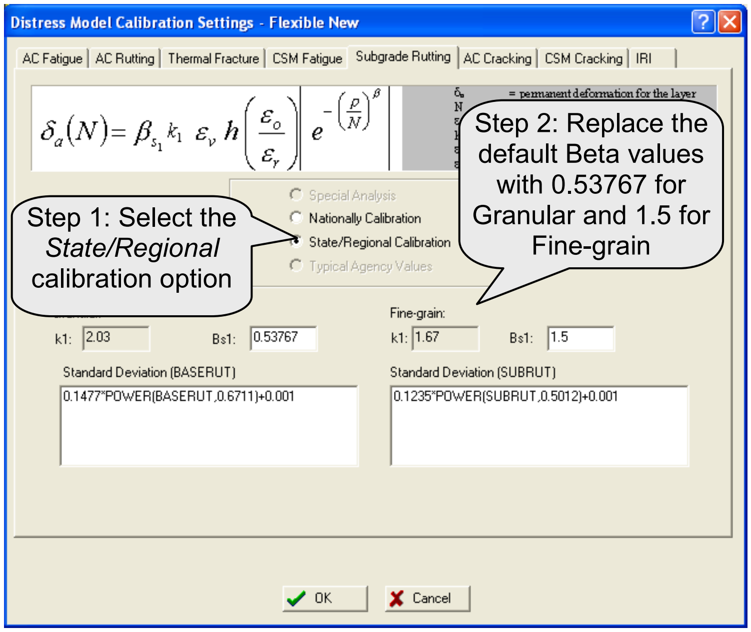

FIGURE 6.8 A screen capture of the unbound base and subgrade materials rutting calibration settings window.

REFERENCES

1) Applied Research Associates, Inc. (2004). *Guide for Mechanistic-Empirical Design of New and Rehabilitated Pavement Structures.* NCHRP 1-37A, Final Report, Part 1, Introduction. Transportation Research Board, National Research Council. Washington, D.C.

2) Zapata, C. E. (2010). *A National Catalog of Subgrade Soil Water Characteristic Curve (SWCC) Default Input and Selected Soil Properties for Use with the MEPDG.* NCHRP 9-23A, final Report. National Cooperative Highway Research Program, Washington, DC.

3) Applied Research Associates, Inc. (2007). *Calibration of Rutting Models for HMA Structural and Mix Design*. National Cooperative Highway Research Program, NCHRP 9-30A. Transportation Research Board, Washington, DC.

4) Applied Research Associates, Inc. (2004). *Guide for Mechanistic-Empirical Design of New and Rehabilitated Pavement Structures.* NCHRP 1-37A, Final Report, Part 2, Chapter 4 Traffic. Transportation Research Board, National Research Council. Washington, D.C.

5) Stone, J. R., Kim, Y. R., List, G. F., Rasdorf, W., Sayyady, F., Jadoun, F. M., and Ramachandran, A. N.. (2010). *Development of Traffic Data Input Resources for the Mechanistic Empirical-Pavement Design Process*. Final Report for Project No. HWY-2008-11, under review by the North Carolina Department of Transportation, Raleigh, NC.

6) United States Geological Survey (USGS). *Groundwater Levels for the Nation.* http://nwis.waterdata.usgs.gov/nwis/gwlevels?search_criteria=lat_long_bounding_box&submitted_form=introduction. Last accessed August 24, 2010.

7) Barbour, S. L. (1998). *The Soil–Water Characteristic Curve: a Historical Perspective*. 19th Canadian Geotechnical Colloquium. Canadian Geotechnical Journal 35 (5): 873–894.

8) Jadoun F. M. and Y. R. Kim (2011). *GIS-Based Implementation Methodology for the NCHRP 9-23A Recommended Soil Parameters for Use as Input to the MEPDG in North Carolina*. Presented at the 90th TRB Annual Meeting, Washington, DC.

9) Beyer, H. *Hawth's Analysis Tools for ArcGIS.* http://www.spatialecology.com/htools/download.php. Accessed June 24, 2010.

APPENDIX I DYNAMIC MODULUS (|E*|) DATABASE

Mix ID	Temp (°F)	|E*| (psi)					
		0.1 Hz	0.5 Hz	1 Hz	5 Hz	10 Hz	25 Hz
S9.5A	14	3,179,855	3,601,671	3,763,157	4,089,808	4,210,292	4,352,114
	40	1,471,473	1,968,367	2,190,486	2,701,885	2,913,534	3,180,038
	70	324,882	539,393	660,249	1,010,286	1,189,285	1,447,937
	100	62,797	109,193	139,235	243,781	308,188	415,665
	130	19,817	30,738	37,856	63,720	80,726	111,134
S9.5B	14	2,899,388	3,299,058	3,450,426	3,753,103	3,863,378	3,992,102
	40	1,331,997	1,811,959	2,026,158	2,515,590	2,715,931	2,965,832
	70	288,772	492,081	608,736	950,779	1,126,667	1,380,661
	100	57,431	100,916	129,578	231,313	295,013	402,352
	130	19,139	29,463	36,289	61,535	78,414	108,968
S9.5C	14	3,477,881	3,841,349	3,978,499	4,253,698	4,354,765	4,473,690
	40	1,915,519	2,416,838	2,629,637	3,099,006	3,286,307	3,517,430
	70	548,155	851,110	1,009,796	1,435,346	1,637,966	1,917,046
	100	116,295	200,761	253,085	424,099	522,833	679,183
	130	32,804	53,196	66,459	113,843	144,196	196,949
S12.5B	14	3,178,414	3,586,118	3,739,780	4,046,213	4,157,675	4,287,727
	40	1,452,961	1,964,701	2,191,357	2,706,541	2,916,672	3,178,440
	70	307,341	531,349	659,089	1,030,335	1,219,596	1,491,335
	100	58,842	109,831	143,798	264,458	339,549	464,961
	130	18,682	32,139	41,344	76,329	100,049	143,076
S12.5C	14	3,340,219	3,700,879	3,837,932	4,114,968	4,217,531	4,338,902
	40	1,851,067	2,331,465	2,535,961	2,988,577	3,169,989	3,394,700
	70	561,247	849,585	1,000,516	1,405,293	1,598,028	1,863,503
	100	141,662	224,805	275,254	437,969	531,270	678,717
	130	51,511	73,340	86,887	133,214	161,962	211,080
S12.5D	14	3,739,485	4,152,910	4,313,858	4,647,005	4,773,395	4,925,452
	40	2,066,922	2,578,282	2,799,001	3,297,101	3,501,255	3,758,382
	70	641,318	955,516	1,116,352	1,542,608	1,745,059	2,025,161
	100	141,206	239,633	298,200	481,749	584,142	743,059
	130	33,509	57,493	72,870	126,352	159,616	216,050
I19.0B	14	3,516,178	3,903,750	4,045,263	4,319,631	4,416,711	4,528,028
	40	1,761,953	2,331,003	2,573,455	3,102,926	3,310,402	3,562,090
	70	398,660	678,231	836,324	1,286,905	1,510,664	1,824,379
	100	85,424	146,350	186,846	331,286	421,602	572,740
	130	33,955	49,287	59,464	97,304	122,704	168,762

Appendix I (Continued)

I19.0C	14	2,687,128	3,190,620	3,396,983	3,839,790	4,012,382	4,222,536
	40	1,292,943	1,756,971	1,973,450	2,494,634	2,720,108	3,012,654
	70	337,491	540,185	653,306	981,402	1,150,628	1,397,794
	100	69,380	116,300	145,516	243,427	302,122	398,769
	130	18,774	28,708	34,962	56,666	70,324	93,956
I19.0D	14	3,732,648	4,127,058	4,276,441	4,576,884	4,687,380	4,817,439
	40	2,090,704	2,622,913	2,849,303	3,350,128	3,550,608	3,798,493
	70	627,698	958,895	1,130,474	1,587,023	1,803,342	2,100,782
	100	136,257	233,058	292,170	482,360	590,704	760,845
	130	36,807	59,968	74,913	127,697	161,124	218,706
B25.0B	14	3,650,444	4,020,452	4,155,821	4,419,026	4,512,461	4,619,839
	40	1,944,851	2,505,635	2,741,078	3,251,255	3,450,356	3,691,698
	70	484,380	806,122	980,709	1,458,624	1,688,168	2,003,978
	100	94,819	172,359	223,463	401,314	509,155	684,735
	130	30,392	48,917	61,491	109,004	141,091	199,100
B25.0C	14	3,634,329	4,064,777	4,223,683	4,535,081	4,646,578	4,775,552
	40	1,751,551	2,341,438	2,598,012	3,167,991	3,394,699	3,672,163
	70	392,383	655,843	806,164	1,243,391	1,465,658	1,782,844
	100	79,950	137,614	175,094	306,900	389,089	527,423
	130	26,235	40,078	49,126	82,174	104,067	143,532
RS9.5A	14	2,652,862	2,938,077	3,043,194	3,248,638	3,321,872	3,406,206
	40	1,335,698	1,742,148	1,917,017	2,303,982	2,457,826	2,646,312
	70	323,879	525,164	636,486	950,654	1,106,696	1,326,855
	100	74,396	123,046	154,024	259,781	323,709	428,679
	130	28,873	42,180	50,680	80,856	100,284	134,453
RS9.5B	14	2,994,001	3,295,937	3,408,431	3,631,035	3,711,516	3,805,146
	40	1,631,285	2,060,809	2,243,381	2,645,422	2,805,211	3,001,505
	70	467,391	715,439	846,604	1,202,304	1,373,449	1,610,725
	100	115,248	184,433	226,695	364,161	443,673	570,244
	130	42,367	61,224	72,961	113,264	138,370	181,385
RS9.5C	14	3,076,920	3,348,575	3,447,891	3,641,252	3,710,078	3,789,381
	40	1,784,319	2,214,005	2,391,607	2,772,542	2,920,152	3,098,577
	70	542,946	826,221	972,886	1,359,879	1,540,724	1,786,023
	100	134,092	217,396	268,328	432,943	527,062	674,956
	130	48,675	71,277	85,499	134,786	165,655	218,591

Appendix I (Continued)

RI19.0B	14	3,295,213	3,616,694	3,735,321	3,968,100	4,051,584	4,148,228
	40	1,810,157	2,289,367	2,490,990	2,930,009	3,102,462	3,312,643
	70	518,508	804,845	956,408	1,365,502	1,560,713	1,829,143
	100	130,213	212,930	264,011	431,275	528,177	682,015
	130	49,848	73,991	89,288	142,681	176,313	234,205
RI19.0C	14	3,369,350	3,637,481	3,734,781	3,923,087	3,989,741	4,066,284
	40	2,065,381	2,513,600	2,695,550	3,080,064	3,227,100	3,403,450
	70	685,031	1,020,556	1,189,208	1,621,306	1,817,882	2,079,961
	100	169,710	279,048	344,847	552,396	667,988	845,847
	130	56,206	85,941	104,757	169,925	210,484	279,401
RB25.0B	14	3,543,504	3,834,812	3,937,512	4,130,374	4,196,413	4,270,517
	40	2,055,852	2,573,375	2,783,651	3,223,782	3,389,326	3,584,872
	70	581,526	911,190	1,086,270	1,555,770	1,776,690	2,075,807
	100	141,975	226,810	280,188	459,151	565,053	735,463
	130	57,972	79,657	93,363	141,518	172,259	226,015
RB25.0C	14	3,045,763	3,285,924	3,368,299	3,518,942	3,569,082	3,624,287
	40	1,775,014	2,238,695	2,423,937	2,803,199	2,942,207	3,103,301
	70	489,990	790,201	951,598	1,384,941	1,587,373	1,858,502
	100	121,781	198,475	247,940	417,632	519,581	684,498
	130	52,846	73,271	86,496	134,265	165,497	220,972

APPENDIX II   COMPLEX SHEAR MODULUS (G*) DATABASE

Binder Grade	Temperature (°F)	|G*| (Pa)	Phase Angle (degree)
PG64-22	50.0	15,600,000	36.8
	77.0	1,668,000	58.2
	104.0	144,000	68.6
	147.2	4,500	82.4
PG70-22	50.0	17,800,000	33.5
	77.0	2,175,000	54.5
	104.0	211,750	64.1
	140.0	13,700	75.5
	158.0	3,843	81.0
PG76-22	50.0	24,582,328	42.5
	66.2	6,146,101	50.3
	86.0	1,118,810	57.9
	104.0	245,433	61.5
	122.0	63,015	63.9
	140.0	19,482	63.6
	158.0	6,403	66.2
	168.8	3,529	66.7